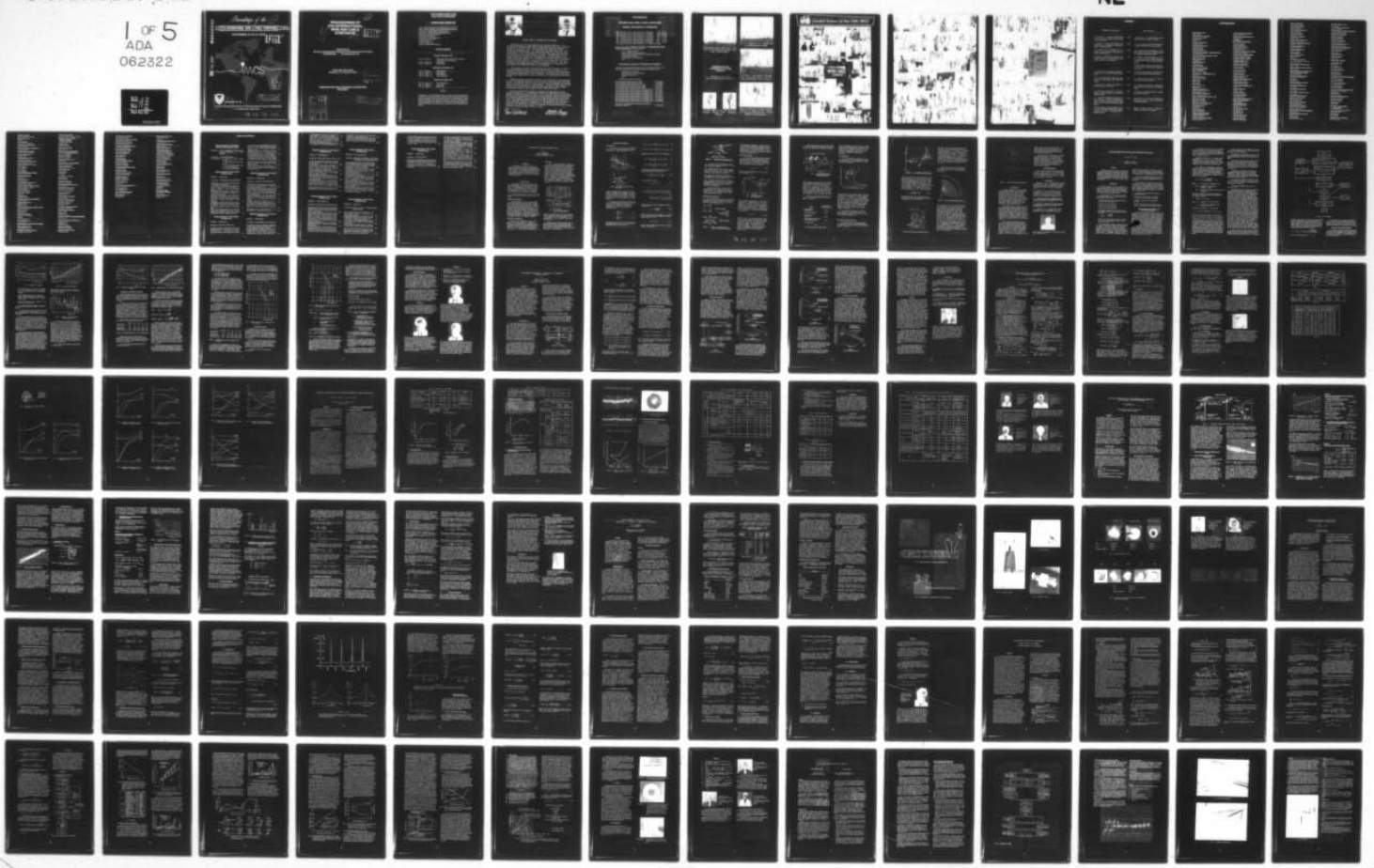
AD-A062 322 ARMY COMMUNICATIONS RESEARCH AND DEVELOPMENT COMMAND --ETC F/G 13/9
PROCEEDINGS OF THE INTERNATIONAL WIRE AND CABLE SYMPOSIUM (27TH--ETC(U)
NOV 78 E F GODWIN

UNCLASSIFIED NL

1 OF 5
ADA
062322



AD A062322

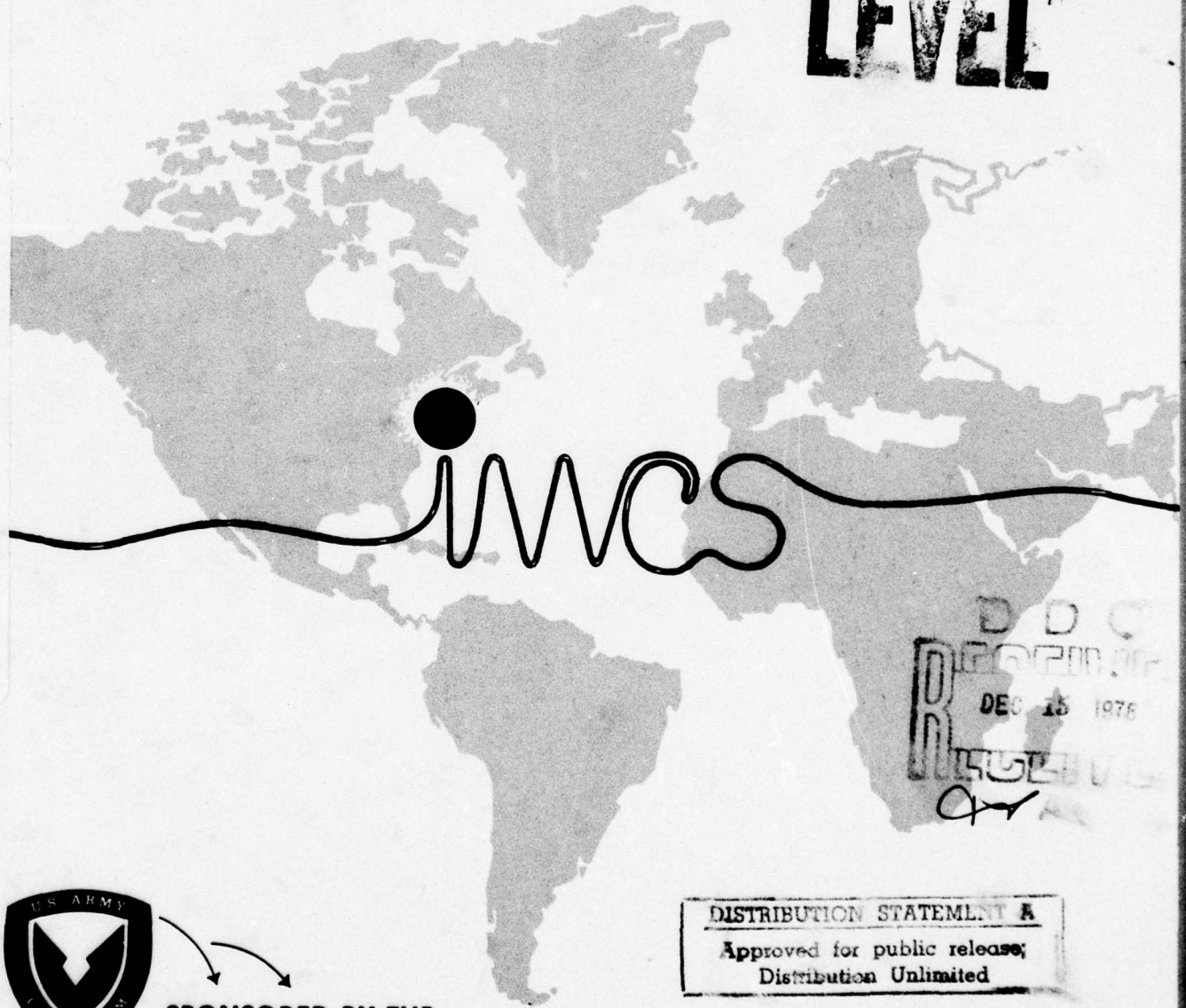
DDC FILE COPY

Proceedings of the (12)

27th INTERNATIONAL WIRE & CABLE SYMPOSIUM

NOVEMBER 14-15-16 1978

LEVEL II



DDC
RECEIVED
DEC 15 1978
B

DISTRIBUTION STATEMENT A
Approved for public release;
Distribution Unlimited

SPONSORED BY THE

U S Army Communications Research and Development Command (CORADCOM)

Fort Monmouth, New Jersey

78 12 15 042

(12)

PROCEEDINGS OF 27th INTERNATIONAL WIRE AND CABLE SYMPOSIUM

See back page for #1473

AD A047609

LEVEL II

Sponsored by
US Army Communications Research and Development Command
(CORADCOM) Fort Monmouth, N.J.

Cherry Hill, New Jersey
November 14, 15 and 16, 1978

DDC
DEC 15 1978
A

APPROVED FOR PUBLIC RELEASE: DISTRIBUTION UNLIMITED

ACCESSION for
NTIS White Section
DDC Buff Section
UNANNOUNCED
JUSTIFICATION
BY
DISTRIBUTION/AVAILABILITY CODES
Dist. AVAIL. and/or SPECIAL
A

DISTRIBUTION STATEMENT A
Approved for public release;
Distribution Unlimited

27th INTERNATIONAL WIRE AND CABLE SYMPOSIUM

SYMPOSIUM COMMITTEE

Elmer F. Godwin, Chairman, USA CORADCOM (201) 544-2770
Milton Tenzer, Co-Chairman, USA CORADCOM (201) 544-4834
Adolf Asam, ITT Electro-Optical Products Division
M. A. DeLucia, David W. Taylor Naval Ship R & D Ctr.
Marta Farago, Northern Telecom Ltd.
F. M. Farrell, 3M Company
Irving Kolodny, General Cable Corp.
K. Bow, Dow Chemical, USA
Joe Neigh, AMP Inc.
Frank Short, Belden Corp.
George H. Webster, Bell Laboratories

TECHNICAL SESSIONS

Tuesday, 14 November 1978

9:30 a.m.	Session I:	Tutorial-Advanced Communications Networks-Responding to Future Demands
2:00 p.m.	Session II:	Cable Design I
2:00 p.m.	Session III:	Manufacturing

Wednesday, 15 November 1978

9:00 a.m.	Session IV:	Cable Materials I
9:00 a.m.	Session V:	Cable Design II
2:00 p.m.	Session VI:	Cable Materials II
2:00 p.m.	Session VIII:	Cable Applications

Thursday, 16 November 1978

9:00 a.m.	Session VIII:	Fire Considerations
9:00 a.m.	Session IX:	Optical Fiber
2:00 p.m.	Session X:	Optical Cable

PAPERS

Responsibility for the contents rests upon the authors and not the symposium Committee or its members. After the symposium all the publication rights of each paper are reserved by their authors, and requests for republication of a paper should be addressed to the appropriate author. Abstracting is permitted, and it would be appreciated if the symposium is credited when abstracts or papers are republished. Requests for individual copies of papers should be addressed to the authors.





MESSAGE FROM THE CHAIRMAN AND CO-CHAIRMAN

Welcome to the 27th International Wire and Cable Symposium. It is extremely gratifying to report that the 26th symposium last year was equally successful as the 25th Silver Jubilee celebration, which was the most successful symposium to date. The attendance was greater than 1600. The international representation from twenty-seven countries increased significantly (210 vs. 170). Twenty-nine of the fifty-five papers presented were by representatives from ten different countries. The symposium, with its large national and international representation, provides attendees with the most effective procedure for reviewing and discussing latest developments in the wire/cable industry. It also provides a convenient media for the exchange of related technical information of special interest. The quality of the technical papers continues to be outstanding and is considered the key element to the continued growth of the symposium.

The response to the call for papers was excellent this year. A total of fifty-three technical papers covering topics of current interest will be presented, following the opening tutorial session, entitled "Advanced Communication Networks Responding To Future Demands". The timely topic and distinguished panel members should make the tutorial an interesting and stimulating session.

Committee members Joe Neigh of AMP Inc. and Tim Farrell of the 3M Company are retiring from the Committee after four years of dedicated and outstanding service. Joe and Tim, by their efforts and specialized knowledge, contributed significantly to the success of the symposium. Needless to say, they will be missed, and, on behalf of the Committee, we thank them for their valuable contributions and wish them success in their future activities.

We wish to take this opportunity to express our appreciation to all Committee members for their unstinting efforts and cooperation in making the symposium a continued success each year, and to the many individual governmental and industrial organizations for their continued support and/or contributions. The symposium cannot prosper without their sustained participation and attendance. The Committee continues to look for ways to improve the activities of the symposium, therefore, suggestions or recommendations are requested for promoting the interchange of information and the technical growth of the symposium. We solicit the support of all members of the wire and cable industry to insure continued success in years to come.

ELMER F. GODWIN, Chairman

MILTON TENZER, Co-Chairman

PROCEEDINGS

INTERNATIONAL WIRE & CABLE SYMPOSIUM

BOUND—AVAILABLE AT CORADCOM

20th	International Wire & Cable Symposium Proceedings	—	1971 —	$ 4.00
21st	International Wire & Cable Symposium Proceedings	—	1972 —	$ 5.00
22nd	International Wire & Cable Symposium Proceedings	—	1973 —	$ 6.00
23rd	International Wire & Cable Symposium Proceedings	—	1974 —	$ 7.00
24th	International Wire & Cable Symposium Proceedings	—	1975 —	$ 7.00
26th	International Wire & Cable Symposium Proceedings	—	1977 —	$ 8.00
*27th	International Wire & Cable Symposium Proceedings	—	1978 —	$10.00

*Extra Copies 1-3 $10.00; Next 4-10 $8.00; next 11 and above $5.00 each.

Make check or bank draft **PAYABLE** in **US dollars** to the **INTERNATIONAL WIRE & CABLE SYMPOSIUM** and forward request to:

Mr. E. F. Godwin, Chairman
International Wire & Cable Symposium
US Army Communications Research & Development Command
ATTN: DRDCO-COM-RM-1
Fort Monmouth, New Jersey 07703
USA

PHOTOCOPIES—AVAILABLE AT DEPARTMENT OF COMMERCE

Photocopies are available for complete sets of papers for 1964 and 1966 thru 1976. Information on prices and shipping charges should be requested from the:

US Department of Commerce
National Technical Information Service
Springfield, Virginia 22151
USA

Include Title, Year and "AD" Number.

13th Annual Wire & Cable Symposium (1964)	— AD 787164
15th Annual Wire & Cable Symposium (1966)	— AD A006601
16th International Wire & Cable Symposium (1967)	— AD 787165
17th International Wire & Cable Symposium (1968)	— AD 787166
18th International Wire & Cable Symposium (1969)	— AD 787167
19th International Wire & Cable Symposium Proceedings 1970	— AD 714985
20th International Wire & Cable Symposium Proceedings 1971	— AD 733399
21st International Wire & Cable Symposium Proceedings 1972	— AD 752908
22nd International Wire & Cable Symposium Proceedings 1973	— AD 772914
23rd International Wire & Cable Symposium Proceedings 1974	— AD A003251
24th International Wire & Cable Symposium Proceedings 1975	— AD A017787
25th International Wire & Cable Symposium Proceedings 1976	— AD A032801
26th International Wire & Cable Symposium Proceedings 1977	— AD A047609
Kwix Index of Technical Papers, International Wire & Cable Symposium (1952-1975)	— AD A027558



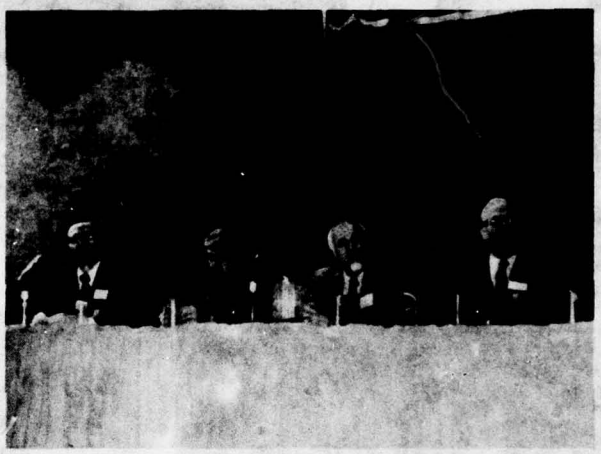
Guest Speaker, Major General Jack L. Hancock, U.S. Army Computer Systems Command, Ft Belvoir, Virginia



Col. D. A. Slingerland, Dir. of COMM/ADP Lab introducing Guest Speaker

Highlights of the 26th International Wire and Cable Symposium

November 15, 16, 17, 1977
Cherry Hill Hyatt House, Cherry Hill, N.J.



Panel Members-Tutorial Session, Wilson MaGruder, REA, Jim Egan, AMP Inc., John Haas, Navy, and Bruce Tyrell, Northern Telecom



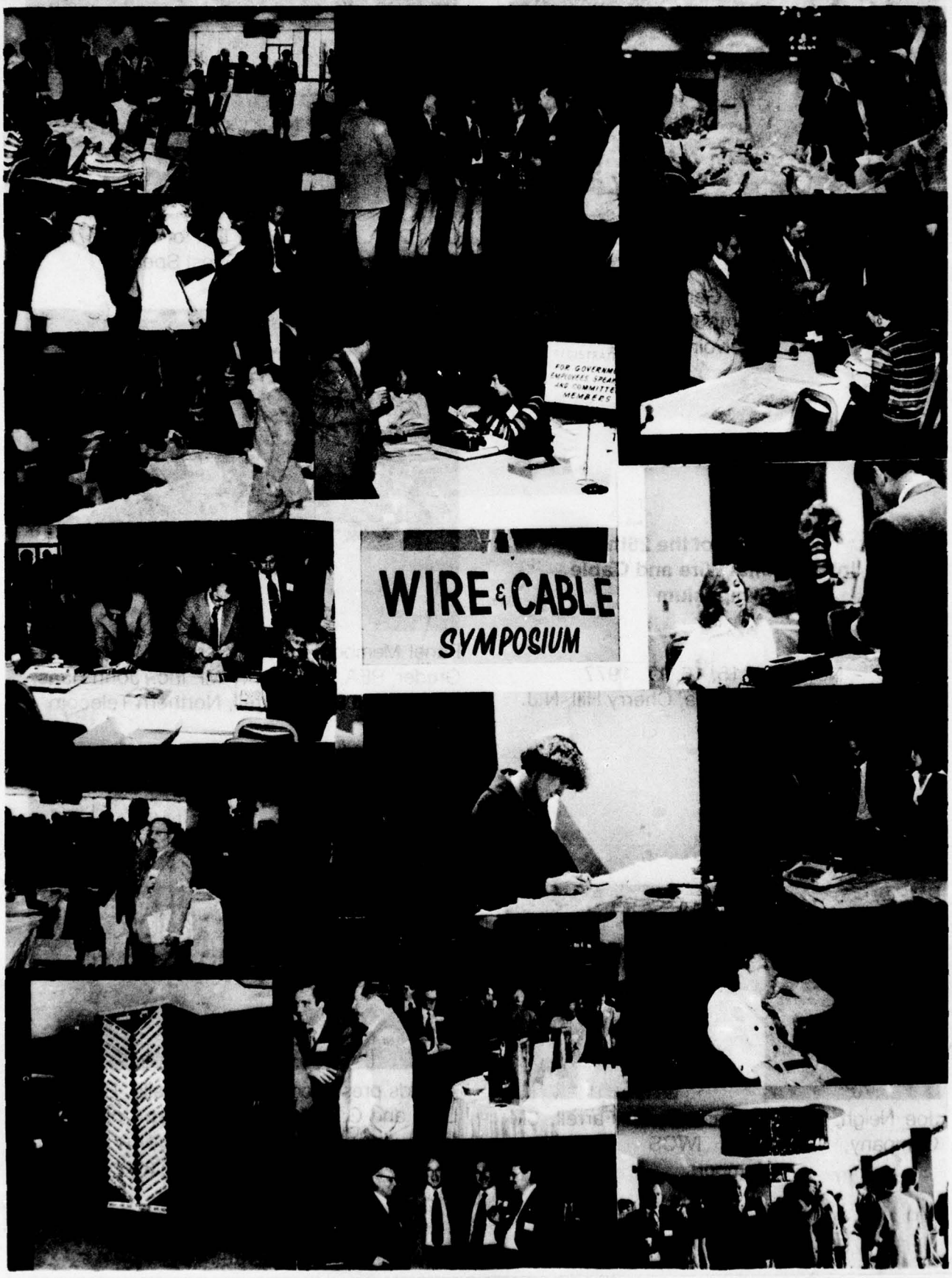


Joe Neigh, AMP Inc. and F. M. Farrell, 3M Company, Retiring IWCS Committee Members.

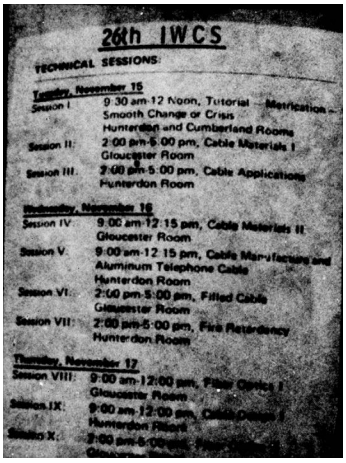


Awards presented to N. J. Cogelia, Bell Tele. Labs and G. K. Lavoie, U.S. Dept. of Interior for outstanding technical paper; and M. Delucia, for best presentation

Candid Scenes at the 26th IWCS







26th IWCS

TECHNICAL SESSIONS:

Tuesday, November 15

Session I: 9:30 am-12 Noon, Tutorial — Metrication — Smooth Change or Crisis
Hunterdon and Cumberland Rooms

Session II: 2:00 pm-5:00 pm, Cable Materials I
Gloucester Room

Session III: 2:00 pm-5:00 pm, Cable Applications
Hunterdon Room

Wednesday, November 16

Session IV: 9:00 am-12:15 pm, Cable Materials II
Gloucester Room

Session V: 9:00 am-12:15 pm, Cable Manufacture and Aluminum Telephone Cable
Hunterdon Room

Session VI: 2:00 pm-5:00 pm, Filled Cable
Gloucester Room

Session VII: 2:00 pm-5:00 pm, Fire Resistance
Hunterdon Room

Thursday, November 17

Session VIII: 9:00 am-12:00 pm, Fiber Optics I
Gloucester Room

Session IX: 9:00 am-12:00 pm, Cable Design I
Hunterdon Room

Session X: 2:00 pm-5:00 pm, [illegible]
[illegible]

AWARDS

	Outstanding Technical Paper	*Best Presentation*
1968	H. Lubars and J. A. Olszewski, General Cable Corp—"Analysis of Structural Return Loss in CATV Coaxial Cable"	N. Dean, B.I.C.C.—"The Development of Fully Filled Cables for the Distribution Network"
1969	J. B. McCann, R. Sabia and B. Wargotz, Bell Laboratories—"Characterization of Filler and Insulation in Waterproof Cable"	J. D. Kirk, Alberta Government Telephones—"Progress and Pitfalls of Rural Buried Cable"
1970	D. E. Setzer and A. S. Windeler, Bell Laboratories—"A Low Capacitance Cable for the T2 Digital Transmission Line"	Dr. O. Leuchs, Kable and Metalwerke—"A New Self-Extinguishing Hydrogen Chloride Binding PVC Jacketing Compound for Cables"
1971	R. Iyenger, R. McClean and T. McManus, Bell Northern Research—"An Advanced Multi-Unit Coaxial Cable for Tool PCM Systems"	S. Nordblad, Telefonaktiebolaget LM Ericsson—"Multi-Paired Cable of Nonlayer Design for Low Capacitance Unbalance Telecommunication Network" N. Kojima, Nippon Telegraph and Telephone—"New Type Paired Cable for High Speed PCM Transmission"
1972	J. B. Howard, Bell Laboratories—"Stabilization Problems with Low Density Polyethylene Insulations"	S. Kaufman, Bell Laboratories—"Reclamation of Water-Logged Buried PIC Telephone Cable"
1973	Dr. H. Martin, Kabelmetal—"High Power Radio Frequency Coaxial Cables, Their Design and Rating"	R. J. Oakley, Northern Electric Co., Ltd.—"A Study into Paired Cable Crosstalk"
1974	D. Doty, AMP Inc.—"Mass Wire Insulation Displacing Termination of Flat Cable"	G. H. Webster, Bell Laboratories—"Material Savings by Design in Exchange and Trunk Telephone Cable"
1975	T. S. Choo, Dow Chemical U.S.A.—"Corrosion Studies on Shielding Materials for Underground Telephone Cables"	J. E. Wimsey, United States Airforce—"The Bare Base Electrical Systems"
1976	N. J. Cogelia, Bell Telephone Laboratories and G. K. Lavoie and J. F. Glahn, US Department of Interior—"Rodent Biting Pressure and Chemical Action and Their Effects on Wire and Cable Sheath"	Michael DeLucia, Naval Ship Research and Development Center—"Highly Fire-Retardant Navy Shipboard Cable"
1977	Thomas K. McManus, Northern Telecom Canada Ltd. and R. Beveridge, Saskatchewan Telecommunications, Canada—"A New Generation of Filled Core Cable"	William L. Schmacher, AMP Inc.—"Design Considerations for Single Fiber Connector"

CONTRIBUTORS

Abbey Plastics Corp.
Hudson, Mass.
Allied Chemical Corporation
Morristown, New Jersey
Amerace Corp.
Union, NJ
American Cyanamid Co.
Bound Brook, NJ
American Hoechst Corp.
Leominster, Mass.
AMP Incorporated
Harrisburg, Pennsylvania
The Anaconda Company - Aluminum Division
Louisville, Kentucky
Anaconda Telecommunications - Cable
Overland Park, Kansas
ARCO Chemical Co.
Philadelphia, PA
ARCO/Polymers, Inc.
Philadelphia, Pa.
Arvey Corporation
Cedar Grove, New Jersey
Austral Standard Cables
Pty Ltd., Maidstone
Melbourne, Vic., Australia
Autometrix-Div. of Systems Res. Lab.
Dayton, Ohio
Bakelite Xylonite Ltd.
Grangemouth, Scotland
Belden Corp.
Geneva, Illinois
Bell Canada
Toronto, Ontario, Can.
Berk-Tek, Inc.
Reading, Pennsylvania
Berkshire Electric Cable Co.
Leeds, Massachusetts
BICC Telecomm. Cables Ltd.
Prescot, Merseyside, Eng.
Boston Insulated Wire & Cable Co. Ltd.
Hamilton, Ont. Canada
Brand-Rex Company
Willimantic, Connecticut
Breen Color Concentrates, Inc.
Lambertville, New Jersey
The Bridge Mfg. Co.
Enfield, Conn.
Burndy Corporation
Norwalk, Connecticut
Cabel, Industria Venezolana
de Cables Electricos, C.A.
Caracas, Venezuela
Cable Consultants Corporation
Larchmont, New York
Cable Equipment Corporation
New York, New York
Cables De Comunicaciones, S.A.
Zaragoza, Spain
Cabletronix
Div. of Strom King Industries
Newburgh, New York
Cabot Corporation
Billerica, Massachusetts
Camden Wire Co., Inc.
Camden, New York
Campbell Technical Waxes Limited
Crayford, Kent, England
Canada Wire and Cable Limited
Winnipeg, Manitoba, Canada
Canadian Industries Limited
Brampton, Ontario, Canada
Canadian Pacific Ltd.
Montreal, Quebec, Canada
Carlew Chemicals Ltd.
Montreal, Quebec, Canada
R. E. Carroll, Inc.
Trenton, New Jersey
Cary Chemicals, Inc.
Edison, New Jersey
Chase & Sons Inc.
Randolph, Massachusetts
Colorite Plastics Co.
Division of Dart Industries, Inc.
Ridgefield, New Jersey
Comm/Scope Company
Catawba, North Carolina
Commonwealth Telephone Co.
Dallas, Pa.
Conoco Chemicals
Houston, Texas
Continental Oil Co.
Ponca City, Oklahoma
Corning Glass Works
Corning, New York
Dart Chemical Specialties, S.A.
Wilson Products Division
Assess, Belgium
Davis-Standard Div. of
Crompton & Knowles
Pawcatuck, CT
DCM International Corp.
San Leandro, CA
The Delker Corp.
Branford, Conn.
Delphi Electronics Inc.
Folcroft, Pennsylvania
Diamond Shamrock
Cherry Hill, New Jersey

Disco Incorporated
Ringwood, New Jersey
Dow Chemical U.S.A.
Midland, Michigan
Dow Corning Corporation
Midland, Michigan
Duncan M. Gillies Co.
West Boylston, Mass.
Dussek Bros. Australia
Sydney, Australia
Dussek Bros. (Canada) Ltd.
Belleville, Ontario, Can.
Eastman Chemical Products, Inc.
Kingsport, Tennessee
Electroconductores C.A.
Caracas, Venezuela
Electron Machine Corp.
Umatilla, Florida
The Entwistle Co.
Hudson, Massachusetts
Essex Group, Inc.
Decatur, Ill.
ETS. Pourtier Pere & Fils
c/o Cable Equipment Corporation
New York, New York
Exxon Chemical Company USA
Houston, Texas
Felten & Guilleaume Carlswerk AG
West Germany
Felten & Guilleaume Carlswerk AG
Telecommunication Division
Koln, West Germany
Firestone Plastics Company
Pottstown, Pennsylvania
Formulabs
Escondido, Calif.
Franklin Plastics Corporation
Kearny, New Jersey
The Fujikura Cable Works
Chiba, Japan
The Fujikura Cable Works
Tokyo, Japan
The Furukawa Electric Co. Ltd.
Tokyo, Japan
Gavitt Wire & Cable Co. Inc.
Brookfield, Massachusetts
Gem Gravure Co. Inc.
West Hanover, Mass.
General Cable Corporation
Rahway, New Jersey
General Electric Company
Silicone Products Department
Waterford, New York
General Electric-Insulating Materials
Schenectady, NY
General Engineering USA Ltd.
Stratford, Conn.
G. M. Gest Inc.
Montreal, Quebec, Can.

Gold Star Cable Co., Ltd.
Seoul, Korea
W. L. Gore & Associates, Inc.
Newark, Delaware
Great American Chemical Corporation
Fitchburg, Massachusetts
GTE Service Corporation
Stamford, Connecticut
Harbour Industries
Shelburne, Vermont
Hercules Incorporated
Crowley, Louisiana
Heyman Manufacturing Co.
Kenilworth, New Jersey
High Voltage Engineering Corp.
Burlington, Massachusetts
Hitachi Cable, Ltd.
Tokyo, Japan
Hitemp Wires Inc.
Hauppauge, New York
Hooker Chemical
Hicksville, NY
Hudson Wire Company
Ossining, New York
Ibaraki Elect. Lab.
Tokai, Japan
ICI Americas Inc.
Wilmington, Delaware
Icore International, Inc.
Sunnyvale, CA
Insulated Wire Inc.
Ronkonkoma, NY
International Wire Products Company
Wyckoff, New Jersey
ITT Cannon Electric
Santa Ana, California
ITT Electro-Optical Prod.
Div., Roanoke, Virginia
Judd Wire Division
Turners Falls, Mass.
Kabel-Und Lackdrahtfabriken GmbH
Casterfeldstrasse, Germany
Kabmatik AB
Stockholm, Sweden
Kenrich Petrochemicals, Inc.
Bayonne, New Jersey
Lamart Corporation
Clifton, New Jersey
Laribee Wire
Camden, NY
S.A. Lignes Telegraphiques
ET Telephoniques
Conflans Sainte Honorine, France
Lowe Associates, Inc., J. J.
Bedford Hills, NY
3M Company
St. Paul, Minn.
Madison Wire & Cable Corp.
Worcester, Mass.

Maillefer Company
South Hadley, Massachusetts
Manning Paper Co.
Troy, NY
Micro-Tek Corp.
Cinnaminson, New Jersey
Mohawk Wire & Cable Corp.
Leorminister, Mass.
Monsanto Industrial Chemicals Co.
St. Louis, Missouri
The Montgomery Company
Windsor Locks, Connecticut
Moore & Munger, Inc.
Fairfield, Conn.
H. Muehlstein & Co., Inc.
Montvale, New Jersey
New England Printed Tape Co.
Pawtucket, Rhode Island
Nippon Telegraph & Tel. Corp.
Tokyo, Japan
N.K.F. Kabel b.v.
Delft, Holland
N. L. Industries
Plastics & Speciality Chemicals
Bayonne, New Jersey
Nokia Electronics, Inc.
Atlanta, Ga.
Nonotuck Mfr., Co.
South Hadley, MA
Northeast Wire Company, Inc.
Holyoke, Massachusetts
Northern Telecom Canada Limited
Montreal, Quebec, Canada
NV Habia Benelux
Breda, The Netherlands
Olex Cables Limited
Australia
Omega Wire Inc.
Camden, New York
OY NOKIA AB Finnish Cable Works
Helsinki, Finland
Pacific Electric Wire &
Cable Co., Ltd.
Republic of China
The Pantasote Company of New York Inc.
Passaic, New Jersey
Penn Color, Inc.
Doylestown, Pa.
Pennwalt Corporation
Philadelphia, Pennsylvania
Penreco
Butler, Pennsylvania
A. E. Petsche Co., Inc.
Arlington, Texas
Phelps Dodge Communications Company
White Plains, New York
Phelps Dodge Int. Corp.
Coral Gables, Florida
Philadelphia Insulated Wire Co.
Moorestown, New Jersey
Phillips Cables Limited
Vancouver, British Columbia, Canada
Phillips Chemical Company
A Division of Phillips
Petroleum Company
Pasadena, Texas
Pirelli Cables Ltd.
St. Jean, P. Que., Can.
Pirelli USA Rep. Corp.
New York, NY
Plastic Products & Resins Dept.,
E. I. Du Pont de Nemours & Co.
Wilmington, Delaware
Plastoid Corporation
New York, New York
Plymouth Rubber Co. Inc.
Canton, MA
Plymouth Wire & Cable Company
Worcester, Massachusetts
Polymer Services Inc.
East Brunswick, New Jersey
Prestolite Wire Div.
Hudson, Mass.
Propintel SA,
c/o Cables
Cortaillod SA, Switzerland
Radix Wire Co.
Cleveland, Ohio
Raychem Corporation
Menlo Park, California
RDI (Radiation Dynamics, Inc.)
Long Island, NY
Reichhold Chemicals, Inc.
Hackettstown, New Jersey/
Mansfield, Massachusetts
Reliable Electric Co.
Franklin Park, Ill.
The Rochester Corporation
Culpeper, Virginia
Rohm and Haas Company
Philadelphia, Pennsylvania
Sartomer Company
Westchester, PA
The Seiss Insulating Works Ltd.
Breitenbach, Seitzerland
Shell Chemical Company
Houston, Texas
Siemens AG
Munchen, Germany
Societe Anonyme De Telecommunications
Paris, France
Southwest Chemical & Plastics Co.
Seabrook, Texas
Southwire Co.
Carrollton, Georgia
Sterling Davis Electric
Wallingford, Connecticut
Sumitomo Electric Ind. Ltd
Yokohama, Japan

Sun Chemical Corporation
Paterson, New Jersey
Sun Petroleum Products Company
Philadelphia, Pennsylvania
Superior Cable Corporation
Hickory, North Carolina
The Swiss Insulating Works Ltd.
Breitenbach, Switzerland
Syncro Machine Company
Perth Amboy, New Jersey
Technical Coatings Co.
Nutley, New Jersey
Teknor Apex Co.
Pawtucket, R. I.
Telcom Australia
Lines Construction Branch
Melbourne, Australia
Teledyne Thermatics
Elm City, No. Carolina
Teledyne Western Wire & Cable
Los Angeles, Calif.
Telephone Cables
Dagenham, Essex, England
Tenneco Chemicals, Inc.
Piscataway, New Jersey
Tensolite Company
Division Carlisle Corp.
Buchanan, New York
Thermax Wire Corp.
Flushing, NY
Thermo Conductor Services, Inc.
Prospect, Connecticut
Trea Industries, Inc.
North Kingstown, R.I.
Union Carbide Corporation
Hackensack, New Jersey
USS Chemicals
Pittsburgh, PA
Walter Rose GmbH & Co.
Federal Republic of
Germany
Wardwell Braiding Machine Co.
Central Falls, R. I.
The Ware Chemical Corp.
Stratford, Conn.
Weber & Scher Mfg, Co.
Newark, New Jersey
G. Whitfield Richards Co.
Philadelphia, Pennsylvania
Whitmor Wire & Cable Corp.
North Hollywood, California
Wilcom Products, Inc.
Laconia, New Hampshire
Wilson Products
Assesse, Belgium
The Wire Chemical Corp
Stratford, Conn.
Wire Journal
Guilford, Conn.
Witco Chemical Corp.
New York, N. Y.
Woven Electronics Div.
Mauldin, S. C.
Wyre Wynd Inc.
Jewett City, Connecticut
Wyrough and Loser, Inc.
Trenton, New Jersey
The Zippertubing Co.
Los Angeles, California
LaBarge Inc.
Irvine, CA
Societé Industrielle
De Liaisons Electriques
Paris, France
Wilson Products Co.
Neshanic, N.J.

TABLE OF CONTENTS

Tuesday, November 14, 1978—9:30 am
Hunterdon and Cumberland Rooms

SESSION I: *Tutorial*—Advanced Communication Networks—Responding to Future Demands

Chairperson: F. Farrell, 3M Company
Panel Members: Mr. Howard Anderson, Yankee Group
Mr. Frank Schmicci, GTE Service Corp.
Mr. A. (Tony) Flores, Rural Electrification Administration
Mr. F. M. Banks, Bell Canada

Tuesday, November 14, 1978—2:00 pm
Gloucester Room

SESSION II: Cable Design

Chairperson: Paul Szulborski, Icore, International

GEOMETRICALLY DECOUPLED BALANCED PAIRS, *D. P. Woodard, Bell Laboratories* 1
CAPACITANCE UNBALANCE AND CROSSTALK STUDY FOR SMALL SIZE PLASTIC CABLE, *J. E. Bright, R. A. Clark and P. Nerer, Telecom Australia, Melbourne, Australia* 7
EXPERIMENTAL VERIFICATION OF THEORETICAL LOW FREQUENCY CROSSTALK MODELS, *T. F. McIntosh, Bell Laboratories* 15
COMPLETE ANALYSIS OF THE ELECTRICAL BEHAVIOUR OF A SCREENED QUAD CABLE, *G. C. Groenendaal, Philips' Res. Labs, Eindhoven, Netherlands; and R. R. Wilson, NKF Kabel B. V. Delft, Netherlands* 20
MICROCOAXIAL CABLES INSULATED WITH HIGHLY EXPANDED POLYETHYLENE BY CHEMICAL BLOWING METHOD, *Y. Suzuki, F. Suzuki, A. Mori and S. Sato, Sumitomo Electric Industries, Ltd., Yokohama, Japan* 27
CABLE AND COUPLING DEVICE FOR TELECOMMUNICATION TRANSMISSION IN HIGH-VOLTAGE POWER LINE NETWORKS, *S. Bruggendieck, Felten & Guilleaume Carlswerk AG, Cologne, W. Germany* .. 35

Tuesday, November 14, 1978—2:00 pm
Hunterdon Room

SESSION III: Manufacturing

Chairperson: Frank Short, Beldon Corp.

A NOVEL EXTRUDER SCREW DESIGN FOR THE MANUFACTURE OF A "FOAM SKIN" TELEPHONE WIRE INSULATION, *J. K. Normanton and J. E. Robinson, Bakelite Xylonite Limited, Grangemouth, Scotland, U.K.* 44
RETURN LOSS AND TRANSMISSION DISTORTION DUE TO STRUCTURAL IRREGULARITIES IN COAXIAL CABLE, *L. J. Hall, Telecom Australia, Melbourne, Victoria, Australia* 51
NUMERICAL ANALYSES OF VISCOUS FLOW IN A WIRE COATING DIE, *K. Fuse, K. Orimo, and K. Shibata, The Furukawa Electric Co., Ltd., Tokyo, Japan* .. 62
A NEW PROCESS FOR THE MANUFACTURE OF MAGNET WIRE, *G. Beaud and E. Kertscher, Maillfer, S. A., Ecublens, Switzerland: and B. Schmidt, Kabel & Lackdrahtfabriken GmbH, Mannheim, West Germany* 74
MORE RIGOROUS SHEATHING FOR OUTSIDE PLANT CABLES, *R. Rossi, J. D. Lawler and K. J. Virkus, General Cable Corp.* 84
LARGE SCALE, DYNAMIC CABLE TESTING, *E. A. Falquero, Northern Telecom Canada Limited, Montreal, Quebec, Canada* 92

Wednesday, November 15, 1978—9:00 am
Gloucester Room

SESSION IV: Cable Materials I

Chairperson: Ken Bow, Dow Chemical USA

COPPER DEACTIVATORS FOR POLYOLEFIN INSULATION, *M. G. Chan, H. M. Gilroy, L. Johnson and W. M. Martin, Bell Laboratories* 99
DEVELOPMENT OF NEW COPPER DEACTIVATOR FOR POLYOLEFIN INSULATIONS, *M. Sato, S. Nakagawa, T. Hatta, and H. Noda, Hitachi Cable, Ltd., Hitachi, Japan; and S. Kawawata, Hitachi Densenkako Co., Ltd., Hitachi, Japan* 107
OXIDATIVE STABILITY OF POLYPROPYLENE COMPARED TO HIGH DENSITY POLYETHYLENE, *E. G. Malawer and K. D. Kiss, Phelps Dodge Communications Co.* 116
THERMAL OXIDATIVE STABILITY OF POLY (1-BUTENE), *Ilene P. Heyward, Bell Laboratories* ... 130
THE EFFECT OF FILLING COMPOUND MIGRATION ON CELLUAR INSULATION, *D. Mangaraj, M. C. Biskeborn and K. D. Kiss, Phelps Dodge Communications Co.* 139
THE AGING OF FILLED CABLE WITH CELLULAR INSULATION, *C. K. Eoll, Superior Cable Corp.* 156

Wednesday, November 15, 1978—9:00 am
Hunterdon Room

SESSION V: Cable Design II

Chairperson: George Webster, Bell Laboratories

INSULATION BY POWER AND FIBERS DEPOSITION GIVING WATER BLOCKED TELEPHONE CABLES, *Ph. A. Robert, Propintel SA, Morges, Switzerland* 171
NEW SYMMETRICAL STAR QUAD CABLE FOR SUBSCRIBER LOOPS AND SERVICES, *M. Ohmura, T. Fuchigami and N. Kojima, Nippon Telegraph and Telephone Public Corporation, Tokai, Ibaraki, Japan* 176

AN INCREASED PAIR DENSITY UNDERGROUND FEEDER CABLE, *T. D. Nantz, Bell Laboratories* 187
PETAP CABLE - A NEW CONCEPT IN BURIED CABLE DESIGN, *D. C. Smith, D. R. Bissell and D. Chadwick, British Post Office and BICC Telecommunications Cables Ltd., Wembley, Middx, England* 191
AN IMPROVED SCREENED CABLE DESIGN, *R. Rossi, A. P. Gabriel and J. D. Justiss, General Cable Corp.* 200

Wednesday, November 15, 1978—2:00 pm
Gloucester Room

SESSION VI: Cable Materials II

Chairperson: Marta Farago, Northern Telecom, Ltd.

STUDIES OF INSULATION-CONDUCTOR ADHESION IN VINYL DROP WIRE, *P. C. Warren and J. E. Adams, Bell Laboratories* 206
EVALUATION OF CROSS-LINKED MATERIAL INSULATED ELECTRONIC APPLIANCE HOOK-UP WIRES, *T. Yamamoto, M. Ishibashi and A. Mogi, The Fujikura Cable Works, Ltd., Tokyo, Japan* 213
THE ROLE OF POLYMER PROPERTIES ON PERFORMANCE OF RETRACTILE CORD, *C. C. Ho, Uniroyal Chemical, Division of Uniroyal, Inc.* 220
SHOULDER BREAKING PROBLEMS OF POLYETHYLENE SPECIMENS ON TENSILE STRENGTH TESTS, *J. Cobo and M. Villarig, Cables de Communicaciones, S. A., Zaragoza, Spain* 225
THE RAPID EVALUATION OF THE PROCESSIBILITY OF POLYETHYLENE RESINS FOR USE ON HIGH SPEED INSULATING LINES, *E. P. Marsden, Northern Telecom Canada, Limited, Montreal, Quebec, Canada* 235
BLOWN FILM ANALYSIS OF PVC WIRE AND CABLE COMPOUNDS, *M. F. Marx, Western Electric Co., Inc.* 241

Wednesday, November 15, 1978—2:00 pm
Hunterdon Room

SESSION VII: Cable Applications

Chairperson: Irving Kolodny, General Cable Corp.

IMPROVED RESISTANCE VALUES FOR CRIMPED TERMINATIONS OF NICKEL-PLATED ELECTRICAL WIRE, *R. P. Fialcowitz, M. T. Gromek and N. R. Byrd, Douglas Aircraft Company* 249
NEW JUNCTION CABLE WITH LOADING COILS FOR CABLE TUNNEL USE, *K. Ishizaki and K. Mori, Nippon Telegraph & Telephone Public Corporation, Tokyo, Japan; K. Sugiyama, The Furukawa Electric Co., Ltd., Tokyo, Japan; Y. Iwamoto, Sumitomo Electric Ind., Ltd., Yokohama, Japan; and H. Ishihara, The Fujikura Cable Works, Ltd., Tokyo, Japan* 258
LIGHTNING SURGES IN BURIED, FILLED TELEPHONE DISTRIBUTION CABLE, *J. J. Refi and M. J. Swiderski, Bell Laboratories* 264
LIGHTNING PINHOLES IN CABLE SHEATHS, *H. D. Campbell, Northern Telecom Canada Limited, Montreal, Quebec, Canada; and D. O. Lawrence, Anaconda Telecommunications Cable Products Headquarters* 273
LABORATORY EVALUATION OF BURIED SPLICE CLOSURES, *N. A. Gac, Raychem Corp.* 281
CONECS — A COMPLETE SPLICING SYSTEM FOR AERIAL, BURIED AND UNDERGROUND TELEPHONE PLANT, *D. R. Frey and G. S. Cobb, Bell Laboratories* 281

Thursday, November 16, 1978—9:00 am
Hunterdon Room

SESSION VIII: Fire Considerations

Chairperson: Michael DeLucia, David W. Taylor Naval Ship Research and Development Center

A NON-FLAME PROPAGATING TELEPHONE CABLE FOR INDOOR INSTALLATION, *J. M. Daly, The Okonite Co.; and G. Maltz, Kabel-und Metallwerke Gutehuffnungshuette A.G., Hannover, W. Germany* 293
PYROLYSIS OF PVC AND EXPERIMENTAL PVC COMPOUNDS USING TGA, FURNACE AND OVEN TECHNIQUES WITH RECOVERY STUDIES OF HCl, *A. B. Carel, Continental Oil Co.* 299
FLAME RETARDANTS IN PVC, *E. R. Cox, Conoco Chemicals Research & Development* 306
THE EFFECT OF SILANE COUPLING AGENTS ON FILLED PVC JACKETING FORMULATION PROPERTIES, *J. L. Rodriguez and J. Cobo, Cables de Communicaciones, Zaragoza, Spain* 313
CABLE DESIGN AND MATERIALS FOR HIGH RELIABILITY, SEVERE DUTY AND CIRCUIT INTEGRITY, *R. S. Armstrong, General Electric Co.; and B. C. Milliken, Milibride, Inc.* 321
EFFECT OF FIRE-PROTECTIVE COATING ON AMPACITY OF CABLES IN CABLE TRAYS, *D. V. Paulson, G. C. Gambs, Jr., and S. P. Carfagno, The Franklin Institute Research Laboratories* 325

Thursday, November 16, 1978—9:00 am
Gloucester Room

SESSION IX: Optical Fiber

Chairperson: Adolph R. Asam, ITT Electro-Optical Products Division

EFFECT OF MOISTURE ON THE STRENGTH OF OPTICAL FIBERS, *D. Kalish, B. K. Tariyal and H. C. Chandan, Bell Laboratories* 331
SOME RECENT RESULTS ON FRACTURE STRESS AND MIRROR SIZE FOR OPTICAL FIBERS, *F. Quan, S. T. Gulati and C. B. King, Corning Glass Works* 342
LONG LENGTH, HIGH STRENGTH OPTICAL FIBERS, *M. S. Maklad and A. R. Asam, ITT Electro-Optical Products Division* 346
A SINGLE FIBER ALIGNMENT SYSTEM, *L. M. Borsuk, ITT Cannon Electric; and M. Pomerantz, CORADCOM* 350
SPLICE LOSSES IN FUSION-SPLICED OPTICAL WAVEGUIDE FIBERS WITH DIFFERENT CORE DIAMETERS AND NUMERICAL APERTURES, *D. R. Briggs and L. M. Jayne, Corning Glass Works* 356

STRESS IN FIBERS DURING OPTICAL CABLE MANUFACTURING PROCESS AND INSTALLATION, *T. Kobayashi, Y. Sugaware, R. Yamauchi and K. Inada, The Fujikura Cable Works, Ltd., Chiba-ken, Japan; and N. Uchida, Ibaraki Electrical Communication Lab., Ibaraki-ken, Japan* 362

Thursday, November 16, 1978—2:00 pm
Gloucester room

SESSION X: Optical Cable

Chairperson: Joe Neigh, AMP Inc.

MECHANICAL/ENVIRONMENTAL PERFORMANCE OF RUGGED LIGHTWEIGHT FIBER OPTIC CABLES FOR TACTICAL FIELD APPLICATIONS, *R. J. Freiburger, J. C. Smith and G. A. Gasparian, ITT Electro-Optical Products Division; and M. Pomerantz, CORADCOM* 370

FIBER OPTIC CABLE DESIGN, TESTING AND INSTALLATION EXPERIENCES, *P. R. Bark, Siecor Optical Cables, Inc.; U. Oestreich and Günter Zeidler, Siemens AG, Munich, Germany* 379

DESIGN AND MANUFACTURE OF AN EXPERIMENTAL LIGHTGUIDE CABLE FOR UNDERSEA TRANSMISSION SYSTEM, *R. C. Mondello and R. F. Gleason, Bell Laboratories; and B. W. Fellows and D. A. Hadfield, Simplex Wire and Cable Company* 385

INSTALLATION OF A FIBER OPTIC SYSTEM IN AN ELECTRIC POWER STATION, *O. L. Bishop, ITT Telecommunications Division: and J. C. Smith, ITT Electro Optical Prod. Div* 390

HIGH QUALITY OPTICAL FIBER CABLE FOR TELECOMMUNICATION, *A. Bolza, Pirelli Cables Ltd., Saint Jean, Quebec, Canada; and G. Grasso, M. Pizzorno and A. Portinari, Industrie Pirelli S.P.A., Milan, Italy* 394

UNIT CORE CABLE STRUCTURES FOR OPTICAL COMMUNICATION SYSTEMS, *T. S. Swiecicki, Northern Telecom Canada Limited, Montreal, Quebec, Canada; and F. D. King and F. P. Kapron, Bell-Northern Research, Ottawa, Ontario, Canada* 404

GEOMETRICALLY DECOUPLED BALANCED PAIRS

by

D. P. Woodard
Bell Laboratories
Norcross, Georgia 30071

Abstract

A number of parallel conductor, balanced two-pair cable configurations exist that are inherently decoupled from each other. The principle of decoupling two contiguous pairs geometrically is developed and applied to several configurations for which all pairs are mutually non-interactive.

Introduction

Innumerable technical papers have been included in the International Wire and Cable Symposium Proceedings on crosstalk. This exposure has been such that we know what crosstalk is, how to measure and model it, and how it sometimes limits the use of our wires and cables.

We have learned how to control crosstalk, at least partially; and our ways are these:

Metallic Shielding

The shielded pair is a good example where both electric and magnetic fields can be forced toward zero by the proper choice of shield characteristics. Screens that separate groups of pairs in multiconductor cable is another example; as is the use of ground planes and intervening ground conductors in single plane, multipair configurations. The basic idea is to establish desirable boundaries about pairs or groups of them, so that one neighbor or neighborhood does not disturb another.

Dielectric Shielding

We have also seen how a pair insulated with a low dielectric constant material, polyethylene for example, and overcoated further with a high dielectric constant, high loss material, perhaps a lossy PVC, can be isolated effectively from similar, closely spaced companions.[1,2]

Twisting

This is our standard. Possibly a holdover from earlier textile practice, twisting has permitted us to bundle large groups of pairs into space efficient, low crosstalk cables. Simplistically, if we can maintain perfect twist helices with the correct pitch ratios, the average coupling between geometrically close pairs is vanishingly small. However, the instantaneous electric and magnetic couplings are not small, except at certain points where the couplings reverse. A typical case of coupling between two pairs is shown below.

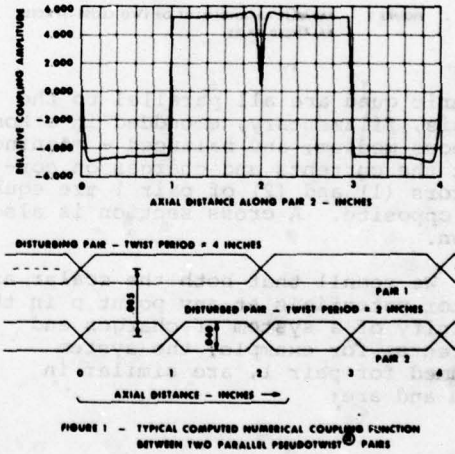


FIGURE 1 - TYPICAL COMPUTED NUMERICAL COUPLING FUNCTION BETWEEN TWO PARALLEL PSEUDOTWIST® PAIRS

Aside from shielding, the only obvious way to diminish coupling magnitudes is to increase the pair separation. Unfortunately, this is not an attractive alternative.

These are the known ways we use to control crosstalk. But another way exists that is particularly attractive for ordered configurations where for some reason the pairs cannot be shielded, twisted, or moved apart.

Geometric Decoupling

Development

We consider conditions required to decouple two contiguous pairs as shown in Figure 2. The conductors of the

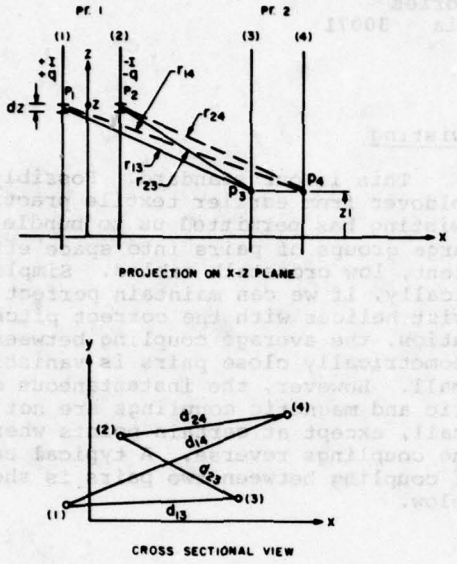


FIGURE 2 – PARALLEL ARRANGEMENT OF TWO CLOSE-SPACED BALANCED PAIRS

generic quad are all parallel to the Z axis, filamentary, embedded in a homogeneous medium, and balanced - meaning that the currents and charges on conductors (1) and (2) of pair 1 are equal and opposite. A cross section is also shown.

We recall that both the scalar and vector potentials at any point p in the vicinity of a system of charges and currents, for example, the system assumed for pair 1, are similar in form and are:

$$V = \sum_{L=1}^{n} \frac{q_i}{4\pi\epsilon r_i} \tag{1}$$

$$\bar{A} = \sum_{k=1}^{n} \frac{\mu I_k}{4\pi r_k} \tag{2}$$

Applying these we write the differential potentials at points P_3 and P_4 at an arbitrary point z_1 on pair 2:

$$(dV_3 - dV_4) = dV_{34}(z_1) = \frac{q\,dz}{4\pi\epsilon}\left[\frac{1}{r_{13}} - \frac{1}{r_{23}} - \frac{1}{r_{14}} + \frac{1}{r_{24}}\right] \tag{3}$$

$$(d\bar{A}_3 - d\bar{A}_4) = d\bar{A}_{34}(z_1) = \frac{\mu I\,dz}{4\pi}\left[\frac{1}{r_{13}} - \frac{1}{r_{23}} - \frac{1}{r_{14}} + \frac{1}{r_{24}}\right] \tag{4}$$

Integration gives the total potentials

$$V_{34}(z_1) = \left(\frac{q}{4\pi\epsilon}\right) \lim_{L\to\infty} \int_{z=-L}^{L} \left(\frac{1}{r_{13}} - \frac{1}{r_{23}} - \frac{1}{r_{14}} + \frac{1}{r_{24}}\right) dz \tag{5}$$

$$\bar{A}_{34}(z_1) = \left(\frac{\mu I}{4\pi}\right) \lim_{L\to\infty} \int_{z=-L}^{L} \left(\frac{1}{r_{13}} - \frac{1}{r_{23}} - \frac{1}{r_{14}} + \frac{1}{r_{24}}\right) \bar{a}z \tag{6}$$

The integral similarity results in a geometric potential function

$$\phi(z_1) = \int_{z=-L}^{L} \left(\frac{1}{r_{13}} - \frac{1}{r_{23}} - \frac{1}{r_{14}} - \frac{1}{r_{24}}\right) dz \tag{7}$$

From Figure 2 since

$$r^2_{ij} = d_{ij}^2 + (z - z_1)^2 \tag{8}$$

$$\phi(z_1) = \lim_{L\to\infty} 2\left\{ \int_0^L \frac{dz}{\left[d_{13}^2 + (z-z_1)^2\right]^{1/2}} - \int_0^L \frac{dz}{\left[d_{23}^2 + (z-z_1)^2\right]^{1/2}} \right. \tag{9}$$
$$\left. - \int_0^L \frac{dz}{\left[d_{14}^2 + (z-z_1)^2\right]^{1/2}} + \int_0^L \frac{dz}{\left[d_{24}^2 + (z-z_1)^2\right]^{1/2}} \right\}$$

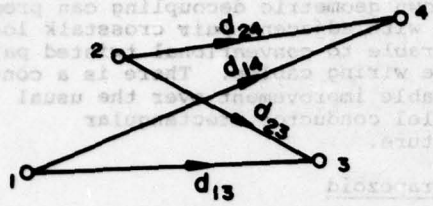
This is a well known integral with the solution[3,4]

$$\phi(z_1) = 2 \ln \frac{(d_{13}d_{24})}{(d_{14}d_{23})} \tag{10}$$

Since z_1 is arbitrary on pair 2, a sufficient condition for decoupling the two pairs ($\phi(z_1) = 0$) is

$$d_{13}d_{24} = d_{14}d_{23} \tag{11}$$

This is our decoupling rule and is illustrated in Figure 3.



$$d_{13}\, d_{24} = d_{14}\, d_{23}$$

FIGURE 3 – GEOMETRIC DECOUPLING RULE

In view of the assumptions, there are some practicalities implicit in (11) that should be stated:

(a) Quadrilaterals with vertex separations that satisfy (11), if any exist, should be such that pair conductors are balanced with respect to ground;

(b) Conductor shapes and dielectric inhomogenities and boundaries will alter the idealistic rule given by (11);

(c) It may not be possible to achieve perfect electric and magnetic decoupling simultaneously with a given geometry because of conductor finite size and dielectric boundaries.

These items have not been studied in any depth. We have concentrated instead on purely geometric interpretations of (11) to see what useful cable configurations may exist.

Simple Configurations

We note first that both the standard quad and "tee" configurations, shown below and with which we are all familiar, satisfy the decoupling rule.

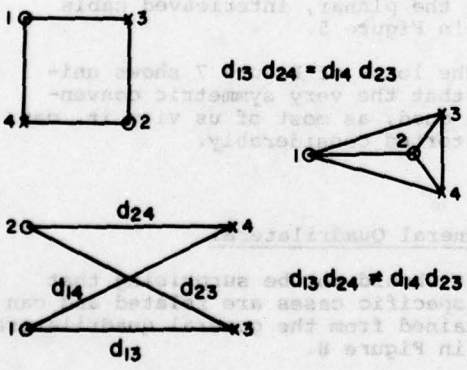


FIGURE 4 – SIMPLE 2 PAIR GEOMETRIES THAT ILLUSTRATE GEOMETRIC DECOUPLING

A rectangular conductor arrangement, however, does not decouple, except in the limit as the diagonal distances approach equality with the side distances. But the concept is consistent with our earlier observations relative to crosstalk reduction by separating pairs.

The Parallelogram

A little distortion of the rectangle produces a very useful geometry - the parallelogram. Applying the decoupling rule (11) to this configuration with a little algebra, it is easy to show that the decoupling locus is given by

$$x = (2 \cos 2\alpha)^{1/2} \qquad (12)$$

The locus and geometry are both shown below, Figure 5.

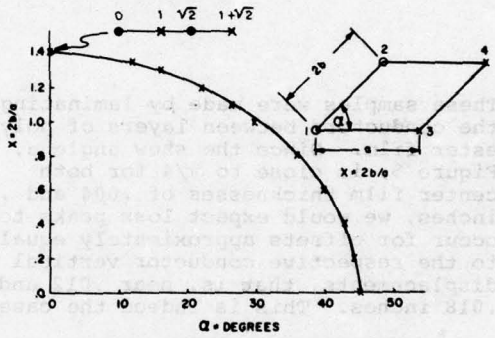


FIGURE 5 – NORMALIZED DECOUPLING LOCUS FOR THE PARALLELOGRAM

α is the skew angle and x is the side to side ratio. α approaches π/4 as the structure becomes very thin, or conversely, as the pair spacing increases. Shown also is the planar, interleaved cable that results when $x = \sqrt{2}$ and $\alpha = 0$. For this case it is quite easy to show that the mutual inductance linking the two pairs is

$$L_m = \frac{u}{2\pi} \ln (x^2 - 1) \qquad (13)$$

which is zero for the normalized dimensions given. Except for the flat case, all parallelograms represented by the locus are "open" in the sense that another adjacent decoupled pair can always be added. The two pair flat cable is "closed" in that it does not have this geometric characteristic. We will encounter other "closed" geometries.

78 12 15 042

Some experimental results are given in Figure 6 that shows near end crosstalk loss as a function of conductor offset.

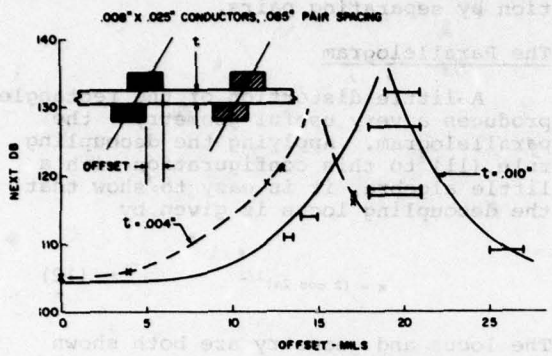


FIGURE 6 – MEASURED NEAR END CROSSTALK (NEXT) LOSS FOR TWO PAIR PARALLELOGRAM GEOMETRY EXPERIMENTAL CABLES

These samples were made by laminating the conductors between layers of polyester film. Since the skew angle α, Figure 5, is close to $\pi/4$ for both center film thicknesses of .004 and .010 inches, we would expect loss peaks to occur for offsets approximately equal to the respective conductor vertical displacements, that is, near .012 and .018 inches. This is indeed the case.

Repeating the parallelogram structure for 25 pairs gives the results shown in Table 1.

CABLE	TYPICAL NEXT dB/10FT./600Ω/1KHz
PARALLEL COND. FLAT (RECT. GEOMETRY)*	90–100
2 PAIR INSIDE WIRE (QUAD.)	120–130
25 PAIR INSIDE CABLE (TWISTED PAIR)	120–140
25 PAIR GEOMETRICALLY DECOUPLED PARALLEL CONDUCTOR CABLE*	110–150

* .085" PAIR SPACING

TABLE I

NEXT LOSS COMPARISON FOR DIFFERENT CABLES

As shown geometric decoupling can produce cable with adjacent pair crosstalk loss comparable to conventional twisted pair inside wiring cables. There is a considerable improvement over the usual parallel conductor, rectangular structure.

The Trapezoid

The trapezoidal configuration is a generalization of the conventional quad; its cross section and decoupling locus is shown in Figure 7.

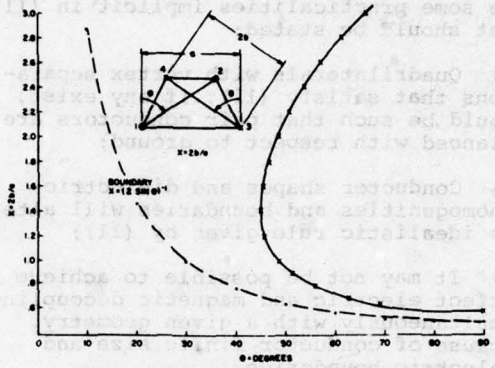


FIGURE 7 – NORMALIZED DECOUPLING LOCUS FOR THE ISOSCELES TRAPEZOID

Geometrically one can shown that the distance between conductors 2 and 4, d_{24}, is zero when $x = (2\sin\theta)^{-1}$. This boundary is shown. Since all x that satisfy the decoupling rule are greater than $(2\sin\theta)^{-1}$ for $0 \leq \theta \leq \pi/2$, the pair axes must cross and the structure is closed, i.e., an adjacent decoupled pair cannot be added. When $x = \sqrt{2}$ and $\theta = \pi/4$, we have the conventional quad; when $\theta = \pi/2$, we obtain the planar, interleaved cable shown in Figure 5.

The locus of Figure 7 shows uniquely that the very symmetric conventional quad, as most of us view it, can be distorted considerably.

The General Quadrilateral

It should not be surprising that these specific cases are related and can be obtained from the general quadrilateral shown in Figure 8.

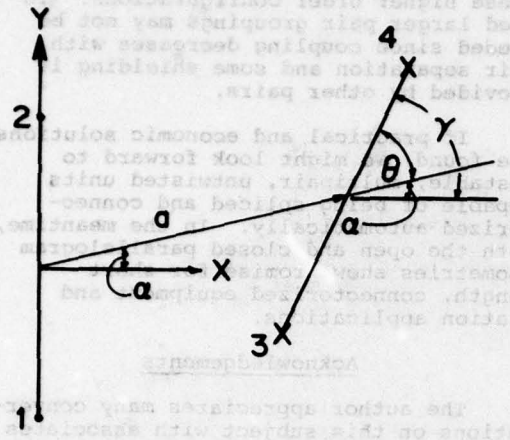


FIGURE 8 – THE GENERAL QUADRILATERAL

As far as possible, we retain our original notation: 2b is the intrapair conductor separation; the center to center pair axis separation is a; and $x = 2b/a$ is still the normalized variable. The axis center of pair 1 is fixed at the (x-y) origin; pair 2 is allowed to translate (distance a, azimuth α) and to rotate (angle γ). With these variables the decoupling rule (11) requires that

$$x = \sqrt{2}\left[\frac{2\cos\theta\sin\alpha}{\sin\gamma} - 1\right]^{1/2}. \qquad (14)$$

The resulting loci can be shown in a variety of ways. An example is Figure 9 drawn for $\alpha = 60°$ and $2b = 1$.

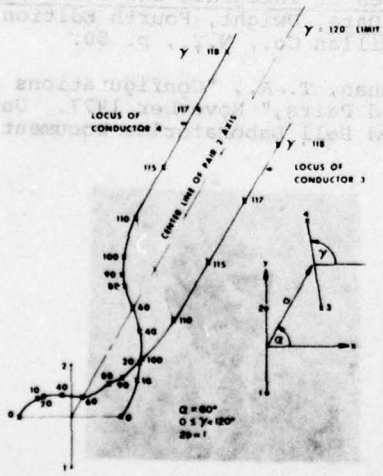


FIGURE 9 – PAIR 2 CONDUCTOR LOCI FOR CONSTANT AZIMUTH ANGLE – α

The two loci are the positions of conductors 3 and 4 required to decouple the two pairs for $a \geq 0$ and $0 \leq \gamma < 120°$. Connecting equal γ on the two loci defines the axis of pair 2. The conventional quad occurs when $a = 0$ and $\gamma = 0$; a trapezoid when $\gamma = 20°$, for example; and a parallelogram for $\gamma = 90°$. Various nonsymmetrical quadrilaterals result with $\gamma > 90°$. The limiting value of γ is 2α which occurs when the pairs are spaced relatively far apart (i.e., $x \cong 4$).

Axis center line loci for pair 2 are shown in Figure 10 for variations in both α and γ, pair 1 remaining at the origin.

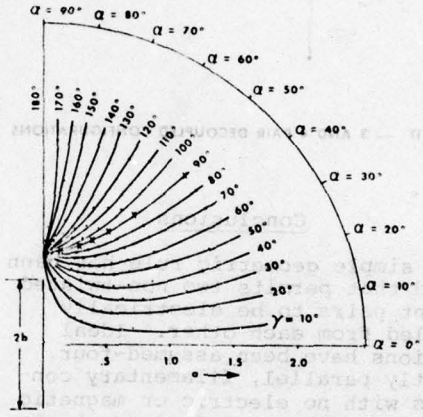


FIGURE 10 – PAIR 2 AXIS CENTER LINES FOR CONSTANT γ

This construction is a direct application of (14). If the axis of pair 2 is centered on a given γ locus, it must also be inclined at the same angle γ from the horizontal to be decoupled from pair 1. The locus $\gamma = 90°$ is easy to visualize as the axis center for all possible parallelograms. For any α, the limiting value of γ is 2α. The center line loci all converge to a common "focal" point ($x = 0$, $y = 1/\sqrt{2}$) when $\alpha = \pi/2$. This is exactly the axis center for pair 2 for the planar intermeshed cable. With pair 2 centered at this point, there is no restriction on γ. An interesting result is the three mutually decoupled pairs shown in Figure 11. A four pair, double parallelogram arrangement is also shown.

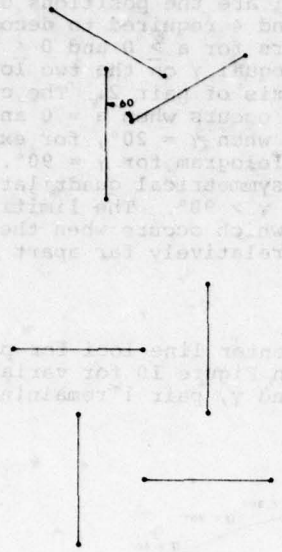


FIGURE 11 – 3 AND 4 PAIR DECOUPLED CONFIGURATIONS

Conclusions

A simple geometric rule has been derived that permits two non-twisted adjacent pairs to be electrically decoupled from each other. Ideal conditions have been assumed-four perfectly parallel, filamentary conductors with no electric or magnetic boundaries. These conditions, however, do not preclude the realization of practical cable configurations with crosstalk losses comparable to conventional twisted-pair cables.

The quadrilaterals that have been discussed are related geometrically. Some are "closed" in the sense that no other adjacent, decoupled pair can be added; the conventional quad and the interleaved, planar, two pair cable are examples. The "open" property of the parallelogram geometry permits the construction of a true multipair cable, albeit the configuration is essentially planar.

More complex structures can be built from this basic quadrilateral concept; mutually decoupled three and four pair structures have been shown. For a grouping of n decoupled pairs, the decoupling rule must apply simultaneously $n(n-1)/2$ times. Lenahan[5] suggests that up to seven pairs in a single ensemble can be mutually decoupled. We have not attempted to find these higher order configurations. Indeed larger pair groupings may not be needed since coupling decreases with pair separation and some shielding is provided by other pairs.

If practical and economic solutions are found, we might look forward to nestable, multipair, untwisted units capable of being spliced and connectorized automatically. In the meantime, both the open and closed parallelogram geometries show promise for short length, connectorized equipment and station applications.

Acknowledgements

The author appreciates many conversations on this subject with associates at Bell Laboratories. In addition, help has been provided by Messrs. C. J. Lever, B. C. Vrieland, and C. A. Elliott of the Western Electric Company.

References

1. Marshall, J. B., "The Uni-Field (Black Magic™) Flat Cable, A New Multi-Signal Transmission Line," Proceedings of 20th International Wire and Cable Symposium, 1971.

2. Marshall, J. B., Linville, R. B., "Explanation for the Dual Dielectric Phenomenon in Differential Crosstalk Control," Proceedings of 21st International Wire and Cable Symposium, 1972.

3. Fields and Waves in Modern Radio, Ramo and Whinnery, Second Edition, John Wiley & Sons, N.Y., p. 100.

4. Tables of Integrals and Other Mathematical Data, Dwight, Fourth Edition, The MacMillan Co., N.Y., p. 50.

5. Lenahan, T. A., "Configurations of Decoupled Pairs," November 1977. Unpublished Bell Laboratories Document.



Dan Woodard is a Member of Technical Staff, Bell Laboratories.

CAPACITANCE UNBALANCE AND CROSSTALK STUDY FOR SMALL-SIZE PLASTIC CABLE

by

R.A. Clark, P. Nerer

Telecom Australia
Melbourne, Australia

Abstract

Telecom Australia has studied the relationship between pair-to-pair capacitance unbalance in individual drumlengths of cable and the near-end crosstalk attenuation on long routes. The study showed that specifying the maximum or RMS unbalance for individual drumlengths is not the best way of controlling crosstalk. A new specification method is described.

Introduction

Telecom Australia, like most telephone administrations, includes in its specification for cable, requirements for pair-to-pair capacitance unbalance. The prime purpose of these requirements is to ensure that occurrences of intelligible crosstalk in the network are rare.

For small-size (6 to 100-pair, in 10-pair units) plastic cable, prior to this study, the specification required that :

- The corrected capacitance unbalance between any pairs shall not exceed:

  210 pF for 0.40 mm conductors

  120 pF for 0.64 mm conductors

  100 pF for 0.90 mm conductors

- The measured capacitance unbalance shall be corrected to the equivalent 1000 metre length as follows :

$$K_{1000} = K\sqrt{\frac{1000}{\ell}}$$

  where K is the measured capacitance unbalance in pF and ℓ is the length in metres of the cable being tested.

The specification aimed to ensure that, when the cable is jointed and loaded with 88 mH coils at 1830 metre spacing, the near-end crosstalk attenuation at 1.6 kHz, arising from capacitance unbalance, should exceed 70 dB for route lengths equal to Telecom's customers' (subscribers') transmission limit. Transmission limits for loaded lines for the very sensitive telephone[1] extensively used for long rural lines are 37 km for 0.90 mm conductor cable and 20 km for 0.64 mm conductor cable. The 0.40 mm conductor cable is used mostly in unloaded form for a maximum distance of 5.7 km.

The 70 dB crosstalk standard is severe but the information in CCITT Recommendation G116 indicates that the standard is appropriate for that telephone.

The limits for 0.40 mm cable proved readily achievable but factory rejections of 0.64 mm and 0.90 mm cable were too frequent. Doubts were held about the impact of rejections and of the diverse manufacturing processes being used, on the achievement of adequate crosstalk performance on the very long routes involved.

The study of this problem has involved three separate phases -

- estimation of the crosstalk performance of individual manufacturing processes.
- analysis of statistics for capacitance unbalance.
- impact of various acceptance limits on the crosstalk performance of the accepted product.

Computer Program for Estimation of Crosstalk Performance

This phase was undertaken with the help of a computer program performing so called "monte carlo" simulation. For simplicity and ease of modification BASIC language was used. Hypothetical routes are created and the near-end crosstalk attenuation (NEXTA) arising from the pair-to-pair capacitance unbalance of the drumlengths used is calculated. Raw pair-to-pair capacitance unbalances (C… …iety of drumlengths as produced by …y preferably with the inclusion of … that the present specification would …ct. The study is conducted separately for results from each factory, for various methods of unit stranding used in that factory and for each conductor size. Where the data supplied was the corrected CU it was converted back to uncorrected data. Approximately 100 lengths were considered adequate for each type of cable.

Input block of data is a set for each length. Each set contains the set number, the length of cable and the values of the capacitance unbalance for all combinations in one unit. For lengths in which a second unit is measured that unit is treated as a separate length.

Normally, CU values are in sequence of pair combinations (1-2, 1-3, 1-4, ..., 9-10), and where data are not in that sequence a routine to re-sequence data is applied. Each block of data contains initial information being manufacturer's identification, pair size and conductor size.

In a typical run the computer creates hypothetical routes of the predetermined length for a particular pair combination by random selection of sets (= drumlengths) and performing straight (colour) jointing. All capacitance unbalances are considered to be located in the centre of each length. They are transformed to equivalent crosstalk ratio by formula :

$$N_i = 20 \log_{10} \left| \frac{8 \times 10^{12}}{\omega K_i |Z_o|} \right| \quad \text{dB}$$

where ω = 2 πf where f is frequency in Hz

$|Z_o|$ = modulus of characteristic impedance in ohms

K_i = capacitance unbalance in pF of the ith drumlength

The NEXTA contribution from that drum length is calculated utilising transmission parameters of the cable as follows :

$$NEXTA_i = N_i + 2\alpha\ell_i$$

where α = attenuation of cable in dB/km

ℓ_i = distance of the unbalance from the near end in km

The phase of the $NEXTA_i$ is calculated by :

$$\phi_i = \Delta\beta_i \pm \frac{\pi}{2} \quad \text{where } \Delta\beta_i = 2 (\beta\ell_i + n\beta_{LC})$$

where $\Delta\beta_i$ is the phase change for the distance ℓ_i made of line phase coefficient and phase shift at loading coil β_{LC}. The term $\pm \frac{\pi}{2}$ is the phase change associated with the capacitance unbalance. As the capacitance unbalance can be either positive or negative, the sign of the phase change is selected by the computer randomly and with equal probability. This is necessary since the factory measurement of CU normally provides only the magnitude and ignores the sign, and it is well known that the mean value of CU when signed is zero. Contributions from all drumlengths are then added on a vectorial basis (as voltages) to give the total NEXTA.

Normally the analysis is conducted at 1.6 kHz and all line parameters and crosstalk calculations are related to that frequency.

The simulation is performed a number of times and the associated statistics program is used to evaluate mean, RMS, min, max, etc., values of the NEXTA.

The computer program is very flexible and it can readily evaluate any selected combination or all possible pair combinations, 45 for 10-pair units and 15 for 6-pair cable. Capacitance unbalances between units in 20-pair and larger cables are known to be insignificant and are therefore not considered.

Furthermore the program can evaluate the crosstalk-frequency response for any selected combination. Random jointing is not used for small-sized cables in Australia, but the program has also been used to assess the crosstalk benefit conferred by random jointing.

A routine for checking data files for possible errors (typing mistakes, too much data, etc.) has been created and it should be used before the main program is operated.

The computer programme block diagram is depicted in Fig. 1.

To determine how many repeats are sufficient for statistical evaluation, 100, 200 and 500 repeats were tried with all combinations being analysed for 6-pair 0.90 mm cable. Results indicated that 100 repeats, which is equivalent to 100 routes and hence 600 pairs and 1500 combinations, will produce crosstalk information with required accuracy but slightly pessimistic results for low values, as more repeats tend to improve results in the 99 to 100% region of the lower end of the pair crosstalk distribution. Thus for any further analysis 100 repeats were used. In this context, 99% has been defined as the sixth worst crosstalk result out of 600 pairs. This result is at the 99.6% point of the crosstalk results for the 1500 combinations. Similarly for 100 routes of 10 pairs, the 99% point is defined to be the tenth worst result out of 1000 pairs and 4500 combinations. This definition may marginally overestimate the quantity of poor crosstalk performance since, in any particular trial,a specific pair may have two or more pairs to which it has poor crosstalk performance. Note also that the definition could be judged as underestimating the performance by a factor of two, since two pairs are involved in each result, and in a network where, as in Australia, customers' cables are not field tested for crosstalk performance, two customers' lines would be exposed to that particular NEXTA. However, if the problem were detected by field testing,only one pair would need to be taken out of service.

As each route is created from 500 to 2000 m lengths and 100 repeats are used and as the transmission limit for 0.90 mm cables is 37 km the procedure becomes computer time and cost consuming.

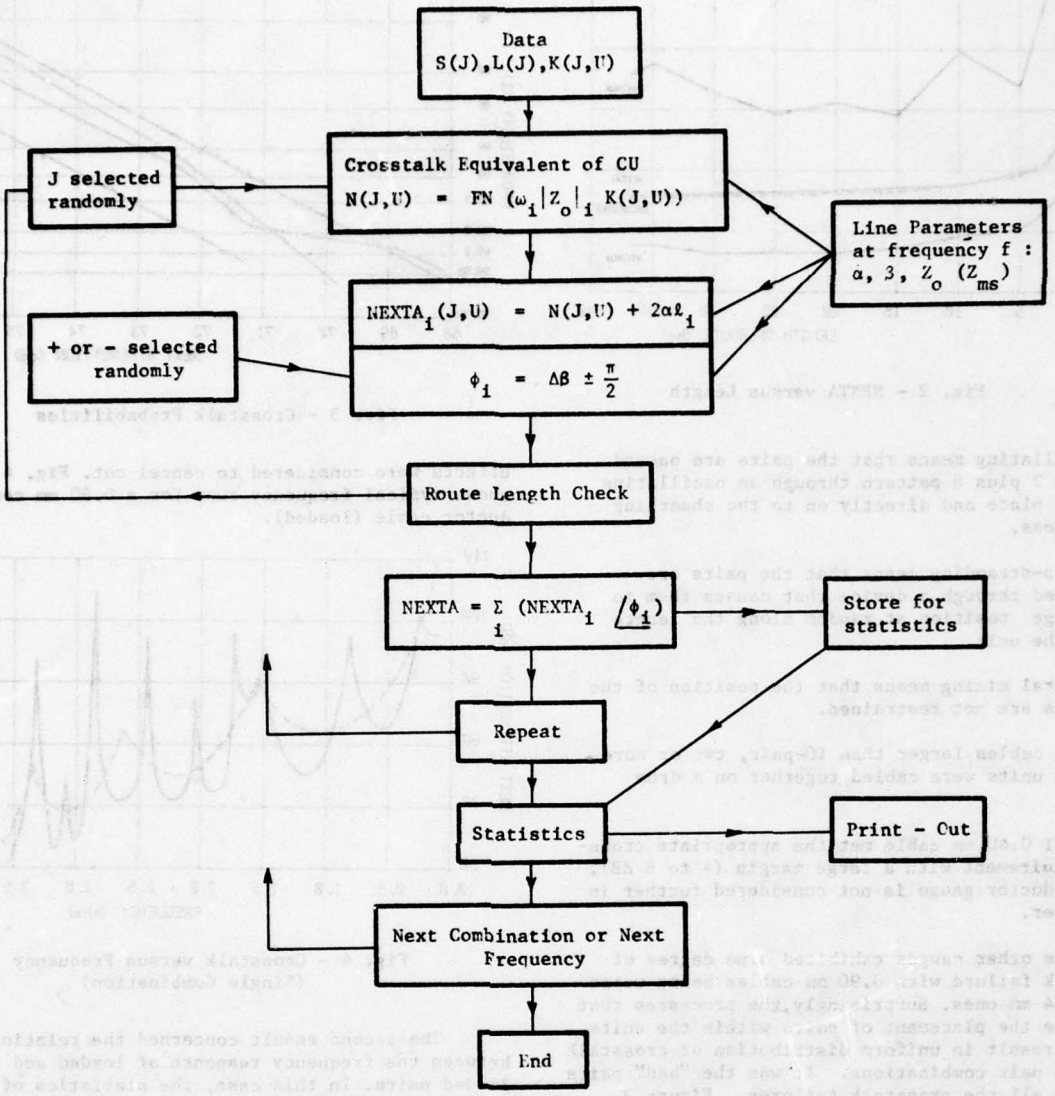


Fig. 1 - Block Diagram

To reduce that, 6-pair 0.64 mm and 0.90 mm conductor cables were analysed at various route lengths to find the correlation between the NEXTA and the route length. Results for 6-pair 0.90 mm cable are presented in Fig. 2 and it can be seen that the shape of the curves closely agrees with the theoretical length correction factor for the NEXTA :

$$N = N_{\ell_o} - 10 \log_{10} \left| \frac{1 - e^{-0.46 l \alpha \ell}}{1 - e^{-0.46 l \alpha \ell_o}} \right|$$

In our calculated example ℓ_o = 1 km

It was found that a route length of 10 km was sufficient for the statistical evaluation provided 72 dB is used for 0.90 mm and 71 dB for 0.64 mm conductor cables in place of the 70 dB objective for NEXTA for the maximum route length.

Results of Crosstalk Simulation

Two companies supplied sufficient data for various methods of manufacture and various conductor sizes. The methods of unit production involved included oscillating, cross-stranding and natural mixing where :-

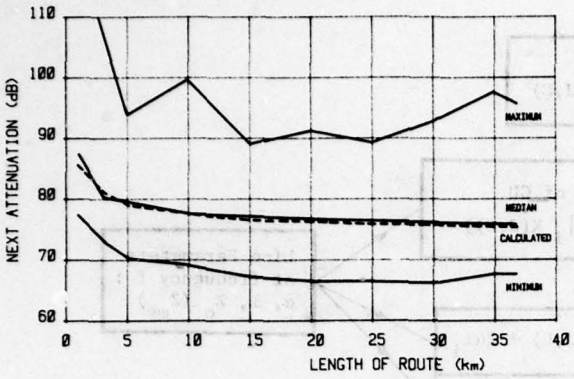


Fig. 2 - NEXTA versus Length

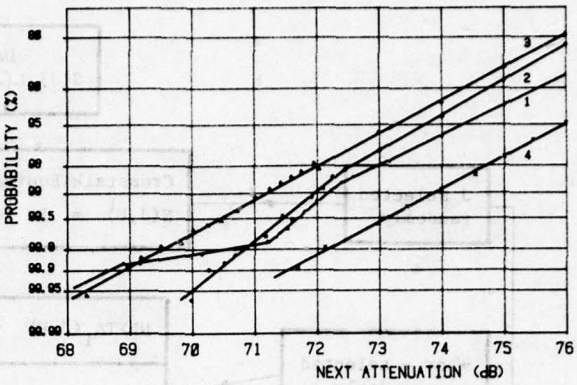


Fig. 3 - Crosstalk Probabilities

- oscillating means that the pairs are passed in a 2 plus 8 pattern through an oscillating face plate and directly on to the sheathing process.

- cross-stranding means that the pairs are passed through a device that causes them to change position at random along the length of the unit.

- natural mixing means that the position of the pairs are not restrained.

In cables larger than 10-pair, two or more of these units were cabled together on a drum twister.

*All 0.40 mm cable met the appropriate cross-*talk requirement with a large margin (4 to 6 dB). This conductor gauge is not considered further in this paper.

The other gauges exhibited some degree of crosstalk failure with 0.90 mm cables being worse than 0.64 mm ones. Surprisingly,the processes that randomise the placement of pairs within the units, did not result in uniform distribution of crosstalk over the pair combinations. It was the "bad" pairs that had all the crosstalk failures. Figure 3, curves 1, 2 and 3 show typical pair-crosstalk probabilities. Irregularities in the shape of curve 1 suggested that not all the data were supplied by the manufacturer.

During this phase of the study crosstalk-frequency runs were made and these exhibited two interesting characteristics. First, for any individual combination, the response had the expected peaks and troughs and the frequency spacing between these became shorter as the length studied was increased. On the "bad" side,the troughs were quite broad and shallow while on the "good" side,the peaks were sharp. Thus,it appears that some of the crosstalk failures found earlier would be the result of fortuitously encountering the "bad" area for that combination,but also some of the good results would be from combinations that might be judged "bad" by a frequency run. These opposing effects were considered to cancel out. Fig. 4 shows typical frequency runs for a 0.90 mm conductor cable (loaded).

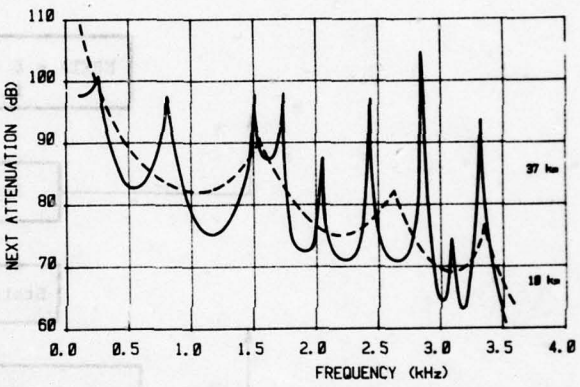


Fig. 4 - Crosstalk versus Frequency (Single Combination)

The second result concerned the relation between the frequency response of loaded and unloaded pairs. In this case, the statistics of multiple runs were compared with the surprising result depicted in Fig. 5. At 1.6 kHz the loading deteriorates the mean crosstalk performance by approximately 15 dB and the difference increases rapidly with frequency,since the loaded pairs deteriorate at 12 dB/octave from 1.6 kHz to 3.2 kHz compared with 2 dB/octave for the unloaded. These results,when considered with the aims of the crosstalk objective (to minimise the incidence of intelligible crosstalk) and the sensitivity of the ear and telephone at the higher VF frequencies, suggest that a higher crosstalk objective may be necessary for loaded pairs. This aspect is not further considered here.

Fig. 5 shows the comparison between loaded and unloaded pairs.

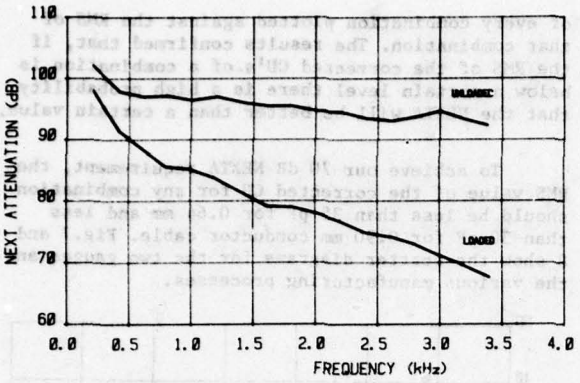


Fig. 5 - Comparison between Loaded and Unloaded Pairs

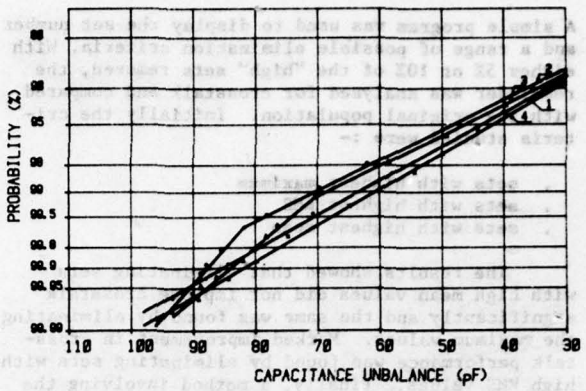


Fig. 6 - Probabilities of the Capacitance Unbalance

Statistics of Capacitance Unbalance

Various programs for the analysis of the raw data of the capacitance unbalance were designed to provide some insight into the statistical distribution of the capacitance unbalances to allow a correlation between them and the crosstalk results to be sought.

At first, all corrected CU's associated with all pair combinations were analysed as one group, and the total distribution produced. This has been compared to the single-sided normal distribution with a standard deviation equal to the RMS of the total population. All types of cables exhibited an excess of high values of capacitance unbalance in the 95-100% region as compared to the normal distribution. Sometimes, but not always, cables with the greatest excess of high values had low values of crosstalk. No correlation between maximum unbalances and low crosstalk has been found.

Table 1 shows the method used to review the normality of the corrected CU distribution.

	RMS/MEAN	90%	95%	99%	99.5%
ONE-SIDED NORMAL DISTRIBUTION	1.254	1.645	1.960	2.576	2.807
NATURAL MIXING	1.324	1.604	2.041	3.085	3.368
CROSS-STRANDING	1.415	1.708	2.146	3.278	3.451
OSCILLATING	1.499	1.723	2.256	3.356	3.809
OSCILL.+ STRANDING	1.384	1.658	2.134	3.070	3.430

Table 1 - Statistical Normality of CU Distributions

Example from Table. The 99% point of a single sided normal distribution occurs at 2.576 times the RMS whereas for the naturally mixed cable the point is at 3.085 times the RMS indicating an excess of high values.

Fig. 6 shows typical probabilities of the capacitance unbalance.

Comparing Figures 3 and 6, it can be seen that the cables exhibited marked differences in crosstalk at the lower end but had similar maximum unbalances. One version (curve 2) had more higher unbalances than another (curve 3) but in crosstalk their performance was reversed.

As some reservations were held about the CU correction factor for length, further investigation was conducted in which each manufacturing method was separately analysed in individual drumlength groups (500 m, 1000 m and 2000 m). Three correction factors for length were used:-

Linear $K_{1000} = K_\ell \times \frac{1000}{\ell}$

Square Root $K_{1000} = K_\ell \sqrt{\frac{1000}{\ell}}$

Composite $K_{1000} = K_\ell \times \frac{1}{2}\left[\sqrt{\frac{1000}{\ell}} + \frac{1000}{\ell}\right]$

With one exception, it was found that the square-root corrected results for all drumlength groups for a particular manufacturing method, were consistent with the hypothesis that they were samples from a single population. The exception was a sample that had exhibited poor crosstalk performance. It was then found that the data had come from two groups separated by a change in manufacturing process and with one group being almost all 1000 m lengths and the other 2000 m lengths. One group contained all the "bad" crosstalk results with two particularly "bad" combinations. The cable manufacturer confirmed manufacturing problems in the past and supplied new data. Results of the new analysis are curves 4 in Fig. 3 and 6. The square root correction factor applied to the new data.

As the objective of any rejection criterion is to improve crosstalk performance, and knowing that "bad" crosstalk is caused by an excess of "high" values of capacitance unbalance, some method of eliminating these "high" values is required.

A simple program was used to display the set number and a range of possible elimination criteria. With either 5% or 10% of the "high" sets removed, the remainder was analysed for crosstalk and compared with the original population. Initially the criteria studied were :-

- sets with highest maximum
- sets with highest RMS
- sets with highest mean

The results showed that eliminating sets with high mean values did not improve crosstalk significantly and the same was found by eliminating the maximum values. Marked improvement in crosstalk performance was found by eliminating sets with high RMS values. Finally, a method involving the computation of the RMS of the four highest unbalances in the set and using this value as the elimination criterion proved to be the most successful for all cables.

Overall, we were still surprised by the small crosstalk improvement achieved by the elimination of such high proportions - perhaps a manifestation of the adage that quality cannot be tested into a product. Moreover we were still confronted by the anomaly that we could not review blocks of CU data and assess which would give acceptable crosstalk and which would not.

As mentioned before, we have found that the total CU distribution was not normal and that poor crosstalk performance often involved only a few "bad" combinations. Our breakthrough came with the separate analysis of the corrected CU of each pair combination.

Our program analysed each combination over the whole data block (100 or so sets) and the mean, RMS, 90%, 95%, 99%, and maximum values for each combination were obtained. It was found that the distribution of unbalances for any combination was close to the normal one. All unbalances were then normalised (e.g. expressed as standard deviations of the particular combination) and the total population of all "normalised" unbalances observed. All types of cables analysed then exhibited normal distribution. Table 2 shows results and indicates that the normality remains at least up to the 99.5% level.

	RMS/MEAN	90%	95%	99%	99.5%
ONE-SIDED NORMAL DISTRIBUTION	1.254	1.645	1.960	2.576	2.807
NATURAL MIXING	1.257	1.650	1.950	2.500	2.740
CROSS-STRANDING	1.322	1.650	2.000	2.690	2.980
OSCILLATING	1.301	1.550	1.900	2.780	3.140
OSCILL.+ STRANDING	1.317	1.640	2.020	2.860	3.160

Table 2 - Normalised Values of the Capacitance Unbalance

Thus, for any combination, the RMS of the corrected CU of a reasonably sized data block completely characterises the CU distribution and combinations with similar RMS's should exhibit similar statistics of crosstalk. To check this, scatter diagrams were produced for selected NEXTA statistics of every combination plotted against the RMS of that combination. The results confirmed that, if the RMS of the corrected CU's of a combination is below a certain level there is a high probability that the NEXTA will be better than a certain value.

To achieve our 70 dB NEXTA requirement, the RMS value of the corrected CU for any combination should be less than 35 pF for 0.64 mm and less than 30 pF for 0.90 mm conductor cable. Fig.7 and 8 show the scatter diagrams for the two gauges and the various manufacturing processes.

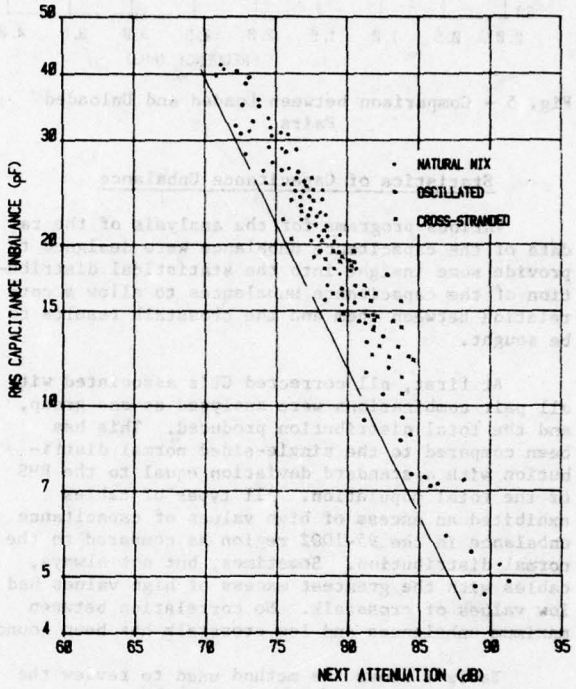


Fig. 7 - NEXTA versus RMS of corrected CU for 0.64 mm cable

New Acceptance Limit

The above was for a block of data - 100 or so drumlengths. This is acceptable in order to demonstrate the adequacy of the cable design, manufacturing processes and production approvals. But for acceptance of an individual drumlength of a cable some method of assessing its corrected CU's in relation to the total population's RMS is required.

The theory of discrete time series, where the data are discrete observations, has been consulted and the exponential smoothing method accepted[3]. This method produces an average in which past observations are geometrically discounted according to their age.

The general formula for exponential smoothing is :

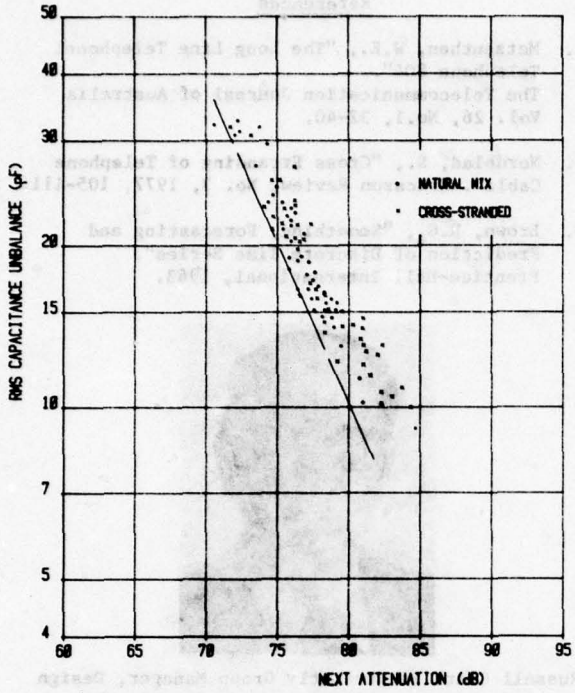


Fig. 8 - NEXTA versus RMS of corrected CU for 0.90 mm cable

$$S_t(x) = X_t + (1 - \alpha)\ S_{t-1}(x)$$

where $S_t(x)$ is the smoothed function after the tth observation of data

$S_{t-1}(x)$ is the previous value of the smoothed function

X_t is the value of the tth observation

α is the smoothing constant.

Adapting the formula for the RMS of the corrected CU we can write :

$$RMS_t = \sqrt{\alpha K^2 + (1-\alpha)\ RMS^2_{t-1}}$$

where K is the corrected CU of the tth drumlength.

Various test runs were performed in order to study the effect of various values of the smoothing constant and the range within which the smoothed RMS moves when data sets are selected at random from a data block. It has been found that, with smoothing constants of 0.02 and 0.01, the smoothed RMS for any "bad" combination varied by approximately 3 pF and 2pF respectively around some average value.

Both results seemed satisfactory and 0.01 was chosen and the limits were set at 2 pF above the previously determined 30 and 35 pF. Checks showed that, if the RMS of the data block was, for example, 31 pF, the 32 pF limit rejected a high proportion of the product and the crosstalk performance of the accepted product remained satisfactory. Thus the method is very sensitive and appears to be fair to both producer and customer.

The new method has been applied successfully for a trial period on the following basis :-

- Acceptance of individual drumlengths is determined directly from the square root of the exponentially smoothed RMS value of the corrected capacitance unbalance determined separately for each within-unit pair combination.

  Provided the result for each within-unit pair combination is below the limit, the drumlength is acceptable. The upper limits are :

  70 pF for 0.40 mm

  37 pF for 0.64 mm

  32 pF for 0.90 mm conductor cables.

- The formula for determining each new average is

$$A_t = \sqrt{0.01\ (K_1^2 + K_2^2 + ..+ K_n^2) + (1-0.01n)\ A^2_{t-1}}$$

  where A_t is the new exponentially smoothed RMS for a combination

  A_{t-1} is the RMS for that combination after acceptance of the previous drumlength

  n is the number of units tested in the drumlength being offered. (In 30,50,70 and 100-pair cables only two units are normally tested.)

  $K_1, K_2, ..K_n$ are the corrected CU's for that combination in the units tested.

- In determining the acceptability of the initial production, the starting value of A_{t-1} is taken as 3 pF below the upper limits quoted before.

- A drumlength not initially accepted may be re-offered at any time and is acceptable if the resultant smoothed average at that time is satisfactory but the manufacturer has to report, monthly, the number of re-offered drumlengths.

The manufacturers involved use test equipment under computer control and this readily allows the drumlength-by-drumlength surveillance of the smoothed RMS values so that there is no

cost penalty for testing. In this regard the exponential smoothing technique has the benefit of being relatively economical of computer memory.

Other Applications

As indicated earlier, it is possible to assess the benefit of random jointing within 10-pair units with the crosstalk simulation program. With our data sets, a benefit of 2 to 3 dB was found but, we suspect, the benefit arose because our manufacturers' products always exhibited some "bad" pair combinations, presumably arising from the twist lengths used. In these products, 10 twist lengths are used and each pair retains the same twist length. If all combinations were equal, random jointing would confer no benefit.

Application to 25-pair units is also possible but here the test equipment has to provide the smoothed RMS results for each of the 300 combinations. We feel that some of the factors unearthed in this study are even more significant with straight (colour) jointed 25-pair units. Hence we believe that the specifications we have examined do not assure the user of adequate crosstalk performance for his telephone in his network.

Conclusion

The paper has outlined the study that has resulted in a method whereby the capacitance unbalance results obtained on drumlengths can be used to predict the crosstalk performance of routes using that cable. The method has been adapted to provide a specification that ensures that the crosstalk objective of the user is achieved.



Pavel Nerer is presently Engineer, Cable Design, Lines Construction Branch, Telecom Australia. He has a MS Degree in Electrical Engineering from the S.V.S.T. (Slovenska Vysoka Skola Technicka) of Bratislava, (Czechoslovakia) His early experience included medical electronics and teaching (Czechoslovakia and industrial electronics (South Africa). After joining Telecom Headquarters in 1972 he worked in an area of the line transmission theory, computer programmes and various aspects of cable design.

References

1. Metzenthen, W.E., "The Long Line Telephone: Telephone 804". The Telecommunication Journal of Australia Vol. 26, No.1, 32-40.

2. Nordblad, S., "Cross Stranding of Telephone Cable". Ericsson Review, No. 3, 1977, 105-111.

3. Brown, R.G., "Smoothing, Forecasting and Prediction of Discrete Time Series". Prentice-Hall International, 1963.



Russell Clark is presently Group Manager, Design and Provisioning, Lines Construction Branch, Telecom Australia. He joined Telecom in 1950 after graduation as Bachelor of Engineering, University of Tasmania. His early experience covered field supervision of a construction, operations and maintenance work force. After joining Telecom Headquarters and working in various areas, he joined the section responsible for cable design and the technical aspects of provisioning. In this position he worked on aluminium conductor cables, nylon jacketting for insect protection, filled and foam plastic insulated cables and initiated the study reported here.



John Bright was born in Brisbane in 1942 and obtained an Electrical Engineering Degree in 1963 from the University of Queensland. He spent the first five years after qualifying working as a field engineer for Telecom Australia where he gained experience in external plant practices. He moved to Headquarters in 1968 and has worked in a number of areas concerned with external plant matters. He is currently the Section Manager Cable Provisioning, Lines Construction Branch, Telecom.

EXPERIMENTAL VERIFICATION OF THEORETICAL LOW-FREQUENCY CROSSTALK MODELS

by

Thomas F. McIntosh
Bell Laboratories
Norcross, Georgia 30071

Abstract

Results are presented from a continuing measurement program to characterize low frequency crosstalk in multipair cables and to verify the mathematical models for crosstalk prediction. Specifically, crosstalk measurements are discussed for two 900-pair 26-gauge multiunit pulp cables for the frequency range from 2.1 to 772 kHz and for both the balanced-to-balanced and longitudinal-to-balanced modes. Mean, standard deviation and 1% crosstalk statistics are presented. Comparisons are made between crosstalk measurements and analytical predictions for specific termination conditions. Differences between the measurements and predictions are typically within 1.0 dB, with maximum differences at specific frequencies of approximately 1.6 dB. The variation of predicted crosstalk loss with the level of termination impedance is discussed.

Introduction

The increasing presence of signals with significant frequency content outside the voice band continues to emphasize the need for crosstalk characterization of multipair telephone cable in the range below a few hundred kHz. Although the cables are designed to operate in an electrically balanced configuration, some of the signals may contain a dominant longitudinal component. This gives rise to the additional need for characterization of the crosstalk coupling between a disturbing longitudinal circuit and a disturbed balanced circuit.

Previous crosstalk data have been limited principally to the frequency range above 100 kHz, and have included only the balanced-to-balanced coupling mode. Since the characteristic impedance of a cable pair changes rapidly with frequency below 100 kHz, it is impossible to approximately match the pairs with fixed terminations except over a relatively narrow bandwidth. The resulting mismatches in impedance between the cable and the terminations produce reflections which can significantly alter measured crosstalk. Thus a prohibitively large amount of crosstalk data measured under various termination conditions would be required for adequate characterization.

A theoretical model for crosstalk prediction which accounts for the effects of nonmatched terminations has been reported.[1] This model has been extended to include the longitudinal-to-balanced crosstalk case. Crosstalk measurements on two 26-gauge pulp cables are discussed as a part of a continuing program of model verification and of low frequency crosstalk characterization. Crosstalk predictions are presented for a range of nonmatched terminations.

Low Frequency Crosstalk Model

In the following, the theoretical model presented previously[1] is reviewed briefly and the modifications required to extend the analysis to the longitudinal-to-balanced mode are identified.

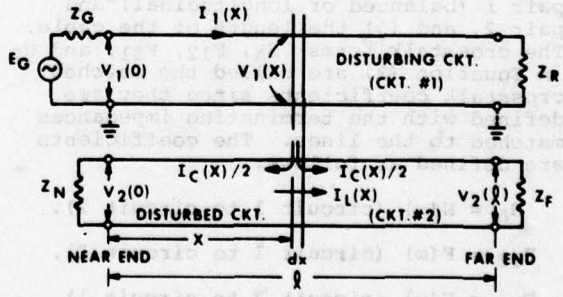


FIGURE 1
CROSSTALK CIRCUIT MODEL

Figure 1 shows the circuit diagram for any two pairs of a multipair cable. At a given point x along the circuit, voltages and currents are induced in

the disturbed circuit through capacitive and inductive coupling (see Reference 2). If the near-end crosstalk, $N(\omega)$, and the equal-level far-end crosstalk, $F(\omega)$, are defined as (see Figure 1)

$$N(\omega) \triangleq \frac{V_2(0)}{V_1(0)} \qquad (1a)$$

and

$$F(\omega) \triangleq \frac{V_2(\ell)}{V_1(0)e^{-\Gamma_1 \ell}} \qquad (1b)$$

then a reflection analysis of the disturbed circuit yields the following basic model formulas:

$$N(\omega) = K_N\left[C_{N1}N_A(\omega)+C_{N2}F_{12}(\omega)+C_{N3}F_{21}(\omega)+C_{N4}N_B(\omega)\right] \qquad (2a)$$

$$F(\omega) = K_F\left[C_{F1}N_A(\omega)+C_{F2}F_{12}(\omega)+C_{F3}F_{21}(\omega)+C_{F4}N_B(\omega)\right] \qquad (2b)$$

In Equation (1), Γ_1 is the propagation constant of the disturbing pair, Pair 1, and ℓ is the length of the line. For the case of longitudinal-to-balanced coupling, $V_1(0)$ is a longitudinal voltage and Γ_1 is the longitudinal propagation constant.

Referring to Equation (2), the complex constants K and C are functions of frequency but are deterministic from (1) the known terminations Z_N and Z_F, (2) the normalized amplitudes of the forward and backward traveling waves in pair 1 determined by the terminations Z_G and Z_R, (3) the propagation constants of pair 1 (balanced or longitudinal) and pair 2, (4) the characteristic impedances of pair 1 (balanced or longitudinal) and pair 2, and (5) the length of the cable. The crosstalk terms N_A, F_{12}, F_{21}, and N_B in Equation (2) are called the matched crosstalk coefficients since they are defined with the terminating impedances matched to the lines. The coefficients are defined as follows:

$N_A = N(\omega)$ (circuit 1 to circuit 2).

$F_{12} = F(\omega)$ (circuit 1 to circuit 2).

$F_{21} = F(\omega)$ (circuit 2 to circuit 1).

$N_B = N(\omega)$ (circuit 1 to circuit 2). Measured at the opposite end of the cable from which N_A is measured.

The definitions are valid for both balanced-to-balanced and longitudinal-to-balanced crosstalk.

Given the propagation constants and the characteristic impedances of both pairs, Equation (2) indicates that $N(\omega)$ and $F(\omega)$ can be calculated for any set of terminating conditions if the matched crosstalk coefficients are known. Conversely, these coefficients can be evaluated by measuring $N(\omega)$ and/or $F(\omega)$ under four sets of terminating conditions, and performing the necessary matrix inversion. Notice that all the terms in Equation (2) are complex, and that both the loss and phase of the crosstalk signals must be measured.

In summary, the theoretical models permit the prediction of pair-to-pair near-end or far-end crosstalk for any balanced-to-balanced or longitudinal-to-balanced termination condition from a basic set of measurements. This set consists of four crosstalk measurements for nonmatched terminations, plus the propagation constants and characteristic impedances of the pairs. This technique can greatly reduce the number of measurements required for crosstalk characterization for a variety of termination conditions.

Crosstalk Measurements

Crosstalk measurements are performed utilizing a Computer-Operated Transmission Measuring Set (COTMS).[3] COTMS permits the rapid measurement of near-end or far-end crosstalk loss and phase for a wide range of frequencies from 1 kHz to 10 mHz. A recently improved computer-controlled pair switch automatically selects the pair combination and sets the terminations (longitudinal or balanced) for each of the 1225 combinations in a 50-pair unit.[4] Corrections due to mismatched terminations are made to the measured insertion ratio to obtain crosstalk loss and phase.[1] The near-end and far-end crosstalk losses are expressed as positive numbers by

$$N(\omega)_{dB} = -20 \log_{10}|N(\omega)| \qquad (3a)$$

$$F(\omega)_{dB} = -20 \log_{10}|F(\omega)| \,, \qquad (3b)$$

where $N(\omega)$ and $F(\omega)$ are defined in Equation (1). Crosstalk phase is the angle of either $N(\omega)$ or $F(\omega)$.

Crosstalk measurements were collected on two 900-pair 26-gauge multiunit pulp (MUP) cables. The MUP design breaks the standard 900-pair pulp construction into 100-pair multiunits composed of four 25 pair primary units. This is a recently introduced design which facilitates splicing, rearranging and restoring pulp cables when using modular connectors. Data were collected on two 25-pair primary units (50

pairs) near the center of the cable core and on two units (50 pairs) adjacent to the shield. Each set consisted of 1225 pair-to-pair combinations. The lengths of cables 1 and 2 were approximately 2000 and 2300 feet, respectively.

Fine gauge conductors were selected for initial measurements to permit reasonable cable lengths on a reel, and simultaneously to have a pair count large enough to distinguish between units near the center of the core and those near the shield. Pulp insulation was chosen for the first phase of measurements because previous data had shown that the longitudinal-to-balanced crosstalk losses were lower for pulp than for corresponding PIC cables. Future measurements as currently envisioned will include 26-gauge PIC, and 22-gauge pulp and PIC cables, including DEPIC designs.

Model Verification

Figure 2 shows a simplified data flow involved in the model verification program. Four nonmatched near-end and far-end measurements (loss and phase) utilizing open and short circuit conditions[1] were made by COTMS for each pair combination for 10 frequencies from 2.1 to 772 kHz, for both balanced-to-balanced and longitudinal-to-balanced coupling. These measurements, along with the propagation constants and characteristic impedances of each pair, were processed on a general purpose computer to derive the four matched crosstalk coefficients (using Equation (2)) for each pair combination at each frequency. The coefficients are universal in the sense that they characterize 26-gauge MUP cable for these cable lengths and for these frequencies, and they can be used to predict crosstalk for any configuration of balance or longitudinal (disturbing pair only) terminating impedance. As a test of model validity, both measurements and predictions were generated for an all 78-ohm termination case. This termination condition represents the standard COTMS configuration and was selected for convenience. Previous studies have verified that the model accuracy is insensitive to termination level.

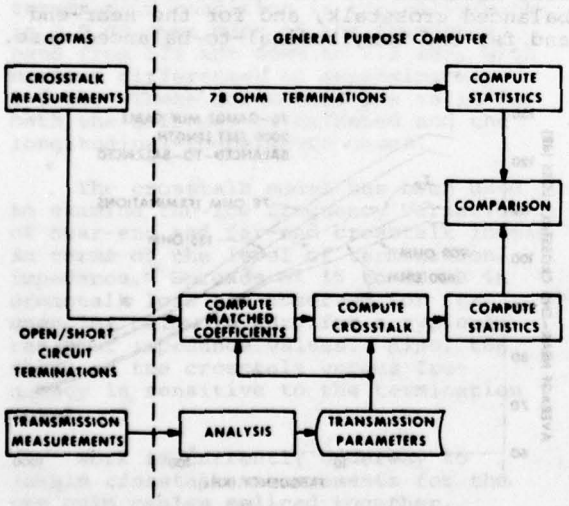


FIGURE 2
SIMPLIFIED DATA FLOW CHART

Figures 3, 4, and 5 summarize the pertinent statistics for the near-end measurements and predictions for 78-ohm terminations. These data represent the composite averages of both 50-pair groups (core center and core edge) for both MUP cables. The accuracy of the models for any individual group for either cable was not significantly different from that illustrated in these figures. Both balanced-to-balanced and longitudinal-to-balanced data are presented. 1% crosstalk loss is of interest in specific transmission system studies. This represents the point on the crosstalk distribution for which only 1% of all measured values are poorer (lower crosstalk loss).

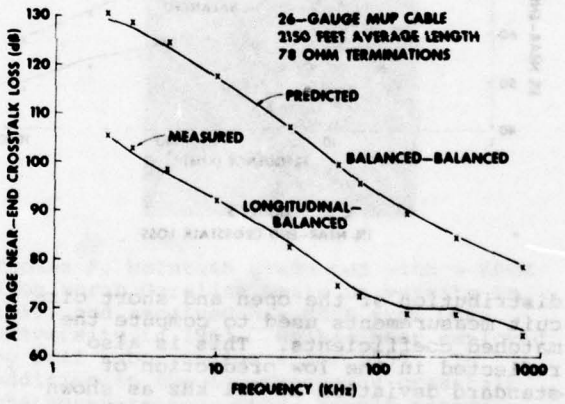


FIGURE 3
AVERAGE NEAR-END CROSSTALK LOSS

For the balanced-to-balanced case, the difference between the measured and predicted average and 1% losses are generally less than 1.0 dB, with a maximum difference of 1.6 dB for the average at 2.1 kHz. This difference is attributed to a limitation of the COTMS measurement sensitivity, which has the effect of distorting the high loss end of the

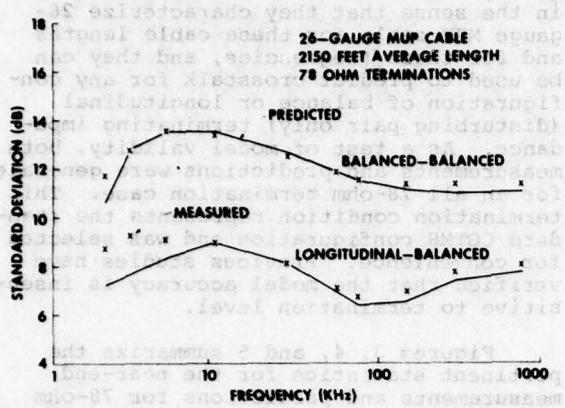


FIGURE 4
STANDARD DEVIATION

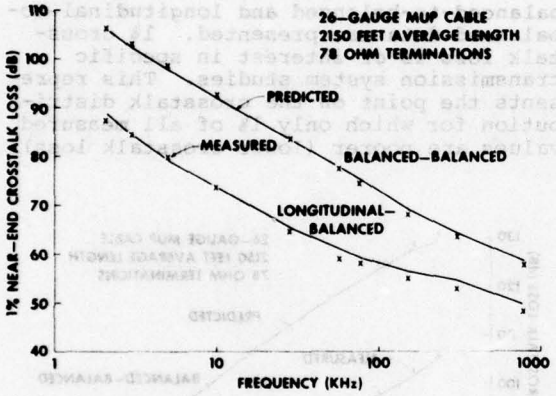


FIGURE 5
1% NEAR–END CROSSTALK LOSS

distribution of the open and short circuit measurements used to compute the matched coefficients. This is also reflected in the low prediction of standard deviation at 2.1 kHz as shown in Figure 4. Agreement between the average and 1% near-end crosstalk losses for the longitudinal-to-balanced case is also typically less than 1.0 dB, with maximum differences of approximately 1.6 dB.

The tests of model validity for far-end crosstalk losses produced results which were very similar to those shown for near-end crosstalk. These data have been omitted here for space reasons.

The following comments can be made concerning these low frequency crosstalk measurements for 78-ohm terminations. First, no significant differences were observed between the data for the 50-pair group near the core center and those for the group near the shield. This is true for both balanced-to-balanced and longitudinal-to-balanced. Second, the difference between the average near-end balanced-to-balanced and longitudinal-to-balanced crosstalk loss varies between approximately 26 dB at 2.1 kHz and 20 dB at 150 kHz. The corresponding values for the average far-end crosstalk loss are 24 dB at 2.1 kHz and 26 dB at 150 kHz. And third, over the frequency range from 2.1 to 150 kHz, the slopes of average near-end crosstalk loss versus frequency are approximately -24 dB/decade and -21 dB/decade for balanced-to-balanced and for longitudinal-to-balanced, respectively. The corresponding slopes for average far-end crosstalk are about -26 and -28 dB/decade.

Crosstalk Predictions

Although the measurements for 78-ohm terminations are useful for model verification, it is of interest to examine the crosstalk levels for terminations which more closely match the cable characteristic impedances at low frequency. The matched crosstalk coefficients for both 50-pair groups of cable 1 (2000 feet) were used to predict near-end and far-end crosstalk loss for a range of termination levels. Figure 6 illustrates the type results observed. Shown here are the average balanced-to-balanced near-end crosstalk profiles when both the disturbing and disturbed pairs are terminated in the fixed resistive values shown. Similar data were obtained for far-end balanced-to-balanced crosstalk, and for the near-end and far-end longitudinal-to-balanced case.

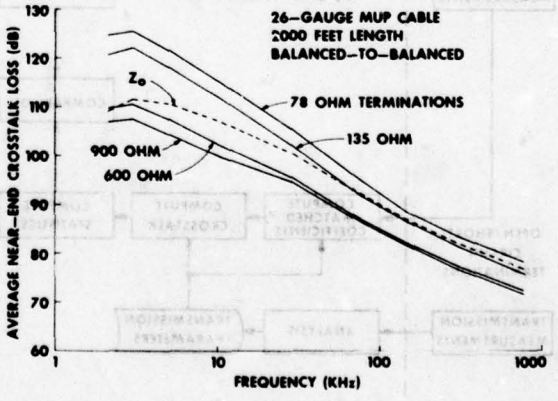


FIGURE 6
AVERAGE NEAR–END CROSSTALK LOSS

Notice the decreasing slope versus frequency as termination levels increase. Also shown by the dashed curve in Figure 6 is the average near-end crosstalk loss when the pairs are terminated in the characteristic impedance. Over the frequency range between 10 kHz and 1 MHz, this dashed curve has an approximately -17 dB/decade slope, which can be compared to -15 dB/decade as theoretically predicted for matched crosstalk at higher frequencies.[5] Similarly, for the same frequency interval, the average matched far-end crosstalk loss also exhibits a slope of -17 dB/decade compared to -20 dB/decade as theory predicts at higher frequencies. However, since the pairs are matched by fixed terminations which equal the characteristic impedance over limited frequency bands, the -17 dB/decade slopes are not valid over wide bandwidths under practical conditions.

Summary

Crosstalk measurements on two 900-pair 26-gauge multiunit pulp cables have been described. These data are a part of a continuing verification program for the low frequency crosstalk model. The model is useful for predicting near-end and far-end crosstalk loss for any nonmatched termination condition, which can greatly reduce the number of measurements required for crosstalk characterization in the low frequency range down to voice frequencies. The model has been extended to include the longitudinal-to-balanced coupling mode. For these standard pulp cables, agreement between model predictions and measurements for a fixed termination condition is typically within 1.0 dB over most of the frequency band from 772 kHz down to 2.1 kHz, with maximum differences of approximately 1.6 dB. These accuracies are valid for both the balanced-to-balanced and the longitudinal-to-balanced cases.

The crosstalk model has been used to examine the low frequency variation of near-end and far-end crosstalk losses in terms of the level of termination impedance. Spreads of 15 to 20 dB in crosstalk loss are observed for frequencies below 10 kHz, for a typical range of impedance values. Also, the slope of the crosstalk versus frequency is sensitive to the termination level.

Work is currently underway to obtain crosstalk measurements for the two pulp cables spliced together. These data will provide insights into the effects of the splice and to length scaling relationships for nonmatched conditions. Future work will expand the model verification to other gauges and cable types (for example, DEPIC). When the laboratory phase is complete, the feasibility of making confirming field measurements will be explored.

References

1. J. C. Isaacs, Jr., T. F. McIntosh, and T. D. Nantz, "Characterization of Crosstalk in Twisted Pair Telephone Cables with Nonmatched Terminations," 25th International Wire and Cable Symposium, November, 1976.

2. Campbell, G. A., "Dr. G. A. Campbell's Memorandum of 1907 and 1912," BSTJ, October, 1935.

3. Anderson, R. E., "Computer Controlled Cable Measurements," 21st International Wire and Cable Symposium, December, 1972.

4. T. D. Nantz, Bell Laboratories, unpublished work.

5. H. Cravis and T. V. Crater, "Engineering of T1 Carrier System Repeatered Lines," Bell System Technical Journal, March, 1963.



Thomas F. McIntosh graduated with a BSEE from North Carolina State University in 1959, and received his MSEE from Duke University in 1961. He has been employed by Bell Laboratories since 1959. In addition to the low-frequency crosstalk characterization, other recent assignments have included computer modeling of electrical performance and costs of multipair cables.

COMPLETE ANALYSIS OF THE ELECTRICAL BEHAVIOUR OF A SCREENED QUAD CABLE

G.C. Groenendaal
Philips Res. Labs., Eindhoven, Netherlands

R.R. Wilson
NKF Kabel B.V., Delft, Netherlands

Abstract

Based on previous publications we have set up a computer program which enables us to calculate the primary and secondary parameters of transmission circuits in ordinary subscriber cables. The program has been applied to a screened quad cable. The numerical results are verified by measurements. There is a very good agreement.

I Introduction

For future communication services such as high-speed data, facsimile and viewphone a bandwidth exceeding the usual 4 kHz is needed. From economical point of view it is worthwhile to investigate whether the existing subscriber cables are suitable or not. Another attractive proposition would be the development of new types of broadband cables. Both alternatives should be investigated. For this reason we have derived a mathematical model describing the electrical behaviour of circuits in twisted multiwire cables [1].

In this paper we apply the mentioned model to the accurate computation of the primary and secondary parameters of a screened quad cable (see fig. 1) by means of a digital computer. The dimensions of the cable are also indicated in this figure. These dimensions are slightly different from the ones under ref. 4 because of a more accurate measurement and a higher ambient temperature (25°C instead of 20°C). In order to facilitate the set up of the computer program we have worked out the formulae of [1] and added some new details too. Section II is devoted to the calculation of the resistance and inductance and section III gives the formulae for the capacitance of the side, phantom and asymmetric circuits. Comparison of measurements and numerical results, will be presented in section IV.

II Calculation of resistance and inductance

A great deal of insight into the contribution of skin and proximity effect to the total resistance and inductance can be gained by calculation the sub-contributions defined as :

$$\frac{R_{tot}}{R_o} = R^{skin} + R^{prox} + R^{screen} + (R^{out}), \quad (1)$$

$$\frac{L_{tot}}{L_o} = L^{skin} + L^{prox} + L^{screen} + L + (L^{out}) \quad (2)$$

with $R_o = \Theta \frac{1}{\pi a^2 \sigma}$ and $L_o = \Theta \frac{\mu}{8\pi}$ (3)

where R_o is the d.c. resistance per unit length of the circuit deduced from the resistance $1/\pi a^2\sigma$ per wire. L_o is deduced from the low frequency value $\mu/8\pi$ per wire.
We introduce [4]:

$$\Theta = \begin{cases} 2 & \text{for symmetric circuits} \\ 1 & \text{for phantoms} \\ \frac{1}{4} & \text{for asymmetric circuits} \end{cases} \quad (4)$$

Losses per wire due to skin effect are represented by

$$Z_1^{skin} = R_1^{skin} + j\omega L_1^{skin} = -\frac{j\omega\mu}{2\pi ka} \frac{J_0(ka)}{J_1(ka)} \quad (5)$$

where $k = \sqrt{-j\omega\mu\sigma}$ (σ = conductivity, μ = permeability). The separation of (5) into real and imaginary parts can be performed very easily by using the Kelvin functions [2].

The theory of the proximity effect is described in [3, 4]. Although, we have proved in [4] that separation of the proximity losses in a part representing the losses in the wires (Z^{prox}) a second part giving the losses in the screen (Z^{screen}) is not physically meaningful, we still follow the notation of Kaden [5].
For all circuits we have derived in [3, 4]

$$\frac{R^{prox}}{R_o} = \frac{\omega\mu\sigma}{2} a^2 \, Im\left[\sum_{n=1}^{\infty} Q_n \delta^{2n}\right], \quad (6)$$

$$\frac{L^{prox}}{L_o} = -4 \, Re\left[\sum_{n=1}^{\infty} Q_n \delta^{2n}\right] \quad (7)$$

with Q_n as given in [3] and $\delta = \frac{a}{D}$.
The normalized values of R^{screen} and L^{screen} are given in Table I. Moreover, the principal values of the inductance L, as given by Kaden [5] are shown too ($u = (\frac{D}{2a_o})^2$).

The terms R^{out} and L^{out} only contribute in the asymmetric mode of transmission.
In [4] we have derived

$$Z^{out} = \frac{j\omega\mu}{2\pi} \frac{X}{ka_o} \quad (8)$$

with

$$X = \frac{J_o(ka_o)Y_1(kb) - J_1(kb)Y_o(ka_o)}{J_1(ka_o)Y_1(kb) - J_1(kb)Y_1(ka_o)}. \quad (9)$$

Hence

$$\frac{R^{out}}{R_o} = -\frac{2a^2}{a_o} Re[kX], \quad (10)$$

$$\frac{L^{out}}{L_o} = \frac{16}{a_o}\, Im\left[\frac{X}{k}\right]. \qquad (11)$$

X can easily be calculated by using the Kelvin functions as defined in [2].

III Calculation of the capacitance

Let us consider the screened quad cable of fig. 1. For the potentials $U_1, U_2, \ldots U_4$ on the four conductors with charges $q_1, q_2, \ldots q_4$ we can write the set of linear equations [6]:

$$\begin{aligned} U_1 &= K_1 q_1 + K_2 q_2 + K_3 q_3 + K_2 q_4, \\ U_2 &= K_2 q_1 + K_1 q_2 + K_2 q_3 + K_3 q_4, \\ U_3 &= K_3 q_1 + K_2 q_2 + K_1 q_3 + K_2 q_4, \\ U_4 &= K_2 q_1 + K_3 q_2 + K_2 q_3 + K_1 q_4. \end{aligned} \qquad (12)$$

The coefficients K_1, K_2 and K_3 are the coefficients of potential. In his book [6] Klein has derived formulae for the capacitances of the three independent circuits in a quad, viz. side (S), phantom (F) and asymmetric (A) :

$$\begin{aligned} C_S &= \frac{1}{2(K_1 - K_3)} = \frac{1}{K_S}, \\ C_F &= \frac{1}{K_1 - 2K_2 + K_3} = \frac{1}{K_F}, \\ C_A &= \frac{4}{K_1 + 2K_2 + K_3} = \frac{1}{K_A}. \end{aligned} \qquad (13)$$

The computation of K_1, K_2 and K_3 for thin wires is straightforward.
We start from (96) of [3] with $A_n = 0$.

$$2\pi\varepsilon U_s = q_s \ln\left|\frac{1 - \frac{D_{os} D_{os}^*}{a_o^2}}{a_s/a_o}\right| + \sum_{\substack{t=1 \\ t\neq s}}^{N} q_t \ln\left|\frac{1 - \frac{D_{os} D_{ot}^*}{a_o^2}}{D_{st}/a_o}\right| \qquad (14)$$

s = 1, 2, 3, 4.
Note that all dimensions are normalized with respect to a_o. With the notation of (25), (26) and (27) of [4], after comparison with (12) we obtain:

$$\begin{aligned} 2\pi\varepsilon K_1 &= \ln\left(\frac{1-u}{2\delta\sqrt{u}}\right), \\ 2\pi\varepsilon K_2 &= \frac{1}{2}\ln\left(\frac{1+u^2}{2u}\right), \\ 2\pi\varepsilon K_3 &= \ln\left(\frac{1+u}{2\sqrt{u}}\right). \end{aligned} \qquad (15)$$

Combining (15) and (13) yields :

$$\begin{aligned} 2\pi\varepsilon K_S &= 2\ln\left(\frac{1}{\delta}\,\frac{1-u}{1+u}\right), \\ 2\pi\varepsilon K_F &= \ln\left(\frac{1}{2\delta}\,\frac{1-u^2}{1+u^2}\right), \\ 2\pi\varepsilon K_A &= \frac{1}{4}\ln\left(\frac{1-u^4}{8\delta u^2}\right). \end{aligned} \qquad (16)$$

These values can also be found in Kaden [5]. In [4] the values of Z^{prox} to the order of δ^2 are given (Table II one page 421). These results can be applied in order to obtain our first correction for thick wires of the coefficients K_S, K_F and K_A. Therefore, in Table II of [4] we put $\lambda_1 = 1$ and $w_r = 1$. Performing the summations gives

$$\begin{aligned} 2\pi\varepsilon\,\Delta K_S &= -\delta^2\left\{\left(1+\frac{8u^3}{1-u^4}\right)^2 + \left(3-\frac{8u}{1-u^4}\right)^2\right\}, \\ 2\pi\varepsilon\,\Delta K_F &= -\delta^2\left(1-\frac{8u^2}{1-u^4}\right)^2, \\ 2\pi\varepsilon\,\Delta K_A &= -\delta^2\left(3+\frac{8u^4}{1-u^4}\right)^2. \end{aligned} \qquad (17)$$

For our screened quad cable, it therefore follows that

$$\begin{aligned} \delta &= 0.1810, \\ u &= 0.1225. \end{aligned} \qquad (18)$$

In Table II the calculations of the "thin wires approach" are given based on (16). The results given are valid for $\varepsilon_{eff} = 1$, but the cable of fig. 1 has an inhomogeneous dielectrum, viz. a combination of polythene and air. The ε_r of pure polythene is 2.3. Because of the small air slots we expect an effective dielectric constant which is a little bit lower. Comparison of the measured capacitances, which are $C_S = 54.07$ (nF/km), $C_F = 129.58$ (nF/km) and $C_A = 140.08$ (nF/km), give effective dielectric constants as shown in Table II. We conclude that the approximation for thin wires is very inaccurate. Adding the correction for thick wires (17) gives excellent results as shown in Table II. An ε_{eff} of 2.24 is very realistic.

IV Practical example

We have set up a computer program based on the formulae of sections II and III. This program is applied to the screened quad cable, as shown in fig. 1. Results are shown in figs. 2 to 7. From the figures we conclude that losses due to skin effect play a dominant role, but for higher frequencies (>100 kHz), the proximity effect also becomes important. In these figures the normalized inductance and resistance are given, which makes mutual comparison difficult. Hence we have also computed the real values of the primary parameters. The results are presented in figs. 8 to 10. From the primary parameters we easily obtain the secondary parameters, viz.

$$Z_o = Re\, Z_o + j\, Im\, Z_o = \sqrt{\frac{R_{tot} + j\omega L_{tot}}{G + j\omega C}}, \qquad (19)$$

$$\gamma = \alpha + j\beta = \sqrt{(R_{tot} + j\omega L_{tot})(G + j\omega C)}. \qquad (20)$$

These quantities are also given in figs. 8 to 10. It appears that the asymmetric circuit has the lowest attenuation. Another important conclusion is that for all three circuits the phase constants are equal. Hence, we expect a very low cross-talk between those three circuits because the waves are propagating at the same speed.

Finally we want to compare the measured and calculated attenuation for several frequencies. In practice it is impossible to measure α as given in figs. 8 to 10, because the terminating networks of

the transmission line are in general resistors (e.g.R=75Ω), which give rise to reflections. Since our measuring set (Walter & Golterman PM-7) measures the insertion loss, the most convenient way is to correct the calculated α as follows :

$$\alpha_{cor.} = \alpha_{cal.} + 20\ ^{10}\log\left|\frac{1-\rho^2 e^{-2\gamma l}}{1-\rho^2}\right| \qquad (21)$$

where $\rho = \frac{R - Z_o}{R + Z_o}$ and l = length of transmission line. Expression (21) has been well-known to telephone engineers for 50 years (Zobel, B.S.T.J. July 1928). It is also evident that the computations have to be performed for the correct ambient temperature of the cable, because the conductivity of copper is a function of temperature, viz.

$$\sigma_T = \frac{58 \times 10^6}{1 + 0.00396\,(T-20)} \quad (S/m) \qquad (22)$$

where T = temperature in °C.

We have carried out the computations for σ_{25}= 56.87×10^6(S/m) and l = 1211 m. The results are given in Table III. Comparison with measurements gives the relative deviation as shown. From Table III it follows that the approximations are good since we have a maximum error of 1.5 % for the side and phantom and 2.5 % for the asymmetric circuit.

V Conclusions

This paper has indicated how the primary and secondary parameters of the side, phantom and asymmetric circuits of a screened quad cable can be calculated. Use has been made of formulae derived in several previous papers. The cable model was verified by comparing the computed and measured results of the insertion loss. There is good agreement between the results (maximum difference 2.5 %).

VI Acknowledgement

The authors are grateful to V. Belevitch (MBLE Res. Lab.) for suggestions and corrections.

VII References

1. V. Belevitch, G.C. Groenendaal, R.R. Wilson, "On the computation of primary parameters of circuits in twisted multiwire cables", Proc. of 26th Int. Wire & Cable Symp., Cherry Hill, N.J., pp. 338-342, Nov. 1977.

2. M. Abramowitz, I.A. Stegun, "Handbook of Mathematical Functions", Dover Publications, Inc., New York, 1968.

3. V. Belevitch, "Theory of the proximity effect in multiwire cables", part I+II, Philips Res. Repts., Vol. 32, pp. 16-43 and pp. 96-117, 1977.

4. G.C. Groenendaal, R.R. Wilson, V. Belevitch, "Calculation of the proximity effect in a screened pair and quad", Philips Res. Repts., Vol. 32, pp. 412-428, 1977.

5. H. Kaden, "Wirbelströme und Schirmung in der Nachrichtentechnik, 2-te Auflage, Springer, Berlin, 1959.

6. W. Klein, "Die Theorie des Nebensprechens auf Leitungen", Springer, Berlin, 1955.

Authors



Gradus C. Groenendaal was born in Est, The Netherlands, on March 14, 1943. He received the degree in electrical engineering from Eindhoven University of Technology, in 1968. From 1968 to 1970 he served with the Royal Netherlands Air Force. In 1970 he joined the Philips Research Laboratories, Eindhoven, The Netherlands, where he is engaged in research on systems for broadband transmission via cables including related electromagnetic field problems and computer-aided-design tools. He is a member of IEEE and of the Netherlands Electronics and Radio Society.



René R. Wilson received his electrical engineering degree from Delft University of Technology, The Netherlands, in 1951. From 1951 to 1961, he was with Draka Kabel, Amsterdam. From 1961 to 1971 he was head of the Telecommunication Laboratory of NKF Kabel, Delft, The Netherlands. He is currently engaged in research and development activities on telecommunication cables at NKF Kabel. He is a member of the Royal Netherlands Institute of Engineers.

	side	phantom	asymmetric
R^{screen}/R_o	$\omega\mu\sigma a^2 \mathrm{Im}\left[\sum_{r=1,3,5,..}^{\infty} \frac{w_r u^r}{r}\right]$	$2\omega\mu\sigma a^2 \mathrm{Im}\left[\sum_{r=2,6,10}^{\infty} \frac{w_r u^r}{r}\right]$	$2\omega\mu\sigma a^2 \mathrm{Im}\left[\sum_{r=4,8,12}^{\infty} \frac{w_r u^r}{r}\right]$
L^{screen}/L_o	$-\delta \mathrm{Re}\left[\sum_{r=1,3,5,..}^{\infty} \frac{w_r u^r}{r}\right]$	$-16\mathrm{Re}\left[\sum_{r=2,6,10,..}^{\infty} \frac{w_r u^r}{r}\right]$	$-16\mathrm{Re}\left[\sum_{r=4,8,12,..}^{\infty} \frac{w_r u^r}{r}\right]$
L/L_o	$-4\ln\delta$	$-4\ln(2\delta)$	$-4\ln(8\delta u^2)$

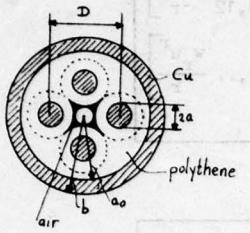
Table I.

	thin wires			thick wires		
	$2\pi\varepsilon K_{S,F,A}$	$C_{S,F,A}$ (nF/km)	ε_{eff}	$2\pi\varepsilon K_{S,F,A}$	$C_{S,F,A}$ (nF/km)	ε_{eff}
side	2.9266	18.9830	2.37	2.7593	20.1339	2.24
phantom	0.9864	56.3215	2.30	0.9610	57.8108	2.24
asymmetric	0.9573	58.0336	2.41	0.8835	62.8791	2.23

Table II.

f(kHz)	side circuit (R=150Ω)			phantom (R=50Ω)			(R=75Ω) asymmetric circuit		
	$\alpha_{cor.}$ (dB)	$\alpha_{meas.}$ (dB)	$\Delta\alpha$(%)	$\alpha_{cor.}$ (dB)	$\alpha_{meas.}$ (dB)	$\Delta\alpha$(%)	$\alpha_{cor.}$ (dB)	$\alpha_{meas.}$ (dB)	$\Delta\alpha$(%)
10	1.06	1.07	-0.93	1.39	1.38	+0.72	0.92	0.94	-2.13
20	1.30	1.32	-1.52	1.59	1.61	-1.24	1.79	1.81	-1.10
30	1.58	1.59	-0.63	1.85	1.86	-.054	2.58	2.59	-0.39
40	1.84	1.85	-0.54	2.12	2.10	+0.95	3.00	3.01	-0.33
50	2.04	2.04	0	2.36	2.33	+1.29	2.98	2.99	-0.33
60	2.18	2.17	+0.46	2.56	2.52	+1.59	2.62	2.66	-1.50
70	2.27	2.27	0	2.73	2.71	+0.74	2.17	2.22	-2.25
80	2.37	2.40	-1.25	2.88	2.85	+1.05	1.98	2.03	-2.46
100	2.69	2.72	-1.10	3.23	3.23	0	2.81	2.83	-0.71
200	3.79	3.82	-0.79	4.56	4.63	-1.51	3.93	3.96	-0.76
300	4.52	4.52	0	5.49	5.57	-1.44	3.86	3.89	-0.77
400	5.11	5.15	-0.78	6.28	6.36	-1.26	3.57	3.62	-1.38
500	5.71	5.75	-0.70	7.00	7.13	-1.82	4.21	4.23	-0.47
600	6.29	6.35	-0.94	7.68	7.80	-1.54	5.09	5.10	-0.20
700	6.77	6.78	-0.15	8.27	8.37	-1.19	5.27	5.28	-0.19
800	7.18	7.21	-0.42	8.81	8.95	-1.56	5.00	4.99	+0.20
900	7.59	7.67	-1.04	9.33	9.43	-1.06	5.20	5.13	+1.36
1000	8.03	8.11	-0.99	9.84	9.98	-1.40	5.93	5.86	+1.19

Table III.



a_o=5.10 mm
b_o=5.23 mm
D =3.57 mm
a =0.646 mm
tanδ=2.10^{-4}

Fig.1. Cross-section through a screened quad cable.

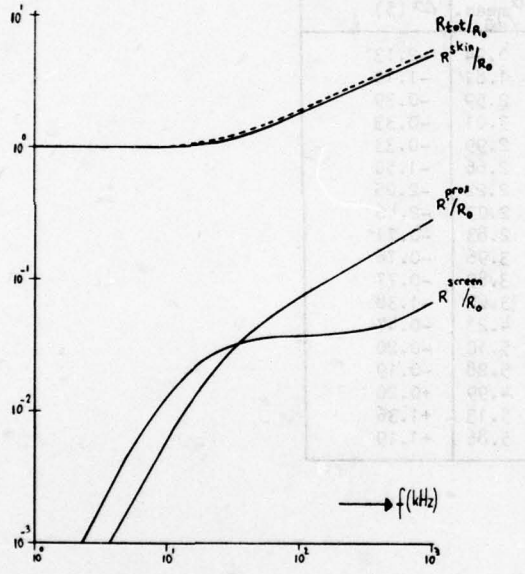


Fig. 2. Normalized resistance versus frequency for side circuit.

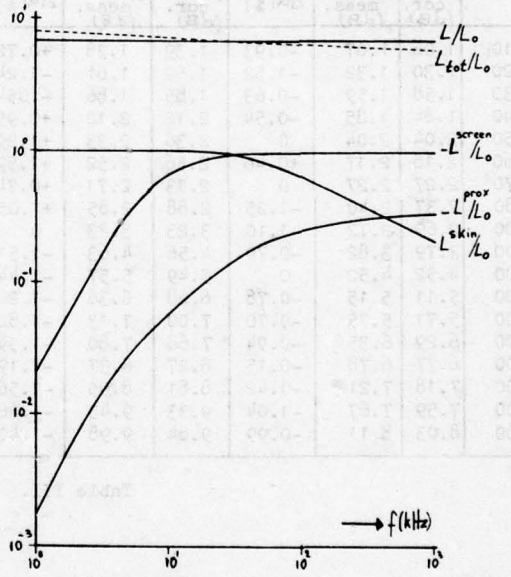


Fig. 3. Normalized inductance versus frequency for side circuit.

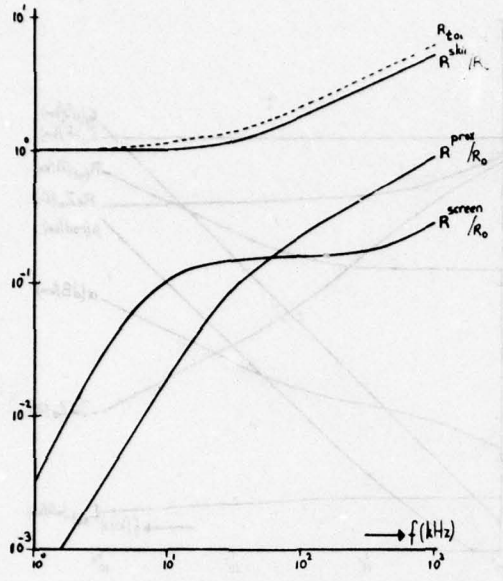


Fig. 4. Normalized resistance versus frequency for phantom circuit.

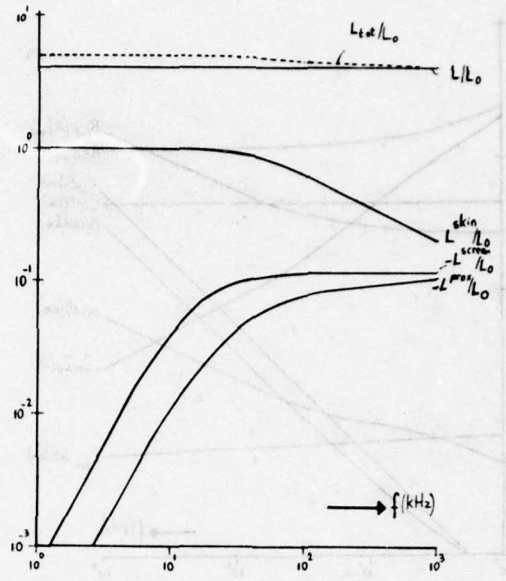


Fig. 5. Normalized inductance versus frequency for phantom circuit.

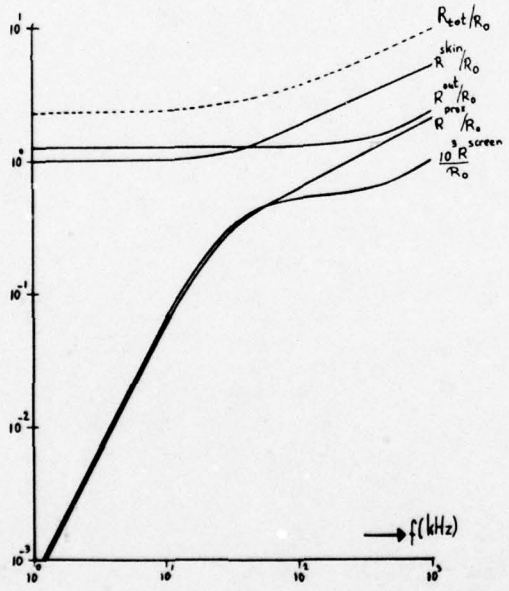


Fig. 6. Normalized resistance versus frequency for asymmetric circuit.

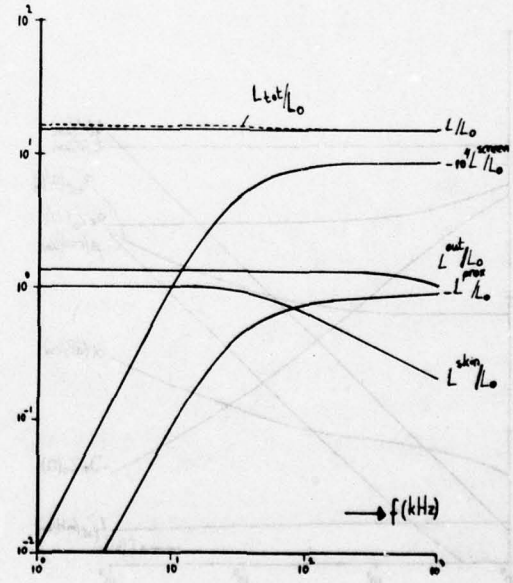


Fig. 7. Normalized inductance versus frequency for asymmetric circuit.

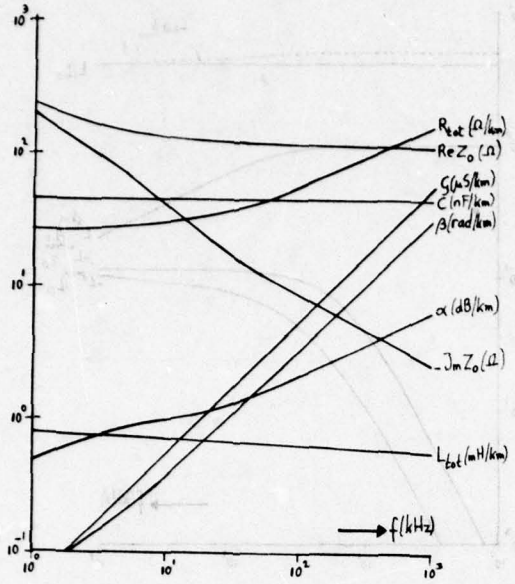


Fig. 8. Primary and secondary parameters versus frequency for side circuit.

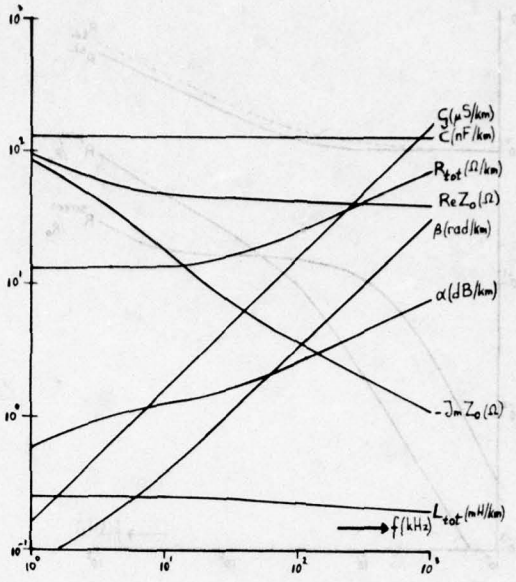


Fig. 9. Primary and secondary parameters versus frequency for phantom circuit.

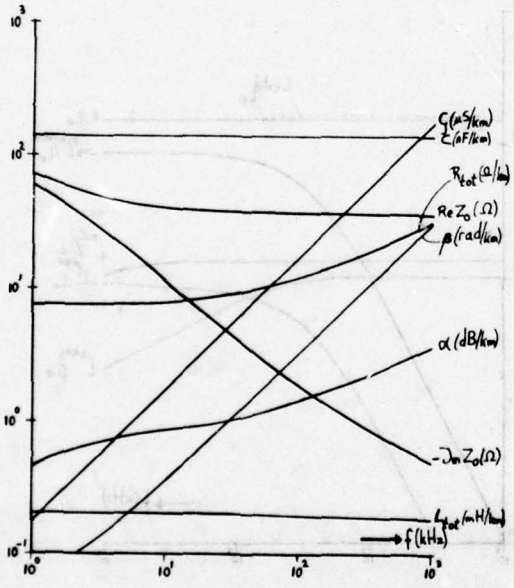


Fig. 10. Primary and secondary parameters versus frequency for asymmetric circuit.

MICROCOAXIAL CABLES INSULATED WITH HIGHLY EXPANDED POLYETHYLENE BY CHEMICAL BLOWING METHOD

F. Suzuki, A. Mori, S. Sato and Y. Suzuki

Sumitomo Electric Industries, Ltd.
Yokohama, Japan

Summary

This paper describes the new chemical blowing method to produce expanded polyethylene insulation with about 65% expansion and its application to microcoaxial cables with low attenuation. The chief characteristic of this method is to use a polypropylene modified polyethylene mixed with a conventional chemical blowing agent (azodicarbonamide).
The new developed microcoaxial cable with expanded polyethylene insulation of 65% expansion has an attenuation constant equal to that of cable provided with a conventional air-dielectric-type insulation. The insulation also has more desirable flexibility and shrinkage properties.

1. Introduction

Commercially available coaxial cables are generally insulated by an air-dielectric-type insulation, by an expanded polyethylene with about 50% expansion, or by solid polyethylene. Many types of the air-dielectric-type insulation have been widely applied to coaxial cables with low attenuation. One of them is helical dielectric insulation which is composed of polyethylene string wound helically around the inner conductor and polyethylene pipe extruded around the helical string. As well known, however, it is difficult to economically produce microcoaxial cables having the air-dielectric-type insulation with diameter of insulation smaller than about 3 mm. If an extrusion technique of highly expanded polyethylene for such small cores could be developed, it would be very useful for making a microcoaxial cable with low attenuation.

At present, conventional chemical blowing methods can not be applied to obtain expanded polyethylene insulation over 50% expansion. The extrusion process using a liquid blowing agent has already been developed,[1), 2)] but unfortunately the process has the disadvantage that the uniform insulation cores of small diameter are unable to be extruded because of the difficulty in obtaining small and uniform cells.

Under such circumstances, a new chemical blowing method for making insulation over 65% expansion has been investigated and microcoaxial cables with low attenuation have been successfully developed. The new microcoaxial cables have been already in practical application to MATV (Master Antenna Television) systems and many other usages.

2. Extrusion of expanded insulation

2-1 Selection of material

Selecting a suitable chemical blowing agent and polyethylene was an important problem for obtaining highly expanded insulation. It is well known that azodicarbonamide and p, p'-oxybis (benzene sulfonyl hydrazide) are the most preferable chemical blowing agents. On the preliminary extrusion test for the core of a microcoaxial cable, the comparison of both chemical blowing agents described above was carried out employing commercially available low density polyethylene for wire insulation. The conductor diameter and the overall diameter of the insulation were 0.73mm and 3.1mm, respectively. As a result of the test, it was shown that azodicarbonamide has fine cell structure, higher expansion, and a smoother insulation surface. The result of this test suggested that azodicarbonamide should be selected for this purpose.

Following the selection of the chemical blowing agent, three kinds of polyethylene compounds with 2% azodicarbonamide content were evaluated. The results are shown in Table 1, illustrating that resin A gives the most desirable expansion and cell structure. In Table 1, resin B and resin C are low density polyethylene (LDPE) and high density polyethylene (HDPE), respectively, now in use in our company as insulation for telecommunication cables. Resin A is a specially formulated polyethylene compound, which is comprised of LDPE with unique arrangement of side chains and some amounts of polypropylene.
The polypropylene is mixed to obtain fine cell structure, to increase the mechanical strength of expanded insulation and to improve the extrudability of the LDPE. Based on additional experiments, it was found that the addition of polypropylene of 20 - 30% exhibited the best performance.

Figure 1 shows the relationship between expansion rate and blowing agent concentration in the case of resin A. In the extrusion test, temperature profile of extruder, die design, and preheating condition of conductor were kept constant in all runs. By observing Figure 1, it was finally decided that the best concentration of azodicarbonamide is 1.4%.

Table 1. Properties of polyethylene

Materials / Items	Resin A (New Material)	Resin B	Resin C	Remarks
Density (g/cm^3)	0.916	0.920	0.945	ASTM-D-1505
Melt Index (g/10 min.)	1.4	0.21	0.45	ASTM-D-1238
Expansion Rate (%)	67	60	51	Specific Grarity Method
Cell Structure	Fine	Coarse	Coarse	

Note: Conductor diameter : 0.73 mm
Insulation diameter : 3.1 mm
Chemical blowing agent : Azodicarbonamide 2.0%

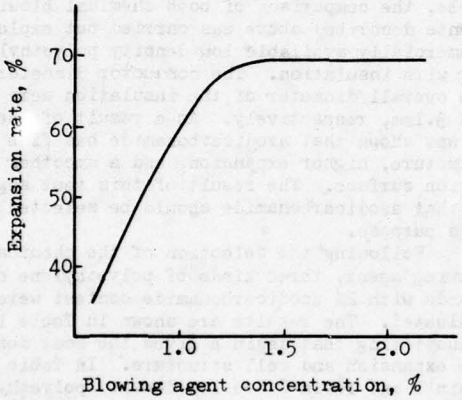
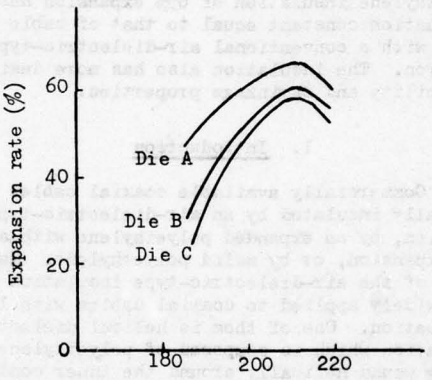


Figure 1. Effect of blowing agent concentration on expansion rate



Exit diameter of die
Die A : 2.0 mm
Die B : 2.35mm
Die C : 2.50mm

Figure 2. Effect of the exit diameter of die

2-2 Extruder and die

The conventional extruder was applied to produce the core of microcoaxial cable. The diameter and L/D of the screw are 65 mm and 24, respectively. The die was the same as that for solid insulation except that it was designed so the exit diameter of the die would be as small as possible in order to release the pressure of the polymer in die suddenly, producing high expansion. Figure 2 illustrates the effect of die diameter on expansion rate, with changing stock temperature.

2-3 Temperature profile

The melt viscosity of molten polyethylene affects the expansion rate and cell structure. Therefore, the temperature at the front end of the extruder was set lower so as to increase the melt viscosity. Table 2 shows the most preferable temperature profile for producing the maximum expansion rate.

Table 2. Temperature profile

Feed zone	Compression zone	Metering zone		Crosshead	Die
		1	2		
175°C	188°C	213°C	182°C	160°C	160°C

2-4 Conductor pre-heating

The conductor pre-heating temperature also affects the expansion rate and cell structure of the insulation. Figure 3 shows the effect that pre-heating temperature has on expansion rate. The pre-heating temperature of 110 - 120°C was selected for suitable condition. According to the microscopic observation of the insulation's cross section, it was found that the cell structure of the core extruded at a pre-heating temperature over 130°C was very coarse.

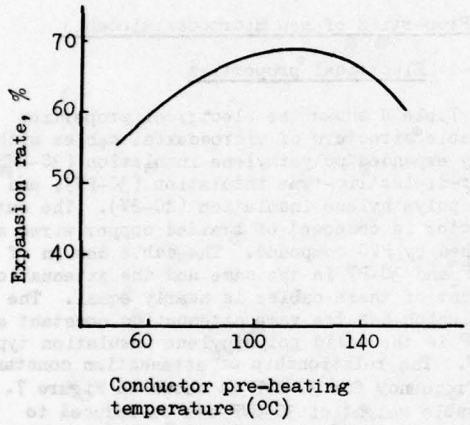


Figure 3. Effect of pre-heating temperature on expansion rate

3. Cable Manufacturing

3-1 Comparison of single layer and double layer insulation

Two trial types of microcoaxial cables shown in Table 3 were manufactured. The construction of the cables was designed so as to obtain the same attenuation constant as that of the cable with an air-dielectric-type insulation, which was composed of polyethylene string helically wound around the inner conductor and polyethylene pipe covered over the polyethylene string. The double layer insulation was formed of a solid polyethylene layer over the expanded polyethylene. It was produced in order to compare the capacitance change of its core —after extruding, after braiding copper wires, and after sheathing with polyvinyl chroride (PVC) compound— with that of the single layer insulated core. The foaming extrusion conditions such as the formulation of polyethylene and temperature profile, etc. were the same as those for single layer insulation.

Table 3. Cable core design

Items \ Type			Single Layer Insulation	Double Layer Insulation
Diameter of Inner Copper Conductor, mm			0.73	0.73
Insulation	Inner Insulation	Material	New Material	New Material
		Diameter, mm	3.1	2.9
		Dielectric Constant	1.39	1.36
	Outer Insulation	Material	-	HDPE
		Thickness, mm	-	0.10
	Outer Diameter, mm		3.1	3.1
	Dielectric Constant		1.39	1.39
Outer Conductor			Braided Copper Wires	
Jacket	Material		PVC compound	
	Outer Diameter, 1 mm		5.0	5.0

In the extrusion, the capacitance of the double layer insulation was controlled within ± 0.5 pF/m at line speeds of 300 m/min. compared with ± 1 pF/m of the single layer insulation. The fluctuations of capacitance are shown in Figure 4. The change of capacitance after braiding copper wires and subsequently sheathing PVC compound is shown in Figure 5, illustrating that the double layer insulation exhibits a more preferable performance. The decrease of capacitance in double layer insulation after braiding occurs as a result of the space gap between the core and braided copper wires.

In the case of single layer insulation, the capacitance change in the core after braiding is attributed to the deformation of the insulation by the braided copper wires. It is clear that the mechanical strength of double layer insulation was improved enough to cause no capacitance change

in cable making process. Cross section of the double layer insulation is shown in Figure 6.

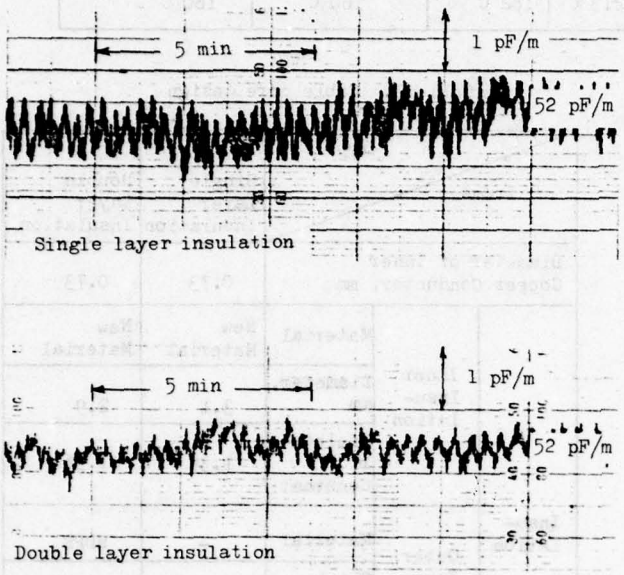


Figure 4. Fluctuations of capacitance

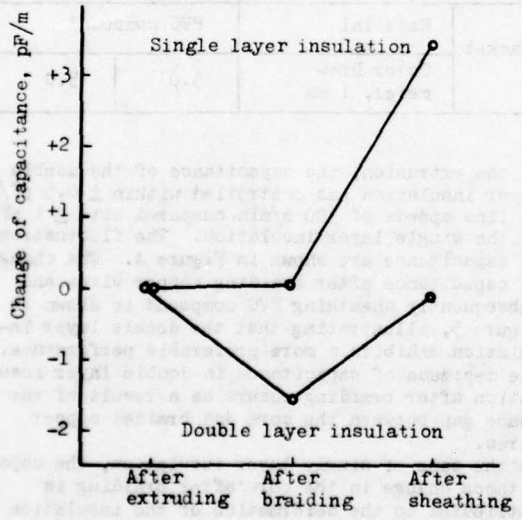


Figure 5. Change of capacitance during cable making

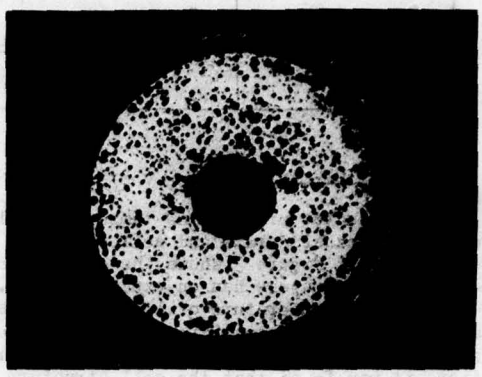


Figure 6. Cross section of double layer insulation

3-2 Properties of new microcoaxial cable

3-2-1 Electrical properties

Table 4 shows the electrical properties and cable structure of microcoaxial cables with highly expanded polyethylene insulation (3C-SVF), an air-dielectric-type insulation (3C-PV), and solid polyethylene insulation (4C-2V). The outer conductor is composed of braided copper wires and sheathed by PVC compound. The cable design of 3C-SVF and 3C-PV is the same and the attenuation constant of these cables is nearly equal. The cable which has the same attenuation constant as 3C-SVF is the solid polyethylene insulation type, 4C-2V. The relationship of attenuation constant and frequency for 3C-SVF is shown in Figure 7. The cable weight of 3C-SVF can be reduced to approximately 90% of 3C-PV and to 63% of 4C-2V.

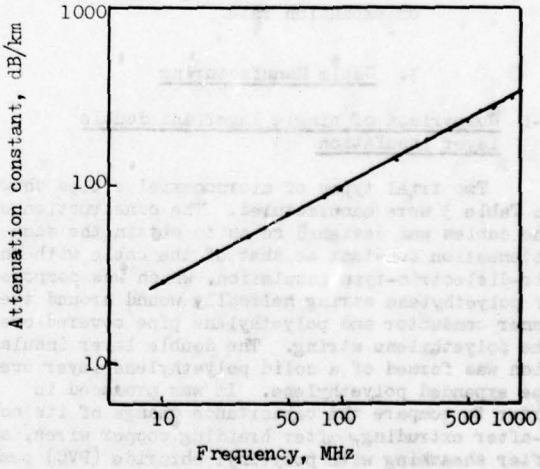


Figure 7. 3C-SVF: Attenuation constant vs. frequency

Table 4. Cable structure and electrical properties

Items \ Type			3C-SVF	3C-PV	4C-2V
Cable Structure	Diameter of Inner Copper Conductor, mm		0.73	0.73	0.65
	Insulation	Material	Highly Expanded Polyethylene (Expansion Rate 65%)	Air-Dielectric-Type	Solid Polyethylene
		Outer Diameter, mm	3.1	3.1	4.0
	Outer Conductor	Material	Braided Copper Wires		
	Jacket	Material	PVC Compound		
		Outer Diameter, mm	5.0	5.0	6.4
	Cable weight, kg/km		36	40	57
Electrical Properties	Cable Capacitance, nF/km		52	53	67
	Characteristic Impedance at 10 MHz, Ω		75	75	75
	Attenuation Constant at 10 MHz		29	30	30
		at 100 MHz	98	110	113
		at 1000 MHz	350	360	370
	Permittivity at 20°C		1.38	1.39	2.30

3-2-2 Physical properties

Several physical properties were tested.

(a) Minimum bending radius

The bending radius is defined as the minimum bending radius when V.S.W.R. is not changed by a bend in the cable.

(b) Pull-out strength between the inner conductor and the insulation

The inner conductor was pulled out from the insulation by the tension tester. The magnitude of the strength was recorded on the chart and the maximum strength read. The cable sample was 50 mm long.

(c) Flexibility

Flexibility is evaluated as the drooped distance (H) of the free end with a 10 g weight attached, as shown in Figure 8.

(d) Shrinkage after heat cycle test

Cables were submitted to a heat test in an oven. The temperature was programmed from 60°C to -20°C at 6 hours/cycle. After the exposure for 30 cycles, the shrinkage of the insulation from the end of the outer conductor was measured. The cable sample was 50 cm long.

The test results are listed in Table 5. 3C-SVF is superior to 3C-PV and is most excellent in flexibility.

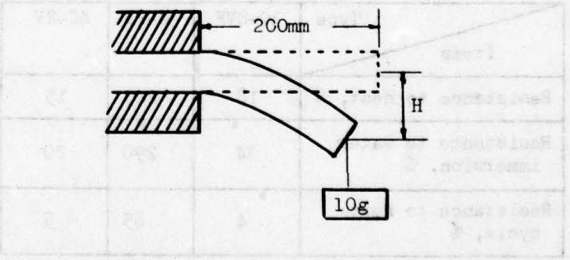


Figure 8.

3-2-3 Aging properties

Table 6 shows the maximum change ratio of attenuation constant after aging in the frequency range of 1 - 800 MHz.

(a) Resistance to heat
Cables were put in an oven at 98°C for 20 days. Then the attenuation constant of the cables was measured.

(b) Resistance to water immersion
Cables were exposed in 70°C water for 20 days.

(c) Resistance to heat cycle
Heat cycle test was performed in an oven as described 3-2-2(d).
Cables were exposed for 40 cycles.

The results of the tests show that the properties of 3C-SVF are superior to 3C-PV and equal to 4C-2V.

Table 5. Physical properties

Items \ Type	3C-SVF	3C-PV	4C-2V
Minimum bending radius, mm	19	21	15
Pull-out strength between inner conductor to insulation, kg/50mm	3.2	1.6	10.0
Flexibility, mm	120	95	80
Shrinkage after heat cycle, mm	5	11	1

Table 6. The change ratio of attenuation constant in aging test

Items \ Type	3C-SVF	3C-PV	4C-2V
Resistance to heat, %	18	245	15
Resistance to water immersion, %	34	290	20
Resistance to heat cycle, %	4	65	5

4. Application of the new material to other cables

The new extrusion technique of highly expanded polyethylene is applicable to the manufacture of various types of cables. Table 7 shows examples of other highly expanded polyethylene insulated cables. The three cables shown in Table 7 have low-capacitance. 7/0.128-PEFXSV meets UL Specification "FR-1" regarding the flame retardancy. 1.5C-SXV and 7/0.128-PEFXSV fulfill the requirements specified in UL style 1550 and 1691, respectively. These cables can be used for MATV systems, internal wiring of electronics equipment, and other purposes.

5. Conclusion

An extrusion technique of highly-expanded polyethylene by a chemical blowing method has been developed and applied to microcoaxial cables with diameter of insulation smaller than about 3 mm. In this process, a specially formulated polyethylene in combination with a conventional chemical blowing agent are used. The new cable insulated by a foamed polyethylene with about 65% expansion has excellent properties when compared to conventional cables. This new method makes it possible to produce various types of microcoaxial cables.

6. References

1. Y. Toda and T. Nakahara, et al., "A Highly Expanded Polyethylene Insulated CATV Coaxial Cable" 22nd International Wire and Cable Symposium, 1973.

2. M. Yuto and T. Nakahara, et al., "Novel Extrusion Process For Robust Highly Expanded Polyethylene Insulated Coaxial Cables" 25th International Wire and Cable Symposium, 1976.

Table 7. Structures and properties of highly expanded PE insulated cable

Items \ Type		1.5c - SXV (Coaxial cable)	7/0.128 - PEFXSV (Shielded cable)	7/0.1 - PEFXSV (Shielded cable)
Inner Conductor	Material	Copper	Tin-coated Copper Wire	Copper-alloy
	Strand	1	7/0.128	7/0.10
	Diameter, mm	0.40	0.38	0.32
Inner Insulation	Material	Highly Expanded PE (Expansion Rate 67%)	Highly Expanded PE (Expansion Rate 60%)	Highly Expanded PE (Expansion Rate 67%)
	Diameter, mm	1.6	0.8	2.3
Outer Insulation	Material	HDPE	PVC	HDPE
	Thickness, mm	0.05	0.1	0.1
Outer Diameter of Insulation		1.7	1.0	2.5
Irradiation of Insulation		Irradiate	Irradiate	Irradiate
Outer Conductor	Material	Braided Copper Wires	Tin-coated Copper Wires (Spiral Wrapped)	Tin-coated Copper Wires (Spiral Wrapped)
	Diameter, mm	2.2	1.2	2.7
Jacket	Material	PVC	PVC	PVC
	Diameter, mm	3.0	1.7	3.8
Dielectric Strength, 0.5 KV rms, 1 min		Passed	Passed	Passed
Insulation Resistance, Megohms/km		> 1,000	> 1,000	> 1,000
Capacitance, pF/m, at 1 KHz		51	100	37
Use		MATV systems, Internal wiring of TV, audio machine, etc.	Internal wiring of audio machine and other electronics equipment	Accessary code connected between amplifier and player



Fumio Suzuki

Sumitomo Electric
Industries, Ltd.
1, Taya-cho,
Totsuka-ku,
Yokohama,
Japan

Fumio Suzuki finished the Chemical Engineering Course of Arai High School in Niigata Prefecture in 1958.
He joined the Research Division of Sumitomo Electric Industries, Ltd. in 1958, and worked on application research of high polymers especially polyvinyl chroride for wire and cables.
Mr. Suzuki is now Senior Engineer of Communications R & D Department and a member of the Society of Polymer Science of Japan.



Akinori Mori

Sumitomo Electric
Industries, Ltd.
3-3, Satsuki-cho,
Kanuma-city,
Tochigi-prefecture
Japan

Akinori Mori received his B.S. degree in mechanical engineering from Kyushu University in 1970. He then joined Sumitomo Electric Industries, Ltd., and engaged in manufacturing of plastic cables. Mr. Mori is now a member of Electronics Wire Division.



Shizuyoshi Sato

Sumitomo Electric
Industries, Ltd.
3-3, Satsuki-cho,
Kanuma-city,
Tochigi-prefecture
Japan

Shizuyoshi Sato graduated from Tsuyama Technical College majoring electrical engineering in Okayama Prefecture in 1968. In 1969, he joined Sumitomo Electric Industries, Ltd., and engaged in development and design of various kinds of coaxial cables. Mr. Sato is now a member of Electronics Wire Division.



Yoichi Suzuki

Sumitomo Electric
Industries, Ltd.
1, Taya-cho,
Totsuka-ku, Yokohama,
Japan

Yoichi Suzuki received his B.S. degree in applied chemical engineering from Tohoku University in 1971. He then joined Sumitomo Electric Industries, Ltd., and engaged in research of plastic materials and manufacturing of plastic cables. Mr. Suzuki is now a member of Communications R & D Department.

CABLE AND COUPLING DEVICE FOR TELECOMMUNICATION TRANSMISSION IN HIGH-VOLTAGE POWER LINE NETWORKS

S. Brüggendieck

Felten & Guilleaume Carlswerk AG
Cologne, West Germany

Summary

An overhead communication power line system has been developed for the transmission of carrier channels in high-voltage overhead line networks. It combines a phase conductor with a telecommunication cable in one unit. At the ends of the transmission line a coupling device provides inductive connection of the telecommunication facilities on the low-voltage side.

A number of trial lengths have been installed in the 20 kV overhead line network. The results of the field measurements and the problems of interference are considered in detail.

Finally, the economic aspects of the new telecommunication system in power line networks are discussed with special reference to its advantages in the 20 kV overhead line network.

1. Introduction

The supply of electrical energy by high-voltage power lines for large areas is so extensive that a comprehensive telecommunication network has become indispensable for operational purposes.

Besides telephone calls data and remote-control signals for the automatic control of the networks, for monitoring the system and localization of trouble in the power supply have to be transmitted. Depending on the telecommunication requirements of the network the following transmission systems have been used up to now:

- radio link
- power line carrier-frequency system
- self-supporting aerial telecommunication cables
- buried telecommunication cables

The first two transmission methods offer economic advantages over long distances such as, for instance, in high-voltage power line networks for 110 kV and above. However, they are not suitable for the medium voltage networks with nominal voltages from 20 kV and medium distances of about 10 km on account of the numerous branch lines.

Self-supporting aerial telecommunication cables mounted on the pylon hangers, either as earth conductor or otherwise, meet the requirements for economic transmission of information in the medium-voltage network. The necessary separation to the phase conductors and the additional strain on the pylons caused by self-supporting cables, however, often involve elaborate measures for the hangers. Subsequent installation on existing, often older overhead lines can, therefore, mean considerable difficulties.

For the medium-voltage networks an economic transmission of information within a phase conductor of the high-voltage overhead line has been developed[1]. It is known as the phase conductor telecommunication cable.

2. Description of the System

The basic design of an overhead communication power line is given in Figure 1. The most important components in this transmission system are the phase conductor telecommunication cable and the coupling device. The cable consists of a combination of a phase conductor with a star quad in its core. The wires of the phase conductor forming the armouring over the core conduct the high-voltage power. The construction of the phase conductor telecommunication cable can be adapted in design to all phase conductor types so that the new cable assumes both the mechanical and electrical functions of the phase conductor. It is installed instead of one of the phase conductors on the pylons of the overhead power line.

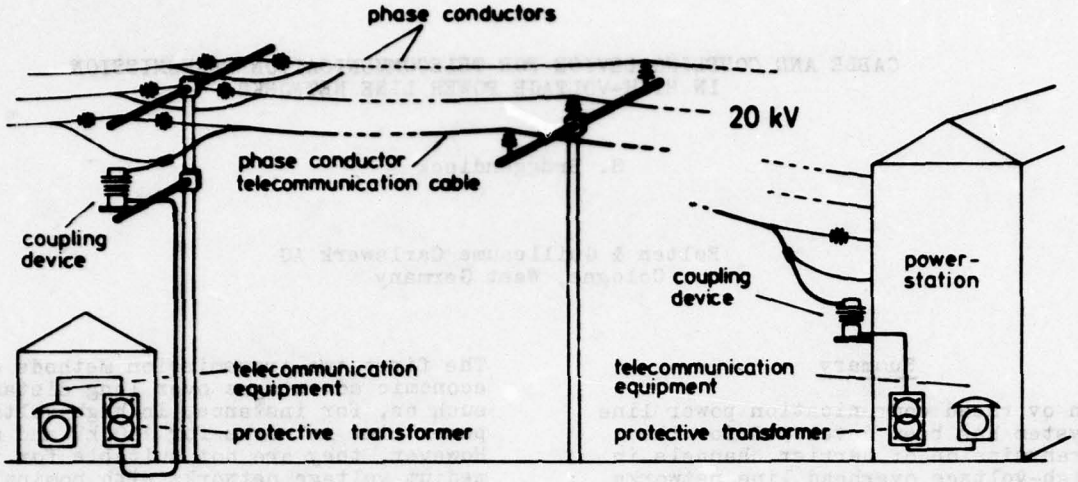


Figure 1. Overhead Telecommunication Power Line Network

The coupling devices at the ends of the cable permit low-loss, trouble-free transmission of telecommunication signals and guarantee the reliable protection of the operating personal and the telecommunication equipment against high-voltage influence. In the 20 kV medium-voltage network the coupling devices consist essentially of high-voltage transformers which isolate the high-voltage potential of the overhead line from the earth potential of the telecommunication equipment. The voltage strength requirements for this coupling device are, therefore, particularly stringent. It must also be capable of transmitting at minimal attenuation a frequency band up to at least 120 kHz for 12 channel carrier-frequency systems (Z 12).

3. Phase Conductor Telecommunication Cable

3.1. Cable Design and Electrical Properties

A compromise had to be found in the dimensions of the cable regarding the low attenuation and small cable cross-section requirements, so that the cable can conform in its outer dimensions to the other phase conductors.

For a maximum transmission distance of 15 km the attenuation of the route must be only about 60 dB at 108 kHz for the 12-channel carrier-frequency system Z 12 or 50 dB at 48 kHz for the 4-channel carrier frequency system Z 4, newly developed by F&G-TEKADE. This attenuation requirement can be easily met with 0.9 mm copper conductors. This also includes adequate reserve for the transformer attenuation of the coupling devices at either end of the transmission line and for by-passing circuit breakers along the route.

Figure 2 shows an example of the construction of a cable in a 20 kV overhead power line system, adapted to the conventional Al/St 95/15 phase conductor according to DIN 48 204.



Figure 2. Phase Conductor Telecommunication Cable

As is shown in Figure 2, the cable consists of a star quad with 0.9 mm PE-insulated copper conductors. Plastic tapes are wrapped over the star quads. The core is protected by a PE-sheath of 2 mm thickness. An 0.2 mm aluminium tape is wrapped over the sheath in order to improve the transmission characteristics. The armouring consists of 11 3.3 mm aluminium alloy wires and three 3.3 mm Alumoweld wires.

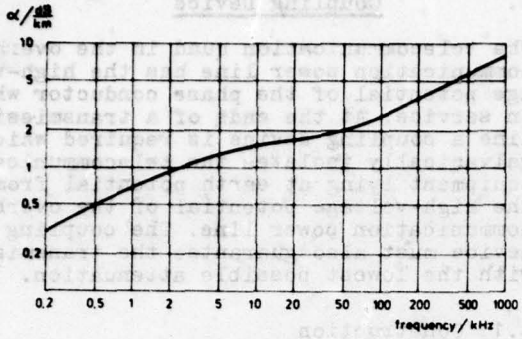


Figure 3. Attenuation α of the 0.9 mm star quad, t = 20°C

Particular importance must be attached to minimize pair-to-ground capacitance unbalances of the star quads, in order to prevent any external interference. The crosstalk between the side circuits of the quads is not critical due to the segregated band system on two wires and the short sections. In normal cable production the stipulated values can be easily adhered to.

The high-voltage requirements on the phase conductor telecommunication cable are the same as those for the phase conductors. Special attention must be given, however, to their influence on the star quad and in the selection of the material for the telecommunication core.

The thermal short-circuit strength required by VDE 0103 [2] means a significant temperature rise inside the cable core. Tests on the thermal short-circuit strength have yielded the temperature curve given in Figure 4 for the phase conductor and star quad.

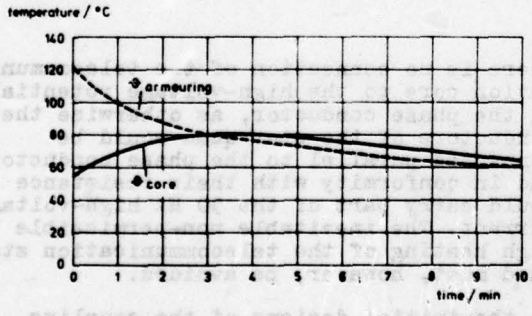


Figure 4. Temperature of the Core and the Armouring after loading with short-circuit Current

Table 1

Electrical and Transmission Characteristics of the Cable

A. Power Transmission at 50 Hz

resistance of armouring	0,3 Ohm/km
long-term current loading at final rope temperature ϑ_E = 80°C	340 A
short-term current at final rope temperature ϑ_E = 160°C	7 kA
screening factor	0,39
dielectric strength conductor/conductor	3 kV (10 s)
core/armouring	20 kV (10 s)
impulse withstand voltage (waveform 1.2/50 µs)	120 kV

B. Telecommunication Transmission up to 120 kHz of the Quad at 20°C

insulation resistance	≧ 10	GOhm · km
loop resistance	≦ 56.6	Ohm/km
mutual capacitance (800 Hz)	≦ 45	nF/km
attenuation α at 108 kHz	≦ 2,9	dB/km
impedance Z at 108 kHz	= 135	Ohm
near-end crosstalk a_n	≧ 65	dB
far-end crosstalk a_f-a	≧ 65	dB(1 km)

Table 2

Mechanical properties of the Cable

	Unit	Phase Conductor with telecom. core	
outer diameter	mm	18,4	13,6
weight	kg/m	0,570	0,383
max. tensile strength	N	18720	13160
every day stress	N	5768	3982
calculated breaking load	N	58100	35750

Table 1 lists those electrical properties which are decisive for the operation of the phase conductor telecommunication cable. The relevant rope requirements are given in Table 2 in comparison with the Al/St 95/15 phase conductor.

Owing to the thermal stress of the cable in the event of a short-circuit high-density polyethylene was chosen for the insulation of the star quad conductors and the sheath. These bare Cu-conductors are tinned in order to eliminate any possibility of catalytic oxydation of the insulation at higher operating temperatures.

The construction of the cable over the communication core is determined by rope requirements, whereby it must be remembered that the cross section of the armouring wires must have the same conductance as the other two phase conductors of the overhead power line. This provides balance of the three-phase system.

3.2 Accessories and Joints

Preformed dead ends normally used for self-supporting aerial cables are also used for this cable. These fittings minimize the surface pressure on the cable and provide protection against damage due to vibrations.

The joints of the phase conductor telecommunication cable (Figure 5) are installed in the strain-relieved current loops of the anchoring mast.

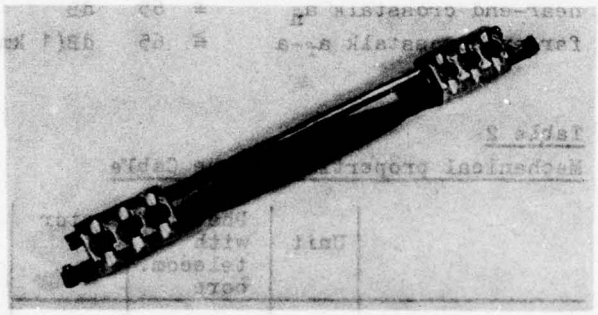


Figure 5. Joint of Phase Conductor Telecommunication Cable

The telecommunication cores are connected with solder joints which are protected against moisture by a lapping of self-welding plastic tapes. This guarantees the strength of the star quad against the phase conductor. A shrink hose over the lapping provides the mechanical protection for the telecommunication splice. The galvanic joint is resistant to short-circuits and continuous-current. It consists of two clamps normally used in overhead line systems, which are joined by a solid aluminium bar. This means the joint is also mechanically stabilized.

4. Coupling Device

The telecommunication quad in the overhead communication power line has the high-voltage potential of the phase conductor when in service. At the ends of a transmission line a coupling device is required which galvanically isolates the telecommunication equipment lying at earth potential from the high-voltage potential of the overhead communication power line. The coupling device must also guarantee the transmission with the lowest possible attenuation.

4.1 Construction

The construction of the coupling device is shown in Figure 6. The coupling device incorporates two high-voltage-proofed toroidal transformers for the inductive coupling to the two side circuits of the star quad in the phase conductor telecommunication cable. The transformer centre taps on the low-voltage side are earthed.

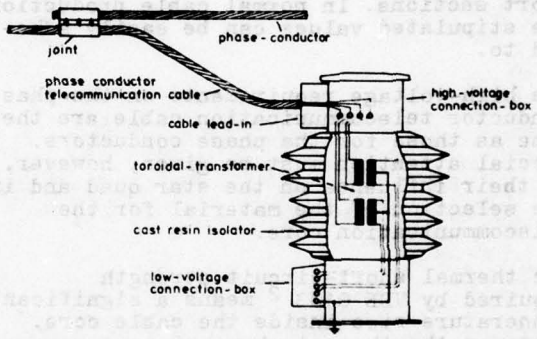


Figure 6. Basic Construction of the 20 kV Coupling Device

There is no connection of the telecommunication core to the high-voltage potential of the phase conductor, as otherwise the conductors of the star quad would be connected parallel to the phase conductor and in conformity with their resistance would carry part of the 50 Hz high-voltage current. The inevitable non-permissible high heating of the telecommunication star quad must, however, be avoided.

In the initial designs of the coupling device transformer insulating oil was used. A cast resin encapsulated design has meanwhile been developed, which has advantages in regard to weight, installation and service reliability. Cycloaliphatic cast-

resin used as insulation is very resistant to atmospheric influences. The coupling device is therefore suitable for outdoor and indocr use. In its high-voltage design it corresponds essentially to an outdoor 20 kV current transformer.

4.2 Transmission- and High-Voltage Characteristics

The coupling device meets all the high-voltage requirements stipulated in VDE 0414 [3], the standard for the corresponding current transformer.

Table 3 lists the high-voltage and telecommunications data of the cast-resin encapsulated coupling device.

Table 3

Electrical and Mechanical Properties of the Coupling Device

nominal voltage	20 kV, 50 Hz
dielectric strength	55 kV, 50 Hz, 1 min.
impulse-withstand-voltage	125 kV (waveform 1,2/50 µs)
	145 kV (cut-off waveform)
ionisation voltage	>14 kV

Attenuation

carrier-frequency band (Z = 150 Ohm)

Z4 - system	12 kHz-	48 kHz	<1 dB
Z12 - system	6 kHz-	108 kHz	<1 dB

audio-frequency band (Z = 600 Ohm) at 1 kHz	<4 dB
crosstalk attenuation between the two transformers (0.3 ... 120 kHz)	≧ 85 dB
transformation ratio	1:1
weight	46 kg
total height	520 mm
overall diameter	340 mm

In order to use as many channels as possible the coupling device must be able to transmit at least carrier-frequency systems up to 120 kHz. Transmission in the audio-frequency range should also be possible.

Realization of these requirements with due allowance for the high-voltage aspects led to a transformer with a frequency characteristic of the attenuation as given in Figure 7. The marked increase in the attenuation at very low frequencies is acceptable, as the attenuation of the cable decreases the lower the frequency and thus compensates the transformer attenuation to a certain extent.

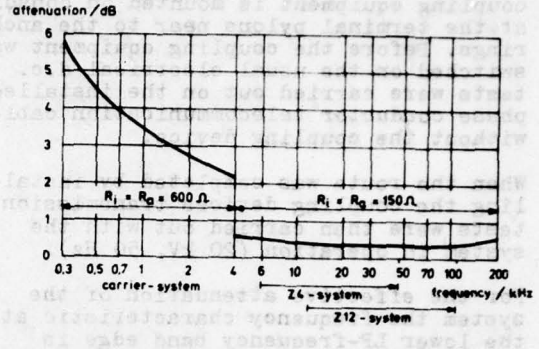


Figure 7. Attenuation of the Coupling Device

4.3 Installation of the Coupling Device

The coupling device is usually mounted on the hangers of the final pylon. During installation the overhead communication power line is lead into the head of the coupling device in a waterproof manner and connected to the connecting terminals of the high-voltage winding of the two transformers. The ends and centre tap of the two low-voltage windings, joined to the terminals of the terminal box, are connected to the insulated conductors of the outgoing telecommunication cable or earth.

Although appropriate measures were taken in the construction of the coupling unit so that in the unlikely case of a voltage breakdown this can only occur to earth, isolating transformers must be provided as additional protection directly in front of the telecommunication equipment.

In addition to coupling devices at the ends of the routes they are also required at both sides of any circuit breakers in the phase conductor line, as during switching or work on the line the phase conductor and telecommunication conductor must be put at equal and defined potential.

5. Field Tests

In autumn 1976 the first overhead communication power line system in the 20 kV medium-voltage network was taken into service on a 5 km route of the Badenwerk AG. For various reasons, this route consists of nine anchor sections and termi-

nates at both ends at cable terminal pylons. The overhead communication power line was installed in lengths of about 1000 to 1450 m at a rate of 60 m/min. The overhead communication power line was treated as a phase conductor of corresponding diameter in regard to installation technique, equipments and tools. Joints were installed on three anchor pylons. The coupling equipment is mounted on consoles at the terminal pylons near to the anchorings. Before the coupling equipment was switched on the usual electrical d.c. tests were carried out on the installed phase conductor telecommunication cable without the coupling device.

When the route was completed by installing the coupling devices transmission tests were then carried out with the system in operation (20 kV, 50 Hz).

For the effective attenuation of the system the frequency characteristic at the lower LF-frequency band edge is essentially determined by the coupling device and at the upper frequency band edge by the cable:

at 300 Hz : a = 17 dB

at 108 kHz: a = 16 dB

The near- and far-end crosstalk at values above 70 dB are so good that balancing measures were not necessary.

The noise voltage was measured at <0.03 mV with a psophometer. The limit value in the public network lies at < 2 mV.

The interference on the route does not show any value below 70 dB during selective measurement in the frequency range up to 120 kHz (Figure 8).

In general the noise level depends essentially on local conditions and should be checked before the route is taken into service. Particularly in the case of carrier-frequency transmission on high-voltage systems along parallel routes the interference level on the overhead communication power line must be measured.

Besides this route eight others have meanwhile been taken into service. Their performance has been very satisfactory.

6. Influence Hazards

Owing to its more exposed installation this new type of transmission system is at a greater risk from electromagnetic influence and interference.

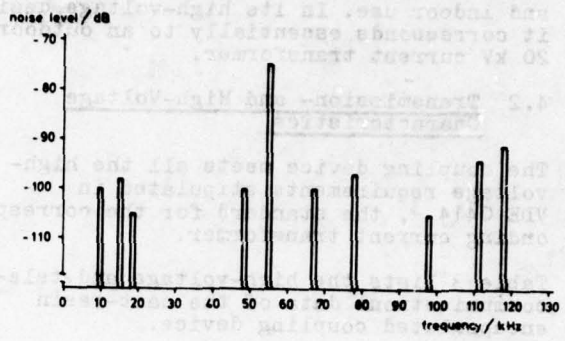


Figure 8. Measured Noise Levels on an Installed Route (Length: 5 km)

6.1 Influence on the overhead Communication Power Line during a Short-Circuit

In studying power current influence of the telecommunication core the double pole earth short-circuit must be considered for the 20 kV-network without rigid star point earthing.

According to the equivalent-circuit diagram (Figure 9) the voltage stress caused by the initial double short-circuit current I''_{KEE} is

$$U_M = I''_{KEE} (R + j\omega L_E) \cdot l$$

$$U_E = I''_{KEE} \; j\omega M \cdot l$$

$$U_A = I''_{KEE} \; R \cdot l$$

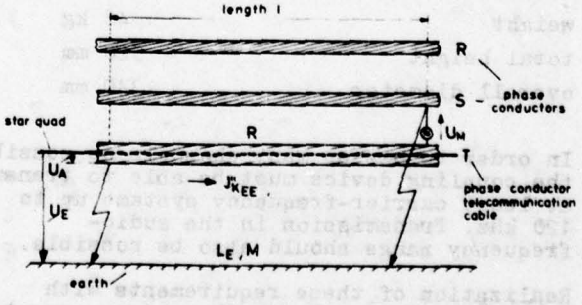


Figure 9. Short-Circuit Conditions in a 20 kV-line network

As the core/earth circuit, which is influenced, is inductively very closely coupled to the armouring/earth circuit causing the influence, the mutual inductance M is equivalent to the earth circuit inductance L_E. The core/earth voltage is thus

$$U_E = I'_{KEE}\, j\omega\, L_E \quad . \quad 1$$

If the ratio U_a/U_m is given, the screening factor r of the cable is

$$r = \frac{U_A}{U_M} = \frac{R}{R+j\omega L_E}$$

This yields for the voltages:

$$U_A = U_M \cdot r$$

$$U_E = U_M \cdot (1-r)$$

For the 20 kV medium-voltage network is

$$U_M = 20 \text{ kV}$$

With a screening factor of r = 0,17-j0,38 for the phase conductor telecommunication cable the following voltages can be calculated:

core/armouring: U_A = 8 kV

core/earth : U_E = 18 kV

According to [2] the short-circuit surge current exceeds the short-circuit a.c. current I'_{KEE} 2,5 times. This results in a short term surge voltage stress effective for the cable

core/armouring: $\hat{U}_A$ = 20 kV

and effective for the coupling device

core/earth : $\hat{U}_E$ = 45 kV

The voltage stresses on the insulation core and coupling device therefore lie below the test voltage levels (Table 1+3).

6.2 Influence of Lightning

Basically, the same conditions apply for the influence of lightning on an overhead communication power line as for the conventional overhead power line. Years of experience and study are available on the behaviour of overhead lines when struck by lightning [4].

When lightning strikes the overhead line, the surge impedance of the phase conductor earth circuit, which is about 400 ohms, becomes effective. Analogous to the short rise time of the lightning a voltage-to-earth of some megavolts occurs on the phase conductor. This causes a flashover to earth at the next pylon, due to the surge withstand voltage of the 20 kV-isolators. Thus the voltage is reduced to the value given by the lightning current and earth resistance of the pylon. The lightning current is therefore essentially reduced at these flashover points.

The effects of the lightning in the influenced armouring/core circuit correspond essentially to those when lightning strikes a cable which is earthed at given distances. The lightning current causes a voltage drop on the phase conductor. This drop occurs on the inside of the armouring and leads to a breakdown between core and armouring if the impact breakdown voltage is exceeded.

A so-called quality factor g has been defined for cables which indicates how far a definite lightning current can pass through the cable without causing a breakdown:

$$g = \frac{U_{st}}{R_K}$$

U_{st}: nominal impulse withstand voltage of the insulation between armouring and telecommunication core,

R_K : coupling resistance of the armouring (in most cases equal to the d.c. resistance).

From Table 1 the following values apply for the phase conductor telecommunication cable:

U_{st} = 120 kV, R_K = 0.3 ohm/km

Therefore, g = 400 kA . km.

Assuming an unusually high lightning current of 100 kA, which is propagated almost equally in both directions when lightning strikes the phase conductor telecommunication cable, the lightning current of 50 kA remaining in one direction can flow about 8 km along the cable without causing a breakdown. If allowance is made for the attenuation of the lightning current along the cable which is caused by flashovers at the pylons, the propagation distances will be far more than 8 km in one direction. In medium-voltage networks the overhead communication power lines have a maximum length of about 15 km, so that breakdowns due to lightning are not to be expected in the phase conductor telecommunication cable.

If there is a coupling device in the immediate vicinity of the point where the lightning strikes the cable, it is endangered by the very steep rise and, as a result of the impulse inertia in overhead lines, the high values of the over-voltage. According to [4] the coordi-

nation of the inner and outer insulation is obtained up to the level of the surge for the 1.2/50 µs impulse wave (cf., Table 3). In extreme cases for voltages with a steeper rise the installation of lightning arresters or parallel spark gaps with arc fittings is recommended.

6.3 Interference

The phase conductor telecommunication cable, like all overhead lines, is subject to various types of interference, e.g., from radio transmitters and CF-transmissions on adjacent high-voltage lines.

In the case of radio transmitters a method is given in 5, whereby the level of interference at the ends of an overhead communication power line can be estimated.

Long-wave transmitters, which may cause interference in the CF-range up to 120 kHz are vertically polarized. The electrical field intensity of their radiation field is perpendicular to the earth's surface, provided that the conductivity of the earth is infinite. The actual finite conductivity of the earth together with the increased dielectric constant means that the vector of the electrical field E stands at an angle of <90° to the surface of the earth.

For the vertical field intensity E_A of the transmitter with the power P at point A, which is at a distance r_A from the transmitter (Figure 10), the following equation applies for the remote radiation field:

$$E_A = \frac{C_1 \sqrt{P}}{r_A} \quad \text{with } C_1 = 3\sqrt{10\ \text{Ohms}}$$

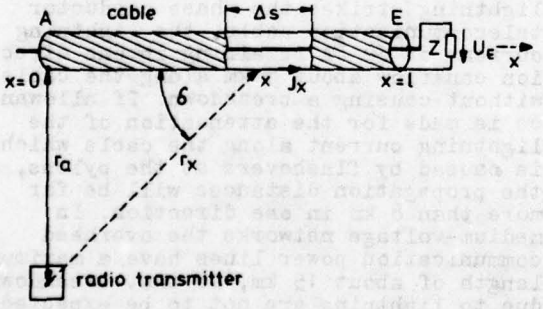


Figure 10. Graphical Illustration of the Calculation

The phase conductor telecommunication cable, which lies in the direction of the wave propagation, also has a sheath current I due to the horizontal field.

The product of sheath current I and coupling resistance R_K of the cable sheath yields the electrical direct-axis field intensity $E_i = I \cdot R_K$ inside the cable.

With increasing distance r from the transmitter the phase of the wave decreases in accordance with $2\pi r/\lambda$ and the amplitude with $1/r$.
Thus for a definite point x along the overhead communication power line the following equation applies:

$$E_x = E_A \frac{r_A}{r_x} e^{-j \frac{2\pi}{\lambda} (r_x - r_A)}$$

The field intensity E_x produces at the field point x the partial sheath current

$$I_x = C_2 \cdot E_x \cdot \cos\delta$$

The factor C_2 is a function of the frequency f and the earth conductivity σ:

$$C_2 = \frac{0{,}6}{\sqrt{f \cdot \sigma}} \text{ in } \frac{A}{V/m} \text{ with } \begin{matrix} f \text{ in Hz} \\ \sigma \text{ in } 1/\Omega m \end{matrix}$$

To calculate the interference, a cable route is divided into partial sections of the magnitude $\Delta s \approx \lambda/10$. With the sheath current at point x and the coupling resistance R_K of the phase conductor telecommunication cable the interference voltages ΔU_x in the telecommunication circuit can be calculated. With allowance for the pair-to-ground capacitance unbalance k_{ui} in the cable the following equation applies:

$$\Delta U_x = R_K \cdot I_x \cdot \Delta s \cdot k_{ui}$$

For k_{ui} a typical value is at least 10^{-3}.

The partial voltage ΔU_x still has to be multiplied by the propagation factor γ in order to obtain the voltage ΔU_E at end E.

$$\Delta U_E = \Delta U_x \, e^{-\gamma l_x}$$

The partial voltages ΔU_E from all calculated sections Δs along the influenced route must be geometrically added to the resultant interference voltage U_E.

This calculation only provides a rough estimation of the level of interference to be expected on the line. In case where the planned route may be subjected to strong interference, noise level measurements will be necessary to confirm the calculation.

7. Economic Aspects

The overhead communication power line system with inductive coupling device was specially developed for the 20 kV medium-voltage network. A telecommunica-

tion system for this network has not been previously installed to any major extent.

Only in a few cases has power line carrier-frequency transmission been used so far in medium-voltage networks. The relatively high costs for the coupling-in and-out of the carrier-frequency, which is necessary at each branching point or breaker, stand in the way of any economic use of this system over short transmission distances.

Self-supporting aerial telecommunication cables have a construction similar to the phase conductor telecommunication cable. Their disadvantage in the medium-voltage network lies in the fact that the self-supporting aerial cables have to be installed both additionally and separately on the pylons, as earth conductors are not required in medium-voltage networks. This involves higher costs as a fourth conductor has to be installed which sometimes requires pylons with a higher effective strength and stronger foundation. In such cases, the additional costs for a transmission system with self-supporting aerial cables can lie about 20% above those for an overhead communication power line system.

9. Conclusion

The described overhead communication power line offers a reliable and economic telecommunication system for the 20 kV medium-voltage network.

The efficient utilization of the cable with a few carrier frequency channels essentially covers the increasing demand for telecommunication facilities on overhead power lines. The field trials show that the new developed cable fulfills the requirements for power and, likewise, telecommunication transmission.

Moreover, the calculations discussed in this paper reveal that there may no problems be expected regarding interference from radio transmitters, lightning or short-circuit in the overhead power line. The many phase conductor telecommunication cables already installed confirm the results in this paper.

References

1. Benndorf, Stichling, Kirch, Levacher: Energie- und Informationsübertragung in 20 kV-Mittelspannungsnetzen mit dem Phasenseilkabelsystem Elektrizitätswirtschaft, Heft 19, September 1977
2. VDE 0103, 5.74: Mechanical and thermal short-circuit strength of electrical power installations
3. VDE 0414, Teil 2, 12.70: Bestimmungen für Meßwandler; Besondere Bestimmungen für induktive Stromwandler
4. Baatz: Gewitterschutz und Wirksamkeit direkter Schutzmaßnahmen in Netzen ETZ-A, Heft 9, 1961
5. W. Wild, W. Vogl: Die Beeinflussung von Fernmeldekabeln durch Starkstromleitungen und durch Hochfrequenzsender Knebel, Verlag Herzog, Goslar 1957



Siegfried H. Brüggendieck
Felten & Guilleaume Carlswerk AG
D 5000 Cologne 80
West Germany

Mr. Siegfried H. Brüggendieck studied communication engineering at Technische Hochschule Stuttgart. In 1964 he joined Felten & Guilleaume Carlswerk AG. He is now Manager of the Department for Telecommunication Cables Research and Development.

A NOVEL EXTRUDER SCREW DESIGN FOR THE MANUFACTURE OF A 'FOAMSKIN' TELEPHONE WIRE INSULATION

J.K. Normanton
J.E. Robinson

Bakelite Xylonite Limited,
Grangemouth, Scotland.

ABSTRACT

A process for the extrusion of a 'foamskin' telephone insulation using a single screw extruder has been developed. The cellular "foam" and solid "skin" materials are fed to the screw using a split feed hopper. A twin flighted screw leads to a special nose section where the feed from one flight is channelled to the screw centre. At crosshead entry the melt consists of a cellular core surrounded by solid polymer. Simple, single feed crosshead and die tooling has produced insulation with a clearly defined 'foamskin' laminate. Development continues to improve its concentricity. The properties of insulations produced from medium density polyethylene based compounds are described.

INTRODUCTION

Interest continues in 'foamskin' as a complementary insulation to either solid or cellular polymerics for telephone wires, particularly with petroleum jelly filled cables. This insulation comprises a cellular core, normally produced from a compound containing an azodicarbonamide blowing agent, surrounded by a solid polymer layer. Lamination is achieved during extrusion in the wire making process. Indications are that medium or high density based polyethylene compounds are viable in the application with some experience of polypropylene.[1,2] The 'foamskin' extrusion process normally combines two extruders feeding a common head and die carrying the conductor. The primary extruder serves the cellular core with a second or "piggy back", the solid skin.

Our investigation has shown potential for a 'foamskin' insulation to be produced using a novel single screw design.[3] The paper outlines progress with this development. It covers the screw design, material feed arrangements, together with extruder and die effects. Evaluations on wire covering using medium density based polyethylene compounds are described.

PROCESS DESCRIPTION

Design

The process is based on a standard single extruder wire coating line. Additionally, a metered feed for the cellular compound, split feed hopper, special twin flighted screw having a special nose section and suitable crosshead tooling are required. Fig. 1 & 2.

Split Feed Hopper. The hopper and feed throat of the extruder are divided by a metal plate. This plate in the feed throat has been accurately fitted to the shape of the feed throat in order to avoid any leakage. The solid compound is loaded in the foremost hopper.

Metered Feed. Cellular compound is fed to the rearmost hopper via a small vibratory feeder. The function of this metered feed is to control the proportions of cellular and solid compound entering the extruder. Initially the operation of the feeder was unsatisfactory with poor stability at low output rates $\sim$ 3.0 Kg/hr. This was improved by the addition of baffles in the feed tray. Fig. 3.

Extruder Screw Design. The two polymers are kept essentially separated by means of a twin channelled screw. The first channel starts beneath the rearmost feed hopper, the second beneath the forward hopper. The screw has a special nose which transfers polymer from the first channel to the hollow core of the nose. Both melt streams subsequently combine at the end of the screw with compound from the second channel surrounding compound from the first exiting along the axis of the screw.

For the initial development a screw having equal section channels has been used. Further screws having dissimilar channels to optimise the 'foamskin' ratio are envisaged.

Head Design. For initial laboratory work an in-line head and die extruding a rod section was used. Fig. 4. Further work utilised a simple single entry crosshead with a plugged point. Fig. 5. A similar single entry crosshead was used for wire line trials.

Design Philosophy

It is accepted that the two polymer streams within the screw cannot be kept completely separated. Two potential transfer routes are:

- at the base of the feed hopper.
- screw leakage.

Every revolution the first channel is exposed to the second hopper and some 'topping up' is unavoidable. However, there is no direct path from the first hopper to the second channel and any transfer in this direction must be overflight.

Screw leakage is a phenomenon common to all screw extruders. Generally this is taken into account[4] by modifying the drag flow by the factor $(1 - \delta/H)$

where δ = screw/barrel clearance
H = channel depth.

As the pressure flow is relatively small (<20% x drag flow) the reduction in output due to leakage is only slightly greater than this factor i.e. 7%.

EXPERIMENTAL EXTRUSION WORK

A 60 mm diameter, 21/1 length to diameter ratio, extruder was used having a screw profile as described. The capability of the process to produce a 'foamskin' extrusion was first evaluated on an in-line rod section. Subsequently a crosshead fitted with a plugged point was used before progressing to wire covering using a telephone singles extrusion line.

Table 1: Screw Design for 'Foamskin' Extrusion

	Dimension
Diameter	60 mm
Type	Twin Start
Pitch	2 x 38 mm
Length Feed	280 mm
Transition	190 mm
Meter	794 mm
Meter Channel Depth	2.5 mm
Compression Ratio	3.5:1
Nose Core Diameter	10 mm

Compounds based on low, medium and high density polyethylene have been used in different stages of the work. With cellular insulation compounds containing blowing agent, extrusion temperatures are directly related to blowing agent activation in order to achieve an optimum cellular structure.[5] Except where indicated an extrusion temperature of 210°C was used with compounds containing azodicarbonamide and 150°C with p,p,-oxy-bis (benzene sulphonyl hydrazide). The solid skin compounds were formulated to process at the required temperatures.

Table 2: Polyethylene 'Foamskin' Process Evaluation Compounds

COMPOUND REFERENCE	TYPE	MELT FLOW INDEX	POLYMER NOMINAL DENSITY	BLOWING AGENT CONTENT
		dg/min	gm/cc	%
A	Cellular(1)	2.0	0.917	1.2
B	Cellular(2)	0.7	0.933	0.65
C	Cellular(2)	0.7	0.933	0.71
D	Cellular(2)	0.7	0.933	1.0
E	Solid	2.0	0.917	-
F	Solid	0.3	0.950	-
G	Solid	0.2	0.933	-

Blowing Agents: (1) p,p,oxy-bis (benzene sulphonyl hydrazide).
(2) azodicarbonamide.

In line Rod Section

Clearly defined and concentric 'foamskin' sections were produced using compounds B and G. Fig. 6A. Typically, overall extrudate specific gravities of 0.60 with foam specific gravities of 0.40 have been achieved. The specimen shown (Fig. 5A) has a skin thickness of 10% of the overall diameter which approaches the minimum obtainable with an equal channelled screw.

The significance of varying the extrusion temperature from 200 to 225°C is shown. Fig. 7. As the temperature is increased the specific gravity is lowered.

Coarse cells showing loss of nucleation are observed at 213°C. At higher temperatures these penetrate into the skin material.

Inspection of the screw push outs indicated some cross channel material flow in both directions. Some flow of skin compound into the cellular channel was anticipated; flow in the other direction was not. The cause was identified as material from the first channel feeding up into the throat of the foremost hopper and back down into the second channel. It is thought that this is due to pressure build up during the initial closed half revolution of the first channel. The problem is overcome by metering material in the first channel to less than thirty five percent of the total extrusion output.

Plugged Crosshead

Initial work simulated wire covering by means of a plugged crosshead. Fig. 5. An extrudate comprising cellular compound A and skin compound E is shown. Fig. 6B. The 'foamskin' structure is clearly defined. However, the effect of the particular crosshead is to cause a part of the skin to penetrate to the centre of the extrusion. This penetration occurs diametrically opposite the feed entry point. Similar results were obtained with cellular compound B and skin compound F.

Telephone Singles Extrusion

Cellular compound C and skin material G were used to produce an insulated telephone wire. A capacitance reduction compared with a solid insulation was obtained. The cross section shown in Fig. 6C illustrates the difficulty in maintaining concentricity in the 'foamskin' through a crosshead although the particular design shows improvement over the plugged crosshead. The integrity of the foam and skin is maintained with clearly defined boundaries shown.

Table 3: Extrusion Wire Line Trials

Conditions	
Skin	Compound G
Foam	Compound C
Line Speed	590 m/min
Screw Speed	43 rpm
Vibratory Feeder Rate	6.5 Kg/hr
Extrusion Temperature	210°C
Diameter Conductor	0.63 mm
Insulation	1.04 mm
Capacitance*	242 pF/m
Tensile Strength	13.3 Mn/m^2
Elongation	720%

*Aim Capacitance Solid 278 pF/m
Cellular 227 pF/m

DISCUSSION AND STATUS

At the present stage of development the viability of the process can be assessed. It is shown capable of producing a 'foamskin' insulation achieving a preferred capacitance reduction when compared with solid insulation. Amongst factors influencing capacitance are skin and foam ratio as well as the realised specific gravity. An optimum aim ratio has not been fully defined. However, the process offers scope for adjustment principally by alteration of the width or depth of the twin screw channels and of fine tuning by control in metering the cellular compound. Alteration in expansion capability of the cellular compound by adjustment of its blowing agent content gives further flexibility.

The integrity of the 'foamskin' section is demonstrated and maintained during the extrusion process. Although some loss in concentricity occurs in the crosshead only standard tooling has been used to date. With design development to maintain flow uniformity at this point, improvement to a fully adequate level is envisaged.

REFERENCES

1. E.J.Gouldson et al, "Foam Skin. A composite expanded insulation for use in telephone cables". Proceedings 21st International Wire & Cable Symposium, Atlantic City, N.J., 1972.

2. S.G.Foord, "Compatibility problems in filled cellular polyolefin insulated telephone cables". Proceedings 22nd International Wire & Cable Symposium, Atlantic City, N.J. 1973.

3. British Patent Application No. 34631/76. Bakelite Xylonite Limited, 8 Grafton Street, London, W1A 2LR.

4. W.D.Mohr and R.S.Mallouk, Ind. Eng. Chem. 51, 765 (1959).

5. J.K.Normanton, "Extrusion of telephone cable insulation using expandable medium density polyethylene compounds". Proceedings 21st International Wire & Cable Symposium, Atlantic City, N.J., 1972.

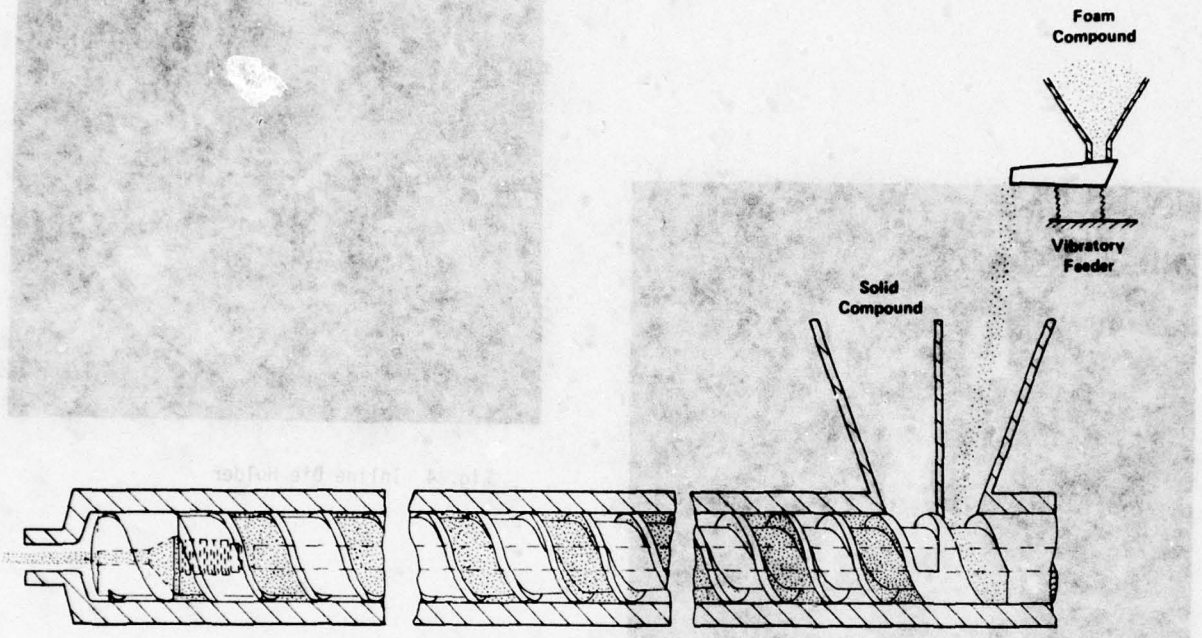


Fig. 1 General Arrangement of Extruder and Vibratory Feeder

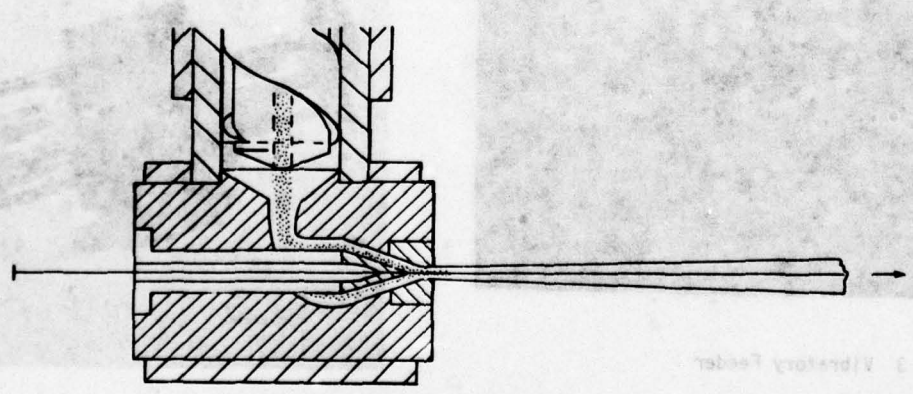


Fig. 2 Typical Single Entry Crosshead used for Foam Skin Development

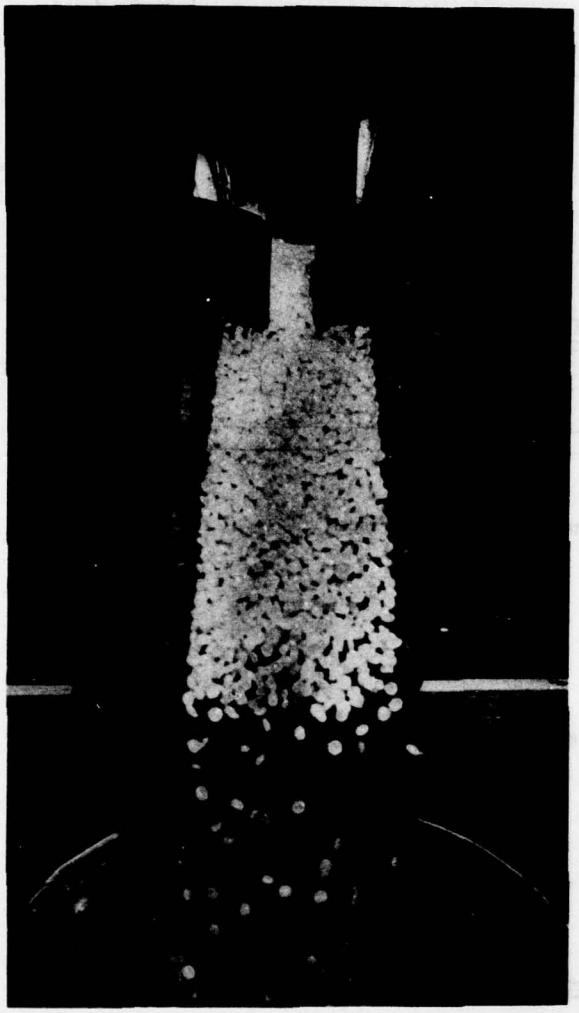


Fig. 3 Vibratory Feeder



Fig. 4 Inline Die Holder

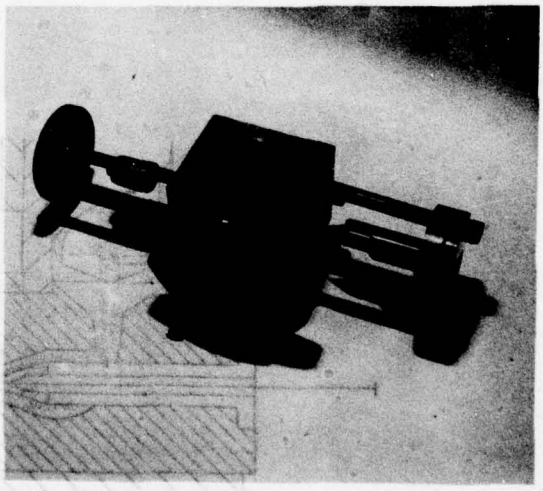


Fig. 5 Plugged Crosshead

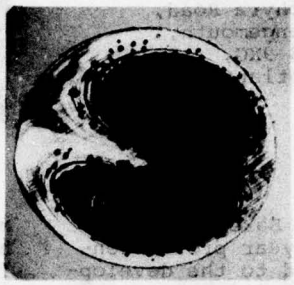
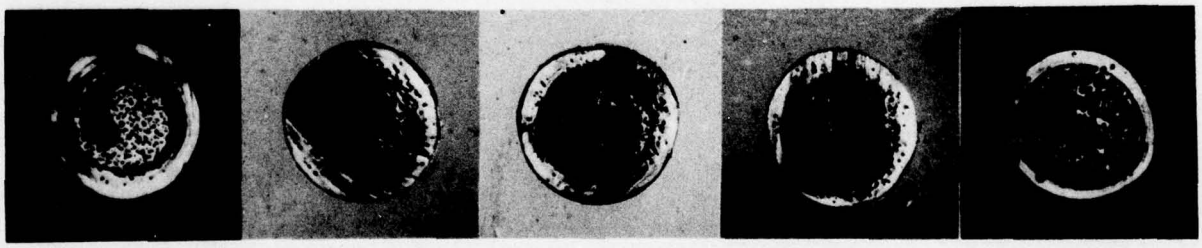
	A. Inline	B. Plugged Crosshead	C. Wire Coating Trial
			
Foam	Compound B	Compound A	Compound C
Skin	Compound G	Compound E	Compound G
Specimen Diameter	2.5 mm	5.5 mm	1.0 mm

Fig. 5 Three Foam Skin Sections

200°C	208°C	210°C	213°C	225°C
				

Foam	Compound B
Skin	Compound G
Specimen Diameter	2.5 mm

Fig. 6 Effect of Increasing Zone 4 Extrusion Temperature on Foam Skin Structure



Mr. J.K. Normanton,
Bakelite Xylonite
Limited,
Inchyra Road,
Grangemouth,
FK3 9XG,
Scotland.



Mr. J.E. Robinson,
Bakelite Xylonite
Limited,
Inchyra Road,
Grangemouth,
FK3 9XG,
Scotland.

Mr. J.K. Normanton joined Bakelite Ltd. in 1950, and his 28 year professional career has been devoted to the development of thermoplastic extruded products for electrical applications. He is currently Group Leader in the Technical Department of BXL Polyethylene Division, responsible for product development and technical service for polyethylene wire and cable compounds.

Mr. J.E. Robinson graduated with an honours degree in mechanical engineering from City University, London, in 1970. He joined Hawker Siddeley Aviation Ltd. and in 1971 was awarded an SBAC scholarship for 1 year to study Materials Technology at Imperial College, London. Since 1974 Mr. Robinson has worked in the Product Development Department of BXL Polyethylene Division specializing in wire and cable process studies.

RETURN LOSS AND TRANSMISSION DISTORTION DUE TO STRUCTURAL IRREGULARITIES IN COAXIAL CABLE

Laurence J. Hall

Telecom Australia
Melbourne, Australia

A unified approach to the problem of return loss and transmission distortion due to structural irregularities, both quasi-systematic and random, is presented. Using a detailed model and a comprehensive theory, measured return loss values are related to estimates of system performance, while the effect of changes in cable production can be evaluated. The theory also has application to crosstalk on symmetric pair cable.

1. INTRODUCTION

An important characteristic of modern wire transmission systems is that they are often required to operate on cables which were designed primarily for transmission at much lower frequencies. Two examples are the use of pulse code modulation systems on symmetric pair cable and high capacity analogue and digital transmission systems on trunk coaxial cable. The large amount of cable already installed necessitates an in-depth investigation of the performance of this valuable resource to determine what limitations on system performance are imposed by its shortcomings. In addition the substantial investment in plant to make current-design cable means that the relationship between production techniques and performance shortcomings should be identified in order to produce the best product for high frequency working with a minimum of plant changes. This paper deals primarily with trunk type coaxial cable (the 2.6/9.5 mm or 1.2/4.4 mm sizes) and the effect of manufacturing irregularities on its high frequency performance. However, the theory and results are equally applicable to CATV type coaxial cable.

The design of trunk coaxial cable adopted four decades ago for what was then high bandwidth transmission (a few MHz) has been shown by detailed measurements to perform very closely to what is predicted by quite simple theory up to a frequency of well over 1 GHz, except in a number of narrow near-harmonically related bands where the insertion loss and phase can show marked deviations from nominal. The reason for these deviations is the presence of near-periodic irregularities in the structure of the coaxial tube, predominantly caused by the stranding process. The problem of "impedance irregularities" in coaxial cable has been considered by a number of authors over a period of 40 years yet no theory has appeared which:

- is theoretically satisfying yet tractable,
- can be used to predict transmission performance from simple measurements, and
- is able to show the sensitivity of transmission performance to manufacturing deviations.

This paper aims to present a unified approach linking the important results on manufacturing irregularities, return loss and transmission distortion from a combined theoretical and practical study. This is achieved by commencing with an adequate model of the cable structure which identifies the important aspects of the manufacturing process, and then producing an electrical model which relates measurable electrical quantities to this process, allowing the effect of design changes to be seen. The final stage is the extension of the model so that system transmission performance can be reliably predicted from routine measurements.

The theoretical concepts developed in conjunction with the coaxial cable analysis can be applied to the study of crosstalk in multipair cable. This is illustrated in the last section of the paper by considering crosstalk coupling due to an unbalanced current flow in an earth circuit. As for the coaxial case, analysis of the model and the results can determine how small changes in cable production and jointing can yield major changes in crosstalk performance.

2. SELECTION OF A MODEL FOR MANUFACTURING IRREGULARITIES

Normal production processes and tolerances result in coaxial cable with a physical structure which is not perfectly uniform with length. Field theory shows that at each point of irregularity, some of the energy in the wave travelling from a source is reflected back towards that source. Normal transmission line theory can be extended to cope with a slightly irregular cable by allowing the primary parameters of inductance, resistance, capacitance and conductance to be functions of distance along the cable; this results in the secondary parameters of attenuation (α) and phase (β) coefficients and characteristic impedance (Z_0) being functions of length. Taking the derivatives of $Z_0(x)$, $\alpha(x)$ and $\beta(x)$ with respect to the

dimensional and physical quantities most subject to irregularities in manufacture shows that the characteristic impedance is the most sensitive to changes; furthermore, the effect of changes in the characteristic impedance is immediately apparent on propagation, while for $\alpha(x)$ and $\beta(x)$ it is the integral with distance which is significant so that short term variations in α and β with length are not considered important. Consequently, the cable with structural irregularities is modelled as having impedance irregularities, i.e. a characteristic impedance which is a function of distance, x, and this characteristic impedance can be considered a mechanical property of the cable.

2.1 Characteristics of Impedance Irregularities

The manufacture of trunk coaxial cable is divided into two basic operations, namely tube fabrication and the stranding of a number of tubes to form a complete cable. In both operations, the irregularities in the characteristic impedance which are introduced can be divided into two categories :-

i. "random" deviations having a correlation length of only a few centimetres.

ii. "quasi-systematic" deviations having a correlation length which is a damped periodic function with a period of a few tens of centimetres or more and an envelope of a few tens of metres or more.

The term correlation length is quantified by introducing a related quality, the power density spectrum $P(\nu)$, the Fourier transform of the auto-correlation function $Z_0(x)$; in the same way that the frequency domain, f, is the transform domain of time t, ν is the transform domain of the distance variable x. The random component of the $Z_0(x)$ process is analogous to white noise and hence has a power density spectrum which is close to being flat from essentially $\nu=-\infty$ to $\nu=+\infty$ while the quasi-systematic component has its power concentrated in a number of peaks in the ν domain.

While a number of sources of quasi-systematic irregularities have been identified, the major one, as far as trunk coaxial cable is concerned, is that produced by cable stranding[1]. The conventional coaxial tube has a longitudinal seam in the outer copper conductor which results in the tube not being uniformly resistant to deformation in the radial direction. Stranding causes a pressure point to move helically along the tube with the resultant deformation being greatest in the vicinity of the seam. The tube does not completely regain its original shape after the pressure point passes and is left with a characteristic impedance function which can be initially modelled as in Figure 1.

2.2 Almost-Periodic Irregularities

However the process is not perfectly periodic as suggested by Figure 1. Analysis of the stranding process indicates that the peak height of the pulse varies about the mean value Z_d shown, while the position of each pulse varies about the mean separation of T metres from the mean position of the previous pulse.

A number of different factors contribute to the variation in pulse height so that a gaussian distribution of height about the mean value Z_d can be assumed. For the pulse position, other factors contribute to the variation, so that the pulse position can be considered to be a gaussian distribution about a mean value of T metres separation. Furthermore, for each pulse, the height and position are assumed uncorrelated, as are the values of one pulse to another. The slope of the sides of the pulse is considered constant, irrespective of the height and position of the pulse. The values of T and S of this "quasi-systematic" or "almost-periodic process", together with other significant features of the random process, will be considered in a later section.

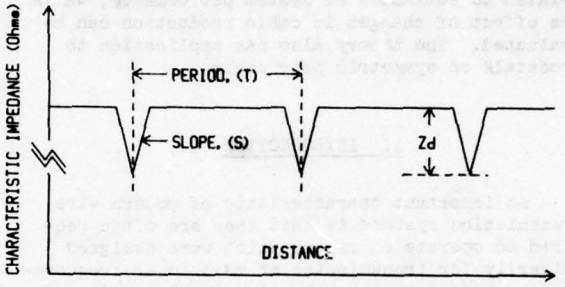


FIGURE 1:
Initial Model of the Systematic Impedance Irregularity Process

At this stage, it is appropriate to introduce an electrical model of the irregular cable which can take a proposed impedance irregularity process and translate it to measurable electrical quantities.

3. DEVELOPMENT OF AN ELECTRICAL MODEL

In the previous section, it was shown that the characteristic impedance process, $Z_0(x)$, is the cable parameter which incorporates all the possible sources of manufacturing irregularities and an examination of the mechanics of cable production gave an initial model for the form of $Z_0(x)$. It must be emphasised, however, that the electrical effect of irregularities is to convert a portion of energy travelling in one direction to the opposite direction of travel, and it is this effect which is responsible for return loss and transmission distortion. The characteristic impedance with its irregularities is thus not so much the cause of the electrical effects but a convenient intermediate point in the development of a suitable electrical model.

3.1 The Reflection Density Process

Consider a cable composed of segments of length dx, with the characteristic impedance constant over each length. The impedance is $Z_0(x)$ from $(x-dx)$ to x and $Z_0(x+dx)$ from x to $(x + dx)$. At x, a uniform line of $Z_0(x)$ is terminated by an

impedance $Z_0(x+dx)$ (the fact that the line of impedance $Z_0(x+dx)$ is not necessarily terminated by $Z_0(x+dx)$ is considered by repeating the analysis at $(x+dx)$). Consequently, conventional transmission line analysis predicts a reflection coefficient at x of :

$$d\rho(x) = \frac{Z_0(x+dx) - Z_0(x)}{Z_0(x+dx) + Z_0(x)} = \frac{dZ_0(x)}{2Z_0}$$

$$\triangleq r(x)dx \qquad (3\text{-}1)$$

which defines $r(x)$ to be the reflection density process, a term initially used by Karbowiak.[2] Electrically, $r(x)dx$ can be considered as the ratio of the infinitesmal reverse travelling voltage wave produced in dx to the incident voltage wave at x. For analytical purposes, this reverse propagating wave can be considered as having been coupled from the original line

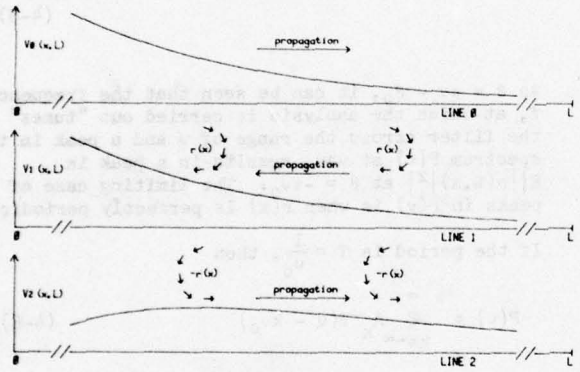


FIGURE 2:
The Three Line Model of an Irregular Cable

(line 0, Figure 2) to a new auxiliary line with propagation in the reverse direction (line 1, Figure 2), via the coupling function $r(x)$. However this signal on line 1 encounters sites of irregularity while propagating back to the origin, and there is coupling of signal onto a second auxiliary line, line 2 of Figure 2. The direction of propagation on line 2 is the same as for line 0. This process of coupling from one line to a higher numbered line can be extended indefinitely; however a total of 3 lines gives a model of suitable accuracy.

3.3 Attenuation Deviation due to Return Loss

The majority of authors who have considered the impedance irregularity problem neglect the fact that the production at a reflection site of a reverse travelling wave on line 1 causes a loss of power in the direct propagating signal on line 0. Similarly, the coupling to line 2 causes a loss of power to line 1 and so on. It will be shown later that this "return loss" is a major component of attenuation deviation. Accordingly, the attenuation on each of the three lines in Figure 2 is increased to account for this power coupling to a higher numbered line.

This enables all three lines in the model to be considered uniform, that is a constant impedance of Z_0, and the impedance irregularity process $Z_0(x)$ is no longer required as $r(x)$ is now the fundamental process. The conversion back to Z_0 after each "reflection site" can be considered to be accomplished by a hypothetical transformer whose effect is included in the attenuation increase.

If $\Delta\alpha_1(L,x)$ represents the increase in attenuation on line 0, (due to power coupling to line 1), at the point x on a cable of total length L, it can be shown that (see Appendix 1):

$$\Delta\alpha_1(L,x) = \frac{-1}{2(1-2|\rho(L,x)|^2)} \frac{d|\rho(L,x)|^2}{dx} + \frac{2\alpha_0|\rho(L,x)|^2}{1-2|\rho(L,x)|^2} \qquad (3\text{-}2)$$

where $\rho(L,x) \triangleq \frac{\text{total line 1 voltage at x}}{\text{line 0 voltage at x}}$

α_0 is the uniform line attenuation.

It can be shown (see Section 4) that if x is not too close to L, the end of the cable,

$$\frac{d}{dx}\left(E\left[|\rho(L,x)|^2\right]\right) = 0, \text{ so that}$$

$$E\left[\Delta\alpha_1(L,x)\right] \cong \frac{2\alpha_0 E\left[|\rho(L,0)|^2\right]}{1-2E\left[|\rho(L,0)|^2\right]} \qquad (3\text{-}3)$$

where $\rho(L,0)$ is the reflection coefficient at the input of the cable, a quantity which is conveniently measured by bridge or directional coupler methods. The variance of $\Delta\alpha_1(L,x)$ is not evaluated because the important quantity for transmission is

$$\int_0^L \Delta\alpha_1(L,x)dx$$

and while the average value of this is $LE[\Delta\alpha_1(L,0)]$ (neglecting the change in $E\Delta\alpha_1(L,x)$ as x approaches L), the integral effectively reduces the variance to a negligible quantity.

The significance of equation (3-3) is that it predicts the attenuation deviation due to return loss using a quantity which is readily estimated from measurements. It will be shown later that there is a simple relationship between this attenuation deviation and that from the signal on line 2 (due to double reflection) adding at the termination with the line 0 process.

At this point, it is appropriate to consider the theoretical derivation of $E\left[|\rho(L,x)|^2\right]$ from the reflection density process and its power density spectrum $P(\nu)$.

4. THE RETURN LOSS

At any point x along the cable, the line 1 signal, $V_1(x,L)$ is a weighted summation of reflection components produced at all points from x to the end of the cable, L, and $\rho(L,x)$ is the ratio of $V_1(x,L)$ to $V_0(x,L)$. In order to relate the attenuation deviation to manufacturing irregularities rather than just to the measured reflection coefficient, $\rho(L,x)$ is required in terms of the power density spectrum $P(\nu)$ of the $r(x)$ process. Using the definition of $r(x)$,

$$\rho(L,x) = \int_{\eta=x}^{L} \exp(-2\alpha_o(\eta-x)-2j\beta_o(\eta-x) - \int_x^\eta \Delta\alpha_1(L,\lambda)d\lambda - \int_x^\eta \Delta\alpha_2(L,\lambda)d\lambda)\, r(\eta)d\eta \tag{4-1}$$

where the excess attenuation due to power coupling is included for both line 0 ($\Delta\alpha_1(L,\lambda)$ and for line 1 ($\Delta\alpha_2(L,\lambda)$).

But $\int_x^\eta \Delta\alpha_1(L,\lambda)d\lambda \cong (\eta-x)\, E\left[\Delta\alpha_1(L,x)\right]$

and $\int_x^\eta \Delta\alpha_2(L,\lambda)d\lambda \cong (\eta-x)\, E\left[\Delta\alpha_1(L,x)\right]$

Therefore,

$$\rho(L,x) \cong \int_\eta^x \exp\left((-2\alpha-2j\beta_o)(\eta-x)\right) r(\eta)d\eta$$

where $\alpha = \alpha_o + E\left[\Delta\alpha_1(L,x)\right]$ (4-2)

Using well known statistical techniques it can be shown :

$$E\left[|\rho(L,x)|^2\right] = \int_{\nu=-\infty}^{\infty} \frac{P(\nu)d\nu}{4(\alpha^2+\beta^2)} \left(1-2\exp(-2\alpha(L-x))\right.$$

$$\left.\cos 2\beta(L-x) + \exp(-4\alpha(L-x))\right) \tag{4-3}$$

where $\beta = \pi\nu + \beta_o$ (4-4)

which, as expected, shows that the mean square reflection coefficient builds up to a constant value as x moves away from L. By analogy to circuit theory, (4-3) shows that this mean square reflection coefficient is the total power of a signal which results from passing an input signal with power density spectrum $P(\nu)$ through a filter with system function

$$|H(\nu)|^2 = \frac{\left|1-2\exp(-2\alpha(L-x))\cos 2\beta(L-x) + \exp(-4\alpha(L-x))\right|}{4(\alpha^2+\beta^2)} \tag{4-5}$$

As $\beta = \pi\nu - \beta_o$, it can be seen that the frequency, f, at which the analysis is carried out "tunes" the filter across the range of ν and a peak in the spectrum $P(\nu)$ at $\nu=\nu_o$ results in a peak in $E\left||\rho(L,x)|^2\right|$ at $\beta = -\pi\nu_o$. The limiting case of peaks in $P(\nu)$ is when $r(x)$ is perfectly periodic.

If the period is $T = \frac{1}{\nu_o}$, then

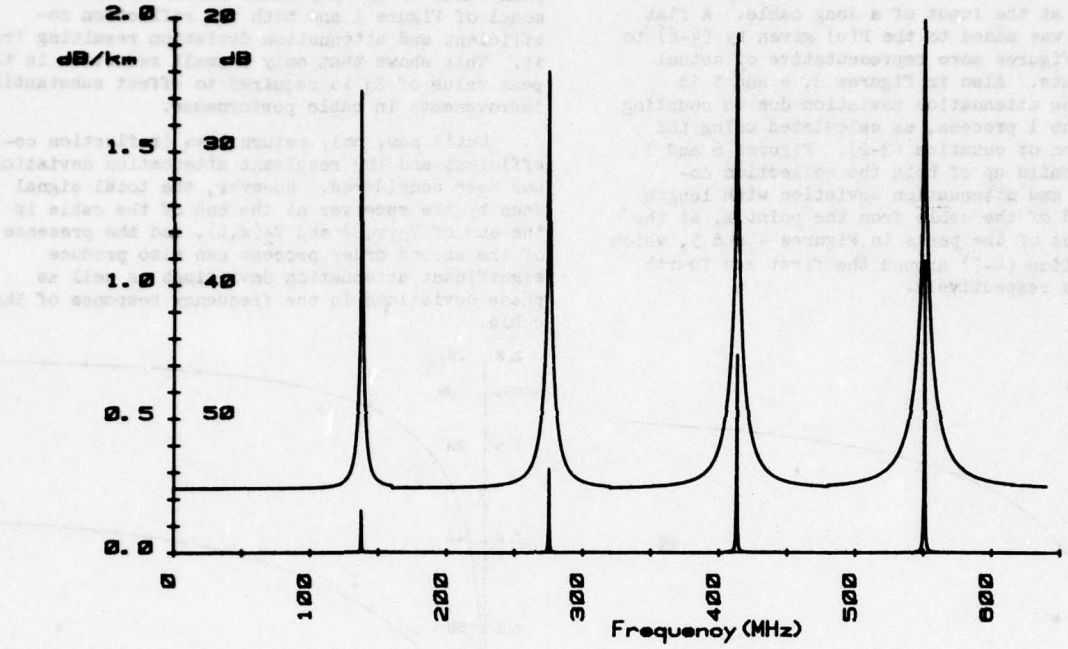
$$P(\nu) = \sum_{k=-\infty}^{\infty} A_k\, \delta(\nu - k\nu_o) \tag{4-6}$$

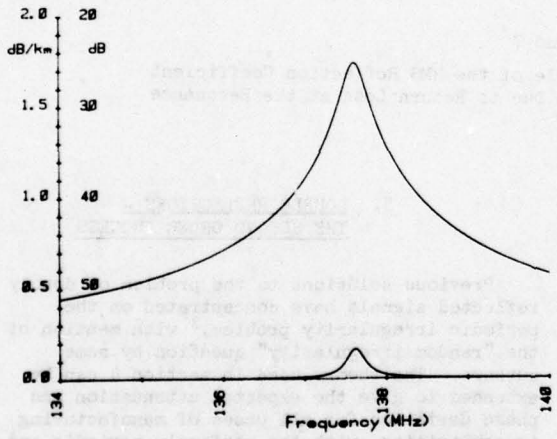
and $\sqrt{E\left[|\rho(L,x)|^2\right]}$

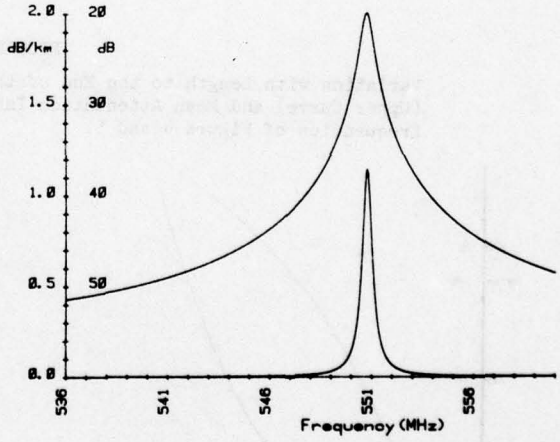
$$= \sqrt{\sum_{k=-\infty}^{\infty} \frac{A_k}{4(\alpha^2+(\pi k\nu_o+\beta_o)^2)}} \cdot \cos\left|2(\pi k\nu_o+\beta_o)(L-x)\right| + \exp(-4\alpha(L-x)) \tag{4-7}$$

which shows that as f is varied, then large peaks in reflection coefficient will occur where $\beta_o = \pi\nu_o, 2\pi\nu_o, 3\pi\nu_o \ldots\ldots$

Equation (4-7) is shown plotted against frequency, f, in Figures 3, 4 and 5 for the model of $Z_0(x)$ shown in Figure 1, for $Z_d=0.3\Omega$, S=10Ω/metre and



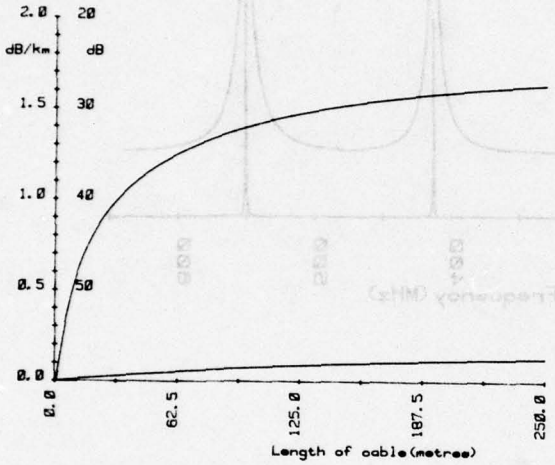


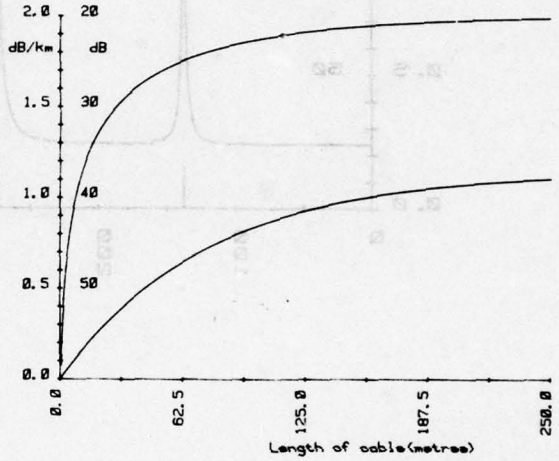


FIGURES 3, 4 and 5

RMS Reflection Coefficient at the Input of a Long Cable (Upper Curve) and Mean Attenuation Increase due to Return Loss. The total attenuation increase is double that shown.

ν_o = 0.956 cycle/metre and with (L-x) set to a very large value to simulate the reflection coefficient at the input of a long cable. A flat component was added to the P(ν) given by (4-6) to make the figures more representative of actual measurements. Also in Figures 3, 4 and 5 is plotted the attenuation deviation due to coupling to the line 1 process, as calculated using the expectation of equation (3-2). Figures 6 and 7 show the build up of both the reflection coefficient and attenuation deviation with length to the end of the cable from the point x, at the frequencies of the peaks in Figures 4 and 5, which show equation (4-7) around the first and fourth resonances respectively.





FIGURES 6 and 7

Variation with Length to the End of the Cable of the RMS Reflection Coefficient (Upper Curve) and Mean Attenuation Increase Due to Return Loss at the Resonance Frequencies of Figure 4 and 5.

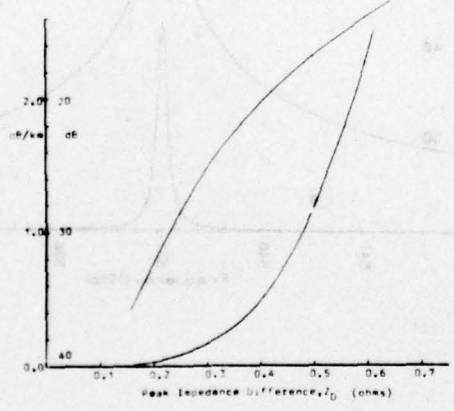


FIGURE 8

RMS Reflection Coefficient (Upper Curve) and Mean Attenuation Increase due to Return Loss Versus the Peak Impedance Deviation in the Model of Figure 1.

Figure 8 shows the relationship between the peak value of the impedance difference for the model of Figure 1 and both the reflection coefficient and attenuation deviation resulting from it. This shows that only a small reduction in the peak value of Z_d is required to effect substantial improvements in cable performance.

Until now, only return loss (reflection coefficient and the resultant attenuation deviation) has been considered. However, the total signal seen by the receiver at the end of the cable is the sum of $V_0(x,L)$ and $V_2(x,L)$, and the presence of the second order process can also produce significant attenuation deviations as well as phase deviations in the frequency response of the cable.

5. DOUBLE REFLECTIONS - THE SECOND ORDER PROCESS

Previous solutions to the problem of doubly reflected signals have concentrated on the periodic irregularity problem,[3] with mention of the "random irregularity" question by some authors. The theory used in section 4 can be extended to give the expected attenuation and phase deviation for all cases of manufacturing irregularities, with the perfectly periodic and random cases being two extremes.

5.1 The Line 2 Reflection Coefficient

At any point x on a cable of length L, the line 2 signal, $V_2(x,L)$, is a summation of all double reflections, where the second reflection point is between the origin and x and the first reflection point is between the second and the end of the cable, L.

Defining $\rho_2(x,L) = \frac{V_2(x,L)}{V_0(x,L)}$ (5-1)

$$\rho_2(x,L) = -\int_{\eta=0}^{x}\int_{\xi=\eta}^{L} r(\eta)d\eta r(\xi)d\xi \exp(-2\alpha(\xi-\eta) - 2j\beta_o(\xi-\eta)) \quad (5-2)$$

where the attenuation on all three lines is approximated by $\alpha = \alpha_o + E[\Delta\alpha_1\ (L,0)]$. (5-3)

Again, using standard techniques and substituting in the power density spectrum of the r(x) process, P(ν)

$$E[\rho_2(x,L)] = -\int_{\nu=-\infty}^{\infty} \frac{P(\nu)d\nu}{2(\alpha-j\beta)}\left(x - \frac{\exp(-2\alpha(L-x)+2j\beta(L-x))}{2(\alpha-j\beta)} + \frac{\exp(-2\alpha L+2j\beta L)}{2(\alpha-j\beta)}\right) \quad (5-4)$$

where $\beta = (\pi\nu-\beta_o)$

For the case of a long cable, the second order process at the end of the cable is

$$E[\rho_2(L,L)] \cong -L\int_{\nu=-\infty}^{\infty} \frac{P(\nu)d\nu}{2(\alpha-j\beta)} \quad (5-5)$$

5.2 Attenuation and Phase Deviations

The total signal received at L is

$$E[V(L)] = V_0(L,L)(1 + E[\rho_2(L,L)])$$

$$= V_0(0)\exp(-\alpha-j\beta_o)L\left(\exp\left(-\alpha L\int_{\nu=-\infty}^{\infty}\frac{P(\nu)d\nu}{2(\alpha^2+\beta^2)}\right)\right.$$

$$\left. - jL\int_{\nu=-\infty}^{\infty}\frac{\beta P(\nu)d\nu}{2(\alpha^2+\beta^2)}\right) \quad (5-6)$$

which indicates that there is an attenuation increase

$$E[\Delta\alpha_s] = \alpha\int_{\nu=-\infty}^{\infty}\frac{P(\nu)d\nu}{2(\alpha^2+\beta^2)} \quad (5-7)$$

and a phase change coefficient deviation of

$$E[\Delta\beta_s] = \int_{\nu=-\infty}^{\infty}\frac{\beta P(\nu)d\nu}{2(\alpha^2+\beta^2)} \quad (5-8)$$

However, equation (4-4) indicates that for a long length of cable,

$$E[|\rho(L,0)|^2] = \int_{\lambda=-\infty}^{\infty}\frac{P(\lambda)d\lambda}{4(\alpha^2+\beta^2)} \quad (5-9)$$

where $\lambda = -\nu$ of equation 4-4.

Thus the total attenuation deviation due to both power coupling from line 0 to line 1 and the second order process is

$$E|\Delta\alpha| = E[\Delta\alpha_1] + E[\Delta\alpha_s] \quad (5-10)$$

$$= \frac{2\alpha_o\ E[|\rho|^2]}{1-2\ E[|\rho|^2]} + 2\alpha\ E[|\rho|^2] \quad (5-11)$$

where subscripts have been omitted as all quantities are invariant with length (except for the small lengths near the ends of the cable). Equation (5-11) can be simplified to :

$$E|\Delta\alpha| \cong 4\alpha\ E[|\rho|^2] \quad (5-12)$$

so that doubling the attenuation deviation values in Figures 3, 4, 5, 6, 7 and 8 yields the total attenuation deviation due to both causes. The deviation in phase change coefficient can be evaluated using equation (5-8) and the appropriate power density spectrum. For the perfectly periodic case,

$$E[\Delta\beta_s] = \sum_{k=-\infty}^{\infty}\frac{A_k\ (\pi\ \nu_o\ \beta_o)}{2(\alpha^2+(\pi k\nu_o-\beta_o)^2)} \quad (5-13)$$

which is zero at the "resonance frequencies" where $E|\Delta\alpha|$ is at a peak. However $E[\Delta\beta_s]$ has a peak on either side of the resonance.

6. MEASUREMENT REQUIREMENTS

The significance of equation (5-12) is that the attenuation deviation due to manufacturing irregularities is given in terms of a cable property which is readily estimated from measurements. It is standard practice in coaxial cable production to measure the magnitude of the reflection coefficient on at least a sampled basis. If these measured values are $|\rho_i|$ for i = 1, 2, 3..., then the estimate of $E[|\rho|^2]$ (the subscripts are omitted as the cable length is assumed long so that $E||\rho|^2|$ is independent of x) is given by:

$$\hat{E}[|\rho|^2] = \sum_{i=1}^{n} \frac{|\rho_i|^2}{n} \qquad (6\text{-}1)$$

Figures 6 and 7 indicate the length of cable required for measurement to ensure that the assumption of independence of $E||\rho|^2|$ with length is valid - alternatively the correction factor for measurements on short lengths is indicated in the Figures.

Figures 3 and 8, together with equation (5-12 indicate that the calculated attenuation deviation is very sensitive to errors in measurement of $|\rho_i|$. In particular, if the measured value is artificially increased by poor connectors etc. then an unduly pessimistic estimate of cable performance is obtained. To obviate this possibility, Telecom Australia developed the carrier burst technique for use in its measurements. This method has the additional advantage that a short length of cable near the sending end, which may be a typical of the body of the cable, may also be omitted.

7. THE ALMOST PERIODIC PROCESS

The equations in Sections 4 and 5 were derived for a general power density spectrum, P(ν), and then evaluated for the special case where the r(x) process was perfectly periodic. Comparing Figure 3 to typical measurement results indicates that there is variation between cables which is not accounted for in the perfectly periodic model. The "almost-periodic" model described in Section 2 was tested by simulation techniques to determine if the amplitude and phase jitter on an otherwise periodic process could account for the observed variation between cables. The results indicated that phase jitter alone could not account for the variation, although amplitude jitter could. Calculation of P(ν) for the jittered process indicated that the resultant P(ν) has peaks which are still much narrower than the filter function described in Section 4 - as a result the values in Figures 3, 4, 5, 6, 7 and 8 are valid for this "almost-periodic" process as well as for the perfectly periodic process. Equation (4-1) indicates that because of attenuation the measured reflection coefficient is determined by an effective length which is quite small in comparison to the length which determines attenuation deviation. This means that the variance of attenuation deviation over a regenerator or repeater length is much less than the variance of $|\rho|$ which is observed in factory measurements. As a consequence, the variance of $\Delta\alpha$ and $\Delta\beta_s$ was considered negligible and has not been calculated.

8. APPLICATION TO MULTIPAIR CABLE

The theory developed in the previous sections, which related coaxial line irregularities to transmission deviations, is directly applicable to multipair cable, particularly with the increasing use of this type of cable at high frequencies for digital transmission. However, the main limitation which a cable imposes on the regenerator span is due to its crosstalk performance and the concept of the coupling of signal from one line to another via a coupling function which is dependent on physical and geometrical properties only is of great utility in relating the resultant electrical performance with the physical structure of the cable. This will be illustrated by applying the theory to the case of far end crosstalk ratio between two pairs due to propagation on a third circuit, the "earth" surrounding the two pairs in question.

8.1 Balanced and longitudinal transmission

Judy and Refi[4] have studied the problem of transmission on a pair with a nearby earth composed of a screen, sheath or other cable pairs. Assuming all parameters are invariant with length, the wire-earth voltage for each wire of the pair is a summation of two travelling waves with differing propagation coefficients. The difference of these voltages is the transverse or balanced transmission voltage, while the sum is the longitudinal voltage, wherein there is current flow in the earth circuit. If the pair is perfectly balanced to earth, the balanced voltage contains only one propagation coefficient, γ_b, while the longitudinal contains the other, γ_ℓ. Further, if balanced excitation is used, the longitudinal component is zero. However, if the pair has any unbalance to earth, for balanced excitation, the balanced signal contains both propagation coefficients while a longitudinal signal (with both propagation coefficients) also propagates. The presence of the two components in the balanced signal, one with γ_b, the other with γ_ℓ, creates a "beat" in the insertion loss and phase versus frequency of the pair which appears as a damped ripple, with an insertion loss peak occuring first. The frequency at which this peak occurs is inversely proportional to the length of the line and the difference in propagation time per unit length for pure balanced and pure longitudinal transmission. In dealing with crosstalk arising from the longitudinal signal, Judy and Refi drop their analytic model in favour of a heuristic model. However, the analytic model can be extended to cover this case by using the coupled line concepts introduced earlier.

For a pair with unbalance to earth represented by two constants K_b' and K_ℓ', excited in the balanced mode at $\eta=0$ by equal and opposite current generators to earth from each wire, the longitudinal current can be shown (by an extension of the theory of Ref[4]) to be :

$$I_L(\eta) = \frac{K_b'(2+K_\ell')}{2 - K_b' + K_\ell'} (1 - e^{-\Delta\gamma\eta}) e^{-\gamma b\eta}$$

where $\Delta\gamma = \gamma_\ell - \gamma_b$ (8-1)

If η is very small,

$$I_L(\eta) = \frac{K_b'(2 + K_\ell')}{2 - K_b' + K_\ell'} (\Delta\gamma\eta) e^{-\gamma_b\eta} \quad (8-2)$$

As far end crosstalk ratio is being considered, the $e^{-\gamma b\eta}$ term is transparent and will be omitted from here on. As equation (8-2) is now proportional to η, if propagation in the balanced mode is considered affected only to the extent of a change in the effective γ_b (c.f. the coaxial case), then the longitudinal current at any point x can be written as

$$I_L(x) = \int_{\eta=0}^{x} \frac{K_b'(2+K_\ell')}{2-K_b'+K_\ell'} \Delta\gamma \; e^{-\Delta\gamma(x-\eta)} d\eta \quad (8-3)$$

where in (8-3) η has been replaced by $d\eta$ thereby making the approximation in equation (8-2) valid. The inclusion of the phasing term in (8-3) results in it being valid for all lengths x. Furthermore, there is now no restriction that the line parameters be invariant with η. Consequently, the unbalance constants can be replaced by a "coupling density" function in a similar manner to the way in which a reflection density function was proposed for the coaxial cable case.

Therefore

$$I_L(x) = \int_{\eta=0}^{x} \Delta\gamma \; K_{TL}(\eta) e^{-\Delta\gamma(x-\eta)} d\eta \quad (8-4)$$

where $K_{TL}(\eta)$ is the coupling density function from transverse to longitudinal propagation. Dimensional changes in the line strongly affect K_b' and K_ℓ' and hence $K_{TL}(\eta)$; however, the effect on γ_b and γ_ℓ is small, and consequently they will be considered invarient with length. Furthermore, $K_{TL}(\eta)$ is very close to being real and independent of frequency, ω.

8.2 Third Circuit Crosstalk

Consider now a second pair in the cable which shares the same earth as the above, or disturbing pair. The longitudinal current produced by the disturbing pair appears as a longitudinal current in the wire-wire-earth circuit of the disturbed pair. Whereas for the disturbing pair in a length $d\eta$, an increment $\Delta\gamma K_{TL}(\eta)d\eta$ was added to the longitudinal current, in a length $d\xi$ an increment of ratio $\Delta\gamma K_{LT}(\xi)d\xi$ is coupled from the longitudinal current to form a balanced current increment in the disturbed pair. In the same manner as for the disturbing pair, a perfectly balanced disturbed pair will have no coupling from a longitudinal current to a balanced current. Consequently, the far end crosstalk ratio after a length L due to third circuit propagation is

$$FEXTR3 = \Delta\gamma^2 \int_{\eta=0}^{L} \int_{\xi=\eta}^{L} K_{TL}(\eta) K_{LT}(\xi) e^{-\Delta\gamma(\xi-\eta)} d\xi d\eta \quad (8-5)$$

where there are no functional restrictions on $K_{LT}(\eta)$ or $K_{TL}(\xi)$.

It is informative to evaluate (8-5) for two special cases, namely, constant coupling with length and purely random coupling, in order to determine the degradation of this third circuit crosstalk with both frequency and length. Oakley and Jaar[5] have previously presented such results for direct pair-to-pair crosstalk.

8.3 Constant Coupling with Length

Let $K_{TL}(\eta) = K_1$ for all η,

$K_{LT}(\xi) = K_2$ for all ξ (8-6)

then, $FEXTR3 = \Delta\gamma^2 K_1 K_2 \int_{\eta=0}^{L} \int_{\xi=\eta}^{L} e^{-\Delta\gamma(\xi-\eta)} d\xi d\eta$

$$= \Delta\gamma K_1 K_2 L + K_1 K_2 (e^{-\Delta\gamma L} - 1)$$

$$= \Delta\gamma K_1 K_2 L \qquad \text{for long lengths L}$$

$$= (\ell_1 \sqrt{\omega} + j\ell_2 \omega) K_1 K_2 L \quad (8-7)$$

where ℓ_1 and ℓ_2 are constants. (8-7) shows that FEXTR deteriorates at the rate of 20 dB/decade with length, 10 dB/decade with frequency for the in phase component and 20 dB/decade with frequency for the quadrature component.

8.4 Random Coupling with Length

For the case of random coupling with length, $K_{TL}(\eta)$ and $K_{LT}(\xi)$ become sample functions from two random processes. However, for the purpose of calculating the degradation of crosstalk with length and frequency, no loss of generality is sufferred by assuming them to be sample functions

of the one process. Taking the ensemble average,

$$E|FEXTR3| = \Delta\gamma^2 \int_{\eta=0}^{L} \int_{\xi=\eta}^{L} E|K_{TL}(\eta)K_{LT}(\xi)|e^{-\Delta\gamma(\xi-\eta)} d\xi d\eta$$

$$= \Delta\gamma^2 \int_{\eta=0}^{L} \int_{\chi=0}^{L-\eta} \int_{\nu=-\infty}^{\infty} P_{KK}(\nu)e^{j2\nu\chi} d\nu \; e^{-\Delta\gamma\chi} d\chi d\eta \qquad (8\text{-}8)$$

where $P_{KK(\nu)}$ is the power density spectrum of the coupling process, $K_{TL(\eta)}$. (8-8) is valid for any power density spectrum. One spectrum often assumed is a flat power spectrum, corresponding to no correlation between couplings. This is given by :

$$P_{KK}(\nu) = K^2 \text{ for all } \nu$$

$$\therefore \text{FEXTR3} = \frac{K^2}{2} (\ell_1^2 \omega - \ell_2^2\omega^2 + 2j\ell_1\sqrt{\omega}\ell_2)L \qquad (8\text{-}9)$$

Once again the crosstalk is degraded 20 dB/decade with length while the in phase component degrades at 40 dB/decade with frequency at high frequencies ($\ell_2^2\omega^2 >> \ell_1^2\omega$), with the quadrature component degrading at 30 dB/decade with frequency. At high frequencies this results in an effective crosstalk degradation of 40 dB/decade with frequency which agrees with results measured by Judy and Refi by their heuristic model assuming constant coupling. This result would suggest that the random coupling is a more valid model, and is the one normally assumed with direct pair-pair crosstalk. However, whereas with direct pair-pair crosstalk the assumption of random coupling gives a degradation of 10 dB/decade with length as compared with 20 dB/decade with length for constant coupling, the third circuit crosstalk deteriorates at 20 dB/decade with length irrespective of the nature of the coupling. It is believed that this result is supported by the mean value achieved by Judy and Refi of 5.3 dB/octave (19.3 dB/decade), with the spread they observed being due to two factors:

(a) the statistics of the random process

(b) the influence of direct pair-pair crosstalk summing with third circuit crosstalk.

9. CONCLUSION

In this paper, a complete theory of transmission distortion on an irregular coaxial cable has been presented. The theory is valid for any form of irregularity process as the description is in terms of its power density spectrum. Attenuation deviation is directly related to reflection coefficient, while the latter is related to the size of the impedance deviations in a proposed model of the irregular cable. The question of cable measurement is also considered in order that cable performance can be accurately predicted.

The theoretical concepts introduced for the coaxial cable case are valid for the study of transmission distortion on a wider range of cables. This is illustrated by considering the case of third circuit crosstalk in symmetric pair cable. The dependence of this form of crosstalk on the length of the cable, the frequency being considered and on the form of the power density spectrum of the coupling process has important implications for manufacture.

10. ACKNOWLEDGEMENT

The permission of the Chief General Manager, Australian Telecommunications Commission, to publish this paper is gratefully acknowledged.

11. REFERENCES

1. J.R. Osterfield, S. Longoni and A. Manilii, "Structural Return Loss Associated with 2.6/9.5 Coaxial Cable for 60 MHz Analogue Systems and Higher Capacity Future Digital Systems", 23rd International Wire and Cable Symposium, 1974.

2. A.E. Karbowiak, "An Investigation of Signal Distortion in Cables Caused by Imperfections in Cable Manufacture", Proc IEE, Vol. 121, No.6, pps 419-431.

3. S.E. McConkey, "Attenuation Irregularities in Coaxial Cables Containing Cyclic Impedance Discontinuities", 22nd International Wire and Cable Symposium, 1973.

4. A.F. Judy and J.J. Refi, "Effect of Pair Unbalance on Carrier Frequency Insertion Loss and Crosstalk in Multipair Cable", 25th International Wire and Cable Symposium, 1976.

5. R.J. Oakley and R. Jaar, "A Study into Paired Cable Crosstalk", 22nd International Wire and Cable Symposium, 1973.

APPENDIX 1

This appendix outlines the derivation of equation (3-2) which gives the increase in attenuation on line 0 at x for a cable of length L, due to coupling to line 1.

Equation (3-2) is simply an expression of conservation of energy in a length dx situated at x. For line 0 the input power at x is P_1, while the output power at (x+dx) is P_2. Line 0 loses power P_3 due to normal attenuation. The power coupled from line 0 to line 1 is P_7. Conservation of power for line 0 requires :

$$P_1 = P_2 + P_3 + P_7$$

For line 1, the power entering dx at (x + dx) is P_4, while the power leaving dx at x is P_5. Normal attenuation on line 1 causes a loss of P_6 while coupling from line 1 to line 2 causes a loss of P_8. Consequently energy conservation requires for line 1 that :

$$P_4 + P_7 = P_5 + P_6 + P_8.$$

P_1, P_2 and P_3 are evaluated from propagation on the uniform line 0; P_4, P_5, P_6 and P_8 are related to line 0 powers by the reflection coefficient $\rho(L,x)$. Consequently,

$$P_7 = P_1 - P_2 - P_3 = P_5 - P_4 + P_6 + P_8$$

which leads to equation (3-2).



Laurence J. Hall
Telecom Australia
Lines Construction
Branch
199 William St.
MELBOURNE 3000
Australia

Laurence J. Hall was born in Sydney, Australia on 17 October, 1952. He joined Telecom Australia in 1971 as a Cadet Engineer, graduating with a B.E. in Electrical Engineering from the University of New South Wales in 1974. From 1974 through 1977, he did postgraduate work at the University of New South Wales in the field of cable propagation. In late 1977 he was appointed to the position of Engineer Class 3, Bearer Characterisation and Measurement, Cable Design and Specifications Section, Telecom Australia, Headquarters.

Numerical Analyses of Viscous Flow in a Wire Coating Die

K. Fuse K. Orimo and K. Shibata

The Furukawa Electric Co., Ltd. Tokyo, Japan

Summary

To make an ultra-high speed wire coating process with stabilized operations, the following technical problems on a cross-head die are discussed.
One is the development of a cross-head die, which is least liable to melt instabilities such as a melt fracture and minimize the back tension exerted on the running wire and another is a self-centering die which needs no centering process between a bare wire and an insulation material. In order to design and develop the above equipments, the relative equations to estimate the melt properties of polymers and the die geometries must be established. However, no significant useful attempts have been made to calculate such relations. In view of the above, numerical analyses of viscous flow in a wire coating die are presented with parameters which are estimated easily on the actual manufacturing processes. The velocity, the pressure distributions and the tension on wire along die are evaluated with varying combinations of the die geometry and the running speed of the wire. Calculated results indicate that the stabilizing flow behaviors in the die land and the lowering of the reduction ratio are essential to realize the high speed coating. As an example of application of the flow analyses, one of the Furukawa's self-centering die, which was developed in consideration of the hydrodynamic forces on the wire and flow properties, is presented.

1. Introduction.

Recent improvement for the speed in wire coating process is remarkable and it is reported that 3000 m/min. is accomplished in the laboratory[1]. The increase, however, in the extrusion speed has raised several important problems: 1) to prevent from melt fracture phenomenon occuring on the surface of an extruded wire, 2) to prevent from the reduction in conductor diameter caused by the increase of back tension working on a running wire in a cross head die, 3) to develop and design a fixed die[2], which requires no centering operations between a wire and an insulation material. In order to solve these problems, it is important to make clear the relation between melt flow properties and die duct geometries and to develop a new cross head die suitable for such a high speed insulation. However, we have not seen any successful report on practically usefull equations to evaluate and review the melt flow properties in insulation die, with existence where a substance like wire is running. So, most of dies and nipples used in manufacturing plants are produced away from optimum design.

This report describes: i) Exploration of die duct geometries suitable for high speed insulation. ii) Introduction of relative equations on flow properties inside of die head by utilizing the practical parameters which enables us to evaluate on manufacturing field, as a first step to make clear the relation ship between processing and melt flow at wire coating process. iii) Simulation using practical die geometry. Alos, we discuss fixed die which was developed as the actual application of these analyses.

2. Analysis.

2.1 Background[3],~[7],

It is very difficult to get exact solution which indicates the flow behaviors in a wire-coating die. One reason is that a flow pattern in a die is one of non-Newtonian fluid in a conical tube, for which complete analytical function has not yet been obtained. Another reason is the existence of running wire in the die that makes analysis much more difficult. Therefore, as far as the authors know no papers for the exact solution regarding these problems have not yet been published. Some trials to get approximate solution are reported, but they are not convenient and practical to be used in manufacturing fields by engineers. In introducing, the relative equation for the analysis of flow in a cross head die, we consider two important factors. First is the capability of evaluation at manufacturing fields. Second is the conveni-

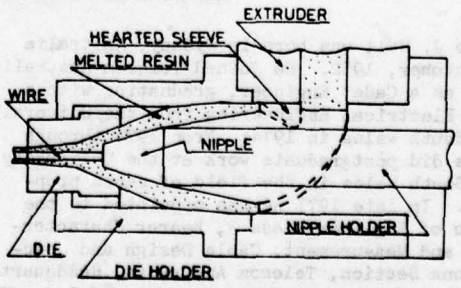


Fig. 1 Schematic representation of wire coating crosshead and die.

ence and practicability of expression. We made analysis on the models and assumptions that will be stated hereinafter.

2.2 Assumptions

(1) In order to analyze the flow in a coss head die during wire coating process, die tube was divided into two parts, as shown in Fig. 1, according to the difference in the driving forces which make the flow to run.

(i) Path enclosed by a die and a nipple. (Flow is assumed to be pressured flow.)

(ii) Path enclosed by a die and a wire. (Composite flow of pressured flow and drag flow.)

As these two tubes are actually a continuous tube, it is considered that moving liquid within these tubes are influencing each other. Here, to make analysis easier, we assume that each flow goes through die tubes which are independent of each other.

(2) When we make a model of flow, we neglect the non-steady flow which is induced by the 90 degree change in the flow angle which comes from extruder to the cross head. We consider the flow to be homogeneous and uniform.

(3) Flow in the path enclosed by a die and a nipple is actually the flow within non-parallel but concentrically tapered tubes. However, as shown in Fig. 2, at minute sections which are equally divided in the direction of flow, the influence of the difference in the angle between taper ange γ of die and taper angle β of nipple and the difference between ζ and β, to the flow is negligibly small. The ratio of the gap Hc between the die and the nipple to the radius of curveture, Hc/rc, is about 0.2. So the influence of side wall of the duct to the flow can be neglected. On these premises, we assume the flow to be the one between two parallel planes.

(4) The flow in the path enclosed between the die and the wire is assumed to be the flow through the area enclosed by the following two planes. One plane is a tilted plane with angle α from the flow direction. Another plane is a parallel plane to the flow direction and is moving at the speed V_0. As is the same with previous flow, within minute sections devided along the direction of flow, the influence of die wall angle α to the flow is small. Hc/rc ration is 0.2 to 0.5. Hence we can assume the flow to be the one between the two paralled planes similarly above mentioned.

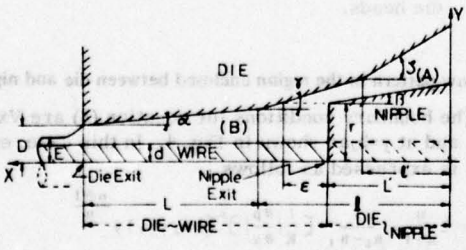


Fig. 2 Cross section of wire coating die, consisting of two convergent channels; (A) clearance between die and nipple, and (B) clearance between die and wire. Die consists of three tapered parts, having angles of 2α, 2γ and 2ζ each. Taper angle of nipple is 2β. ε indicates gam space. d, D and E are radii of wire, die exit, and coated core, respecitively.

(5) The flow is nonelastic, non-Newtonian liquid which composed isothermal, incompressible and steady flow.

(6) Body forces such as gravity are neglected.

(7) Slip in the flow on a duct wall and on a wire is neglected.

(8) Centers of the die, nipple and wire are on the same line. As was stated, flow is axially symmetric.

2.3 Motion equations

Based on the aforesaid assumptions, the die tube of Fig. 2 is considered to be the path between the two parallel planes as shown in Fig. 3. We introduce the x-y-z cartesian coordinates. (It is general to take x axis parallel to the nipple wall for the flow between the die and the nipple. But in this analysis, x axis is on the wire as is the same as the case of the area between the die and the wire. By doing this, it becomes possible to evaluate relative relationship between inlet of the path between the die and the wire and the exit of the path between the die and the nipple.) In this case, minute sections divided equally in the direction of flow are regarded as those between two parallel planes. Velocity components in the direction of y,z coordinate, which is perpendicular to flow, are quite small compared to the velocity component in the direction of x. If the velocity component of the flow direction is independent to z coordinate, speed V is expreseed as follows.

$$V_x = V(x, y), V_y = V_z = 0 \tag{1}$$

X component of the well-known motion equation and the continuous equation are represented as follows.

$$\rho\left(\frac{DV_x}{Dt}\right) = -\left(\frac{\partial p}{\partial x}\right) + \left(\frac{\partial \tau_{xx}}{\partial x} + \frac{\partial \tau_{yx}}{\partial y} + \frac{\partial \tau_{zx}}{\partial z}\right) + \rho g_x \tag{2}$$

$$\frac{D\rho}{Dt} + \rho\left(\frac{\partial V_x}{\partial x} + \frac{\partial V_y}{\partial y} + \frac{\partial V_z}{\partial z}\right) = 0 \tag{3}$$

Here, ρ is density, D/Dt is substantial derivative, $\partial p/\partial x$ is pressure gradient of the flow direction, τ_{xx}, τ_{yx}, τ_{zx} are stress components and g_x is x component of body force. From the previous assumptions,

$$\frac{DV_x}{Dt} = 0, \quad \frac{D\rho}{Dt} = 0, \quad g_x = 0, \quad \rho = 0$$

From equations (1) and (3)

$$\frac{\partial \tau_{xx}}{\partial x} = 0, \quad \frac{\partial \tau_{zx}}{\partial z} = 0$$

If the fluid is presumed to be "power law fluid", following relationship is satisfied.

$$\tau_{xy} = -K \cdot \left|\frac{\partial Vx}{\partial y}\right|^{n-1} \cdot \left(\frac{\partial Vx}{\partial y}\right) \quad (4)$$

(Where, k and n are physical parameters of non-Newtonian fluid).

Then, motion equation (2) will become as this,

$$-\left(\frac{\partial p}{\partial x}\right) + \frac{\partial}{\partial y}\left[K\left|\frac{\partial Vx}{\partial y}\right|^{n-1} \cdot \left(\frac{\partial Vx}{\partial y}\right)\right] = 0 \quad (5)$$

Notice should be made to the sign of $\partial p/\partial x$. As is clear from equation (5), the sign of $\partial p/\partial x$ is obtained by derivation of shear rate by y. So it is expressed in absolute value for convenience.

In solving equation (5), pressure gradient $\partial p/\partial x$ is assumed not to be related to y-coordinate.

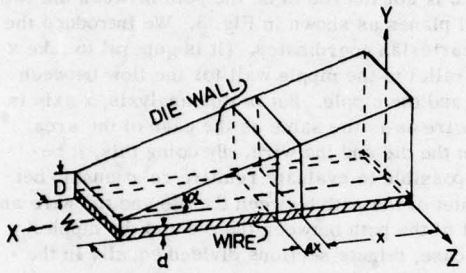


Fig. 3 Idealized slit channel. Within a narrow section of width Δx, the die wall and the wire surface are both assumed to be flat and paralled with each other. Coordinate X is in the running direction of wire.

On that condition, the following equation is derived by integrating the equation by y using integration formulae of a rational function.

$$Vx = \pm \frac{n}{n+1}\left(\frac{1}{K}\right)^{\frac{1}{n}} \frac{\left[\left|\frac{\partial p}{\partial x}\right| y + C_1\right]^{\frac{n+1}{n}}}{\left|\frac{\partial p}{\partial x}\right|} + C_2 \quad (6)$$

Where, $\partial p/\partial x \neq 0$, C_1 and C_2 are integral constants. In general, integral constants C_1 and C_2 can be decided in equation (6). But because of several reasons, it is difficult to decide the integral constants C_1 and C_2 from boundary conditions for the die tube in question. For example, within the die tube enclosed between the die and the nipple, the equation to deside integral constants becomes infinitive and the integral constants cannot be decided. (e.g., the equation which satisfies $Vx = 0$ at $y = h_1, h_2$.) In case of tube between the die and the wire, it is in principle possible to obtain C_1 and C_2 in the equation when $Vx = 0$ at $y = h$ and $Vx = Vo$ at $y = d$ by utilizing computer aided successive approximation method such as the Newtonian method or by using approximation with power series expansion method such as the Taylar series expansion. However, mathematical complications like convergence for the solution or uniformity will accompany to considered to be practical. Here, we propose an approximate method to derive Vx from equation (5).

Although this method is not mathmatically exact, it is useful within the engineering tolerance.

In equation (5), it is considered that shear rate $\frac{\partial vx}{\partial y}$ is decided almost by n-th root of $\frac{1}{k}\frac{\partial p}{\partial x}y$. In order to weaken the influence of this assumption on Vx, the following function C_1 is used.

$$\frac{\partial Vx}{\partial y} = \pm\left(\frac{1}{K}\left|\frac{\partial p}{\partial x}\right| y\right)^{\frac{1}{n}} + C_1 \quad (7)$$

The sign at the right hand side is + when $\frac{\partial vx}{\partial y} > 0$ or − when $\frac{\partial vx}{\partial y} < 0$. In this equation (7), c_1 is actually the variable function consisted with x, y and z. In order to make the following analysis easier, c_1 is assumed to be the function consisted with only x and constants and does not include y. Then we can get the following relative equation by integrating both sides of the equation by y,

$$Vx = \pm \frac{n}{n+1}\left(\frac{1}{K}\left|\frac{\partial p}{\partial x}\right|\right)^{\frac{1}{n}} y^{\frac{n+1}{n}} + C_1 y + C_2 \quad (8)$$

Here, c_2 is an integral constant.

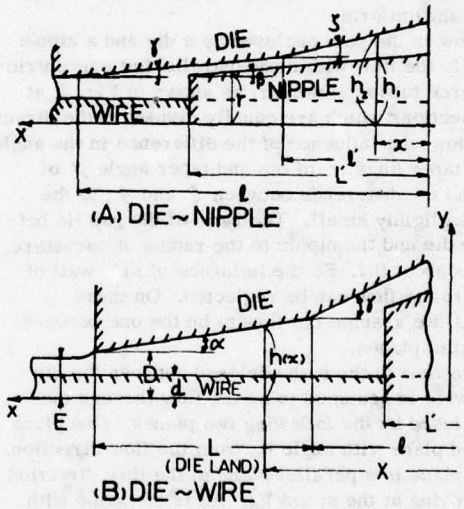


Fig. 4 Geometry of convergent narrow channel of die heads.

2.4 Flow pattern in the region enclosed between die and nipple

The boundary conditions for equation (8) are Vx=0 at $y=h_1$ and at $y=h_2$ as shown in Fig. 4. In this case, equation (8) is expressed as follows.

$$Vx = \pm \frac{n}{n+1} \cdot \frac{1}{h_2 - h_1} \cdot \left[\frac{1}{K}\left|\frac{\partial p}{\partial x}\right|\right]^{\frac{1}{n}} \left[(h_2 - h_1) y^{\frac{n+1}{n}} + \left(h_1^{\frac{n+1}{n}} - h_2^{\frac{n+1}{n}}\right) y - h_1 h_2 \left(h_1^{\frac{1}{n}} - h_2^{\frac{1}{n}}\right)\right] \quad (9)$$

Where h_1 and h_2 satisfy following geometrical relationships.

(i) $0 \leq x \leq \ell'$

$$\begin{cases} h_1 = r + (L' - x)\tan\beta & (10) \\ h_2 = D + L\tan\alpha + (\ell - \ell')\tan\gamma + (\ell' - x)\tan\varphi & (11) \end{cases}$$

(ii) $\ell' < x \leq L'$

$$\begin{cases} h_1 = r + (L' - x)\tan\beta & (12) \\ h_2 = D + L\tan\alpha + (\ell - x)\tan\gamma & (13) \end{cases}$$

L' is the value which does not have practical meaning. So it is to be represented by ε which expresses the distance between the die and the nipple and is of practical importance. In that case, L' is given by the next equation.

$$L' = \ell - \varepsilon - \frac{r - (D + L\tan\alpha)}{\tan\gamma} \quad (14)$$

In equation (9), pressure gradient ($\frac{\partial p}{\partial x}$) in the die is difficult to measure. We should convert this parameter to another one with easely of measurement. In case of the model flow path, shown in Fig. 3, volume per unit width, Q/Wi, at arbitrary position is

$$\frac{Q}{Wi} = \int_{h_1}^{h_2} Vx\, dy \quad (15)$$

In case of an actual tube, flow path width varies with x. In equation (16), the definition of corrected coefficient of flow path width Co is introduced, that means the correction of flow path at slit duct used as model to the actual tubular duct.

$$\frac{Q}{W} = \frac{1}{Co}\int_{h_1}^{h_2} Vx\, dy \quad (16)$$

As it is clear from Fig. 2, Q/W can be expressed by the insulator extruded from the die as eq. (17), defining insulation radius, bare wire radius and wire speed as E, d and Vo respectively.

$$\frac{Q}{W} = (\rho/\rho_m)(E - d)Vo \quad (17)$$

Here, ρ_m is the melt polymer density at temperature T°C. ρ_m is given by the equation derived from experiments.

$$\rho_m = \{1.2566 + 0.936(T - 120)\times 10^{-3}\}^{-1} \quad (18)$$

From equation (9), (16) and (17),

$$\frac{n}{n+1}\left(\frac{1}{K}\left|\frac{dp}{dx}\right|\right)^{\frac{1}{n}} = \frac{2(2n+1)C_o(\rho/\rho_m)(E-d)Vo}{(h_2-h_1)\{(h_1-h_2)(h_1^{\frac{n+1}{n}} + h_2^{\frac{n+1}{n}}) - 2nh_1h_2(h_1^{\frac{1}{n}} - h_2^{\frac{1}{n}})\}} \quad (19)$$

From equation (9), and (19), Vx is given.

$$Vx = -\frac{2(2n+1)Co\{(\rho/\rho_m)(E-d)Vo\}\left(\frac{n+1}{n}\right)^{\frac{n+1}{n}}\{(h_2-h_1)y^{\frac{n+1}{n}} + (h_1^{\frac{n+1}{n}} - h_2^{\frac{n+1}{n}})y - h_1h_2(h_1^{\frac{1}{n}} - h_2^{\frac{1}{n}})\}}{(h_2-h_1)\{(h_1-h_2)(h_1^{\frac{n+1}{n}} + h_2^{\frac{n+1}{n}}) - 2nh_1h_2(h_1^{\frac{1}{n}} - h_2^{\frac{1}{n}})\}} \quad (20)$$

Shear rate γ_n is given by $\gamma_n = \frac{\partial vx}{\partial y}$. So from equation (20),

$$\gamma_N = \frac{2(2n+1)Co\{(\rho/\rho_m)(E-d)Vo\}\left(\frac{n+1}{n}\right)^{n+1}\{(h_2-h_1)y^{\frac{1}{n}} + h_1^{\frac{n+1}{n}} - h_2^{\frac{n+1}{n}}\}}{(h_2-h_1)\{(h_1-h_2)(h_1^{\frac{n+1}{n}} + h_2^{\frac{n+1}{n}}) - 2nh_1h_2(h_1^{\frac{1}{n}} - h_2^{\frac{1}{n}})\}} \quad (21)$$

From the relationship given in equation (19), pressure P is given by, for example, approximation method of Runge-Kutta Method. Corrected coefficient of flow path width Co is determined by pressure P and the pressure around the inlet of the cross head die which is derived from expriments. Shear stress τ_{xy} within the die tube can be calculated by equation (4), where the shear rate given by equation (2) and the material parameter K of non Newtonian fluid derived from experiences are used.

2.5 Flow pattern in the duct enclosed between die and wire

Boundary conditions for the duct shown in Fig. 4 are,

$$Vx = 0 \quad \text{at} \quad y = h(x)$$
$$Vx = V_0 \quad \text{at} \quad y = d$$

With regard to h(x), parameters are changed by the relationship shown in Fig. 4;

(iii) $L' < x \leq \ell$

$$h(x) = D + L\tan\alpha + (\ell - x)\tan\gamma \quad (22)$$

(iv) $\ell < x \leq \ell + L$

$$h(x) = D + (\ell - L - x)\tan\alpha \quad (23)$$

In this case, equation (8) is expressed as follows

$$Vx = \pm\frac{n}{n+1}\left(\frac{1}{K}\left|\frac{dp}{dx}\right|\right)^{\frac{1}{n}}\left\{y^{\frac{n+1}{n}} - h^{\frac{n+1}{n}} + \frac{h^{\frac{n+1}{n}} - d^{\frac{n+1}{n}}}{d-h}(y-h)\right\} + \frac{y-h}{d-h}Vo \quad (24)$$

From equation (16)

$$\frac{n}{n+1}\left(\frac{1}{K}\left|\frac{dp}{dx}\right|\right)^{\frac{1}{n}} = \frac{(2n+1)\{Vo(h-d) - 2Co\frac{Q}{W}\}}{h^{\frac{2n+1}{n}} - d^{\frac{2n+1}{n}} - (2n+1)dh(h^{\frac{1}{n}} - d^{\frac{1}{n}})} \quad (25)$$

If dimensionless factor $\phi = h/d$ is introduced to make calculation easier, Vx of equation (24) is expressed as follows.

$$Vx = \frac{\phi}{1-\phi}\left\{Fo\left(\lambda^{\frac{n+1}{n}} - 1\right)\cdot\phi\cdot(1-\phi) + \left\{1 + Fo\left(\phi^{\frac{n+1}{n}} - 1\right)\right\}(\lambda - 1)\right\}Vo \quad (26)$$

F_0 is non dimentional factor which satisfies the next equation.

$$Fo = \frac{(2n+1)\left[\phi - 1 - 2Co\left(\frac{\rho}{\rho_m}\right)\left(\frac{E}{d} - 1\right)\right]}{\phi^{\frac{2n+1}{n}} - 1 - (2n+1)\phi\left(\phi^{\frac{1}{n}} - 1\right)} \tag{27}$$

From equation (26), shear rate $\dot{\gamma}_D$ is given by next equation.

$$\dot{\gamma}_D = \left[\left(\frac{n+1}{n}\right)Fo(\phi\lambda)^{\frac{1}{n}} + \frac{1+Fo\left(\phi^{\frac{n+1}{n}} - 1\right)}{1-\phi}\right] \cdot \frac{Vo}{d} \tag{28}$$

Calculation of pressure P and shear stress τ_{xy} is the same as in the previous case.

2.6 Back tension due to running wire in a die

Tension produced on running wire in a die is decided by the relative relationship between the speed of a wire and a melt poymer. If the running speed of wire is faster than that of fluid, the flow of melt polymer obviously hampers the run of wire. So the tension will work on wire in a way to prolong the wire toward the running direction. This kind of tension will be generated not only in the cross head die but also in the cooling through, in the capstan or in the take up area. However, these tensions generated in the later processes are less than half of that occurs in the die head. In order to obtain the tension generated at the die, as a first step, it is necessary to obtain the shear stress which works on wire. At previous analysis, shear rate $\dot{\gamma}$ of the running wire within the die is obtained from equation (28) by putting $\phi\lambda = 1$

$$\dot{\gamma}_W = \left[\left(\frac{n+1}{n}\right)Fo + \frac{1+Fo\left(\phi^{\frac{n+1}{n}} - 1\right)}{1-\phi}\right] \cdot \frac{Vo}{d} \tag{29}$$

Both from equations (4) and (29), shear stress τ_w, working on a wire can be calculated from $k\,\dot{\gamma}_w^{\,n-1}\dot{\gamma}_w$. When we consider the total balance of power working on the minute section $\triangle x$ which is open equally through the flow direction, and make shear stress at the wire surface to be τ_{wr} and tension there to be $\triangle T$.

$$\triangle T = -2\pi d \cdot \triangle x \cdot \tau_{wr} \tag{30}$$

Total length of the wire which goes through the die is L+l−L' as can be seen in Fig. 4. Making divided wideth to be m, and $\triangle x = (L+\ell-L')/m$, the increment of tension $\triangle T$ at the i-th minute section is given by

$$\triangle T_i = K \cdot 2\pi d^{1-n} \cdot \left(\frac{L+\ell-L'}{m}\right) \cdot \left[\left(\frac{n+1}{n}\right)Fo + \frac{1+Fo\left(\phi^{\frac{n+1}{n}} - 1\right)}{1-\phi}\right]^n \cdot Vo^n \tag{31}$$

Then tension T which is produced throughout a cross head is calculated by following.

$$T = \sum_{i}^{N} \triangle T_i \tag{32}$$

3. Calculations.

Followings are the examples of calculation. Equations which have been introduced by previous analysis were used. FACOM 230-58 was used for calculation. Cutting length is 0.05cm. Table 1 is the flow chart which is used for calculation. Non-Newtonian melt viscosity K becomes necessary for calculation. It is measured by attaching special designed Rheometer at the head of common extruder. With this, it is possible to measure the value even when shear rate is over 10^4 sec^{-1}. K is obtained from experimental data. Then calculation is conducted. One example of flow curve is shown in Fig. 5. Table 2 shows the geometric para-

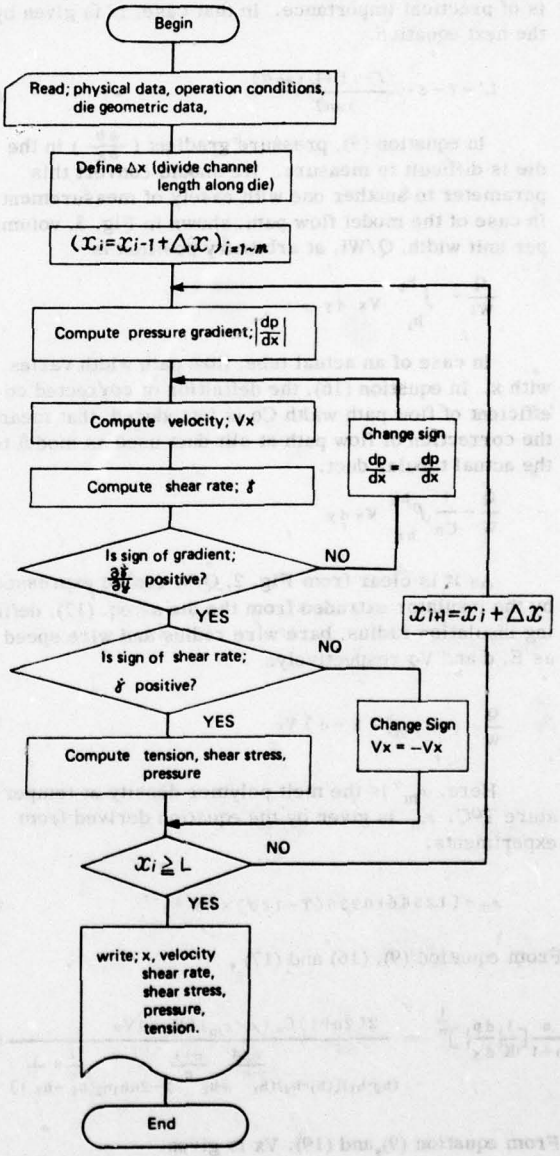


Table 1. Flowchart of computer program for wire-coating die

meters of the die and the nipple used for the calculation and the operating conditions. Insulation material used for the calculation is high density polyethylene for telecommunication wire. MI=0.4 (g/10 min.) and density= 0.945 g/cm^2.

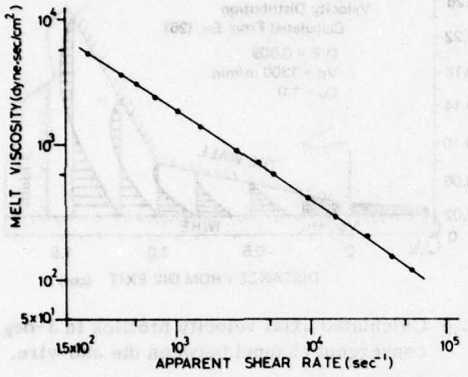


Fig. 5 Flow curve of high density polyethylene for wire insulation (MI 0.4g/10min., density 0.945g/cm^3) at 240°C. Measurements were made with a capillary rheometer having length-to-diameter ratio of 30, and diameter of 1.00mm.

	APPELLATION	KEY	VALUE
DIE	Exit Radius	D	0.035 cm
	Land Length	L	1.000 cm
	2nd Taper Length	ℓ-ℓ'	0.650 cm
	3rd Taper Length	ℓ'	0.700 cm
	Land Tap. Semi angle	α	3.0 deg.
	2nd Tap. Semi angle	γ	20.0 deg.
	3rd Tap. Semi angle	ζ	30.1 deg.
NIPPLE	Exit Radius	r	0.250 cm
	Taper Semi angle	β	20.0 deg.
	Wire Radius	d	0.020 cm
	Insulation Radius	E	0.033 cm
RESIN	Power Law Index	n	0.4
	Density	ρ	0.945 g/cm^3
	Material Temp.	T	240°C
	Die~Nipple Clearance	ε	0.150 cm
	Wire Velocity	V_o	1300 m/min.

Table 2 Geometric parameters of wire coating die.

4. Discussion.

4.1 Velocity profiles in wire coating die

Fig. 6 shows the velocity distribution in the path between the die and the nipple at the cross head die. Fig. 7 shows the calculated result of velocity distribution within the path between the die and the wire.

First, as to the results of calculation of the flow in the path between the die and the nipple, interesting major change was not observed even when geometrical parameters of both die and nipple were changed within practical limitation. We could not get interesting results. However this result is considered to be reasonable when considering past experimental examinations of insulation. That is, geometric parameters of the duct between the die and the nipple will not greatly influence extrusion properties (such as extruded surface roughness, pressure profile in die, reduction in bare wire diameter and so on).

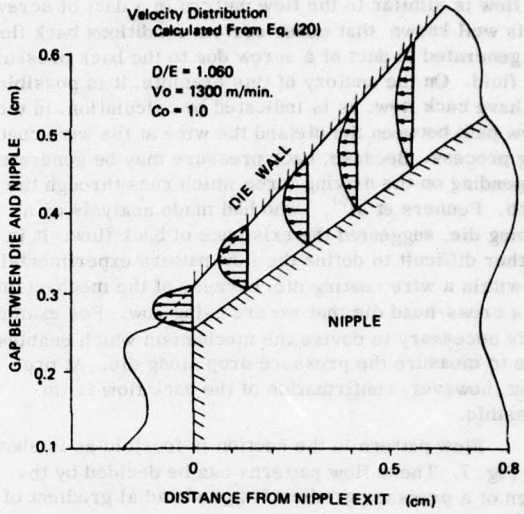


Fig. 6 Axial velocity profiles in convergent channel between die and nipple, calculated from eq. (20) at V_0 = 1,300m/min. .

Based on the assumption of the independent flow path employed for our analysis (assumption is that two paths are independent of each other and they are connected in such a way as only to satisfy the continuous equation), influence of the drag flow due to wire running to the flow patten is not taken into account. Actually, the flow near the exit of nipple differs greatly from calculated results. Results of calculation on the other flow pattern between the die and the wire is important. Fig. 7 is one example. Flow pattern at the exit of the nipple

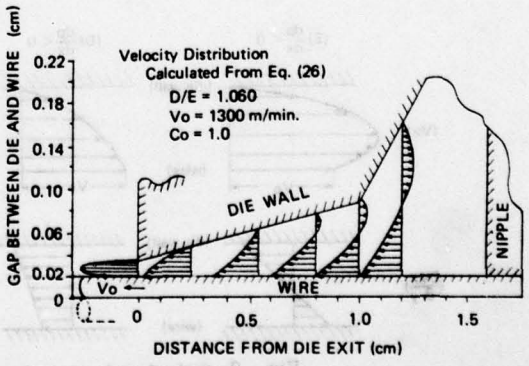


Fig. 7 Calculated axial velocity profiles in 3-deg. convergent channel between die and wire.

is different from that at the exit of die. Back flow opposite to the flow directions was observed at certain length from the exit of the nipple to that of the die. The flow between the die and the wire is considered to be composed of pressure flow and drag flow. Former is cause by a pressure difference generated in the flow path of the extruder itself and at the exit of the die. The latter is generated by the running of wire in the die. This kind of flow is similar to the flow pattern in a duct of screw. It is well known that under certain conditions back flow is generated in duct of a screw due to the back pressure on fluid. On the analozy of this example, it is possible to have back flow, as is indicated by calculation, in the flow path between the die and the wire at the wire coating process. Because, back pressure may be generated depending on the driving force which runs through the path. Fenners et al[5], who had made analysis on a tubing die, suggested the existence of back flow. It is rather difficult to define the flow pattern experimentally within a wire coating die, because of the mechanism of a cross-head die that we are using now. For example, it is necessary to devise the mechanism which enables one to measure the pressure drop along die. At present, however, confirmation of the back flow is impossible.

Flow pattern in the section is fourfold as is shown in Fig. 7. These flow patterns can be decided by the sign of a pressure gradient dp/dx and radial gradient of the shear rate. These flow patterns show strong tendency of dependence on die geometries. We obtained the following results. The flow within a dieland, which is from the exit of a nipple to that of a die, will depend largely on reduction ratio D/E. This D/E is defined by the ratio between radius of die exit D and radius of insulated wire E.

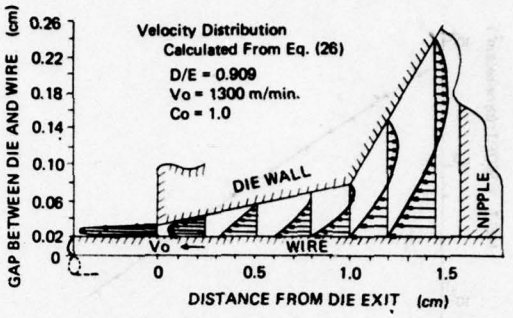


Fig. 8 Calculated axial velocity profiles in 3-deg. convergent channel between die and wire.

4.2 Reduction ratio and velocity profile

In the operation of extrusion for insulation, extrusion properties vary greatly by die geometries. Among these, reduction ratio D/E is the most important factor for the extruder design. In order to infer the influence of D/E ratio to extrusion properties, we examined the relation between reduction ratio D/E and velocity profile. Calculation results for velocity profile at a dieland area differ from the case of reduction in

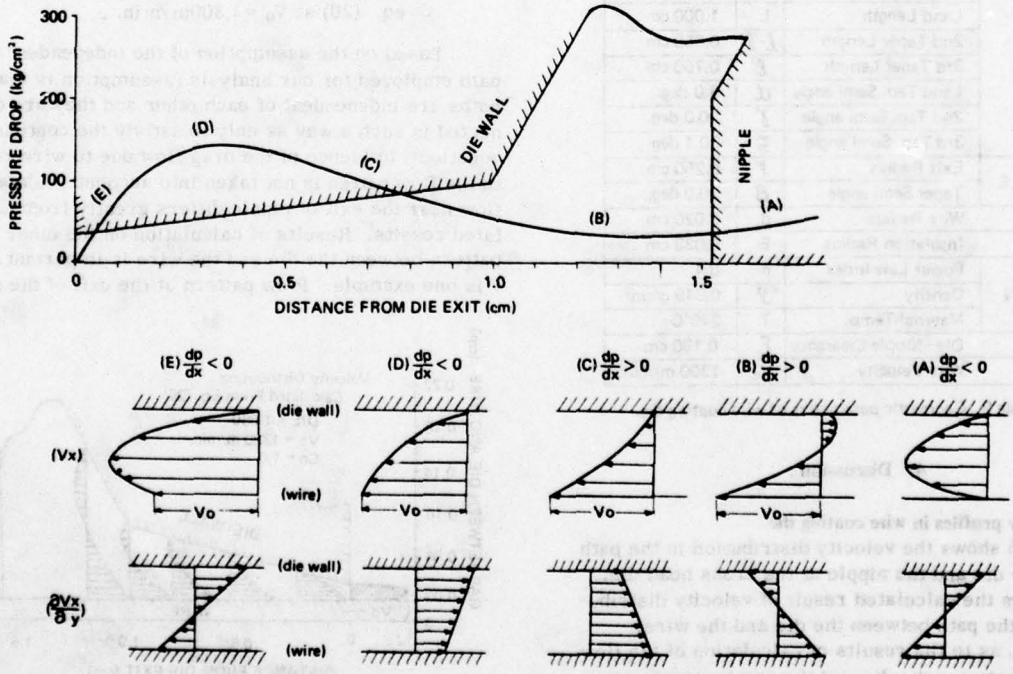


Fig. 9 Calculated axial pressure drops and flow patterns, parameters in eq. (25) : D/E=1.06, $\alpha = 3^{o}$, Co=1.0, and Vo= 1,300 m/min..

the form of D>E to the case of D< E. Former is shown in Fig. 7 and the latter in Fig. 8.

This indicates the possibility of back flow up to the area adjacent to the exit of a die when larger reduction is given at the time of the extrusion. The flow profile, when D/E ratio is increasing, is that the maximum speed of fluid on an arbitraly section occurs on wire.

On the contrary, if the operation is conducted without reduction, the influence of pressure flow which acts the wire pulling to the running direction increases, and pressure flow becomes dominant in the flow profile gradually. Maximum speed of flow, which occurs in the middle of the gap between the wire and the die wall, becomes much faster than wire running speed.

4.3 Pressure drop profiles

Calculated pressure drop along die is quite complex. As shown in Fig. 9, in the flow path between the die and the nipple, pressure decreases monotonously and becomes minimum at the exit of the nipple. However, as it is clear from the calculated velocity profile, back pressure works from the exit of the nipple to the exit of die. So the part of a flow becomes back flow and the pressure becomes maximum just before the exit of die. Then it changes to positive pressure with steep pressure gradient, which forces wire to push out to the exit of die, and then pressure drops toward the atmospheric pressure with rapidity. In case of calculated example, we indicated the case where corrected coefficient of flow path width Co equals to one. When Co equals to one, culculated absolute value of pressure is 1/3 to 1/4 smaller than the value we usually have experiences. The reasons are twoholds. (i) We assumed that the initial condition for the pressure is that pressure at the exist of die equals to the atmospheric pressure ... (Po = 0). But actually, it is probable that a certain degree of residual pressure still remains. (ii) It this analysis, we used slit channel as model.

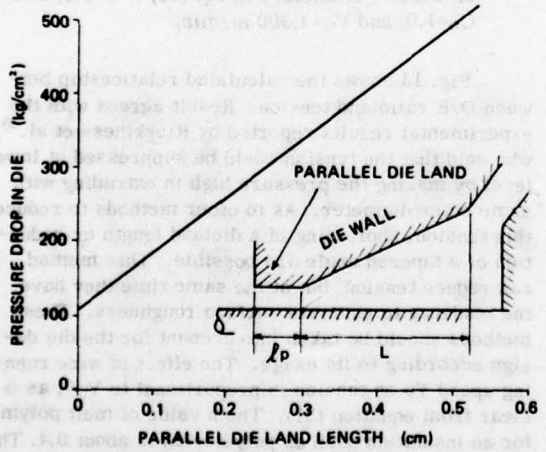


Fig. 10 Calculated maximum pressure in die, changed with an additional a parallel part near the die exit, parameters in eq. (25) : D/E=1.06, L=1.0, α =3°, and V_o= 1,300 m/min..

With this model, pressure was tended to be underestimated, because of the errors occurred from the difference between a cross sectional area of the model and of an actual channel influence the calculation of volume, that is clear from equation (25).

Corrected coefficient Co will deffer depending on the conditions of simulation, but it is considered to be around Co=1 to 2.

Influence of the material parameters K and n for the non-Newtonian fluid is as important as that of die geometries. Due considerations should be given to these parameters when insulation materials for high speed wire-coating is to be selected. Subsequently machining and designing exactness for the die geometries near the exit is important with regard to the value of pressure drops. When there is a parallel part ℓ_p, existed near the die exit, as seen in Fig. 10, the relationship between the calculated maximum value of a pressure and the length of a parallel tube is as follows. If there is 1mm of a parallel section, then that will cause the increase of a pressure by about 70 Kg/cm^2. So when extruding operation is conducted with low pressure, manufacturing of a die should be done quite carefully. Incidentally as it is clear from the result shown in Fig. 11, which decides the effect of a tapered angle to a pressure drop, maximum pressure value in die increases with the decrease of tapered angle markedly. When such a die is used, they should be fully aware of the flow profile with dominant pressure flow as previously mentioned.

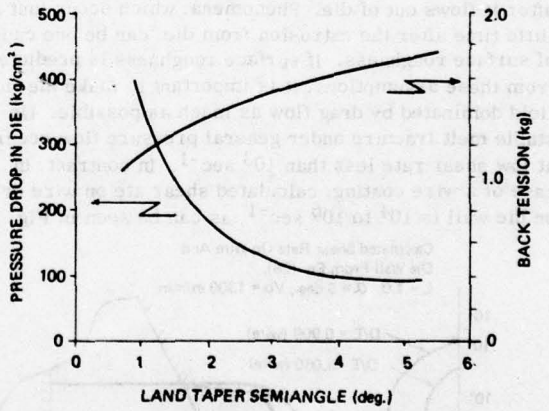


Fig. 11 Effect of tapered semi-angle of die α on pressure drop P and on tension exerted on wire T. Parameters in eq. (25) and (31) : L=1.0, Co=1.0, D/E=1.06, and V_o= 1,300 m/min..

4.4 Extruded surface roughness and die design

In well-known capillary flow consisted with a pure pressure flow, a surface roughness, called as the shark skin, will be generated when a shear rate is above a certain high level [8]. The mechanism of generating such phenomena is complex and satisfactory explanation has not been made. Similar roughness phenomena above mentioned are observed in wire coating processes.

From our experiences so far, we could observe the change in extruded surface roughness by changing the die geometry, not altering other conditions such as material, temperature, wire speed and etc. In order to prevent extruded surface roughness; (i) it is better to have long land length L. (ii) it is said good to have an angle of the dieland α around 3°. (iii) good result is obtained by making reduction large. (iv) Surface roughness is degradated with the increase of wire speed. (v) Result was better for the material with good flow properties. If we analyse the facts based on experiences of the calculated results, we can get the following estimations. The value of a shear rate in die becomes smaller with the increase of a reduction rate D/E, with the lowering of the running speed and with the increase of a tapered angle α in a dieland. It is considered that this serves for the prevention of unsteady melt fractures. However, about the tapered angle α , it becomes too large, sectional area near the nipple exit also becomes too large. Thus effects of a back pressure on flow tends to increase. This result is not facourable for the prevention of a surface roughness. As to tapered angle, from this presume, it should be believed that there are some optimum angle for the best die designs. As stated before, lower the D/E ratio is, more dominat the pressure flow becomes. At the flow near the exit of a die, maximum flow speed which is faster than wire running speed tends to be generated in the gap between the wire surface and the die wall. From this calculating results, we can assume that the melted insulation material which is extruded from die will be continuously drawn by wire after it flows out of die. Phenomena, which occur just a little time after the extrusion from die, can be one cause of surface roughness. If surface roughness is predicted from these assumptions, it is important to make the flow field dominated by drag flow as much as possible. Unstable melt fracture under general pressure flow occurs at low shear rate less than 10^3 sec^{-1}. In contract, in case of a wire coating, calculated shear ate on wire or on die wall is 10^4 to 10^6 sec^{-1}, as can be seen in Fig. 12.

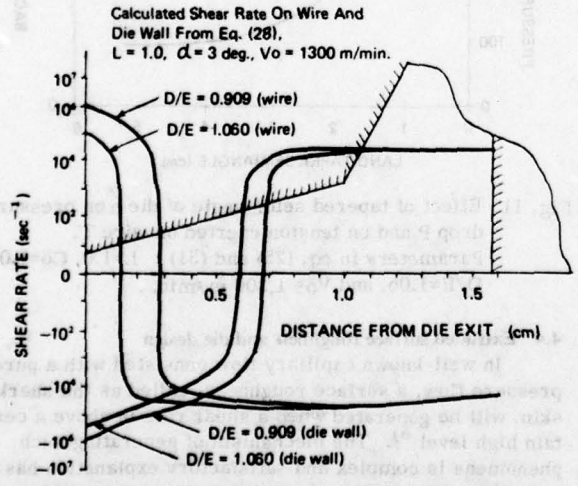


Fig. 12 Calculated variations of shear rate $\dot{\gamma}$ on die wall and wire surface with reduction ratio D/E.

With regard to the extrusion for a wire coating, the surface roughness do not occur up to high shear rate area which is far higher than a melt fracture under a common pressure flow. This means that with the wire coating flow, some important factors which effect on melt polymer in die should prevent the occurance of the surface roughness. It is quite probable that this should be caused by another flow other than the pressure flow. That is drag flow, we suppose. At any rate, the effect of a drag flow on unsteady flow should be further discussed in other opportunities.

4.5 Back tension exerted on wire in die

Tension in die depends on the flow pattern largely. As is clear from Fig. 7 and Fig. 8, with the increase of reduction ratio for the extrusion, drag flow due to a running wire in die becomes more dominant. It becomes more probable to have a maximum speed of running fluid along flow direction on wire. Thus the tension in die becomes higher. But in the flow profile in which the pressure flow is dominant, the tension exerted on wire markedly decreased as the flow drags out the wire to the exit.

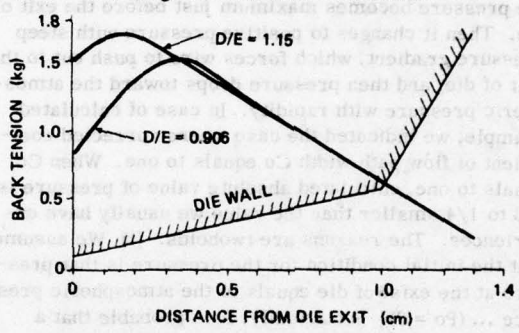


Fig. 13 Effect of reduction ratio D/E on Tension exerted on wire. Parameters in eq. (31) : L=1.0, α=3°, C_o=1.0, and V_o= 1,300 m/min.

Fig. 13 shows the calculated relationship between D/E ratio and tension. Result agrees with the experimental results reported by Riekkiness et al.[9], who said that the tension could be suppressed at lower level by making the pressure high in extruding with same outer diameter. As to other methods to reduce this tension, shortening of a dieland length or reduction of a tapered angle are possible. This method can reduce tension, but at the same time they have the tendency to generate surface roughness. These methods should be taken into account for the die design according to its usage. The effect of wire running speed Vo on tension is proportional to V_s^n, as is clear from equation (31). The n value of melt polymer for an insulation such as polyethylen is about 0.4. The influence of that is smaller than that of the parameters such as D/E, L and others. So with regard to reduction problems of wire, if a die design is correct, high wire running speed will be not limited so critically.

4.6 Future problems.

In this report, velocity profile in die is obtained as a first step for the design of die and cross head which are suitable for high speed insulations. Then by assuming the flow pattern in die, preventive action for surface roughness was considered. Further, we introduced the relative equation for a back tension exerted on running wire in die. Then we simulated to identify the occurance of tension under acutual operational conditions. Calculated results with this numerical methods do not necessarily agree with actually measured value quantitatively. However qualitatively, these two coincide.

With regard to this analytical method, we conducted analysis on the assumption that flow in the duct enclosed by the die and the nipple and the flow enclosed by the die and the wire are independent with each other. So we could not satisfactorily explain the influence of the clearance to extrusion properties, for example. Closer investigation is desired in order to conduct the simulation for the important area where the nipple part changed to the die part. One major method is the use of finite element method (FEM)[10], for example. We would like to report on this method at other occasion.

5. Application.

This chapter is about self-centering fixed die which was designed based on the data obtained from the analytical method. This is one example of application. Three important factors for the design and the development of the fixed die are as follows.

i) preciseness of machine processing.
ii) hydrodynamic effects on wire[11].
iii) thermal stabilities of die material.

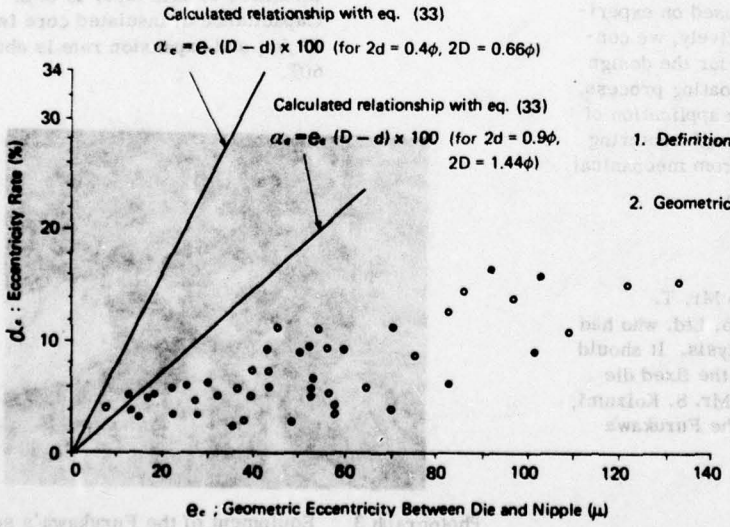
With regard to the influences of a flow on self-centering effects, following two thoughts are important. a) to prepare steady and homogeneous flow as much as possible. b) to consider hydrodynamic forces which hold wire its centric position of die. These factor should be counted for die designs. When wire runs in the duct of a die, it is important to make it run at the centric position of die at all times. In order to maintain the position, the aid of a hydrodynamic force is required.[11], When we designed self-centering die, we explored the duct geometeries with which centripetal forces formed by mechanical effects of a fluid will work on a wire. We developed a new self-centering fixed die with helping a hydrodynamic forces above mentioned. We are now using them in our manufacturing process. Fig. 14 shows the experimental facts which indicate the effects of hydrodynamic forces which bring about self-centering phenomena above mentioned.

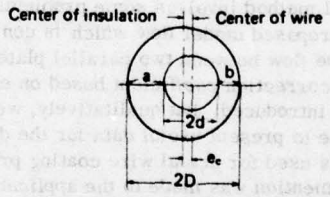
Looking from these results, if an eccentricity of an extruded wire is decided only by the geometrical relationship between the die and the nipple, degree of geometric eccentricity ε_c and eccentric ratio α_c can be expressed as following.

$$\alpha_c = e_c\,(D-d) \times 100 \quad (\%) \tag{33}$$

Here, α_c can be defined by the following equation when maximum insulation thickness is expressed by a and minimum thickness by b.

$$\alpha_c = \frac{a-b}{a+b} \times 100 \quad (\%) \tag{34}$$





1. Definition of an eccentricity rate; α_e is following.

$$\alpha_c = \frac{a-b}{a+b} \times 100\ (\%)$$

2. Geometrical relationship is satisfied with this equation.

$$\alpha_c = e_c\,(D-d) \times 100(\%)$$

○ : 2d = 0.4φ (2D = 0.66φ)
● : 2d = 0.9φ (2D = 1.44φ)

Fig. 14 Plots of eccentricity rate α_c versus geometric mechanical eccentricity between die and nipple e_c, on extruded wire with Furukawa's self-centering fixed die.

However, in case of Furukawa's Fixed Die, it is possible to suppress the eccentricity to smaller degree because of the hydrodynamic effect of a fluid even when they are processed under lesser mechanical accuracy than is difined in equation (33).

This fact tells us that it is possible to produce a fixed die with cheeper price, under mechanical accuracy in the order of 10 ~ 100 u, suitable for the mass production rather than the ultra high exact machining in the order order of μ^2).

It is shown the appearance of the Furukawa's fixed die, at photograph 1. Cross sectional view of insulation extruded with the dixed die is given. This die is necessary for the extrusion of dual insulated wire which is the extension of our present technology. Also the picture of equipment for cross head die is shown. (Photograph 1 ~ 3)

6. Conclusion.

Several equations were introduced which indicated the flow properites within a cross head die for a wire coating process. Simulation was conducted with actual die geometries. In our analysis, the flow between two non-parallel, concentric tube was divided equally into small segments along the die. Flow, in the divided minute sections, was considered to be the flow in the duct enclosed with two parallel plates.

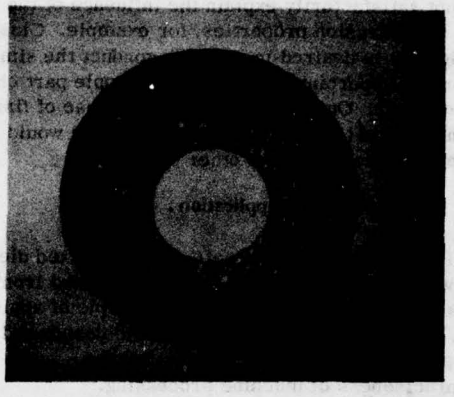
We assumed power law fluid which was composed of steady, incompressible and isothermal fluid. From the proposed equations and numerical calculations, relationship between velocity distribution and pressure profile was estimated. Furthermore, estimation was made on the generated tension. The proposed analytical method involves some problems regarding the proposed model flow which is considered to be the flow between two parallel plates. Quantitatively, correction coefficient based on experiment should be introduced. But qualitatively, we consider it possible to present useful data for the design of a die which is used for actual wire coating process. In this report, mention was made to the application of this analysis, that was the Furukawa's self-centering fixed die for which centripetal forces from mechanical effects of fluid were taken into account.

Acknowledgement

Authors extend sincere thanks to Mr. T. Matsunaga of the Furukawa Electric Co. Ltd. who had assisted us earnestly in doing our analysis. It should be stated here that the development of the fixed die was conducted with the cooperation of Mr. S. Koizumi, Mr. T. Fujimura and Mr. S. Nagai of the Furukawa Electric Co., Ltd.



Photograph 1 The Furukawa's self-centering fixed die for high speed insulations.



Photograph 2 Cross sectional view of dual insulated core, with highdensity polyethylene. Wire diameter is 0.9 mm (19AWG), diameter with cellular is 2.3 mm and thickness of skin layer is 50μ. Capacitance of insulated core is 85 PF/m, and expansion rate is about 60%.



Photograph 3 Equipment of the Furukawa's self-centering fixed die for a dual insulation.

References

1) M. Rokunohe, Y. Ueno, et al., 24th. I.W C.S. Proceedings, 53 (1975)
2) for example, Maillefer S.A. Technical Report No.11
3) Oka, S., J. Phys. Soc. Japan, 19 1481 (1964)
4) K. Ito, Plastics 24 89 (1973)
5) Fenner, R.T. Trans. J. Plastics Inst., 35 701 (1976)
6) K. Hayashida, Kobunshikagaku, 18 190 99 (1961)
7) K. Fuse, K. Orimo, J. Soc. Rheol. Japan 5 2 60 (1977)
8) J.R. Tordella, "Rheology" cuap. 2 (1969) Academic Prees Inco., New York.
9) Riekkinen, A and R. Ekholm, 24th I.W.C.S. Proceedings 43 (1975)
10) B. Caswell, R.I. Tanner, "Wire coating die design using finite element methods" (1977)
11) Z. Tadwor, R.B. Bind, Poly.Poly. Eng. Sci., 14 2 (1974)



KENICHI FUSE
The Furukawa Electric Co., Ltd.
6-1 Marunouch, 2-Chome, Chiyoda-ku, Tokyo, Japan

Mr. Fuse graduated from Keio Univ. 1971 with a M. Sc. degree in mechanical engineering. Then he joined The Furukawa Electric Co., Ltd. and has been engaged in research and development of plastic material and manufacturing methods for telephone cables.

Mr. Fuse is now chief engineer of Material Engineering Section of the Telecommunication Laboralory at The Furukawa Electric Co., Ltd. and a member of the Society of Rheology, Japan.



KATSUMI ORIMO
The Furukawa Electric Co., Ltd.
6-1 Marunouchi 2-Chome, Chiyoda-ku, Tokyo, Japan

Mr. Orimo graduated from Kyoto University in 1966 with a B. Sc. in Applied Chemistry.

Upon graduation he jointed the Furukawa Electric Co., Ltd. and has been engaged in the research and development of plastic materials and manufacturing methods for telephone cables.

Mr. Orimo is now manager of Material Engineering Section of the Telecommunication Laboratory at The Furukawa Electric Co., Ltd. and is also a member of the Society of Materials Science of Japan.



KEIICHI SHIBATA
The Furukawa Electric Co., Ltd.
6-1 Marunouchi, 2-Chome, Chiyoda-ku, Tokyo, Japan

Mr. Shibata graduated from Tokyo Univ. of Education, 1969 with a B. SC. in dep. of Mat..

Then, he jointed the Furukawa Electric Co., Ltd. and has been engaged in analyzing and calculating of technical problems in manufacturing telephone cables and power cables.

Mr. Shibata is now chief engineer of the System's Dept. of the Furukawa Electric Co., Ltd. and a member of the mathematical Society of Japan.

A NEW PROCESS FOR THE MANUFACTURE OF MAGNET WIRE

EBERHARD KERTSCHER

MAILLEFER, S.A.
Ecublens, Switzerland

BRUNO SCHMIDT

KABEL & LACKDRAHTFABRIKEN G mb H
Mannheim, West Germany

SUMMARY

The authorsdescribe a completely new process for manufacturing enamel-insulated magnet wire (so called enamelled wire).Unlike the still generally applied technique of using solvent enamels with subsequent solvent evaporation and hardening of the enamel film using a baking oven, the new process uses a modified and developed form of the extrusion process which has been employed for years in the manufacture of cables and wires.

The process (EMAILEX) and its basic problems are described in detail and explained using the example of a 4 wire system for conductor diameters of .4 to 1.2 mm.

Material selection is also discussed. In this regard, suitable and economical materials were found with which extruded enamelled wire (EXOGAN) was produced. The results of test carried out on that wire as well as first operational trials in relay coils and IEC standard motors are described.

INTRODUCTION

Enamel-insulated magnet wire, commonly called enamelled wire, is widely used in the production of electrical machinery, transformers and electronic systems. The conductor material of such wire, usually copper or aluminum, is insulated with a thin layer of synthetic resin enamel which is highly resistant to mechanical and thermal stresses.

Enamelled wire is manufactured in so-called wire enamelling machines by multiple continuous coating with wire enamel, i.e.the metal wire is coated with a solution of an organic synthetic resin and a solvent (1). In order to achieve a smooth film of enamel which is free from blisters and solvent material, the number of layers of enamel must be increased as far as possible with the individual layers being as thin as possible.

In general, 6 to 10 individual coats (passes) are applied with the necessary thickness depending to a very large extent on the diameter of the wire (see, for example, German Standard DIN 46 435).

The baking process after each coating operation permits the solvent to evaporate and the film of enamel to harden. The resulting solvent vapour is removed from the baking chamber by means of an extractor fan.

For these processes, the baking temperature is between 300 and 550°C and depends on the enamel base, the diameter of the wire, the type of baking oven used and the rate of throughput.

The wire enamels (enamel solutions) contain solid substances to an extent of approx. 15% to approx. 50%, i.e. the proportion of solvents to be evapored is 50% to 85%. Increasing the content of solids results in operationally less favorable conditions since the enamel solutions obtained have too high viscosity.

Owing to their high dissolving capacity, high flow-aiding boiling range, and not least their favourable economic aspects, the solvents used for most wire enamel materials are Cresol and Xylenol compounds extracted from coal or lignite tar, blended with aromatic hydrocarbons; for some special wire enamels, other solvents such as N-methylpyrrolidone and Dimethylformamide are also used.

This process still is widely used for the manufacture of enamel-insulated winding wire and has a number of disadvantages. There is quite clearly room for improvement:

- The application of several very thin individual coats demand high technology and therefore considerable investment.
- Complete removal of the solvents, which is essential if optimum enamelled wire properties are to be obtained, is only possible with considerable energy usage.
- The parallel baking process - with most wire enamel resins, consists of cross-linking involving volatile condensation products splitting off - and also requires large quanties of energy.
- Despite the considerable cost involved, the throughput rates obtained with normal machines are comparatively low due to the necessary reaction times (e.g. with a wire diameter of 1 mm, the throughput is approx. 25 m/min.).

In addition, there is the physiological danger from the solvents used in wire enamels, if they come into contact with human skin or are inhaled as vapour; this may be illustrated with the following data on the most commonly used Cresol and Xylenol materials:

- In accordance with the directions issued by the Commission on Hazardous Operational Materials in 1977, the maximum concentration at a place of work is 5ppm or 22 mg/m^3 (Regulation on Hazardous Operational Materials of 8.3.1975, category 1 b).
- According to the Technical Directive on Air Pollution Measures of 28.8.1974, Cresol and Xylenol materials fall into category 1, i.e. the maximum emission permissible is 20 mg C/m^3. This means that to comply with official regulations, appropriate safety measures are required.

On the currently known enamelled wire machines, solvent vapour are removed from the baking chamber by means of an extractor fan. Installation of combustion catalysts which destroy, i.e. subsequently burn off a large proportion of the solvent vapours produced in the baking chamber, results in considerable expenditure and therefore a significant increase in cost in the finished products.

Whilst the fact that the combustion gas in modern catalytic circulating air ovens is utilised for pre-heating (2) and covers part of the additional cost incurred as a result of the use of solvents as well as their storage and transport, it by no means covers all of that additional cost.

It must also be assumed that the above-mentioned official regulations and the sensitive after-burning systems which only operate correctly when properly maintained, will in time be replaced by even more efficient but also considerable more costly thermal after-burning systems.

In order to overcome the problems resulting from the use of solvents, it has already been suggested that aqueous systems should be used. However, both the use of wire enamel dispersions (3) and the use of wire enamel resins dissolved in water (4,5) include the problems of energy-intensive evaporation of large quantities of water as well as their complete removal so that an efficient enamelled wire insulation may be obtained.

Furthermore, the pollution problems described above cannot be solved in an optimum way by the high-boiling organic additives necessary for aqueous systems, e.g. catalysts, dispersing and thickening agents as well as the amines which aid water solubility.

There is also the method of insulating electrical conductors made of resin melts, in particular of thermosetting Polyesterimides (6,7,8). However, when processing melts of such reactive resins and considering the necessary temperatures, one must remember the limited temperature storage stability over longer periods of time.

Despite an improvement in pollution effects, the throughput rates obtainable with these processes are no higher than those achieved with conventional wire enamels.

BASIC PROBLEMS ENCOUNTERED WITH EXTRUSION ENAMELLING (EMAILEX)

In order to improve the methods used for manufacturing enamelled wire, extrusion technology which has been used for a long time in cable and wire production, was taken as the basis. Previously, the application of such a technology has always foundered because of the very thin layer of insulation required for enamelled wire.

Below, is introduced an extrusion technology - the so-called extrusion enamelling process, EMAILEX, which has been developed from previously known technology but which differs considerably from the basic principles.

a) Instead of conventional wire enamels, extrudable thermoplastics are being used. Since those thermoplastics contain neither solvents nor toxic substances, costly combustion or afterburning facilities as well as other measures required to avoid health hazards are unnecessary.

The new process is thus obviously more favourable regarding environmental considerations than are the processes previously mentioned. Since there is no need for solvent evaporation and because the resulting savings in energy which may be as much as 90%, the process is also considerably more economical.

b) The use of thermoplastics removes the need for the hardening reaction necessary for the processes previously used, which again results in additional and considerable savings in energy.

c) As a result of the above-listed factors, a possible, and therefore, decisive increase in the throughput rate and thus in the economic efficiency of wire coating may be obtained.

As will be shown in detail below, speeds of 250 m/min are in fact practicable with a wire diameter of 1 mm.; this means that compared with the conventional process, the operating speed may be increased by a factor of 10 without problems.

There were a number of basic problems with the new process which had to be resolved:

The operational system of the conventional extrusion technology had to be modified and developed in such a way that wires with wall thicknesses of as little as 15 µ (0.0006") could be coated perfectly and economically.

Furthermore, insulating materials had to be selected and developed which on the one hand were suitable for extruder coating and on the other hand met the usual property requirements for enamelled wire.

There was also the need to integrate the annealing of the wire at the high extrusion speeds to be expected, into the system and at the same time keep the wire surface completely clean and, most importantly, free from residual drawing grease.

Below, is described how these problems were solved, and a discussion of the current state of this new extrusion enamelling (EMAILEX) and the extruded enamelled wire (EXOGAN) manufactured.

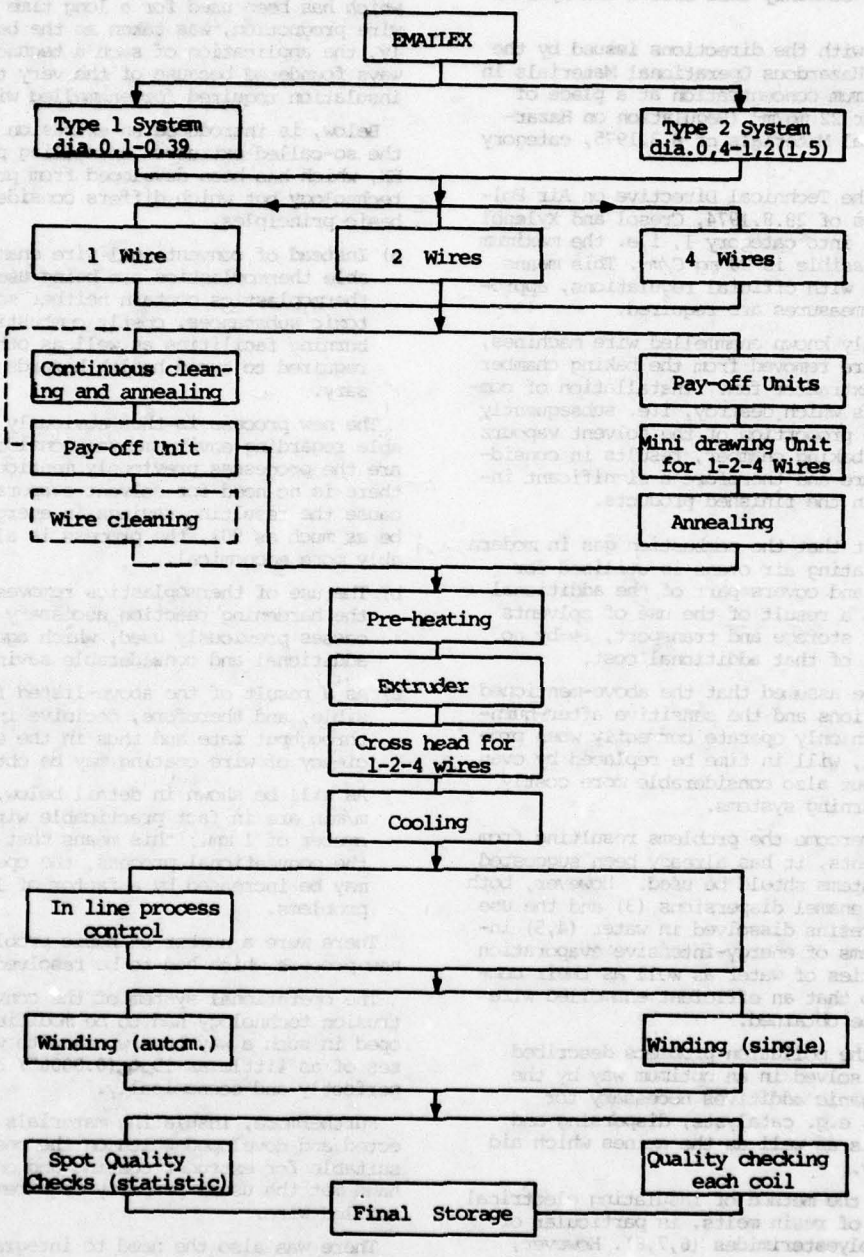


FIG. 1 SYSTEM FLOW CHART

FUNCTIONAL DESIGN OF EXTRUSION SYSTEMS

The systems are designed in such a way as to permit wires with diameters of between 0.1 mm and 1.5 mm to be insulated. Basically, as illustrated in Fig. 1. two system sizes are available for this purpose.

On conventional enamelled wire machines, the wire is annealed either by resistance annealing or with superheated steam with the wire being cleaned and degreased to a large extent by the steam during annealing. If degreasing is not complete, then the film of enamel will have poor adhesive properties after insulating.

The EMAILEX process offers a relatively high safety factor in this respect. If a normal continuously-annealed wire is used, no subsequent cleaning is necessary. Experiments have shown that cleaning is required only if poorly cleaned coils (e.g. pot-annealed coils) are processed. In all cases, any residual drawing grease remaining on the wire will be vapourised due to the high pre-heating temperatures employed in the process.

Another possibility is to connect in series with the system a group of so-called multiple mini-drawing units and to anneal the wire immediately, using a continuous-annealing system. The quality achieved in this way is sufficiently high to ensure good adhesion of the insulation of the conductor.

SYSTEM DESIGN

The design of a 4 wire system, Type 2, for semi-automatic operation for wire diameters of between 0.4 mm and 1.2 (1.5) mm may be seen in Fig. 2. This system is designed in such a way as to ensure consistent continuous operation.

DUAL PAY-OFF UNITS

As can be seen from Fig. 2 the system is equipped with dual pay-off units which are specially designed for controlled wire pay-off. The wire pays off without noise; the change-over from the empty to the full coil is effected without any reduction in line speed.

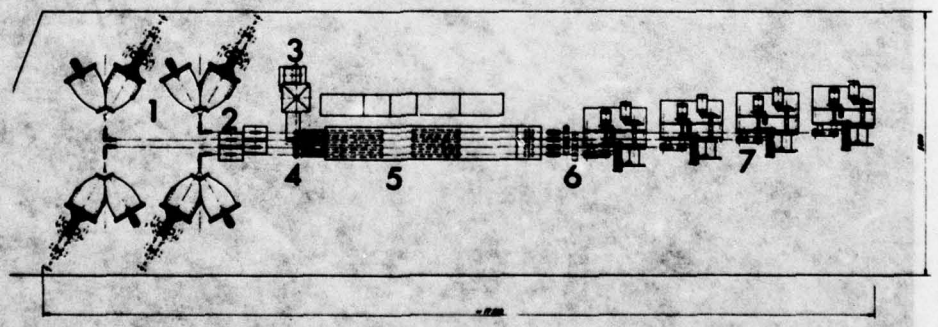
Pre-heating

The pre-heating unit has been designed in such a way that four wires can be brought to a pre-determined temperature simultaneously but independently of each other. This accurate way of pre-heating is essential in order to ensure optimum properties, e.g. adhesion, elongation and surface smoothness.

FIG. 2

SCHEMATIC LAYOUT OF AN EMAILEX SYSTEM, TYPE 2

1 Twin overhead pay-off units
2 Pre-heating
3 Extruder
4 Extrusion cross-head
5 Cooling and drying unit
6 Wire inspection and control
7 Coiling



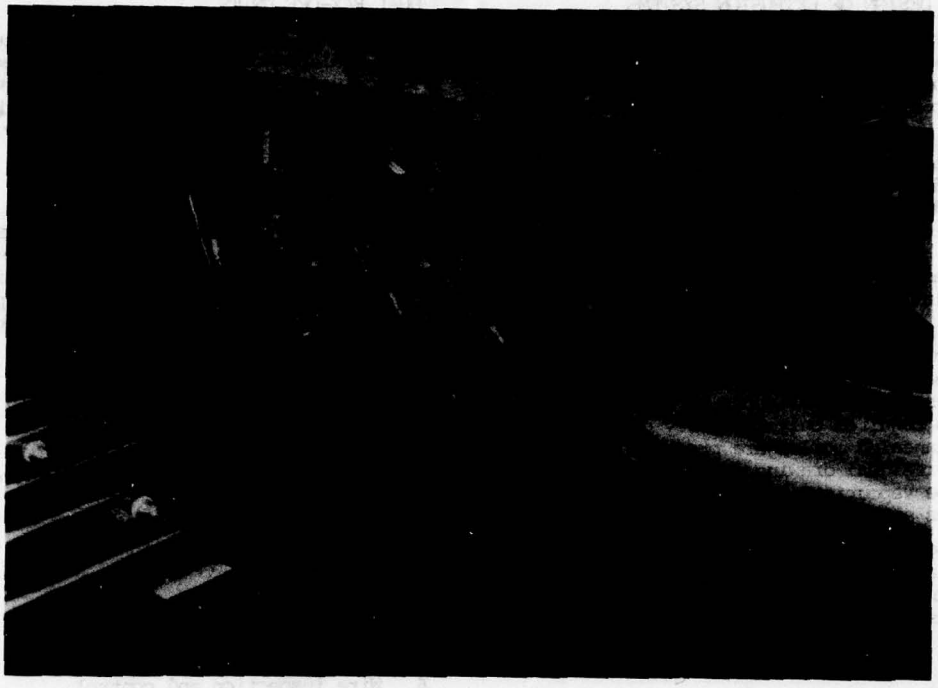


FIG. 4 FOUR WIRE CROSSHEAD

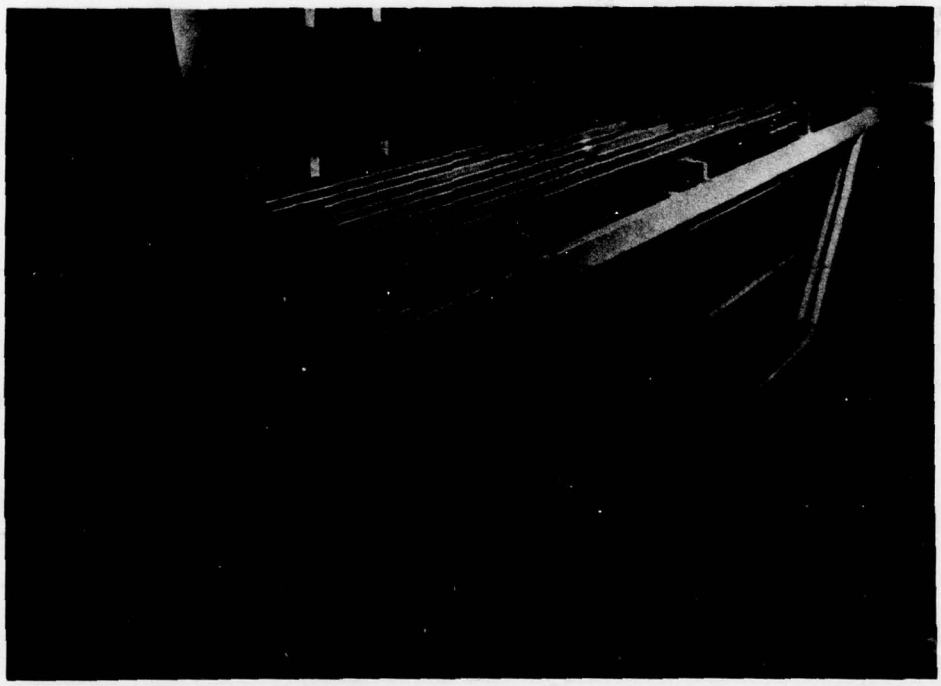


FIG. 5 COOLING & DRYING UNITS

EXTRUDER

To facilitate the production of the extremely thin insulating wall thickness required for winding wire ensuring the highest quality and a high pay-off speed, a special screw and a number of other elements had to be developed in order to obtain absolutely smooth and faultless surfaces. Screw and cylinder are adapted to each other in such a way that the material is drawn in evenly and without any pulsating.

Both the reduction gear and the drive of the extruder ensure a perfectly even rotational speed of the screw without shock or vibration effects.

It is preferable to use thyristor-controlled DC drives which are easily synchronised with the rest of the line and, most importantly, with the capstan. In addition, special care must be taken over regulating both cylinder heating and cooling so as to ensure as perfect a temperature consistency as possible.

The heating zones of the barrels are equipped with special thyristor-controlled thermostats which, if required, provide infinitely variable control for the cooling fans. This system has been proved to give high consistency of temperature and thus an excellent consistency in wire quality.

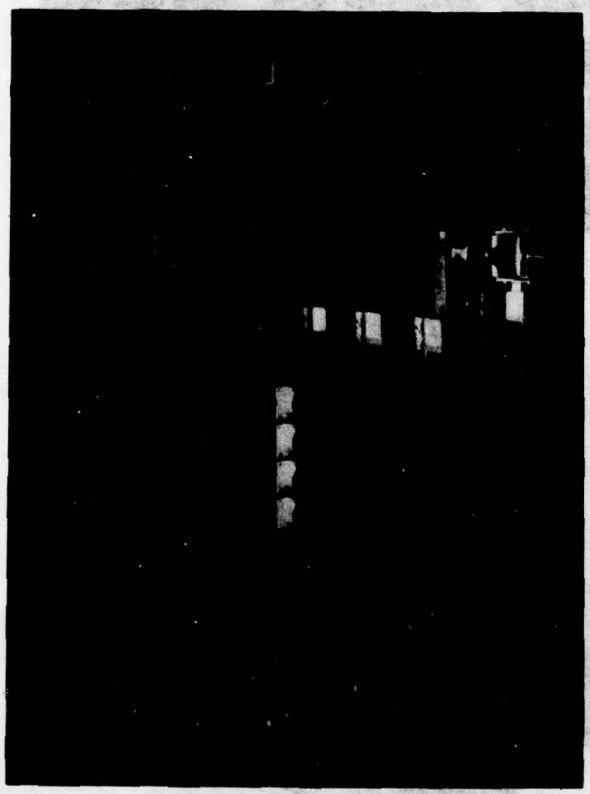


FIG. 3 BM 30 EXTRUDER

METERING CROSS-HEAD

Together with the extruder, the cross-head is one of the main elements of the new process. This unit, too, is a product-specific development. The demands made on this important element are as follows:

- Perfect centering of the wire
- Even and smooth insulation surface
- Smallest possible retention loss in the wire
- Possibility of fast tooling change even if the system is not switched off
- Long operational life of the tools

All the above requirements are met by the metering cross-head illustrated in Fig 4. The design of the head is based on the mechanical assembly technique (MAT), with the body being designed for 1, 2 or 4 positions. The appropriate interchangeable tool carriers are fitted into the body. The tools themselves are precision parts and are made from high wear-resistant materials.

COOLING AND DRYING UNITS

The cooling trough is designed in such a way that the four insulated conductors can be cooled independently of each other. In order to save water, a closed circuit system is provided (see Fig 5).

WIRE CONTROL

After leaving the cooling and drying units, the insulation is continuously checked. Any faults occurring are indicated immediately. In addition, it is possible to equip the system with a process production control facility which allows production and quality data to be instantly available and/or recorded statistically at any time.

A practical solution would be to connect several systems to this unit integrating them into production planning.

COILING

The finished insulated wire may be coiled using single winding machines or automatic winding systems.

In case of the single winding machine, Fig. 6, the processing must be slowed down for the change-over of coils so as to enable the wire to be placed on the new reel.

If automatic winding machines, Fig 7, are used, the change-over from the full to the empty coil takes place at full speed. Both the removal of the full coil and the insertion of the empty reel are also effected automatically.

AD-A062 322 ARMY COMMUNICATIONS RESEARCH AND DEVELOPMENT COMMAND --ETC F/G 13/9
PROCEEDINGS OF THE INTERNATIONAL WIRE AND CABLE SYMPOSIUM (27TH--ETC(U)
NOV 78 E F GODWIN

UNCLASSIFIED NL

2 OF 5
ADA
062322

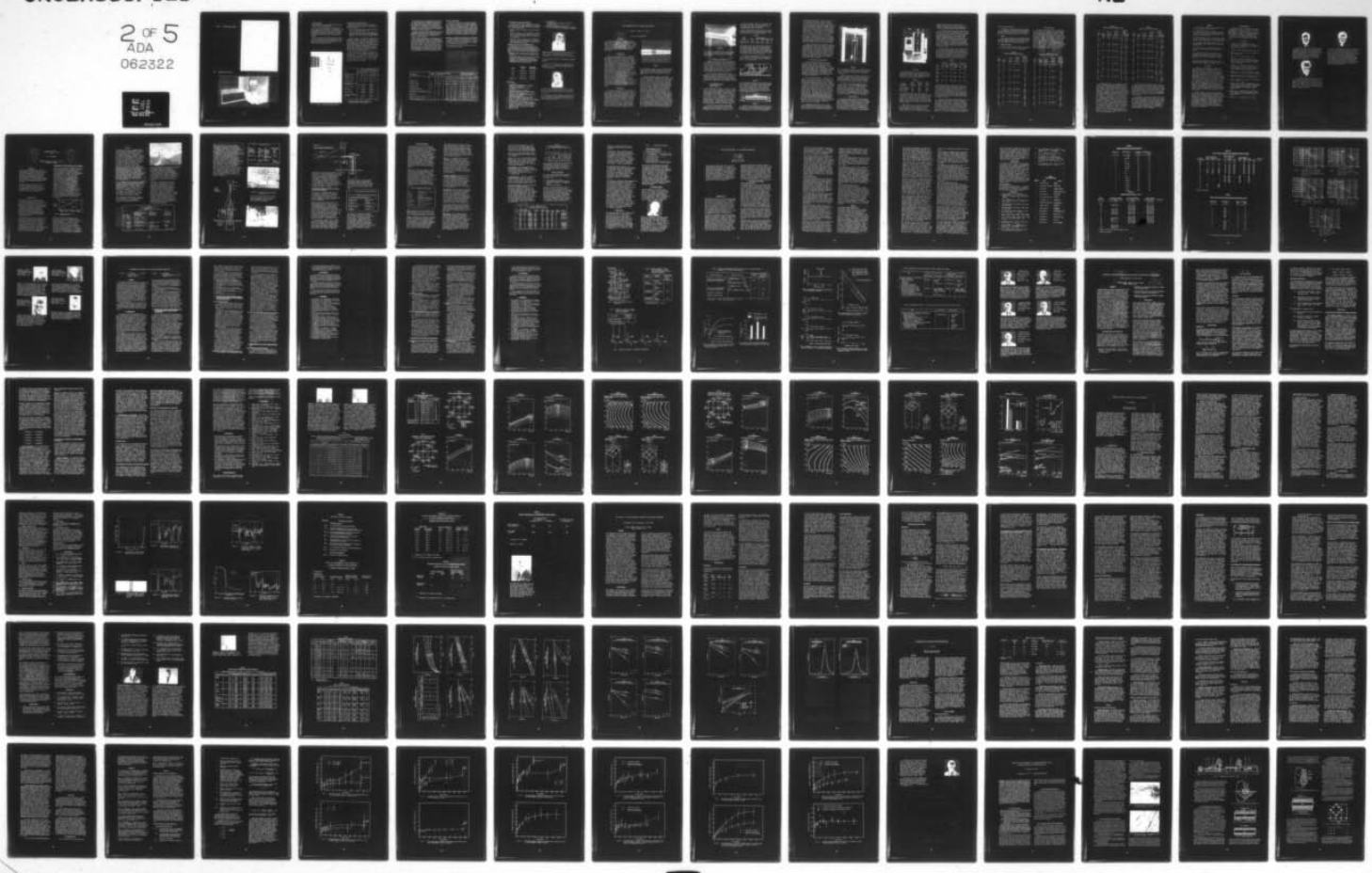


FIG. 6 SINGLE TAKE-UP UNITS

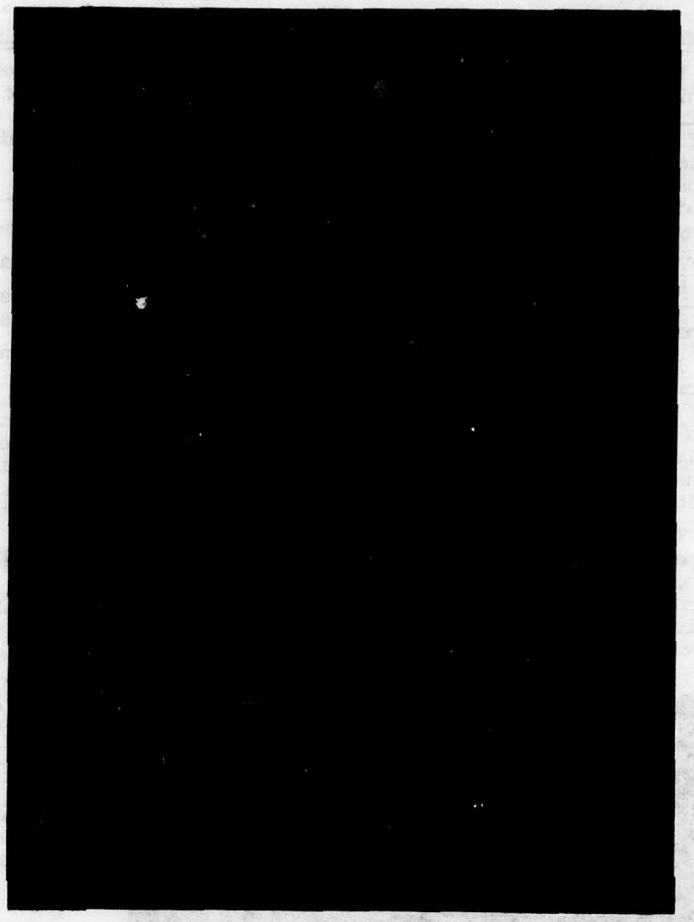
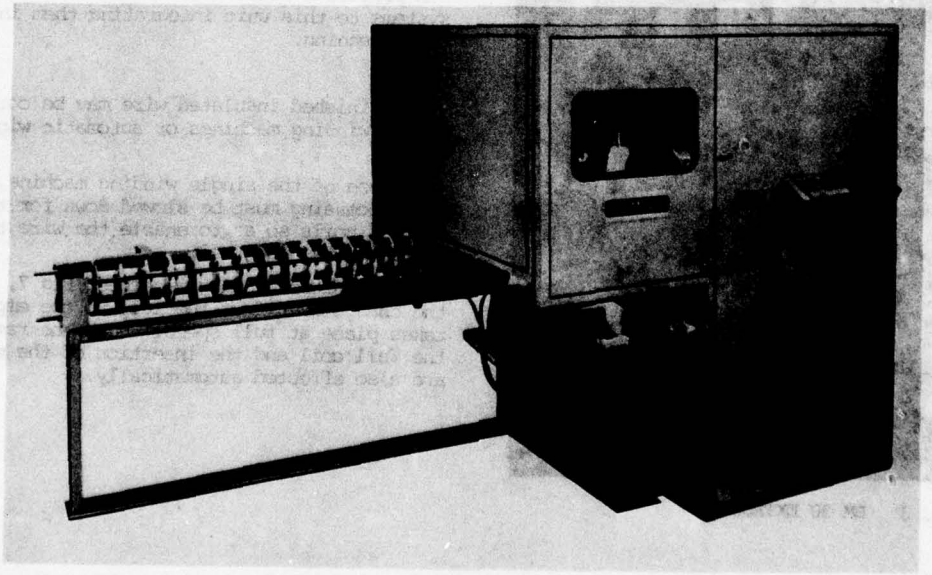


FIG. 7 AUTOMATIC DUAL TAKE-UP



SYSTEM CONTROL

The systems are equipped with DC drives and are fully synchronised.

The control mechanism is designed in such a way that the speed of each wire can be separately controlled. In addition, it is possible with this system to insulate simultaneously four wires with different diameters at different or equal linear speeds.

Should production be changed on one position or the tools require changing, then any one position may be stopped without adversely affecting the operation of the three remaining positions.

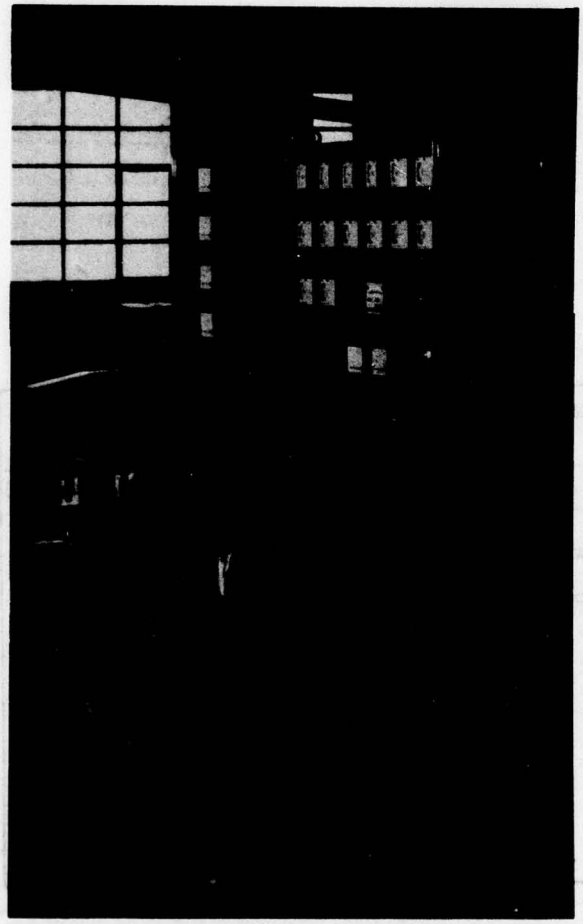


FIG. 8 SYSTEM CONTROL PANEL

MATERIALS AND TEST RESULTS

Regarding materials, the task was to select or develop suitable insulating materials which:

- were suitable for use in the extrusion system described above and
- met the enamelled wire requirements as imposed, for example, by German Standards DIN 46 435, DIN 46 416 and Din 46 453.

A large number of possible products were tested in order to arrive at a choice of materials which promised a maximum level of success. Successful application trials were completed using the insulating material wire resin 350-100 (a terephthalate resin) and further developments - e.g. wire resin 350-101. The final products fulfilled the objectives set and were also economically satisfactory.

The following table shows the results of two successfully completed series of experiments. The property patterns (tested according to DIN 46 453 / DIN 46 416) for extruded enamelled wire (EXOGAN) with conductor diameters of .4 - .6 mm, with an increase of 1 L (grade 1) are in accordance with DIN 46 435.

	Dimension	Trial Series* wire resin 350-100	Trial Series* wire resin 350-101
Adhesion, RT	-	1xd,20% VD	1xd,20% VD
Thermal shock	°C	1xd, 200	1xd, 220
Fusing point	°C	240-260	250-270
Breakdown Voltage Twists, RT	KV	≥ 4.5	≥ 4.5
do. at 155°C	KV	≥ 3	≥ 3
Hardness	-	≥ H	≥ 2 H
do. Solvent	-	≥ HB	≥ H
Tinning capacity, 375°C	S	≤ 3	≤ 2

* Products of BASF Farben + Fasern AG, Unternehmensbereich Lackchemine (9)

With modifications to both materials and extrusion technology, it was possible to achieve for extruded enamelled wire (EXOGAN), essentially, a heat class W 155 according to DIN 46 416 Part 4 and DIN 46 453, together with the additional advantages of very high enamel film flexibility and compliance with the tinning capacity requirements according to DIN 46 416 Part 2.

A number of products showed excellent results in temperature stability tests. Materials were tested which in aged condition at 250°C and over a period of 20 000 hours still possessed 90% of their original properties.

Since the products tested were thermoplastics or border products between thermo- and duroplastics, the main difficulty of course proved to be achieving of the fusing points of heat category W 180 as specified in DIN 46 416 Part 5 and DIN 46 453, i.e. 265°C. Further trials have been initiated in this respect so as to round off the improved properties compared with conventional heat - resistant enamelled wire (flexibility, thermal shock, tinning capacity), with an adequate fusing point.

RESULTS OF PROCESSING

In addition to the actual extrusion experiments and the tests carried out on extruded enamelled wire (EXOGAN), processing trials were completed on relay coils and IEC standard motors. These tests which are being continued with the possible limit diameters resulting from the system design and using materials suitable for obtaining higher fusing points showed the perfect utilisation of extruded enamelled wire (EXOGAN) in accordance with heat category W 155 as specified by DIN 46 416 Part 4.

PROPERTIES OF ENAMELLED WIRE TESTED FOR PROCESSING

For the processing trials, enamelled wire with a diameter of .6 mm and an increase of 1 L (grade 1) in accordance with DIN 46 435 was used in comparison to conventional enamelled wire.

The following table shows selected properties of the enamelled wire tested.

PROPERTIES	DIMENSION	EXTRUDED ENAMELLED WIRE TRIAL SAMPLE			COMPARISON ENAMELLED WIRE ACC. TO DIN 46 416	
		No. 3	No. 6	No. 8	Type V (1)	Type W 155 (2)
Adhesion, RT	-	1xd,5% VD	1xd,5% VD	1xd,0% VD	1xd,0% VD	1xd,0% VD
Thermal shock	°C	1xd,240	1xd,180	1xd,240	1xd,150	1xd,180
Fusing Point	°C	245	270	275	≥ 210	≥ 280
Scraping strength	N	7.4	5.8	7.8	≥ 6.5	≥ 6.5
Breakdown voltage Twists, RT	KV	8.4	4.0	3.6	≥ 2.5	≥ 2.5
Hardness	-	2H	HB	HB	≥ 3H	≥ 3H
Number of faults per 30 m.	-	4	6	13	≤ 15	≤ 15
Tinning capacity, 375°C	S	4	> 20	> 20	≤ 6	-

PROCESSING TRIALS ON RELAY SWITCHES

In comparison with Type V enamelled wire, extruded enamelled wire as described above was used to wind relay switches (BBC), Type SIA 63, and assessed or tested as follows:

- Winding trials: no difference could be found to exist
- Switching cycles, Uc, 3000 switching cycles per hour, 25 and 55°C ambient temperature, a total of 10 millions switching cycles : no change in coil properties
- Heat test, 1.1 Uc, 1000 hrs with switching cycles, 160°C ambient temperature : no failures although some of the coil forms (duroplast material) had become distorted.

PROCESSING TRIALS ON IEC STANDARD MOTORS

In comparison with Type W 155 enamelled wire, extruded enamelled wire as described above was used to wind stators for IEC standard motors (BBC), Type QU 100 L4 AC, and assessed or tested as follows:

- Winding trials : no differences could be found to exist.
- Heating measurement, electrical heating through the influence of current up to failure or breakdown ; The measured breakdown times and temperatures basically reflect the measured breakdown values and fusing points.

SAMPLE	BREAKDOWN TIMES	BREAKDOWN TEMPERATURES
No.3	40-45 min.	200-230°C
No.6	80-100 min.	230-260°C
No.8	20-30 min.	180-220°C
Type W 155	120-140 min.	270-330°C

BIBLIOGRAPHY

1) H.J. Reiser: Herstellung, Eigenschaften und Wickelhalten von Lackdrahten Drahtfachzeitschrift 1975, Vol 4, pp 153-159
2) B.Hinsch, G.Rinne, H.J. Reiser: Experimenteller Vergleich zweier Messverfahren zur Ueberwachung der Emission von Kohlenwasserstoffabgasen an Lackdraht-Einbrennofen Drahtfachzeitschrift 1975, Vol 1,pp6-11
3) DOS 23 51 078 BASF AG,Inventors : Dr. Kovacs, Dr. Marx, Dr. Spoor, Dr.Jung, W.Roschke
4) DOS 26 05 790 Dr. Beck & Co. AG Inventors: Dipl.-Ing. Hansch, Dr.Janssen
5) DP 2135157 Dr. Beck & Co. AG Inventors: Dr. Janssen DOS 2401 027 Dr. Beck & Co.AG Inventors: Dipl.-Ing Hansch, Dr. Janssen
6) DT-OS 2 135 157
7) DT-OS 2 401 027
8) K. Scharfner : Fabrication de fils emailles a l'aide de resines fusibles Le Trefile 1976, Vol 7, pp 127-129
9) OS 26 38 763 Company Maillefer S.A., Dr. Beck & Co. AG Inventors : Dr. Janssen, E. Kertscher



Eberhard Kertscher was born in 1939 and in 1962 was graduated from the Staatliche Fachschule für Betriebstechnik located in Stuttgart, West Germany.

He was employed by Lonza S.A. in Basle as a Process Engineer.

In 1968 he joined Maillefer S.A. where today he is responsible for the process development and the technical marketing.



Bruno Schmidt was born in Mönchen-Gladbach, Federal Republic of Germany, on May 5, 1931. He received the Diploma of Physical Science at the University of Cologne, Germany, in 1955 and took his Degree of Doctor at the same University in 1959.

He is presently employed at Kabel- und Lackdrahtfabriken GmbH (Kabel + Draht), Mannheim, Federal Repbulic of Germany, as Managing Director and is responsible for all technical affairs of cables and wires in this company, which belongs to the German Brown, Boveri Group.

MORE RIGOROUS SHEATHING FOR OUTSIDE PLANT CABLES

J. D. Lawler; R. Rossi; K. J. Virkus

General Cable Corporation

Abstract

In order to minimize incidence of sheath damage during installation and handling of filled cable, various designs have been considered. This paper will deal with one such possibility - namely, a jacket in the mid density range. The paper will also present various tests and test methods as a possible prediction of filled cable handling performance.

Introduction

Over the recent number of years, the design of outside plant telephone cable has changed dramatically, filled cable being the most prominent example. During this evolutionary transition, it became apparent that, in some cases, filled cable behaved quite differently from the unfilled variety, especially during handling at relatively high temperatures. Occasional problems with sheath damage at high temperatures gave emphasis to the fact that in the more demanding direct burial environment, a more rigorous sheath would be of advantage in minimizing installation problems with filled cable. This paper will concern itself with filled cable mechanical characteristics and the means by which these characteristics may give rise to sheath damage problems. In addition, sheath evaluation procedures will be discussed, along with their relative merits. Finally, this paper will present the rationale, along with the raw material criteria, for selecting an intermediate density polyethylene jacket as a sheath improvement for filled telephone cables over the currently employed low-density polyethylene jacket.

Background

Prior to the introduction of filled cable in the telephone system direct buried plant, the predominant cable for such application was Double Sheath Alpeth such as shown in Figure 1. In some cases, copper shielding was employed instead of aluminum to provide added mechanical protection and/or improved corrosion resistance. The two jackets were thought to be necessary to provide a satisfactory impediment to the entrance of moisture into the cable core. With the introduction of adhesive copolymer coated aluminum tape, it became the shielding material of choice in much of the Independent Telephone Industry.

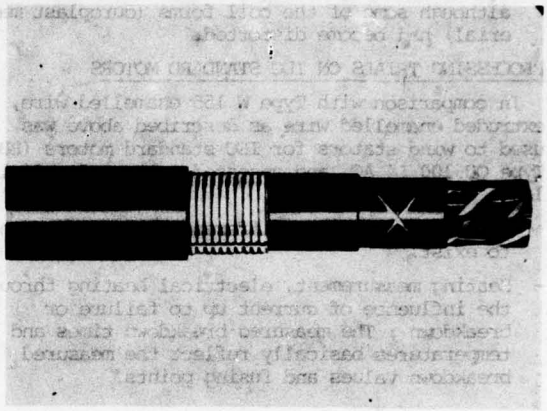


Figure 1

From a handling viewpoint, no major problems were encountered with double jacketed cable, and sheath damage during installation resulted mainly from rough plowing terrain or inadvertent mechanical abuse.

The basic premises for the use of filled cable in direct buried telephone plant have, by now, been well-documented. The many years of experience since its introduction have also verified the projected savings in system maintenance. Since the industry now had a cable with moisture blocking properties, it was determined that an inner jacket on a direct burial cable was an unnecessary cost and was, therefore, eliminated. In a relatively few number of years, however, it became quite apparent that the handling properties of filled cable differed from the air-core variety[1]. In addition to the points raised by Pehrson[2], it has also been shown that, at relatively high temperatures, a filled cable jacket has a greater tendency to move independent of the shield. The mechanism for this phenomenon will be discussed in another section of this paper, but when coupled with rigorous handling, the result can be observed in Figure 2. In a very simplistic manner, then, we can say that sheath buckling may be minimized by restricting the motion of the jacket relative to the shield. This may be accomplished by increasing and maintaining the intimate contact bond between the jacket and

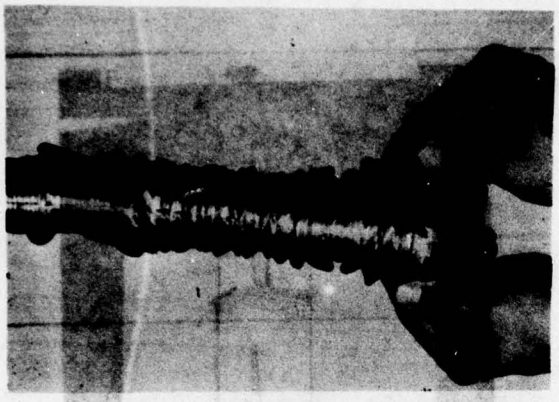


Figure 2

the shield, or by minimizing the tendency of the cable jacket to deform. In this paper, we will restrict ourselves to the latter of the two alternatives.

Sheath Failure Mechanism

Defined very basically, cable jacket buckling occurs when the longitudinal forces external to the jacket exceed the bond strength at the shield/jacket interface, jacket yield strength and the column strength of the jacket. We will define the column strength to be the resistance of the jacket to deformation when subjected to a compressive force parallel to the axis of the cable.

As stated above, sheath buckling occurs primarily at elevated temperatures. Experience has shown[3] that, when cable temperature exceeds 120°F (approximately 49°C), there is greater susceptibility to sheath buckling during rigorous handling. In addition to temperature, other elements involved are:

Cable Thermal History
Plowing Conditions
Sheath Design

As cable temperature increases, a number of events occur. First, the cable components expand, and this includes the filling compound. As an example, the thermal expansion of commonly employed PE/PJ filling compound is in the order of 2% for a temperature increase of 40°C. Depending on the stiffness of the shield, and its thermal expansion, a significant amount of filling compound can "extrude" through the shield overlap area into the shield/jacket interface.[4]. This added material may then be susceptible to softening, acting as a potential lubricant between the shield and cable jacket.

It has also been shown that polyethylene jacket will swell when in contact with filling compounds currently employed.[5] This is due to absorption of oils into the jacket wall. The swelling will normally reach an equilibrium condition after a period of time, but the rate is accelerated by increase in temperature. The following example will illustrate:[6]

A ring of jacket material from a 150 pair 22 AWG cable was immersed in filling compound at various temperatures, with the following results:

Table 1

Aging Temp.	Ring Diameter Orig	1 Day	3 Days	Final	% Chg.
100°F (37.8°C)	1.492"	1.502"	1.505"	1.514"	1.5
140°F (60 °C)	1.493"	1.508"	1.511"	1.530"	2.5

If the cable, then, has been exposed to relatively high temperatures, there may be a possibility of excessive filling compound in the shield/jacket area, and the jacket may have swelled, eliminating the intimate jacket/shield bond. The jacket, then, is relatively free to move over the shield without the physical restriction of the shield.

The cable plow configuration is also a significant factor in the potential for the jacket to buckle. Figure 3 depicts a schematic diagram of a typical plow employed today.



Figure 3

In the path from the pay-off reel to the plow chute exit, the cable is subjected to frictional forces which ultimately contribute to the cable tension as it leaves the plow chute. These frictional forces are a function of cable back tension, jacket material, bending radius and chute design. A simple representation of the various forces involved would be as follows:

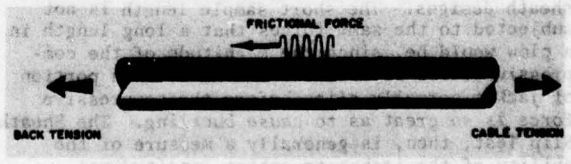


Figure 4

While the forces acting on the cable are much more complex, the representation above will suffice for our discussion. The longitudinal component of the frictional force is, then, the longitudinal

force on the cable sheath, and can be taken to be the approximate difference between the final cable tension and the back tension. The back tension is a function of the cable package weight and frictional forces between the reel and the support shaft and is, therefore, variable. Depending whether manual assistance is provided to the pay-off reel, the back tension may vary between almost zero lb. to over 100 lb. In many plowing configurations, the back tension has a significant effect on final cable tension. In one series of tests, an increase of 30 lb. in back tension resulted in an increase of 250 lb. in cable pull-out tension.[7] The major portion of this increase is reflected in frictional force and is a significant contributor to sheath buckling. Depending on cable plow configuration then, frictional forces anywhere between 10 and 700 lb. may be realized.

If the cable sheath is constructed such that the longitudinal force on the jacket is transmitted to the underlying shield, the combined strength of the sheath will, in most cases, be sufficient to resist buckling. As given above, however, forces within the cable may weaken the intimate contact between the jacket and shield, leaving the jacket alone to withstand the longitudinal forces caused by friction. When these forces exceed the longitudinal compression resistance of the jacket, buckling is a likely result.

Sheath Design Considerations

Because of the possibility that, due to design or internal cable stresses, the jacket alone may have to bear the frictional forces inherent in the cable plowing process, a jacket material was sought, which was sufficiently rugged to withstand these forces. Before proper materials could be selected, however, a meaningful sheath evaluation technique had to be developed. This technique would also have to be translated into raw material requirements which would result in the desired sheath design.

The first consideration was a Sheath Slip Test[8] as illustrated in Figure 5. The test itself consists of pulling the shielded core through an opening which permits the shield to pass through yet is smaller than the jacket diameter. The basis of the test is to determine the lbs.-force required to cause a 12-inch portion of jacket to slip on the shielded core. While the test does in a fashion, simulate the compressive forces on the jacket, it became evident that the results do not easily lend themselves to a comprehensive analysis of possible sheath designs. The short sample length is not subjected to the same forces that a long length in a plow would be, since the magnitude of the compressive force is much less. The 12-inch portion of jacket normally slips before the compressive force is so great as to cause buckling. The Sheath Slip Test, then, is generally a measure of the ability of the jacket to resist longitudinal motion relative to the shield.

As described previously, however, another factor, perhaps more significant, is the column strength of the jacket. The cable jacket buckles when its resistance to compression is overcome.

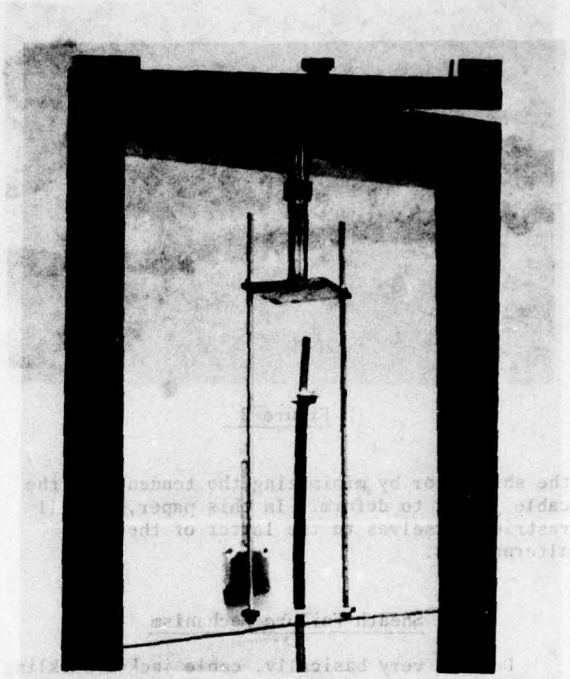


Figure 5

In a very primitive analogy, if the jacket consisted of a rigid metallic tube, it would not buckle even though it could move independently of the underlying shield.

A test was then devised[9] which would recognize the column strength of the jacket, and yet not discriminate against a sheath system utilizing an adhesive bond between the shield and the jacket. An illustration of this test is shown in Figure 6.

The primary difference between the Column Strength Test as shown and the Sheath Slip Test shown in Figure 5 is that the upward movement of the top portion of the jacket is restricted, increasing the longitudinal compressive forces. This more closely simulates a long cable length, since in the cable plowing process jacket buckling occurs when it is pushed back toward the pay-off reel and, ultimately, its motion is restricted.

Jacket Material

Low density, high molecular weight polyethylene jacket material currently employed in outside plant telephone cable sheathing is a tough material and has performed its function admirably. In evaluating the causes of occasional jacket buckling, however, it was determined that some properties of the jacket were quite sensitive to temperature, and significantly in the area over 120°F (48.9°C). Since jacket buckling is primarily a manifestation

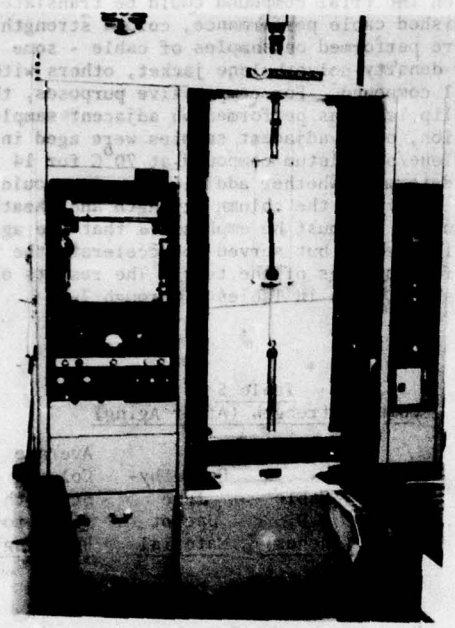


Figure 6

of jacket deformation, it seemed reasonable to study the basic physical characteristics of the jacket material over a broad temperature range. Results for the most commonly employed jacketing material at the time were as follows:[10]

Table 2

Test Temperature	Elongation (Percent)	Tensile Strength (Psi)	Tensile Yield (Psi)
73.4°F (23°C)	720	2620	1400
100 °F (37.8°C)	720	2120	1180
140 °F (60°C)	700	1560	880
158 °F (70°C)	519	950	667

As is readily apparent, while the elongation remained fairly stable, the jacket tensile strength and tensile yield deteriorated approximately 50%. Of particular significance are the tensile yield results, since tensile yield is a measure of the tendency of the jacket to deform. Once the jacket deforms, slippage and resultant buckling are more likely to occur.

In the area of jacket swelling, tests have also shown that currently employed low density polyethylene jacket may increase up to 10% in volume, depending on the temperature or time involved, when exposed to filling and/or flooding compounds employed in filled cable today. This tendency to swell results in jacket diameter increase, with possible resultant deterioration of the intimate contact between jacket and shield.

As a result of these evaluations, another test program was initiated to determine whether a higher density jacket would provide the properties desired. Past experience with notch sensitivity on high density polyethylene jacket for telephone cable mandated a cautious approach, and our initial studies, therefore, centered around a polyethylene jacket material in an intermediate density range. It was hoped that such a material would provide some of the toughness of high density polyethylene without the attendant drawback mentioned previously. As such, we selected a material in the 0.94 - 0.95 final density range.

The initial test results were extremely promising and met our expectations. After satisfying ourselves that notch sensitivity and environmental stress crack resistance paralleled low density polyethylene material, further tests revealed that the primary physical properties were much improved in the temperature range over 120°F (48.9°C). The following comparative results will illustrate:[11]

Table 3

Test Temp	Elongation (%)		Tensile Strength (Psi)		Tensile Yield (Psi)	
	L.D. Poly	Trial Compd	L.D. Poly	Trial Compd	L.D. Poly	Trial Compd
73.4°F (23°C)	720	930	2620	4071	1400	2908
100°F (37.8°C)	720	1067	2120	3957	1180	2370
140°F (60°C)	700	1350	1560	3550	880	1681
158°F (70°C)	519	912	950	2965	667	1160

Of particular interest to note here is that the tensile strength and tensile yield results for the trial compound are significantly better than for low-density polyethylene jacketing material. In fact, the trial compound performs as well at 70°C as the low density polyethylene at room temperature (23°C). This result gains particular significance when coupled with the fact that sheath buckling has not been experienced when cable temperatures were below 120°F (48.9°C).

In the area of filling compound absorption, the trial compound exhibited 50% less weight increase and 45% less volume change. With less swelling, the jacket will have less of a tendency to increase in diameter, thereby better maintaining an intimate shield/jacket interface. An interesting by-product of the reduced oil absorption into the jacket is that, after absorption equilibrium, the trial compound lost little of its original physical properties, whereas the low density polyethylene lost 40% of its

original 70°C elongation.[12]

In addition to the positive results obtained above, following is a brief listing of other properties which bear on the ability of the sheath to withstand rugged handling during installation:[11]

A) Creep

Creep can be defined as the permanent deformation of a material under stress. Test results on the trial compound indicate insignificant tensile creep after 1000 hours under 250 psi load.

B) Notch Resistance

The trial compound exhibited the same excellent notch resistance as low density polyethylene.

Cable Evaluation

In order to determine whether the excellent results on the trial compound could be translated into finished cable performance, column strength tests were performed on samples of cable - some with low density polyethylene jacket, others with the trial compound. For comparative purposes, the Sheath Slip Test was performed on adjacent samples. In addition, other adjacent samples were aged in polyethylene/petrolatum compound at 70°C for 14 days to determine whether additional aging would have any effect on the column strength and sheath slip results. It must be emphasized that the aging process is severe, but served to accelerate the effects for purposes of the test. The results of the tests are given in Tables 4 through 7.

Table 4
Column Strength (Before Aging)

Test Temp (°C)	Sheath Type	Cable O.D. (Inches)	Polyethylene Jacket Material	Average Column Strength (Lbs. to Buckling)
23	FPA	0.560	Low Density	140
50	"	"	" "	89
60	"	"	" "	80
70	"	"	" "	66
23	ASP	0.640	Low Density	165
50	"	"	" "	136
60	"	"	" "	115
70	"	"	" "	86
23	ASP	1.01	Low Density	267
50	"	"	" "	194
60	"	"	" "	138
70	"	"	" "	114
23	ASP	0.940	Mid Density	360
50	"	"	" "	292
60	"	"	" "	248
70	"	"	" "	210
23	ASP	1.250	Low Density	362
50	"	"	" "	283
60	"	"	" "	194
70	"	"	" "	163
23	ASP	1.250	Mid Density	395
50	"	"	" "	338
60	"	"	" "	286
70	"	"	" "	240
23	FPA	1.230	Low Density	226
50	"	"	" "	182
60	"	"	" "	159
70	"	"	" "	101

Table 5
Column Strength (After Aging)

Test Temp (°C)	Sheath Type	Cable O.D. (Inches)	Polyethylene Jacket Material	Average Column Strength (Lbs. to Buckling)
23	FPA	0.560	Low Density	128
50	"	"	" "	73
60	"	"	" "	81
70	"	"	" "	82
23	ASP	0.640	Low Density	162
50	"	"	" "	128
60	"	"	" "	110
70	"	"	" "	89
23	ASP	1.01	Low Density	245
50	"	"	" "	171
60	"	"	" "	140
70	"	"	" "	150
23	ASP	0.940	Mid Density	383
50	"	"	" "	---
60	"	"	" "	264
70	"	"	" "	203
23	ASP	1.250	Low Density	371
50	"	"	" "	223
60	"	"	" "	173
70	"	"	" "	160
23	ASP	1.250	Mid Density	439
50	"	"	" "	349
60	"	"	" "	269
70	"	"	" "	254
23	FPA	1.230	Low Density	215
50	"	"	" "	135
60	"	"	" "	114
70	"	"	" "	136

Table 6
Sheath Slip Test (Before Aging)

Test Temp (°C)	Sheath Type	Shield O.D. (Inches)	Polyethylene Jacket Material	Average Sheath Slip Lbs	Average Sheath Slip Lbs/Inch Circumf.
23	FPA	0.460	Low Density	115	79.6
50	"	"	" "	89	61.6
60	"	"	" "	66	45.7
70	"	"	" "	39	30.0
23	ASP	0.480	Low Density	40	26.5
50	"	"	" "	16	10.6
60	"	"	" "	10	6.63
70	"	"	" "	10	6.63
23	ASP	0.885	Low Density	184	66.2
50	"	"	" "	106	38.1
60	"	"	" "	48	17.3
70	"	"	" "	39	14.0
23	ASP	0.820	Mid Density	144	55.9
50	"	"	" "	113	43.9
60	"	"	" "	85	33.0
70	"	"	" "	68	26.4
23	ASP	1.09	Low Density	88	25.7
50	"	"	" "	63	18.4
60	"	"	" "	47	13.7
70	"	"	" "	41	12.0
23	ASP	1.14	Mid Density	212	59.2
50	"	"	" "	158	44.1
60	"	"	" "	96	26.8
70	"	"	" "	92	25.7
23	FPA	1.09	Low Density	60	17.5
50	"	"	" "	37	10.8
60	"	"	" "	21	6.13
70	"	"	" "	19	5.54

Table 7
Sheath Slip Test (After Aging)

Test Temp (°C)	Sheath Type	Shield O.D. (Inches)	Polyethylene Jacket Material	Average Sheath Slip Lbs	Average Sheath Slip Lbs/Inch Circumf.
23	FPA	0.460	Low Density	5	3.46
50	"	"	" "	<5	<3.46
60	"	"	" "	<5	<3.46
70	"	"	" "	<5	<3.46
23	ASP	0.480	Low Density	11	7.29
50	"	"	" "	13	8.62
60	"	"	" "	<5	<3.32
70	"	"	" "	<5	<3.32
23	ASP	0.885	Low Density	18	6.47
50	"	"	" "	6.4	2.30
60	"	"	" "	8	2.88
70	"	"	" "	10	3.60
23	ASP	0.820	Mid Density	128	49.7
50	"	"	" "	---	----
60	"	"	" "	52	20.2
70	"	"	" "	74	28.7
23	ASP	1.09	Low Density	42	12.3
50	"	"	" "	28	8.18
60	"	"	" "	23	6.72
70	"	"	" "	16	4.67
23	ASP	1.14	Mid Density	166	46.4
50	"	"	" "	102	28.5
60	"	"	" "	100	27.9
70	"	"	" "	88	24.6
23	FPA	1.09	Low Density	17	4.96
50	"	"	" "	11	3.21
60	"	"	" "	<5	<1.46
70	"	"	" "	<5	<1.46

Reviewing the data, it is apparent from Table 4 that the column strength for the Mid-Density jacket is significantly higher than for Low Density Polyethylene. In the upper temperature regions, where field problems are more likely to occur, the higher column strength results are of even greater importance. In Table 5, the column strength results for the aged samples are basically similar to unaged. Both these results were predicted by tests on the raw material. In the first case, tensile yield for Mid-Density Polyethylene was much better than for Low Density Polyethylene. This is reflected in column strength. In the second case, it was shown that 70°C aging in filling compound produced no deleterious effect on Mid-Density Polyethylene, nor on the tensile strength and tensile yield for Low Density Polyethylene. The ultimate elongation for Low Density Polyethylene, however, decreased by 40% from its unaged value. While this is not reflected in the column strength test, one may predict that, once jacket buckling commences, rupture of the cable sheath is more probable for the Low Density Polyethylene jacket.

From the slip test results in Table 6 and 7, the wide variation in jacket/shield bond is apparent. The aged results show yet further reduction in the shield/jacket interface bond, yet the column strength did not deteriorate. It is felt that the slip test results may be a good indicator of initial bonding between shield and jacket, however, aging phenomena make this test an unreliable indicator of possible field problems.

The results of the column strength test become meaningful when related to actual field conditions. For a given thickness of jacket, the column strength will be fairly consistent for a given material at a given temperature and is, therefore, fairly predictable on a worst case basis. With a knowledge of the friction forces developed during plowing and, using the column strength results, a cable for minimum damage risk may be designed.

Summary

Based on the results of the evaluations, one may draw some general conclusions.

a) Sheath buckling, in filled cable, is a manifestation of excessive friction within the cable path in the plow; of sheath design weaknesses; of excessive cable temperature.

b) Unfilled cable is not as susceptible to sheath buckling as filled cable due to the greater bond between sheath components and lack of jacket swelling.

c) The potential for sheath buckling increases significantly as cable temperature increases over 120°F (48.9°C).

d) The potential for sheath buckling may be reduced by increasing the column strength of the sheath.

e) The column strength of the sheath may be improved by increasing the bond between sheath components (which may deteriorate with time), or by increasing the column strength of the jacket alone.

f) The column strength of the jacket may be improved by increasing its thickness, or by increasing its tensile strength and tensile yield.

Conclusion

Necessity is, of course, the proverbial mother of invention. The impetus, then, for our paper grew out of field experience with filled cable under specific conditions, and attempts to solve existing problems. We have presented here, hopefully, an analysis of one such problem and a highly probable solution. Within the cable handling environment, however, there are a number of factors which bear significantly on the ultimate success of an installation. Reduction of cable friction and cable temperature also play a major role. Lacking full control of the friction to which a cable is subjected, or the temperature, our approach was to improve cable ruggedness. Again, there may be a number of approaches to improving cable ruggedness. In light of field experience and laboratory studies, however, the more immediate solution lay with the cable jacket.

In this area, our results indicate definite relationships between polyethylene compound density and ability to withstand rigors of handling. This, however, may not be the significant design criteria to consider. Our studies indicate that, from a performance viewpoint, the jacket column strength is of primary importance, with polyethylene compound tensile strength and tensile yield to be a good barometer of success in this endeavor. It goes without saying that this must be achieved without adversely affecting other important cable performance requirements.

Acknowledgements

The authors wish to acknowledge the valuable contributions of a number of people in bringing this paper to a successful conclusion. For the many long hours spent in preparing and testing the cable samples, we express our deep gratitude to E. R. Babulski, H. Gongora, K. Korbelak and J. Peveler. We also express our appreciation to Ms. D. Tunnell for the preparation of the manuscript.

References

1. Pehrson, V. W., "Engineering for Cable Installation", Proceedings, 24th International Wire and Cable Symposium, pp. 260 - 269. Cherry Hill, N.J. 1975.

2. Rossi, R., Field Evaluation Report, July 1976.

3. Goodell, R., Field Trial Notes, San Angelo, Texas, August 1976.

4. Pehrson, V. W., Notes, December 1976.

5. Bostwick, R., "Effect of Petroleum Jelly Filler on Low-Density Polyethylene Telephone Cable Jacketing", Kabelitems No. 146, Union Carbide Corporation.

6. Virkus, K. J., "Swelling of Low Density Polyethylene Jacket After Contact with Cable Filling Compound," General Cable Corporation Research Report 34661-C, August 1976.

7. Maguire, C. V., "ASP Cable Evaluation, Plowing Characteristics", Internal Report, August 1976.

8. Specification, REA PE-39, Appendix II, Para. 2.5, "Jacket Slip Strength Test", November 1976.

9. Kaye, J., Maguire, C. V., "ASP Cable Evaluation", Internal Report, March 1977.

10. Lang, R., "The Influence of Temperature on the Yield Strength, Tensile Strength and Elongation of LDPE Telephone Cable Jackets." General Cable Corporation Research Report 34669-C, September 1976.

11. Virkus, K. J., "Medium Density Polyethylene Jacket Compound, Evaluation Summary", General Cable Corporation Research Report 34869, August 1977.

12. Virkus, K. J., Research Notes, July 1978.



Richard Rossi has been with General Cable Corporation since 1963. Since then he has had assignments in the Product Design and Product Engineering Departments. He is currently Senior Application Engineer in the Communications Products Operation, Application Engineering Department, concentrating on outside plant telephone cable design. Mr. Rossi has been a member of IEEE since 1972.



K. J. Virkus, a native of Estonia, received a B.S. Degree in Chemical Engineering from Worcester Polytechnic Institute in 1961. He has worked for a number of wire and cable companies, and began his employment at General Cable Corporation in 1974. He is currently Research Group Manager at the General Cable Corporation Research Center in Union, New Jersey.



John D. Lawler has been on the R & D Staff of the General Cable Corporation Research Center since 1967. Since joining the Research Center he has been involved primarily in outside plant cable and cable accessories, holding several patents in this area. More recently he has assumed product responsibilities for filled telephone cable and cable hardware. Mr. Lawler attended both Staten Island Community College and the County College of Morris County and is currently attending Fairleigh Dickenson University. Prior to joining General Cable Corporation, he was employed by the Western Electric Company.

LARGE SCALE, DYNAMIC CABLE TESTING

BY

E.A. FALQUERO

NORTHERN TELECOM CANADA LIMITED
MONTREAL, QUEBEC

ABSTRACT

Large scale dynamic cable testing was created to bridge the gap between the laboratory and a field installation. In these tests cable are pulled around pulleys or through and under controlled forward and back tensions. A conditioning chamber houses the give-up and permits testing over the temperature range - 50 to 50°C.

Though primarily proving test for new cable designs the facility is also a valuable development and troubleshooting device by virtue of its versatility and the analytical nature of the data generated.

INTRODUCTION

The suitability of a cable design for handling and installation is only fully proven by field experience. Usage over a period of time will expose a cable to normal and abnormal conditions, revealing any weaknesses in design or material selection. But before marketing a product, or even releasing prototypes for field trial, the manufacturer must establish through experimentation that the new product will perform satisfactorily.

A comparison to existing, time-proven designs is useful. But this is not enough, particularly where novel materials are involved. A sheath is a composite unit and the ensuing synergistic effects do not favour extrapolation. Thus, to bridge the gap between design and installation performance the Large Scale, Dynamic Cable Testing Facility, generally known as the RIG, was developed.

DEVELOPMENT OF MECHANICAL CABLE TESTING

Cable is a material intensive product and materials testing plays a critical role in research and manufacture. In developing new designs laboratory testing permits a rapid and inexpensive optimization of material selection. Such tests are wide ranging and comprehensive, e.g. heat ageing, creep, stress cracking sensitivity, low temperature properties, and, of course, tensile and elongation tests. However, they do not help predict with great accuracy the behaviour of a composite structure. Material tests can be backed by static tests on a finished cable, such as pressurization trials, cold bending, impact etc. These generate a much better appreciation of the cable's potential performance but the gap between this characterization and installation conditions is still large, as indicated schematically in Figure 1.

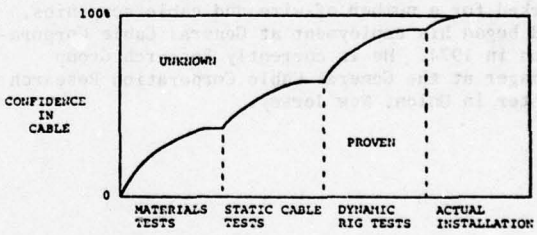


FIGURE 1: DIAGRAMATIC REPRESENTATION OF THE ACCUMULATION OF DATA

The RIG test was developed to fill this gap. Cables at temperatures ranging from -50 to 50°C can be pulled around sheaves or through a curved guide at speeds up to 800 ft./min. under controlled forward and back tensions. The test cannot reproduce all the unusual hazards which might occur in an installation. In contrast many relevant parameters are measured and the test is considered a dependable indicator of installation performance.

THE RIG

In the early 1970's a comprehensive investigation was conducted with the aim of solving a serious problem of low temperature jacket fractures in Stalpeth cables. Extensive laboratory tests on homopolymers, blends, and various copolymers of polyethylene had lead to the selection of a particular copolymer LDPE with excellent low temperature properties for use in cable. However, jacket failures in cold installation persisted. Impact and bend tests were then performed on cables using different flooding compounds. Such tests gave some indication of the importance of flooding compound on the jacket failure mechanism but it was only after dynamic tests simulating installation conditions that the mechanism was fully understood. These tests were performed on the RIG, which had been specifically constructed for this purpose.

In its embryonic state the RIG comprised a large, angle iron frame supporting two large pulleys, over which a cable could be pulled. Figure 2 shows the device at the La Tuque test site. Cables were pulled by trucks and winches and shipping reels were the give-ups. Test temperature was determined by the weather, to which the several men needed to operate the trials were equally exposed.

The La Tuque site had been chosen for those tests as the most reliably cold location at an accessible distance to the Lachine Plant.



FIGURE 2:
THE RIG AT LA TUQUE

Though rudimentary by current standards, the tests lead to a solution of the sheath cracking problem and proved the value of the apparatus. In the course of the investigation a large number of cables of different constructions and using a variety of materials were tested. Performance was judged by visual examination of the type and severity of sheath damage.

The cause of the problem proved to be the interaction of the cold temperature brittleness of the flooding compound and the notch sensitivity of the polyethylene, illustrating the complex effects which can occur in a composite structure. This is illustrated by the data shown in Table I. Black flooding compound resulted in jacket cracks at -30°C, and at -40°C the jacket shattering was dramatic. No cracks were observed with white compound, except at excessively high speeds at -35°C, a performance which was easily matched by the Sealpeth construction.

TABLE I
SUMMARY OF STRAIGHT PAY-OUT DATA,
LA TUQUE TRIALS
CABLE DIAMETER 3 IN.

TEMP °C	SPEED ft/min	STALPETH BLACK (CONVENTIONAL) FLOODING CPD. LDPE JACKET	STALPETH WHITE (LOW TEMP.) FLOODING CPD. LDPE JACKET	SEALPETH (PULP CORE) MDPE JACKET
-20	600-850	Buckles; no cracks	—	—
-25	0 - 250	No damage	—	—
-30	0 - 250	Buckles; cracks	—	No damage
	350-500	No buckles; cracks	Buckles; no cracks	Small kinks
	600-850	—	No damage	—
-35	0 - 250	Buckles; cracks	No damage	Kinks
	350-500	—	Buckles; no cracks	Kinks
	600-850	—	Buckles; cracks	—
-40	350-500	Jacket shatters	Buckles; no cracks	Kinks, no cracks

The La Tuque trials also showed that open field testing was uncomfortable, uneconomic and difficult to schedule because of the dependence on the weather. Thus the RIG was installed at Lachine and several refinements made, as shown schematically in Figure 3. The cables are now given-off from an environmental chamber so that tests could be made at -50°C one day and 50° a couple of days later with no interference from the weather. A wire rope attached to a winch pulls the cable out of the chamber, around the pulleys and onto the lawn. Only an operator and a safety-lookout man are now needed. During a test tension, speed, and sidewall pressure are recorded on a chart for later analysis. The measurable parameters and a typical set of data are shown in Table II. Several aspects of the facility are shown in Figure 4.

TABLE II TEST CAPABILITY OF RIG

Parameter	Range	Type	Typical Stalpeth 1100 pr. 22 Ga.
Cable Diameter	3-1/4" Max.	Independent	3.02 in.
Cable Length	120 ft Max.	Independent	120 ft.
Temperature	-50 to 50°C	Independent	-40°C
Pulley Diameter	40 in.	Independent	40 in.
Back Tension	5000 lbs. Max.	Generally Independent	960 lbs.
Speed	800 fpm Max.	May be	400 fpm
Forward Tension	10,000 lbs. Max.	independent or dependent, also affected by cable size	2070 lbs.
Sidewall Pressure	2000 lbs Max	Dependent	N.A.
Condition	Visual assesment	Dependent	No Damage, occasional small buckles

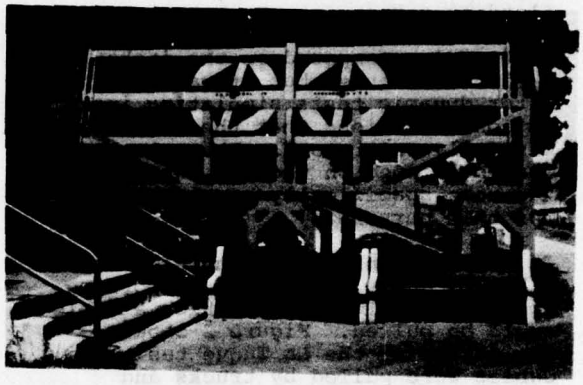


FIGURE 4: The RIG at the Lachine installation.

Upper photograph shows main frame.

Lower photograph shows environmental chamber, controls and refrigeration equipment.

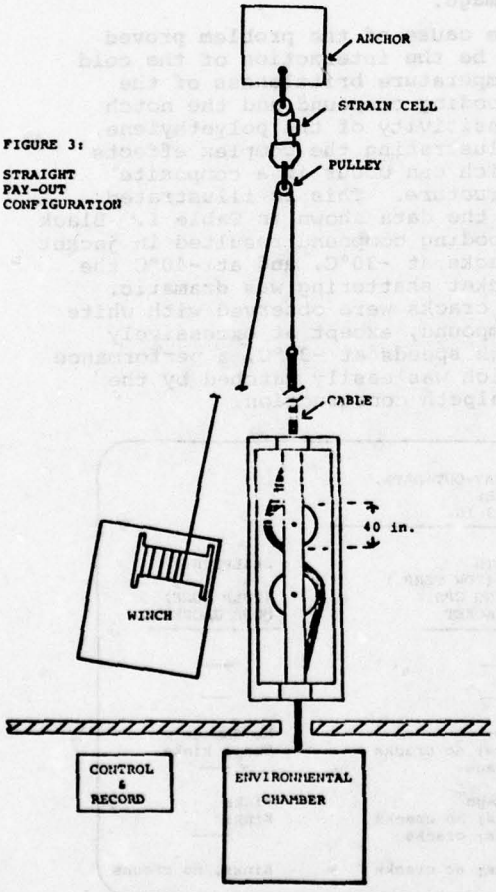


FIGURE 3:

STRAIGHT PAY-OUT CONFIGURATION

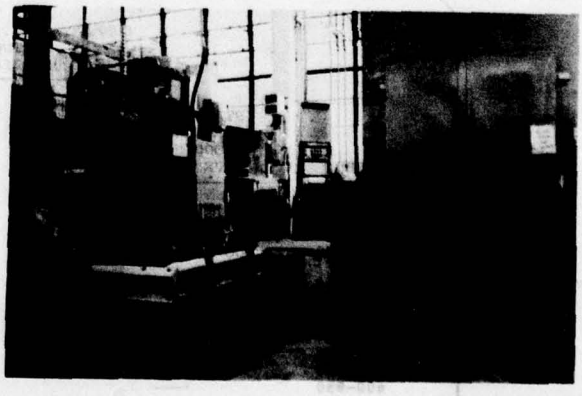
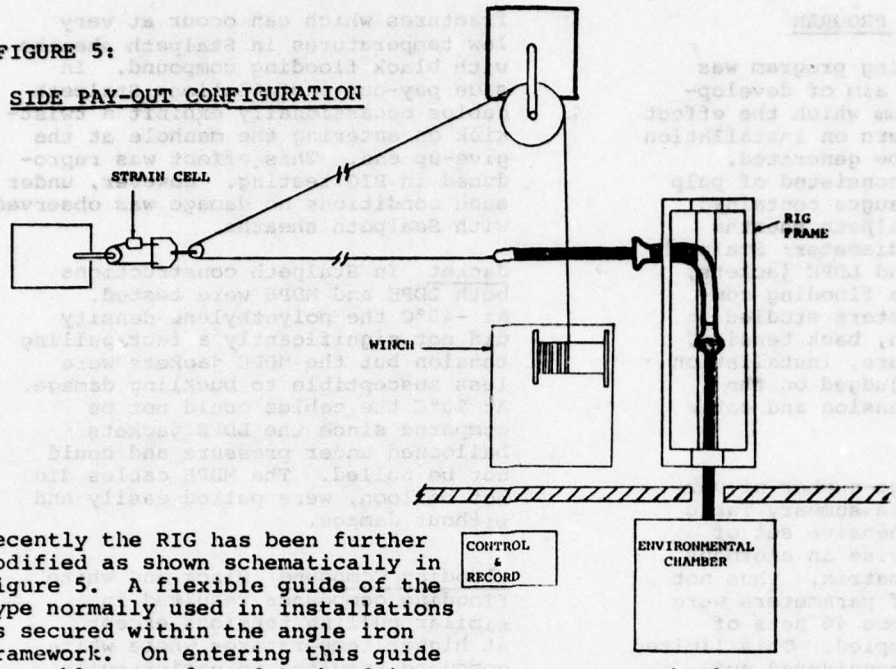


FIGURE 5:

SIDE PAY-OUT CONFIGURATION



Recently the RIG has been further modified as shown schematically in Figure 5. A flexible guide of the type normally used in installations is secured within the angle iron framework. On entering this guide the cables are forced to bend in a plane approximately at right angles to the plane of the give-up, which is geometrically a very close simulation of the side pay-out configuration frequently used in Canada.

CORRELATION BETWEEN MATERIAL, STATIC AND RIG TEST RESULTS

In Figure 1, reference was made to the concept of building up data by a sequence of tests i.e. material, static cable, and RIG tests. As in any sequence or chain, correlation between different stages can and must be expected.

Material data and static cable data were compared on the basis of a bending beam model. Stress analysis techniques permit the derivation of a complex bending beam equation based on the dimensions of all the components and material characterization data. Alternately, the cable may be bent and the required load measured. Bending load ratios of two cables are shown in Table III: the correlation between calculated and measured values is extremely close.

In an analogous manner, static cable and dynamic RIG results may be compared. In passing over the pulleys in the RIG a cable is alternately bent and straightened. Using static test results for cable bending and applying stress analysis the work required to pass a cable through the pulleys may be calculated. Examples of this, compared to the work performed by the winch during a RIG test, is shown in Table III. Again very close correlation was found.

TABLE III COMPARISON OF MATERIAL AND STATIC CABLE RESULTS

Cables Compared: Sealpeth 1100 pr. 22 ga. pulp 2.77 in. dia.
Stalpeth 1800 pr. 24 ga. pulp 2.99 in. dia.

F = Force to bend end of 18 in. cable by 6 in.
W = Work required to pass a cable through RIG.

FROM MATERIAL TESTS AND STRESS ANALYSIS	FROM DIRECT STATIC MEASUREMENT
$\frac{F\ (Sealpeth)}{F\ (Stalpeth)} = 2.15$	$\frac{F\ (Sealpeth)}{F\ (Stalpeth)} = 2.2$
FROM DIRECT STATIC DATA AND STRESS ANALYSIS	**FROM RIG DATA, I.E. TENSION X SPEED**
$\frac{W\ (Sealpeth)}{W\ (Stalpeth)} = 1.497$	$\frac{W\ (Sealpeth)}{W\ (Stalpeth)} = 1.520$

The practice of comparing ratios was chosen in order to minimize errors from assumptions or approximations made in stress analysis calculations. Nonetheless, the correlation between sets of data is compelling, indicating that mathematical modelling techniques may be applicable to mechanical cable testing. Perhaps in the future a complete mathematical stress model of an installation may be possible.

RIG TEST PROGRAM

A large cable testing program was initiated with the aim of developing a data base from which the effect of various parameters on installation performance could be generated. The cables tested consisted of pulp cores of various gauges contained in Stalpeth and Sealpeth sheaths about 3 inches in diameter; Stalpeth cables used MDPE and LDPE jackets, and black and white flooding compounds. The parameters studied were pressurization, back tension, speed and temperature, installation performance being judged on the basis of pulling tension and cable damage.

Because of the large number of variables involved (see summary Table IV) a fully comprehensive set of results would comprise an enormous multi-dimensional matrix. Thus not all combinations of parameters were tested; instead, some 40 sets of conditions were sampled. This limited data base was not considered sufficient for a full mathematical modelling, but it adequately identified general trends, as described below.

TABLE IV Variables in Data Base Study

Core	Pulp 300 pr 26 ga; 1800 pr 24 ga; 110 pr 22 ga
Sheath	Stalpeth, Sealpeth
Jacket	LDPE; MDPE
Flooding	Conventional black and low temperature white compounds
Orientation	Straight and side pay-out.
Temperature	-40°C to +50°C
Speed	200 ft./min. to 400 ft. min.
Back Tension	600 lbs. to 1000 lbs.
Pressurization	0 and 15 psig

Core The pair count and gauges used were selected to give similar cable diameters and the type of core used had no perceptible effect on pulling.

Sheath Stalpeth and Sealpeth sheaths resulted in similar pulling tensions both in straight and side pay-out configurations. In straight pay-out Stalpeth with white flooding compound and Sealpeth are considered equivalent: both exhibit small kinks when tested at -40°C but do not suffer from the dramatic sheath fractures which can occur at very low temperatures in Stalpeth sheaths with black flooding compound. In side pay-out installations Stalpeth cables occassionally exhibit a twist-kink on entering the manhole at the give-up end. This effect was reproduced in RIG testing. However, under such conditions no damage was observed with Sealpeth sheaths.

Jacket In Stalpeth constructions both LDPE and MDPE were tested. At -40°C the polyethylene density did not significantly affect pulling tension but the MDPE jackets were less susceptible to buckling damage. At 50°C the cables could not be compared since the LDPE jackets ballooned under pressure and could not be pulled. The MDPE cables did not balloon, were pulled easily and without damage.

Flooding Compound Black and white flooding compounds resulted in similar pulling tensions except at higher temperatures where white compound resulted in easier pulls. From the point of view of damage the effect of flooding compound is very pronounced, and this is further discussed under the heading of Temperature.

Orientation Both straight and side pay-out installation were simulated on the RIG. The pulling tensions measured were generally 2000 to 3000 lbs. for straight pay-out and 1000 to 2000 lbs. for side pay-out. It should be noted that orientations only simulate field conditions so a comparison of straight and side results may not truly reflect a comparison under field conditions.

Where sheath damage occured buckles (perpendicular to cable axis) were observed for straight pay-out and twisting-kinks (buckles 45° to cable axis) seen in the case of side pay-out.

Temperature In straight pay-out the pulling tension decreased as temperature increased, as might be expected; pulling tension at 50°C was about half that experienced at sub-zero temperatures. However little change was seen over the range 0 to -40°C. In contrast the trend was reversed in side pay-out, but this effect may be due to condensation on the cable exiting the environmental chamber and acting as a lubricant.

Twist-kinks were observed in side pay-out on all Stalpeth cables at -30°C but at -20°C and higher temperatures were only observed on some cables with white flooding compound.

At -40°C, as mentioned above, shattered jackets occur with black flooding compound.

Speed Most of the testing was carried out at near 300 ft./min. For large differences (eg. 200 vs. 400 ft./min.) higher pulling tensions and more damage occured at the faster speeds, as might be expected.

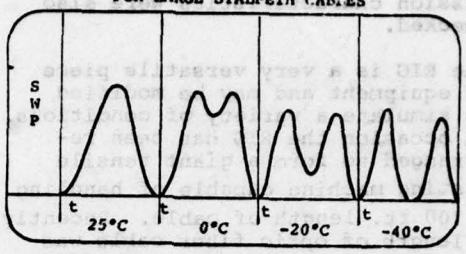
Back Tension This parameter had remarkably little systematic effect on pulling tension. The ratio Pulling Tension/Back Tension was 2 or 3 in straight pull-out and 1.5 or 2 in side pay-out.

Pressurization This had no significant effect on pulling tension. However, under marginal damage conditions pressurized cables performed better than unpressurized cables.

Side Wall Pressure This was measured by a strain cell embedded in a pulley; a continuous trace of the sidewall pressure on the cable as it rounded the pulley was obtained. At high temperatures this was a single pulse (shown schematically in Figure 6) but as the temperature fell the pulse divided into two. Thus, the shape of the pulse gave an indication of stiffness and the possibility of cable damage could be judged on the pressure at the valley compared to the peaks.

FIGURE: 6

SCHEMATIC OF SIDE WALL PRESSURE PULSES FOR LARGE STALPETH CABLES



These general conclusions were derived from several tables of data such as that shown in Table V, which also illustrates the large amount of information available from current RIG tests.

USES OF THE RIG

The RIG has many functions and uses, but most fall within four general headings, viz.

1. Final test of a cable
2. Development test for materials
3. Versatile hardware for special tests
4. Fault investigation

Perhaps the most important use of the RIG is that of a final test for any new cable design. All recent designs such as *Hi-Fill Pulp*, *Dri-Fill* and Optic Fiber cables have been pulled through the RIG under severe temperature and tension conditions. The physical performance of the cable was compared to that of existing designs to verify their ability to withstand normal installation

TABLE V
SUMMARY OF SIDE PAY-OUT DATA
TAKEN FROM CONTEMPORARY (1978) DATA

TEMP. °C	PAIR COUNT	GAUGE AWG	SHEATH	FLOODING COMPOUND	PULLING TENSION Lbs.	BACK TENSION Lbs.	SPEED ft/min	PRESSURE psig	COMMENTS
-30	3000	26	Stalpeth	White	1500	600	300	0	Twist-Kink
	3000	26	Stalpeth	White	1000	600	300	15	Twist-Kink
	1800	24	Stalpeth	Black	1000	750	250	0	Twist-Kink
	1100	22	Stalpeth	Black	1100	1000	200	0	Cracks
-20	3000	26	Stalpeth	White	1100	900	300	0	Twist-Kink
	3000	26	Stalpeth	White	1400	850	350	15	No Damage
	3000	26	Stalpeth	Black	1800	1100	320	0	" "
	1800	24	Stalpeth	Black	1000	700	260	0	" "
	1100	22	Stalpeth	Black	1400	800	320	0	" "
+10	3000	26	Stalpeth	White	1500	600	300	15	Minor T-K
	3000	26	Stalpeth	White	1700	600	230	0	Twist-Kink
	3000	26	Stalpeth	White	1700	1000	360	0	No Damage
	1800	24	Stalpeth	Black	1750	700	330	0	No Damage
	1100	22	Stalpeth	Black	1800	920	300	0	No Damage
	1100	22	Sealpeth	NIL	1200	800	250	0	No Damage

handling. Electrical and transmission characteristics were also checked.

The RIG is a very versatile piece of equipment and may be modified to simulate a variety of conditions. On occasion the RIG has been rearranged to form a giant tensile testing machine capable of handling a 300 ft. length of cable. Recently a length of optic fiber cable was thus tested in tension to measure the effect of load on attenuation.

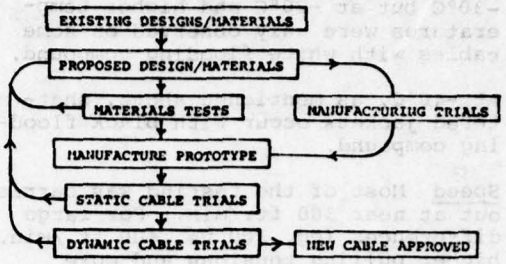
In developing new materials or designs the RIG testing of prototypes is extremely useful in optimizing a selection. The data generated permits an analysis of the cable performance far beyond that possible by simple visual examination. An example of this is the sidewall pressure measurement mentioned earlier.

Also when an existing design experiences installation problems in the field the RIG may be used to simulate the conditions leading to the problem, and thus help provide a better understanding of the process involved. In particular, there have been occasional reports of a twist-kink fault in Stalpeth cables, forming at the give-up end during side pay-out installation. Using the simulated side pay-out as described before these faults may be reproduced. This matter is still under study and no fully acceptable solution has yet been identified. The incidence of twist-kink faults may be particularly prevalent in the Canadian environment due to the frequent use of side pay-out and the necessity for using a low temperature grade of flooding compound.

CONCLUSION

Material and static cable tests play an important part in cable manufacture but it is the simulated installation or RIG test that is the final reference regarding the suitability of the cable. The multiple parameters accumulated in a RIG test also permit an analytical approach and appears to be amenable to mathematical modelling techniques. In developing a new cable all type of tests are inter-related as shown in Figure 7.

FIGURE 7: DEVELOPMENT OF A NEW CABLE



Regarding installation performance of existing designs several general conclusions may be made. For low temperature application white compound is essential to avoid sheath cracking problem; however in side pay-out such a compound is more likely to cause twist-kinks than black compound. For high black body temperatures (60°C) ballooning of pressurized cables may occur with LDPE jackets though this problem does not affect MDPE jackets under similar conditions. Sealpeth sheaths exhibit superior behaviour to optimized Stalpeth sheaths.

ACKNOWLEDGEMENTS

The development of the RIG test set as it is today is not attributable to any single individual, but rather to a series of researchers who, at different times, worked on the project and added refinements to the apparatus. The particular contribution made by R. Williams and F. Jodoin is acknowledged.



Emilio A. Falquero is Manager Cable Materials, Research and Development, Cable Division, Northern Telecom Canada Limited. In 1969 he received the degree of Ph.D. in Metallurgy at the University of Windsor, Ontario, Canada, and in 1971 he joined the Cable Division R & D. Dr. Falquero has worked on numerous developments of materials, processes and test methods in Communication Cables and Wires, and Optic Fibers.

COPPER DEACTIVATORS FOR POLYOLEFIN INSULATION

M. G. Chan
H. M. Gilroy
L. Johnson
W. M. Martin

Bell Laboratories
Murray Hill, N.J.

Copper deactivators are used to stabilize polyolefin insulation in contact with copper conductors. A number of new commercial deactivators have been evaluated in polyethylene and polypropylene insulation. Several of these deactivators performed adequately in laboratory tests and full-scale plant extrusion trials with polyethylene formulations and are considered to be viable alternatives to the deactivators currently specified for wire insulation.

INTRODUCTION

Polyolefins used for wire insulation must be stabilized against thermal oxidation, particularly that catalyzed by copper.[1,2] The stabilizers currently specified[3,4] for use in Bell System insulation are commercial grades of primary and secondary antioxidants of which many are specified, and copper deactivators, which until recently were limited to two, N,N´-dibenzal oxalyldihydrazide (B, Table I) and N,N´-bis(3,5-di-tert-butyl-4-hydroxyhydrocinnamyl) hydrazine (C).

In order to increase the availability of copper deactivators for Bell System applications, we began a program to test additional deactivators. Additive manufacturers were asked to submit samples of copper deactivators which were available commercially or which were being considered for commercialization because of promising laboratory results. These copper deactivators were incorporated into polyethylene or polypropylene wire formulations, extruded onto 22 AWG copper wire, and tested in the Experimental Pedestal Installation Complex (EPIC)[5] test program and by the usual oxygen- absorption technique. As a result of these studies, several promising deactivators were selected for further testing under standard manufacturing conditions. They were compounded into polyethylene by the duPont Company, extruded onto wire at Western Electric, and tested in the EPIC program. Several deactivators performed well and are specified now for use in Bell System polyethylene wire insulation.

MATERIALS AND METHODS

Copper Deactivators

The copper deactivators tested are identified in Table I. All were used as received from the manufacturer. Deactivators A through E were available commercially at the start of the tests. One of these additives, C, is a bifunctional stabilizer which functions both as a chain terminator of the hydrogen donor type and as a copper deactivator.[6,7,8] Additives B and E are marketed as copper deactivators and benzotriazole (A) is widely used to retard copper corrosion. Deactivator D is marketed as an antioxidant but its structure suggests that it should deactivate copper. The remaining deactivators, F through O, are laboratory samples which performed well in laboratory tests of the manufacturers.

The deactivators (Table I) have similar structures and most are derivatives of oxamide or diformyl hydrazine. Infrared spectra of the deactivators all have absorptions in the N-H (3350-3140 cm-1) and C=O (1730-1560 cm-1) regions. These absorptions are complex and suggest that the deactivators have several isomeric forms.

Melting points to 290°C were obtained on a Mettler FP51 apparatus and those above 290°C on an Electrothermal apparatus (Table II). All of the deactivators except A and D melt above 200°C. Many discolor and decompose upon melting and most have a broad melting range which is probably due to the presence of impurities

as well as to the different isomeric forms of the deactivators. For example, when the melting point of B is measured by differential thermal analysis (DTA) three distinct melting endotherms at 330, 337, and 342°C are observed.

The thermal decomposition temperatures of the deactivators were obtained by thermogravimetric analysis (TGA) on a duPont Model 951 analyzer. The samples were heated in nitrogen and temperatures at which initial and 10% weight (t_{10}) losses occurred were recorded (Table II). All of the samples, except A, have t_{10} values greater than 300°C indicating that the deactivators should be thermally stable during processing. There is a small initial weight loss in most of the samples above 200°C. Deactivators G and A are exceptions. They have initial weight losses at 80°C and 130°C respectively.

Wire Formulations

The copper deactivators were tested at a concentration of 0.1 weight percent in commercial, unstabilized polyethylene and polypropylene resins, to which we added selected antioxidants. The polyethylene was a high density (.945) ethylene-olefin copolymer, duPont Alathon 6600. The polypropylene was a propylene-ethylene copolymer, Hercules SB 272. Antioxidants were commercial grades and used as received.

All polyethylene formulations contained 0.1 weight percent tetrakis [methylene-3(3',5'-di-tert-butyl-4'-hydroxyphenyl)propionate] methane (THPM), an antioxidant commonly used in Bell System wire insulation. The antioxidant and the deactivators were premixed into the polyethylene on a two-roll mill before extrusion.

Two polypropylene formulations were tested: one containing 0.25 weight percent of the bifunctional additive, C, (Table I), the other containing 0.5 weight percent of an oligomer of 4,4'-thiobis(3-methyl-6-tert-butyl phenol) (OTBP).[9] These antioxidants had been recommended previously for use in polypropylene insulation.[6] The antioxidants and deactivators were dry-blended into polypropylene powder in a Waring blender before extrusion.

Laboratory wire samples were prepared by extruding the pre-blended polyolefins onto 22 AWG copper wire using a twin-screw extruder and conditions designed to simulate plant extrusions.[10] The extruder was purged after extrusion of each deactivator formulation. Formulations containing deactivators A through J (except D) were extruded as a group. Samples containing deactivators D, and K through O, were extruded later as they became available. Additional control samples containing deactivator B were prepared during these later extrusions.

Test Methods

Oxygen absorption tests were run at 140°C on the wire formulations. Wires were cut to lengths containing 0.1 grams of polymer insulation. They were oxidized in the usual fashion[11] and data reported in the form of average extrapolated induction times.

EPIC tests were run on all the wires in the temperature range of 90 to 110°C. Samples were stressed periodically and time to first observation of cracking due to oxidation reported. Samples were placed in the EPIC pedestals shortly after extrusion. Hence, formulations containing deactivators A through J (except D) were placed in one series of pedestals while those containing D, and K through O were tested in other sets of pedestals. Care was taken not to mix antioxidant formulations or resins in a single pedestal.

Full Scale Extrusion Trails

Full scale extrusion trials of resins containing several of the copper deactivators were made at the Western Electric Product Engineering Control Center (PECC) laboratory in Atlanta. Lots (150 lbs) of Alathon 6600 polyethylene resin containing the selected formulations (see below) were compounded by the duPont company. The resins were extruded onto 26 AWG copper wire on a 2 1/2 inch production extruder using operating conditions normal to Western Electric. The extruded wires were placed under test in the EPIC program.

RESULTS

Laboratory Scale Extrusions

In analyzing the results of the oxygen absorption (Table III) and EPIC tests for copper deactivator performance (Table IV) we use the formulations containing deactivator B as standards. Results for these standard formulations are shown in Figure 1 and appear as standard curves in Figures 2, 3 and 4. The polypropylene-C (Table I) formulation clearly outperforms the polypropylene-OTBP and polyethylene-THPM formulations. The latter formulations give almost identical results in the oxygen absorption test but differ somewhat in the EPIC tests, with the polypropylene system the better of the two. The performance of the polypropylene systems in the EPIC tests may be due to better retention of the stabilizers by the polypropylenes.

The superior performance of the polypropylene-C formulation occurs with all of the copper deactivators. Most of the deactivators tested enhance the stability of the 0.25% base formulation. Results for several of the deactivators are illustrated in Figure 2. The long term stability of these formulations in the EPIC program is particularly impressive. Many of the samples are still under test at 90°C after two years.

Interestingly one of the best formulations in all the tests is that of polypropylene with 0.35% C, the bifunctional additive. This system outperforms every other system tested. Polypropylene containing 0.35%C is three to four times more stable than the standard polyethylene insulation containing THPM and B. For example at 140°C the polypropylene- 0.35%C formulation lasts 469 hours while the polyethylene-THPM-B formulation lasts 178 hours (Table III).

Because C is itself a copper deactivator it is difficult to draw conclusions about the performance of other copper deactivators in formulations containing C. Hence, we must examine individual deactivators in systems free of other metal deactivators such as the OTBP and THPM formulations. The oxygen absorption data at 140°C (Table III) for most of these formulations are similar. A poor deactivator, G, is weak in both systems while good deactivators, B, F, I, J, and L perform well in both systems.

The EPIC tests for the polypropylene-OTBP formulations (Table IV) give somewhat different results than are found in the higher temperature oxygen absorption tests. Failure times for the polypropylene formulations in EPIC cluster around the failure time for the weakest sample (Table IV, Figure 3). Once one formulation fails in a pedestal containing polypropylene samples, the other formulations in that pedestal fail shortly afterwards. A similar effect was observed previously in multiple DTA tests on polypropylene resins.[12] Apparently oxidation products from a failed sample can catalyze the failure of adjacent samples. In the longer EPIC tests, e.g., polypropylene-C samples lasting more than a year, wires were removed as soon as failure was observed.

The spread in the data is much greater for the polyethylene-THPM formulations (Table IV, Figure 4) and the lower temperature EPIC data reflect the oxygen absorption data with one exception. The sample containing G which is weak in the 140, 110, and 100°C tests has the same stability as the sample containing B in the 90°C test. The samples containing I and J give outstanding results in this test.

On the basis of these tests we believe that a number of deactivators show promise for use as copper deactivators in the Bell System. Four deactivators are weak; A, E G and M. The other deactivators perform as well as B and two, I and J, appear superior to B. In general, we have found that the hydrazines slightly outperform deactivators derived from oxamides.

The commercial availability of the deactivators now becomes important. Several of the deactivators are eliminated from further consideration because at present we do not believe that they will be available commercially. They are: H, I, K, L and M. Two deactivators, N and O, are being evaluated by their manufacturer,[13] and we are awaiting their commercialization before evaluating them further. The rest of the deactivators are either commercially available now or will be shortly.

Full-Scale Extrusion Trials

Before specifying new deactivators we must be sure that they will not interfere with the wire extrusion process and that they will remain active after exposure to normal processing conditions. Three of the new deactivators, F, G and J, were tested under plant extrusion conditions at Western Electric, Atlanta and their performance compared to that of one of the deactivators currently specified, C. The deactivators were tested in high density polyethylene, the insulation most widely used in the Bell System. Formulations were prepared by the duPont Company in polyethylene containing several different antioxidants (Table V). All of the formulations extruded smoothly.

EPIC data (Table V, Figure 5) for the plant wires shows that formulations containing the deactivator, G, are less stable than those containing the other deactivators while formulations containing F and J perform well. Similar conclusions can be reached from the results of the laboratory trials (Table IV). In addition the plant wire data indicate that OTBP and C are acceptable antioxidants for high density polyethylene.

It is interesting to compare the data from the plant extrusion trials with some of our older EPIC data. Included in Figure 5 are failure points for low density polyethylene wire insulations tested in EPIC pedestals. These wire samples are representative of materials that failed in field installations in less than five years in some hotter regions of the country.[14] Any formulation that performs

nearly an order of magnitude better than the low density polyethylene samples in Figure 5 is considered to be adequately stabilized for maximum design life in field installations. Insulations containing both F and J meet this requirement in these tests and therefore, these deactivators have now been specified for use in high density polyethylene wire insulations.

CONCLUSIONS

As a result of the tests reported here we believe that we have a comprehensive evaluation of all copper deactivators potentially available commercially. No one of them is outstanding but several perform adequately. We have added two, F and J, to our high density polyethylene specification. Several others, currently available commercially, E and D, are somewhat weaker but might be adequate under some conditions, for example at a higher concentration. One deactivator O is very promising in high density polyethylene and will be tested further should it become available commercially.

Acknowledgments

We gratefully acknowledge I. P. Heyward for providing several of the infrared spectra and E. J. George for conducting the full scale extrusion trials.

REFERENCES

1. R. H. Hansen, C. A. Russell, T. DeBenedictis, W. M. Martin and J. V. Pascale, J. Polym. Sci., A-2, 587 (1964).
2. W. L. Hawkins, M. G. Chan and G. L. Link, Polym. Eng. Sci., 11, No. 5, 377 (1971).
3. Western Electric Material Specification MS59062.
4. Western Electric Material Specification MS59056.
5. H. M. Gilroy, Proc. 23rd Int. Wire and Cable Symp., 42 (1974).
6. M. G. Chan, R. A. Powers, Proc. 33rd ANTEC., Soc. Plast. Eng., 292 (1975).
7. D. D. O'Rell and A. Patel, Proc. 24th Int. Wire and Cable Symp. 231 (1975).
8. A. Patel, Proc. 26th Int. Wire and Cable Symp., 83 (1977).
9. W. H. Selcer, J. T. Renshaw, R. H. Hirsch, Proc. 35th ANTEC, Soc., Plast. Eng., 403 (1977).
10. E. T. Kokta, Proc. 24th Int. Wire and Cable Symp. 220 (1975).
11. W. L. Hawkins, R. H. Hansen, W. Matreyek and F. H. Winslow, J. Appl. Polym. Sci., 1, 37 (1959).
12. J. B. Howard, Polym. Eng. Sci., 13, No. 6, 429 (1973).
13. K. Yamaguchi, T. Yoshikawa, N. Sakamoto, S. Ohtomo, K. Kanda, S. Oh-e and T. Imaoka, Proc. 26th Int. Wire and Cable Symp., 87 (1977).
14. J. B. Howard, Proc. 21st Int. Wire and Cable Symp., 329 (1972).

TABLE I
COPPER DEACTIVATORS

DESIGNATION	SOURCE	STRUCTURE
A	SHERWIN-WILLIAMS CO.	
B	EASTMAN CHEMICAL PRODUCTS, INC.	
C	CIBA-GEIGY CORP.	
D	CIBA-GEIGY CORP.	
E	ARGUS CHEMICAL CORP.	
F	EASTMAN CHEMICAL PRODUCTS, INC.	PROPRIETARY
G	R.T. VANDERBILT CO., INC.	
H	MONSANTO INDUSTRIAL CHEMICALS CO.	
I	AMERICAN CYANAMID CO.	
J	AMERICAN CYANAMID CO.	
K	UBE INDUSTRIES, LTD.	
L	UBE INDUSTRIES, LTD.	
M	UBE INDUSTRIES, LTD.	
N	UBE INDUSTRIES, LTD.	PROPRIETARY
O	UBE INDUSTRIES, LTD.	

TABLE II

THERMAL PROPERTIES OF COPPER DEACTIVATORS

Deactivator	Melting Point	Decomposition Temperature	
		Initial	t_{10}
A	97-100	130	190
B	333-336	210	340
C	231	235	400
D	161-162	275	347
E	307-310	220	314
F	276-286	210	323
G	295	80	335
H	286	280	340
I	249	283	345
J	252-257	230	355
K	206-208	255	315
L	279-281	270	338
M	302-305	270	338
N	303-307	290	340
O	281-283	230	305

TABLE III

OXYGEN ABSORPTION RESULTS - 140°C

Copper Deactivator	Polyethylene-THPM Average[a] Induction Time-Hours	Polypropylene-OTBP Average Induction Time-Hours	Polypropylene-C Average Induction Time-Hours	Experiment
None	-	39 ± 5 (4)	253 ± 6 (3)	
A	3 ± 1 (2)	-	-	
B[b]	178 ± 21 (2)	169 ± 26 (4)	282 ± 4 (3)	
C	-	172 ± 13 (7)	469 ± 14 (3)	
E	-	84 ± 17 (3)	197 ± 48 (6)	1
F	179 ± 74 (2)	187 ± 21 (4)	330 ± 44 (5)	
G	10 ± 8 (2)	91 ± 9 (3)	298 ± 14 (6)	
H	131 ± 1 (2)	135 ± 17 (4)	267 ± 12 (6)	
I	34 ± 8 (2)	179 ± 17 (4)	433 ± 21 (3)	
J	229 ± 76 (2)	238 ± 5 (4)	380 ± 8 (4)	
D	-	119 ± 10 (4)	300 ± 15 (4)	
K	163 ± 21 (4)	137 ± 4 (4)	317 ± 8 (4)	
L	180 ± 49 (3)	165 ± 16 (4)	431 ± 62 (4)	2
M	<21	106 ± 13 (4)	315 ± 4 (4)	
N	123 ± 9 (3)	173 ± 14 (4)	28 ± 37 (4)	
B[b]	-	241 ± 10 (4)	279 ± 17 (4)	
N	225 ± 29 (2)	-	-	
O	355 ± 0 (2)	-	-	3
B[b]	199 ± 19 (3)	-	-	

[a] Numbers in parentheses indicate number of runs

[b] Control extrusions

TABLE IV

TIME TO INITIAL FAILURE IN EPIC LABORATORY EXTRUSION SAMPLES

Copper Deactivator	Polyethylene-THPM Time to Failure-Days 110°C	100°C	90°C	Polypropylene-OTBP Time to Failure-Days 110°C	100°C	90°C	Polypropylene-C Time to Failure-Days 110°C	106°C	100°C	90°C	Experiment #
None	-	-	-	56	119	208	-	209	342	491	
A	9	34	53	-	-	-	-	-	-	-	
B[a]	50	53	149	62	132	274	-	233	406	742	
C	-	-	-	62	132	288	-	531	544	>742	
E	-	-	-	58	126	244	-	434	544	>742	1
F	74	60	193	73	153	317	-	317	531	614	
G	10	29	149	48	132	244	-	244	320	742	
H	126	127	350	57	119	274	-	273	320	531	
I	126	339	350	69	145	317	-	365	544	742	
J	151	338	350	71	153	288	-	365	406	742	
D	-	-	-	122	>160	-	156	-	287	-	
K	-	-	-	122	>160	-	156	-	211	-	
L	-	-	-	122	>160	-	156	-	211	-	2
M	-	-	-	102	>160	-	156	-	287	-	
N	-	-	-	>122	>160	-	156	-	199	-	
B[a]	-	-	-	122	>160	-	156	-	287	-	
N	67	-	195	-	-	-	-	-	-	-	
O	77	-	>195	-	-	-	-	-	-	-	3
B[a]	77	-	>195	-	-	-	-	-	-	-	

[a] Control extrusions

TABLE V

TIME TO INITIAL FAILURE IN EPIC FULL-SCALE EXTRUSION TRIALS[a]

Deactivator 0.1 Wt. %	Antioxidant 0.1 Wt. %	Failure Time-Days 110°C	100°C
F	THPM	37	85
G	THPM	13	38
J	THPM	49	97
C	THPM	48	99
C	C	56	92
F	OTBP	52	98
G	OTBP	30	53
J	OTBP	49	73
C	OTBP	51	83

[a] All formulations are in high density polyethylene

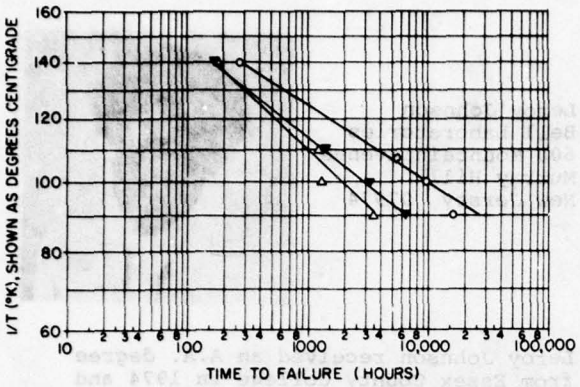


Figure 1 Samples with 0.1% B. Δ HDPE - THPM ▼ PP - OTBP; O PP-C. 140°C Data by oxygen uptake. Lower temperatures in EPIC static air ovens.

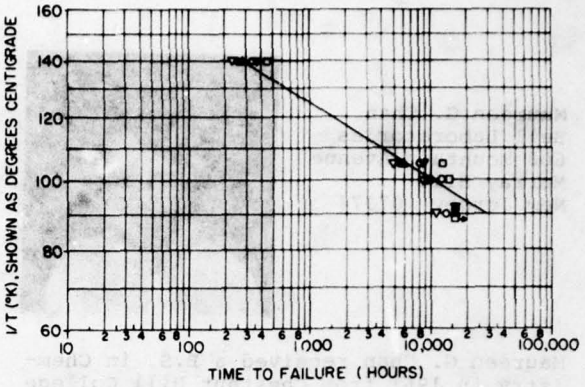


Figure 2 PP with 0.25% C. (▽ 0.25% C alone, □ 0.35% C, ● B, O F, ▲ G, ▼ J). Testing same as in Figure 1.

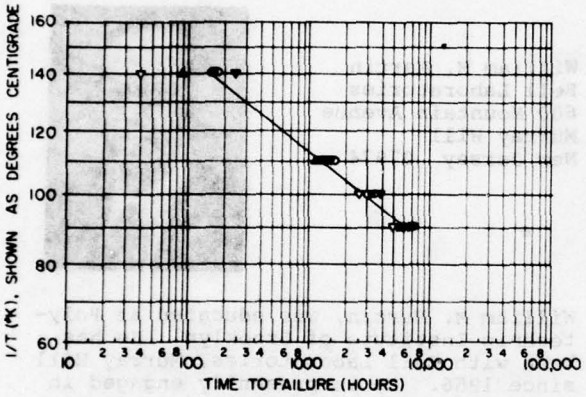


Figure 3 PP with 0.5% OTBP. (▽ OTBP alone, ● B, ■ C, O F, ▲ G, ▼ J). Testing same as Figure 1.

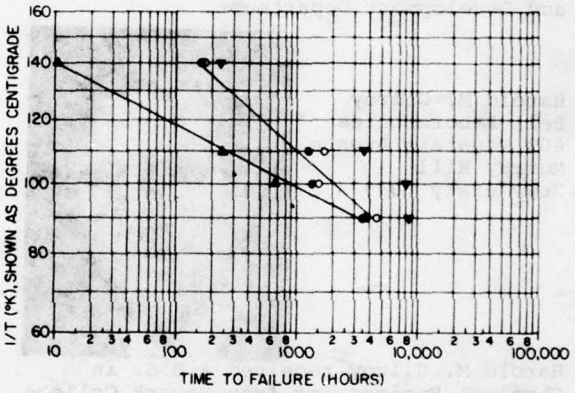


Figure 4 HDPE with 0.1% THPM. (● B, O F, ▲ G, ▼ J). Testing same as in Figure 1.

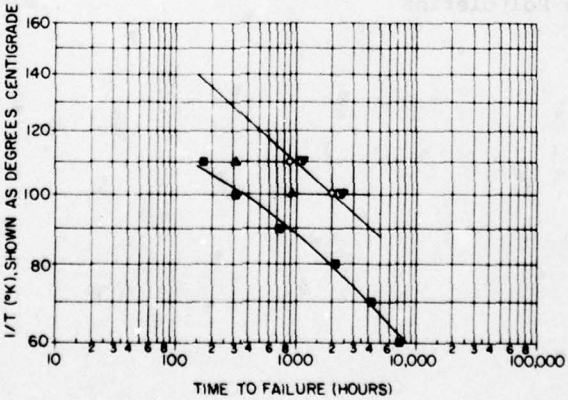


Figure 5 HDPE with 0.1% THPM. ■ C, O F, ▲ G, ▼ J, ■ LDPE control samples). All samples tested in EPIC.

Maureen G. Chan
Bell Laboratories
600 Mountain Avenue
Murray Hill
New Jersey 07974



Maureen G. Chan received a B.S. in Chemistry in 1961 from Chestnut Hill College and an M.S. in Chemistry in 1965 from Stevens Institute of Technology. She joined Bell Laboratories in 1962 when she began research on the deterioration and stabilization of polyolefins. At present, she is a Member of Technical Staff in the Plastics Chemistry Research and Development Department.

Harold M. Gilroy
Bell Laboratories
600 Mountain Avenue
Murray Hill
New Jersey 07974



Harold M. Gilroy received a B.S. in Chemical Engineering from Newark College of Engineering and has been at Bell Laboratories since 1955. He has been involved in many phases of research and development on thermoplastics for wire and cable applications. At present he is Supervisor of the Polyolefins Wire and Cable Group.

Leroy Johnson
Bell Laboratories
600 Mountain Avenue
Murray Hill
New Jersey 07974



Leroy Johnson received an A.A. degree from Essex County College in 1974 and is currently attending New Jersey Institute of Technology. He joined Bell Laboratories in 1970 and is currently involved in studies on the thermal properties of polyolefins for wire and cable.

William M. Martin
Bell Laboratories
600 Mountain Avenue
Murray Hill
New Jersey 07974



William M. Martin, was educated at Polytechnic Institute of Brooklyn. He has been with Bell Laboratories, Murray Hill since 1956. He is presently engaged in the development and application of polyolefins for wire and cable.

DEVELOPMENT OF NEW COPPER DEACTIVATOR FOR POLYOLEFIN INSULATIONS

M. Sato S. Nakagawa T. Hatta
Hitachi Cable, Ltd.
Hitachi, Japan

H. Noda S. Kawawata
Hitachi Densenkako Co., Ltd.
Hitachi, Japan

SUMMARY

The thermal oxidative degradation of polyolefins is accelerated by a direct contact with copper. The present research deals with the influence of aromatic dibasic acid dihydrazides and their derivatives on this copper-accelerated degradation and their efficiency as copper deactivators. Out of this investigation there emerged an excellent copper deactivator, N, N'-di-α-phenoxypropionyl-(isophthalyl dihydrazide). Even a small amount of this new copper deactivator added to polyolefins was found to be highly effective in inhibiting their degradation. It was further observed that the deactivator is thermally stable in high temperatures up to about 350°C and has almost no effect on the color or physical properties of polyolefins.

The new copper deactivator was applied with good results to insulations of solid and formed polyolefin-insulated communication cables, cross-linked polyethylene-insulated control cable and polyvinyl chloride-insulated electric equipment wires.

1. INTRODUCTION

Polyolefins such as polyethylene, cross-linked polyethylene, and polypropylene are widely used as insulating material for wire and cable. When used at high temperatures, these polyolefins are affected by the oxygen in air and undergo a thermal oxidative degradation, which impairs their mechanical and electrical properties. When polyolefins are in direct contact with a transition metal such as copper, the thermal oxidative degradation is markedly accelerated. In wires and cables in which the copper conductor is directly covered with a polyolefin insulation, this copper-accelerated degradation is a major factor in determining the performance and life of the cable.

R.H. Hansen et al [1~3] were the first to study the copper-accelerated thermal oxidative degradation of polyolefin insulations in datail and to describe copper deactivators. Since then, many studies have been made in different parts of the world, aiming at developing more effective copper deactivators. By now, many kinds of materials such as oximide, triazole and hydrazide derivatives are known to have an inhibiting effect and thus to serve as copper deactivators [1~5]. At the past symposiums, methods of testing the accelerated aging, the relationship between the efficiency and the chemical structure of copper deactovators, and the synergistic action of antioxidants and copper deactivators were reported [6~9].

Yet, very few copper deactivators have been applied practically because a stabilizer added to wire and cable insulations is required to ensure various properties of the insulation in addition to inhibition of copper-accelerated degradation.

This paper describes the results of research on aromatic dibasic acid dihydrazides and their derivatives.

Aromatic dibasic acid dihydrazides exhibit an inhibiting effect on copper-accelerated degradation. This effect was found to change according to the position of the substituted group. Isophthalyl dihydrazide with two hydrazide groups in a meta position showed an outstanding performance in this respect. Among the derivatives, N,N'-di-α-phenoxypropionyl-(isophthalyl dihydrazide), which has phenoxy groups at both of the ends, proved to be an ideal additive for wire and cable insulations satisfying all the requirements of a stabilizer in addition to being a powerful copper deactivator.

2. MECHANISM OF THERMAL OXIDATIVE DEGRADATION OF POLYOLEFINS AND ACTION OF COPPER DEACTIVATORS

The past decades have seen much progress in the study of the mechanisms of thermal oxidative degradation and the stabilization of polyolefins. Today, it is recognized that the oxidation reaction of polyolefins is based on a radical chain reaction such as shown in Fig. 1. [10, 11]

Under the influence of heat or another energy, a polyolefin generates a polymer radical, which then reacts with oxygen to produce a peroxy radical. The peroxy radical receives hydrogen from another polymer, to produce hydroperoxide. At the same time, a polymer radical is formed. The hydroperoxide dissociates into alkoxy radicals and hydroxy radicals. Thus, as this radical chain reaction proceeds, the molecular chain of the polyolefin is severed and polar molecules are formed.

This oxidative degradation of polyolefins can be inhibited by adding an antioxidant such as a radical chain terminator or a hydroperoxide decomposer.

In an oxidative degradation where the polyolefins are in contact with copper, however, the cupric ion prcduced by oxidation of copper reacts readily with the hydroperoxide. This reaction produces radicals, and thus the oxidative degradation proceeds at such a high velocity that an ordinary oxidation inhibitor cannot suppress the degradation. In order to prevent copper-catalyzed degradation, it will be necessary to

use a ligand, which is capable of arresting the cupric ion in a chemically stable state. Such a ligand should readily form a complex with cupric ion and the formed complex should be chemically stable.

On the other hand a wire and cable insulating material must meet various performance requirements in addition to resisting thermal oxidative degradation. Therefore, a copper deactivator to be added to an insulation should have the following characteristics:

(1) Effective inhibition of degradation by a small amount added to the insulation.
(2) No vaporization or chemical change during processing and the use of the polyolefin.
(3) Good dispersion in polyolefins and good compatibility.
(4) No effect on the color of polyolefins.
(5) No adverse effects on electrical and mechanical properties of polyolefins.
(6) No adverse effects on the action of other additives.
(7) Good resistance to water and oil

3. INHIBITION OF COPPER-ACCELERATED DEGRADATION BY AROMATIC DIBASIC ACID DIHYDRAZIDES AND THEIR DERIVATIVES

3.1 Oven aging life test

In the present study the inhibition of copper-accelerated degradation was evaluated by the oven aging life test using a copper dish. This is a simple test, which however allows a direct observation of the state of degradation.

Test pieces were prepared in the following manner: 0.1 phr of antioxidant, tetrakis [methylene (3,5-di-t-butyl-4-hydroxyhydrocinnamate)] methane, and 0.1 phr of copper deactivator were added to low density polyethylene, which was then mixed for 10 minutes in a mixing roll at 140°C. The rolled sheet was pressed for 3 minutes in a hot press at 180°C, to produce a pressed sheet of 0.5mm thickness. From this sheet, five rectangular pieces measuring 10 mm by 3.0 mm were prepared. Each of the five pieces were placed on a copper dish, which had been washed thoroughly.

The five test pieces were placed in an air oven at 150 °C and observed visually for signs of discoloration and embrittlement. Since stabilized polyethylene usually undergoes local degradation, the time elapsed before discoloration or embrittlement occurred in three of the five pieces was measured and defined as the oven aging life.

Table 1 shows the oven aging life of low-density polyethylene containing only an antioxidant and compares the results of a test using copper dishes as described above with another test using aluminum dishes. It will be seen that the oven aging life with copper dishes is about one-fourth of that with aluminum dishes. This is obviously the result of an acceleration of thermal oxidative degradation by copper.

3.2 Effect of aromatic dibasic acid dihydrazides

With respect to the dihydrazides of the aromatic dibasic acids of phthalic acid, isophthalic acid and terephthalic acid, the influence of these materials on the inhibition of copper-accelerated degradation was investigated and the results are summarized in Table 2.

It is recognized from these data that the inhibiting effect of three isomers is markedly different. The highest effect was obtained with isophthalyl dihydrazide, in which the substituted groups are at a meta position in the benzene nucleus. The second highest effect was shown by phthalyl dihydrazide and the lowest by terephthalyl dihydrazide. It is considered that the catalytic action of the cupric ions is inhibited by the formation of a complex between the hydrazide group and the ion. Therefore inhibition will increase with the stability of the complex, which inturn increases with the electron density of oxygen and nitrogen atoms in the hydrazide group.

With respect to the interaction between the lone-pair electrons in the hydrazide group and the π -electrons in the benzene nucleus in isophthalyl dihydrazide, it is assumed that both of the two hydrazide groups have a high electron density due to the resonance structure shown in Fig. 2. On the other hand, in phthalyl dihydrazide and terephthalyl dihydrazide, in which the two substituted groups are in ortho and para positions, respectively, it is assumed that the hydrazide group has a low electron density because the two substituted groups influence each other.

3.3 Effect of isophthalyl dihydrazide derivatives

The above data show that isophthalyl dihydrazide has the highest effect of inhibiting copper-accelerated degradation among all aromatic dibasic acid dihydrazides, subsequently a few derivatives of isophthalyl dihydrazide were synthesized and investigated for their efficiency, in an attempt to improve thermal and chemical stability.

Of the various derivatives, the most effective one was N,N'-di-α -phenoxypropionyl-(isophthalyl dihydrazide), which has phenoxy groups at the ends of the molecule. The test results are shown in Table 3.

By adding 0.1 phr of this copper deactivator to low-density polyethylene, the oven aging life can be increased by about 4 times of that of nontreated polyethylene. This results in a higher oven aging life than in the test with aluminum dishes, where accelerated degradation does almost not occur. Such a high inhibiting effect is not seen in conventional copper deactivators available on the market.

4. CHARACTERISTICS OF THE NEW COPPER DEACTIVATOR

4.1 Degradation inhibiting effect

The influence of different amounts of the copper deactivator on extending the oven aging life of low-density polyethylene were measured and the results are shown in Fig. 3.

of the copper deactivator in addition to stabilizers and antioxidants results in an estimated service life of at least 40,000 hours at the rating temperature of 105°C.

6. CONCLUSIONS

In an attempt to prevent thermal oxidative degradation of polyolefin insulators in contact with copper, the effect of aromatic dibasic acid dihydrazides and their derivatives on the inhibition of copper-accelerated degradation was investigated.

It was demonstrated that N,N'-di- α -phenoxypropionyl-(isophthalyl dihydrazide) not only is highly effective in inhibiting copper-accelerated degradation but also has good properties as an additive to be used in wire and cable insulations.

Good results were obtained by applying the new copper deactivator to insulations of communication and control cables and electric equipment wires.

7. REFERENCE

1. R.H. Hansen, T. De. Benedictis, W.M. Martin; Transaction of the Institution of the Rubber Industry, 39, (6), T290 (1963).
2. R.H. Hansen, C.A. Russell, T.De. Benedictis, W.M. Martin, J.V. Pascale; Journal of Polymer Science, Part A, 2, 587 (1964)
3. C.A. Russell, J.V. Pascale; Journal of Applied Polymer Science, 7, 959 (1963)
4. R.H. Hansen, T.De. Benedictis, W.M. Martin; Polymer Engineering Science, 5, (4), 223 (1965)
5. C.E. Tholstrup: Proceedings of the Battelle Symposium on Thermal Stability of Polymers, P-1 (1963)
6. J.M. Fabar, W.H. Brown, A.DiBattista, P.P. Klemchuki; Proceedings of the 21th International Wire and Cable Symposium 361 (1972)
7. G.A. Schmidt; Proceedings of the 22th International Wire and Cable Symposium 11 (1973)
8. K. Yamaguchi, T. Yoshikawa, H. Kishi, M. Masaki, N. Sakamoto; Proceedings of the 23th International Wire and Cable Symposium, 97 (1974)
9. K. Yamaguchi, T. Yoshikawa, N. Sakamoto S. Ohtomo, K. Kanda, S. Ohe, T. Imaoka; Proceedings of the 26th International Wire and Cable Symposium, 87 (1977)
10. W.L. Hawkins, F.H. Winslow; Chemical Reactions of High Polymers, E.M. Fettes, Ed., Interscience, New York (1964)
11. W.L. Hawkins; Jorunal of Polymer Science, Symposium No. 57, 319 (1976)

The oven aging life increases initially with the amount of the deactivator added but saturates for high doses. Thus for each copper deactivator, there seems to be a limit in oven aging life. One reason for this is that the complex, which is formed between the deactivator and the cupric ion, has a residual action of accelerating the oxidative degradation of polyolefins. With an amount of 0.5 phr of the new copper deactivator, the oven aging life is extended about six times over that without any deactivator, and the effect of copper is almost completely eliminated.

The copper deactivator was also tested with high-density polyethylene and polypropylene, in addition to the previous low-density polyethylene. The results are shown in Fig. 4. While each polymer uses a different antioxidant a similar inhibiting effect was obtained for all three polyolefins.

4.2 Thermal stability

The thermal stability of the new copper deactivator was tested with a differential scanning calorimeter and the results are shown in Fig. 5.

An endothermic peak due to crystalline melting is observed at 225°C. Otherwise, no thermal change is noted in the temperature range between 50 and 350°C. Therefore this copper deactivator will not cause vaporization or thermal decomposition even when exposed to high temperatures during processing and under the normal operating conditions of the polyolefins.

4.3 Effect on physical properties of polyolefins

Low-density polyethylene containing up to 0.5 phr of the new copper deactivator was tested for flow, mechanical and electrical properties. The results are shown in Fig. 6.

It is seen that the melt index, the tensile strength, and the elongation of the polyethylene remain almost unchanged regardless of the amount of the deactivator. These results confirm that the deactivator disperses well in the polyethylene, has good compatibility and causes no chemical change.

As for dielectric properties, an addition of the copper deactivator results in a slight increase in the dielectric constant and the dissipation factor. This is because the deactivator is a polar substance. At low amounts, no problem will be encountered for all practical purposes.

5. APPLICATION TO WIRE AND CABLE INSULATION

5.1 Foamed polyolefin-insulated communication cable

In local telephone cables, multi-pair cables with small size-conductors, which allow the installation of a large quantity of communication circuits in cable ducts of limited size, and petroleum jelly-filled cables, in which the reliability is improved by blocking the penetration of water, are required in the world. Recentry 26AWG x 4800 pairs cable and 0.4mm x 2000 pairs jelly-filled cable were developed to fulfill these requirements. The new copper deactivator was applied to the formed polyolefin insulations of these cables.

The cores of these cables consisted of copper wires having a 0.4 mm diameter covered with insulations of about 0.15 mm thickness. Table 4 lists the results of tests on the properties of these cables. It will be seen that addition of the copper deactivator has no effect on the extrudability or other properties of the foamed polyolefin insulation.

Results of a thermal aging life test made with the cores of these cables are presented in Fig. 7. Two different samples were used. One was an untreated core, while the other was a core immersed for 14 days in a petroleum jelly water-blocking compound at 70°C. These cores were heated in an air oven and wound on a rod with the same diameter as the core. Thermal aging life was taken as the time required to initiate cracking or discoloration

Extrapolation of the data in Fig. 7 to an operating temperature of 60°C shows that a life of at least 40 years is assured when the copper deactivator is used.

5.2 Crosslinked polyethylene-insulated control cable

Control cables to be used in high-temperature environments have to be crosslinked polyethylene-insulated cables with improved heat resistance. The newly developed copper deactivator was used to stabilize the insulation of such a cable.

Table 5 shows the properties of an experimentally manufactured 600V 7 x 2 SQ control cable. The cable core consists of a copper strand conductor (outside diameter: 1.8 mm) covered with a crosslinked polyethylene insulation of 0.8 mm thickness containing antioxidants and the copper deactivator. It was manufactured by the atmospheric pressure crosslinking method.

It will be seen that the cable has good mechanical, heat deformation, and electrical properties. Fig. 8 shows the change in the electric breakdown voltage during long-term immersion of the cable core in water. Both AC and DC breakdown voltages remain stable. It is thus estabilished that this copper deactivator does not undergo any chemical change even when in contact with water.

In a accelerated aging test, it was verified that the maximum operating temperature of this cable can be set at 90°C.

5.3 Polyvinyl chloride-insulated electric equipment wire

Copper-accelerated degradation was also found in plasticized polyvinyl chloride insulations. Therefore the new copper deactivator was applied to polyvinyl chloride-insulated wire having a bare or tinned copper conductor to be used at high temperature.

For instance in a crosslinked polyvinyl chloride-insulated electric equipment wire, accelerated aging tests showed that the use

of the copper deactivator in addition to stabilizers and antioxidants results in an estimated service life of at least 40,000 hours at the rating temperature of 105°C.

6. CONCLUSIONS

In an attempt to prevent thermal oxidative degradation of polyolefin insulators in contact with copper, the effect of aromatic dibasic acid dihydrazides and their derivatives on the inhibition of copper-accelerated degradation was investigated.

It was demonstrated that N,N'-di- α -phenoxypropionyl-(isophthalyl dihydrazide) not only is highly effective in inhibiting copper-accelerated degradation but also has good properties as an additive to be used in wire and cable insulations.

Good results were obtained by applying the new copper deactivator to insulations of communication and control cables and electric equipment wires.

7. REFERENCE

1. R.H. Hansen, T. De. Benedictis, W.M. Martin; Transaction of the Institution of the Rubber Industry, 39, (6), T290 (1963).
2. R.H. Hansen, C.A. Russell, T.De. Benedictis, W.M. Martin, J.V. Pascale; Journal of Polymer Science, Part A, 2, 587 (1964)
3. C.A. Russell, J.V. Pascale; Journal of Applied Polymer Science, 7, 959 (1963)
4. R.H. Hansen, T.De. Benedictis, W.M. Martin; Polymer Engineering Science, 5, (4), 223 (1965)
5. C.E. Tholstrup: *Proceedings of the* Battelle Symposium on Thermal Stability of Polymers, P-1 (1963)
6. J.M. Fabar, W.H. Brown, A.DiBattista, P.P. Klemchuki; Proceedings of the 21th International Wire and Cable Symposium 361 (1972)
7. G.A. Schmidt; Proceedings of the 22th International Wire and Cable Symposium 11 (1973)
8. K. Yamaguchi, T. Yoshikawa, H. Kishi, M. Masaki, N. Sakamoto; Proceedings of the 23th International Wire and Cable Symposium, 97 (1974)
9. K. Yamaguchi, T. Yoshikawa, N. Sakamoto S. Ohtomo, K. Kanda, S. Ohe, T. Imaoka; Proceedings of the 26th International Wire and Cable Symposium, 87 (1977)
10. W.L. Hawkins, F.H. Winslow; Chemical Reactions of High Polymers, E.M. Fettes, Ed., Interscience, New York (1964)
11. W.L. Hawkins; Jorunal of Polymer Science, Symposium No. 57, 319 (1976)

Chain reaction

Initiation

$$RH \longrightarrow R\cdot + H\cdot$$

Propagation

$$R\cdot + O_2 \longrightarrow ROO\cdot$$

$$ROO\cdot + RH \longrightarrow ROOH + R\cdot$$

$$ROOH \longrightarrow RO\cdot + HO\cdot$$

Termination

$$R\cdot + R\cdot \longrightarrow RR$$

$$R\cdot + ROO\cdot \longrightarrow \text{Inert products}$$

$$ROO\cdot + ROO\cdot \longrightarrow \text{Inert products}$$

Stabilization by antioxidant

Chain inhibition

$$ROO\cdot + HA \longrightarrow ROOH + A\cdot \text{ (Stable)}$$

$$RO\cdot + HA \longrightarrow ROH + A\cdot \text{ (Stable)}$$

$$HO\cdot + HA \longrightarrow HOH + A\cdot \text{ (Stable)}$$

Peroxide decomposition

$$ROOH + RSR \longrightarrow \text{Inert products}$$

Effect of copper

Catalytic peroxide decomposition

$$Cu \longrightarrow Cu^{++} + 2e$$

$$ROOH + Cu^{++} \longrightarrow ROO\cdot + Cu^{+} + H^{+}$$

$$ROOH + Cu^{+} \longrightarrow RO\cdot + Cu^{++} + OH^{-}$$

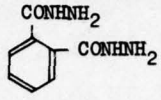
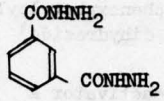
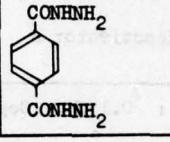
Stabilization by copper deactivator

Complex formation

$$Cu^{++} + n\cdot L \longrightarrow \left[Cu\ (L)n\right]^{++}$$

Fig. 1 Mechanism of thermal oxidation of polyolefins

Table 2 Effect of aromatic dibasic acid dihydrazides in copper-accelerated degradation of low-density polyethylene

Copper deactivator	Chemical structure	Oven aging life at 150°C (hours)
Phthalyl dihydrazide		230
Isophthalyl dihydrazide		460
Terephthalyl dihydrazide		170

Antioxidant: 0.1 phr
Copper deactivator : 0.1 phr

Table 1 Influence of copper on thermal oxidative degradation of low-density polyethylene

Test method	Oven aging life at 150 °C (hours)
Copper dish method	150
Aluminum dish method	540

Antioxidant : 0.1 phr

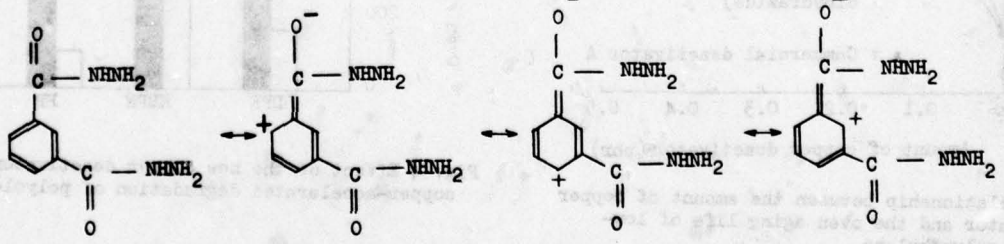
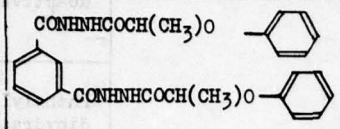
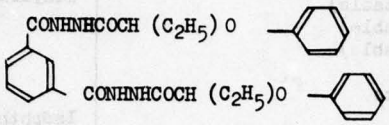


Fig. 2 Resonance structure of isophthalyl dihydrazide

Table 3 Effect of isophthalyl dihydrazide derivatives in copper-accelerated degradation of low-density polyethylene

Copper deactivator	Chemical structure	Molecular weight	Oven aging life at 150°C (hours)
N,N'-di- α -phenoxypropyonyl-(isophthalyl dihydrazide)		490	570
N,N'-di- α -phenoxybutyloyl-(isophthalyl dihydrazide)		518	550
Commercial deactivator A	-	-	400
Commercial deactivator B	-	-	310

Antioxidant : 0.1 phr, Copper deactivator : 0.1 phr

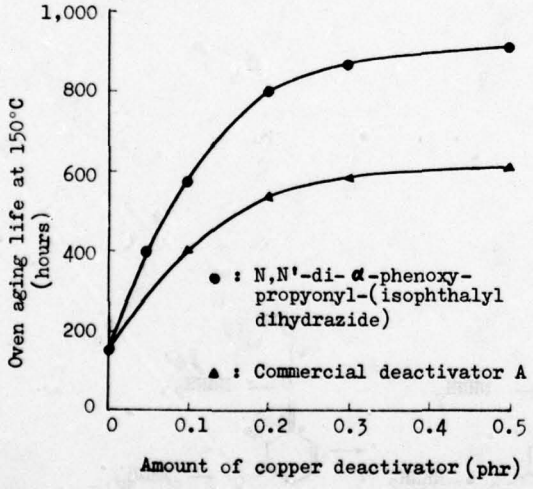


Fig. 3 Relationship between the amount of copper deactivator and the oven aging life of low-density polyethylene

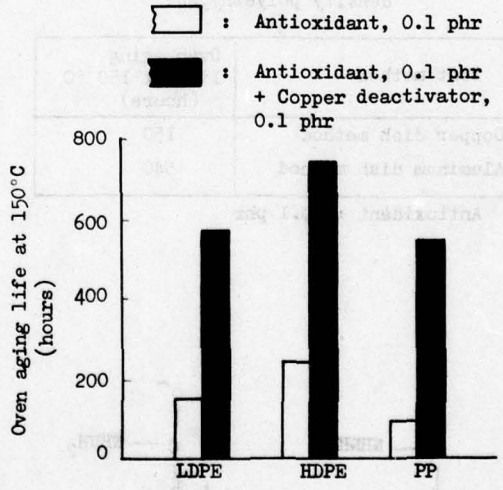


Fig. 4 Effect of the new copper deactivator on copper-accelerated degradation of polyolefins

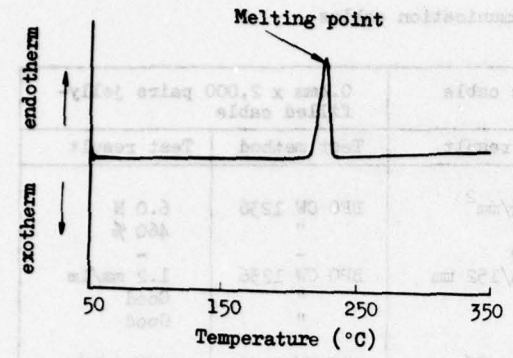


Fig. 5 Differential scanning calorimetry curve of the new copper deactivator

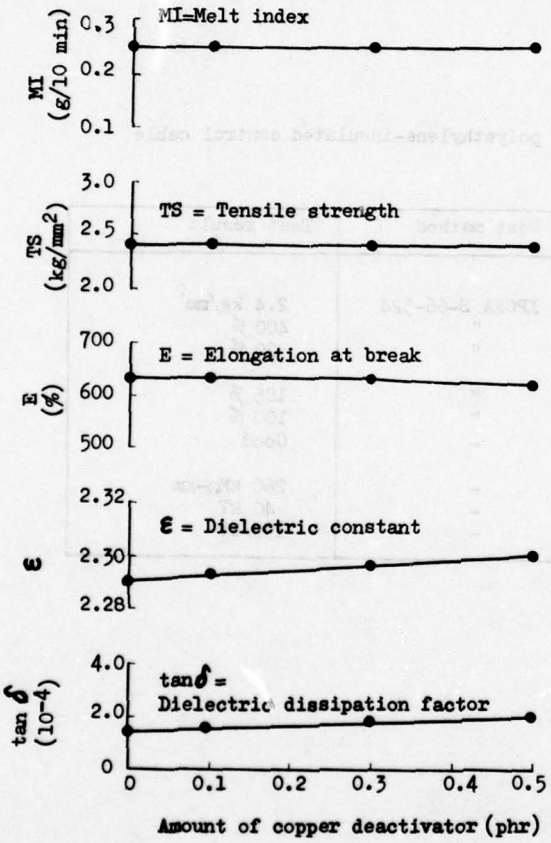


Fig. 6 Influence of the new copper deactivator on physical properties of low-density polyethylene

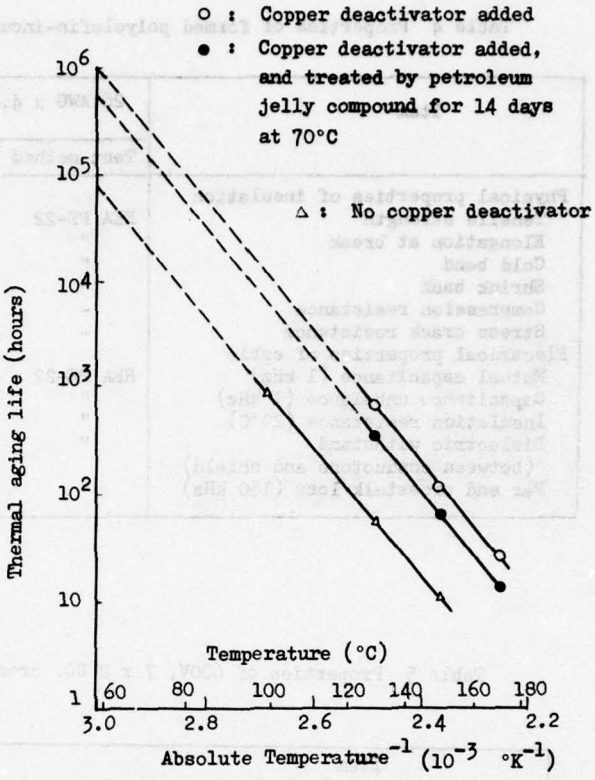


Fig. 7 Thermal aging life of formed polyolefin-insulated communication cable core

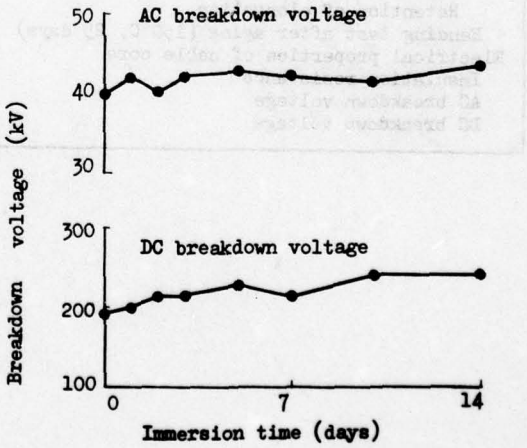


Fig. 8 Electrical breakdown properties of cross-linked polyethylene-insulated cable core after immersion in water

Table 4 Properties of formed polyolefin-insulated communication cables

Item	26 AWG x 4,800 pairs cable		0.4mm x 2,000 pairs jelly-filled cable	
	Test method	Test result	Test method	Test result
Physical properties of insulation				
Tensile strength	REA PE-22	2.6 kg/mm^2	BPO CW 1236	6.0 N
Elongation at break	"	450 %	"	460 %
Cold bend	"	0/10	-	-
Shrink back	"	1.7 mm/152 mm	BPO CW 1236	1.2 mm/1m
Compression resistance	-	-	"	Good
Stress crack resistance	-	-	"	Good
Electrical properties of cable				
Mutual capacitance (1 kHz)	REA PE-22	Ave.53 nF/km	BPO CW 1236	Avg.52 nF/km
Capacitance unbalance (1 kHz)	"	RMS 19 PF/305m	"	MAX.50 PF/500m
Insulation resistance (20°C)	"	Above 100 kMΩ-km	"	Above 50 kMΩ-km
Dielectric withstand (between conductors and shield)	"	Good	-	-
Far end crosstalk loss (150 kHz)	"	RMS 74 db/305m	-	-

Table 5 Properties of 600V, 7 x 2 SQ. crosslinked polyethylene-insulated control cable

Item	Test method	Test result
Physical and aging properties of insulation		
Tensile strength	IPCEA S-66-524	2.4 kg/mm^2
Elongation at break	"	400 %
Heat deformation (121°C, 500 g, 1 hr.)	"	20 %
Aging test (121°C, 168 hrs)		
Retention of tensile strength	"	105 %
Retention of elongation	"	100 %
Bending test after aging (150°C, 25 days)	-	Good
Electrical properties of cable core		
Insulation resistance	-	260 kMΩ-km
AC breakdown voltage	-	40 kV
DC breakdown voltage	-	190 kV



Masakatsu Sato
Research Laboratory
Hitachi Cable, Ltd.
5-1 Hitaka-cho,
Hitachi-shi
Ibaraki-ken, Japan

Graduated from the Chemical Science Department, Tohoku University in 1961, thereupon joining Hitachi Cable, Ltd., where he has been engaged in research and development work on insulating materials for power cable. Now, as senior researcher at Research Laboratory, he is working on research and development of plastic insulating materials for wire and cable, he is a member of the Institute of Electrical Engineers of Japan and the Society of Polymer Science, Japan.



Hajime Noda
Hitaka Works
Hitachi Cable, Ltd.
5-1 Hitaka-cho,
Hitachi-shi
Ibaraki-ken, Japan

Graduated from the Electronic Engineering Department, Osaka University in 1958, He joined Hitachi Cable, Ltd., where he has been engaged in development and design of communication cable. Now, as Deputy Manager at Communication System Design Department, Hitaka Works, he is taking charge of management on development and design of communication cable. He is a member of the Institute of Electric and Communication Engineers of Japan.



Shinkichi Nakagawa
Research Laboratory
Hitachi Cable, Ltd.
5-1, Hitaka-cho,
Hitachi-shi, Ibaraki-
ken, Japan

Graduating from the Chemistry Course Hitachi Technical School in 1957, he joined Hitachi Cable, Ltd., where his research and development efforts have been directed at insulations of communication cable. Now he is researcher at Research Laboratory, taking charge of work on flame resistant materials. He is a member of the Institute of Electrical Engineers of Japan and the Society of Polymer Science, Japan.



Shichiro Kawawata
Hitachi Densenkako
Co., Ltd.
5-1, Hitaka-cho,
Hitachi-shi, Ibaraki-
ken, Japan

Graduating from the Chemistry Course, Hitachi Technical School in 1939, he joined Hitachi Ltd.. He has been engaged in research and development of insulating materials for wire and cable at Hitachi Ltd. and then Hitachi Cable Ltd.. Now he is Board Manager at Hitachi Densenkako Co., Ltd., managing on manufacture of wire and cable accessories. He is a member of the Institute of Electric Engineers of Japan and the Society of Polymer Science, Japan.



Toshimasa Hatta
Research Laboratory
Hitachi Cable, Ltd.
5-1 Hitaka-cho,
Hitachi-shi, Ibaraki-
ken, Japan

Upon gradation from the Polymer Science Department, Hokkaido University, in 1971, he entered Hitachi Cable, Ltd., where he has been engaged in research and development work on insulating materials for communication cable. He is now researcher at Research Laboratory and is involved in above work.

OXIDATIVE STABILITY OF POLYPROPYLENE COMPARED TO HIGH DENSITY POLYETHYLENE

E.G. Malawer and K.D. Kiss

Phelps Dodge Communications Company
White Plains, N.Y.

Summary

A statistically designed experimental grid program was utilized to characterize the effect of foaming agent as well as incremental antioxidant and metal deactivator upon the stability of a commercially available polypropylene resin. A mathematical approach was used to quantify the primary effects of these additives and their interactions. The method is applicable to define the most cost efficient compositions for a wide range of performance levels. The results of this study are compared to similar work on high density polyethylene (HDPE) reported by this laboratory in 1977. The OIT stability of commercial polypropylene is significantly higher than that of HDPE both for solid and foamable grades. Both materials show increased stability with additions of incremental antioxidant. Incremental addition of metal deactivator had a definite and beneficial effect on the stability of foamable polypropylene in the absence of copper, but had no effect on the foamable HDPE. Either the foaming agent or the presence of copper alone lowers the stability of polypropylene while HDPE is affected only by the combination of these two factors.

Introduction and Objectives

This paper represents the conclusion of a two-part work on the oxidative stability of the two polyolefins most commonly used today as primary insulation for conductors in communications cable. The first part concerned itself with high density polyethylene (HDPE) exclusively and was presented at this symposium in 1977.[1] The objectives of the present work were to:

- Quantify the antioxidant - metal deactivator - foaming agent interaction for polypropylene.
- Estimate the limiting stability of foamable polypropylene.
- Establish the cost of stability improvement for foamable polypropylene.
- Compare the stability behavior of HDPE and polypropylene.

Background

Low density polyethylene (LDPE), high density polyethylene (HDPE) and polypropylene (PP) are the resins traditionally used to insulate telephone conductors. Interest in foamed insulation within the past two decades has stemmed from its potentially lower cost and higher pair density per unit cable cross-sectional area, especially in filled cables. A foamable HDPE using azobisformamide as the blowing agent first appeared around 1960.[2]

It has been reported that the blowing agent or its reaction products reduces the thermal stability of HDPE insulation.[3,4] Foamed HDPE insulation was found to have poorer stability when compared to solid HDPE insulation in the presence of copper[5,6] but not in the absence of copper.[1] One worker has postulated that the cellular structure itself may contribute to reduced stability in the foam by facilitating an increased rate of oxygen diffusion into the matrix.[7] The authors' own work has led them to the opposite conclusion.[1]

IPCEA Working Group 434 has recently reported on life prediction studies of solid and foam HDPE and PP commercial insulations by oven-aging, DTA, and a variety of physical tests.[5] Petrolatum exposure has been found to reduce the stability of HDPE but not that of the low or medium density polyethylenes.[8] The mechanism of the catalytic effect of copper oxide upon the oxidation of polypro-

pylene has received further attention.[9,10] Other workers have concentrated on optimizing the efficiency of stabilizers, particularly metal deactivators,[11] including a bifunctional metal deactivator - antioxidant.[12,13] A number of patents have been recently granted for a variety of polyolefin - stabilizer packages.[13-18]

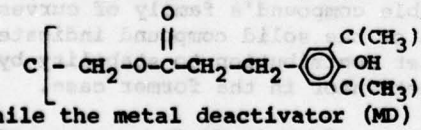
The effect of temperature upon the stability of HDPE as measured by the DSC-oxidative induction time method has been found to be non-linear in the melting region using an Arrhenius plot,[19] so that the technique is unsuitable for service temperature life prediction. It has also been observed that a variety of stabilizer systems tested at several temperatures by DSC showed crossover in performance upon comparison of the high and low temperature results.[20] However, for a single stabilizer package, the order of stability, as measured by TGA-oxygen uptake, for a series of polyethylene samples did not change in the range of 115-200°C.[21]

In this work, the authors used a three-dimensional experimental grid program of DSC -oxidative induction times for polypropylene to quantify the interactions of antioxidant, metal deactivator and foaming agent and show the relationship between the desired stability level and the lowest possible cost at that level. It was assumed that the stability order determined for a variety of additive concentrations at 200°C will be the same at typical service temperatures.

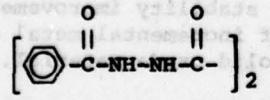
Experimental

Materials

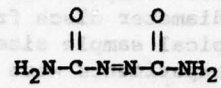
The polypropylene compound utilized was a commercially available product in pellet form. The antioxidant (AO) employed was tetrakis [methylene 3 - (3',5'-di-tert-butyl-4'hydroxyphenyl) proprionate] methane:



while the metal deactivator (MD) was N,N'-dibenzal oxalyl dihydrazide:



and the foaming agent (FA) was azobisformamide (also known as azodicarbonamide or azodicarboxylic acid diamide):



The commercial grade of polypropylene used is stabilized with unknown quantities of antioxidant and metal deactivator but contains no foaming agent. The experimental compositions that were produced for this study contained known incremental concentrations of antioxidant (ΔAO) and metal deactivator (ΔMD) (over and above the unknown amount in the base resin). The various levels of foaming agent represented total concentrations (FA) of that particular additive.

Procedure

The experimental compositions were produced in a two-step process. Masterbatches of antioxidant and metal deactivator were compounded at 2.4% w/w in polypropylene. The foaming agent masterbatch was compounded at 5.8% w/w in solid grade HDPE so that this initial compounding could take place at a temperature (160°C) sufficiently low to minimize decomposition of the blowing agent. These masterbatches were in turn compounded with polypropylene to achieve the final formulations specified in the grid program. HDPE was added at this stage as necessary in order to bring all of the final formulations to the same concentration in HDPE (i.e. 10% w/w). The exact concentrations of ΔAO, ΔMD, and FA in each experimental composition are specified in Table 1.

Compounding was performed in a Brabender Plasticorder equipped with a roller 5-type measuring head. The final compositions were mixed in 40 gram batches at 182°C (360°F) and 50 rpm for 10 minutes. Masterbatches and experimental formulations were each passed once through a Farrel two-roll mill (6 x 13 inches) at 104°C (220°F). A Wabash hydraulic press set at 175°C and 5500 lbs./sq.in. was used for 3 minutes to press each of the 15 experimental formulations to 8 mil thick films. Compositions containing foaming agent were not allowed to foam by performing the compounding below the blowing temperature.

The oxidative induction times (OIT) were determined on a Perkin-Elmer model 1B Differential Scanning Calorimeter (DSC)

at 200°C in oxygen. Samples were prepared by punching 3mm diameter discs from the films to give typical sample sizes of 1.4 to 1.7 mg. All experiments were performed in duplicate and the averages were employed in the statistical treatment.

Experimental Design

The experimental grid program used to evaluate the stability optimization of polypropylene was identical to that already employed to characterize HDPE and has been described in great detail.[1] The grid was designed to assess the following variables:

X_1 = incremental antioxidant concentration (ΔAO), ranging from 0 to 0.24% w/w.

X_2 = incremental metal deactivator concentration (ΔMD), ranging from 0 to 0.24% w/w.

X_3 = total foaming agent concentration (FA), ranging from 0 to 0.58% w/w.

The responses of interest were:

Y_A = OIT in copper contact measured in minutes.

Y_B = OIT in the absence of copper measured in minutes.

Y_C = Relative cost of added (incremental) stabilizers on an arbitrary scale of 0 for the commercial compounds to 100 for the combination of 0.24% antioxidant + 0.24% metal deactivator.

The experimental grid (Figure 1) is a three-variable, multilevel, center weighted, patched orthogonal design and requires 15 experiments. The variables are on 5 levels (designated as very low, low, medium, high and very high in Figure 1 and Table 1) and expressed in "experimental units" ranging from -1.215 e.u. for very low levels to +1.215 e.u. for very high levels.

The generalized equation for a given response is:

$$Y = a_o + a_1X_1 + a_2X_2 + a_3X_3 + a_{11}X_1^2 + a_{22}X_2^2 + a_{33}X_3^2 + a_{12}X_1X_2 + a_{13}X_1X_3 + a_{23}X_2X_3$$

where the X's are the additive concentrations expressed in experimental units. The experimentally determined responses Y_A, Y_B, and Y_C were used to generate the coefficients of the three response equations which are listed in Table 2.

The coefficients were then used to back calculate the predicted or "computed" responses for each experiment. Figure 2 and Table 1 compare the "computed" Y_A values for each experiment with the "actual" values. The difference between the computed and actual values is a measure of "fit" or validity of the approximation. The standard deviation and the relative error, other measures of the "fit", are both given in Table 2. The relative cost, Y_C, whose linear equation requires only three coefficients is not differentiated with respect to "actual" or "computed" values.

Discussion

Polypropylene Stability in Copper Contact

The primary effects of the three variables, incremental concentrations of antioxidant and metal deactivator, and foaming agent level are presented in Figures 3-7. Figure 3 shows the effect of antioxidant in the solid compound (i.e., FA = 0%) while Figure 4 shows the same additives effect in the foamable compound (i.e., FA = 0.58%). In both cases there is a monotonic increase in stability with increase in ΔAO. This indicates that both compositions could be further stabilized by adding more than 0.24% incremental antioxidant. The increased "spread" in the foamable compound's family of curves over that of the solid compound indicates the greater contribution to stability by metal deactivator in the former case.

The symmetry and absence of curvature of the family of curves in Figure 5 are indicative of no stability improvement with the addition of incremental metal deactivator in the solid grade material.

The primary effect of incremental metal deactivator in the foamable grade material is to improve stability up to a concentration of 0.18%. The decline of the curves in Figure 6 to the right of this value should be interpreted to be actually asymptotic with the maximum stability value. The decline appears to be due to the forced use of the second order approximation.

Figure 7 depicts the destabilizing effect of foaming agent which is partially offset by the addition of antioxidant or, to a lesser extent, of metal deactivator. For example, the addition of 0.24% MD alone raises the OIT of the foamable grade from 117 to 131 minutes while the addition of the same amount of antioxidant raises the stability from 117 to 146 minutes.

The curves depicted in Figures 3 through 7 can be used to choose the relative amounts of incremental stabilizers needed to reach a specified level of stability. To achieve a level of stability for the foamable grade corresponding to an OIT of 150 minutes, any of the following incremental stabilizer concentrations may be utilized (taken from Figure 6):

0.24%△AO + 0.018%△MD

0.22%△AO + 0.026%△MD

0.20%△AO + 0.036%△MD

0.16%△AO + 0.058%△MD

0.12%△AO + 0.088%△MD

The interactions of the variables are presented graphically in Figures 8 and 9 wherein the equal performance contours represent plots of one variable versus the second keeping the third constant. Figure 8 depicts these equal performance curves for the solid compound (FA = 0%). Each curve is labeled with its corresponding stability value (OIT in minutes). The absence of a saddle-type configuration indicates that limiting stability has not been reached for the combination of the two stabilizers. A similar set of plots for the foamable grade material again indicates the lack of limiting stability. These plots may also be used to select compositions for a given performance. The 150 minutes line in Figure 9 defines all incremental stabilizer combinations providing this level of stability and includes those combinations deduced earlier from Figure 6.

Isometric response surfaces are depicted in Figures 10 and 11 and represent another way to visualize the interaction of two variables. The two surfaces presented in each of these figures represent the responses of polypropylene and HDPE under the same experimental conditions. The latter is reprinted from earlier work[1] and is shown on the same scale as polypropylene. The two resins will be compared later. The OIT values for a given foaming agent level are plotted on the vertical axis. The surfaces depicted can be visualized as the conversion to three-dimensionality of the sets of contour lines presented in Figures 8 and 9. The response surface for solid grade polypropylene (Figure 10) shows the limiting effect of incremental metal deactivator while the addition of antioxidant is effective in increasing stability for virtually every stabilizer combination over the 0%△AO - 0%△MD case. The surface for the foamable grade polypropylene (Figure 11) shows much the same behavior with a marked shift to lower overall stability. One obvious difference in the latter case is the increased effectiveness of incremental metal deactivator. In neither response surface is there any hint of synergistic behavior in the combined effect of the two stabilizers.

Polypropylene Stability in the Absence of Copper.

The catalytic effect of copper on the stability as determined by OIT can be assessed by comparing the previously described results with those generated in the absence of copper. Actual and computed OIT values, Y_B, for the 15 compositions are given in Table 1 and Figure 12 and the coefficients for the second order equation in Table 2.

Primary effects. The addition of incremental antioxidant results in stabilization improvement both in the solid (Figure 13) and foamable (Figure 14) grade compounds. Figure 15 shows that the metal deactivator in the solid grade reduces stability as its concentration increases. This anomalous result can be viewed either as a real effect with limiting stability already reached at 0%△MD or as an artifact caused by the forced use of a second order approximation. In

the case of the foamable grade, addition of metal deactivator has a positive effect upon stability which appears to reach a limiting level at approximately 0.24%△MD (Figure 16). This is surprising since the purpose of the MD is to act as a chelating agent to tie up catalytic cupric ions.[11] Aluminum is not expected to exhibit the same degree of catalytic behavior as copper. Another surprising result was that increasing the foaming agent concentration beyond roughly 0.20% causes a dramatic decrease in stability as shown in Figure 17. This decrease in stability can again be partially offset by the addition of either stabilizer.

Interactions of variables. The curvature of the equal performance contour lines for the solid grade (Figure 18) shows that limiting stability was not reached. Addition of antioxidant beyond the 0.24% level is expected to increase the stability while incremental metal deactivator promises no beneficial effect. The equal performance plot for the foamable grade (Figure 19) indicates that limiting stability has not been reached at the 0.24% △AO - 0.24%△MD stabilizer point. The relative planarity of the isometric response surfaces for polypropylene in Figures 20 and 21 is indicative of little or no interaction between antioxidant and metal deactivator.

Relative Cost

The relative cost of incremental additives Y_C, is computed for the antioxidant and metal deactivator alone (i.e., the stabilizers). Computed values of the relative cost (scaled to a maximum of 100 arbitrary units) for the 15 compositions are presented in Table 1. The additive nature of the relative cost manifests itself in a linear correlation with both stabilizers as shown in Figure 22. This equal cost contour diagram is similar to the equal performance contour diagrams presented in Figures 8, 9, 18, and 19.

Determination of Most Cost Effective Systems

The combination of equal stability and equal cost contour line diagrams may be used to determine the minimum cost composition at a given stability level. In the cases of solid and foamable grades in the absence of copper and solid grade in the presence of copper, it can be shown that the minimum cost compositions are achieved at 0%△MD with the addition of appropriate amounts of antioxidant. The case of the foamable grade in the presence of copper is depicted in Figure 23 which is an overlay of Figures 22 and 9. The dotted line is the locus of all tangential points of the two sets of contour lines, the path of the minimum cost compositions, as has been described in detail in the earlier publication.[1]

Comparison of Polypropylene and HDPE

The relative stabilities of the commercial HDPE and polypropylene resins studied in both the previous[1] and current works are presented in histogram form in Figure 24. The OIT stability of the solid grade polypropylene resin is 3.6 times as great as its HDPE counterpart in the absence of copper. This relative stability does not reflect any intrinsic property of these polymers but is a result of the higher level of additives in the commercial polypropylene.[5] It is well known that the presence of a high number of tertiary hydrogens along the polypropylene backbone (which are easily abstracted by free radicals) results in a higher susceptibility to oxidation as compared to HDPE.[22] It can be seen that polypropylene is affected by either copper contact or foaming agent alone while HDPE was affected only by the combination of these two conditions. It should be noted that even in the presence of copper, the stabilities of the solid and foamable grades of polypropylene are 3 times and 5.5 times greater respectively than those of the corresponding HDPE grades.

The effect of incremental stabilizers was illustrated by the isometric response surfaces in Figures 10, 11, 20, and 21. The response-response correlation, the comparison of OIT stabilities with and without contact to copper is depicted in Figure 25. This figure shows that even after the addition of 0.1% of either MD or AO, HDPE is still lower in stability than polypropylene. As indicated earlier,[1] the addition of 0.1% AO improves stability either in the presence or in the absence of copper for the solid and foamable grades of HDPE. In polypropylene, 0.1% △AO improves stability in all cases and the improvement continues at a level of 0.24% △AO.

The effect of incremental metal deactivator on stability in the solid grades of both resins is negligible. At the 0.1% Δ MD level, stability of the foamable HDPE was improved only in the presence of copper whereas in polypropylene improvement was noted in the presence or absence of copper. This is presumably due to differences in the nature of the base resins' stabilizer systems.

The cost efficiency of incremental additives is presented in Figures 26 and 27 for both resins. The relative cost values for HDPE were recalculated in order to conform to the corresponding polypropylene scale by multiplying the original HDPE values[1] by (0.1/0.24) or 0.417. The cost effectiveness of either additive in improving OIT in contact with or in the absence of copper is very low as reflected in the moderate slopes of the response lines in Figures 26 and 27 respectively. Since the points depicting the effect of incremental stabilizers in HDPE are significantly lower than those for the commercial polypropylene resin, it can be concluded that the stability gap between the two resins cannot be bridged without major cost increase.

Conclusions

- The addition of antioxidant to either resin was found to be more efficient than the addition of an equal amount of metal deactivator in improving stability.
- Incremental antioxidant is more cost effective than incremental metal deactivator.
- The addition of metal deactivator to the foamable grade resins improved stability in HDPE only in the presence of copper while it proved beneficial in polypropylene either in the presence or absence of copper.
- No evidence of synergistic behavior was observed between antioxidant and metal deactivator in either resin.
- The commercial grade polypropylene studied was found to have much higher OIT stability than its HDPE counterpart.
- Either the foaming agent or the presence of copper alone lowers the stability of polypropylene while HDPE is affected only by the combination of these two factors.

Acknowledgements

The authors would like to express their gratitude to Dr. M.C. Biskeborn and Mr. R.M. Morgan for providing stimulation and helpful suggestions in this work, and to Ms. J. Amato, Mr. E. Armour, and Mr. C. Nigro for performing the experimental work.

Their contributions are gratefully acknowledged.

References

1. Kiss, K.D. and Malawer, E.G. Proc. 26th IWCS, P. 68 (1977).
2. Pusey, B.B., Proc. 10th IWCS (1961).
3. Marshall, D.I. et.al., Proc. 23rd IWCS P. 63, (1974).
4. Robinson, M., SPE, ANTEC, Vol. XXI, 390 (1975).
5. Schmidt, G.A., Proc. 26th IWCS,P. 161 (1977).
6. Gesner, B.D. and Harmel, R.J., SPE, ANTEC, Vol. XXI, 286 (1975).
7. Wight, F.R., J. Cellular Plastics, P. 317. (Nov./Dec. 1976).
8. Grill, K., Wire Technology, 9, 223 (Oct. 1977).
9. Czanderna, A.W. et.al., Annual Report, INCRA Project No. 224, July 31, 1977.
10. Czanderna, A.W. et.al., Industrial Research, 20(1), 62, (Jan. 1978).
11. Yamaguchi, K., et.al., Proc. 26th IWCS, P. 87, (1977).
12. Patel, A., Proc. 26th IWCS, P. 83, (1977).
13. Kiss, K.D., U.S. Pat. 4,065,635, Dec. 27, 1977.
14. Kiss, K.D., U.S. Pat. 3,951,911, April 20, 1976.
15. Turbett, R.J., U.S. Pat. 4,044,200, August 23, 1977.
16. Scardiglia, F. and Kiss, K.D., U.S. Pat. 4,049,751, Sept. 20, 1977.
17. Kiss, K.D., Allan, J.H.L. and Fein, M.M., U.S. Pat. 4,066,610, Jan. 3,1978.
18. Kiss, K.D., U.S. Pat. 4,075,146, Feb. 21, 1978
19. Bernstein, B.S. and Lee, P.N., Proc. 24th IWCS, P. 202 (1975).
20. Chan, M.G., et.al., SPE 36th ANTEC, Vol. 24, 381 (1978).
21. Bair, H.E., SPE 31st ANTEC, P. 613, (1973).
22. Abramoff, C.S., "Antioxidants", Modern Plastics Encyclopedia, P. 144 (1977-78).



EDWARD G. MALAWER is a Research Chemist in charge of the Analytical Instrumentation Laboratories of Phelps Dodge Cable & Wire Company. He received a B.S. in Chemistry from the City College of New York in 1970, a Ph.D. in Physical Chemistry from New York University in 1976 and performed a post-doctoral study at the State University of New York, Albany. His areas of interest include instrumental analysis, optical and scanning electron microscopy, thermal analysis, stabilization, polymer degradation and morphology of solid dielectrics. His thesis involved the characterization of molecular motion in molten salts by Fourier-transform NMR spectrometry, and his work on the development of a DTA system for the teaching laboratory was published in the Journal of Chemical Education.



KORNEL D. KISS is the Manager of the Materials Research Laboratory at the Phelps Dodge Cable & Wire Company. He received a B.S. in Chemical Engineering in 1944 and a D.C.E. in 1947 from the Polytechnical University of Budapest. His past experience includes organic and polymer synthesis research, supervision of product and process development on a variety of polymers, polymer aging, degradation and stabilization. He is the author of five textbooks, and the inventor of over 40 patents, about half of them in the additives and polymer stabilization field. His interests include the optimization of insulating materials, thermal analysis, process miniaturization, statistics and laboratory scale simulation of polymer aging.

TABLE 1

Variables and Responses

Variables: X_1=Incremental Antioxidant concentration, % by weight, ΔAO
X_2=Incremental Metal Deactivator concentration, % by weight, ΔMD
X_3=Total Foaming Agent concentration, % by weight, FA
L = Low, M = Middle, H = High, V = Very, α = 1.215

Responses: Y_A=OIT in copper, minutes
Y_B=OIT in absence of copper, minutes
Y_C=Relative Cost
ΔY=Actual Value-Computed Value

	VARIABLES									RESPONSES						
	Levels			Experimental Units			% By Weight			Y_A=OIT in Copper			Y_B=OIT in Aluminum			Y_C=Relative Cost
Exp. No.	ΔAO X_1	ΔMD X_2	FA X_3	ΔAO X_1	ΔMD X_2	FA X_3	ΔAO X_1	ΔMD X_2	FA X_3	Act.	Comp.	ΔY_A	Act.	Comp.	ΔY_B	Act.=Comp.
1	L	L	L	-1	-1	-1	0.0216	0.0216	0.0522	156.6	157.6	-1.1	193.8	195.7	-1.9	8.5
2	H	L	L	1	-1	-1	0.216	0.0216	0.0522	198.0	189.6	8.4	231.4	221.8	9.6	43.8
3	L	H	L	-1	1	-1	0.0216	0.216	0.0522	153.9	155.4	-1.5	196.3	190.0	5.4	55.8
4	H	H	L	1	1	-1	0.216	0.216	0.0522	185.1	192.3	-7.2	201.0	208.2	-7.2	91.1
5	L	L	H	-1	-1	1	0.0216	0.0216	0.522	132.2	126.8	5.4	153.0	143.3	9.7	8.5
6	H	L	H	1	-1	1	0.216	0.0216	0.522	151.1	151.5	-0.4	175.5	178.3	-2.8	43.8
7	L	H	H	-1	1	1	0.0216	0.216	0.522	127.4	137.7	-10.3	154.1	161.1	-7.0	55.8
8	H	H	H	1	1	1	0.216	0.216	0.522	166.5	167.3	-0.8	191.7	187.3	4.4	91.1
9	VL	M	M	$-\alpha$	0	0	0	0.12	0.29	148.6	143.1	5.5	184.2	188.6	-4.4	28.3
10	VH	M	M	α	0	0	0.24	0.12	0.29	179.8	180.5	-0.7	217.6	220.3	-2.7	71.2
11	M	VL	M	0	$-\alpha$	0	0.12	0	0.29	139.9	150.8	-10.9	183.9	195.3	-11.4	21.0
12	M	VH	M	0	α	0	0.12	0.24	0.29	174.7	159.1	15.6	202.1	197.8	4.3	78.5
13	M	M	VL	0	0	$-\alpha$	0.12	0.12	0	187.2	186.7	0.5	214.6	202.3	12.3	49.8
14	M	M	VH	0	0	α	0.12	0.12	0.58	157.1	152.8	4.3	171.4	157.8	13.6	49.8
15	M	M	M	0	0	0	0.12	0.12	0.58	157.6	164.5	-6.9	179.5	201.3	-21.8	49.8

TABLE 2

Coefficients of Second Order Equation and Measure of Fit

DESIGNATION		RESPONSES Y_A	Y_B	Y_C	Coefficient For
Coefficient	a_o	164.518	201.3191	1.5	
	a_1	15.4043	13.0552	0.532	X_1
	a_2	3.40413	1.0512	0.713	X_2
	a_3	-13.9492	-18.3243	0	X_3
	a_{11}	-1.82170	2.1268	0	X_1^2
	a_{22}	-6.49344	-3.2220	0	X_2^2
	a_{33}	3.56096	-14.4022	0	X_3^2
	a_{12}	1.225	-2.225	0	X_1X_2
	a_{13}	-1.825	2.225	0	X_1X_3
	a_{23}	3.25	5.65	0	X_2X_3
Standard Deviation		6.93	9.43	0	
Relative Error, %		4.21	4.68	0	

Figure 1

PARTIAL FACTORIAL GRID DESIGN FOR 3 VARIABLES

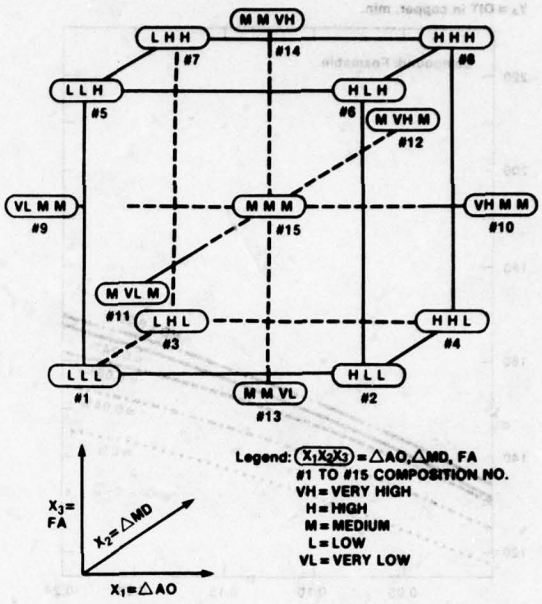


Figure 2

COMPARISON OF "ACTUAL" AND "COMPUTED" VALUES

Display: Y_A, OIT in copper, minutes

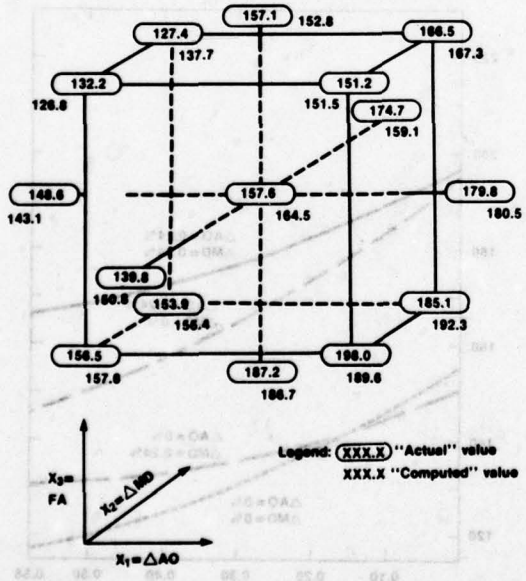


Figure 3

EFFECT OF ANTIOXIDANT

Y_A = OIT in copper, min.

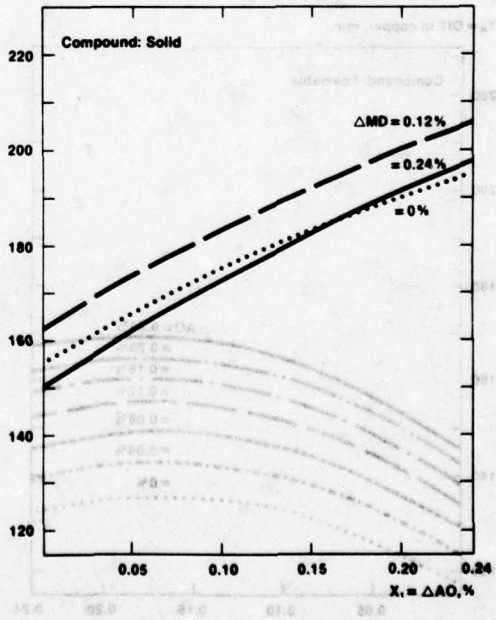


Figure 4
EFFECT OF ANTIOXIDANT

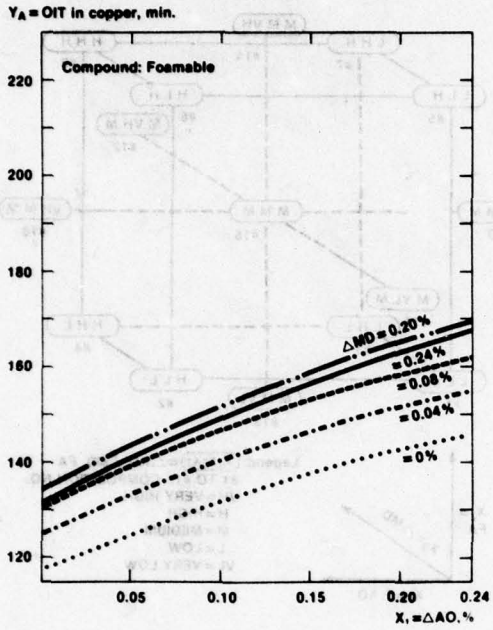


Figure 5
EFFECT OF METAL DEACTIVATOR

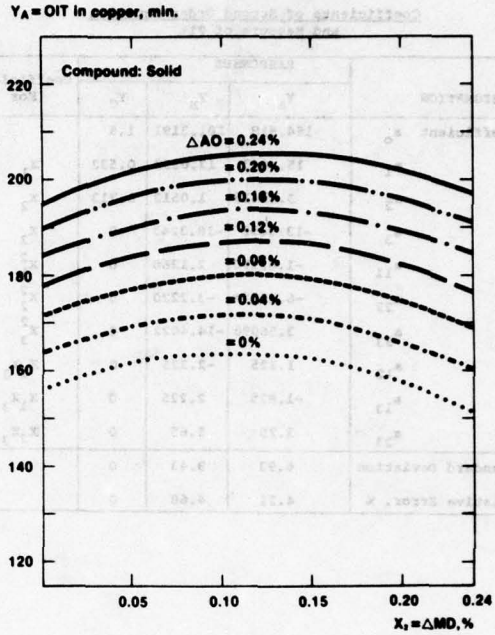


Figure 6
EFFECT OF METAL DEACTIVATOR

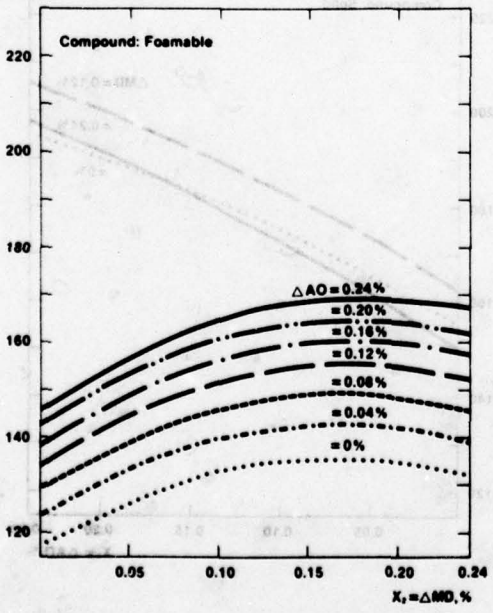


Figure 7
EFFECT OF FOAMING AGENT

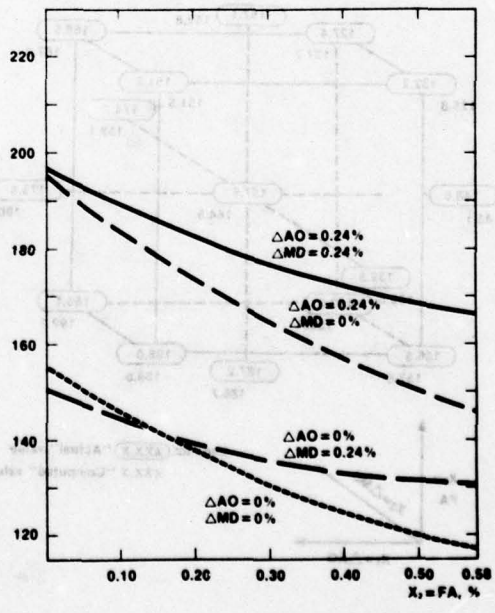


Figure 8

EQUAL PERFORMANCE COMPOSITIONS

Display: Y_A, Equal OIT Times in copper, minutes
Compound: Solid

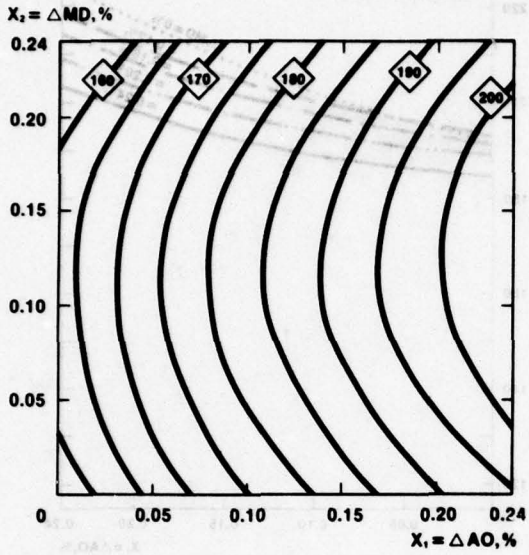


Figure 9

EQUAL PERFORMANCE COMPOSITIONS

Display: Y_A, Equal OIT Times in copper, minutes
Compound: Foamable

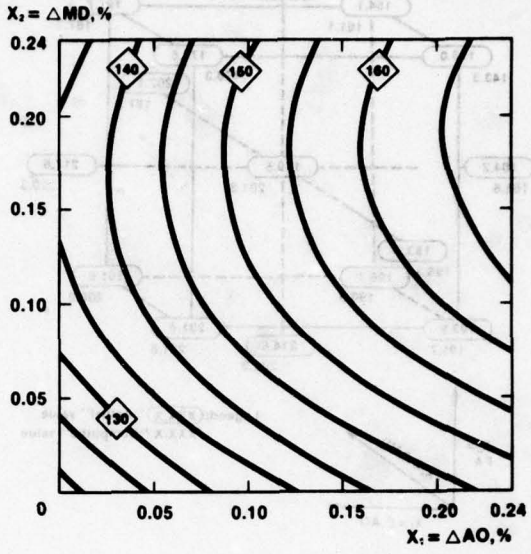


Figure 10

ANTIOXIDANT – METAL DEACTIVATOR INTERACTION

Y_A = OIT in copper, minutes
Compound: Solid

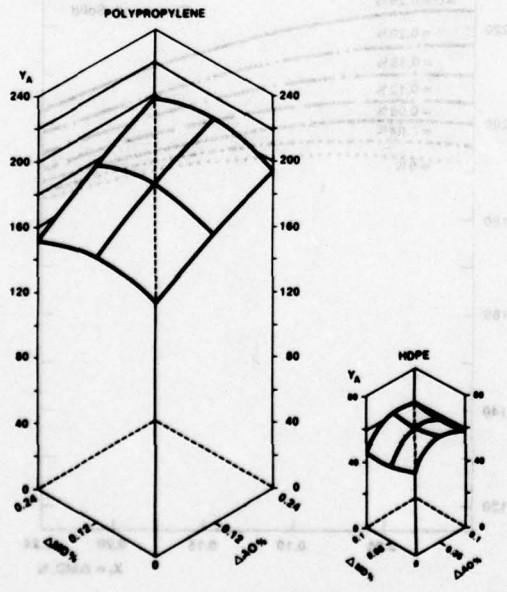


Figure 11

ANTIOXIDANT – METAL DEACTIVATOR INTERACTION

Y_A = OIT in copper, minutes
Compound: Foamable

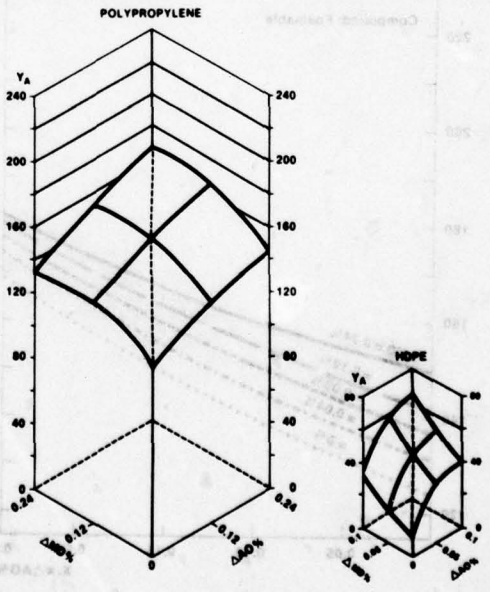


Figure 12

COMPARISON OF "ACTUAL" AND "COMPUTED" VALUES

Display: Y_B, OIT in absence of copper, minutes

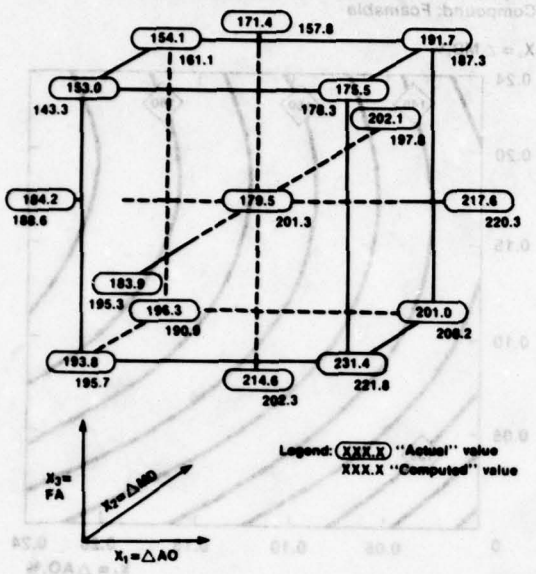


Figure 13

EFFECT OF ANTIOXIDANT

Y_B = OIT in absence of copper, min.

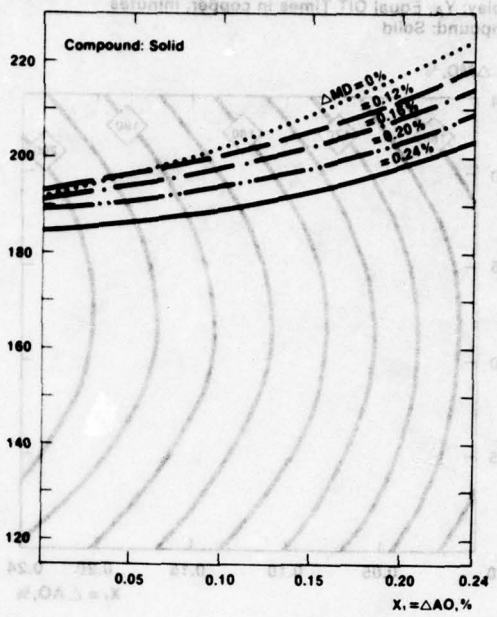


Figure 14

EFFECT OF ANTIOXIDANT

Y_B = OIT in absence of copper, min.

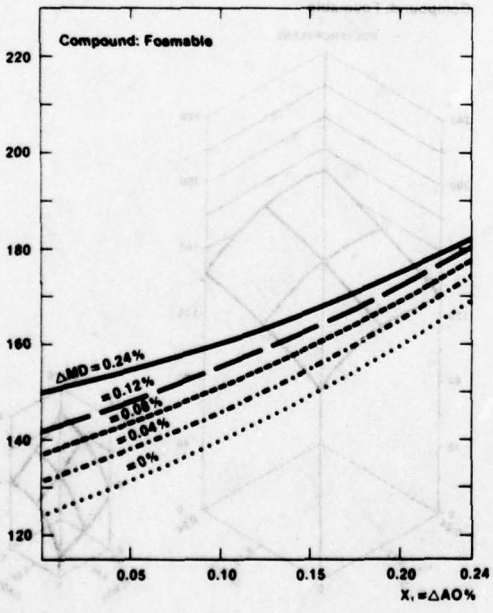


Figure 15

EFFECT OF METAL DEACTIVATOR

Y_B = OIT in absence of copper, min.

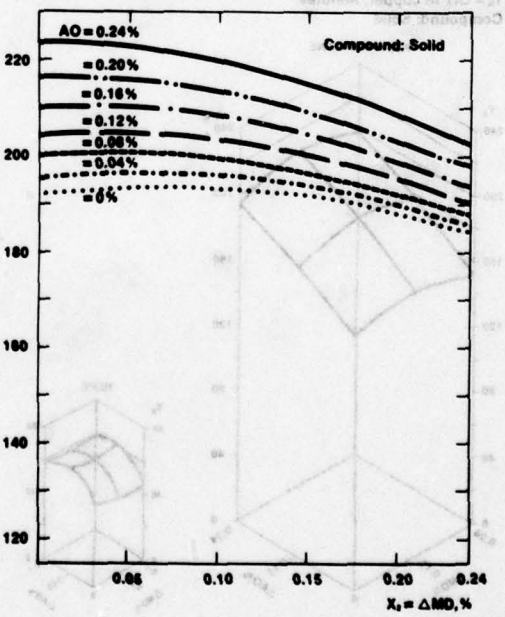


Figure 16
EFFECT OF METAL DEACTIVATOR

Y_B = OIT in absence of copper, min.

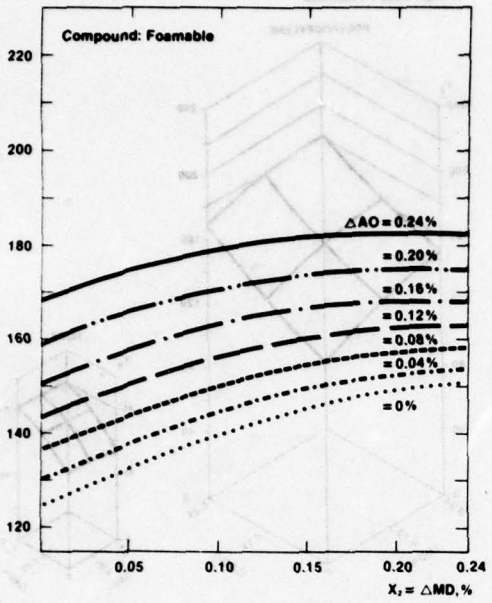


Figure 17
EFFECT OF FOAMING AGENT

Y_B = OIT in absence of copper, min.

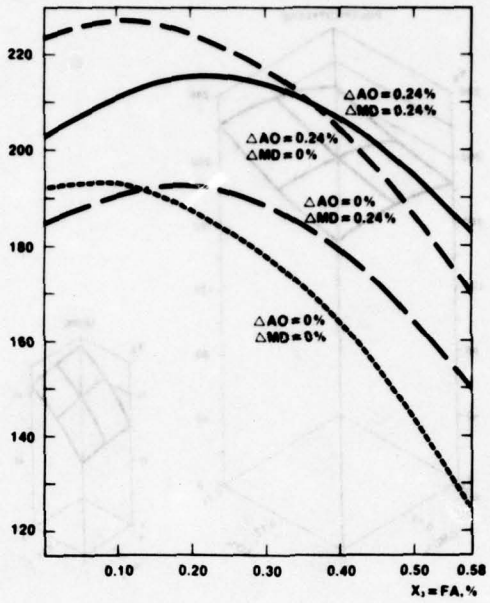


Figure 18
EQUAL PERFORMANCE COMPOSITIONS

Display: Y_B, Equal OIT Times in absence of copper, minutes
Compound: Solid

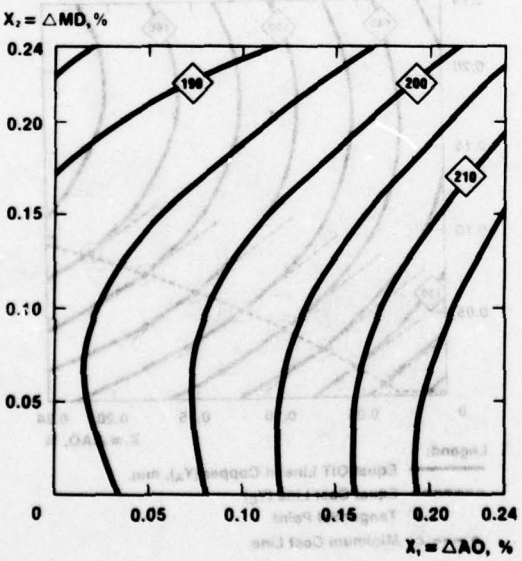


Figure 19
EQUAL PERFORMANCE COMPOSITIONS

Display: Y_B, Equal OIT Times in absence of copper, minutes
Compound: Foamable

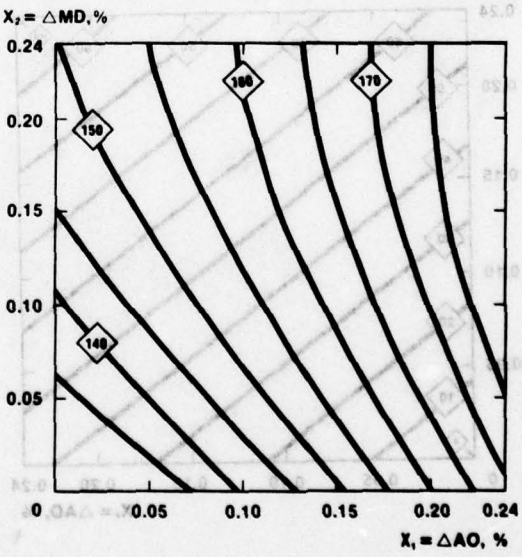


Figure 20

ANTIOXIDANT – METAL DEACTIVATOR INTERACTION

Y_B = OIT in absence of copper, minutes
Compound: Solid

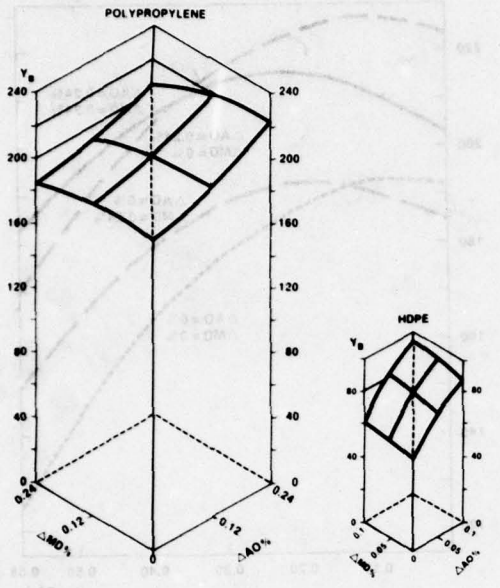


Figure 21

ANTIOXIDANT – METAL DEACTIVATOR INTERACTION

Y_B = OIT in absence of copper, minutes
Compound: Foamable

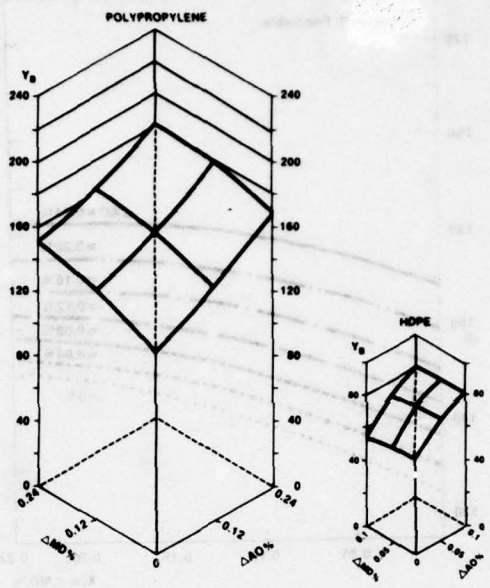


Figure 22

EQUAL COST COMPOSITIONS

Display: Y_C, Relative Cost

X_2 = △MD, %

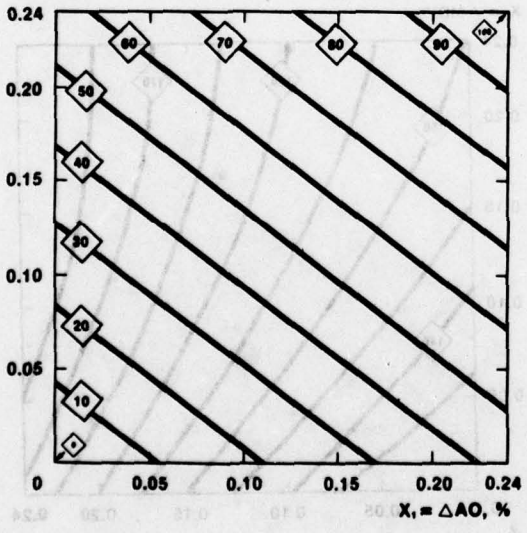
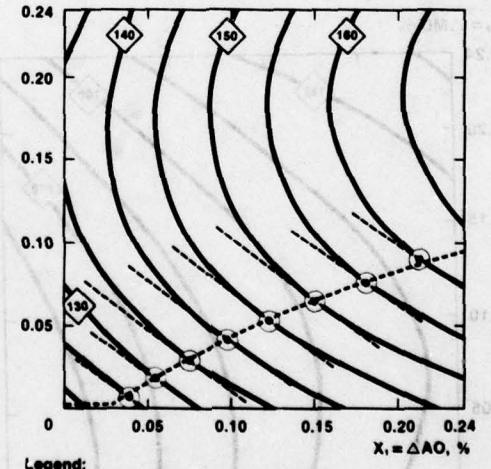


Figure 23

MINIMUM COST COMPOSITIONS

Compound: Foamable

X_2 = △MD, %



Legend:
- Equal OIT Line in Copper (Y_A), min.
- Equal Cost Line (Y_C)
- Tangential Point
- Minimum Cost Line

Figure 24
COMPARISON OF POLYPROPYLENE AND HDPE

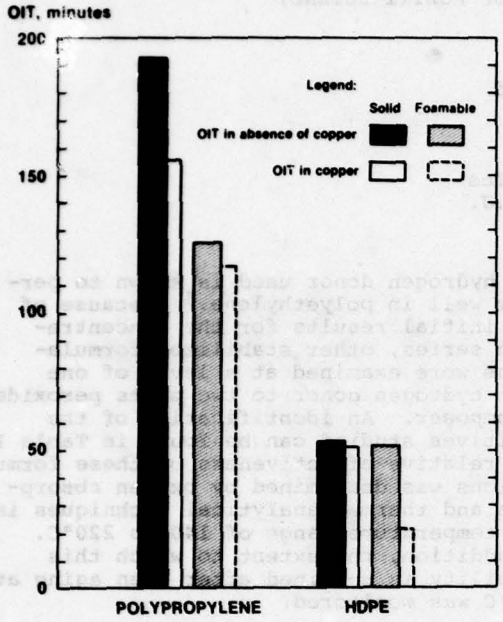


Figure 25
CORRELATION BETWEEN OIT VALUES

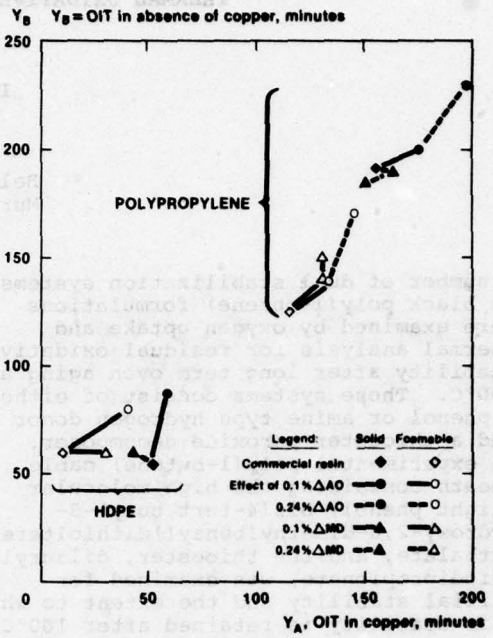


Figure 26
CORRELATION BETWEEN RELATIVE COST AND OIT IN COPPER

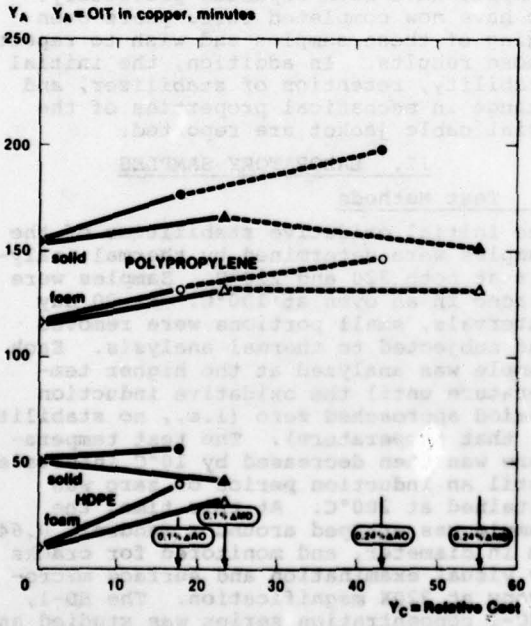
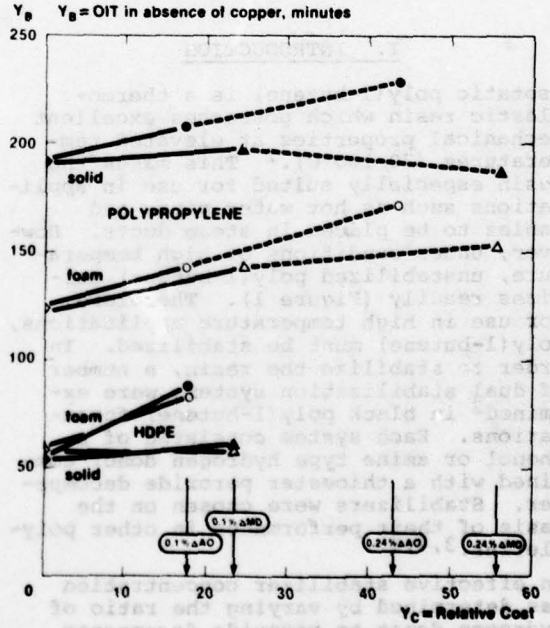


Figure 27
CORRELATION BETWEEN RELATIVE COST AND OIT IN ABSENCE OF COPPER



THERMAL OXIDATIVE STABILITY OF POLY(1-BUTENE)

I. P. Heyward

Bell Laboratories
Murray Hill, N.J.

A number of dual stabilization systems in black poly(1-butene) formulations were examined by oxygen uptake and thermal analysis for residual oxidative stability after long term oven aging at 100°C. These systems consist of either a phenol or amine type hydrogen donor and a thioester peroxide decomposer. An experimental poly(1-butene) cable sheath containing the high molecular weight phenol, bis(4-tert.butyl-3-hydroxy-2,6-dimethylbenzyl)dithioltere-phthalate, and the thioester, dilauryl-thiodipropionate, was examined for initial stability and the extent to which this stability is retained after 100°C oven aging. Changes in the physical properties of the sheath accompanying aging were also studied.

I. INTRODUCTION

Isotatic poly(1-butene) is a thermoplastic resin which possesses excellent mechanical properties at elevated temperatures (70-100°C).[1] This makes the resin especially suited for use in applications such as hot water pipes and cables to be placed in steam ducts. However, under conditions of high temperature, unstabilized poly(1-butene) oxidizes readily (Figure 1). Therefore, for use in high temperature applications, poly(1-butene) must be stabilized. In order to stabilize the resin, a number of dual stabilization systems were examined[2] in black poly(1-butene) formulations. Each system consisted of a phenol or amine type hydrogen donor combined with a thioester peroxide decomposer. Stabilizers were chosen on the basis of their performance in other polyolefins.[3,4,5]

An effective stabilizer concentration was determined by varying the ratio of hydrogen donor to peroxide decomposer. The hydrogen donor used is known to perform well in polyethylene.[4] Because of the initial results for the concentration series, other stabilizer formulations were examined at a level of one part hydrogen donor to two parts peroxide decomposer. An identification of the additives studied can be found in Table I. The relative effectiveness of these formulations was determined by oxygen absorption and thermal analytical techniques in the temperature range of 140 to 220°C. In addition, the extent to which this stability is retained after oven aging at 100°C was monitored.

On the basis of initial effectiveness and the results of one year's aging at 100°C, several systems were selected to be included in a material specification. One system containing HD-6 and DEC-1 was incorporated into a trial cable jacket.

Initial results for the laboratory samples have been reported previously.[2] We have now completed three years oven aging of these samples and wish to report those results. In addition, the initial stability, retention of stabilizer, and change in mechanical properties of the trial cable jacket are reported.

II. LABORATORY SAMPLES

A. Test Methods

The initial oxidative stabilities of the samples were determined by thermal analysis at both 220 and 210°C. Samples were placed in an oven at 100°C. At 30 day intervals, small portions were removed and subjected to thermal analysis. Each sample was analyzed at the higher temperature until the oxidative induction period approached zero (i.e., no stability at that temperature). The test temperature was then decreased by 10°C intervals until an induction period of zero was attained at 200°C. At this time, the sample was wrapped around a mandrel, 0.64 cm in diameter, and monitored for cracks by visual examination and surface microscopy at 320X magnification. The HD-1, DEC-1 concentration series was studied as

well as samples containing diverse hydrogen donors. The residual stabilities of all the laboratory samples were determined at 161°C by oxygen absorption and at 210°C by thermal analysis.

B. Effect of Concentration

The residual oxidative stabilities of poly(1-butene) formulations containing HD-1 and DEC-1 at various concentrations are found in Table II. After three years of aging, three of the samples have attained a zero oxidative induction time at 210 and 200°C. Two of these samples containing either 0.5 or 1.0 percent hydrogen donor and 1.0 percent peroxide decomposer still have measurable induction times at these temperatures. Only two of the samples have cracked. The sample containing no HD-2 or DEC-1 embrittled at the surface after 60 days of aging at 100°C and completely fractured after 8 months at this temperature and the sample containing 0.3 percent of stabilizer showed visible cracks after 2.5 years of aging at 100°C. Complete fracture has not occurred in this sample to date. Both of the samples which cracked attained zero oxidative-induction periods at 200°C after relatively short periods of aging (Table II).

The rapid loss of oxidative stability of the sample containing 0.5 percent hydrogen donor and 2.0 percent peroxide decomposer might be due to the high concentration of the thioester. This additive has been found[2] to exude to the surface. The additive on the surface may oxidize and then act as a prooxidant or the migration of the thioester could act as a carrier for the phenol HD-2 causing physical depletion of the additive. None of these formulations containing HD-2 and DEC-1 appear to impart good long term stability to the resin compared with most of the other hydrogen donors examined.

C. Effectiveness of Other Hydrogen Donors

The residual oxidative stabilities of various phenols in poly(1-butene) formulations are shown in Table III. Since most of these formulations have residual oxidative stability at 200°C, induction times are reported at 210 and 161°C. Two of these formulations containing either HD-6 or HD-3 were included in a material specification based upon initial stability and residual stability after one year of aging at 100°C.[2]

The initial stability measurements in that study indicated that the most effective stabilization systems at the lower test temperatures (161 and 140°C) were those containing either HD-6, HD-7 or HD-8. The initial high (220 and 210°C) and low (161 and 140°C) temperature data for all the formulations were in good agreement with the exception of the two containing either HD-1 or HD-4. The amine HD-1 was very effective at the higher temperatures while the hydrazine HD-4 performed quite well at the lower temperatures. This can be seen in Table III where the initial stabilities are reported at 210 and 161°C. Upon oven aging for one year, however, poly(1-butene) containing HD-7 rapidly lost oxidative stability compared with the other formulations. Conversely, the resin containing either HD-1, HD-3 or HD-6 showed very good retention.

In general, the three-year data correlate well with the one-year test results. After three years of aging, stabilization systems containing HD-1, HD-3 or HD-6 continue to impart some oxidative stability to the resin. However, several formulations which did not appear to be retained well after one year of aging now appear promising. For example, the hydrazine, HD-4, which did not seem particularly effective after a year, now appears to give good results. Additionally the sample containing the thiobisphenol HD-8, has retained a substantial degree of stability compared with initial values at 161°C. These two hydrogen donors, HD-4 and HD-8, have been found[3] to perform very well in formulations of a similar polyolefin, polypropylene. Interestingly, the HD-8 sample retained oxidative stability to a much greater extent than the sample containing HD-7, the monomeric form of this additive.

III. EXPERIMENTAL CABLE

A. Oxidative Stability

An experimental cable with a poly(1-butene) jacket containing 0.5% HD-6 and 1.0% DEC-1 was successfully extruded at Western Electric in Atlanta, Georgia. The initial oxidative stability of the cable jacket and the extent to which this stability is retained on aging were examined by thermal analysis. The values are shown in Table IV where they are compared with the original laboratory samples containing this formulation. The initial oxidative induction periods for the laboratory samples are about two-to-one greater than those of the cable sheath. This may be due to loss of the additives under the extreme thermal conditions of extrusion. After oven aging at 100°C, the oxidative induction periods at 220 and 210°C are essentially zero. The loss of stability accompanying aging is due in part to additive migration. Infrared reflection

spectroscopy and surface microscopy were used to study this migration.

B. Surface Studies

Micrographs of the cable sheath surface were taken at 320X magnification. These micrographs indicated that a residue similar to that shown in Figure 2 was present on the surface. To further investigate the migratory behavior of the additives in the cable sheath, sections of the jacket were aged at both 100°C and ambient temperature and their surfaces were examined by internal reflection spectroscopy. The additives were identified using characteristic bands in the C=O region from 1800 to 1600 cm^{-1} The phenol HD-6 has a doublet phthalate band at 1645 and 1635 cm^{-1} (Figure 3) while DEC-1 has an ester carbonyl at 1735 cm^{-1} (Figure 4). Internal reflection spectra of the sheath taken after 30 days of aging at 100°C indicate that the surface layer contains larger amounts of the hydrogen donor HD-6, while the amount of thioester appears to be moderate (Figure 5). Conversely, the thioester DEC-1 is very noticeable after aging at ambient temperature while little hydrogen donor can be observed. This result could be attributed to the higher volatility and lower molecular weight of the thioester compared with the hydrogen donor. Thermogravimetric analysis shown in Figure 6 demonstrates this phenomena where at 350°C, 60% of the thioester is lost compared with only 20% of the hydrogen donor. Durmis, et al.,[6] found that surface films of additives will be formed if the volatilization process occurs more slowly than the diffusion process.

Reflection spectra of the cable sheath taken after two years of aging are shown in Figure 7. Both the thioester DEC-1 and the phenol HD-6 are present after aging at ambient temperature as indicated by the C=O bands at 1735 cm^{-1} and 1645, 1635 cm^{-1} respectively. Unfortunately, it is difficult to determine if hydrogen donor or thioester are present on the surface of the sheath aged at 100°C due to the broadening of the C=O 1700-1600 cm^{-1} region. In addition, the baseline in the C-O 1200-1300 cm^{-1} region has dropped. It has been shown[7] that these changes are indicative of surface oxidation.

In order to determine the effect of the surface oxidation observed spectroscopically upon the physical properties of the sheath, the tensile properties were studied.

C. Mechanical Properties

The tensile properties of the poly(1-butene) cable sheath aged at 100°C for two years were determined according to ASTM D1708. These values were compared with measurements made on the sheath aged at ambient temperatures, which showed no signs of surface oxidation spectroscopically (Figure 7). The results are shown in Table V. After two years of aging at 100°C, the value of the tensile strength at break of the sheath has decreased by about 11 percent. In addition, the elongation value has dropped by about 18 percent compared with values obtained for the sample aged at room temperature. Changes in elongation values can be indicative of surface oxidation. However, these changes are slight. Analogously, Gesner[8] et al., have shown that poly(1-butene) can withstand substantial amounts of surface oxidation with little change in physical properties.

IV. CONCLUSIONS

The oxidative stability of the experimental cable sheath significantly decreases after two years of oven aging at 100°C. This loss is, in part, due to the migration of additives from the bulk of the resin to the surface. Infrared reflection spectra indicate the presence of some surface oxidation after two years at 100°C. However, this oxidation is found to cause only minor changes in the physical properties of the sheath.

A substantial decrease in most of the residual oxidative stabilities of black poly(1-butene) laboratory formulations also are observed after three years of oven aging at 100°C. However, the formulation containing the phenol HD-6 and DEC-1 continues to impart oxidative stability to the resin. In addition, stabilization systems containing either the phenols HD-4 or HD-8 and the thioester DEC-1 appear to impart good long-term oxidative stability to the resin. These systems did not appear particularly effective in the early stages of aging but now appear promising as alternative stabilization systems for the resin. The use of a polymeric additive such as the thiobisphenol, HD-8 may be the key to good long-term stability of resins used for high temperature applications.

V. EXPERIMENTAL

A. Materials

The poly(1-butene) was a homopolymer (M.I. 0.4) supplied by the Witco Chemical Corporation. Initial oxidative

stability (Figure 1) was determined on an additive-free resin. All other studies were on resin containing 0.1 weight percent di-tert.-butyl-p-cresol (BHT). A Witco masterbatch of poly (1-butene) containing 25 percent furnace black (80 mμ particle size, pH 8.5) was used to fabricate black formulations. Additives (Table 1) were commercial samples used as received.

B. Sample Preparation

Stabilizers were incorporated into poly(1-butene) by mixing on a Brabender plasticorder. The samples (35g) were compounded under nitrogen at 165°C and 50 rpm. The resin was masticated for one minute, removed from the Brabender for addition of stabilizers, and then mixed for an additional three minutes. Black samples were fabricated from 31.5g of clear poly(1-butene) and 3.5g of black masterbatch. Fifty mil films of the compounded resins were prepared by molding the samples for one minute at 165°C and then cooling under pressure.

C. Oxidation

The unstabilized resin (10 mil films) were oxidized at 100°C using the standard oxygen absorption method of Hawkins and coworkers.[5] The compounded resin (50 mil films) were oxidized at 161°C using the Hawkins method.[9] Samples weighed 0.1 ± .01g. Multiple (3-4) runs were made for each formulation. Data are reported as average extrapolated induction times.

D. Aging

Strips (1" x 6" x .05") of the stabilized poly(1-butene) laboratory samples were aged by suspending in a 100°C forced air oven. Samples were removed periodically and subjected to thermal analysis (see below). Sections of the cable sheath were aged 100°C and ambient temperature in open beakers. Tensile bars were punched from the sheath and measurements made as described below.

E. Tensile Tests

Tensile properties were measured using T-50 tensile specimens.[10] A minimum of five measurements were made for each sample. Crosshead speeds of 20"/min. were used.

F. Thermal Analysis

Oxidative stabilities were determined at 210°C on a duPont 990 thermal analyzer equipped with a DSC cell. Samples were analyzed on aluminum pans in an oxygen environment (flow rate - 200 ml/min) using a standard procedure.[11]

The volatilization behavior of HD-6 and DEC-1 were examined on a duPont 951 thermogravimetric analyzer. The samples were heated from ambient temperature to 1000°C at 100°C/min in a nitrogen atmosphere.

G. Microscopy

Specimen surfaces were examined on a Reichert microscope at 125 and 320X magnification.

H. Infrared Analysis

Internal reflection spectra were obtained on a Perkin Elmer 621 spectrophotometer equipped with a Wilks Model 50 internal reflection device. Samples were analyzed on IRS-5 reflection elements (20 x 20 x 2mm) using a 45° angle of incidence and standard instrument conditions. Transmission spectra of polymer additives were obtained with nujol mulls on NaCl crystals.

Acknowledgment

The author wishes to acknowledge L. Lewin and M. G. Chan for sample preparation and initial oxygen absorption studies, and L. Johnson for thermogravimetric analysis.

REFERENCES

1. C. R. Lindengren, Polymer Eng. and Sci., 10, 165 (1970).
2. I. P. Heyward, M. G. Chan and L. Lewin, Presented at the 35th ANTEC, Soc. Plast. Eng., Montreal, (1977).
3. M. G. Chan and R. A. Powers, Proc. 33rd ANTEC, Soc. Plast. Eng., 292 (1975).
4. J. B. Howard, Proc. 21st Int. Wire and Cable Symp., 329 (1972).
5. W. L. Hawkins, V. L. Lanza, B. B. Lloeffler, W. Matreyek and F. H. Winslow, J. Appl. Pclym. Sci., 1, 37 (1959).
6. J. Durmis, M. Korvăs, P. Căučík and J. Holčík, European Polymer Journal, 11, 222 (1975).
7. J. P. Luongo, J. Polym. Sci., 42, 139 (1960).
8. B. D. Gesner and R. J. Harmel, Proc. 35th ANTEC, Soc. Plast. Eng., 407, (1977).
9. W. L. Hawkins, R. H. Hansen, W. Matreyek and F. H. Winslow, J. Appl. Polym. Sci., 1, 37 (1959).
10. ASTM D1708.
11. J. B. Howard, Proc. 31st ANTEC, Soc. Plast. Eng., 408 (1973).

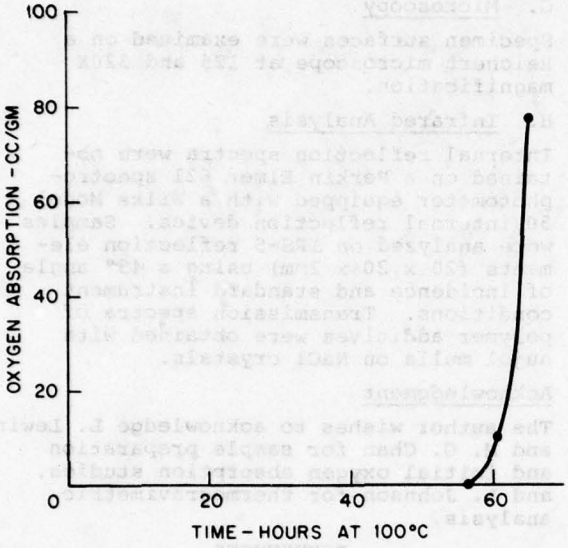


Figure 1. Oxidation of unstabilized poly(1-butene) at 100°C.

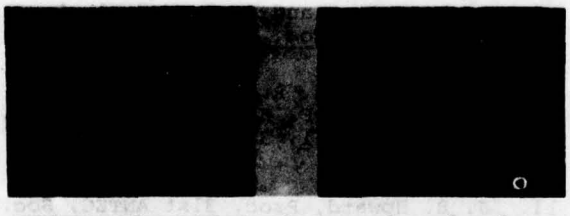


Figure 2. Photomicrographs of poly (1-butene) cable sheath surface at 320X magnification.

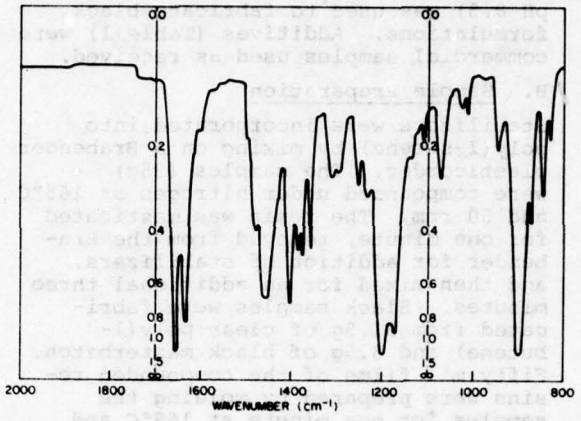


Figure 3. Transmission spectrum of phenol HD-6 (2000-800 cm^{-1}).

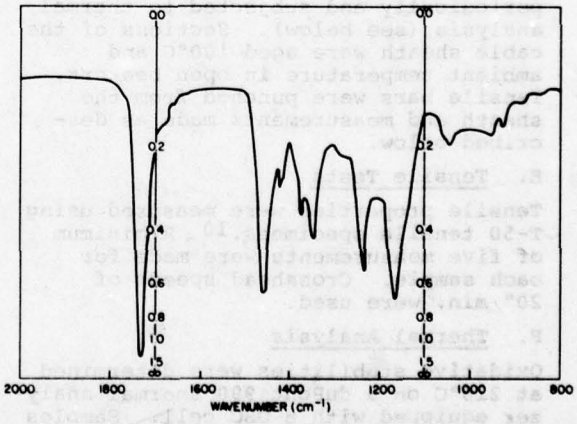


Figure 4. Transmission spectrum of thioester DEC-1 (2000-800 cm^{-1}).

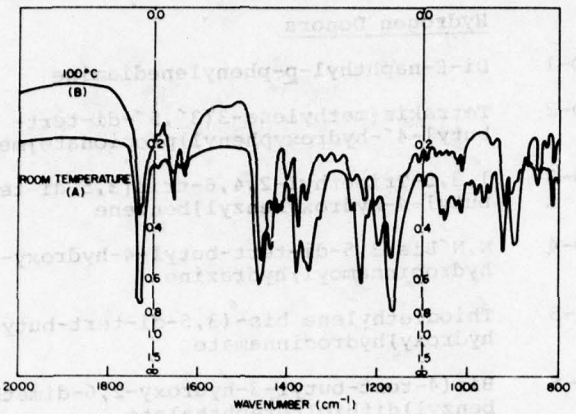


Figure 5. Reflection spectra of poly (1-butene) aged at (A) room temperature and (B) 100°C for 30 days.

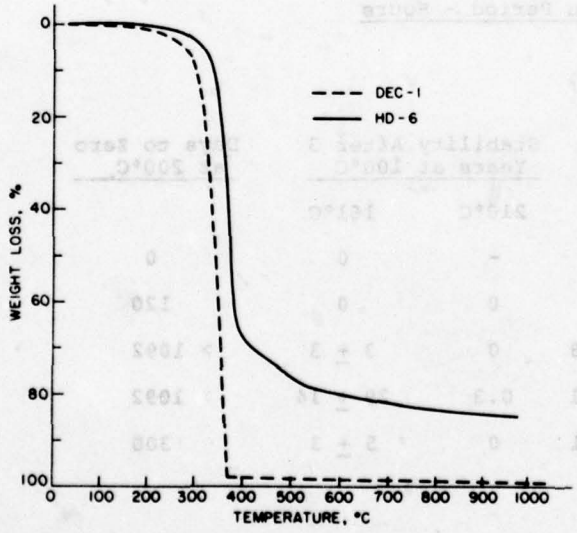


Figure 6. Thermogravimetric analysis of HD-6 and DEC-1.

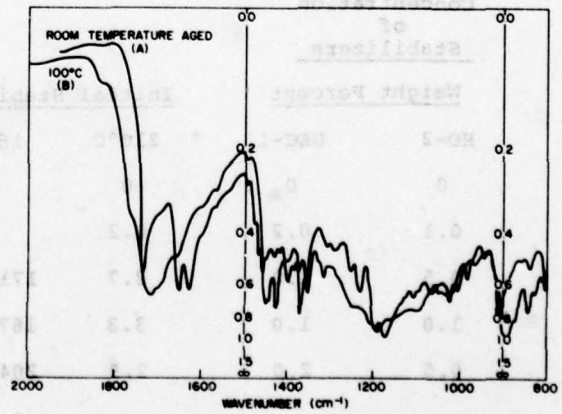


Figure 7. Reflection spectra of poly (1-butene) aged at (A) room temperature and (B) 100°C for 2 years.

TABLE I

ADDITIVES FOR POLY(1-BUTENE)

Additive	Chemical Structure
	Hydrogen Donors
HD-1	Di-β-naphthyl-p-phenylenediamine
HD-2	Tetrakis[methylene-3(3′,5′-di-tert-butyl-4′-hydroxyphenyl)propionate]methane
HD-3	1,3,5-Trimethyl-2,4,6-tris[3,5-di-tert-butyl-4-hydroxybenzyl]benzene
HD-4	N,N′Bis(3,5-di-tert-butyl-4-hydroxy-hydrocinnamoyl)hydrazine
HD-5	Thiodiethylene bis-(3,5-di-tert-butyl-4-hydroxy)hydrocinnamate
HD-6	Bis(4-tert-butyl-3-hydroxy-2,6-dimethyl-benzyl)dithiolterephthalate
HD-7	4,4′-Thiobis(3-methyl-6-tert-butylphenol)
HD-8	Polymeric thiobisphenol
	Peroxide Decomposer
DEC-1	Dilaurylthiodipropionate

TABLE II

EFFECT OF CONCENTRATION ON THE RETENTION OF OXIDATIVE STABILITY OF POLY(1-BUTENE)

Concentration of Stabilizers, Weight Percent		Average* Induction Period - Hours				
		Initial Stability		Stability After 3 Years at 100°C		Days to Zero at 200°C
HD-2	DEC-1	210°C	161°C	210°C	161°C	
0	0	0	-	-	0	0
0.1	0.2	0.2	-	0	0	120
0.5	1.0	2.7	171 ± 28	0	3 ± 3	> 1092
1.0	1.0	3.3	167 ± 21	0.3	29 ± 14	> 1092
0.5	2.0	2.9	204 ± 11	0	5 ± 3	300

* Average of 3-5 samples analyzed

TABLE III

RESIDUAL OXIDATIVE STABILITY OF HYDROGEN DONORS AT 0.5 WEIGHT PERCENT CONCENTRATION

Average* Induction Period - Hours

Stabilizer		Initial Stability		Stability After 3 Years at 100°C	
Hydrogen Donor	Peroxide** Decomposer	210°C	161°C	210°C	161°C
HD-1	DEC-1	2.8	124 ± 12	.13	0
HD-2	DEC-1	2.7	171 ± 28	0	3 ± 3
HD-3	DEC-1	2.2	171 ± 32	.20	5 ± 5
HD-4	DEC-1	1.0	196 ± 2	.10	31 ± 11
HD-5	DEC-1	2.5	198 ± 34	.03	0
HD-6	DEC-1	3.9	219 ± 28	.48	56 ± 16
HD-7	DEC-1	2.2	248 ± 43	.05	18 ± 9
HD-8	DEC-1	2.3	321 ± 78	.10	85 ± 20

* Average of 3-5 samples analyzed

** At 1.0 weight percent concentration

TABLE IV

OXIDATIVE STABILITY OF EXPERIMENTAL CABLE SHEATH

Average* Induction Period - Hours

	Initial Stability		Stability After 2 Years at 100°C	
	220°C	210°C	220°C	210°C
Laboratory Sample**	3.9	-	.28	.97
Experimental Cable**	1.9	-	0	.07

* Average of 5 samples analyzed

** Contains 0.5 percent HD-6 and 1.0 percent DEC-1

TABLE V

TENSILE PROPERTIES OF EXPERIMENTAL CABLE SHEATH

	Tensile Strength (psi)*		Elongation Percent at break*
	Yield	Break	
Room temperature aged sheath**	2800	4300	300
100°C aged sheath**	2800	3800	240

* Average of 3-5 samples

** Aged for 2 years



Ms. Heyward is a member of the Polymer Chemistry Research and Development Department at Bell Laboratories, Murray Hill, New Jersey, where she has been employed since 1976. During this time, she has been involved with various aspects of the stabilization and degradation of polyolefins used for wire and cable applications.

THE EFFECT OF FILLING COMPOUND MIGRATION ON CELLULAR INSULATION

D. Mangaraj, M.C. Biskeborn, & K.D. Kiss

Phelps Dodge Communications Company
White Plains, N.Y.

Summary

The migration of petrolatum based filling compounds into cellular polyolefin insulations was studied on a laboratory scale. Weight gain was monitored as a function of time and temperature using commercially available single insulated conductors and filling compounds. Linear correlations were established for the results on a logarithmic scale. Migration rates and filler absorption levels were determined for several systems and the saturation levels estimated for solid insulations. The extent of migration at ambient temperature was estimated using Arrhenius plots, and the results compared to those in commercial cables using solvent extraction. Gel permeation chromatography was applied to characterize the filling compounds used in the experiments and those retrieved from commercial cables. A simple model involving both permeation and cell filling has been suggested for the migration process. The experimental results are in satisfactory agreement with the model both with respect to the rate of absorption and their temperature dependence. The overall conclusion is that permeation and cell filling take place in all types of cellular insulations. Further, cell filling in plain and skin foam can reach stages where it may affect cable performance depending on the degree of blowing as well as the nature of the filling compound.

Introduction

The purpose of this paper is to present the results of a study of cell filling of foam and skin/foam insulations for waterproof telephone cables. Whereas cellular insulation provides advantages such as economy in raw materials[1] and smaller cable diameter for a given number of pairs, lingering questions[2] remain regarding the migration of filling compound into the cells of foam and skin/foam insulations. The major question is the impact on cable performance[3] of void spaces among the wires of the core created when the filling compound migrates into the cells. The reduction in cable fill is believed significant when a substantial proportion of the cells becomes filled with the filling compound.

Numerous studies around the world on the interaction of filling compound and insulation, both cellular and solid, have led to conflicting conclusions. For example, work by Foord[4] presents data on cell filling approaching saturation levels within 100 days, whereas Verne et al[5] find evidence of cell filling no higher than two percent.

The conclusions regarding cell filling are further complicated because the rate as well as the level of absorption depends on the cell size, density, molecular weight and molecular weight distribution of the insulating materials, the nature of the filling compound, including additives, and its molecular weight. Techniques for monitoring the rate of migration of cable filling compound into the cells of the insulation have not been standardized and are believed responsible for some of the conflicting conclusions.

We believe that understanding of the cell filling process is important and relevant to success in the introduction of foam and skin/foam insulations in waterproof telephone cables. Therefore more than

one year ago, we initiated a systematic program to evaluate the rate of migration of filling compounds into cellular insulation both plain and skin/foam, employing weight gain as the fundamental measurement. Further, we have developed an extraction procedure for estimating the level of cell filling in field samples of various ages.

Scope

The results of migration studies for solid high density polyethylene, polypropylene, high density polyethylene plain foam and skin/foam over a temperature range from 30°C to 70°C are presented herein with extrapolation to 20°C. The 20°C values are compared with the levels of migration found in cable samples made by several different manufacturers, after storage in a warehouse for various periods. Commercially available and industry approved wire insulating materials and cable filling compounds were employed throughout the test program. The insulating materials and the cable filling compounds in the warehouse cables by different manufacturers were also identified. Gel permeation chromatography (GPC) provided aid in the characterization of the filling compounds.

Experimental

Materials

Single wires having the following constructions were used for the migration experiments:

Insulation Types	Base Resin	Wire Sources	% Air	DOD Mils
Plain foam	HDPE	A	30	47
Skin/ foam	HDPE	A	47	47
Skin/ foam	HDPE	B	50	43.5
PE Solid	HDPE	A	--	51
PP Solid	PP	A	--	50

All wires were 22 gauge. The skin/foam samples include a 2 mil thick outer solid PE layer.

The extraction experiments were carried out with singles removed from cables obtained from different manufacturers and stored in a warehouse for 8 to 36 months. Control wires of the same design but not exposed to the filling compound were also put through the extraction process for comparison with wires from the cables. Some of the single samples after exposure to filling compound in our laboratory and for which initial and swollen weights were accurately known served to determine the efficiency of the extraction process, as well as to develop the details of the extraction technique.

Filling compounds A, B, and C were obtained from domestic suppliers, compound D from a foreign source. Compounds E to I were retrieved from cables made by manufacturers A to F and stored in warehouses for 8 to 36 months. N hexane, n heptane and petroleum ether were used as solvents in the extraction studies, hexane being the preferred one. Acetone, methyl ethyl ketone,benzene, n hexane and petroleum ether (boiling range 30 - 60°C) were used to clean the surface of the insulated wires. All solvents were of high purity commercial grades and were used without further treatment.

Procedures

Migration rates were determined by measuring the weight gain after different exposure times in filling compound at various temperatures. Preliminary experiments showed that a given sample could not be used repeatedly because exposure to filling compound softened the insulation. The cleaning procedure was carefully standardized. The initial weight was determined after a one second dip in the filling compound maintained at 70°C. The purpose of this initial quick dip was to establish a "zero time" reference weight, based on the same cleaning steps to which the insulation is subjected after the immersion cycle. Part of the problem is that wiping with dry soft paper tissue (Kimwipes), and then with tissue saturated in a solvent, may extract some of the lower molecular weight components and remove some surface

"bloom" of the insulation. Cleaning only with dry paper tissue was found to give erratic results, when comparing the initial weight of a given wire sample to that after the one-second dip. Use of paper tissue saturated in a solvent reduced the spread to an acceptable value. Different solvents were tried during the exploratory stage, including acetone, methyl ethyl ketone, hexane and petroleum ether. The spread in the initial and dipped weights was lowest for petroleum ether, which was then chosen for the migration studies.

The migration experiments were based on three 16" length wires each bent into U-shape and inserted into a 25x200 mm test tube containing the desired filling compound. The two ends of each wire were kept half an inch over the highest level of the filling compound. Forty-five of these test tubes were mounted in a plexiglass frame, in one temperature controlled waterbath. This made it possible to maintain the insulations in one bath which provided good comparability of heat histories. One test tube was taken out at each time interval, the three wires carefully cleaned with paper tissues soaked with petroleum ether, dried out for 10 minutes at room temperatures and weighed.

The filling compounds were extracted from the filled polyethylene wires using the Soxhlet technique. Three 27" long pieces of the filled or unfilled wires were coiled and placed in the upper part of the Soxhlet extractor without a thimble. They were taken out at regular intervals, dried in a vacuum oven at 70°C to constant weight (4 to 5 hours) and weighed. They were then put back in the extractor for another 24 hours and the process of drying and weighing was repeated until the weight of the wires became constant.

Equipment

Standard laboratory equipment was used in both migration and extraction experiments. They included test tubes, controlled temperature baths, drying ovens, Soxhlet extractors and an analytical balance of 0.1 mg sensitivity. Gel permeation chromatography was performed on a Waters instrument equipped with a refractometer detector.

Data Processing

The weight gain values for the triplicate specimens at each period were expressed as % of the original weight of the insulation. They were averaged and these averaged values are plotted in Figures 1 to 7 for each temperature. Figure 1 is the linear scale presentation of weight gain as a function of time and temperature for the HDPE foam insulation-filling compound A combination. The same data are plotted on logarithmic scales in Figure 3. The lineup of the data points implies linear correlation and regression analysis was performed to assess the "fit" or validity of the linearity. The slope and intercept values of best fitting linear regression lines (based on the least squares principle) and the correlation coefficients (r) are listed in Table 1. The high values of r support the validity of this approach. In the regression analysis the individual values were used for the replicates, and not the average values, to assure fair representation of the spread of the data points. The regression lines or isotherms for 30 to 70°C are shown as solid lines within the actual range of experiments, and are extended as broken lines to represent extrapolation. The dotted line for 20°C is based on values calculated from Arrhenius plots and is discussed later. Figures 2 to 7 present time weight gain correlations for various insulation-filling compound combinations.

The results of the regression analyses and the computed percent weight gain values at 10, 100 and 300 days exposure time are summarized in Table 1. These computed values are used in the Arrhenius plots in Figures 8 to 13. Regression analysis determined the best fitting linear correlation between reciprocal temperature (expressed as °K) and ln percent weight gain. These linear correlation lines were then extended to 0.00341 on the X axis representing 20°C. The corresponding Y values, i.e., the extrapolated % weight gain data at 20°C were then used to construct the 20°C isotherms represented by dotted lines in Figures 2 to 7. The characteristics of linear regression analysis on the Arrhenius correlations, the re-computed values for % weight gain at 10, 100 and

300 days exposure, and the extrapolated values for 20°C are summarized in Table 2. The extrapolated 20°C correlation lines are also presented in Figure 14, and are extended to 1825 and to 3650 days to estimate the % weight gain values at 5 and 10 years respectively.

Results and Discussion

Migration

A brief discussion of the mechanism of absorption and the physical parameters involved should help the appreciation of the present results. It is well known that the rate and the level of absorption of a liquid by a polymer matrix is governed by the twin processes of solubilization and diffusion. If a plastic pipe is surrounded by a liquid, the outer surface is immediately saturated and the concentration level is equal to the solubility of the liquid in the polymer. The inner surface has zero liquid concentration. The resulting concentration gradient initiates the diffusion of liquid into the polymer. Simple derivations[6] based on Fick's equation for diffusivity gives the flux (F)

$$F = \frac{2\pi DS}{\ln(b/a)} \qquad (1)$$

where D is the diffusivity constant,
S is the solubility at the particular temperature, and
a and b are inner and outer radii.

The process of solubilization of a liquid in the polymer matrix occurs spontaneously due to a negative change in free energy of mixing ($-\Delta G^1_m$). The magnitude of the latter is controlled mostly by the difference in solubility parameters[8] (δ_p and δ_l) of the polymer[7] and solvent. If the difference is small, $-\Delta G^1_m$ is large whereas if the difference is large, the solubility is limited. The preferred insulating materials for telephone cables are high density polyethylene and polypropylene having solubility parameters of 7.9 to 8.2 $(cal/cm^3)^{\frac{1}{2}}$. The petrolatum based filling compounds consist of paraffinic and napthenic hydrocarbons. The solubility parameters[9] of simple hydrocarbons C_8 to C_{14} range from 7.6 to 7.9, those of higher hydrocarbons approach a limiting value of 8. Hence, the mixing of amorphous polyolefins with petrolatum presents a case of regular solution[10], where $-\Delta G^1_m$ is high; ΔH^1_m and ΔV^1_m, the heat and volume change on mixing respectively, are negligibly small. However, the polyolefins used for insulations are crystalline. The highly organized structures of crystallites are impervious to liquid below the melting point and hence the solubility is reduced[11]. The crystallites also reduce the diffusivity as they make the path of migration tortuous.[12] Given sufficient time, the twin processes of diffusion and solubilization lead to an equilibrium state where the polymer matrix is completely saturated. The equilibrium absorption in this case would be low because of high crystallinity and should be fairly independent of temperature because ΔH^1_m is small and should not be accompanied by a change in density as ΔV^1_m is almost zero.

In case of cellular insulation this process will be superimposed by a process of cell filling. As the polymer matrix becomes saturated, the cell walls will be completely wetted by the permeant liquid, and a hydrostatic pressure will develop due to the difference in liquid head in the solid matrix and in the cellular space. This will induce oozing of the liquid into the empty cells. Verne[5] et al have suggested that this process is similar to capillary filling and the time required to fill the cell so that its initial radius r_o is reduced to r_i is given by the equations:

$$t = 2\left(\frac{1}{A} + 2\eta\right)(r_o - r_i)\frac{1}{T} + t_s \qquad (2)$$

1/A in the above equation is a resistance term depending on the permeability coefficient and geometry of the insulation,
η is the viscosity of the permeant,
T is the surface tension of the permeant with respect to the matrix and
t_s is the time required for the permeant to wet the inner surface of the cells.
Since the migrating hydrocarbons readily wet the PE surface, t_s may be assumed to be zero. Further, the rate of cell filling should be inversely proportional to the time of cell filling in equation (2). The rate of migration R which depends both on permeation and cell filling may therefore be given by the equation:

$$R = \frac{2\pi DS}{\ln(b/a)} + \frac{KAT}{2(1+A\eta)(r_o - r_i)} \qquad (3)$$

where K is a proportionality constant.

On the basis of experiments, Hagger[5] et al conclude that the process is viscosity controlled and for high viscosity of the permeant solution, only a small amount of cell filling is to be expected. Our experimental data support the conclusion that a substantial degree of cell filling does occur. We infer that the factor A is not negligible and that cell filling is not limited by η alone.

The migration of filling compound A into solid HDPE and PP insulations is presented by Figures 2 and 4 and that of compound B into solid HDPE by Figure 7. The slope of ln percent absorption against ln time are appreciably smaller for 70°C compared to that at 30°C. This anomaly is due to the fact that within the time period covered the absorption at 70°C has approached the saturation level (W_o while that for lower temperatures is progressively further and further away from the equilibrium state. Since the initial rate in any absorption process is very high[13] and since this decreases as equilibrium is approached, the overall slopes as given by the logarithmic plots in Figures 2, 4 and 6 are higher at lower temperatures. As the experiments at lower temperatures progress, the level of absorption will approach W_o and the overall slopes in the logarithmic plots will be smaller as shown in Figure 2 for HDPE foam.

The small slope at 70°C in Figure 2 suggests that the absorption by solid HDPE has almost reached equilibrium around 11%. This value is close to the 10% value obtained by Anderka[14] et al and 9% value obtained by Foord[4]. The high slopes at lower temperatures may indicate that W_o values at these temperatures are not far from the 11% value estimated above for 70°C and the temperature dependence of W_o is small due to small ΔH^1_m as discussed earlier.

The rate and level of absorption of compound A into solid polypropylene (Figure 4), is very close to that for solid polyethylene and the W_o value may be close to 11%. Foord[4] estimated 5% for equilibrium absorption by polypropylene. It may however, be pointed out that W_o is largely a function of amorphous content and an appreciable amount of atactic polypropylene is included in the isotactic polypropylene. The compound used in our work may differ in the atactic content as a result of which W_o in this case could be twice as that obtained by Foord.[4] The apparent higher slopes at low temperature again suggest that the W_o value is fairly temperature independent as mentioned above.

The migration of filling compound B into solid polyethylene proceeds about 30% faster compared to that of A (Figure 7). The equilibrium absorption, W_o may be approximately 13 to 14% compared to 11% for A. It is known that compound A contains a polymeric additive and hence, the chemical potential of the migrating component in this compound is somewhat smaller than in compound B which does not contain such an additive. The apparent anomaly of high slopes at lower temperature persists to a greater degree in this case.

The migration into cellular insulations is distinctly different both with respect to migration rates and weight gains. Generally, compound A migrates into HDPE foam faster than into solid HDPE as reflected by the comparison of Figures 3 and 2. The somewhat higher slopes at low temperatures for HDPE solid are anomalous. The weight gains are higher at the temperatures and times tested. Since there is no reason to assume higher solubility of the filling compound in the matrix of the foam, the higher weight gain indicates that at least part of the filling compound has migrated into the cells. The higher slopes can also be interpreted as an indication of cell filling.

Figure 5 shows the migration of the same filling compound into skin/foam insulation. The percent weight gain data are lower for comparable periods than those for the plain foam. The higher slopes represent higher migration rates, and imply that in due time the skin/foam may absorb more filler. The relative proximity and parallel position of lines for

70 and 30°C indicates moderate temperature dependence and that the migration proceeds at a steady rate for the entire range. This also implies that the permeation and cell filling are taking place simultaneously. At the initial stage the rate of permeation is very high due to higher concentration gradient. The rate of cell filling is lower because the smaller hydrostatic head of the absorbed liquid in the matrix as compared to the empty cells. As the time proceeds, the concentration gradient becomes smaller giving lower rate of permeation, but the rate of cell filling becomes faster due to higher hydrostatic pressure. Since the rate of weight gain at any time is the sum of the twin processes of permeation and cell filling, it remains steady over the entire period covered.

Filling compound B migrates much faster into skin/foam insulation than compound A. Figure 6 shows 2 to 3 fold increase in percent weight gain for compound B at comparable times. This is in line with the difference between these compounds with solid insulations as discussed earlier (Figures 2 and 7). The high levels of weight gains and high slopes of the isotherms indicate high migration rates for the skin/foam systems and are surprising. Simple logic could predict values between those for solid and plain foam systems. One possible explanation involves the difference in cell sizes between foam and skin/foam. The latter ones are much larger and may accumulate the penetrant faster than the small cells of the plain foam.

Effect of Temperature

The temperature dependence of the rate of absorption of filling compound by insulating material has been studied with a view to understand the mechanism as well as to make extrapolations to service temperature. The conventional method is to treat the rates of migration on the basis of Arrhenius correlation. However, the petrolatum based filling compound is not a homogeneous material[15] and its portion available for migration into the insulation may vary with temperature. Hence, any treatment over a range of temperatures will involve different species. These species are similar in chemical structure and the diffusing unit, which, according to Allen et al[16], is small and similar for all species and diffuses unit by unit. Hence. Arrhenius plot may be justified. As noted earlier, instead of plotting the rate of absorption against reciprocal temperature, the amounts of filling compound absorbed at 10, 100 and 300 days have been plotted in Figures 8 to 13. The apparent activation energies computed from these slopes are presented in Table 2.

The temperature dependence of the rate of absorption of compound A into solid PE and PP is given in Figures 8 and 10 and that for compound B into solid PE in Figure 13. They are fairly linear and the correlation coefficients in all cases are fairly high. One of the common features of the 3 diagrams is the gradual decrease in the slopes with increasing time. This is due to the fact that at the initial stage both the rates and their temperature dependence are high. At the latter stage when the level of absorption approaches the equilibrium value, the rate as well as the temperature dependence aresmaller.

The temperature dependence for compound A into PE foam and skin/foam is given in Figures 9 and 11 and that for compound B in Figure 13. The slopes for 10, 100 and 300 days are similar in Figures 9 and 11 and smaller than those for solid insulations. As mentioned earlier, both permeation and cell filling take place simultaneously in case of cellular insulations. Hence, the temperature dependence represents the combined temperature dependence of permeation and cell filling. An analysis of equation (3) shows that in the second term, A occurs both in the numerator and denominator and hence its temperature dependence tends to cancel out. On the other hand, the temperature dependence of η is positive and the overall activation energy will be the activation energy due to permeation minus the activation energy of the viscous flow. This explains the lower slope and the lower activation energy for absorption of filling compound into cellular insulation. The temperature dependence of absorption of compound B into skin/foam at 100 and 300 days are similar to compound A whereas that for 10 day period is somewhat higher.

Extraction

The objective of extraction experiments is the development of a technique permitting determination of the actual weight gain of cable samples exposed to actual aging. The types of wires, the details of the extraction process and the results are summarized in Table 3.

Controls not exposed to filling compounds yielded some extractable component. Virgin HDPE lost 0.5 to 0.8% in petroleum ether and 1 to 1.4% in n hexane, polypropylene lost 5.1% in hexane. Additives, such as stabilizers, and carriers used in the color concentrates are believed to be extracted from HDPE while PP is known to contain a few percent atactic polymer which could be extracted with hydrocarbons. The efficiency of the extraction was established with wires of known filling compound content from the migration experiments. Petroleum ether extracted only 60 to 70% of the known filler content (Experiment Nos. 5 and 2 in Table 3 respectively). N hexane gave extraction efficiencies of over 80% (Nos. 8, 12 and 17 in Table 3).

The comparisons are based on normalized weights, with the weight of insulation before extraction being 100. The weight loss due to extraction and the known filling compound content of insulations impregnated in the laboratory are therefore weight percent of the unextracted insulation. The "apparent filler recovery %" column in Table 3 is the ratio of extracted material and known filler content. The estimated filler recovery is based on analogy with the closest known composition. The "estimated filler recovery, %" values were applied to calculate the estimated filler level. As an example, in experiment #2, a laboratory HDPE skin/foam sample containing 6.4% filling compound A was extracted with petroleum ether. After the extraction, the weight of the insulation decreased to 95.6% and 4.4% was extracted. This represents 69% of the original 6.4% filling compound A, and is designated as "apparent filler recovery". Using 69% as "estimated filler recovery" on the 10% weight loss in experiment #3, the estimated filler level is calculated as 14.5%. This in turn, is converted into "estimated age of cable" using isotherm #4 in Figure 14 as 32 months, and compared to the actual age of 25 months. The extraction results reveal significant filling compound migration for HDPE cables stored in unheated warehouses, as shown below

Age Mo.	% Weight Gain Solid PE	Foam	S/F
Extraction Data			
14	5.1	---	7.8
30	---	8.9	11.6
Weight Gain Data for 20°C			
14	7.6	---	11
30	---	14	14

The agreement between extraction and migration data is about as good as can be expected, considering that the average warehouse storage temperature is probably less than 20°C.
Both filler levels and cable ages are estimated as ranges for PP insulations, due to the high extractable component in the PP (Nos. 20 to 23). The low end of the estimated ages equates the filler content with the difference between extraction losses of the wire recovered from a filled cable and the virgin wire (e.g., 7.9 - 5.1 = 2.8% for experiment #20). The high end of the range assumes all extraction loss consists of filling compound.

Gel Permeation Chromatographic Analysis

Nine filling compound samples (A to I) and one low molecular weight polyethylene sample, suitable for use as a thickening agent were subjected to GPC analysis. Filling compounds A to D are commercially available materials, E to I were retrieved from cables stored in warehouses.

The objectives of the study were threefold:

1. To determine whether the polyethylene thickener incorporated into compounds A, C and D could be readily distinguished from the petrolatum fraction.

2. To establish whether filling compounds of various manufacturers could be differentiated by this technique.

3. To determine if any component in

the filling compound is depleted during storage.

Typical chromatograms are presented in Figures 15 and 16. Although their two peaks overlap slightly (Figure 16), it was found that petrolatum and polyethylene fractions are quite well resolved. It is therefore, quite easy to distinguish a PE containing compound like A, C or D from one which lacks polyethylene. In addition, the chromatogram of a low molecular weight PE alone was compared to that of the high molecular weight fraction of Compound A and was found to be identical.

Figure 15 depicts the superposition of three chromatograms: that of Compound B (taken at two substantially different times but from a total of only several grams of sample) and F, the filler retrieved from a cable from manufacturer B, which is believed to correspond originally to Compound B. The three curves have been normalized with respect to total area. The two Compound B curves are quite similar except that one shows a smaller low molecular weight tail than the other (which is compensated for by an increase in the area directly under the peak). This discrepancy could be viewed as the combination of two effects: the repeatability of the experimental method as well as the inhomogeneity within the sample.

The chromatogram for Compound F shows a further loss of low molecular weight tail with respect to the two Compound B curves and a significant loss of the high molecular weight tail. The latter implies a preferential migration of the high molecular weight component which is contrary to common sense. However, it is clear that there is no evidence of preferential migration of the low molecular weight component particularly in light of the rather narrow molecular weight distribution of the petrolatum fractions (corresponding to a range in carbon chain lengths of roughly 20 to 80). Similar effects can be noted in comparing the normalized chromatograms of Compounds A and G (a retrieved sample from manufacturer A) in Figure 16.

It was determined that filling compounds A, C and D (all containing PE) have chromatograms too similar to resolve with any degree of certainty. Compound E, retrieved from a cable by manufacturer E, appears to contain a much higher molecular weight tail in the distribution of its polyethylene fraction, and more of the low molecular weight fraction of the petrolatum (Figure 16).

Effect of Filler Migration on Waterproofness

One of the consequences of the migration of the filling compound is that its depletion in the interstices among wires may create voids, which in turn, can be filled with ingressing water.[17] The assessment of the correlation between percent weight gain of insulation and the decrease in cable fill level is therefore of major concern. The data generated on migration are applied to estimate this correlation.

Though subject to variations with construction, the combined cross section of wires amount to about 52% of the total cross section, leaving about 48% as the combined cross section of interstices. Ideally, this area is completely filled with the filling compound resulting in 100% cable fill. When the filling compound migrates into solid insulation, swelling occurs. It is generally assumed the increase in the cross section of wires due to swelling is comparable to the decrease in the cross section of the compound in the interstices, which in turn implies no major change in cable fill.

The effect of filler migration into solid insulation on cable fill level is assessed on a qualitative basis. The migration is expected to progress to the saturation level at the rate shown by the 20°C isotherms Nos. 1, 3 and 6 in Figure 14. The saturation level is estimated at somewhat in excess of 11%, and the change in cable fill is small (Table 4).

In cellular insulations, the migrating compound may replace the gas in the cells, which in turn, replaces the filling compound in the interstices. This process depletes the filling compound and causes a decrease in cable fill. The extent of this decrease is estimated for two specific cases.

In plain foam (0.047" DOD, 22 AWG conductor, 30% blow) the cross section area of cells amounts to 21.2% of the cross section of a single wire and 0.52 x 21.2 = 11.2% of the cable cross section

area. The plastic portion of the foam is 50.2% of the single wire's cross section and 26.1% of the total cables' cross section. Assuming that all the migrated filler is located in the cells, and no increase in DOD of the single wire occurs, and ignoring the difference in the specific gravities of insulation and filling compound, 1% weight gain of the insulation results in 0.54% decrease in cable fill.

In the skin/foam construction used in these experiments, the cross section area of the plastic portion of the insulation amounts to 44.8% of that of a single wire, and 23.3% of the cross section of the cable. One percent weight increase therefore, may decrease the cable fill level by 0.49% under the conditions stipulated for plain foam.

The estimated effect of migration in 5 and 10 years is presented in Table 4. The percent weight gain is estimated from isotherm Nos. 2, 4 and 5 in Figure 14 for the 3 cellular insulation - filling compound combinations, and the results multiplied by the applicable factor of 0.54 or 0.49. The migration of filling compound A may cause 9.1% decrease in cable fill in 5 years and 11.8% in 10 years. While no rigid limits are established for acceptability in this respect, generally 6% decrease in cable fill is considered to result in substantial deterioration in cable quality. Filling compound A in combination with HDPE skin/foam insulation is comparable to the plain foam after 5 and 10 years. Compound B migrates faster into skin/foam and may result in 16 and 22.5% cell fill decrease in 5 and 10 years respectively.

These estimates are based on extrapolations and assumptions, and their validty depends on the validity of these assumptions. At this time, they are considered as indications of potential deterioration of waterproofness.

Conclusions

1. Filling compounds migrate into solid insulations even at temperatures as low as 30°C. This process is limited by the mutual solubilities of the compound and the insulation.
2. Migration into cellular insulations progresses beyond the solubility limit of the solid polyethylene matrix. Time temperature correlations support the model of simultaneous permeation of solid matrix and cell filling.
3. The extent of migration depends on cell dimensions, the nature of the filling compound and temperature.
4. Extraction with hydrocarbon solvents confirms the cell filling indicated by weight gain measurements.
5. The molecular weight distribution determined by gel permeation chromatography is helpful in characterizing the cell filling tendencies of the different filling compounds.
6. Depending on the insulation type and the nature of the filling compound, the migration into cellular insulations may decrease the cable fill sufficiently to cause a deterioration in waterproofness.

Acknowledgements

The authors acknowledge their appreciation to Mr. R. Morgan and Mr. W. J. O'Grady for their stimulating discussions and helpful suggestions; to Dr. E. Malawer for the GPC work and to Mrs. J. Amato, Mr. E. Armour, Mr. P. Kerchick, Mr. E Smith and Mrs. M. Szakolczay for carrying out the experimental work.

References

1. E.D. Metcalf - 23rd International Cable and Wire Symposium 1974. p. 46
2. C.J. Aliosio and E.D. Nelson - 22nd International Cable and Wire Symposium 1973. p. 261
3. S.M. Beech, D.F. Cretney and J. Ruskin - Ibid. p. 292
4. S.G. Foord - 22nd International Cable and Wire Symposium 1973. p. 23
5. S. Verne, A.A. Pinching and J.M.R Hagger - Ibid. p. 244
6. J. Crank and G.S. Park - Diffusion in Polymers. Academic Press. 1968. p. 5

7. D. Mangaraj-Die Makromol Chemie 65. 1963. p. 29

8. O. Griffin Lewis-Physical constants of linear homopolymers. Springer Verlag, N.Y. 1968. p. 76.

P.J. Small-J. Applied Chem.3. 1953. p. 71.

9. D. Mangaraj-Ph.D. Thesis, University of Manchester, U.K., 1959.

10. Hildebrand and Scott-Solubility of Nonelectrolytes, Reinhold, N.Y. 1950.

11. J. Crank & G.S. Park-Diffusion in Polymers. Academic Press, 1968 p.208

12. A.S. Michels and H.J. Bixler-J. Poly. Sci. 50. 1961. p. 413

13. D. Mangaraj, K.D. Kiss and H.C. Doepken-Proceedings of National Research Council Conference on Dielectric Phenomenon, Oct., 1978.

14. H. Mayer, J.J. Anderka and H.G. Dagetrarde-24th International Cable and Wire Symposium 1975. p. 265.

15. J.J. Kaufman and T.E. Luisi-23rd International Cable and Wire Symposium 1974. p. 76

16. D. Mangaraj and G. Allen-Polymer 1. 1960. p. 1.

17. M.C. Biskeborn and D.P. Dobbin, 18th International Wire & Cable Symposium, 1968.



DURYODHAN MANGARAJ is a Senior Research Chemist in charge of the Advanced Materials Research Laboratory at the Phelps Dodge Cable and Wire Company. He received his B.S. (Hon.) and M.S. Degrees in Chemistry from the Ravenshaw College, Cultack, India, and his Ph.D. in Polymer Science from the University of Manchester, U.K. He organized research and training in Rubber and Polymer Technology in India and subsequently worked at the Polymer Institute, University of Massachusetts, Amherst and City University of New York. He was Project Manager at Polymer Research Corporation of America before he joined PDCW in 1976. Raj's areas of specialization are polymer synthesis and modification, physical properties as related to molecular structure, phase transition and morphology, graft polymers, transport processes and dielectrics. He has 27 publications and 7 patents to his credit.



M.C. BISKEBORN received his BSEE in 1930 and an honorary Doctor of Engineering degree in 1961 from the South Dakota School of Mines and Technology. He also attended Johns Hopkins University Graduate School in 1948 and 1949. As a Member of the Technical Staff at Bell Telephone Laboratories from 1930 to 1972, Dr. Biskeborn was active in the development of multipair cable, coaxial cable, high frequency measurement techniques, ocean cable, B-wire connectors, waterproof telephone cable, and microwave coaxials and radar during World War II. He was the Head of the Cable Department at Bell Telephone Laboratories for many years and holds twelve patents in the wire and cable field. After leaving the Bell System, Dr. Biskeborn joined Phelps Dodge and is currently Director of Research and Development for Communications Cable.



KORNEL D. KISS is the Manager of the Materials Research Laboratory at the Phelps Dodge Cable & Wire Company. He received a B.S. in Chemical Engineering in 1944 and a D.C.E. in 1947 from the Polytechnical University of Budapest. His past experience includes organic and polymer synthesis research, supervision of product and process development on a variety of polymers, polymer aging, degradation and stabilization. He is the author of five textbooks, and the inventor of over 40 patents, about half of them in the additives and polymer stabilization field. His interests include the optimization of insulating materials, thermal analysis, process miniaturization, statistics and laboratory scale simulation of polymer aging.

TABLE 1

EFFECT OF TIME AND TEMPERATURE ON FILLER MIGRATION

(Linear regression analysis of data. X = ln days, Y = ln % weight gain)

Insulation	Filler	Temp. °C	Linear Regression Analysis			Calculated % Wt. Gain, days		
			Intercept	Slope	Corr. Coef., r	10	100	300
HDPE solid	A	30	0.8931	0.4944	0.94	1.28	3.97	6.89
		40	0.3591	0.3155	0.94	2.94	6.11	8.62
		50	0.5363	0.3011	0.91	3.42	6.82	9.49
		60	1.891	0.0833	0.43	8.00	9.68	10.70
		70	1.994	0.0748	0.69	8.76	10.38	11.25
HDPE foam	A	30	0.7838	0.2878	0.98	4.26	8.25	11.36
		40	0.7686	0.3038	0.95	4.35	8.76	12.18
		50	1.045	0.2828	0.98	5.47	10.49	14.30
		60	1.179	0.2828	0.95	6.23	11.94	16.28
		70	1.458	0.2548	0.94	7.69	13.87	18.36
PP solid	A	30	-1.371	0.5978	0.97	1.00	3.97	7.69
		40	-0.9801	0.5654	0.98	1.38	5.05	9.39
		50	0.6889	0.2820	0.92	3.82	7.32	9.97
		60	1.2970	0.1762	0.95	5.47	8.25	9.97
		70	2.3360	0.0343	0.87	11.13	12.06	12.56
HDPE skin/foam	A	30	-0.0945	0.4170	0.92	2.38	6.23	9.78
		50	0.2521	0.4131	0.95	3.32	8.58	13.60
		70	0.2953	0.4129	0.93	3.49	9.02	14.15
HDPE skin/foam	B	30	0.5226	0.4256	0.66	4.48	11.94	19.11
		50	2.242	0.1640	0.95	13.74	20.08	24.05
		70	2.790	0.1763	0.72	24.53	36.97	44.70
HDPE solid	B	30	-1.639	0.7762	0.88	1.16	6.96	16.28
		50	2.1017	0.0762	0.13	9.78	11.59	12.68
		70	2.280	0.0779	0.80	11.7	14.01	15.18

TABLE 1

EXTRACTION OF FILLING COMPOUNDS

Exp. No.	Single Wire: Insulation	Source	Treatment	Filling Compound: Type	%	Extraction	Norm. Weight after Extraction: Insulation	Weight Loss	Filler Recovery, %: Apparent	Filler Recovery, %: (Estimated)	Filler Level (est)	Age of Cable months: (Est.)	Age of Cable months: Actual	% Filler at Actual Age (From Figure 14)
1	HDPE, skin/foam	A	-	-	-	Petroleum ether @37°C	99.5	0.5						
2	HDPE, skin/foam	A	11L[1]	A	5.4		95.6	4.4	69					
3	HDPE, skin/foam	B	SW[2]	?[3]	?		90.0	10.0		(69)	(14.5)	(32)	25	13
4	HDPE, foam	A	-	-	-		99.2	0.8						
5	HDPE, foam	A	11L	A	12.1		93	7	58					
6	HDPE, foam	A	SW	A	?		92	8		(58)	(13.8)	(30)	30	13.6
7	HDPE, solid	A	-	-	-	N hexane @ 48°C	98.6	1.4						
8	HDPE, solid	A	11L	A	6.4		93.4	6.6	103					
9	HDPE, solid	A	SW	A	?		94.7	5.3		(103)	(5.1)	(7)	14	7.6
10	HDPE, solid	C	SW	?	?		96.1	3.9		(103)	(3.8)	(4)	10	6.2
11	HDPE, skin/foam	A	-	-	-		98.8	1.2						
12	HDPE, skin/foam	A	11L	A	7.7		93.7	6.3	82					
13	HDPE, skin/foam	A	SW	A	?		93.6	6.4		(82)	(7.8)	(5)	14	10.7
14	HDPE, skin/foam	B	-	-	-		98.2	1.8						
15	HDPE, skin/foam	B	SW	?	?		90.5	9.5		(82)	(11.6)	(14)	30	14
16	HDPE, foam	A	-	-	-		99	1						
17	HDPE, foam	A	11L	A	11.4		89.7	10.3	90					
18	HDPE, foam	A	SW	A	?		91.6	8.4		(90)	(8.9)	(9)	30	13.6
19	PP, solid	A	-	-	-		94.9	5.1						
20	PP, solid	A	SW	A	?		92.9	7.9			(>2.8)	(4-12)	14	9
21	PP, solid	E	SW	?	?		91.1	8.9			(>3.8)	(5-13)	<12	<8.2
22	PP, solid	F	SW	?	?		92.0	8.0			(>2.9)	(4-12)	12-18	8.2-12
23	PP, foam	F	SW	?	?		90.7	9.3			(>4.2)	(6-15)	12-18	8.2-12

(1) Impregnated in Laboratory
(2) Stored in Warehouse
(3) ? designates unknown type or %

TABLE 2

EFFECT OF TEMPERATURE ON MIGRATION

(Linear regression analysis, $X = T^{-1}(^{o}K)$, $Y = \ln$ % weight gain)

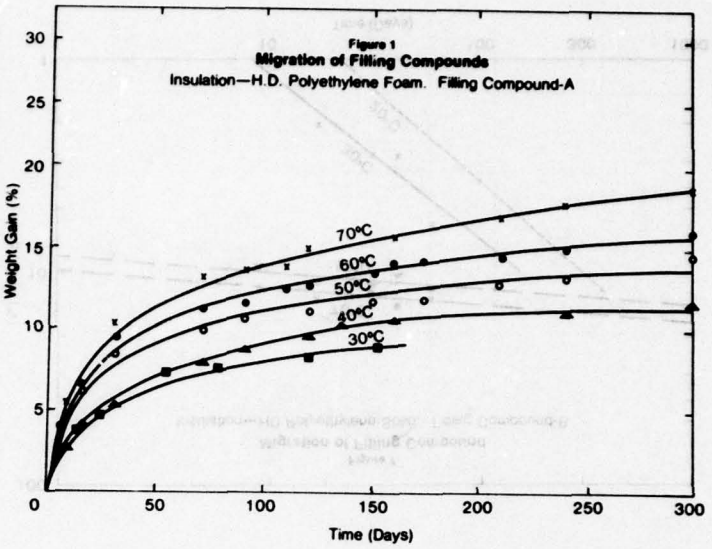
Insulation	Filler	Temp. °C	%Weight Gain at Days: 10	100	300	Linear Regression n: Days	Intercept	Slope	Correlation Coefficient	Activation Energy Kcal/mole
HDPE solid	A	20	(0.799)	(3.20)	(6.27)	10	17.11	-50.80	0.97	10.1
		30	1.41	4.24	7.21	100	9.69	-25.00	0.98	5.0
		40	2.47	5.58	8.28	300	6.11	-12.52	0.98	2.5
		50	4.00	7.07	9.32					
		60	6.48	8.97	10.50					
		70	9.93	11.09	11.68					
HDPE foam	A	20	(3.33)	(6.77)	(9.52)	10	6.62	-15.88	0.97	3.1
		30	3.97	7.92	11.01	100	6.67	-13.86	0.99	2.8
		40	4.73	9.23	12.70	300	6.67	-12.96	0.99	2.6
		50	5.50	10.54	14.36					
		60	6.40	12.03	16.24					
		70	7.33	13.55	18.13					
PP solid	A	20	(0.427)	(2.83)	(6.99)	10	21.07	-64.26	0.98	12.7
		30	.877	3.87	7.89	100	10.65	-28.17	0.99	5.6
		40	1.78	5.28	8.88	300	5.64	-10.83	0.94	2.1
		50	3.28	6.90	9.35					
		60	6.03	9.02	10.92					
		70	10.41	11.46	11.97					
HDPE skin/ foam	A	20	(2.21)	(5.80)	(9.14)	10	4.24	-10.09	0.93	2.0
		30	2.48	6.47	10.18	100	5.09	- 9.75	0.94	1.9
		50	3.05	7.91	12.45	300	5.54	- 9.74	0.93	1.9
		70	3.65	9.42	14.83					
HDPE skin/ foam	B	20	(2.910)	(8.39)	(13.96)	10	16.22	-44.40	0.99	8.8
		30	2.48	11.64	17.83	100	12.11	-29.26	1.00	5.8
		50	3.05	21.21	27.89	300	10.08	-21.82	0.96	4.3
		70	3.65	35.91	41.31					
HDPE solid	B	20	(2.910)	(5.92)	(9.24)	10	20.57	-61.04	0.91	12.1
		30	4.79	7.26	--	100	8.03	-18.33	0.98	3.6
		50	11.90	10.58	12.68	300	5.63	-10.00	1.00	2.0
		70	26.48	14.71	15.18					

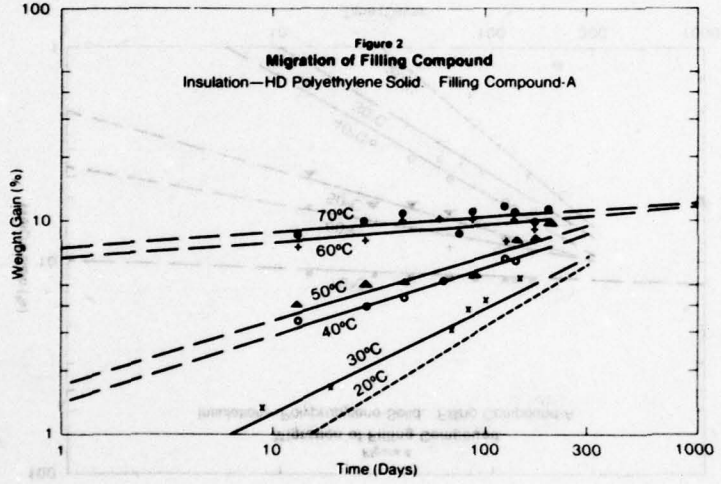
TABLE 4

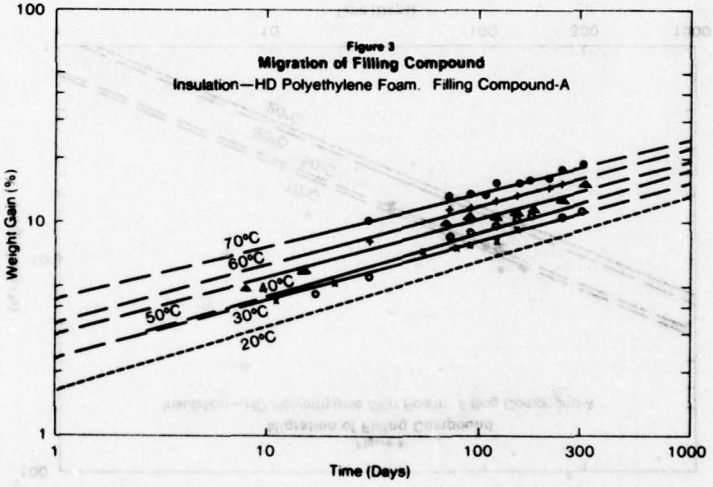
EFFECT OF FILLER MIGRATION ON CABLE FILL

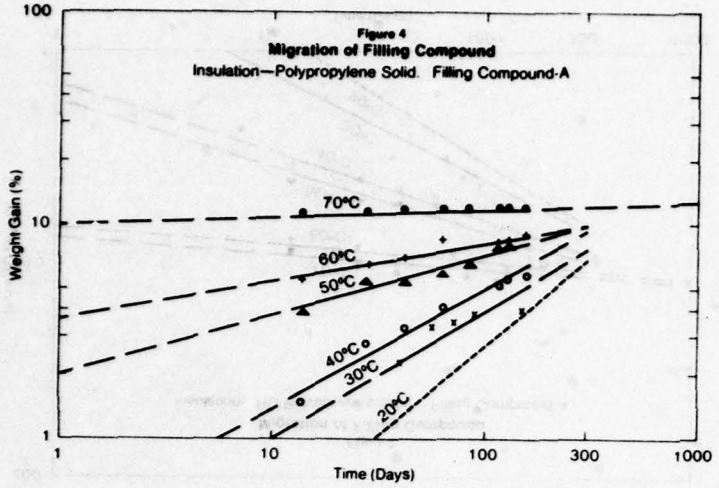
Insulation	Filler	After 5 Years		After 10 Years	
		% weight gain of insulation	decrease in cable fill,%	% weight gain of insulation	decrease in cable fill,%
HDPE, solid	A	>11	small	>11	small
HDPE, foam	A	17.1	9.3(1)	20.8	11.3(1)
PP, solid	A	>11	small	>11	small
HDPE, skin/foam	A	19.5	9.4(1)	26	12.7(1)
HDPE, skin/foam	B	33	16(1)	46	22.5(1)
HDPE, solid	B	>11	small	>11	small

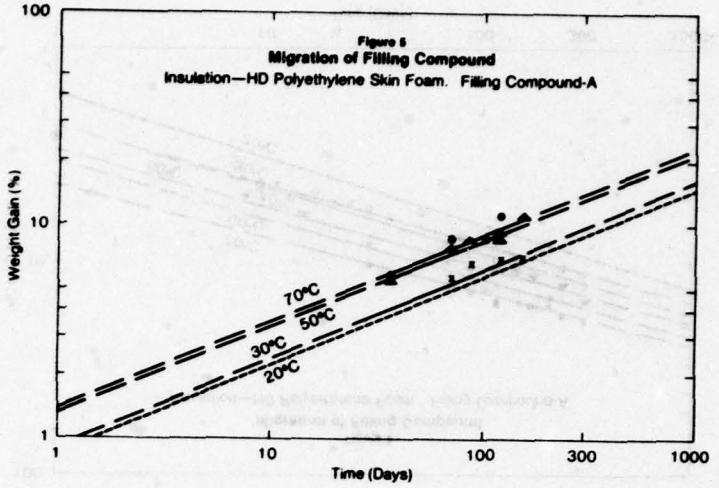
(1) assuming no increase in DCD

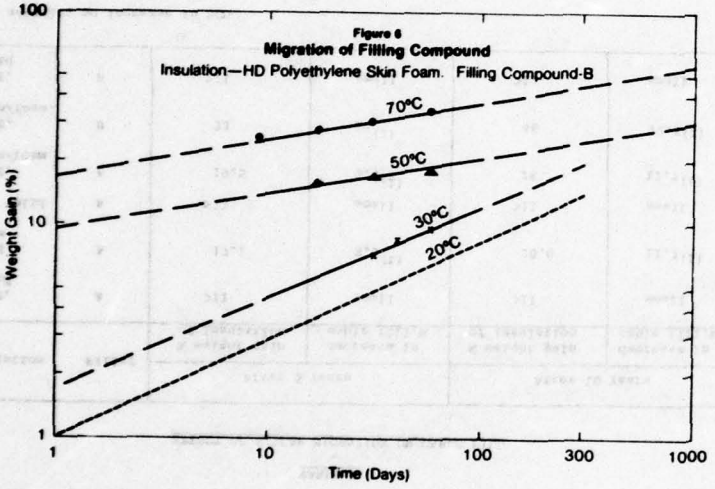


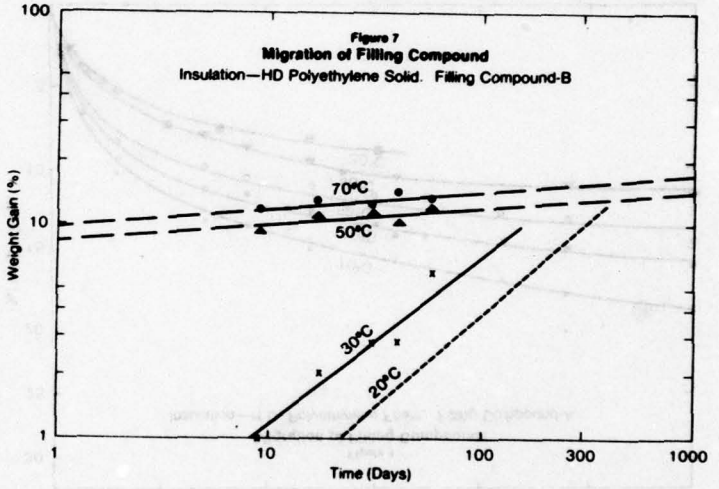


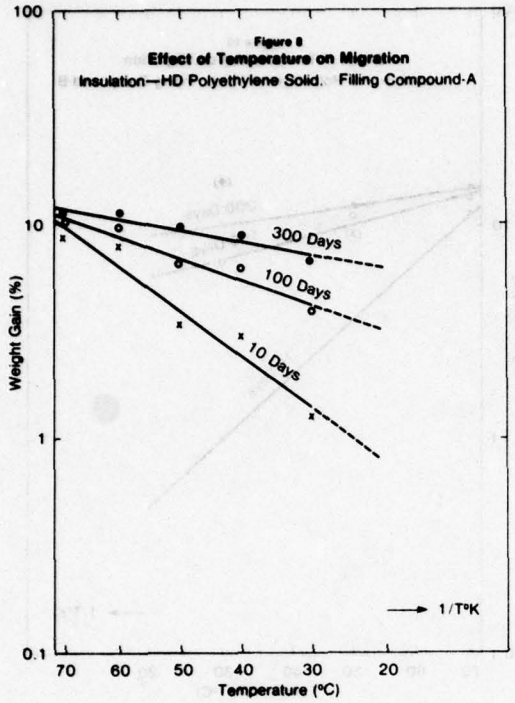


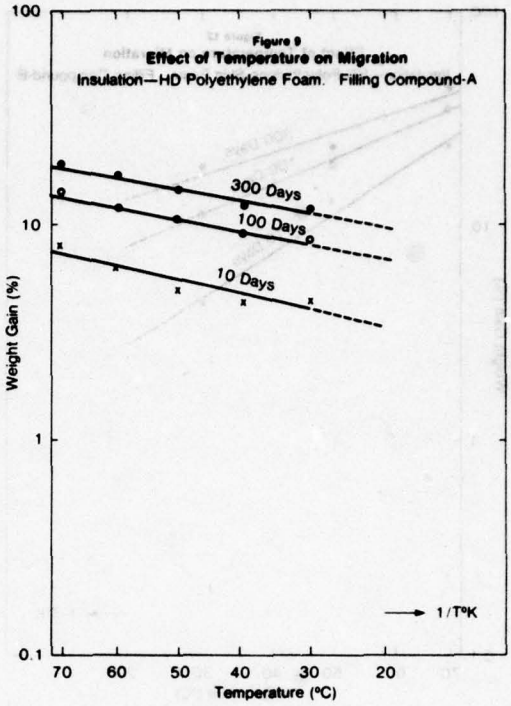

Figure 4
Migration of Filling Compound
Insulation—Polypropylene Solid. Filling Compound-A
Weight Gain (%)
100
10
1
70°C
60°C
50°C
40°C
30°C
20°C
1
10
100
300
1000
Time (Days)

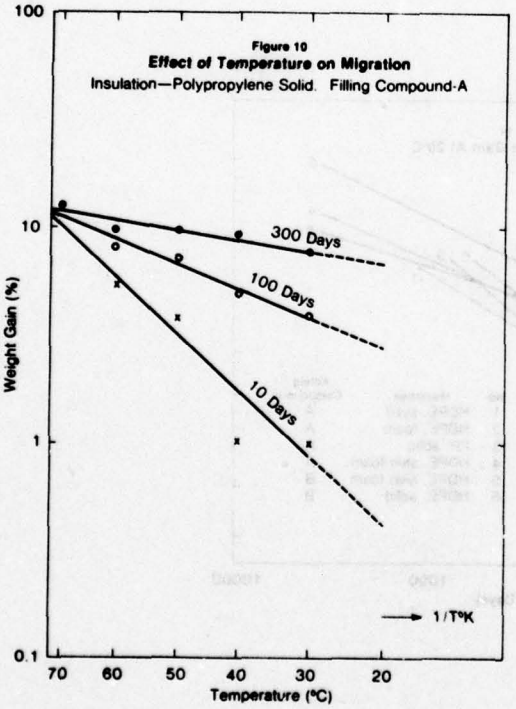

Figure 5
Migration of Filling Compound
Insulation—HD Polyethylene Skin Foam. Filling Compound-A
Weight Gain (%)
100
10
1
70°C
50°C
30°C
20°C
1
10
100
300
1000
Time (Days)

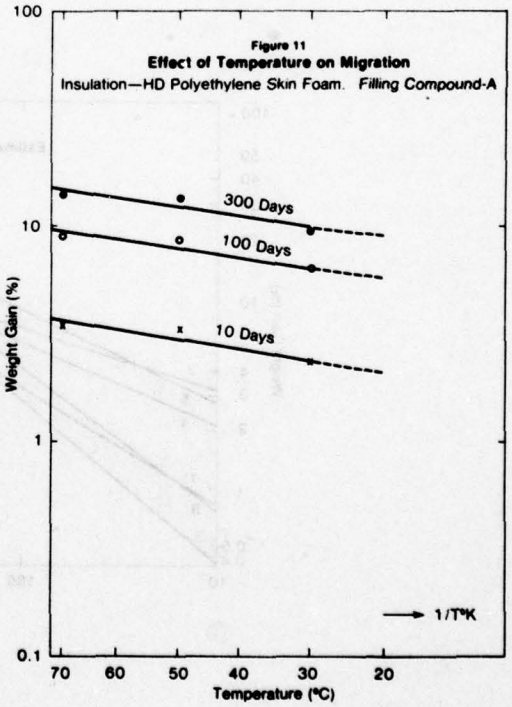

Figure 6
Migration of Filling Compound
Insulation—HD Polyethylene Skin Foam. Filling Compound-B
Weight Gain (%)
100
10
1
70°C
50°C
30°C
20°C
1
10
100
300
1000
Time (Days)

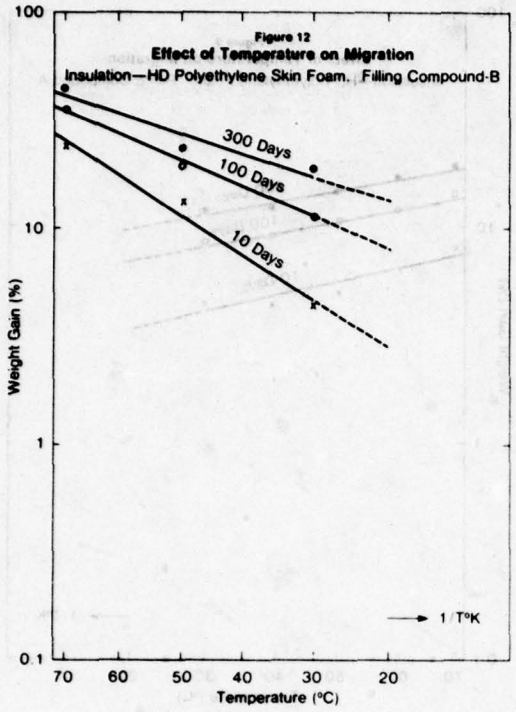

Figure 7
Migration of Filling Compound
Insulation—HD Polyethylene Solid. Filling Compound-B
Weight Gain (%)
100
10
1
70°C
50°C
30°C
20°C
1
10
100
300
1000
Time (Days)

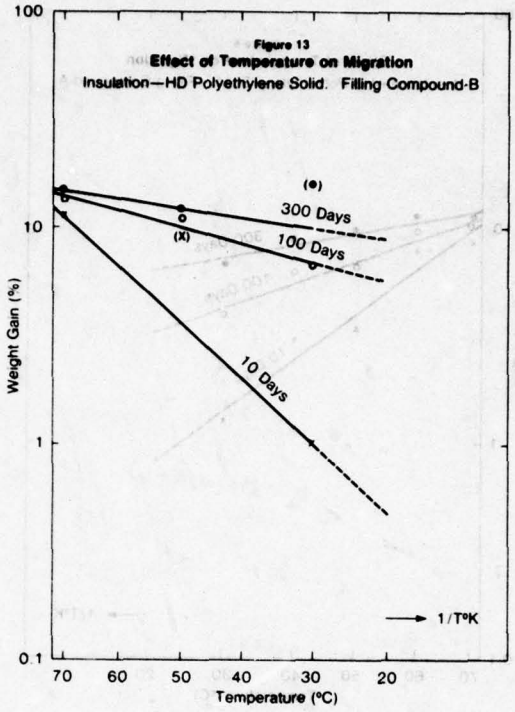

Figure 8
Effect of Temperature on Migration
Insulation—HD Polyethylene Solid. Filling Compound-A
Weight Gain (%)
100
10
1
0.1
300 Days
100 Days
10 Days
1/T°K
70 60 50 40 30 20
Temperature (°C)

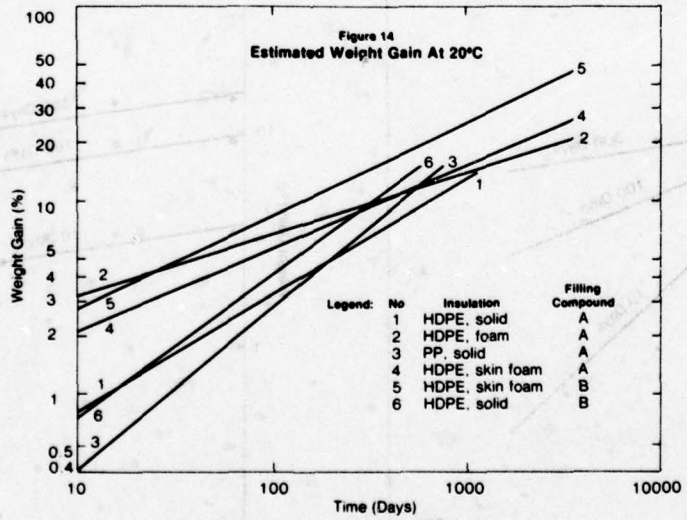

Figure 9
Effect of Temperature on Migration
Insulation—HD Polyethylene Foam. Filling Compound-A
Weight Gain (%)
100
10
1
0.1
300 Days
100 Days
10 Days
1/T°K
70 60 50 40 30 20
Temperature (°C)

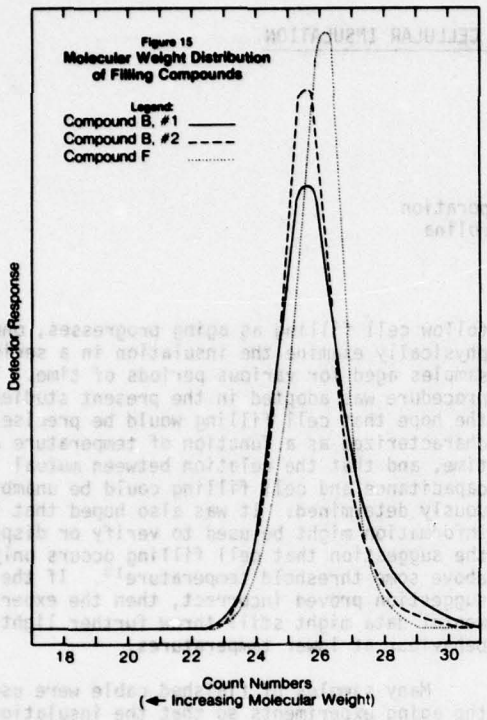

Figure 10
Effect of Temperature on Migration
Insulation—Polypropylene Solid. Filling Compound-A
Weight Gain (%)
100
10
1
0.1
300 Days
100 Days
10 Days
1/T°K
70 60 50 40 30 20
Temperature (°C)

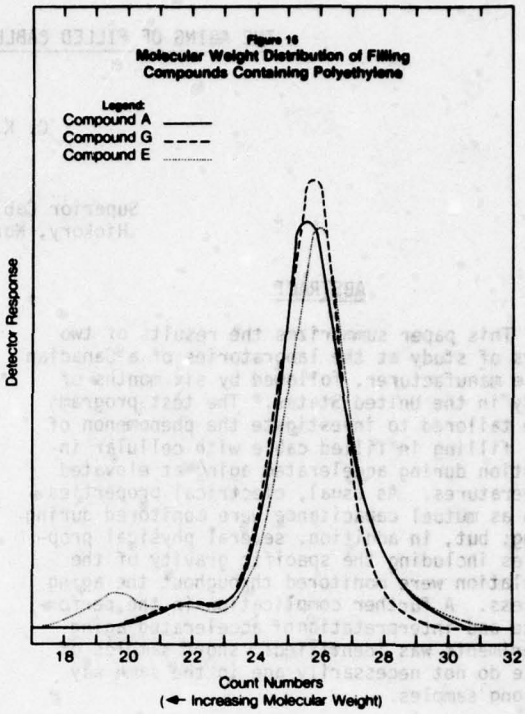

Figure 11
Effect of Temperature on Migration
Insulation—HD Polyethylene Skin Foam. Filling Compound-A
Weight Gain (%)
100
10
1
0.1
300 Days
100 Days
10 Days
1/T°K
70 60 50 40 30 20
Temperature (°C)


Figure 12
Effect of Temperature on Migration
Insulation—HD Polyethylene Skin Foam. Filling Compound-B
300 Days
100 Days
10 Days
Weight Gain (%)
100
10
1
0.1
→ 1/T°K
70 60 50 40 30 20
Temperature (°C)


Figure 13
Effect of Temperature on Migration
Insulation—HD Polyethylene Solid. Filling Compound-B
(•)
300 Days
(x)
100 Days
10 Days
Weight Gain (%)
100
10
1
0.1
→ 1/T°K
70 60 50 40 30 20
Temperature (°C)


Figure 14
Estimated Weight Gain At 20°C
Weight Gain (%)
100
50
40
30
20
10
5
4
3
2
1
0.5
0.4
Legend: No Insulation Filling Compound
1 HDPE, solid A
2 HDPE, foam A
3 PP, solid A
4 HDPE, skin foam A
5 HDPE, skin foam B
6 HDPE, solid B
10 100 1000 10000
Time (Days)


Figure 15
Molecular Weight Distribution
of Filling Compounds
Legend:
Compound B, #1
Compound B, #2
Compound F
Detector Response
18
20
22
24
26
28
30
Count Numbers
(← Increasing Molecular Weight)


Figure 16
Molecular Weight Distribution of Filling
Compounds Containing Polyethylene
Legend:
Compound A
Compound G
Compound E
Detector Response
18
20
22
24
26
28
30
32
Count Numbers
(← Increasing Molecular Weight)

THE AGING OF FILLED CABLE WITH CELLULAR INSULATION

C. K. Eoll

Superior Cable Corporation
Hickory, North Carolina

ABSTRACT

This paper summarizes the results of two years of study at the laboratories of a Canadian cable manufacturer, followed by six months of study in the United States. The test programs were tailored to investigate the phenomenon of cell filling in filled cable with cellular insulation during accelerated aging at elevated temperatures. As usual, electrical properties such as mutual capacitance were monitored during aging; but, in addition, several physical properties including the specific gravity of the insulation were monitored throughout the aging process. A further complication in the performance and interpretation of accelerated aging experiments was identified: short samples of cable do not necessarily age in the same way as long samples.

INTRODUCTION

Many laboratories around the world have studied filled cable with cellular insulation. In particular, they have investigated the tendency of oils in filling compounds to migrate into the cells of foam insulation during accelerated aging at elevated temperatures[1,2,...,11]. Extrapolating the results of such tests to service conditions, however, is by no means straightforward. Thus, definitive laboratory proof that cell filling will never become a problem during the service life of filled cellular cable has not, in fact, been forthcoming. Field experience is gradually verifying the suitability of the cable for buried installations; but experience with aerial installations which, of course, reach much higher temperatures, is still limited. All in all, even a slight risk seems undesirable, and further lab work appears appropriate.

As the plastic in cellular insulation absorbs filling compound at elevated temperatures, the plastic swells causing an increase in insulation diameter. This results in a drop in mutual capacitance. But if filling compound displaces air in the cells, the effective dielectric constant of the insulation increases and the mutual capacitance goes up. Therefore, the observed capacitance is the sum of at least two effects, and capacitance does not provide a direct measure of cell filling. In order to follow cell filling as aging progresses, one can physically examine the insulation in a series of samples aged for various periods of time. This procedure was adopted in the present studies in the hope that cell filling would be precisely characterized as a function of temperature and time, and that the relation between mutual capacitance and cell filling could be unambiguously determined. It was also hoped that this information might be used to verify or disprove the suggestion that cell filling occurs only above some threshold temperature[10]. If the suggestion proved incorrect, then the experimental data might still throw further light on behaviour at lower temperatures.

Many samples of finished cable were used in the aging experiments so that the insulation being aged would be exposed only to the amount of filling compound normally present in cable. In addition, however, individual insulated conductors obtained by dissecting finished cable were aged in an "unlimited" supply of filling compound for purposes of comparison. Dealing with singles is more convenient, and it was hoped to find a correlation between the aging of the insulation on singles and the aging of the insulation in samples of finished cable.

Because of the nature of the study, a large number of cable samples were required. In the case of the 25 pair, 22 AWG cable with cellular medium density polyethylene insulation and petroleum jelly filling compound, more than two hundred samples were cut from a cable 9000 feet in length. In all, the number of individual laboratory measurements numbered in the tens of thousands. In some instances, possible aging effects were masked by experimental error. The results which are more or less unequivocal are presented below.

THE TEST PROGRAM

Description of Cables

The most extensive series of tests involved medium density polyethylene foam insulation, where the specific gravity of the base resin was 0.935. The associated filling compound was a petroleum jelly with no polymers added. (The

Table I: Types of Test Cables

Designation	Wire Size (AWG)	No. of Pairs	Type of Insulation	Percentage of Gas in Unaged Insulation	Type of Filling Compound
A	22	25	Foam MDPE	40.0*	PJ
B	26	50	Foam MDPE	30**	PJ
C	22	25	Solid MDPE	0	PJ
D	22	12	Foam PP	-	PJ + polymers
E	24	50	Foam HDPE	40*	PJ + polymers

*measured average
**nominal

nominal specific gravity of the jelly was 0.91, and the minimum drop melting point using ASTM D-127 was specified to be 180°F.) Two types of cable with these materials were tested, namely 25 pair, 22 AWG and 50 pair, 26 AWG. Let us designate the two types as "A" and "B", respectively. It is noteworthy that the percentage of gas in the unaged insulation of type A was somewhat higher than would be tolerated in normal production.

To provide a reference, a very limited amount of testing was also performed on a filled cable with solid insulation. This cable, to be called cable "C", was insulated with a material that was identical to the base resin in cables A and B; and there was no change in the filling compound. A, B and C all had aluminum shields bonded to the jacket.

Cable "D" will refer to a filled cable made with foam polypropylene insulation. In the unaged state, the average specific gravity of the foam was found to be 0.65. This cable was commercially available in 1975; but, apart from the possible implications of this date, no information is available on the type of polypropylene involved. The filling compound was a very tacky polymer-modified petroleum jelly, and it was in contact with the jacket because the aluminum shield was not bonded thereto.

Finally, some testing was also performed on cable "E", a filled cable with foam high density polyethylene insulation, where the specific gravity of the base resin was 0.95; as in the case of cable A, the degree of expansion of the cellular material was greater than normally desirable. The filling compound was a polymer-modified petroleum jelly, with a specified minimum drop melting point of 198°F (ASTM D-127), and the aluminum shield was bonded to the jacket. Further details may be found in Table I.

Test Method

Aging Temperatures. Samples were aged at four temperatures: 65°C, 60°C, 55°C and about 23°C (room temperature). Test temperatures of about 70°C or higher were avoided so that the experiment would not be complicated by the second order transition point of the medium density polyethylene at 69 to 70°C.

In order to ensure that samples were aged at constant temperature, thermocouples were installed in several places within each oven and the temperatures were monitored on a regular basis. It was hoped to keep variations within 1/2°C, and, in practice, no variations as great as 1/2°C were recorded.

Preparation of Cable Samples for Aging. All cable samples destined to be dissected and examined after oven aging were capped on both ends and coiled, and the coils were placed vertically, with ends up, in the appropriate ovens.

Where mutual capacitance was to be monitored, each sample was treated similarly, except, of course, that only one end was capped, and the pairs at the other end were brought through a port in the oven wall to be connected to a terminal board mounted on the side of the oven close to the port. The exposed pairs were not disturbed during the course of the experiment. One long sample of cable A on a reel in the oven at 65°C was terminated at both ends so that attenuation could be measured.

Preparation of Singles for Aging. For insulated conductors which were to be aged in an "unlimited" supply of filling compound, unaged cable samples were dissected and appropriate singles were removed and placed in open pans containing a large amount of the same filling compound that the cable contained originally.

The grease was packed all around the singles except for the ends; these were not submerged.

Length of Samples. Except for the sample of cable E which was 91m in length, and the reel holding 1355m of cable A, all samples used to monitor mutual capacitance were either 10m or 5m in length. Five meter lengths were used in the small ovens that were held at 55°C and 60°C, whereas ten meter lengths were used in the large oven at 65°C and in the open laboratory where potential capacitance changes at room temperature were monitored.

All cable samples available for destructive testing after various periods of aging were either 5m or 2.5m long. Again, the shorter samples were used only in the ovens at 55°C and 60°C; however, the samples used to determine the insulation densities reported in Fig. 11 for 55°C were 5m in length.

Finally, singles for aging in excess filling compound were all 5m long.

Choice of Pairs. Every pair was monitored in the samples prepared for the measurement of mutual capacitance, except for the 50 pair 26 AWG cables with medium density polyethylene foam insulation where only 10 pairs were monitored.

Usually, ten wires from five pairs were tested when aged samples were examined for physical changes. For each cable type, the same five pairs were always chosen. With the exception of the twelve-pair cable, all ten colours of insulation were included in the five pairs.

Physical Measurements Performed. The following weights and dimensions were measured for each sample of insulated conductor after excess filling compound had been removed from its surface by wiping with a soft cloth dampened by a chlorinated solvent: weight of insulated conductor in air and in water, weight of the copper conductor alone in air and in water, and insulation and conductor diameters (using a micrometer). Conductor diameters were found to be so uniform that the best measure of length proved to be conductor weight.

RESULTS

Changes in Transmission Properties

Mutual Capacitance. The nominal capacitance of all the cables under test was 83 nF/mile as manufactured. Figures 1 to 5 present the percentage change in capacitance as a function of time for the four types of filled foam cable that were subject to accelerated aging. Before the ovens were turned on, the initial capacitance of each pair was determined; then for any given individual pair, the difference between each subsequent reading and the initial reading was expressed as a percentage of the initial reading for that particular pair. Finally, for each cable sample at each stage of aging the average and standard deviation of these percentages were calculated for all the pairs monitored in the sample.

The points plotted on the graphs are, of course, the averages, and the error bars plotted above and below any given average indicate plus and minus one standard deviation, respectively. These error bars represent, in some sense, the magnitude of real variations from pair to pair in addition to variations due to experimental error.

Let us consider the behaviour of all the samples which were five or ten meters in length (i.e. all samples except for the long sample of cable A and the sample of cable E). If these results are taken at face value, MDPE appears to be in trouble at 65°C, and the particular polypropylene in cable D appears in trouble even at 55°C. However, according to Fig. 1 (which compares the effect of aging short and long samples of the same cable), 1355m of cable A with MDPE insulation aged at 65°C with no significant degradation in the capacitance.

A sample of cable C with solid MDPE insulation was also monitored for capacitance changes at 65°C. It is noteworthy that twenty-four hours after the oven was turned on, the average capacitance had dropped by 4.8%.

Other Parameters. The attenuation at 150 and 772 kHz, the capacitance unbalance pair-to-pair and pair-to-shield, and the mutual conductance of a limited number of pairs in the long sample of cable A were measured at room temperature before and after aging for thirteen weeks at 65°C. Considering the accuracy of the measurements, no significant changes were observed. In the case of the attenuation measurements, actual changes must have been less than 1% and 2½% at 772 kHz and 150 kHz, respectively.

Changes in Physical Properties of Insulation

Weight of Insulation. In the unaged state, the weight per unit length of the insulation in cable A was found to be relatively uniform from wire to wire and along the length of any given wire. Because of this, all changes in weight after aging were calculated as percentages of the average weight per unit length before aging, namely 0.378 gm/m. Fig. 6, Fig. 7 and Fig. 8 present the results of accelerated aging of short samples of cable A and of singles from A in a large amount of filling compound.

At 55°C, the weight increase of the insulation in cable A was somewhat greater for insulation that aged within cable samples than for insulation that aged in an excess of filling compound; but the increase appeared less uniform in the former case than in the latter case. At

60° such distinctions became cloudy.

Fig. 9 presents results for the polypropylene insulation. Here, all percentages are based on the average weight per unit length for the unaged insulation of 0.424 gm/m.

It should be mentioned that all the results in Figs. 6 to 9 are based on measurements made on pieces of insulated wire roughly 0.5m in length. One of these samples was cut from each of the relevant 2.5 or 5m lengths of aged wire.

The error bars in Fig. 6 to Fig. 9 have the same meaning as they do in Figs. 1 to 5. In fact, the error bars in all figures indicate plus and minus one standard deviation.

Finally, the solid insulation in a sample of cable C increased in weight by 5.4% after aging for 13 weeks at 65°C.

Density of Insulation. Changes in the density of the MDPE foam in cable A are plotted in Fig. 10 and Fig. 11. The percentages are based on the average unaged density of 0.561 gm/cm^3.

Both at 65°C and 55°C, insulation that aged in the short cable samples showed a greater average increase in density than insulation that aged in an excess of filling compound.

The measurements on which the densities in Figs. 10 and 11 are based were performed on almost the entire 5m length of each of the relevant aged wires.

Diameter of Insulation. Using measurements by micrometer, the average diameter of the unaged insulated conductors in cable A was found to be 44.3 mils (1.125mm). The same figure was obtained from calculations starting with insulation weights and densities. Since the wire diameter was 25.2 mils (0.640mm), the initial thickness of the MDPE foam was 9.55 mils (0.243mm).

For aged insulation, however, almost every average diameter was based on the observation of only ten wires, and in most cases accurate values of diameter did not seem attainable. For the short samples of cable A aging at 65°C, a believable estimate of diameter was obtained by averaging measured and calculated values. (Diameters were calculated using insulation weight per unit length and density, where each density was calculated using data from the same 0.5m length of wire that was used to obtain the corresponding insulation weight.) As shown in Fig. 12, the diameter appeared constant at approximately 45.5 mils (1.156mm) from about 2 weeks to 13 weeks; full diameter was not reached until after the first week. In the case of aging the short samples of cable A and the singles from A at 55°C, there appeared to be little usable information in the results because the experimental error seemed to be larger than the possible effects of aging; however, the mean value of the diameter throughout the period of aging after the first three weeks was probably within the range from 45.0 to 45.2 mils (1.143 to 1.148mm) for both cable samples and singles.

Insulation in Long Sample of A. After the reel holding 1355m of cable A had aged for 13 weeks at 65°C and the electrical measurements were complete, 18 meters of cable were cut from the outside end and the remainder was examined in some detail. In particular, insulation diameter and density were measured for all fifty wires in a sample taken from somewhere near the outside end of the remainder of the reel. The average diameter was found to be 44.9 mils (1.140mm) and the average density was found to be 0.62 gm/cm^3, i.e. 10.5% above the unaged density of 0.561 gm/cm^3. These numbers should be compared with the results obtained for the insulation in cable A when 5m samples were aged in the same way: 45.5 mils (1.156mm) and 16.8% above the unaged density.

Samples at Room Temperature

Throughout two years of observation of cable A, no statistically significant changes were found either in mutual capacitance or in the physical properties of the insulation.

DISCUSSION

End Effects

Comparison of the results of aging short and long samples of cable A suggests that insulation within a few meters of the end of a cable ages more severely than insulation that is not exposed to end effects.

Let us consider the observed changes in insulation weight in short samples of cable A as shown in Figs. 6 to 8. As previously mentioned, each individual measurement was made on a piece of insulated conductor only 0.5m or so in length, and this piece was not always cut from the same place within the 2.5 or 5m length of the wire. Now the determination of insulation weight per unit length is quite an accurate procedure, even for wires only 0.5m in length, so that the observed weights must be indicative of the true weights for the pieces of wire measured. Thus, the apparent irregularity from week to week in the weight changes for 2.5m cable samples at 55°C is presumably the result of variations in the place from which the 0.5m pieces of wire were cut. One may therefore conclude that, for cable A at 55°C, the importance of end effects varies significantly within 1.25m of the end of a cable sample. At 65°C, however, the measured changes in weight increased quite smoothly as a function of time; this suggests, though does not prove, that end effects must have been relatively

uniform throughout each five meter sample. Thus, end effects at 65°C are probably important for more than 2.5m from the end of a cable.

Support for the above arguments is also provided by the results for singles that aged in an excess of filling compound. The weights per unit length plotted for singles in Fig. 8 show uniform behaviour as a function of time even though weights were again measured on pieces roughly 0.5m in length. In addition, the densities plotted in Fig. 11 (and Fig. 10) for samples of cable A exhibit fairly smooth variations as a function of time. These densities were measured using nearly the full 5m length of each wire, so that variations along the length of the wires would have been averaged away. Since the results were so uniform, it is evident that aging did not proceed in a significantly different way from cable sample to cable sample. It is therefore reasonable to assume that variations along the length of each sample explain the irregular behaviour of the insulation weight for short cable samples at 55°C.

Aging Singles in Excess Filling Compound

At least for foam MDPE insulation in petroleum jelly filling compound, the effect of aging insulated conductors in an excess of filling compound is not drastically different than the effect of aging insulated conductors within cables.

Insulation densities tended to be lower for insulation exposed to an excess of filling compound than for insulation exposed to end effects in cable samples; but, at least at 65°C, the densities for aging in a cable core and in an excess of filling compound were nearly identical when the insulation in the cable did not see end effects.

Weight increase was lower overall for insulation exposed to an excess of PJ at 55°C than for insulation in cable experiencing end effects, but the increase was comparable at 60°C. Presumably, therefore, insulation diameter was greater for the insulation in excess PJ at 60°C.

Cell Filling

Degree of Void Filling. As described in the Appendix, when insulation has swollen as a result of absorbing the mobile fraction of a filling compound, and equilibrium has been reached to the extent that the plastic in the matrix has swollen to the same degree throughout the thickness of the insulation, then the inside diameter of the insulation will have increased by the same percentage as the outside diameter, and a gap will have opened up between insulation and conductor. In addition, considering a cross-section of the insulation, the area of the gas cells will have increased by the same percentage as the percentage increase in the cross-sectional area of the insulation as a whole. Others[10] have expressed the degree of cell filling as a percentage of the final volume of the gas cells after swelling is complete. Here we shall not limit ourselves to the volume of mobile fraction in the cells alone. We shall include any filling material under the insulation, and we shall express the degree of void filling as a percentage of the sum of the final volume of the cells and the volume of the gap between insulation and conductor. This is done because of the importance to mutual capacitance of voids immediately next to the conductors. It may very well be important to know what fraction of all voids have been filled, not just what fraction of the gas cells.

Using the above definition of the degree of void filling and starting with observed insulation densities and diameters, the appropriate formula in the Appendix gives the following estimates of the degree of void filling in the foam MDPE insulation in samples of cable A after thirteen weeks at 65°C: 18% when end effects are *not* involved, and 29% when they are. (For the latter case, an estimate of 27% is obtained by starting with the observed increase in weight rather than density, and using Equation [2] instead of [1].)

The Onset of Cell Filling. There is considerable evidence that cells actually begin to fill before swelling of the solid matrix is complete. Considering the short samples of cable A at 65°C, for example, the diameter of the insulation continued increasing for more than one week after the oven was turned on, whereas the mutual capacitance, after its initial fall, had started increasing again before the oven had been on for a week. In addition, after one week the insulation had increased in weight by 9%, while the appropriate formula in the Appendix suggests that, even if the solid matrix was already swollen to its maximum diameter of 45.5 mils (1.156mm) and void filling was zero, the insulation would have increased in weight by only 5.5%.

With respect to the existence of a threshold temperature below which no cell filling can occur[10], the present study does not provide a definite answer; however, the percentage increase in insulation weight for samples of cable A reached figures in the twenties for both 55°C and 60°C as well as for 65°C, though of course longer periods of aging were involved at the first two temperatures. This observation suggests that no true threshold exists; cell filling just takes longer at lower temperatures.

Availability of Mobile Fraction. The results obtained for insulation aged in an "unlimited" supply of filling compound imply that the presence of a large amount of filling compound does not result in extra cell filling, at least for foam MDPE in PJ at temperatures up to 65°C. Nevertheless, the amount of mobile fraction available for cell filling in actual cables is still of interest. In few cables does the ratio of the volume of filling compound to

the volume of insulation exceed two by a significant amount. If the mobile fraction represents 30 or 40% of the filling compound, the ratio of the volume of mobile fraction to the volume of cells in the insulation will also be little more than two at most. Therefore, in order for the cells in the insulation to become entirely filled as the cable approaches its equilibrium state, at least half of the oil in the filling compound would have to diffuse from the filler into the insulation.

Another factor is well-known[4]. As temperature increases, the percentage of the filling compound that is "mobile" will normally increase. For example, in petroleum jelly more waxes will dissolve in the oils as the temperature goes up. But when the chemical nature of the mobile fraction changes with changes in temperature, the qualitative nature of the aging process can change, and one must be careful drawing conclusions about behaviour at temperatures that are different from those at which observations are made.

Several Mechanisms that Probably Affect Aging. When a cellular insulation absorbs filling compound the effective volume of the insulation increases by an amount that is greater than the volume of filling compound absorbed unless void filling is well advanced. This is a result of the increase in volume of the gas cells and the formation of a gap under the insulation proper as the plastic matrix swells. According to the Appendix, before the onset of void filling the volume of filling compound absorbed by the insulation in short or long samples of cable A would be just 42% of the resulting increase in the effective volume of the insulation, where the effective volume includes the gap between the insulation proper and the conductor. (If for some reason there actually was a significant increase in the density of the polymer upon absorption of filling compound, the 42% ratio would be larger; but for reasonable estimates of possible density changes, the ratio remains far less than 100%.) Thus as the insulation attempts to absorb the mobile fraction, pressures must build up in the core except possibly near the cable ends where pressure could be relieved by movement of the unabsorbed filling compound.

In addition, gas pressure in the cells would rise as the temperature of the insulation increases; but it would tend to drop again as the insulation swells and the cells expand. The pressure in the void forming between each conductor and its insulation would, of course, tend to be very low until a significant amount of gas from the cells diffuses into the void and/or a significant amount of gas (air) diffuses along the conductor from one end of the cable or the other. Presumably, any movement of gas in or out of the cable along the voids next to the conductors would be most significant near the ends of a cable.

It is not clear how the above mechanisms would account for the detailed differences in aging between short and long cable samples. Evidence that the expansion of insulation inside cable cores is constrained by some mechanism may readily be found in the experimental results: at 65°C the insulation diameter at a point well removed from the ends of the long sample of cable A was considerably less than the diameter observed in short samples, and at 60°C the insulation diameter was inferred to be less for insulation in short cable samples than for insulation on singles aging outside the confines of a cable sheath. These differences in diameter may possibly be caused by the different pressures seen by the insulation as it starts to swell in the three different circumstances: away from the end of a cable the pressure on the outside of the insulation will be high, whereas under the insulation the pressure will be very low; near the end of a cable, the pressure on the outside of the insulation will be lower than at a point further removed from the end, while the pressure under the insulation will be close to atmospheric pressure; finally, the insulation in the bath of filling compound would see approximately atmospheric pressure on both sides. With respect to the process of cell filling, however, the consequences of the effects discussed in this section are obscure.

CONCLUSIONS

End effects have been found to exist when cable insulated with cellular medium density polyethylene and filled with petroleum jelly undergoes accelerated aging. Thus, results based on aging samples a few meters in length are not necessarily representative of the behaviour of longer lengths; the aging of short lengths can be more severe.

Little attention has been paid in the literature to the influence of pressures generated in the cable core, or to the significance of the void that forms around the conductor. Both factors seem to be important to an understanding of the aging process.

Nothing in the reported results should be cause for alarm with respect to the use of filled cable with cellular medium or high density polyethylene insulation in buried applications, though of course this investigation does not provide positive proof of the suitability of the cable. In many aerial installations, however, cable temperatures could reach 55°C for extended periods of time[10]. In this case, the laboratory aging experiments cannot really be considered "accelerated" tests. The fact that a cable does not degrade significantly when it is kept at 55°C for 35 weeks does not give the author confidence in the use of such a cable in aerial applications.

ACKNOWLEDGEMENTS

The author should like to thank Superior

Cable Corporation and Canada Wire & Cable Ltd. for permission to publish this paper. He is also indebted to P. Reimer, B. Das, M. Stearns, P. Garmon and L. Davis for making the many measurements that led to the results reported herein. Finally, thanks are due to J. Lail for typing the manuscript.

REFERENCES

[1] S. Verne, R. T. Puckowski and A. A. Pinching, "Long Term Stability of Polyethylene Insulated Fully-filled Telephone Distribution Cables," *Proceedings of the Twentieth International Wire and Cable Symposium*, pp. 218-228, 1971.

[2] E. J. Gouldson, M. Farago and G. D. Baxter, "Foam-skin, a Composite Expanded Insulation for Use in Telephone Cables," *Proceedings of the Twenty-first International Wire and Cable Symposium*, pp. 158-172, 1972.

[3] S. G. Foord, "Compatibility Problems in Filled Cellular Polyolefin Insulated Telephone Cables," *Proceedings of the Twenty-second International Wire and Cable Symposium*, pp. 23-29, 1973.

[4] S. Verne, A. A. Pinching and J. M. R. Hagger, "Long-term Stability of Fully-filled Cables," *Proceedings of the Twenty-second International Wire and Cable Symposium*, pp. 244-260, 1973.

[5] C. J. Aloisio and E. D. Nelson, "Effect of Water and Petroleum Jelly Migration on Capacitance of Plastic Insulated Cables," *Proceedings of the Twenty-second International Wire and Cable Symposium*, pp. 261-269, 1973.

[6] S. M. Beach, D. F. Cretney and J. Ruskin, "Cellular Polyethylene Insulated Fully-filled Cable with High Dielectric Strength," *Proceedings of the Twenty-second International Wire and Cable Symposium*, pp. 292-301, 1973.

[7] H. Repp, "Wechselwirkung verzellter, polyäthylenisolierter Nachrichtenadern mit Petrolaten," *Siemens Forsch.-u. Entwickl.-Ber.*, Bd. 4, Nr. 5, pp. 295-300, 1975.

[8] J. Pritchett, E. L. Mather and S. Verne, "Fully-filled Telephone Cable with Cellular Polyethylene Insulation after 10 years Service," *Proceedings of the Twenty-fourth International Wire and Cable Symposium*, pp. 347-360, 1975.

[9] H. J. Anderka, H. G. Dageförde and H. A. Mayer, "Change of Crosstalk Properties in Correlation to the Interaction of Polyethylene/Petroleum-Jelly," *Proceedings of the Twenty-fourth International Wire and Cable Symposium*, pp. 365-373, 1975.

[10] S. M. Beach, K. R. Bullock and D. F. Cretney, "The Properties of Cellular Polyethylene Insulated Filled Communication Cable and its Increasing Use," *Proceedings of the Twenty-fourth International Wire and Cable Symposium*, pp. 379-398, 1975.

[11] L. M. Molleda and E. Used, "Filled Cable for Aerial Installation," *Proceedings of the Twenty-fifth International Wire and Cable Symposium*, pp. 158-173, 1976.

APPENDIX

Isotropic Expansion in Two Dimensions

Isotropic expansion in the plane perpendicular to the axis of the conductor is commonly assumed[10] when cellular insulation absorbs filling compound. If each incremental volume of solid polymer in the matrix of the insulation absorbs oils and swells to the same extent no matter where it is in the insulation, and if the swelling of each increment occurs without preference for one direction or another in the perpendicular plane, swelling of the cross-section will be isotropic. Every dimension in the perpendicular plane will be scaled upwards by the same factor. This implies that the ratio of the new to old overall diameters of the cellular insulation will equal the ratio of the new to old inside diameters which will equal the ratio of the new to old radial diameters of any particular gas cell.

Obviously, the swelling will be isotropic only if the insulation is not distorted by external influences during expansion. In particular, we shall assume that other insulated conductors in the core do not interfere significantly with the expansion of the insulation on the wire being analyzed.

In practice, of course, the mechanism of absorption may possibly leave the insulation in a stressed state where, for example, the expansion of the insulation may be greater near its outer surface than near the conductor, or the expanded insulation may be badly distorted by interference from neighbouring wires. Thus the following formulas based on isotropic expansion in two dimensions should be used with circumspection.

Formulas Pertinent to Aged Insulation

Notation and Definitions.

a, a' = cross-sectional area of void between insulation and conductor (before and after swelling, respectively).

A' = cross-sectional area of insulation, excluding area of void under insulation proper (after swelling).

d = diameter of conductor.

D, D' = diameter over insulation (before and

after swelling, respectively).

F = ratio of volume of gas cells to total volume of insulation (before swelling).

R = density of insulation (before swelling).

R' = effective density of insulation (after swelling), i.e. effective insulation weight per unit length, where effective weight includes the weight of any mobile fraction between conductor and insulation proper, divided by effective insulation volume per unit length, where effective volume includes the void under the insulation proper.

V = ratio of the volume of mobile fraction in all voids to the total volume of all voids.

W = weight of insulation per unit length (before swelling).

W' = effective weight of insulation per unit length including weight of any mobile fraction under insulation proper (after swelling).

ρ_f, ρ_f' = density of filling compound between insulated conductors (before and after swelling, respectively).

ρ_m = density of mobile fraction found in voids.

ρ_p, ρ_p' = density of solid plastic that forms the matrix in the cellular insulation (before and after swelling, respectively).

The effective density R' and the effective weight per unit length W' of aged insulation are defined above in such a way that they represent the quantities which are actually determined in the lab.

Throughout the derivation of the formulas in the next section it is assumed that a=o, i.e. that there is no void next to the conductor in the unaged state.

$$f \equiv D'/D$$

$$c \equiv a'/A' = \frac{1-(1/f)^2}{(D/d)^2-1}$$

$$x \equiv R'/R$$

$$y \equiv W'/W$$

$$Z \equiv \rho_p'/\rho_p$$

All diameters must be expressed in the same units. Similar statements apply to weights, etc. Otherwise, units are of little concern.

Formulas. The percentage of the volume of the voids that is filled with mobile fraction is given by

$$V = 100\,(\rho_p/\rho_m)(1-F)\left[\frac{(1+c)x-Z}{F+c}\right] \%, \quad [1]$$

or by $$V = 100\,(\rho_p/\rho_m)(1-F)\left[\frac{(y/f^2)-Z}{F+c}\right] \%. \quad [2]$$

(If one ignores the existence of the void between the insulation proper and the conductor, that is if one sets c=o, then equation [1] reduces to the formula presented in Appendix 4 of reference[10].)

If the insulation expands on aging, but void filling has not yet begun, then

$$y = f^2 Z \quad . \quad [3]$$

This formula may be used to calculate the weight uptake that would be expected for a given change in insulation diameter if there has been no void filling.

When the insulation is beginning to expand and void filling is not yet significant, one may use the following formula to estimate the ratio, which we shall call "γ", of the volume of filling compound absorbed by the insulation to the increase in effective volume of the insulation:

$$\gamma = 100(\rho_p/\rho_f)(1-F)\left(\frac{D^2-d^2}{D^2}\right)\cdot\left(\frac{Zf^2-1}{f^2-1}\right) \%. \quad [4]$$

(In deriving this relation, it was assumed that, at least approximately, $\rho_f'=\rho_f$.)

When these formulas were used in practice for cable with foam MDPE insulation and PJ filling compound, the assumption was made that there would be little if any change in the density of the polymer as it swells, and Z was set equal to unity. This assumption was made because of the lack of conclusive evidence otherwise. (One reference[10] suggests the figure 1.025 for the same type of materials, but it does not indicate the type of measurements that led to the number. On the basis of a limited amount of testing using wire insulated with solid MDPE, it appeared that Z should be closer to one; it is not clear, however, that plastic forming the matrix in a cellular insulation should be expected to behave in the same way as plastic in solid insulation.) Finally, in using the formulas it was also assumed that $\rho_m = \rho_f$ at least approximately.

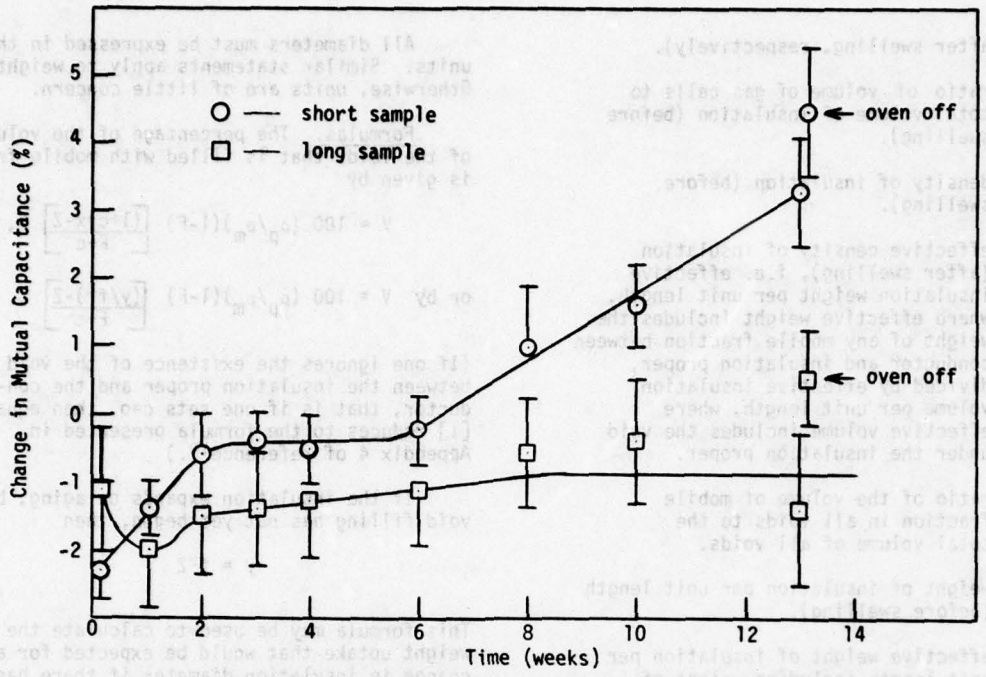


Fig. 1. Percentage Change in Mutual Capacitance as a Function of Time for Long and Short Samples of Cable A at 65°C.

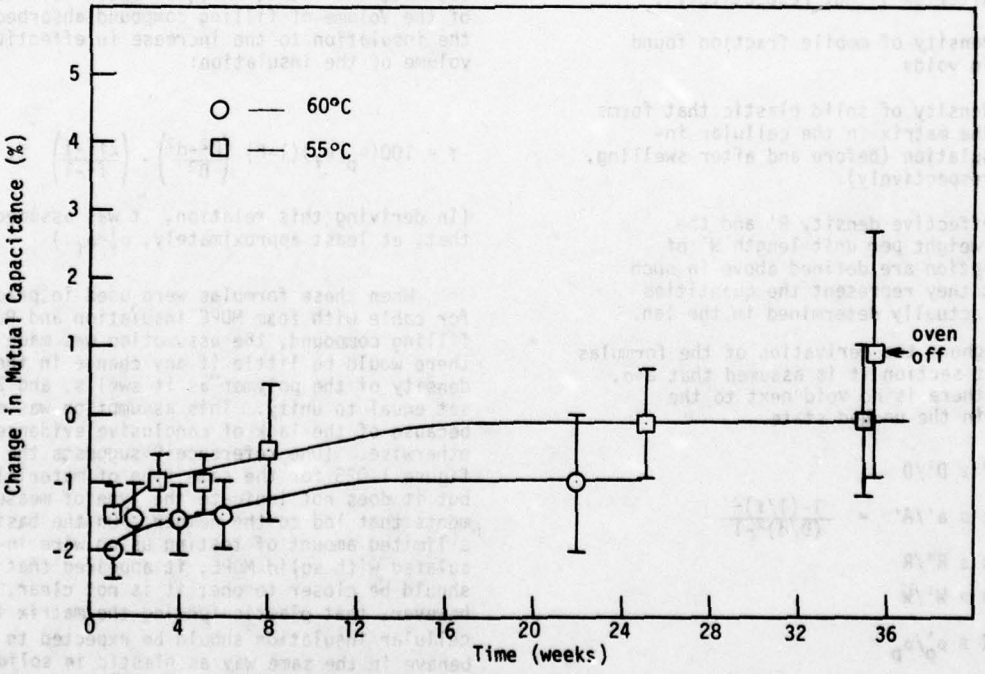


Fig. 2. Percentage Change in Mutual Capacitance as a Function of Time for Short Samples of Cable A at 55 and 60°C.

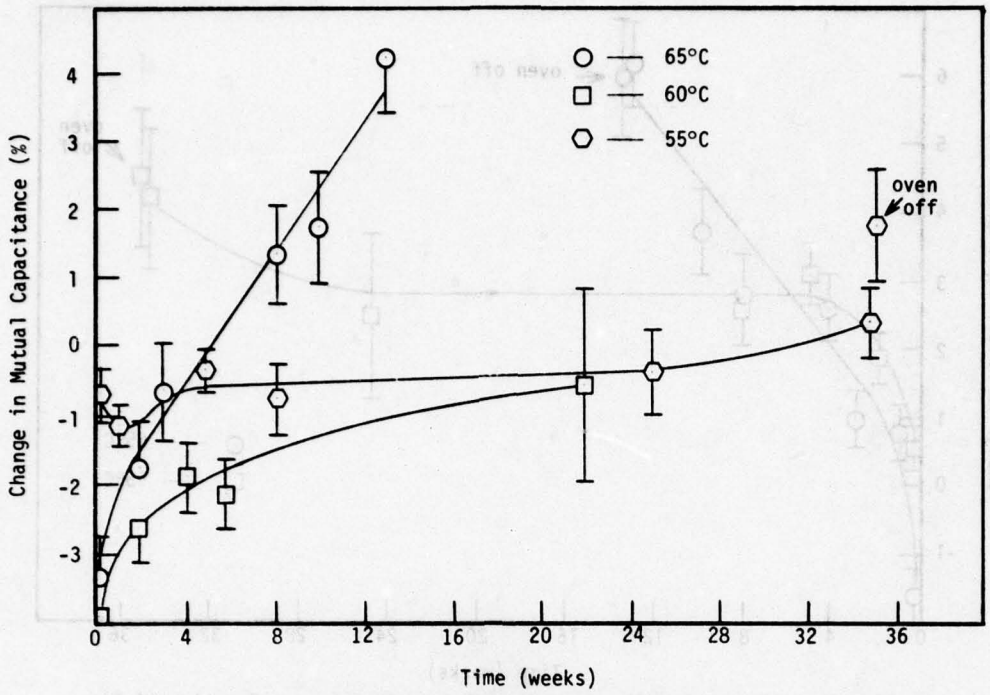


Fig. 3. Percentage Change in Mutual Capacitance as a Function of Time for Short Samples of Cable B.

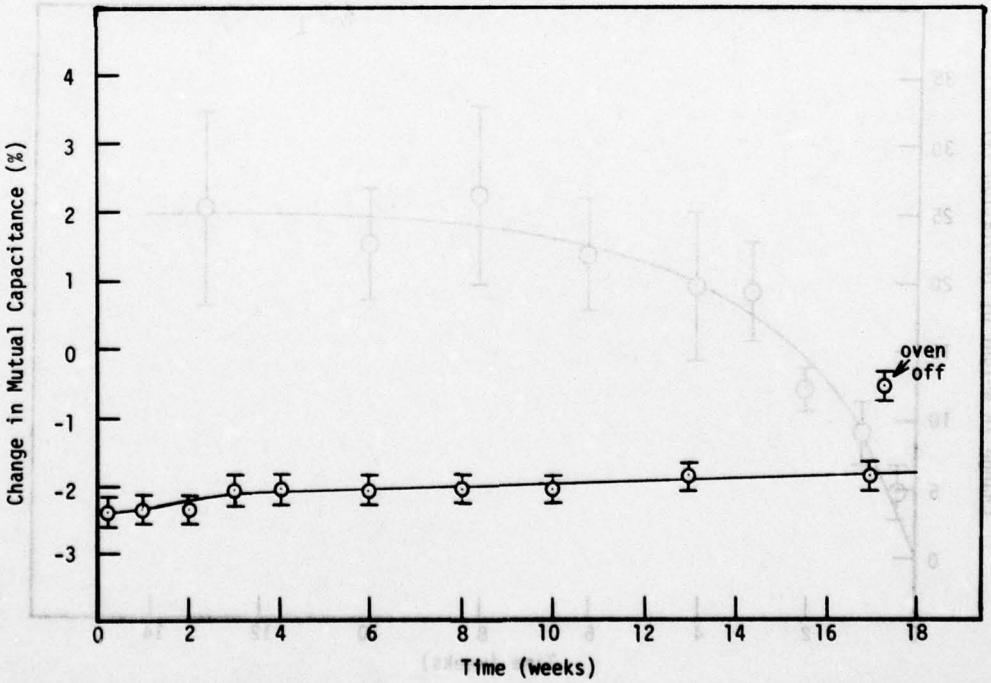


Fig. 4. Percentage Change in Mutual Capacitance as a Function of Time for a Long Sample of Cable E at 65.5°C.

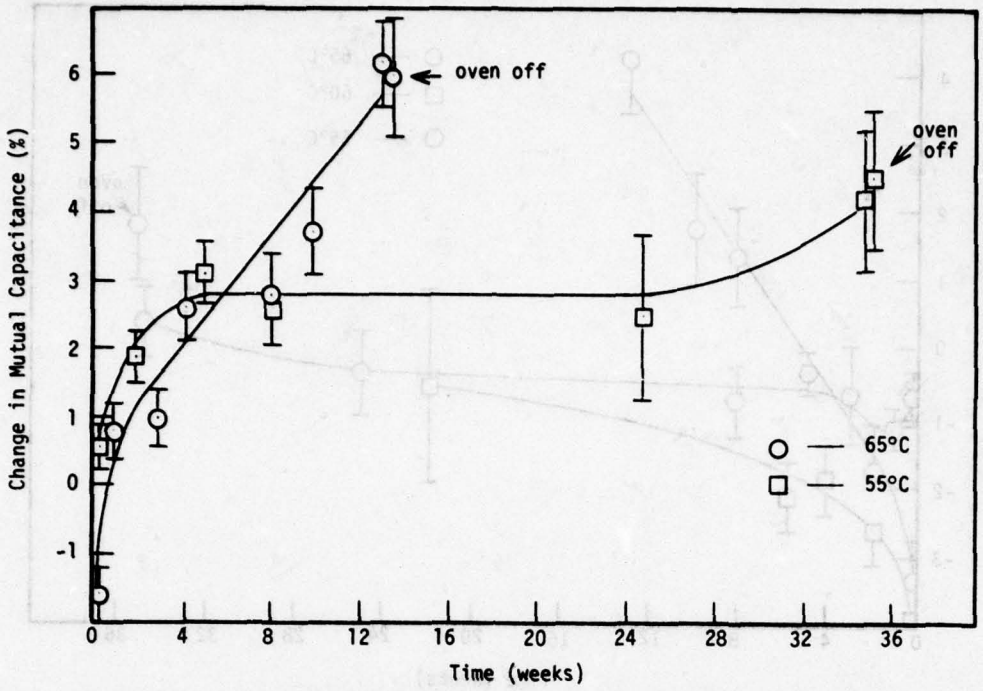


Fig. 5. Percentage Change in Mutual Capacitance as a Function of Time for Short Samples of Cable D at 55 and 65°C.

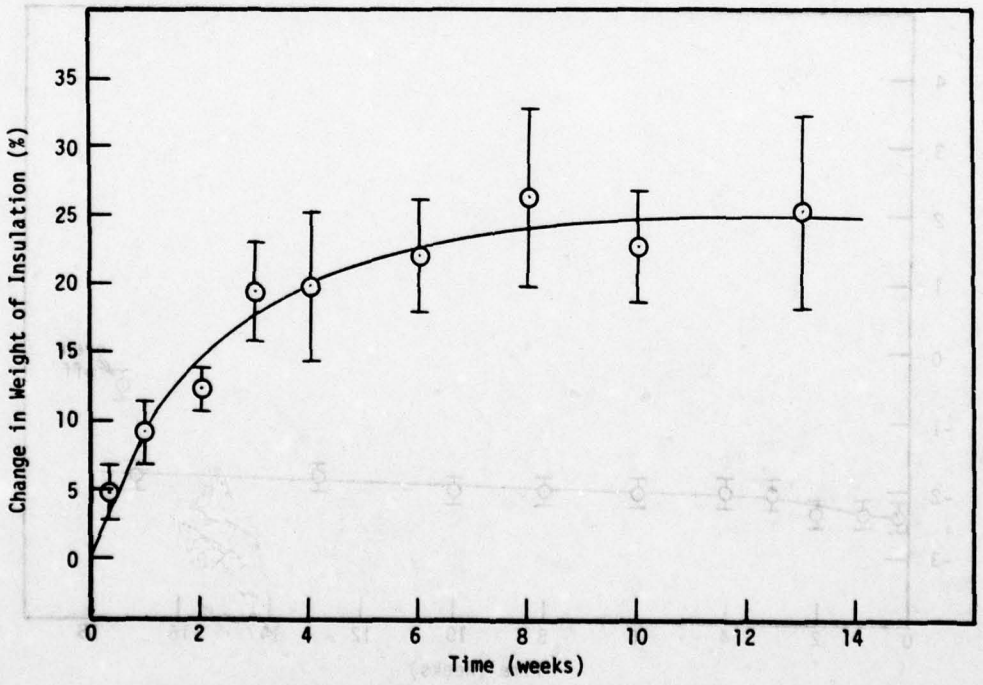


Fig. 6. Percentage Change in Weight of Insulation as a Function of Time for Short Samples of Cable A at 65°C.

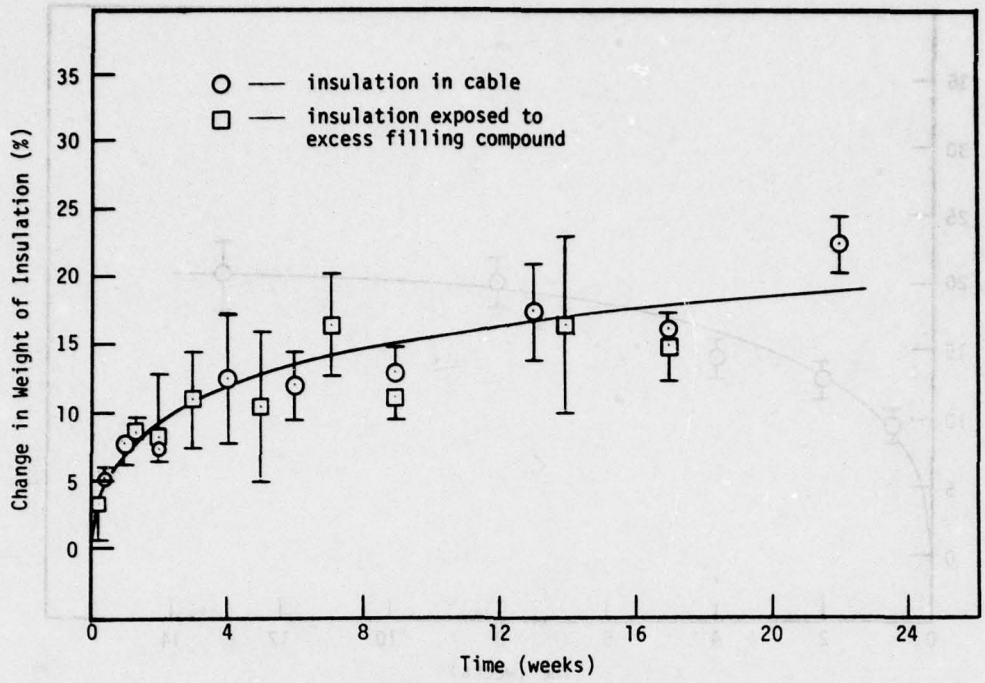


Fig. 7. Percentage Change in Weight of Insulation as a Function of Time for Short Samples of Cable A, and for Singles from Cable A in Excess Filling Compound, at 60°C.

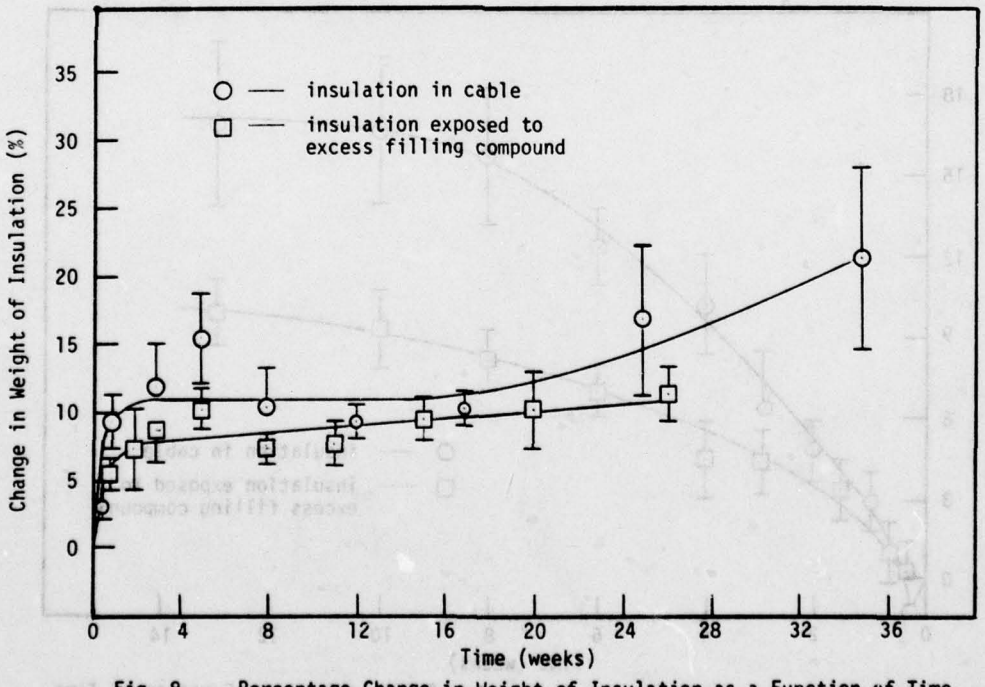


Fig. 8. Percentage Change in Weight of Insulation as a Function of Time for Short Samples of Cable A, and for Singles from Cable A in Excess Filling Compound, at 55°C.

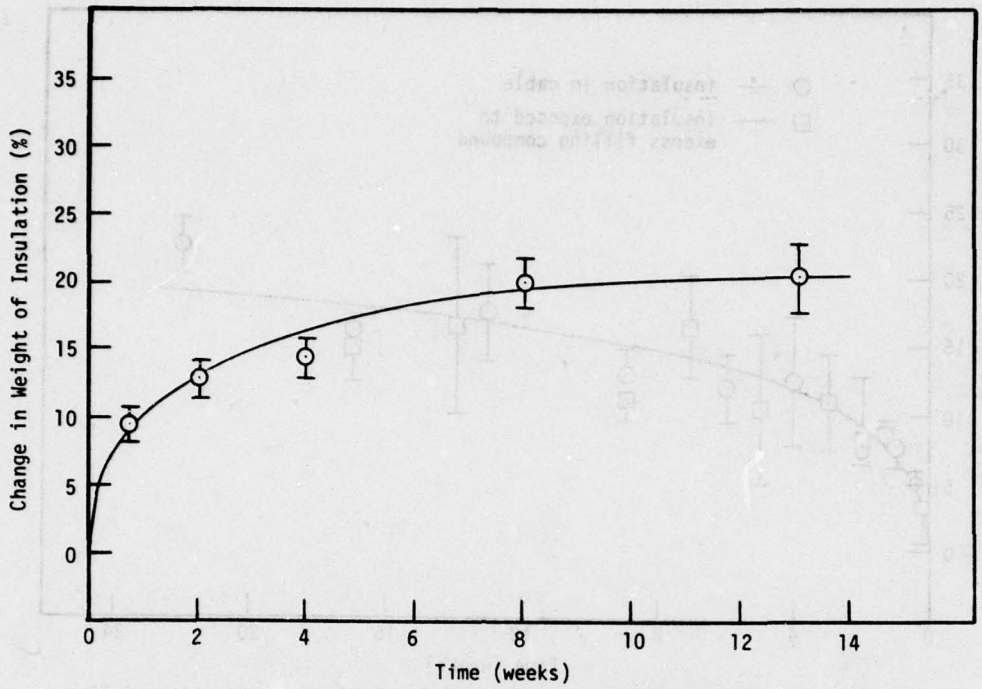


Fig. 9. Percentage Change in Weight of Insulation as a Function of Time for Short Samples of Cable D at 65°C.

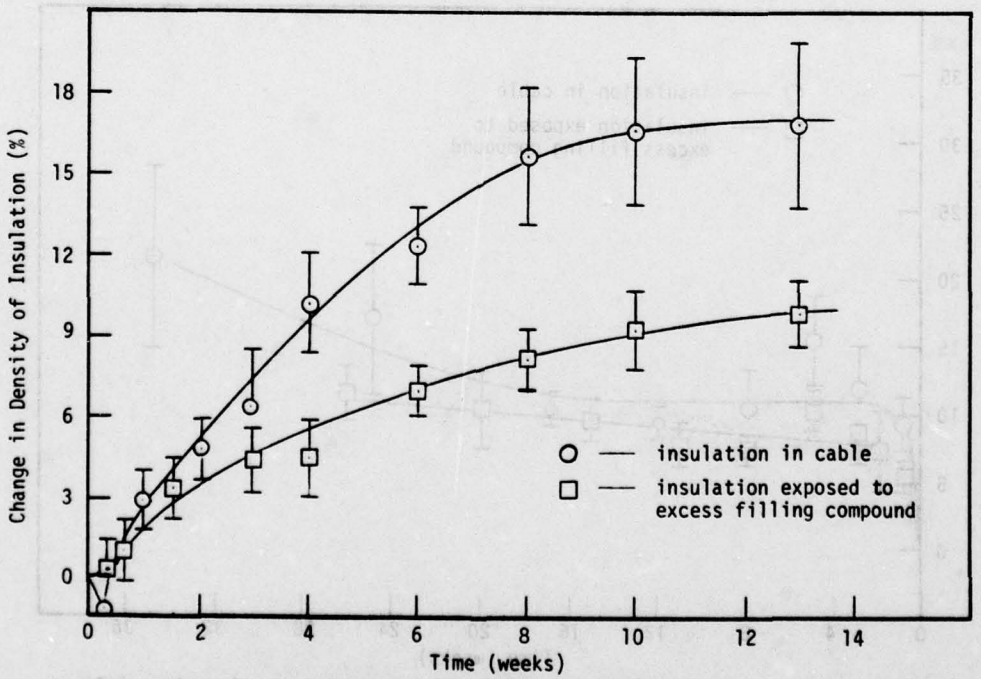


Fig. 10. Percentage Change in Density of Insulation as a Function of Time for Short Samples of Cable A, and for Singles from Cable A in Excess Filling Compound, at 65°C.

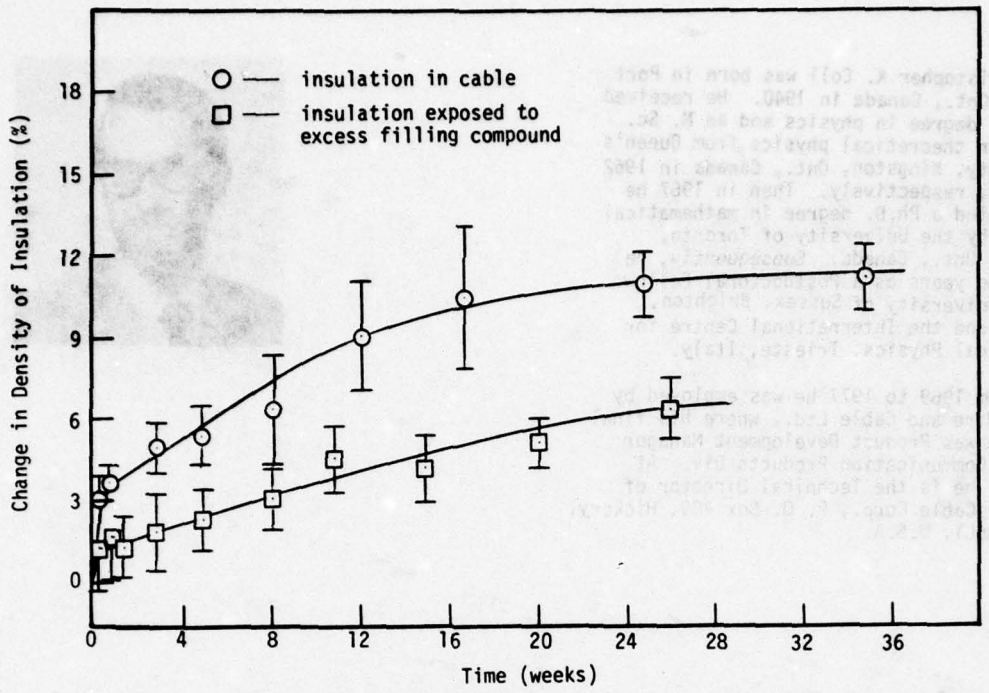


Fig. 11. Percentage Change in Density of Insulation as a Function of Time for Short Samples of Cable A, and for Singles from Cable A in Excess Filling Compound, at 55°C.

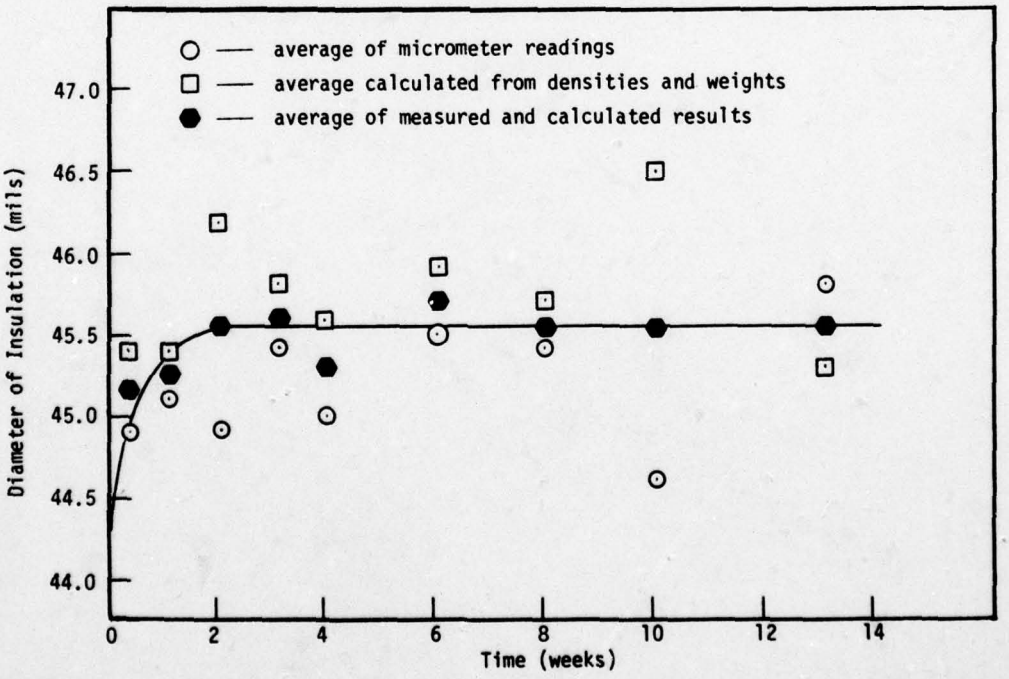


Fig. 12. Average Outside Diameter of Insulation as a Function of Time for Short Samples of Cable A at 65°C.



Christopher K. Eoll was born in Port Arthur, Ont., Canada in 1940. He received a B. Sc. degree in physics and an M. Sc. degree in theoretical physics from Queen's University, Kingston, Ont., Canada in 1962 and 1964, respectively. Then in 1967 he was granted a Ph.D. degree in mathematical physics by the University of Toronto, Toronto, Ont., Canada. Subsequently, he spent two years as a Postdoctoral Fellow at the University of Sussex, Brighton, England and the International Centre for Theoretical Physics, Trieste, Italy.

From 1969 to 1977 he was employed by Canada Wire and Cable Ltd., where his final position was Product Development Manager for the Communication Products Div. At present, he is the Technical Director of Superior Cable Corp., P. O. Box 489, Hickory, N. C. 28601, U.S.A.

INSULATION BY POWDER AND FIBERS DEPOSITION GIVING WATER BLOCKED TELEPHONE CABLES

Philippe A. Robert

Propintel S.A. CH - 1110 Morges Switzerland

Abstract - The technique presented provides water blockage along underground telephone cables the jacket of which has been accidentally damaged. The insulation consists in a thin layer of expanded polyethylene in which cellulose fibers are embedded. The raw material of paper insulated cables and plastic insulated cables are thus simultaneously used. This permits to obtain at the same time the advantages of both technologies without the inconveniencies of either one. For instance detection and location of possible defects in jacket, steady electric properties, reduced capacitance unbalances, easy splicing, high capacity to resisting mechanical stress. Towards the end of 1976, the Swiss Administration of PTT decided to progressively introduce cables made in accordance with this process in its network.

I. INTRODUCTION

The insulation of telephone wire serves several purposes. In particular it has to :

(i) act as a dielectric between the conductors ;
(ii) serve as a mechanical separator between the wires in order to maintain the required distance between them ;
(iii) preserve the shape of twisted pairs or quads which has to be perfectly constant and regular along the complete length of the cable.

When these points are correctly worked out, and provided that all the conductors are of the same type, namely present equal resistances per unit length, the cable constitutes a balanced transmission line. The capacitances of one conductor against others are balanced and the crosstalk is theoretically zero.

A telephone cable must not only satisfy such electrical requirements. Other aspects are equally important, to ensure that it can be laid, installed and used under the best possible conditions, with assured reliability. These aspects are its mechanical strength, lightness, flexibility, the ease with which splicing can be carried out (especially using automatic machines), its resistance to different external agents, such as corrosive environments, rodents, etc. and the ease with which repairs can be carried out, following accidental damage.

II. THE WATER PROBLEM

A critical situation occurs in case the cover has been accidentally pierced, allowing water to enter the cable. With cables having air core plastic insulation, it is possible for the water to be propagated along the wires over great distances, even several kilometres, before the fault is detected. The DC voltage used for the bell circuit can then create, through porosity in the insulation a DC current which will lead to electrolytic erosion of the conductors, and finally their rupture. Even where the conductors are not broken, variations in capacitance and the appearance of capacitance unbalances due to the presence of water will adversely affect the operation of the cable.

In any case, a great length of cable would have to be replaced.

With a cable whose characteristics would allow both to quickly detect the fault and to prevent propagation of water, a few meters of cable only would have to be replaced.

III. CURRENT STATE OF TECHNOLOGY

For many years, all telephone cables have been insulated using dry paper. This type of insulation provides in itself a rapid indication of water penetration by immediate reduction of the insulation resistance. The water propagation is stopped by the swelling of the paper, which is highly absorbent.

So the water problem begins with the outset of the plastic insulation technology. To counter the disadvantage of water penetration along plastic-insulated cables, different solutions are proposed. But no one gives complete satisfaction, as demonstrated be the great number of patents published every year on this subject. These solutions can be

classified into four categories, briefly described below with their advantages and disadvantages.

(i) The cable can be internally gas-pressurized. This solution is a costly one which may only be used for large cables. Localisation of the defect is laborious, its presence only is readily detectable. Should the pressurization system fail, water will enter the cable via small, unrepaired faults which may even have remained undetected.

(ii) The empty spaces in the cable can be filled with an expanded polyester of the closed pore type. The entry of water into the cable is completely prevented only if the filling is complete. Now it is difficult to archieve complete filling of large cables. The cable presents a considerable reduction in flexibility. It is not easy to remove the polyester from the wires for splicing operations.

(iii) Instead of polyester a viscous fluid non-soluble in water can be used. The most famous example is petroleum jelly. As with polyester,the filling of large cables is problematic. The permitivity of the filler increases the capacitance of the circuits, so that it becomes necessary to increase the diameter of the cable in order to maintain the same attenuation coefficient. The handling of the cable for splicing operations is messy and time consuming. It is difficult to find a jelly and an expanded plastic insulant which are mutually compatible.

(iv) The cable can be filled with material that swells when wet, usually in powder form. This method is safer than the previous ones, because it does'nt need a 100 % filling ratio. However there remains the risk of uneven distribution of the powder, which reduces its effectiveness, and can unfavourably affect the direct capacitances of the conductors and especially the capacitance unbalances.

IV. NEW TYPE OF INSULATION

The state of art briefly described above shows that dry paper technology retains some unique valuable features compared to the plastic technology, which offers its specific advantages. This led a group of Swiss Cableworks to launch a research programm in order to find an insulation for telephone cables combining the advantage of both technologies and avoiding the inconveniences of either one. The basic objectives were :

- an adequate restraint to the propagation of water along the cable, due to a protection built into each wire separately
- an immediate indication of the accidental entry of water into the cable, with the possibility to rapidly locate the fault
- a low permittivity
- a physical solidity of the insulation facilitating splicing operation and allowing direct connections to a junction box.

Since 1970 manufacturing techniques employed in the textile industry appeared to be attractive. In 1971, a first sample of wire is insulated. Its length does not exceed 30 cm. In 1973, a first cable of ten star quads, 0.4 mm Cu, 250 m length is manufactured. Its properties are very close to the specifications of the Swiss Administration of PTT. The way to put the process on an industrial production level is open.

The solution lay in creating an insulation consisting of a thin layer of expanded polyethylene, in which cellulose fibers are embedded (Fig. 1 and 2).

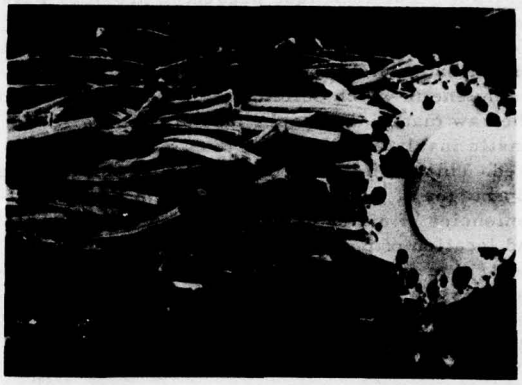


Fig. 1 PEC insulated wire, transverse section
Diameter of copper : 0.6 mm

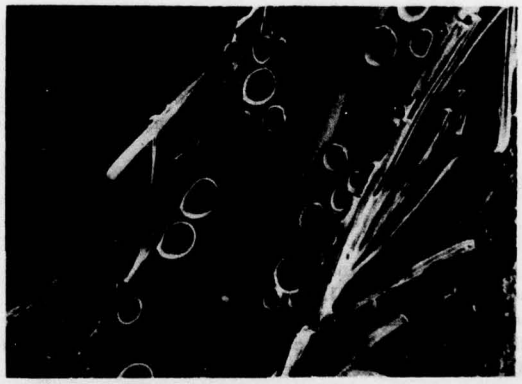


Fig. 2 PEC insulated wire, longitudinal section
Diameter of copper : 0.6 mm

The polyethylene layer provides good mechanical strength as well as sufficient dielectric strength. The fibers, in the dry state, offer adequate insulation resistance. On the other hand, should water penetrate the outer cover, absorption of water by the fibers greatly reduces the insulation resistan-

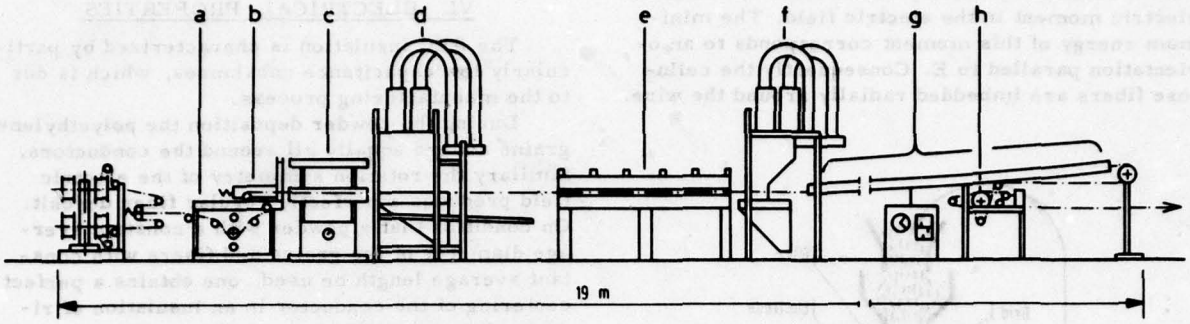


Fig. 3 Diagramm of a production unit

ce between conductors, giving immediate detection of the fault, with its exact location. In addition, absorption of the water causes the fibers to swell, preventing propagation of the water along the cable.

The fibers act also as separators between the wires, carefully dimensioned so as to maintain them at a certain separation and give the required capacitance. Interweaving of the fibers maintains the shape of the quad, facilitating cabling operations by preventing the appearance of capacitance unbalances due to distortion of the quad.

This new type of insulation has been called TELEFLOC, and will be termed PEC (PolyEthylene-Cellulose) below.

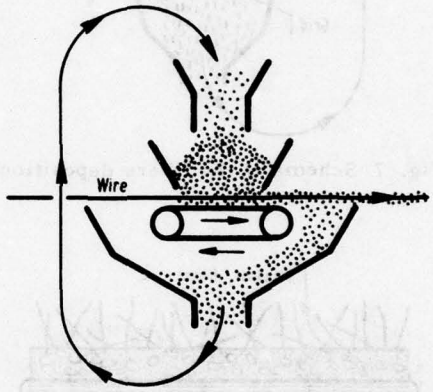


Fig. 4 Schéma of the powder deposition unit

V. PROCESS OF MANUFACTURE

The PEC insulation process uses powder and fibers deposition techniques. It comprises three phases as shown on figure 3. One production unit insulates simultaneously four parallel wires, assembled by means of an inline SZ quadder.

(i) The bare wire is introduced in the machine through an input capstan (a) whose speed is monitored by a force transducer (b). It then runs through a gas preheater (c) and enters the powder deposition unit ((d) and Fig. 4). There a polyethylene powder is carried at the speed of the wire by a belt. The grains of the powder in contact with the wire melt and adhere to the wire. The conditions of the thermic exchange are such that a sole layer of grains is deposed. At the output of the powder deposition unit the wire presents itself as shown schematically in figure 5.

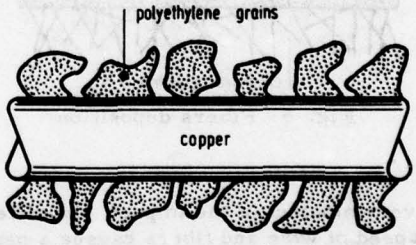


Fig. 5 One layer powder deposition

(ii) The layer of grains is then melted in an oven (e) in order to become a solid and regular layer (Fig. 6).

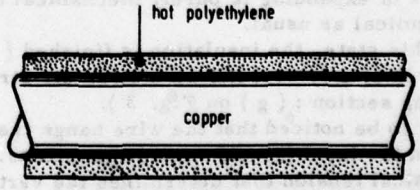


Fig. 6 Melting operation

(iii) On emergence from the oven the wire enters the fibers deposition unit (f). This consists (Fig. 7) of two grids controlling the flow of the cellulose fibers between the electrodes. The voltage applied between the electrodes and the wire produces around the wire a highly inhomogeneous electric field E . The ratio of the distance of the electrodes to the diameter of the wire is high enough for E to present immediately around the

wire a rotation symmetry. Each fibre becomes an electric moment in the electric field. The minimum energy of this moment corresponds to an orientation paralled to E. Consequently the cellulose fibers are imbedded radially around the wire.

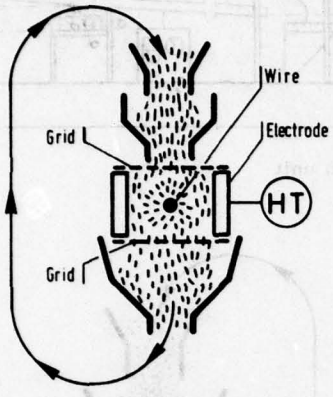


Fig. 7 Schéma of the fibers deposition unit

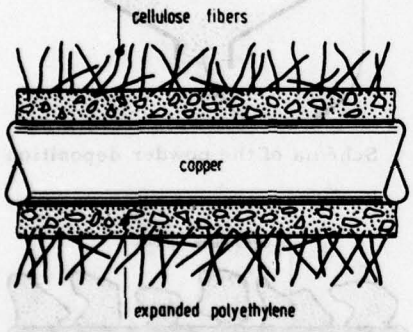


Fig. 8 Fibers deposition

At the very moment of the impact, the difference of the speed of wire and fibers causes a perturbation on the surface of the hot polyethylene, generating bubbles in the polyethylene. Thus the process of expanding is purely mechanical and not chemical as usual.

At this state, the insulation is finished (Fig. 8), there remains to cool the wire by an air stream. (cooling section : (g) on Fig. 3).

It is to be noticed that the wire hangs freely between the input (a) and ouput (h) capstans. The mechanical tension that determines the vertical position of each wire in the machine has to be monitored continuously with great accuracy. This is why each wire is introduced in the machine by an independant capstan. The output capstan however is the same for the four wires.

VI. ELECTRICAL PROPERTIES

The PEC insulation is characterized by particularly low capacitance unbalances, which is due to the manufacturing process.

During the powder deposition the polyethylene grains adhere equally all around the conductors. Similary the rotation symmetry of the electric field produces a perfectly regular fiber deposit. On condition that a powder with a constant average diameter of the grains and fibers with constant average length be used, one obtains a perfect centering of the conductor in an insulation of rigorously constant thickness. The properties required for the fibers and the powder are guaranteed by their manufacturing process.

The classical problems encountered with extruded insulation (variations in thickness and eccentricity) are totally absent in PEC insulation.

More over the interweaving of the fibers belonging to adjacent wires confers to the quad a great stability of shape.

As an example, the capacitance unbalances in a sample of PEC insulated cables are compared to the capacitance unbalances in a similar paper insulated sample in table 1 (about 650 quads distributed over eight cables for each sample Ø Cu = 0.6 mm).

The capacitance unbalances between the pairs of two adjacent quads are called k_9 , k_{10}, k_{11} , k_{12} . The capacitance of each pair is called C_n.

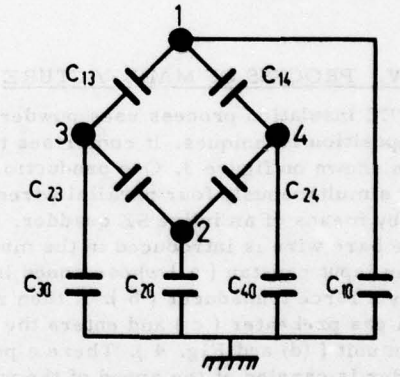


Fig. 9 Direct capacitances in a quad

$$k_1 = C_{14} + C_{23} - (C_{13} + C_{24}) \quad (1)$$

$$e_1 = C_{20} - C_{10} \quad (2)$$

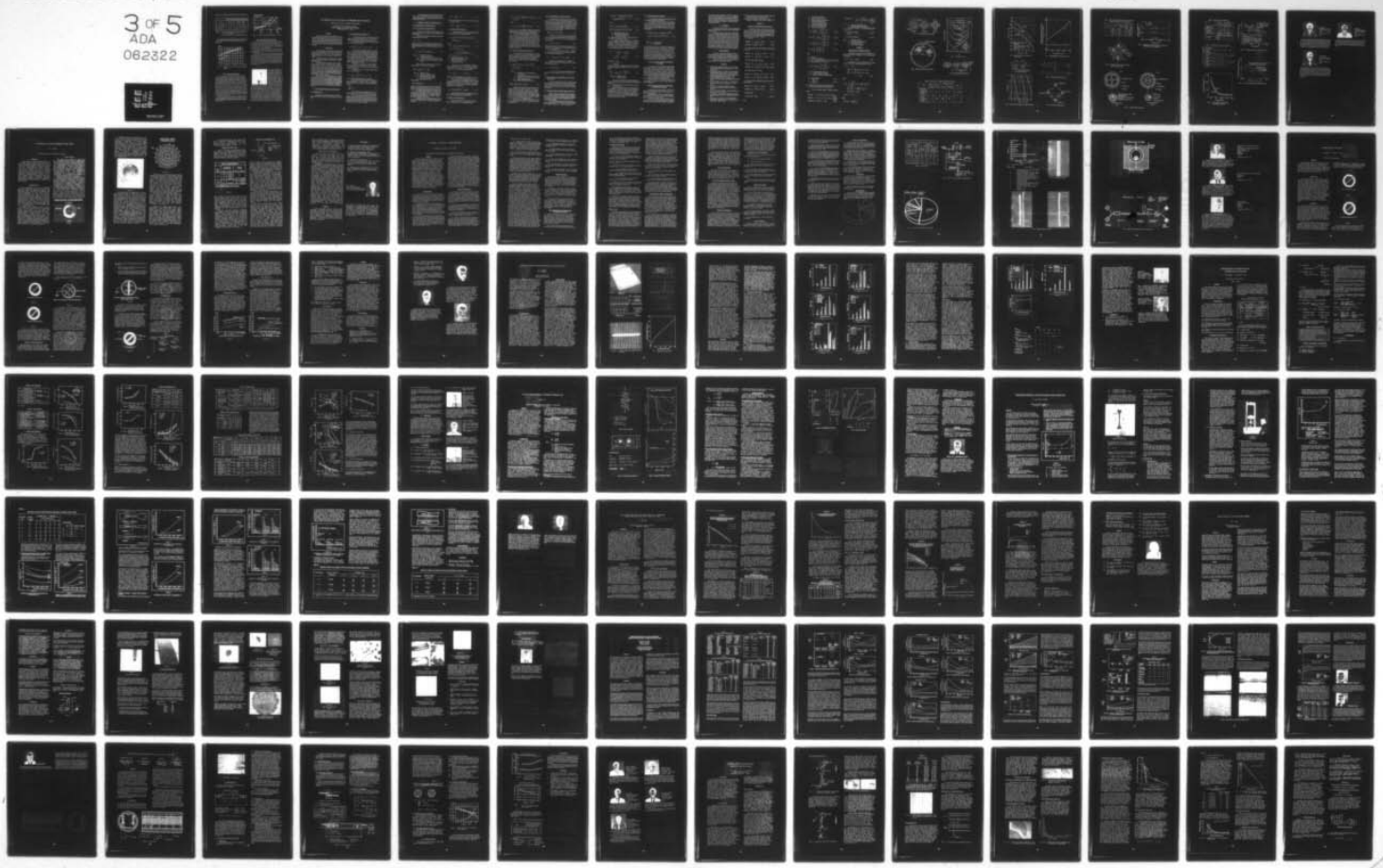
$$e_3 = C_{40} - C_{30} \quad (3)$$

The F test shows that, with a confidence level greater than 0, 998, the dispersion is lower in PEC insulation than in paper insulation as far as capacitance unbalances are concerned. The most remarkable figures concern k_1 . These are the

AD-A062 322 ARMY COMMUNICATIONS RESEARCH AND DEVELOPMENT COMMAND --ETC F/G 13/9
PROCEEDINGS OF THE INTERNATIONAL WIRE AND CABLE SYMPOSIUM (27TH--ETC(U)
NOV 78 E F GODWIN

UNCLASSIFIED NL

3 OF 5
ADA
062322



result of the specific properties mentioned above.

	PEC insulation		Paper insulation	
	m	σ	m	σ
k_1 pF/Km	8, 9	52, 7	12, 6	106
e_1 , e_2 pF/Km	37, 7	198	-8, 8	355
$k_9 \rightarrow k_{12}$ pF/Km	-0, 7	30, 6	0, 4	46, 7
C_n nF/Km	36, 6	0, 71	31, 8	1, 13

Table 1 : Comparison of typical parameters for 0. 6 mm Cu cables.
m = mean value σ = standard deviation

The attenuation obtained with PEC insulation is very similar to that of paper cable as shown in figure 10.

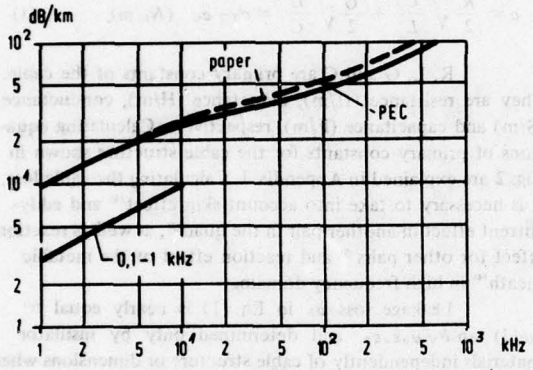


Fig. 10 Attenuation of 0. 6 mm Cu 35 nF/Km cables

VII. WATER BLOCKING

The comparison of the water blocking effect shows that the PEC insulation affords a significantly better protection than the paper insulation. The longitudinal permeability to water has been measured using direct injection of water through the entire surface of the end of the cable. The pressure corresponds to 1 m of water. The migration of water has been monitored by two methods. One of these is time domain reflectometry. The other one consists in pouring water simultaneously into several samples of different length cut into the same cable and to measure the time needed for the water to travel to the free end. Typical results are shown in figure 11.

As soon as the water enters the cable the insulation resistance drops by several orders of magnitude allowing immediate detection and location of the defect.

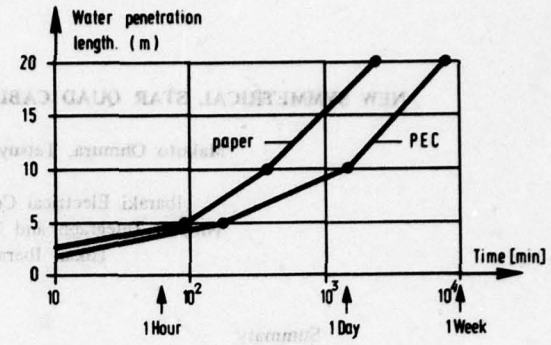


Fig. 11 Water penetration length vs. time

VIII. THE SITUATION TODAY

Since 1973 the Swiss Administration of PTT has closely examined PEC insulated cables. In 1975 a first pilot network has been built at Rovray. It consists of 15 cable lengths whose compositions range between 1 and 100 quads.

Towards the end of 1976 this Administration decided to progressively introduce this cable type in its network.

A first line capable of insulating simultaneously four wires (Fig. 3) of different colours and of assembling them into one quad (SZ system) has been in operation since May 1977. Its performance amounts to 200 m/min. of 35 nF/Km - 0. 4 mm Cu quad. The building of new improved machines is in course. The first will be in operation at the beginning of 1979.



Philippe A. Robert received his Diplôme d'Ingénieur Physicien in 1961 as well as his Ph.D. in 1968 from the Federal Institute of Technology of Lausanne Switzerland, (EPFL). Since 1968, he has been with Les Câbleries et Tréfileries de Cossonay where his research interests lay in specialized electromagnetic measurements and new manufacturing processes. Since 1971 he has been in charge of research and development of PEC insulation. He is the author and co-author of twelve publications, and the inventor and co-inventor of four patents. Dr Robert is a lecturer in Materials Science at the EPFL. He is a member of the Swiss Physical Society and the Swiss Electrotechnical Institution. Mailing address : Câbleries et Tréfileries de Cossonay, CH-1305 Cossonay-Gare, Switzerland.

NEW SYMMETRICAL STAR QUAD CABLE FOR SUBSCRIBER LOOPS AND SERVICES

Makoto Ohmura, Tatsuya Fuchigami, Nobuya Kojima

Ibaraki Electrical Communication Laboratory
Nippon Telegraph and Telephone Public Corporation
Tokai, Ibaraki, 319-11 Japan

Summary

This paper describes technical feasibilities of new symmetrical star quad cable used for subscriber loops, which will meet future digitalization of local networks. Loss minimization design method, required crosstalk characteristics, relation between star quad structure and crosstalk characteristics, and manufactured cable transmission characteristics are stated.

1 Introduction

Outside plant for local network has been originally constructed for telephone service. Recently, demands for digital communication services, such as data and facsimile telecommunications, as well as telephone service, have increased.

Thus, it is necessary to develop a new economical cable with excellent transmission characteristics for digital signal transmission.

In the high frequency domain, such as in digital signal transmission, there is an optimum ratio of distance between wires to conductor radius to minimize symmetrical star quad cable loss. This ratio is fairly large, compared with ordinary telephone cables. Based on these results, it is possible to reduce conductor radius and cable loss. Moreover, if the crosstalk characteristics are improved, economical cable for digital signal transmission, which can accommodate systems using all the pairs, can be realized.

New local cable described in this paper is a symmetrical star quad cable which aims to reduce cable cost and loss by applying loss minimization design method to various different conductor radii, and by insulating conductors thickly by highly expanded polyethylene. By improving crosstalk characteristics, this cable makes it possible for all the pairs to accommodate digital signals transmission systems handling various kinds of services.

2 Designing New Symmetrical Star Quad Cable

2.1 Twisting Structure

This paper describes symmetrical star quad cable, which takes advantage of better spatial efficiency than paired cable.

2.2 Loss Minimization Design Method [1][2]

Loss minimization design is a method which determines wire structure minimizing cable loss, when distance between wires is constant. Figure 1 shows this concept.

Symmetrical star quad cable loss in the high frequency domain is expressed as follows:

$$\alpha = \frac{R}{2}\sqrt{\frac{C}{L}} + \frac{G}{2}\sqrt{\frac{L}{C}} = \alpha_R + \alpha_G \quad (N_p/\mathrm{m}). \tag{1}$$

R, L, G and C are primary constants of the cable. They are resistance (Ω/m), inductance (H/m), conductance (S/m) and capacitance (F/m), respectively. Calculating equations of primary constants for the cable structure shown in Fig. 2 are explained in Appendix 1. Calculating the cable loss, it is necessary to take into account skin effect[3] and eddy-current effect in another pair in the quad[3], as well as reaction effect for other pairs[3] and reaction effect of the metallic sheath[4] in high frequency domain.

Leakage loss α_G in Eq. (1) is nearly equal to $(\omega/2)\tan\delta\sqrt{\mu_0\varepsilon_0\varepsilon_r}$ and determined only by insulator materials independently of cable structure or dimensions when frequency is constant.

Conductor loss α_R can be expressed as the following equation from Appendix 1.

$$\alpha_R = \frac{1}{2d\delta_i\sigma_i}\sqrt{\frac{\varepsilon_0\varepsilon_r}{\mu_0}}\, f_\alpha\left(\frac{d}{r_i},\ C_p,\ r_c,\ r_c',\ R_c\right) \tag{2}$$

f_α is a function of each parameter in the parentheses.

When metallic cable sheath diameter and number of pairs accommodated in the cable are given, wire dimensions minimizing cable loss are obtained by solving the following equations.

$$\frac{\partial \alpha_R}{\partial (d/r_i)} = 0 \tag{3}$$

The numerical results of relations between d/r_i and cable loss are shown in Fig. 3 when frequencies are varied.

Since d/r_i gives minimum cable loss is fairly large, compared with ordinary symmetrical star quad cable, it is advisable to design symmetrical star quad cable on the basis of these results for digital signal transmission. Based on the loss minimization design, low loss and economical symmetrical star quad cable can be brought to realization.

The cable designed on the basis of loss minimization concept is temporarily called LM cable. Effect of this design method applied to existing paper insulated star quad cable is shown in Table 1.

3 Designing on Signal to Crosstalk Power Ratio

3.1 Required Signal to Crosstalk Power Ratio

3.1.1 Noise Power at Pulse Detection Point

Noise power is discussed at a pulse detection point affecting pulse error rate in a model of pulse equalizing section shown in Fig. 4.

The expected value of total Gaussian noise power at detection point σ_G is given by

$$\sigma_G^2 = \sigma_x^2 + \sigma_B^2 \tag{4}$$

where σ_x^2 is the expected crosstalk power value at a pulse detection point and σ_B^2 is the expected thermal noise power value and equalizer noise at a pulse detection point. σ_B^2 is as follows:

$$\sigma_B^2 = \frac{1}{2\pi}\int_0^\infty KTF(\omega)\,|E(\omega)|^2\,d\omega \tag{5}$$

where K : Boltzmann's constant
T : Absolute temperature (°K)
$F(\omega)$: Noise figure for equalizing amplifier circuit
$E(\omega)$: Transfer function for equalizing amplifier circuit.

When the following overall transfer function of rational function is used for wave equalization,[5]

$$W(\omega) = \left(\frac{j\omega}{j\omega+\omega_L}\right)^M \Big/ \left(1+\frac{j\omega}{\omega_H}\right)^N \tag{6}$$

where ω : Angular frequency
M : Order of low frequency cutoff
ω_L : Low angular frequency cutoff
N : Order of low frequency cutoff
ω_H : High frequency cutoff.

$E(\omega)$ is given by

$$E(\omega) = W(\omega)/L(\omega) \tag{7}$$

where $L(\omega)$ is transfer function of cable. Characteristics of signal to thermal noise power ratio $10\log(r_0/\sigma_B)^2$ are shown in Fig. 5. r_0 is equalized pulse amplitude at a detection point.

The required signal to Gaussian noise power ratio $10\log(r_0/\sigma_G)^2$ is 32 dB, as mentioned in 3.1.2. In case of low speed PCM signal transmission σ_B^2 is a negligible order for σ_x^2, and it is possible to take into account only crosstalk noise power as Gaussian noise power.

It is assumed that the probability density function of crosstalk voltage amplitude y is given by the following equations.

$$P(y) = \frac{1}{\sqrt{2\pi}\,\sigma_x} e^{-\frac{y^2}{2\sigma_x^2}} \tag{8}$$

Then, probability density function of crosstalk noise power $|y|^2$ is given as follows:

$$P_{\sigma_x^2}(x) = \frac{1}{\sqrt{2\pi x}\,\sigma_x} e^{-\frac{x}{2\sigma_x^2}}. \tag{9}$$

(1) Far-end crosstalk noise power

The expected value of far-end crosstalk noise power at detection point σ_F^2 is expressed as follows:

$$\sigma_F^2 = \frac{1}{2\pi}\int_0^\infty P(\omega)\,|W(\omega)|^2 n_F k_{xF} (l/l_0)^q (\omega/\omega_0)^2\,d\omega$$
$$= n_F k_{xF} (l/l_0)^q \sigma_{F0}^2 \tag{10}$$

where

$$\sigma_{F0}^2 = \frac{1}{2\pi}\int_0^\infty P(\omega)\,|W(\omega)|^2 (\omega/\omega_0)^2\,d\omega \tag{11}$$

$$P(\omega)^{(6)} = \frac{2m(1-m)}{\tau_0}\,|G(\omega)|^2 \cdot\left\{\frac{1-\cos\omega\tau_0}{1+2(2m-1)\cos\omega_0\tau_0+(2m-1)^2}\right\}$$

$$G(\omega) = \frac{1}{j\omega}(1-e^{-j\pi\omega/\omega_0}) \tag{12}$$

ω_0 : Clock angular frequency ($=2\pi f_0$)
τ_0 : Pulse repetition period ($=1/f_0$)
l : Repeater spacing cable length
n_F : Disturbing pair number.

In Eq. (10), k_{xF} is an antilogarithm of signal to far-end crosstalk power ratio at clock frequency f_0 and cable length l, and q is usually equal to 1. The probability density function of k_{xF}, $P_k(x)$, can be expressed as follows:

$$P_k(x) = \frac{\lambda^\nu}{\Gamma(\nu)} x^{\nu-1}\cdot e^{-\lambda x} \quad (\nu>0,\ \lambda\geqq 0) \tag{13}$$

where $\Gamma(\nu)$ is Gamma function. In Eq. (13), if we put $\nu=1/2$, $\lambda=1/2\sigma_x^2$, $P_k(x)$ is expressed in the same form as Eq. (9).

This equation gives probability density function of antilogarithm of signal to far-end crosstalk power ratio obtained when the induced currents of the disturbed pairs are normally distributed with an average of zero. In this case, the standard deviation for k_{xF} in dB is given by

$$\sigma_{k_{xF}} = 10\log e\cdot\left[\Psi'\left(\frac{1}{2}\right)\right]^{\frac{1}{2}} = 9.65\ \text{dB}. \tag{14}$$

These results mean that the assumption of Eq. (9) is valid, when standard deviation in dB is 9.65 dB.

(2) Near-end crosstalk noise power

The expected value of near-end crosstalk noise power at detection point σ_N^2 is expressed as follows:

$$\sigma_N^2 = \frac{1}{2\pi}\int_0^\infty P(\omega)\left|\frac{W(\omega)}{L(\omega)}\right|^2 n_N k_{x_N}\left(\frac{\omega}{\omega_0}\right)^p d\omega \qquad (15)$$
$$= n_N k_{x_N}\sigma_{N_0}^2$$

where

$$\sigma_{N_0}^2 = \frac{1}{2\pi}\int_0^\infty P(\omega)\left|\frac{W(\omega)}{L(\omega)}\right|^2\left(\frac{\omega}{\omega_0}\right)^p d\omega. \qquad (16)$$

In Eq. (15), k_{xN} is an antilogarithm of signal to near-end crosstalk power ratio at clock frequency f_0. p nearly equals 3/2 in high frequency domain and 2 in low frequency domain.

In case of near-end crosstalk, the phase of the induced currents of the disturbed pairs to the phase of the currents of disturbing pairs distribute uniformly between 0 and 2π. Real part and imaginary part of the induced currents are normally distributed, respectively. This is the case where $\nu = 1$ is put into Eq. (13), and the standard deviation of k_{xN} in dB is 5.56 dB. If we assume that the induced voltage (current) distributes normally like far-end crosstalk, we can estimate the required near-end crosstalk power ratio safer from engineering standpoint.

3.1.2 Error Rate in Bipolar Pulse Transmission

We assumed that crosstalk noise voltage at detection point may be approximated by normal distribution. In bipolar pulse transmission, error probability P_e per repeater spacing, which takes into account crosstalk noise, intersymbol interference and probability of mark for bipolar pulse, is given as follows: [7]

$$P_e = m\Phi\left(\frac{\zeta - r_0 + \Gamma_0}{\sigma_x}\right) + (1-m)\left[\Phi\left(-\frac{\zeta+\Gamma_0}{\sigma_x}\right) + \Phi\left(-\frac{\zeta-\Gamma_0}{\sigma_x}\right)\right] \qquad (17)$$

where

- m : Probability of mark for bipolar pulse
- ζ : Threshold level
- r_0 : Equalized pulse amplitude at detection point
- Γ_0 : Absolute value of worst intersymbol interference at detection point
- $\Phi(\zeta)$: Normal distribution function for ζ

$$\Phi(\zeta) = \frac{1}{\sqrt{2\pi}}\int_{-\infty}^{\zeta}\exp\left(-\frac{1}{2}\eta^2\right)d\eta. \qquad (18)$$

Equalized pulse amplitude at detection point r_0 is obtained from Eq. $r(t)$ shown in Appendix 2. The relation between order of high frequency cutoff N and r_0 is shown in Table 2. The desirable order of high frequency cutoff N is about 15, from the hardware viewpoint. The optimum threshold level exists in the vicinity of $0.5\,r_0$.[8] It is safer to consider Γ_0 as $\Gamma_0 = 0.3r_0$ for engineering the repeater line. m is about 0.5, using scramblers[9] in the transmission line.

Under the above conditions, relations between signal to crosstalk power ratio $10\log(r_0/\sigma_x)^2$ and error rate P_e are shown in Fig. 6.

3.1.3 Required Signal to Crosstalk Power Ratio

Required signal to crosstalk power ratio at detection point $10\log(r_0/\sigma_x)^2$ is 30 dB for allowable error rate 10^{-9} in equalized section and intersymbol interference 30% from Fig. 6. However, in actual subscriber loops, it is necessary to take into account induced noise and impulsive noise as well as crosstalk noise. Then, if we add 2 dB to signal to crosstalk power ratio as the margin, the required signal to crosstalk power ratio at detection point is given as follows:

$$10\log(r_0/\sigma_x)^2 = 30+2 = 32\ \text{dB}. \qquad (19)$$

When there exist simultaneously both far-end crosstalk power and near-end crosstalk power in the transmission line, total crosstalk noise power σ_x^2 for repeater spacing l is given as follows:

$$\sigma_x^2 = n_F k_{xF}\sigma_{F0}^2 + n_N k_{xN}\sigma_{N0}^2. \qquad (20)$$

Since we can obtain σ_x^2 from the required $10\log(r_0/\sigma_x)^2$ for allowable error rate from Fig. 6, we can calculate required k_{xF} and k_{xN} for designated r_0.

In case that near-end crosstalk power is negligible, the required signal to multiple far-end crosstalk power ratio X_{MF} for repeater spacing is given by

$$X_{MF} = 32 - 10\log\left(\frac{r_0}{\sigma_{F0}}\right)^2 = 32-14 = 18\ (\text{dB}). \qquad (21)$$

When far-end crosstalk power is negligible, the required multiple near-end crosstalk power ratio X_{MN} is given by the following equation

$$X_{MN} = 32 - 10\log\left(\frac{r_0}{\sigma_{N0}}\right)^2. \qquad (22)$$

X_{MN} is a function of cable loss. Relations between cable loss at clock frequency f_0 and X_{MF}, X_{MN} are shown in Fig. 7.

3.2 Relation between Star Quad Structure and Crosstalk Characteristics

Excellent crosstalk characteristics are required for the new symmetrical star quad cable to accommodate transmission systems for all pairs. The relation between quad structure and near-end crosstalk characteristics within the quad are described in this section.

3.2.1 Random Variation in Distance between Conductors

Random variation in distance between conductors, due to conductor eccentricity in insulated wire and insulator distortion, causes crosstalk increase within quad. The influence of this random variation on near-end crosstalk power ratio within quad is considered.

In the crosstalk coupling model shown in Fig. 8, near-end crosstalk power ratio $-10\log K_N$, is expressed as follows, when coupling coefficient is $k_c(x)$ at arbitrary position x[10]

$$-10\log K_N = -10\log\left\{\left(\frac{\omega Z_0}{4}\right)^2 \frac{1-e^{-4\alpha l}}{\alpha}\right\} -10\log\left\{\bar{k}_c^2 \Phi\left(\frac{2\omega}{v}\right)\right\} \quad (23)$$

where

$$\Phi\left(\frac{2\omega}{v}\right) = 2\int_0^\infty \varphi(\delta)\cos\frac{2\omega\delta}{v}\,d\delta \quad (24)$$

$$\varphi(\delta) = \frac{1}{\bar{k}_c^2}\lim_{L\to\infty}\frac{1}{2L}\int_{-L}^{L} k_c(x)\,k_c(x+\delta)\,dx \quad (25)$$

$\bar{k}_c^2$: Mean square value of $k_c(x)$
v : Propagation velocity in cable
Z_0 : Characteristic impedance.

It is possible to estimate near-end crosstalk power ratio $-10\log K_N$ by calculating $\bar{k}_c^2$ and $\Phi(2\omega/v)$.

Generally, coupling coefficient $k_c(x)$ consists of capacitive coupling and magnetic coupling. Since the latter is negligible at low frequency, only the capacitive coupling is discussed. Let distance between conductors at x be $d_{12}(x)$, $d_{23}(x)$, $d_{34}(x)$, $d_{41}(x)$, as shown in Fig. 9. Coupling coefficient $k_c(x)$ is approximately given by the following euqation

$$k_c(x) = c\left\{\frac{1}{\log\frac{d_{12}(x)}{r_i}} - \frac{1}{\log\frac{d_{23}(x)}{r_i}} + \frac{1}{\log\frac{d_{34}(x)}{r_i}} - \frac{1}{\log\frac{d_{41}(x)}{r_i}}\right\} \quad (26)$$

where $d_{ij}(x) = d_a(x)$
$(i, j = 1, 2, 3, 4)$
c : constant.

It is assumed that $d_a(x)$ distributes normally along the cable length. Then, probability density function $P(d_a)$ is given as follows:

$$P(d_a) = \frac{1}{\sqrt{2\pi}\,\sigma_{da}}\exp\left\{-\frac{(d_a-\bar{d}_a)^2}{2\sigma_{da}}\right\} \quad (27)$$

where $\bar{d}_a$: Average d_{ij} value
σ_{da} : Standard deviation.

$d_a(x)$ can be estimated by computer simulation, using normal random numbers with average value $\bar{d}_a$ and standard deviation σ_{da}.

Applying this $d_a(x)$ to Eqs. (26) and (25), $\bar{k}_c^2$ and $\Phi(2\omega/v)$ can be estimated.

Based on this procedure, near end crosstalk power ratio dependency on variation of distance between conductors is discussed. Table 3 shows $\bar{k}_c^2$, $\Phi(2\omega/v)$ and $-10\log K_N$ calculated by the procedure mentioned above, when $\bar{d}_a$ is 1.25 mm and σ_{da} is varied. The allowable variation in distance between conductors for required near-end crosstalk power ratio can be estimated from Table 3.

3.2.2 Periodic Wire Structure Variation

Let us discuss the crosstalk characteritics when four conductors are eccentric in the insulator.

It is assumed that the conductors are at distance ξ from the insulator center, and rotate about the center with period p by quad twisting, where the insulator centers always locate at the verteces of the square. As shown in Fig. 10, for this case, distance between adjacent conductors d_{ij} is given by the following:

$$d_{ij}^2 = 4\xi^2\sin\frac{\varphi_i-\varphi_j}{2} + 4\sqrt{2}\,\xi R_i\left\{\cos\left(px+\frac{\varphi_i+\varphi_j}{2}\right) + \sin\left(px+\frac{\varphi_i+\varphi_j}{2}\right)\right\}\sin\frac{\varphi_i-\varphi_j}{2} + 4R_i^2 \quad (28)$$

where R_i : Insulator radius
φ_i, φ_j : Initial phase.

From Eqs. (23), (24), (25), (26) and (28), it is possible to estimate the relation between twisting period p and near-end crosstalk power ratio. Figure 11 shows degradation value of near-end crosstalk power ratio due to p from the near-end crosstalk power ratio for the case of $p = 0.1$ mm and $\xi = 0.01$ mm. When the wire backtwisting rate is 100%, period p becomes equal to quad twisting physical pitch. Therefore, it is advisable to select a shorter quad twisting pitch to improve near-end crosstalk power ratio within quad.

4 New Symmetrical Star Quad Cable Transmission Characteristics

To confirm the loss minimization design method experimentally, cables were manufactured in which the conductor radius was varied from 0.32 mm to 0.65 mm, while distance between wires d remained constant (1.77 mm). Calculated and measured values are shown in Fig. 3. Figure 3 shows that there is an optimum ratio of distance between wires to conductor radius to minimize symmetrical star quad cable loss.

Based on these results, two kinds of cables, A and B shown in Fig. 12 and Table 4, were manufactured.

Measured cable loss, characteristics impedance and crosstalk power ratio results are shown in Table 5, Fig. 13 and Fig. 14, respectively.

5 Application of New Symmetrical Star Quad Cable to Digital Signal Transmission

Summarizing the foregoing studies, a survey is presented of the new symmetrical star quad cable application to digital signal transmission.

Maximum repeater spacing of unit shielded cable A and nonshielded cable B, when accommodating transmission systems for all pairs, are shown in Fig. 15.

For cable A, repeater spacing is determined by only repeater gain. In case of repeater gain 90 dB at f_0 the crosstalk power ratio leaves a margin at less than 20 MHz clock frequency.

For example repeater spacing for 1.5 MHz clock frequency bipolar pulse transmission becomes 6 km. In nonshielded cable B, near-end crosstalk power ratio limits the repeater spacing. The allowable cable loss for the bipolar pulse transmission of 200 kHz clock frequency is 67 dB and repeater spacing is about 7 km.

6 Conclusion

This paper described design concept and engineering method of new symmetrical star quad cable for future digital subscriber loops.

Loss minimization concept was experimentally confirmed, required crosstalk characteristics for allowable error rate were clarified and dependency of near-end crosstalk within quad on variation of distance between conductors and quad twisting pitch was estimated. Furthermore, transmission characteristics of manufactured cable were obtained. Based on these results admissible clock frequency for 6 km repeater spacing is considered to be about 1.5 Mb/s for one way transmission within a shielded unit. For 10 km repeater spacing, the admissible clock frequency is considered to be about 64 Kb/s for two way all circuits accommodation transmission.

Acknowledgement

The authors express their gratitude to Mr. H. Fukutomi, Director of Outside Plant Development Division and Dr. Y. Katoh, Deputy Director of Outside Plant Development Division for providing facilities for the investigation.

Thanks are also due to the personnel of Sumitomo Electric Industries who manufactured the cable.

References

(1) N. Kojima, M. Taguchi, M. Ohmura: New Type Paired Cable for High Speed PCM Transmission, Proc. 20th I.W.C.S., 1971.

(2) N. Kojima, M. Ohmura, T. Fuchigami: On the Optimum Ratio of Distance between Wires to Conductor Radius of Symmetrical Star Quad Cable for Digital Signal Transmission, Electronics Letters, Vol. 14, No. 7, 1978.

(3) H. Kaden: Wirbelströme und Schirmung in der Nachrichtentechnik, Abschnitt E, Springer-Verlag, Berlin, 1959.

(4) M. Sugi: Resistance and Inductance of a Multi-paired Telephone Cable, J.I.E.C.E. of Japan, Vol. 37, No. 2, 1954.

(5) H. Fukinuki, Y. Sato: Wave Equalization in PCM Repeatered Line, Review of the E.C.L., NTT, Vol. 17, 56, 1969.

(6) M. R. Aaron: PCM Transmission in the Exchange Plant, B.S.T.J., Vol. 41, No. 1, 1962.

(7) E. Iwahashi: An Analysis of Error Probabilities in Bipolar Pulse Transmission, J.I.E.C.E. of Japan, Vol. 50, No. 9, 1967.

(8) E. Iwahashi, A. Fuji: Theory of Error Probabilities in Bipolar Pulse Transmission, Electr. Commun. Techn. J., NTT, Vol. 17, No. 4, 1968.

(9) Savage: Some Simple Self-synchronization Digital Data Scramblers, B.S.T.J., Vol. 46, No. 2, 1967.

(10) H. Kaden: Das Nebensrechen in Kabeln bei nichtstationären Vorgängen, A.E.Ü., Band 11, Heft 9, 1957.

Appendix 1

Equations for Primary and Secondary Constants

Calculating the primary constants, it is necessary to take into account (i) skin effect, (ii) proximity effect (eddy-current effect in another pair in the quad), (iii) eddy-current effect in the quad, (iv) reaction effect for other pairs, and (v) reaction effect of the metallic sheath. The following equations are used to calculate R, L, G and C.

(i) Skin effect

$$\text{Resistance} \quad R_i = \frac{1}{\pi r_i^2 \sigma_i} f_i^{(R)} \quad (\Omega/\text{m}) \qquad \text{(A1-1)}$$

$$\text{Inductance} \quad L_i = \frac{\mu_i}{2\pi} \cdot f_i^{(L)} \quad (\text{H/m}) \qquad \text{(A1-2)}$$

(ii) Proximity effect (eddy-current effect in another pair in the quad)

$$\text{Resistance} \quad R_n = \frac{1}{\pi \sigma_i} \cdot \frac{1}{d^2} \cdot f_n^{(R)} \quad (\Omega/\text{m}) \qquad \text{(A1-3)}$$

$$\text{Inductance} \quad L_n = -\frac{\mu_0}{2\pi} \cdot \left(\frac{r_i}{d}\right)^2 \cdot f_n^{(L)} \quad (\text{H/m}) \qquad \text{(A1-4)}$$

(iii) Eddy-current effect in the quad

$$\text{Resistance} \quad R_{ns} = \frac{1}{\pi \sigma_i} \cdot \frac{1}{d^2} \cdot 4 f_n^{(R)} \quad (\Omega/\text{m}) \qquad \text{(A1-5)}$$

$$\text{Inductance} \quad L_{ns} = -\frac{\mu_0}{2\pi} \cdot \left(\frac{r_i}{d}\right)^2 \cdot 4 f_n^{(L)} \quad (\text{H/m}) \qquad \text{(A1-6)}$$

(iv) Reaction effect of other pairs

$$\text{Resistance} \quad R_e = \sum \frac{1}{\pi r_i^2 \sigma_i} \cdot f_n^{(R)} \cdot F_e \quad (\Omega/\text{m}) \qquad \text{(A1-7)}$$

$$\text{Inductance} \quad L_e = \sum \left(-\frac{\mu_0}{2\pi} \cdot f_n^{(L)} \cdot F_e\right) \quad (\text{H/m}) \qquad \text{(A1-8)}$$

(v) Reaction effect of the metallic sheath (in case of thin metallic sheath)

$$\text{Resistance} \quad R_h = \frac{2}{\pi \sigma_i} \cdot \frac{1}{t} \cdot F_h \quad (\Omega/\text{m}) \qquad \text{(A1-9)}$$

$$\text{Inductance} \quad L_h = -\frac{\mu_0}{\pi} \cdot F_h' \quad (\text{H/m}) \qquad \text{(A1-10)}$$

Outer inductance

$$L_a = \frac{\mu_0}{2\pi} \cdot \ln \frac{d}{r_i} \quad (\text{H/m}) \qquad \text{(A1-11)}$$

where

r_i : Wire conductor radius (m)
d : Distance between wires (m)
C_p : Distance between other quads (m)
t : Cable sheath thickness (m)
μ_0 : Free space permeability (H/m)
μ_i : Conductor permeability (H/m)
σ_i : Conductor conductivity (S/m)
Σ : Reaction effects summation

$$f_i^{(R)} = R_e\left\{\frac{1+j}{2\delta_i}\cdot r_i \frac{J_0\left(\frac{1+j}{\delta_i}\cdot r_i\right)}{J_1\left(\frac{1+j}{\delta_i}\cdot r_i\right)}\right\} \quad \text{(A1-12)}$$

$$f_i^{(L)} = R_e\left\{-\frac{\delta_i}{(1+j)r_i}\cdot\frac{J_0\left(\frac{1+j}{\delta_i}\cdot r_i\right)}{J_1\left(\frac{1+j}{\delta_i}\cdot r_i\right)}\right\} \quad \text{(A1-13)}$$

$$f_n^{(R)} = R_e\left\{-\frac{1+j}{\delta_i}\cdot r_i\cdot\frac{J_1\left(\frac{1+j}{\delta_i}\cdot r_i\right)}{J_0\left(\frac{1+j}{\delta_i}\cdot r_i\right)}\right\} \quad \text{(A1-14)}$$

$$f_n^{(L)} = R_e\left\{-\frac{J_2\left(\frac{1+j}{\delta_i}\cdot r_i\right)}{J_0\left(\frac{1+j}{\delta_i}\cdot r_i\right)}\right\} \quad \text{(A1-15)}$$

where

R_e : Real part
δ_i : Conductor skin depth (m)
J_0, J_1, J_2 : Bessel's functions of zero, first and second order
F_e : Reaction coefficient for other pairs

$$F_e = 4m\cdot r_i^2\cdot\left(\frac{d}{2}\right)^2\cdot\left[\frac{C_p^2+\left(\frac{d}{2}\right)^2}{\left\{C_p^2-\left(\frac{d}{2}\right)^2\right\}^3}\right] \quad \text{(A1-16)}$$

m : $m=1$ when other pair is pair type,
$m=2$ when other pair is quad type.
F_h, F_h' : Reaction coefficient of metallic sheath.

$$F_h = \frac{R_c(R_c^2+r_c^2)d^2}{2(R_c^2-r_c^2)^3} \quad \text{(A1-17)}$$

$$F_h' = \frac{R_c^2 d^2}{2(R_c^2-r_c^2)^2} \quad \text{(A1-18)}$$

R_c : Distance from cable center to metallic sheath (m)
r_c : Distance from cable center to pair or quad (m)

From these results, primary constants are given as follow:

Resistance $R = 2(R_i+R_n+R_{ns}+R_e+R_h)$ (Ω/m) (A1-19)

Inductance $L = 2(L_a+L_i+L_n+L_{ns}+L_e+L_h)$ (H/m) (A1-20)

Conductance $G = \omega C\tan\delta$ (S/m) (A1-21)

Capacitance $$C = \frac{\pi\varepsilon_0\varepsilon_r}{\ln\frac{d}{r_i} - 5\left(\frac{r_i}{d}\right)^2 - \Sigma F_e - \frac{(d/R_c)^2}{\{1-(r_c/R_c)^2\}^2}} \quad \text{(A1-22)}$$

ε_0 : Free space permittivity (F/m)
ε_r : Effective dielectric constant ratio

Propagation constant γ and characteristic impedance Z_0 are given by

$$\gamma = \sqrt{(R+j\omega L)(G+j\omega C)} = \alpha+j\beta \quad \text{(A1-23)}$$

$$Z_0 = \sqrt{(R+j\omega L)/(G+j\omega C)} \quad \text{(A1-24)}$$

where γ : Propagation constant
α : Attenuation constant (Np/m)
β : Phase constant (rad/m)
Z_0 : Characteristic impedance

Appendix 2

Equalized Pulse r(t) Calculation Equation [5]

The Laplace transform $S(p)$ of the rectangular transmitted pulse $s(t)$ with an amplitude of 1 and a duty factor of 1/2, is given by

$$S(p) = [1-\exp(-\tau_0 p/2)]/p. \quad \text{(A2-1)}$$

Accordingly, the received equalized pulse $r(t)$ can be obtained by the inverse Laplace transform of $W(p)\cdot S(p)$.

$$\gamma(t) = 0 \quad (t<0)$$
$$= \sum_{k=1}^{M}(-1)^{k-1}\binom{M-1}{k-1}h_k(t) \quad (0<t<\tau_0/2)$$
$$= \sum_{k=1}^{M}(-1)^{k-1}\binom{M-1}{k-1}\{h_k(t)-h_k(t-\tau_0/2)\} \quad (t>\tau_0/2) \quad \text{(A2-2)}$$

where

$$h_k(t) = \frac{\left(-\frac{\omega_L}{\omega_H}\right)^{k-1}}{\left(1-\frac{\omega_L}{\omega_H}\right)^{k+N-1}}\left\{e^{-\omega_L t}\sum_{s=0}^{k-1}\binom{k+N-s-2}{N-1}\cdot\frac{(\omega_L-\omega_H)^s t^s}{s!} - e^{-\omega_H t}\sum_{s=0}^{N-1}\binom{k+N-s-2}{k-1}\cdot\frac{(\omega_H-\omega_L)^s t^s}{s!}\right\} \quad (t>0)$$

$$h_k(t) = 0 \quad (t<0) \quad \text{(A2-3)}$$

where

$$\binom{g}{u} = {}_gC_u = \frac{g!}{u!\,(g-u)!}\cdot$$

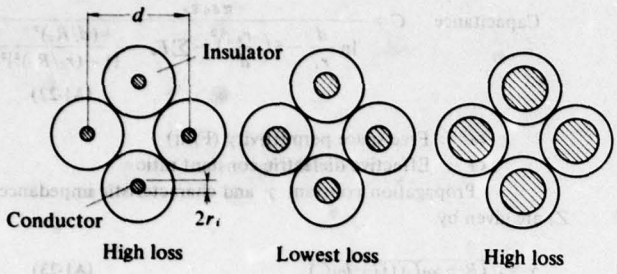


Fig. 1 Loss minimization design concept.

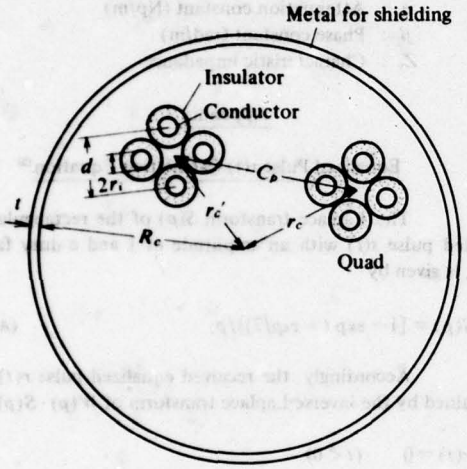


Fig. 2 Symmetrical star quad cable section.

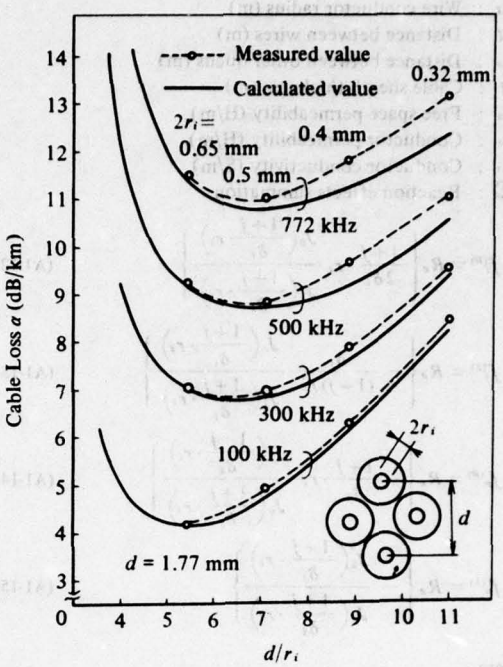


Fig. 3 α dependency on d/r_i.

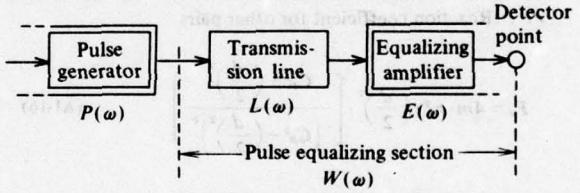


Fig. 4 Pulse equalizing section model.

Table 1. Comparison of Existing Local Cable and LM Cable

Cable	Cable Loss (dB/km)		Characteristic Impedance (Ω)		Note
	1.5 kHz	772 kHz	1.5 kHz	772 kHz	
Local Paper Insulated Cable (Conductor diameter 0.5 mm)	1.8	22.9	611	106	$d = 1.24$ mm, $\epsilon = 1.9$
LM Cable (Conductor diameter 0.4 mm)	1.9	20.4	1030	130	

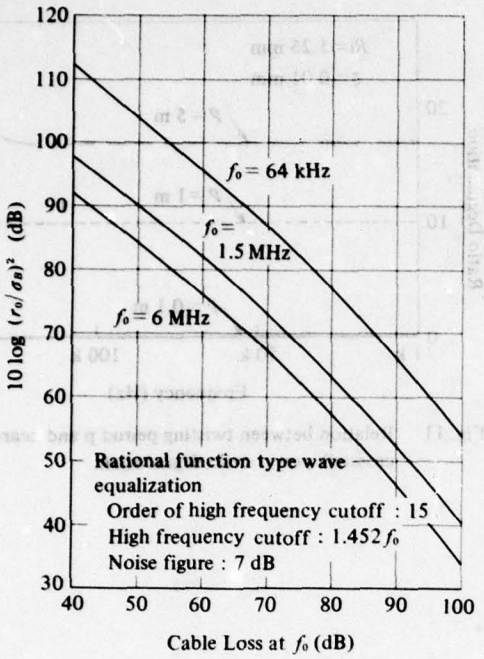


Fig. 5 Signal to thermal noise power ratio characteristics.

Table 2. r_0 due to N

N	r_0	Note
15	0.0443 V	high frequency
20	0.387	cutoff
25	0.348	1.452f_0

N : order of high frequency cut-off
r_0 : equalized pulse amplitude

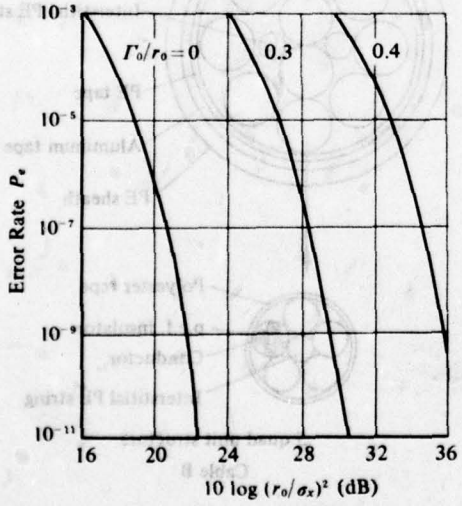


Fig. 6 Error rate due to signal to crosstalk power ratio.

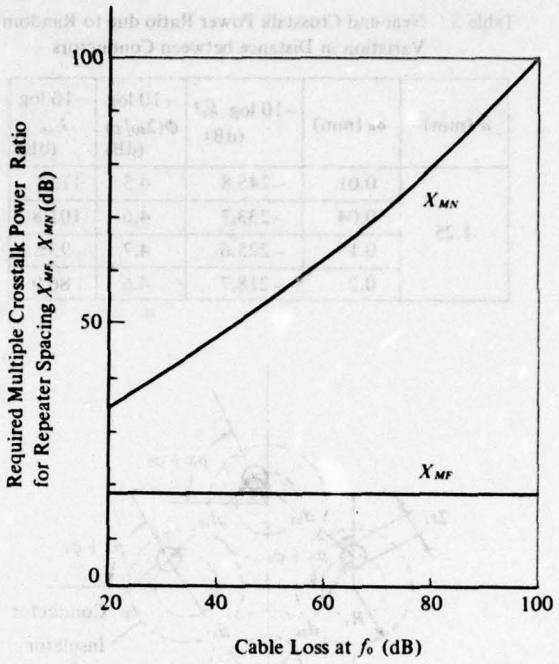


Fig. 7 Required multiple crosstalk power ratio.

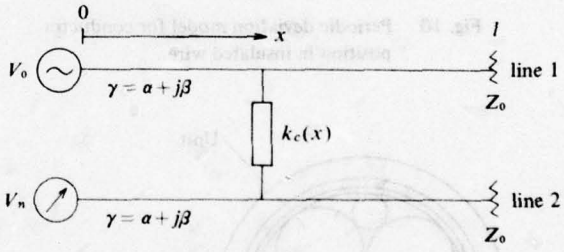


Fig. 8 Near-end crosstalk path model.

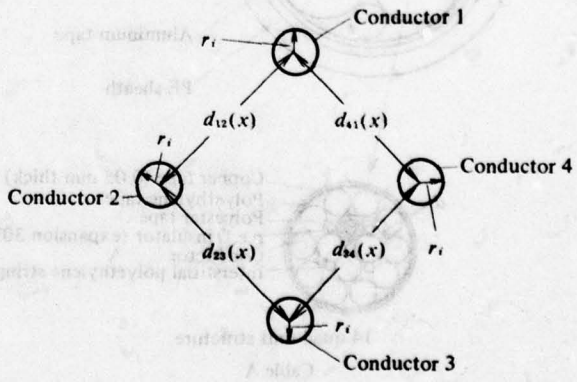


Fig. 9 Star quad structure model.

Table 3. Near-end Crosstalk Power Ratio due to Random Variation in Distance between Conductors

$\bar{d}$ (mm)	σ_d (mm)	$-10 \log \bar{k}_c^2$ (dB)	$-10 \log \Phi(2\omega/v)$ (dB)	$-10 \log k_{xn}$ (dB)
1.25	0.01	−245.8	4.5	113.7
	0.04	−233.7	4.6	101.8
	0.1	−225.6	4.7	93.5
	0.2	−218.7	4.6	86.9

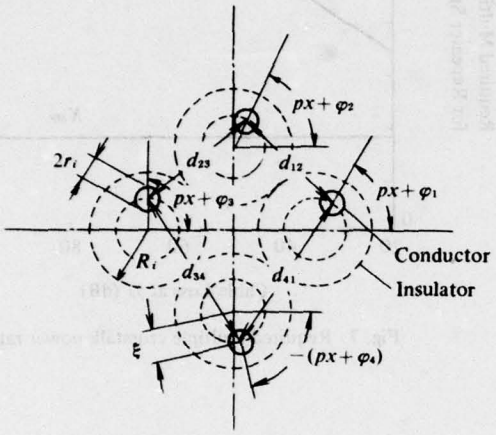


Fig. 10 Periodic deviation model for conductor position in insulated wire.

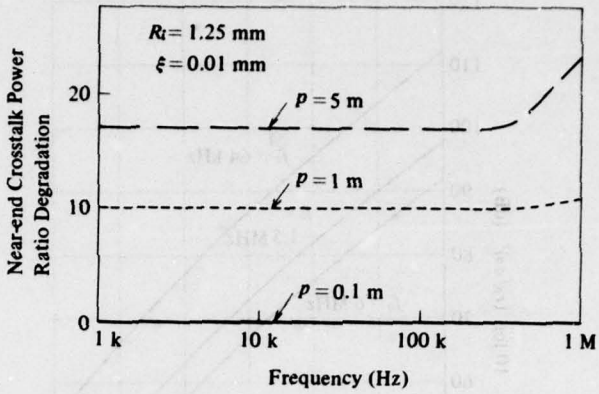
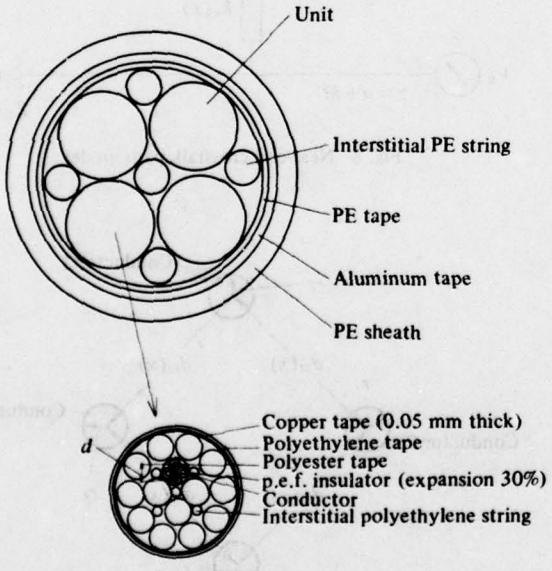
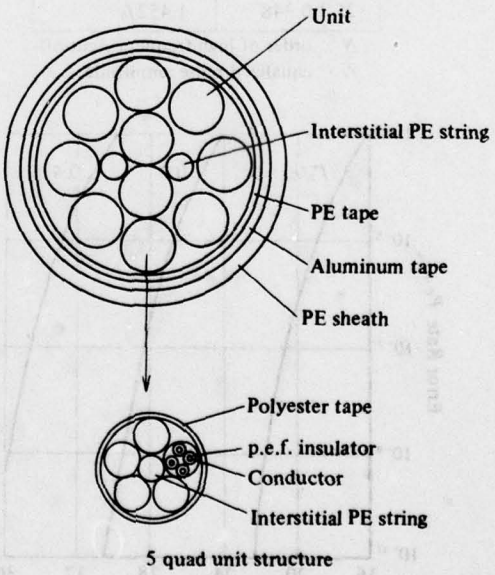


Fig. 11 Relation between twisting peirod p and near-end crosstalk power ratio degradation.



14 quad unit structure

Cable A



5 quad unit structure

Cable B

Fig. 12 Manufactured cable section.

Table 4. Manufactured Cable Structure

	Cable A	Cable B
	$d = 1.77$ mm	$d = 1.13$ mm
Conductor Radius (mm)	0.4	0.4
Free Space Permittivity	1.6	1.6
Number of Pairs	112 (28 pairs/unit)	110 (10 pairs/unit)
Unit Shield	0.05 mm Cu tape	—

Table 5. Manufactured Cable Loss Characteristics

Cable	Frequency (kHz) / Cable Loss (dB/km)	1.5	100	772	1,000	Note
A	Measured value	1.4	5.8	10.8	12.3	$d = 1.77$ mm $\varepsilon_r = 1.9$
	Calculated value	1.4	5.7	10.3	11.6	
B	Measured value	1.8	8.0	16.0	18.2	$d = 1.13$ mm $\varepsilon_r = 1.6$
	Calculated value	1.8	7.5	15.8	17.9	

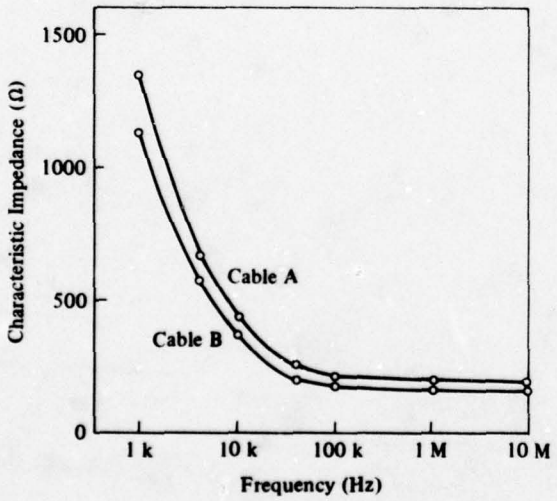
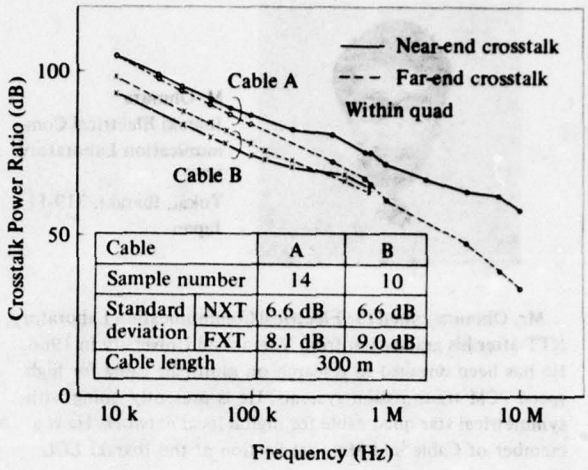


Fig. 13 Manufactured 0.4 mm LM cable characteristics impedance.



Cable		A	B
Sample number		14	10
Standard deviation	NXT	6.6 dB	6.6 dB
	FXT	8.1 dB	9.0 dB
Cable length		300 m	

Fig. 14 Manufactured cable crosstalk characteristic.

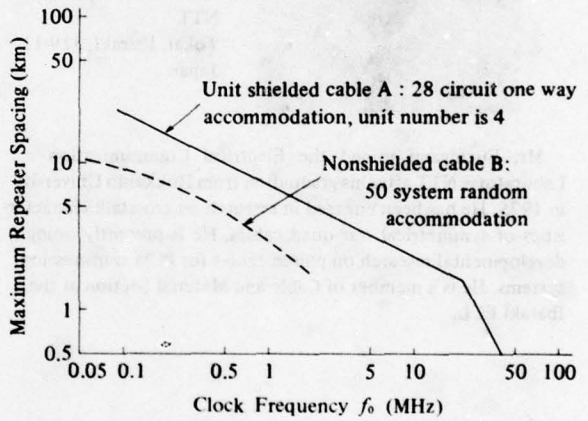


Fig. 15 New cable application to digital transmission.



M. Ohmura
Ibaraki Electrical Communication Laboratory
NTT
Tokai, Ibaraki, 319-11
Japan

Mr. Ohmura joined the Electrical Communication Laboratory, NTT after his graduation from Yamanashi University in 1966. He has been engaged in research on multipair cable for high speed PCM transmission systems. He is presently doing with symmetrical star quad cable for digital local network. He is a member of Cable and Material Section at the Ibaraki ECL.



T. Fuchigami
Ibaraki Electrical Communication Laboratory
NTT
Tokai, Ibaraki, 319-11
Japan

Mr. Fuchigami joined the Electrical Communication Laboratory, NTT after his graduation from Hokkaido University in 1975. He has been engaged in research on crosstalk characteristics of symmetrical star quad cables. He is presently doing developmental research on paired cables for PCM transmission systems. He is a member of Cable and Material Section at the Ibaraki ECL.



N. Kojima
Ibaraki Electrical Communication Laboratory
NTT
Tokai, Ibaraki, 319-11
Japan

Mr. Kojima joined the Electrical Communication Laboratory, NTT after his graduation from Tohoku University in 1959. He is engaged in research on communication cables. He is presently Chief of Cable and Material Section at the Ibaraki ECL.

AN INCREASED PAIR DENSITY UNDERGROUND FEEDER CABLE

T.D. Nantz

Bell Laboratories Norcross, Georgia

Abstract

When conduit runs become congested in a growth area, there may be a need for high pair density cables for feeders (the main subscriber cables leaving the central office). A new 26-gauge cable, DUCTPIC, has been developed to provide 20% increased pair density relative to standard pulp, while maintaining equivalent voice frequency electrical properties. DUCTPIC uses dual expanded plastic insulation. In addition to increased pair density, DUCTPIC affords other advantages such as: color-coding of pairs, improved handling properties, higher dielectric strength, and improved reliability with respect to water entry.

Introduction

The technology of dual expanded plastic insulated conductors (DEPIC) was developed first for waterproof cables and effected major savings of insulation and filling compound. It was next used to develop metropolitan area trunk (MAT) cable producing a 50% saving in copper, increasing by 30% the number of pairs in a sheath, and providing improved T-carrier transmission. Studies of DEPIC being applied to feeder cables did not indicate significant cable material savings, but did show advantages of increased pair density, an opportunity for color coding and other improvements.

Larger pair density cables would defer conduit construction, an expensive outlay of capital. In 1977 the Bell System spent over 300 million dollars to install about 20 thousand miles of ducts. Additionally, some cities are now restricting public utilities to the frequency and hours of duct construction. A new cable, DUCTPIC, uses the DEPIC technology to provide increased pair density relative to standard pulp, and thereby allows the operating telephone companies to defer conduit relief through improved utilization of remaining duct space.

Cable Design

The constraints placed on developing an increased pair density underground feeder cable were that the cable should have the same voice frequency (VF) electrical characteristics as pulp cables, and the insulation should have handling characteristics at least equivalent to pulp. Pulp was used as the baseline since pulp insulation dominates the underground feeder cable market. VF transmission characteristics are controlled by resistance and capacitance. Standard VF cables have an 83 nF/mile capacitance and a resistance proportional to gauge.

The distributions of subscriber loops and congested ducts dictated that a design based on 26-gauge conductors would provide maximum benefits; therefore, the design adopted uses a 26-gauge DEPIC insulated conductor. This insulation consists of an expanded core of plastic material surrounded by a solid skin.[1] DEPIC was selected based on its ability to provide the lower dielectric constant necessary for increased pair density without changing the mutual capacitance, and its overall electrical and mechanical performance.[2] Figure 1 shows a comparison of the DEPIC, solid plastic and pulp insulations for 26-gauge conductors and 83 nF/mile capacitance in an air-core cable design.

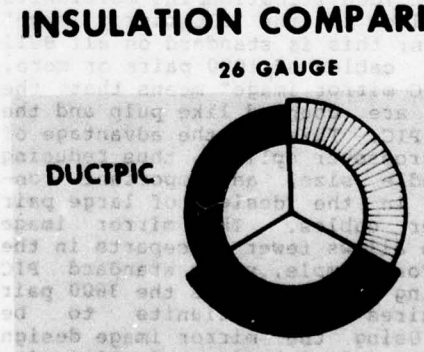


Figure 1

DUCTPIC insulated conductors have an overall diameter over the dielectric (DOD) of 24.5 mils. Extruded over the 15.9 mil, 26-gauge, conductor is a 2.8 mil foamed polyethylene core and a 1.5 mil solid polyethylene skin. The comparable dimensions for DEPIC insulations used in 26 gauge waterproof cable are 4.5 mil foamed core and 2.0 mil skin. Thus the insulation thickness for DUCTPIC is 34% smaller than the insulation for waterproof cable. Figure 2 shows a scanning electron microscope photo of the DUCTPIC insulation and illustrates the dual construction and uniformly sized bubble characteristic of the foamed core.

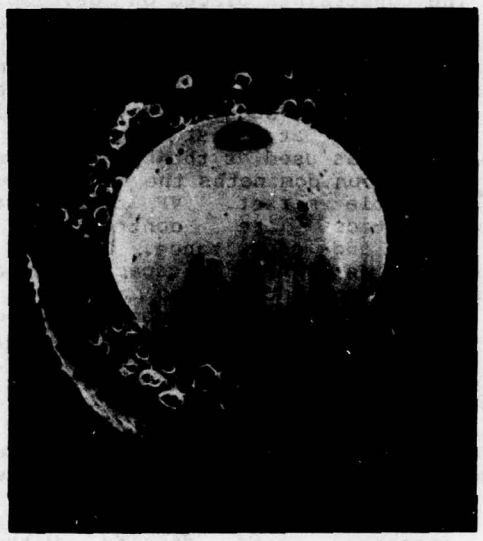


Figure 2

The cable core is composed of 25 pair units and multiunits of 100 pairs (four 25 pair units). Each 25 pair unit has a blue, orange, green, or brown binder to provide unit identification. The multiunits are assembled in the "PIC mirror image" construction; this is standard on all Bell System PIC cables of 1000 pairs or more. Briefly "PIC mirror image" means that the multiunits are counted like pulp and the pairs like PIC. This has the advantage of avoiding crossover splices, thus reducing splice bundle size, an important consideration in the design of large pair count feeder cables. The mirror image design also allows fewer pieceparts in the factory. For example, using standard PIC color coding of multiunits the 3600 pair cable requires 36 multiunits to be stocked. Using the mirror image design requires that only 6 designs of multiunits be stocked. This design still allows any pair in the cable to be uniquely identified, as can be seen from the 3600 pair core construction shown in Figure 3.

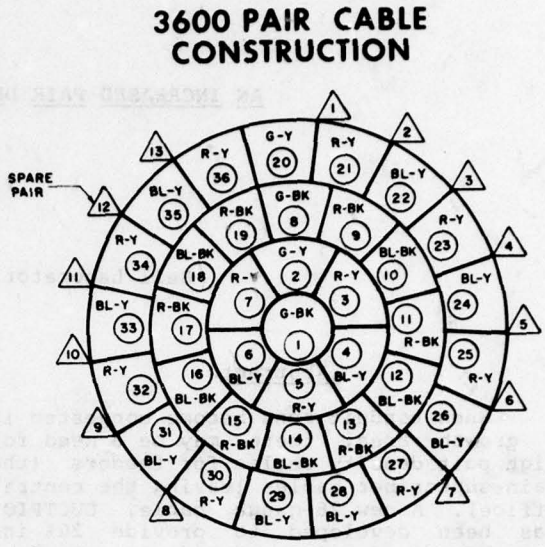


Figure 3

There are two colored plastic binders around each multiunit. One binder defines a multiunit's position within a layer, and the second defines its layer within the cable. The green bound multiunit is the marker in each layer and establishes the starting point for counting in that layer. The green multiunit is flanked on either side by first red multiunits, then blue multiunits, then red, etc. The cable is symmetric about the marker multiunits ; hence, the name "mirror image". The second binder color alternates between yellow and black, starting with yellow for the multiunits in the outermost layer.

The count starts with the center-most marker multiunit. Then with the observer's back to the central office the count proceeds clockwise through that layer's multiunit(s). Counting continues with each layer radially out from the center, starting with the green marker multiunit in that layer and counting clockwise as in Figure 3.

Notice the spare pairs that are positioned in the interstices of the outer multiunits. The need for spare pairs arises because, like pulp-insulated large size cables, there is an economic tradeoff between the manufacturer's cost of guaranteeing the integrity of every conductor and its insulation with the field cost of using and administering spare pairs that replace defective pairs. Each reel with defective pairs has a tag on it to identify the defective pair(s) as to multiunit, unit, and pair. The spare pair colors are unique , avoiding confusion with regular cable pairs.

The requirements on the sheath are that it should be pressurizable and diffusion resistant. Therefore, as with present pulp feeder cables, the time proven stalpeth sheath is used.

Comparison With Pulp

The primary goal in developing DUCTPIC cable is to provide as many pairs as possible for 3-1/2 inch ducts, of which there are many still in place, particularly in central city areas. Table 1 compares the duct compatibility of various sizes of DUCTPIC and pulp cables.

DUCT COMPATIBILITY

Duct Size	DUCTPIC		PULP	
	Dia	Pairs	Dia	Pairs
3.5	2.8	2700		
	2.9	3000		
	3.1	3600	3.0	2700
4.0			3.2	3000
	3.4	4200	3.4	3600

*ALL DIMENSIONS IN INCHES

Table 1

Even though the cable offers about a 20 to 25% increase in pair density over the same diameter pulp cable, the benefit becomes greater when one compares the maximum size pulp and DUCTPIC cables that can be pulled into standard-sized ducts. Because of this "quantization" of conduit sizes, Table I illustrates that DUCTPIC will provide 3600 pairs in the 3-1/2 in. ducts compared to 2700 pulp pairs, a 33% increase.

Because it uses plastic insulated conductors, DUCTPIC has superior handling properties over pulp insulated conductor cables. The conductors can be flexed repeatedly without fear of the insulation unravelling and exposing the conductor. Splicers commonly observe this unraveling of pulp insulation during splice re-entry. To provide a more controlled measure of this characteristic a laboratory experiment was designed where a 25 pair unit of DUCTPIC and a 25 pair unit of pulp were each repeatedly flexed over a 1/2 inch diameter rod as shown in Figure 4.

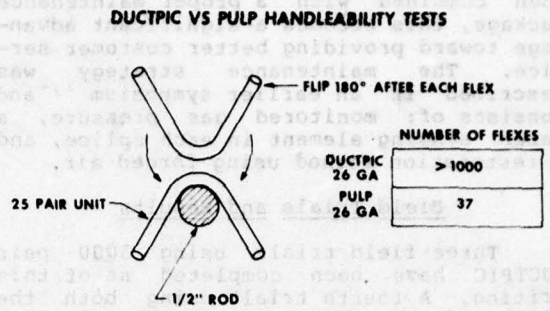


Figure 4

On the average, pulp withstood 37 flexes before copper was exposed, while DUCTPIC exposed no copper after 1000 flexes. This coupled with the fact that the DUCTPIC handling properties are not affected by environmental conditions such as moisture on a splicer's hands means fewer problems in splicing and rearrangements.

DUCTPIC pairs are fully color-coded, which provides advantages of pair identification during clearing, rearrangement, and restoration operations. On the other hand, field and laboratory tests have shown that cable joining rates for PIC color to color splicing are about 40% slower than random splicing pulp. This equates to a wire joining penalty of about nine minutes per 100 pairs joined. Considering the other splicing operations to be constant between the PIC and pulp this penalty means about a 20% increase in time required to splice a 3000 pair DUCTPIC versus the same size pulp.

Dielectric strength measurements on insulated single conductors from pulp and DUCTPIC cables indicate a factor of five increase for DUCTPIC. While lightning and high voltage surges are not considered a problem in the underground, this dielectric strength advantage provides greater margin against damage due to high voltages.

The plastic insulation also offers improved wet circuit reliability. Most DUCTPIC pairs will continue to operate for sometime after the cable is wet. The time to failure is dependent on the insulation condition (number of pinholes) and the connectors used for splicing. The relative insensitivity to water entry was demonstrated by laboratory tests on short lengths of 25 pair units spliced with filled modular connectors which are immersed in water. They show no leakage current for up to eleven hours with 48 volt battery applied. By comparison, leakage current flows immediately when this is done with pulp. Some individuals may consider this insensitivity a disadvantage; they prefer the immediate failure which occurs when pulp gets wet. However,

when combined with a proper maintenance package, this becomes a significant advantage toward providing better customer service. The maintenance strategy was described in an earlier symposium [3,4] and consists of: monitored gas pressure, a water sensing element in each splice, and a restoration method using forced air.

Field Trials and Results

Three field trials using 3000 pair DUCTPIC have been completed as of this writing. A fourth trial using both the 3000 and the 3600 pair designs is underway. The completed field trials have successfully demonstrated the manufacture and installation of over 18000 sheath feet of DUCTPIC cable.

Manufacture of DUCTPIC has presented no fundamantal problems precluding regular commercial manufacture. Installation into ducts and cable racking was satisfactory, as expected from a stalpeth sheathed cable. Generally, the pulling crews felt they could not distinguish between DUCTPIC and pulp. Thirty splices have been made for a total of 180,000 pairs joined. The insulation has performed as predicted by the laboratory handling tests, with fewer insulation defects during splicing than would be expected using pulp cable. Each trial installation resulted in 100% usable pairs, and craft acceptance of the insulation was good. During the DUCTPIC field trials the color code error rate was measured (e.g. splicing blue-white to orange-white). This was done to ascertain whether there were sufficient errors being made to defeat the purpose of color coding the pairs. Errors of this type occurred less than .1% of the time or about 1 per 1000 pairs spliced. The operating companies favor the full color-coding of DUCTPIC pairs even with the possibility for some color splicing errors and the slower wire joining rates. They cite the long-term benefits in clearing troubles, rearrangements, and restorations as reasons for desiring fully color-coded pairs.

Summary

A new, 26-gauge, feeder cable which provides a 20% pair density increase over standard pulp cables has been developed. The design allows up to 3600 pair for 3-1/2 inch ducts and 4200 for 4 inch ducts with standard VF electrical properties. Field trials indicate excellent craft acceptance of the color coding and improved handling properties.

References

1. Mitchell,D.M.,Webster,G.H.,"Material Savings By Design in Exchange and Trunk Telephone Cable," Proc. 23rd, International Wire and Cable Symposium.

2. Baxter,G.D.,Farago,M.,and Gouldson,E.J.,"FOAM-SKIN, A Composite Expanded Insulation for Use in Telephone Cables," Proc. 21st,International Wire and Cable Symposium.

3. DeVeau,G.F.and Dykes,J.D., "Polybutylene Jacketed Air- Core PIC Cable for Use in Steam Exposed Ducts," Proc. 23rd International Wire and Cable Symposium.

4. Hardwick,N.E.,"Restoration of Wet PIC Cable Using Vaporization Drying," Proc. 23rd, International Wire and Cable Symposium.

T.D. Nantz
Bell Laboratories
2000 Northeast Expressway
Norcorss, Georgia 30071



T.D. Nantz recieved the BSEE from the University of Pennsylvania in 1968, and the MSEE form Northeastern in 1973. He is currently a Member of Technical Staff at Bell Laboratories engaged in development of large PIC cables for the underground. Tim is also working on techniques for characterizing multipair cables installed in the field.

PeTAP CABLE - A NEW CONCEPT IN BURIED CABLE DESIGN

D R Bissell, D Chadwick and D C Smith

British Post Office and BICC Telecommunications Cables Ltd

SUMMARY

Cables directly buried in the ground are frequently given protection against damage by the application of steel wire armouring during manufacture. This armouring is expensive and represents a large proportion of the cable cost. A new cable design known as PeTAP - Polyethylene Twin Cable with Annular Protection - offers a similar degree of protection but at a reduced cost. The configuration of the cable design is similar in cross section to a cable in a small duct, and relies on the loose tube to act as an energy absorption medium against impacting or other forces. The main problems of manufacturing this cable with a loose tube have been identified and practical solutions have been obtained. Current production techniques are discussed and the method of manufacture detailed. The design concept of PeTAP allows flexibility in the choice of dimensions, materials and manufacturing techniques to suit any particular application. Thus the principle of PeTAP could be extended to other types of cable and might be used to advantage with small bore coaxial and optical fibre cables.

INTRODUCTION

The British Post Office uses armoured cable, particularly for directly buried cable installation. Most applications are underground feeds from secondary distribution points to customers, particularly on new housing estates. Experience in the UK has shown that unarmoured cables are unsatisfactory for this purpose.

The conventional form of armouring utilises small diameter steel wires helically wrapped around the sheathed cable core. The selection of this type of armouring was a natural choice dictated by the historical method of manufacturing cables, which itself has been based on traditional rope making equipment, and the manufacturing limitations on the application of steel tape armouring to small diameter cables.

Steel wire armouring (SWA) is a satisfactory form of protection on cables and provides an effective guard against most of the hazardous conditions found in this type of installation. However such armouring is expensive relative to the cost of the cable so much so that in some instances, particularly on the smaller sizes, it represents a greater cost than the cable itself.

Early in the 1960's some effort was made by the BPO and the cable manufacturers to breakaway from the SWA concept and various types of alternative armourings were produced. These alternatives all used steel reinforcing in one form or another but none had the general acceptance of steel wire armour. Further work on the problem produced alternatives to steel using various forms of plastic protection, such as thicker sheaths, compound sheaths of different materials, and the use of small bore polyethylene duct into which the cable was inserted prior to installation in the ground. Impact tests-performed using an "Impact Tester" described later - showed that small bore polyethylene duct gave a consistently high degree of protection compared with other forms of armouring. Based on this evidence development work was put in hand to exploit the concept of a loose tube form of armouring and the British Cable Industry undertook to produce a cable meeting these requirements. The success of their efforts is described later in the paper. The final product of this development has now been adopted by the Post Office and is known as cable Polyethylene Twin with Annular Protection or PeTAP for short.

DESIGN CONSIDERATIONS

A statistical survey of the types of damage to directly buried cables on housing estates in the UK was conducted in 1968 and analysed about 250 cases of damage. The results of this survey are shown in the pie diagram (Fig 1) and indicate that the largest proportion of damage to cables can be attributed to hand digging tools. On this evidence the design parameters of protected cable were chosen.

It is virtually impossible to provide protection against damage by mechanical plant at an economical cost, and it was decided at an early stage in the development not to include this as a primary design objective.

There are three possible types of load application to be considered for directly buried cable:- crushing, impact and tensile.

(i) Crushing would normally be caused by pressure from the surrounding earth exerting a force on the cable and can be intensified by additional surface pressure from passing vehicles. Crushing loads are not normally severe unless there are irregularities in the ground, such as sharp stones adjacent to the cable. (Crushing

accounts for 11% of damage cases.)

(ii) Impact loads are generally caused by physical disturbance of the soil by digging implements such as spades, forks, pick-axes, fencing spikes etc. This type of loading is severe and punishing as the implements are sharp and their loading is impulsive generating very high impact forces. (Accounts for 73% of damage cases.)

(iii) Tensile forces are applied during the installation of the cable in the ground or by the occurrence of voids in the ground after laying the cable.

Having established the most likely causes of damage to buried cable it was necessary, before a suitable design of cable could be finalised, to establish a testing procedure which would effectively rank the various alternatives of protection available and provide a standard piece of test equipment for future comparative studies. It will be appreciated that there are many variations of load application and ground conditions to be considered and that no single test can take into account all the pertinent factors.

By referring to the pie diagram (Fig 1) it was decided that impact damage was the major problem area to be considered and therefore a test based on impact performance was devised. Subsequently an impact tester was designed and developed which closely reproduced the types of impact damage experienced under field conditions. (Fig 2.)

The basic element of the impact tester is a pneumatically operated impact cylinder which releases an impulsive force when activated by a push button control. The value of the impulse force is dependent on the pressure of the air supply and the distance through which the impacting ram acts. Pressure is controlled by a regulator valve built into the pneumatic circuit and the distance of travel by adjustment of the height of the cylinder above the sample on test. A variety of impacting heads can be attached to the ram of the cylinder and these simulate the action of a spade, spike or sharp stone. An ionisation tester is connected between the conductors of the sample on test and the bed of the machine. The voltage is set to 2 kV and the tester gives an audible warning when the impacting head breaks through the sheath of the cable into the conductors. This arrangement is employed because visual inspection of damage is not always conclusive and this technique ensures that results are consistent. A compilation of test results, using this equipment, is shown in Fig 3 and indicates that the loose tube cable design (No. 8) offers very good protection against spade damage and compares favourably with steel wire armour protection (No. 9). Other types of protection are shown for comparison and illustrate the various types of protection that have been investigated. The degree of protection has been graded on the diagram as sufficient or insufficient and is directly compared to SWA protection at which the dividing line has been drawn. The loose tube concept for a cable design looked very attractive and a decision was made to design and manufacture a cable meeting this design principle. In preparing this design the following assumptions were made:-

(1) Polyethylene behaves as conventional engineering material and exhibits a Hooke's law characteristic.

(2) Impact damage is the prime cause of cable failure, and in particular spade damage is the most common.

(3) It is considered that in practice spades are not sharp enough to cause pure shear conditions.

(4) The annular protection tube of PeTAP will have constant wall thickness and be circular in section.

(5) Existing steel wire armour constructions give adequate protection against most types of damage.

(6) A cable is considered to fail the impact test when the ionisation tester sounds an audible warning.

PRACTICAL DESIGNS

The current range of PeTAP sizes available for the BPO use is shown in Table 1. The physical dimensions of these have been established on an empirical basis and are the result of comparison tests on the Impact Tester. The degree of protection offered is similar to that of similar size SWA cables but the cost of the items is significantly lower.

Calibration of the Impact Tester was established by comparing the extent of damage caused by the spade attachment with actual spade damage and relating this to samples of cable damaged under field conditions. The calibration sample is shown in Fig 4 and typical damage to cables under test in Fig 5.

It follows from the above that any combination of cable core, tube diameter, tube wall thickness and various materials can be tested in this manner, and by the choice of a suitable calibration sample a whole variety of conditions can be considered. Thus it becomes possible to develop PeTAP designs to suit any particular requirement.

MAJOR PROBLEMS FOR THE MANUFACTURER AND POSSIBLE SOLUTIONS

A choice was made very early in the development stage to use sheathing grade polyethylene (BPO Specification M 132) for the loose tube material. This choice was made to ensure reproducible quality of the tube during the manufacturing development programme, although it was recognised that other materials may ultimately offer a better solution.

The loose tube design poses problems for the cable manufacturer and the two principle difficulties

are (1) the specified 'no adhesion' requirement between the cable sheath and tube and (2) the shape of the tube. These problems and some possible solutions are discussed below.

No Adhesion Requirement

Material to Specification M 132 is also the sheathing material used on the cable core, and since polyethylene is a thermoplastic material there is an obvious prospect of adhesion when extruding the tube over the cable. Two possible solutions to this problem are:-

(1) maintain physical separation between the cable and the tube until the tube has cooled sufficiently to avoid adhesion.

and (2) apply an insulating medium between the cable and the tube.

Solution (1) could be accomplished by way of example, by any of the following means -

(a) an extended core point from the extruder crosshead, possibly water cooled.

(b) separate tube, just bigger than the cable, passing through the crosshead and extending into the cooling section.

(c) long flexible tubular membrane attached to the end of the core point.

Solution (2) could be accomplished by applying either loose material such as talc or grease or a tape such as paper or cotton etc.

All other problems being equal solution (1) would be preferred, as no material is consumed which is superfluous to the function of the cable design. However, there are difficulties in either designing, aligning or starting-up the process with this configuration.

Solution (2) is easier to apply in practice and is a current preferred method of manufacture. Loose material proved difficult to apply consistently and it could be accidentally removed from small areas of the tube by contact with the tooling particularly if the cable tension varied. Utilisation of a paper tape formed as a tube around the cable completely eliminates the adhesion problem and has the virtues of cheapness and availability.

Shape of Tube

In normal tube manufacture it can be difficult to control the shape of the tube during extrusion owing to its weak mechanical strength in the hot condition (extrusion temperature about 200°C). Its own weight can cause sag which results in ovality and variation of wall thickness. The problems of shape control, however, are not too onerous in the PeTAP design because the specified tolerances on the tube allow a reasonable degree of latitude. No joint boxes or fittings are applied to the tube in the field and hence the tolerances on both ovality and wall thickness variation can be much more relaxed compared with, say, water pipe manufacture. Nevertheless the configuration of PeTAP does worsen the likelihood of ovality in the tube and steps have to be taken to control the condition. A water trough is commonly used in cable manufacture as the cooling medium and is applied immediately after the point of extrusion, and as the effective density of the PeTAP tube plus cable core is less than 1.0 it will tend to float. The whole of the tube must be cooled equally otherwise differential cooling will occur which will cause distortion of the tube. Thus the cable must be kept under water and the situation shown in Fig 6 results.

There is an upward force due to buoyancy and a downward force due to the weight of the cable which are acting together to produce ovality. For this reason aluminium cable will generally process better than an equivalent copper cable.

Without the use of a liner it is essential to carefully control the shape of the tube during the initial cool down period. Techniques commonly employed to do this are -

(a) an extended water cooled mandrel from the crosshead

(b) sizing plates with the PeTAP tube pressurised with air from the inside

(c) vacuum forming of the PeTAP tube at the crosshead associated with effective cooling.

The main problem with these systems, besides the added complexity, is the severe restriction on line speed which would generally be limited to about half the normal manufacturing speeds. It should also be noted that both adhesion and shape control problems generally increase with tube size. The alternative is to use a liner with sufficient rigidity to resist the distorting forces.

AN ESTABLISHED METHOD OF MANUFACTURE

One proven way of manufacturing PeTAP cable efficiently was developed by BICC Telecommunication Cables Ltd (see British Patent Application 6220/75). The process uses a paper liner to avoid adhesion problems and to provide a base on which to extrude the tube. This method reduces the capital outlay and enables fairly conventional cable technology to be used. The process utilises a standard sheathing line with some additional plant for the PeTAP process. A schematic diagram of the process is shown in Fig 7 and the additional plant is marked thus*. A description of the process follows.

The stranded cable is sheathed at a previous operation and is supplied to the PeTAP process in long lengths on steel or wooden drums. The drums are loaded into conventional input stands (1) and the inner ends are prepared for changeover. A dual pad pay-off system (2) supplies the paper to a forming system (3) which forms the tape into a tube around the cable. The overlap is glued using propriety equipment (4). The sealed paper tube containing the cable is presented to a conventional

sheathing extruder (5) and the extrusion is made using vacuum techniques. The tubed cable passes into the standard water trough, the first section of which contains a few simple forming dies (6) to help control the shape during the critical initial cool down period. The remainder of the trough has bars spaced at 1-metre intervals to maintain the cable under water. The tubed cable is hauled off by caterpillar (7) and taken up on a dual stand (8).

It will be evident that the whole process is arranged for continuous running. The input cables are easy to changeover due to the relatively large clearance between the cable diameter and the tooling. The PeTAP cables are changed over onto the take up drums in the conventional way. The paper pads can be changed over using an instantaneous jointer (9) and a special high temperature pressure sensitive adhesive tape. The joint produced is hardly perceptible through the natural polyethylene tube.

PLANT CONSIDERATIONS

Two points to note are (1) the extruder output needs to be fairly high (min 250 kg/hr) to achieve reasonable line speeds and (2) adequate cooling capacity must be available in the trough. Unlike normal sheathing there is very little heat sink from the cable itself and hence most of the heat has to flow outwards into the water.

TYPES AND CHARACTERISTICS OF LINER

During the development phase polyethylene coated paper was used and the overlap was heat sealed. This worked quite well but there is a major difficulty in jointing the pads together and reliability problems arose due to the quality of the thin polyethylene coating. It does, however, give a good shape particularly in the overlap area. Mainly because of the jointing difficulty effort was directed to enable the use of plain paper. Initially this did not give such a good shape but significant although small changes in the tooling restored the position. The standard 175 µm high extension belting paper is now used on all sizes manufactured. This paper is used mainly because it is convenient, being used in large quantities for belting cables. It is recognised that perhaps its characteristics are not ideal for the PeTAP process. The high extendible feature is not required and a stiffer side wall property would be more beneficial to the process.

PRODUCTION EXPERIENCE

The process has proved to be very reliable and efficient and has been well accepted by the operatives. Many millions of metres have been manufactured at line speeds within the range 20 to 50 metres/min depending on tube size. Non-stop runs in excess of 24 hours are achieved frequently with finished lengths in the range 500 to 2000 metres. There is an interesting point to note concerning lengths. Normally a length clock is provided immediately prior to the caterpillar, but if this is used it will measure the tube length but not the cable length which will be somewhat shorter unless an input caterpillar is used (not common). This is a fundamental problem which is related to the drum dimensions and the difference in the positions of the centre-line of the cable and the tube. For this reason a measuring clock (10 in Fig 7) is provided at the input end to monitor the cable length and the normal clock is ignored. Alternatively pre-marked input cables could be used but this is not so convenient or secure.

ADVANTAGES OF PeTAP MANUFACTURE

The advantages to the cable manufacturer over the rival SWA system are:

(a) significant raw material savings

(b) one process stage less

(c) capable of greater productivity at the sheathing stage alone (due to continuous run feature)

(d) providing a suitable sheathing line is available, less capital and maintenance costs and more efficient use of floor space.

The only disadvantage is the larger drum size necessary to accommodate the greater overall diameter.

The above features combine to produce a product which is significantly cheaper than an SWA cable.

FURTHER DEVELOPMENTS

PeTAP is a new product and as such it may be capable of improvement with further development. Some possibilities in this area are as follows:-

(a) a more cost effective system could result from an examination of the relationships between basic material costs/dimensions/mechanical properties of such materials as (1) other low density polyethylene compounds including regranulated or waste materials (2) medium or high density polyethylene compounds (3) polypropylene (4) PVC (5) filled materials (6) irradiated materials etc.

(b) the basic construction of the tube could be changed to a corrugated form which generally would be more flexible and use less material for a given strength.

(c) the cable sheath and the tube could be extruded in tandem and hence eliminate a further stage of production although the continuous run feature may be lost.

(d) the paper liner could be modified or eliminated.

FIELD EXPERIENCE

Present specifications for PeTAP cover the range of 2/0.5 mm up to 100/0.5 mm cable and is based on the outside diameter of the cable. The

air space dimension between the tube and the cable and the wall thickness has been selected to provide good mechanical protection.

The majority of uses for this cable in the UK occur on housing estate work but the design is suitable for cable in other situations where conventional SWA cable is used.

So far the cable performance, from a protection aspect, has proved satisfactory and has compared favourably with its SWA counterpart. However the change of type has produced some differences and problems and these relate mainly to handling. The major drawbacks are listed as follows:-

(i) the cable is more bulky (though lighter) and needs larger drums for the same pair size and sheath length. This can cause problems in larger cable sizes since some existing facilities only cater for the smaller drums.

(ii) the cable is more springy than SWA and tends to restore to its coiled shape when laid in trenches or on the ground. Particularly when pulled off over the flange of the drum instead of uncoiling from the barrel drum as normal. SWA cable is of course comparatively dead when laid in the same manner.

These problems have required slight changes in works practices and are not causing any serious disturbance.

The cable can be used successfully for mole-ploughing operations and a number of installations have been completed without problems. Jointing of *PeTAP cable is similar to normal* unarmoured cable except that the outer tube must be removed. This is readily done by methods adopted for the removal of polyethylene cable sheaths and is much easier than the task of removing SWA.

Where the cable is used to lead into dwellings or other structures it is usual to seal the tube to prevent the passage of gas or water along the tube into the structure.

SCOPE FOR FURTHER WORK

The developments reported in this paper are based largely on an empirical design approach and have shown that the loose tube design can effectively reduce cable costs without sacrificing any loss in protection performance.

Further work can be envisaged to establish a more complete theoretical analysis of the subject, particularly as regards the understanding of impact loads on plastic materials. Some work has already been done using the "Thin Ring Theory" as a basis, and it is hoped to develop this to enable predictions of cable performance to be allied to physical dimensions and materials.

The application of loose tube protection to other types of cable core - coaxial optical fibre etc - is possible and to be expected as the need arises in due course.

In the present design of PeTAP normal sheath material has been specified but future developments could aim to use other thermoplastics, either to produce cheaper or more robust designs (or a combination thereof).

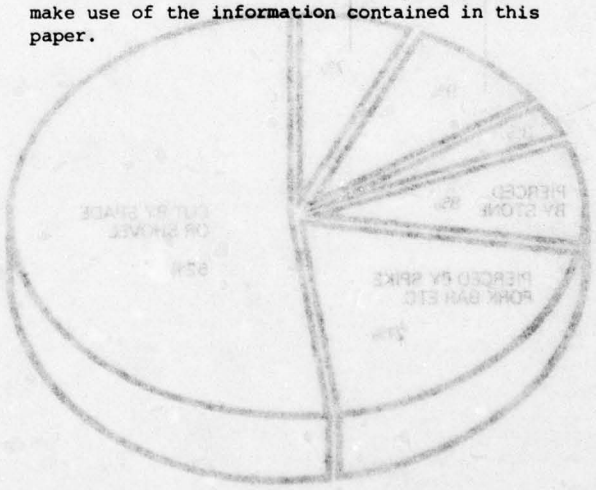
CONCLUSIONS

A new concept in armouring of cable has been described and the considerations leading to its adoption have been discussed. The choice of a practical design with a method of providing a comparative test procedure has been indicated and the method of manufacture with its salient problems and solutions have been outlined.

Practical experience in the field has been itemised and the scope for further development work identified.

ACKNOWLEDGEMENT

The authors wish to express their thanks to the Senior Director of Planning and Provisioning of the Post Office and to the Directors of BICC Telecommunication Cables Ltd for permission to make use of the information contained in this paper.



1	2	3	4	5
Specified Cable Diameter Maximum (mm)	Equivalent cable size 0.5 mm Cond	Annular Protection (mm)		
		Outside diameter	Wall thickness	Outside diameter variation
Inclusive range	Max	Min	Min	Max
- 6.5	2 Pair	18.0	1.7	5.0
6.6 9.5	10 Pair	22.0	2.0	5.0
9.6 16.5	50 Pair	30.0	2.8	5.0
16.6 28.0	100 Pair	44.0	4.1	5.0

TABLE 1 PeTAP Range

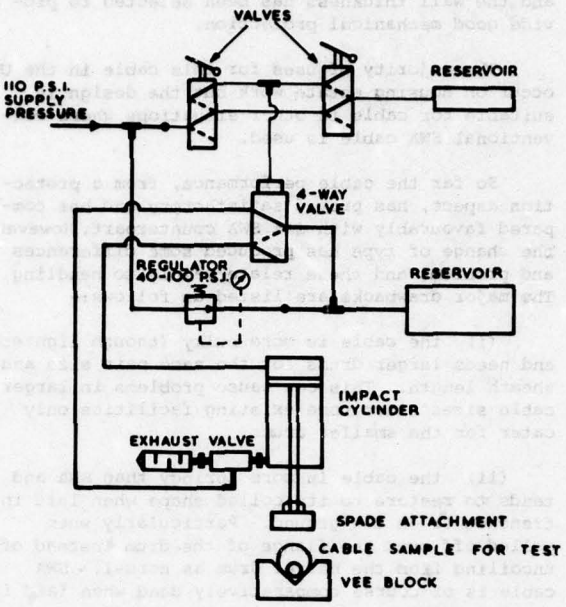


Fig 2 Impact testing machine (diagramatic)

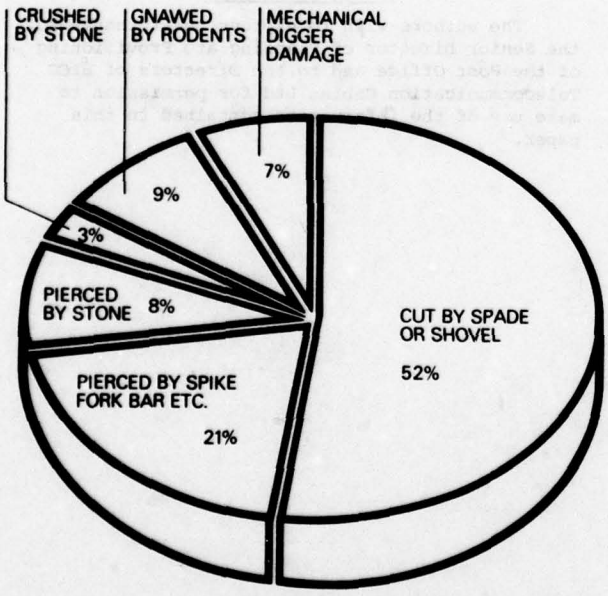


Fig 1 Damage to directly buried cables

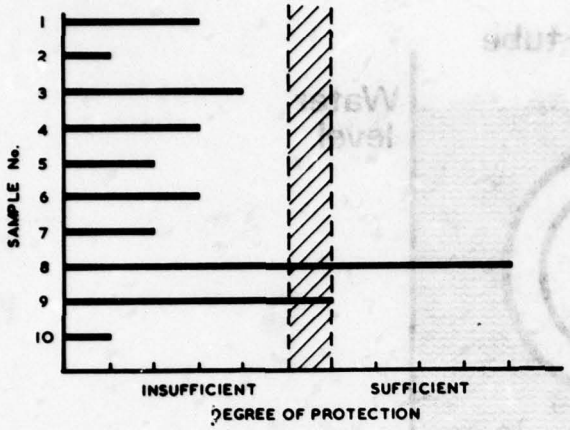


Fig 3 Impact test results

Sample number	Description
1	Ethylene propylene copolymer outer, polyethylene inner
2	Ethylene propylene copolymer sheath
3	Ethylene propylene copolymer outer, cellular polyethylene inner
4	Polyethylene outer, corrugated steel tape inter, polyethylene inner
5	Double thickness ethylene propylene copolymer sheath
6	Polyester sheath
7	Double thickness polyethylene sheath
8	Polyethylene small bore duct with standard cable inside
9	Steel wire armour over standard cable
10	Standard cable

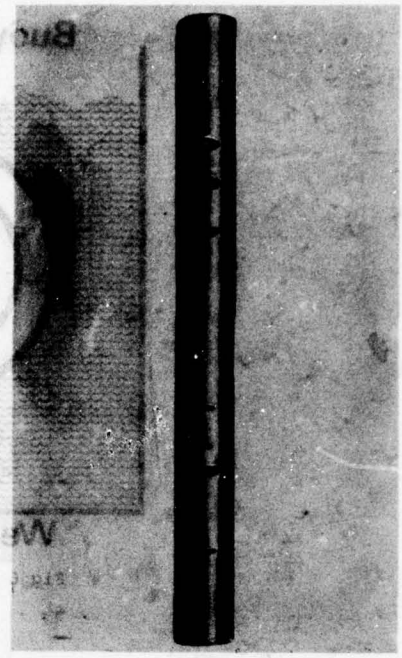


Fig 4 Calibration sample

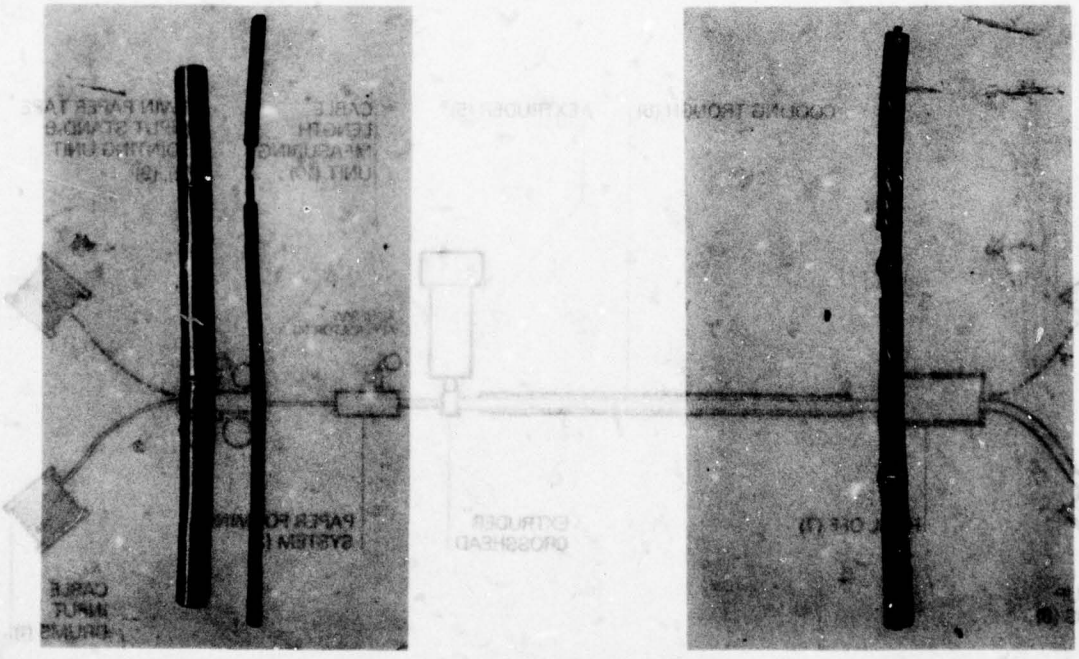


Fig 5 Typical impact results

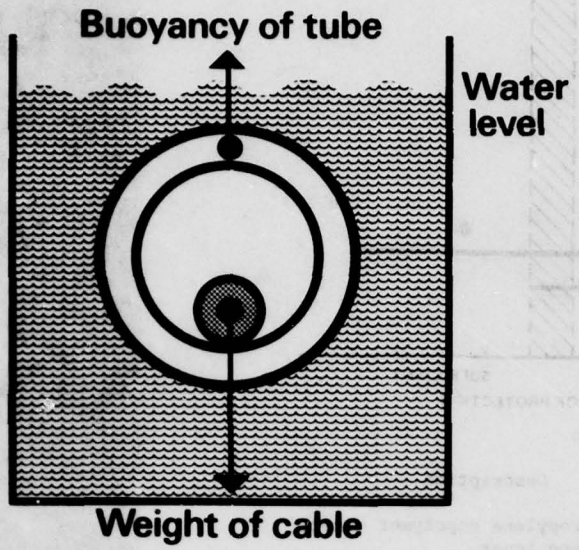


Fig 6 Cooling conditions

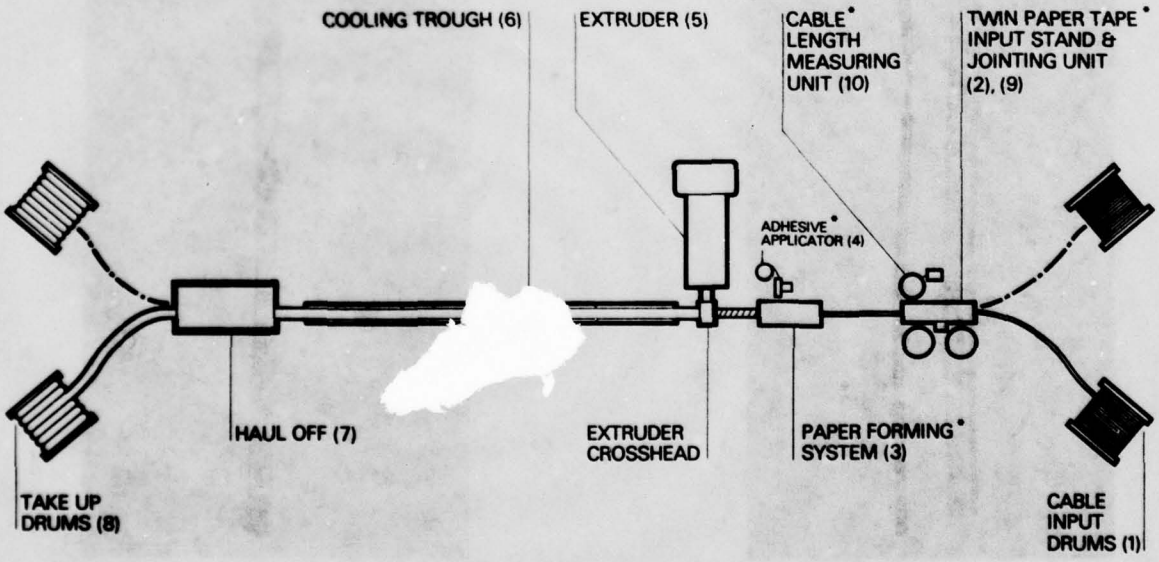


Fig 7 PeTAP manufacturing process (diagramatic)



Mr Bissell works for the British Post Office in the External Plant Development Division and is Head of Group responsible for the mechanical aspects of cable design. He has had many years of practical experience on both development and field work. He is a Chartered Engineer and a Fellow of the Institution of Mechanical Engineers.

External Plant Development Division
OP10.5.3
Operational Programming Department
Carlton House
Carlton Avenue East
WEMBLEY
Middlesex
HA9 8QH

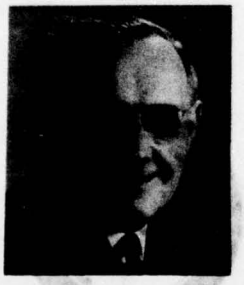
Telephone: 01-90 1176



Mr Chadwick works for BICC Telecommunication Cables Ltd, which he joined in 1966 after 6 years initial service with the British Post Office. He worked in the areas of cable design and process development in telephone cable manufacture at the Prescott plant before transferring to the Blackley, Manchester plant in 1972. In 1975 he became Technical Manager and since become also responsible for Productivity Services. He is a Member of the Institution of Electronic and Radio Engineers.

BICC Telecommunication Cables Limited
Blackley
MANCHESTER
M9 3FP

Telephone: 061-740 9151



Mr Smith is Head of the External Plant Development Division and is responsible for the development of cables, jointing, external plant and practices, and mechanical aids. He joined the BPO in 1939. After war service in the Royal Electrical and Mechanical Engineers where he worked on radar and radio telegraphy, he graduated at London University. From 1947-53 he worked on the design of AC signalling and international dialling and switching. Subsequently he was factories engineer and chief engineer at the Post Office Factories Department before taking up his present post. He is a Fellow of the Institution of Electrical Engineers.

CARLTON HOUSE
Carlton Avenue East
WEMBLEY
Middlesex
HA9 8QH

Telephone: 01-904 9762

AN IMPROVED SCREENED CABLE DESIGN

A. P. Gabriel; J. Justiss; R. Rossi

General Cable Corporation

Abstract

With the rapid acceleration of digital transmission technology, there is a constant need for screened cable which maintains pace with this evolution. To meet this need, a new screened cable has been developed which incorporates a radically new concept in cable screening and shielding. This paper will discuss the details of the new design with the rationale for its selection.

Introduction

The use of internally screened cable for PCM carrier transmission has, by now, become common practice. Initial screened cable designs offered the system designer near-end crosstalk levels which provided adequate safety margins with respect to error rate. With the progression from 24 channel to 48 channel transmission, however, the Near-End Crosstalk (NEXT) margins became uncomfortably low, especially on small pair count cables. In order to increase these margins, the new "Dual D-Shield" cable was developed. This paper will present electrical and mechanical data obtained from initial production, and compare it to current requirements. Finally, the paper will present the general manufacturing steps taken to achieve the required shielding configuration, and some techniques necessary for field splicing of this new cable design.

Background

Since the introduction of screened cable for 100% fill PCM carrier application, the two basic constructions have not substantially changed. The open screen design, introduced in 1970[1], and the closed screen design which soon followed, are with slight modifications, generally the two alternatives of choice today. The modifications which were introduced, concentrated on "state-of-the-art" improvements and also on improving the manufacturing efficiency of the cables. We will review, briefly, the primary designs evaluated since the inception of the screened cable.

The open screen design, shown in Figure 1, was specially designed for the early 24 channel carrier systems.[1] Experience has shown that this original goal was satisfactorily attained. In order to achieve more effective intra-compartmental isolation, the tab ends of the screen were increased in length, giving rise to the extended open screen variety of cable (Figure 2). This approach emerged as a direct result of the progression of carrier systems into the 48 channel transmission mode.



OPEN SCREEN CABLE DESIGN

Figure 1



EXTENDED OPEN SCREEN CABLE DESIGN

Figure 2

The closed screen design, introduced in 1972[2], was a natural progression of the open screen concept. This construction, shown in Figure 3, effectively isolated one core half from the other,

such that 24 and 48 channel transmission is made possible at a greater NEXT safety margin. As given above, other screening methods were evaluated either to improve the "state-of-the-art" and/or improve manufacturing efficiency. Figure 4 illustrates a dual closed screen construction whereby individual screens are placed over each core half of the cable. Although the mechanical integrity of this model was good, there was no tangible benefit in NEXT performance. In addition, the substantial increase in material usage made this design commercially unattractive.



CLOSED SCREEN CABLE DESIGN

Figure 3



CLOSED DUAL SCREEN CABLE DESIGN

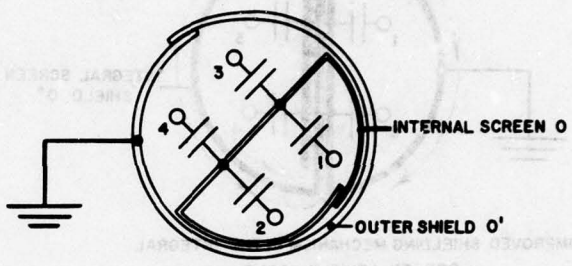
Figure 4

In order to reduce material usage in the two-tape, dual closed screen design, the overall shield was eliminated while the thickness of the screening material was increased to maintain lightning protection in the buried plant environment. This modification reduced material usage somewhat but proved difficult to manufacture and resulted in degradation of the structural integrity of the cable since each core half could move independently of the other.

Integral Screen/Shield Design

During one phase of our study into alternate screened cable designs, the decision was made to evaluate the possibility of merging the internal screen and outer shield into one continuous shielding tape. The rationale for this decision stemmed from earlier NEXT studies, conducted at both 0.772 and 1.576 MHz, which revealed a notable crosstalk level improvement when the screen and outer shield were brought into close proximity. In fact, this improvement could be maximized when these two shielding elements were placed in electrical contact. Although the physical mechanism governing this phenomenon are complex, it is possible to explain the theory in simpler terms by relying on the works of Kaden[3] and Griffith[4].

Kaden, explains the crosstalk mechanism in terms of a capacitance model, such as illustrated in Figure 5.



CROSSTALK MECHANISM IN THE CLOSED SCREEN CABLE

Figure 5

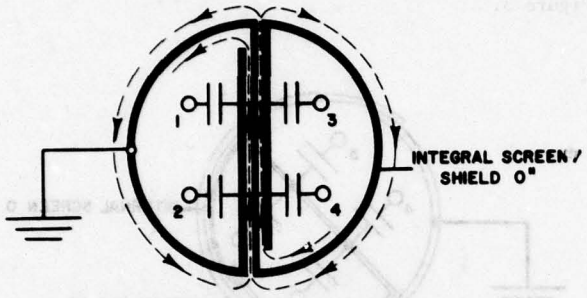
In this model, the mechanism for NEXT is not direct, but rather occurs via intermediate circuitry. Considering pair 3 - 4 outside the inner screen 0, the unbalance capacitances C_{30} and C_{40} give rise to a potential between the pair 3 - 4, considered as a single conductor, and screen 0. Such asymmetrical circuit excitation produces a longitudinal current on screen 0 and, therefore, longitudinal voltage on its inner surface by virtue of its surface transfer impedance. As the screen 0 is brought closer to the overall shield 0', the capacitance of the longitudinal unbalanced circuits of pair 1 - 2 to shield 0 is increased, thereby increasing the attenuation of this circuit. This reduces the longitudinal current and voltage on the screen 0, resulting in an attendant level reduction in NEXT. For conventional open or closed screen designs, this result may be maximized through a physical grounding of the screen.

Although the capacitance model is sufficient to illustrate the Near-End Crosstalk mechanism, the effect of gaps in the screening compartment bear further discussion. Kaden, but more especially Griffith, has illustrated that such gaps (due to shield overlap) in the shield, or the screen in this case, can seriously degrade shielding efficiency at the higher frequencies (depending on the width and length of the gap) due to magnetic flux leakage. For a homogeneous tubular shield, surface transfer impedance will be decreased with increasing frequency. With a gap, however, the inverse occurs at higher frequencies, and the magnitude of the surface transfer impedance becomes a function of the physical size of the shielding overlap gap.

Minimization of the overlap gap can be achieved in two ways:

a) Reduce the cross-sectional overlap area such that it converges to zero.

b) Increase the gap length such that the compartment-to-compartment leakage path is increased, thereby attenuating the interfering signals.

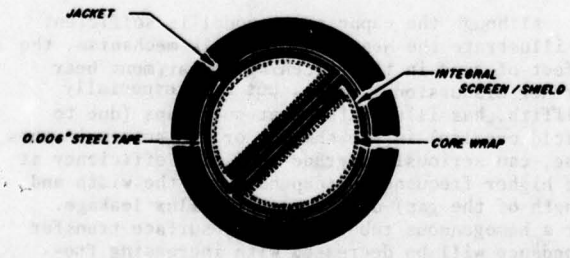


IMPROVED SHIELDING MECHANISM IN THE INTEGRAL SCREEN / SHIELD CABLE

Figure 6

The "Dual-D" Shield model of Figure 6, reflects a minimization of the screen-to-shield separation by making the screen and shield one continuous tape, and it also maximizes the length of the compartment-to-compartment leakage path through overlap placement.

In order to yield a shield resistance equal to, or less than, the combined screen/shield resistance of current designs, the integral screen/shield tape selected was an 0.008" copolymer coated aluminum. This would provide equivalent lightning protection to current screened cable designs. Each compartment half is provided with a high dielectric strength core wrap to minimize potential conductor to shield breakdown during lightning storms. A cable configuration as shown in Figure 7 was the final design selected.



INTEGRAL SCREEN / SHIELD CABLE DESIGN

Figure 7

The cable, as shown, is filled for reasons which will become clear later. The 0.006" steel tape was added for a variety of reasons. One was to facilitate splicing, since intimate bonding of the jacket to the copolymer coated aluminum would increase the difficulty of removing the jacket during the splicing process. This will be explained in greater detail when cable splicing is discussed. A second reasons for the steel tape was to provide increased mechanical protection for critical circuits contained in the cable. What we had, then, was a filled, screened cable with significantly improved shielding capability, and with a sheath providing universal application.

In order to verify the promising transmission performance of the design, prototype cables were manufactured for evaluation. Also, the mechanical performance of the new cable design required evaluation. Certainly, a cable having good electrical performance with weak mechanical properties would not be acceptable. The criteria for mechanical evaluation, therefore, was a performance level at least as good as the current designs.

Mechanical Tests

In addition to the standard industry tests normally required, cable samples, with end blocked, were subjected to temperature cycling. One cycle consisted of a temperature excursion of -40°F to +140°F (-40°C to +60°C) in a time period of 24 hours. Samples were cycled up to 25 days, with some periodically removed at intervals of 4, 11, 15 and 21 days. After removal from the conditioning chamber, cable samples were allowed to stabilize to room temperature and then subjected to bending 180° around a 10X diameter mandrel. The samples were then bent 180° in the opposite direction after which the cable was axially rotated 90° and the process repeated. A standard closed screen cable was also tested for comparison purposes. After the bending test, cable samples were dissected to determine any visible damage to cable components.

It must be emphasized here, that the bending test described above is not industry standard, and the bending diameter was purposely made small to increase the severity of the test. The purpose of the test was to determine relative performance of the new design when compared against current standard cable which has a very satisfactory performance history in the field. The results of the bending test were as follows:

Table 1

Conditioning Cycles/Days	Cable Condition: Current Closed Screen	Cable Condition: Dual D
4	No buckling or damage	No buckling or damage
11	Slight buckling, no damage	"
15	"	Slight buckling, no damage
21	Buckling, no damage	"
25	"	"

No cracking of any cable component was observed in either the current closed screen design, or in the new proposed design. The improved performance of the "Dual-D" shield design, can be attributed to the structure of the screen/shield configuration. Current designs for open screen and closed screen cables permit migration of core filling compound into the shield/jacket interface during broad temperature excursions or severe handling. This has been known to be a factor in occasional cable damage during installation at high temperatures and may occur due to thermal expansion and/or cable deformation. In the "Dual-D" cable, each compartment is mechanically isolated due to the sealed layers in the central partition. The sealing is obtained by means of heat generated by the filling compound. In addition, due to the overlap placement, pressure build-up due to filling compound expansion is effectively contained. This prevents migration of the filling compound into the shield/jacket interface, thereby reducing the effect of one of the major contributions to potential jacket slippage during field handling.

Transmission Testing

For purposes of this series of tests, two cable sizes were tested. One was 24 pair 22 AWG and the other 104 pair 22 AWG. This was done to obtain representative data for both layer and unit type cables. The primary area of interest, of course, was Near-End Crosstalk at both 24 and 48 channel frequencies. Superimposing the results of the tests on previously published graphs[5], the effect of the added screening realized by almost 3 layers of 0.008" copolymer coated aluminum and a notable extension of the overlap length is apparent. Figure 8 displays the results of test at 772 KHz, and Figure 9 at 1.576 MHz.

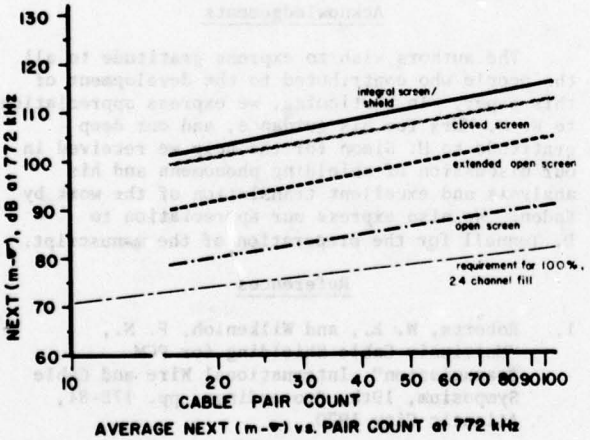


Figure 8

To date, the maximum size manufactured has been a 104 pair 22 AWG cable, which covers the major portion of the screened cable sizes employed today. For this reason, we have not shown data for the larger sizes. The transmission test results show a substantial improvement in Near-End Crosstalk levels over cables in current use, assuring greater safety margins for 48 channel transmission. Other industry electrical tests performed on the prototype cables yielded results substantially equivalent to current standard screened cables.

Cable Manufacture

With any cable construction, one must be able to proceed from the prototype phase to a production mode in a manner which will result in a consistent quality product. Once this possibility was verified, a Patent Application[6] for "Dual-D" was filed and is pending.

Production of the cable presented a unique set of problems. It was mandated at the very outset, that the finished product must be as good, or better than, existing designs in all specification parameters, and significantly better in Near-End Crosstalk. Evaluation testing of the prototype cables verified the last point, but consistent processing techniques are necessary to meet the other goals, particularly Water Flow Resistance and Mechanical Integrity. Of particular significance toward this end was the central screening partition. In order to eliminate potential water flow, and provide a sound mechanical structure, the three layers of 0.008" copolymer coated aluminum tape would have to be physically fused. This is accomplished when the hot filling compound comes in contact with the tape layers. Experience has shown this to be controllable on a consistent

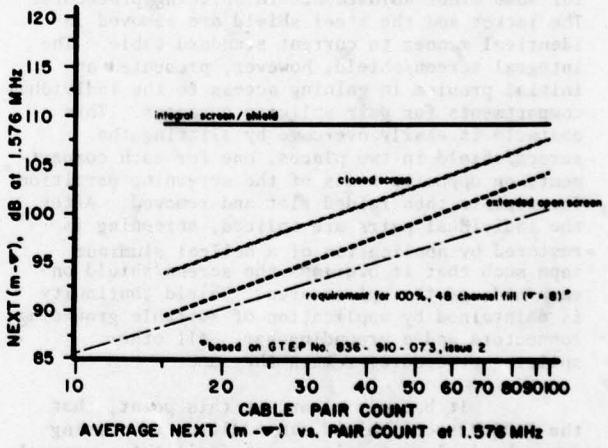


Figure 9

basis. In addition, the filling process mandated that, in one continuous operation, the following must be accomplished:

1) Pay-off two unfilled core halves.
2) Apply filling compound to each core half.
3) Apply core separator tape over each compartment.
4) Apply 0.008" copolymer coated aluminum such that the configuration of Figure 7 is achieved.
5) Apply filling compound at the various sheath interfaces.
6) Apply 0.006" steel tape and flooding compound.
7) Apply jacket.

As can well be imagined, this was quite a formidable task, and with considerable effort, was accomplished. To place this accomplishment into greater perspective, the following had to be considered in the manufacturing process:

a) Fill two separate core halves simultaneously.
b) Core tapes must be properly aligned to result in satisfactory coverage over the core.
c) Core tape overlap must be in proper direction to be compatible with screen/shield bend.
d) Screen/shield must be properly aligned so as to fold in the exact area required. This is important for mutual capacitance control and proper geometric symmetry.
e) Center membrane layers must be placed in close contact for proper fusing.

The equipment for this process is quite complex and is beyond the scope of this paper.

Cable Splicing

The "Dual-D" cable, as designed, is handled basically similar to current standard cable except for some minor adjustments in splicing procedure. The jacket and the steel shield are removed in identical manner to current standard cable. The integral screen/shield, however, presented an initial problem in gaining access to the individual compartments for pair splicing purposes. This obstacle is easily overcome by slitting the screen/shield in two places, one for each compartment, on opposite sides of the screening partition. The tape is then folded flat and removed. After the individual pairs are spliced, screening is restored by application of a helical aluminum tape such that it overlaps the screen/shield on each side of the splice area. Shield continuity is maintained by application of suitable grounding connectors and a grounding bar. All other splicing procedures remain the same.

It becomes clear, at this point, that the 0.006" steel shield, in addition to serving as mechanical protection, also facilitates removal of the outer sheath for easier access to the inner core. Were the steel not there, the adhesion of the jacket to the copolymer coated aluminum integral screen/shield would result in difficulty in gaining access to the pairs for splicing.

Summary

As stated in the foregoing paragraphs, the mechanism for Near-End Crosstalk has been rigorously discussed in other publications. The "Dual-D", integral screen/shield design further reduces the effects of electrostatic and electromagnetic coupling. This has resulted in Near-End Crosstalk improvements at 1.576 MHz (48 channel) transmission by 15 to 20 db, in the cable sizes considered, increasing the margin of safety and further reducing the possible error rate. This has been accomplished without degrading any other cable properties. On the contrary, a more mechanically rugged cable has also been developed.

Conclusions

In this paper, we have presented a cable design for PCM carrier application which represents a significant advance in the "state-of-the-art" for single cable, two-way transmission. In fact, the configuration of the shield member now more closely satisfies the original promise of two cables under one sheath. As has always been demonstrated in the past, technology moves at a rapid pace. Cables originally manufactured for 24 channel, 0.772 MHz transmission, very soon were also required to be compatible with the 48 channel, 1.576 MHz system. Similarly, cable manufactured today must be designed with potential technology improvements in mind. The performance level of the "Dual-D" shield cable, for 48 channel transmission has been shown. Future demands on the carrier cable are not definitely known, but 96 channel duo-binary transmission at 1.576 MHz is becoming a serious topic of discussion. The high NEXT levels of the "Dual-D" shield cable at 1.576 MHz certainly warrant further evaluation for this application.

Acknowledgements

The authors wish to express gratitude to all the people who contributed to the development of this paper. In particular, we express appreciation to W. H. Marx for his guidance, and our deep gratitude to H. Simon for the help we received in our discussion of shielding phenomena and his analysis and excellent translation of the work by Kaden. We also express our appreciation to D. Tunnell for the preparation of the manuscript.

References

1. Roberts, W. L., and Wilkenloh, F. N., "Multipair Cable Shielding for PCM Transmission", International Wire and Cable Symposium, 19th, Proceedings, pp. 175-81, Atlantic City 1970.

2. U. S. Patent 3,603,340. "D" Internal Shield in Telephone Cables. L. Jachimowicz and J. A. Olszewski to General Cable Corporation, April 9, 1974.

3. Kaden, H., "Wirbelstrome und Schirmung in der Nachrichtentechnik", 2nd Edition, pp. 296-301, 327-340, Berlin, Springer, 1959.

4. Griffith, D. E., "Surface Transfer Impedance on Cable Shields Having a Longitudinal Seam", National Electronics Conference, Proceedings, 26, 952-7, 1970.

5. Gabriel, A. P., Woods, J. J. and Peveler, J., "Near-End Crosstalk Properties Compartmentalized PCM Carrier Cables", International Wire and Cable Symposium, 25th, Proceedings, Cherry Hill, New Jersey 1976.

6. U. S. Patent Application, File 15538, Advanced Design Screened Telephone Cable. A. P. Gabriel and J. Justiss, General Cable Corporation, December 1977.



Richard Rossi has been with General Cable Corporation since 1963. Since then he has had assignments in the Product Design and Product Engineering Departments. He is currently Senior Application Engineer in the Communications Products Operation, Application Engineering Department, concentrating on outside plant telephone cable design. Mr. Rossi has been a member of IEEE since 1972.



Anthony P. Gabriel received a B.S. degree in Engineering Science from Richmond College, the City University of New York, in 1972. Employed by the General Cable Corporation since 1967, he holds the position of Research Product Manager, Carrier Telephone Cable. In addition to his responsibilities for the development and analysis of carrier telephone cables, he is also responsible for the development of outside plant wire products. Prior to joining the Research Center, he was affiliated with both Western Electric and the Bell Telephone System.



J. D. (Jimmy) Justiss, a life-long resident of Texas, has been employed at General Cable Corporation's Bonham plant since it was opened in 1957. He has held various technical and supervisory positions related to production and engineering of virtually all types of telephone wire and cable. Mr. Justiss presently holds the position of Assistant Development Engineering Manager for the Communications Products Operation.

STUDIES OF INSULATION-CONDUCTOR ADHESION IN VINYL DROP WIRE

P. C. Warren
J. E. Adams

Bell Laboratories
Murray Hill, N.J.

One method of promoting adhesion of vinyl insulation to the copper-plated steel conductor in drop wire is to selectively preheat the wire immediately before the insulation is applied. We have examined this adhesion phenomenon by constructing a compression mold that closely approximates the bonding conditions encountered in drop wire extrusion.

Our experiments have shown that (1) the adhesion is highly reproducible over the relevant wire preheat range, (2) the highest values are obtained at 275 ± 10°C, (3) there is an upper temperature limit which, when even slightly exceeded, gives irreproducible and inferior insulation-to-conductor bonds, and (4) the bond strength improves slowly but measurably with time. While the mechanism of the adhesion is not understood it apparently depends on dehydrohalogenation of the PVC resin or of an appropriate additive.

INTRODUCTION

An essential element of telephone drop wire design is the adhesion between insulation and the copper-plated steel conductor, thus assuring transfer of load from the clamp to the center strength member during actual service. Some manufacturers of vinyl drop wire achieve the bond by precoating the wire with an adhesive in a separate manufacturing step. Others rely on a simpler method that is done simultaneously with extrusion of the vinyl insulation. It consists of preheating the conductor to 275°C (about 100° hotter than the plastic melt) just before entering the extruder. We have chosen to examine the vinyl-to-copper bond obtained by this latter route with the intent of understanding and hopefully identifying ways to improve it. In particular, we were interested in devising a laboratory scale test that would emulate drop wire extrusion but also consume only a small fraction of the material required in large production machines.

EXPERIMENTAL

In early development work[1] at Bell Laboratories, adhesion between vinyl and copper was promoted in a way that is difficult to relate to drop wire construction. Hot vinyl insulation compound was pressed against solvent-cleaned copper sheets for 1-2 minutes at 220-240°C, after which the laminate was cooled by either water quench or transfer to a cold press. Testing consisted of peeling back a strip of plastic and measuring the required force. While this test method qualitatively predicted adhesion between vinyl and copper, it in no way resembled the thermal history, contact time or metallic surface that was encountered in actual production. Furthermore, it did not provide a way to obtain the thermal differential between conductor and plastic as is essential in actual practice.

We have conceived of a process which is almost identical to drop wire extrusion but can be done on a laboratory scale to fully predict vinyl-copper bonding properties as found in final product. It is modeled after a procedure described in ASTM D1871, "Rubber Property-Adhesion to Single-Strand Wire".[2] A 3/8" wide x 1/4" thick x 6" long compression mold was designed to allow ten conductors spaced 0.5 inches apart to pass through the mold parallel to the first dimension. The wires were electrically insulated from the mold with Teflon bushings and spaghetti tubing, and the ends of each were fastened to a terminal strip. A photograph of the complete mold is shown in Fig. 1. Two 3/8" x 6" strips were cut from a previously prepared 1/8" thick vinyl sheet and placed in the mold, one strip above the wires and one below. The cover was placed on top and the entire assembly heated to 160°C on a steam press. Each of five pairs of wires was connected via knife switches to a "Thermal Monitor" (Joyal Products, Linden, N.J.) which controlled in turn a "Tweezer Weld" Model 10KVA 220 VAC electric welding unit (Arvin Automation, Inc., Cedar Grove, N.J.). A simple schematic is

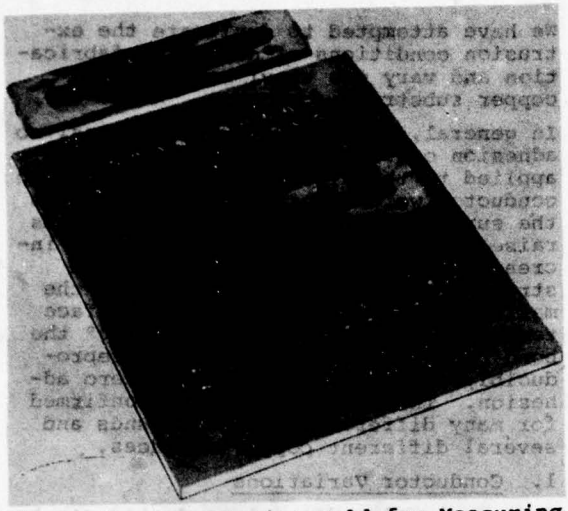


Figure 1 Compression Mold for Measuring Adhesion

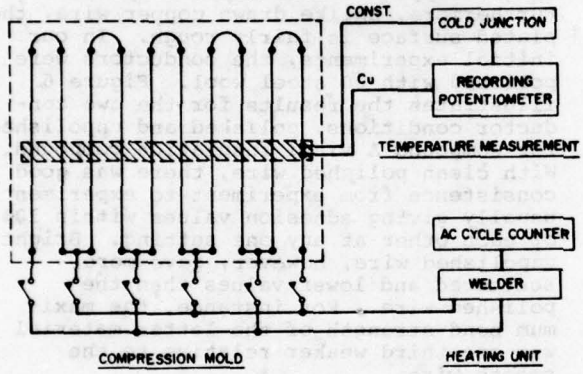


Figure 2 Drop Wire Adhesion Schematic

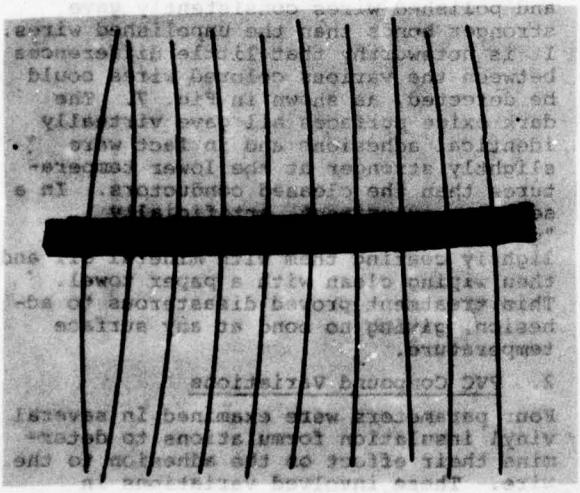


Figure 3 Molded Adhesion Sample Before Testing

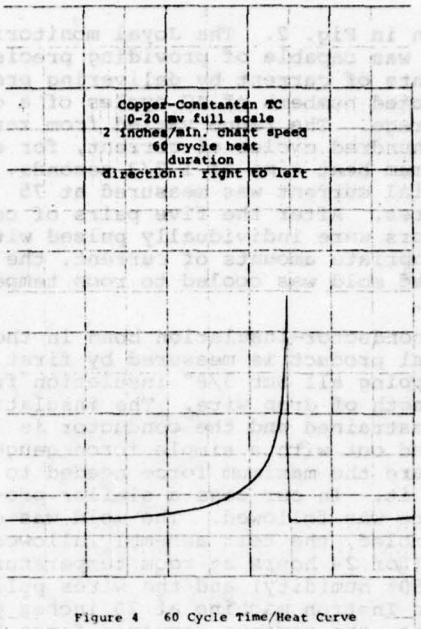


Figure 4 60 Cycle Time/Heat Curve

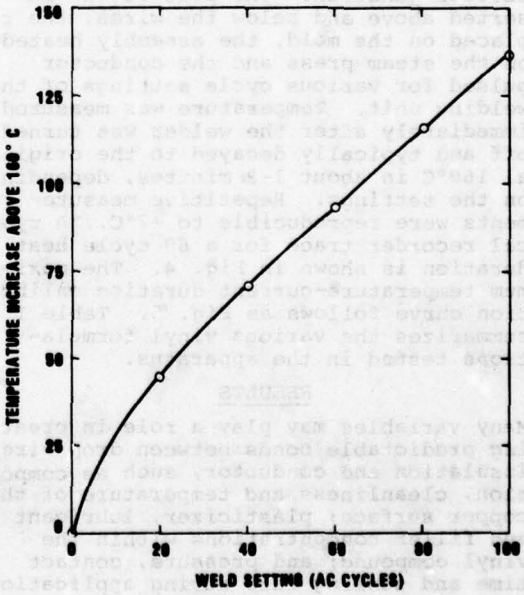


Figure 5 AC Cycle Setting/Wire Surface Temperature Calibration Curve

shown in Fig. 2. The Joyal monitoring unit was capable of providing precise amounts of current by delivering preselected numbers of AC cycles of a given amperage. The range varied from zero to one hundred cycles of current, for a maximum heat time of 1 2/3 seconds. Initial current was measured at 75 amperes. After the five pairs of conductors were individually pulsed with appropriate amounts of current, the heated mold was cooled to room temperature.

The conductor-insulation bond in the actual product is measured by first stripping all but 3/8" insulation from a length of drop wire. The insulation is restrained and the conductor is pulled out with a simple force gauge to measure the maximum force needed to remove it. In our case a similar procedure was followed. The mold was disassembled, the test assembly allowed to age (for 24 hours at room temperature and 50% humidity) and the wires pulled on an Instron machine at 20 inches per minute, the maximum required force being recorded. Figure 3 illustrates the test sample just before measurement. All reported results represent the average of four measurements (two separate experiments each involving one pair of wires).

The wire surface temperature was calibrated with .010" copper-constantan thermocouples; the standard test circuit is diagrammed in the schematic shown in Fig. 2. Three or four turns of constantan wire were wrapped around a conductor inside the mold to form the surface junction. The plastic was inserted above and below the wires, the top placed on the mold, the assembly heated on the steam press and the conductor pulsed for various cycle settings of the welding unit. Temperature was measured immediately after the welder was turned off and typically decayed to the original 160°C in about 1-2 minutes, depending on the settings. Repetitive measurements were reproducible to ± 2°C. A typical recorder trace for a 60 cycle heat duration is shown in Fig. 4. The maximum temperature-current duration calibration curve follows as Fig. 5. Table I summarizes the various vinyl formulations tested in the apparatus.

RESULTS

Many variables may play a role in creating predictable bonds between drop wire insulation and conductor, such as composition, cleanliness and temperature of the copper surface; plasticizer, lubricant and filler concentrations within the vinyl compound; and pressure, contact time and cooling rate during application. We have attempted to duplicate the extrusion conditions of drop wire fabrication and vary the vinyl material and copper substrate.

In general, with very few exceptions, no adhesion occurred when no current was applied to the wire and both plastic and conductor were maintained at 160°C. As the surface temperature of the wire was raised to 250° the adhesion steadily increased. Between 250° and 280° bond strengthened at a more rapid rate, the maximum adhesions occurring at surface temperatures of 275-280°. At ∿300° the bond deteriorated rapidly and irreproducibly, sometimes decaying to zero adhesion. This performance was confirmed for many different vinyl compounds and several different copper surfaces.

1. Conductor Variations

The copper-plated steel conductor can be visually quite variable, ranging from bright copper to dark brown or purple. Furthermore, unlike drawn copper wire, the plated surface is fairly rough. In our initial experiments, the conductors were polished with 00 steel wool. Figure 6 illustrates the results for the two conductor conditions, polished and unpolished, for Compound A vinyl insulation compound. With clean polished wire, there was good consistence from experiment to experiment, usually giving adhesion values within 10% of each other at any one setting. Bright, unpolished wire, however, gave more scattered and lower values than the polished wire. For instance, the maximum bond strength of the latter material was one-third weaker relative to the smooth wire.

Compound B was also tested on several types of conductors, and results were similar to the Compound A experiment. Cleaned and polished wires consistently gave stronger bonds than the unpolished wires. It is noteworthy that little differences between the various colored wires could be detected, as shown in Fig. 7. The dark oxide surfaces all gave virtually identical adhesions and in fact were slightly stronger at the lower temperatures than the cleaned conductors. In a separate experiment, artificially "greasy" conductors were created by lightly coating them with mineral oil and then wiping clean with a paper towel. This treatment proved disasterous to adhesion, giving no bond at any surface temperature.

2. PVC Compound Variations

Four parameters were examined in several vinyl insulation formulations to determine their effect on the adhesion to the wire. These involved variations in

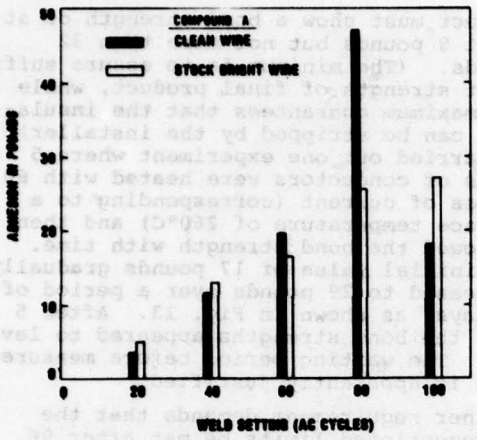


Figure 6 Effect of Cleaned Wire Surface on Adhesion

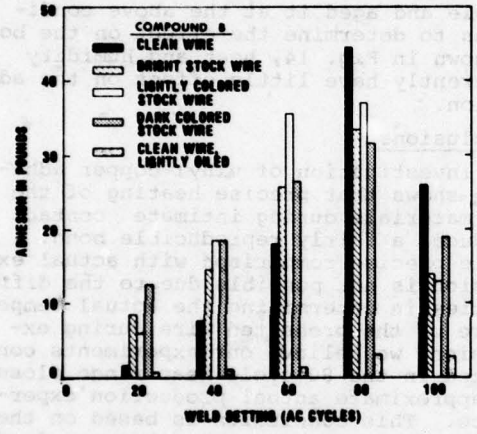


Figure 7 Effect of Various Color Surfaces on Adhesion

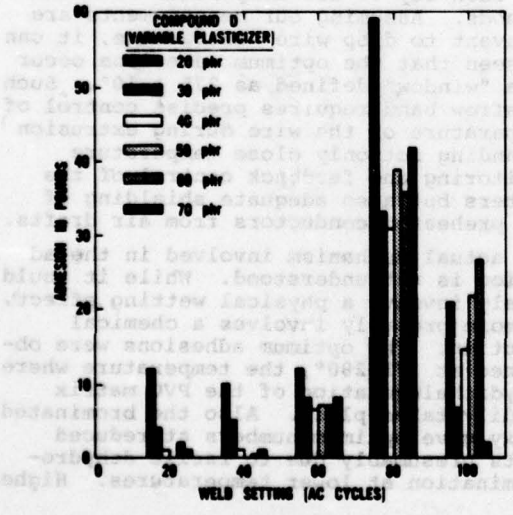


Figure 8 Effect of Variable Plasticizer on Adhesion

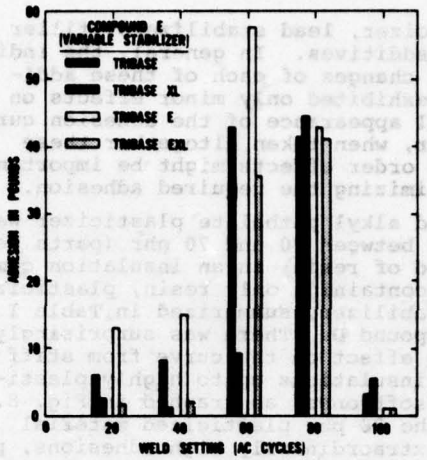


Figure 9 Effect of Several Stabilizers on Adhesion

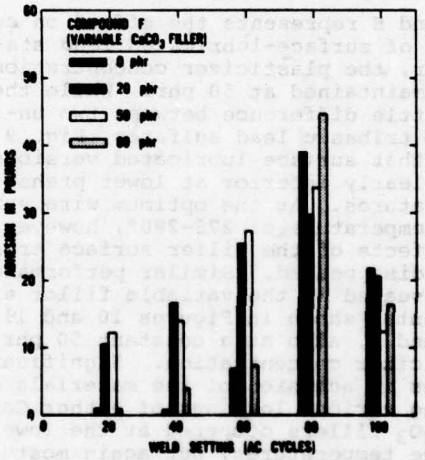


Figure 10 Effect of Variable $CaCO_3$ Filler on Adhesion

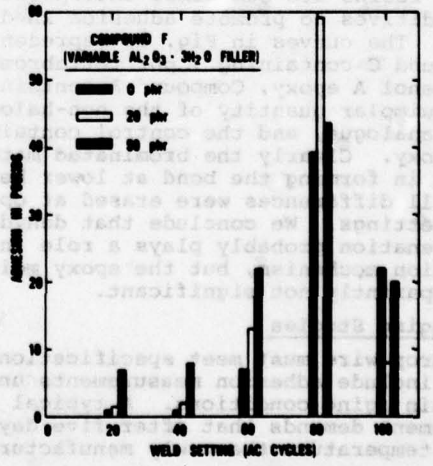


Figure 11 Effect of Variable $Al_2O_3 \cdot 3H_2O$ on Adhesion

plasticizer, lead stabilizers, filler and epoxy additives. In general, the individual changes of each of these additives exhibited only minor effects on the overall appearance of the adhesion curve. However, when taken altogether these second order effects might be important in optimizing the required adhesion.

A mixed alkyl phthalate plasticizer was varied between 20 and 70 phr (parts per hundred of resin) in an insulation compound containing only resin, plasticizer and stabilizer, summarized in Table I as Compound D. There was surprisingly little effect on the curve from stiff semi-rigid insulations up to highly plasticized soft ones, as graphed in Fig. 8. Only the 20 phr plasticized material gave extraordinarily high adhesions, perhaps because the glass transition of the material was near room temperature, reflecting a much higher tensile strength of the compound during measurement.

Compound E represents the effect on adhesion of surface-lubricated lead stabilizer, the plasticizer concentration being maintained at 50 phr. While there was little difference between two uncoated tribasic lead sulfates, Fig. 9 shows that surface lubricated versions were clearly inferior at lower preheat temperatures. At the optimum wire surface temperature of 275-280°, however, the effects of the filler surface treatments disappeared. Similar performance was revealed in the variable filler experiments, shown in Figures 10 and 11 for Compound F, also at a constant 50 phr plasticizer concentration. Significant changes in adhesion of the materials containing various loadings of either $CaCO_3$ or Al_2O_3 fillers occurred at the lower surface temperatures, but again most of these differences disappeared at the optimum setting.

Epoxy resins are sometimes incorporated as additives to promote adhesion in drop wire. The curves in Fig. 12 represent Compound C containing 7 phr tetrabromobisphenol A epoxy, Compound A containing an equimolar quantity of the non-halogenated analogue, and the control containing no epoxy. Clearly the brominated material aided in forming the bond at lower heats, but all differences were erased at optimum settings. We conclude that dehydrohalogenation probably plays a role in the adhesion mechanism, but the epoxy moiety is apparently not significant.

3. Aging Studies

All drop wire must meet specifications that include adhesion measurements under certain aging conditions. A typical requirement demands that after five days at room temperature the newly manufactured product must show a bond strength of at least 8 pounds but not more than 32 pounds. (The minimum is to assure sufficient strength of final product, while the maximum guarantees that the insulation can be stripped by the installer). We carried out one experiment where 5 pairs of conductors were heated with 60 cycles of current (corresponding to a surface temperature of 260°C) and then followed the bond strength with time. The initial value of 17 pounds gradually increased to 29 pounds over a period of 15 days, as shown in Fig. 13. After 5 days the bond strengths appeared to level off. The waiting period before measurement is apparently justified.

Another requirement demands that the aforementioned limits be met after 96 hours at 65°C and 95% humidity. We measured and recorded an adhesion curve for Compound A and then took an identical sample and aged it at the above conditions to determine the effect on the bond. As shown in Fig. 14, heat and humidity apparently have little effect on the adhesion.

Conclusions

Our investigation of vinyl-copper adhesion shows that precise heating of the two materials during intimate contact produces a fairly reproducible bond. While precise comparison with actual extrusion is not possible due to the difficulties in determining the actual temperature of the preheated wire during extrusion, we believe our experiments conducted in the 80 cycle heat range closely approximate actual production experience. This conclusion is based on the temperature of the vinyl, the method of preheating the conductor, the similarity of our values with production numbers and the identity of all components in both methods. Assuming our measurements are relevant to drop wire manufacture, it can be seen that the optimum adhesions occur in a "window" defined as 275 $\pm$ 10°. Such a narrow band requires precise control of temperature of the wire during extrusion demanding not only close temperature monitoring and feedback control of the heaters but also adequate shielding of the preheated conductors from air drafts.

The actual mechanism involved in the adhesion is not understood. While it could merely involve a physical wetting effect, it more probably involves a chemical reaction. The optimum adhesions were obtained at 275-280°, the temperature where dehydrohalogenation of the PVC matrix readily takes place. Also the brominated epoxy gave optimum numbers at reduced heats presumably due to facile dehydrobromination at lower temperatures. Higher

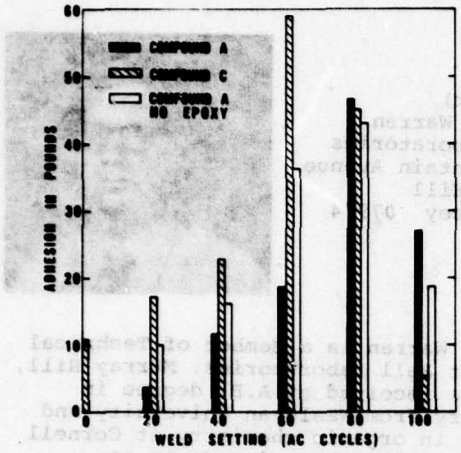


Figure 12 Effect of Several Epoxies on Adhesion

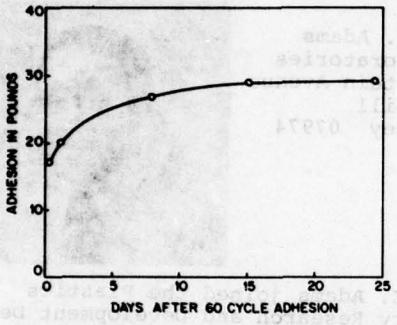


Figure 13 Effect of Aging on Adhesion

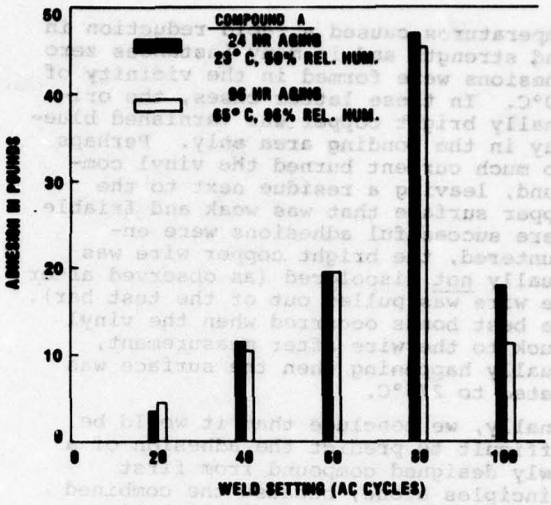


Figure 14 Effect of Heat and Humidity on Adhesion

TABLE I

Resin	A	B	C	D	E	F
GP5-00003	100	100	100	100	100	100
Plasticizer						
Mixed n-alkyl phthalate	66	66	66	See Fig. 8	50	50
Stabilizer						
Tribasic lead sulfate, surface treated	5	5	5	5	See Fig. 9	5
Epoxy						
Epichlorohydrin-bisphenol A resin	4	4	-	-	-	-
Epichlorohydrin-tetrabromo-bisphenol A resin	-	-	7	-	-	-
Filler						
Meta kaolin calcined clay	5	10	5	-	-	-
Fumed silica	5	-	-	-	-	-
Calcium carbonate surface treated	-	-	-	-	-	See Fig. 10
Aluminum oxide trihydrate	-	-	-	-	-	See Fig. 11
Fire Retardant						
Antimony oxide	3	3	3	-	-	-
Weathering Agent						
Furnance black	2.5	2.5	2.5	-	-	-

temperatures caused a rapid reduction in bond strength and in many instances zero adhesions were formed in the vicinity of 300°C. In these latter cases, the originally bright copper was tarnished blue-gray in the bonding area only. Perhaps too much current burned the vinyl compound, leaving a residue next to the copper surface that was weak and friable. Where successful adhesions were encountered, the bright copper wire was usually not discolored (as observed after the wire was pulled out of the test bar). The best bonds occurred when the vinyl stuck to the wire after measurement, usually happening when the surface was heated to 275°C.

Finally, we conclude that it would be difficult to predict the adhesion of a newly designed compound from first principles alone, because the combined variations due to filler, plasticizer, lubricant and other additives are too complex to explain. We prefer to simply test the new material by the new method to determine its adhesion performance. If the extrusion can be run with preheated wire maintained at 275-280° the adhesion will be more or less independent of the particular formulation anyway. Temperatures lower than this will produce bonds whose quality is highly dependent on the compound ingredients and temperatures higher than this will give irreproducible bonds all the way down to zero adhesion.

REFERENCES

1. J. B. DeCoste, U.S. Patent No. 3,579,608 dated 5/18/71.
2. ASTM D1871-68 (Reapproved 1975) "Rubber Property - Adhesion to Single-Strand Wire", Part 37, American Society for TEsting Materials, 1916 Race Street, Philadelphia, Pa. 19103.



(Speaker)
Paul C. Warren
Bell Laboratories
600 Mountain Avenue
Murray Hill
New Jersey 07974

Paul C. Warren is a Member of Technical Staff at Bell Laboratories, Murray Hill, N.J. He received an A.B. degree in chemistry from Wesleyan University and a Ph.D. in organic chemistry at Cornell in 1969. His recent interests at Bell Labs have focused on more efficient designs of PVC wire and cable.



Joseph E. Adams
Bell Laboratories
600 Mountain Avenue
Murray Hill
New Jersey 07974

Joseph E. Adams joined the Plastics Chemistry Research and Development Department at Bell Laboratories, Murray Hill, N.J. in 1973. Previously he was associated with General Cable at Union, N.J. At Bell Labs he has done extensive testing of new PVC insulation and jacket compounds.

EVALUATION OF CROSS-LINKED MATERIAL INSULATED ELECTRONIC APPLIANCE HOOK-UP WIRES

M. Ishibashi, T. Yamamoto, A. Mogi

The Fujikura Cable Works, Ltd

Tokyo, Japan

ABSTRACT

Hook-up wires have become much finer, along with the recent tendency to miniaturise electronic appliances. On the other hand, with the demand for higher reliability, material property improvements have been required. We have evaluated the hook-up wires insulated with cross-linked polyethylene (XLPE) and cross-linked polyvinylchloride (XLPVC) for general purposes. We have obtained some typical comments in addition to the various results for designing or using them.

1. INTRODUCTION

There are two ways to achieve the miniaturization and the property improvements of hook-up wires. One is to utilize newly developed insulating materials of high quality such as fluorinated polymers. The other is to modify the properties of conventional insulating materials by such means as cross-linking. We have manufactured hook-up wires insulated with XLPE and XLPVC which are commonly used for insulation, and have evaluated the thermal, mechanical, electrical, and chemical properties as follows:

(1) Dependence of properties on percent gels which show the degree of cross-linking.

(2) Comparison of properties of irradiated XLPE which is commonly used for general purposes with those of siloxane XLPE which has been recently developed.

(3) Evaluation of various properties with optimum percent gels.

These are summerised in the results and discussion.

2. MECHANIZM OF CROSS-LINKING

There are two principal manufacturing methods for cross-linking polymers. One is irradiated cross-linking using electron beams. The other is chemical cross-linking using, for example, peroxide. The difference between both methods depends on the mechanisms of formation of the polymer radicals which cause the reaction of cross-linking in polymers. In irradiated cross-linking, the polymer radicals are formed by irradiation energy of electron beams. But in chemical cross-linking, the polymer radicals are formed by thermal decomposition of peroxide.

On the other hand, the degradation of polymers by scission of chains of polymer molecules is caused at the same time. Polymers are classified into cross-linking types and degradation types according to the difference of the reaction rate between cross-linking and degradation. The molecular weight of polymers increases in cross-linking types, but decreases in degradation types by irradiation.

Table 1 Classification of radiation effect on polymers

Radical \ Types	Cross-linking types	Degradation types
-H	Polyethylene	—
$-CH_3$	Polypropylene	Polyisobuthylene
$-C_6H_5$	Polystylene	Polymethylstylene
$-\overset{\overset{O}{\|}}{C}-OCH_3$	Polymethyl-acrylate	Polymethylmeth-acrylate
$-\overset{\overset{O}{\|}}{C}-NH_2$	Polyacrylamide	Polymethylmeth-acrylate
-Cl	Polyvinyl-chloride	Polyinyliden chloride
-OR	Polyvinylallyl-ester	—

2-1 XLPE

Cross-lining mechanism in XLPE, such as irradiated cross-linking and chemical cross-linking by silane, is described in this paragraph.

(A) Irradiated XLPE

The mechanism is as follows:

(1) $\{CH_2-CH_2\}_n + e^- \longrightarrow \{CH_2-CH_2\}_n^{**}$

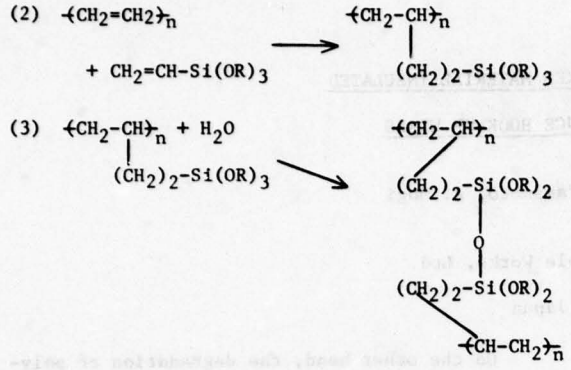
(2) $\{CH_2-CH_2\}_n^{**} \longrightarrow \{CH_2-\dot{C}H\}_n + H$

(3) $\{CH_2-\dot{C}H\}_n + \{\dot{C}H-CH_2\}_n \longrightarrow \{CH_2-CH\}_n$ with $\{CH-CH_2\}_n$ branch

(B) Siloxane XLPE

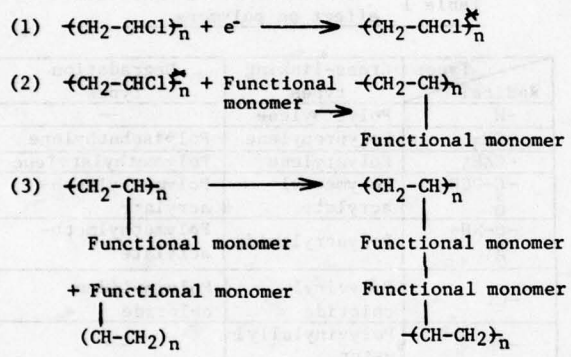
The mechanism is as follows:

(1) $\{CH_2-CH_2\}_n$ + Peroxide $\longrightarrow \{CH_2-CH_2\}_n^{**}$



2-2 XLPVC

Polyvinylchloride is cross-linked by irradiation of electron beams in a vacuum or inert gases. In air, decomposition is mainly caused by oxidation. For the purpose of preventing this decomposition, functional monomers are introduced and added to polyvinylchloride.
The mechanism is as follows:



Typical functional monomers are shown in Table 2. The acrylic functional monomers such as TMPTA, TMPTM, and TMGDM are effective.

Table 2 Functional monomers

TMPTA	Trimethylolpropane triacrylate
TMPTM	Trimethylolpropane trimethacrylate
TMGDM	Tetraethylene glycol dimethacrylate
TAIC	Triallyl cyanulate
DAP	Diallyl phtalate
TEGDM	Tetraethylene glycol diacrylate

3. PROPERTY IMPROVEMENT BY CROSS-LINKING

By cross-linking polymers, the following properties are improved:

(1) Thermal properties
(2) Mechanical properties
(3) Chemical properties

When we use cross-linked insulation for hook-up wires, we mainly aim to improve the thermal and mechanical properties.
Polyethylene and polyvinylchloride have their own melting point and softening temperature originally. If they are heated to more than these temperatures, they will melt or soften and be deformed. To improve these properties the structure of molecules is changed into gels by cross-linking. Cross-linked polymers become more resistant to melt and soften.
Because of the above mechanism, the thermal and mechanical properties of hook-up wires are improved.
The chemical properties are also improved, because polymers become more resistant to disolving in various solvents.
As for the thermal properties, there are two typical improvements. One is the improvement of the property of heat shock and the other is that of long term heat stability.

The above property improvements depend on percent gels of insulation. The percent gels are defined as follows:

(A) Percent gels of XLPE

$$\text{Percent gels} = \frac{\text{Weight of the residue after immersion}}{\text{Weight before immersion}} \times 100\ (\%)$$

Immersion: In 80°C xylene for 24 hours

(B) Percent gels of XLPVC

$$\text{Percent gels} = \frac{\text{Weight of the residue after immersion} - \text{Weight of fillers}}{\text{Weight before immersion} - \text{Weight of fillers}} \times 100\ (\%)$$

Immersion: In 50°C tetrahydroflan for 24 hours

Generally, the higher the percent gels, the better the thermal and mechanical properties are improved. However, when they become too high, the mechanical properties deteriorate-especially elongation. This shows that cross-linking is a certain process of degradation of polymers. It is very important to fully understand the relation of the properties with percent gels, and to utilize them effectively.

4. EXPERIMENTAL

4-1 Test specimens

Test specimens are as shown in Table 3 with various gels.

Table 3 Test specimens

PE	Polyethylene insulated wire	Conductor diameter: 0.5 mm
I-XLPE	Irradiated XLPE insulated wire	
S-XLPE	Siloxane XLPE insulated wire	Insulation thickness: 0.25 mm
PVC	Polyvinylchloride insulated wire	
XLPVC	Irradiated XLPVC insulated wire	Overall diameter: 1.0 mm

4-2 Tests

Table 4 Test methods

	Items	Methods
1	Melting point test	ASTM-D-2117
2	Heat deformation test	JIS C 3005
3	Tensile test	ASTM-D-1248
4	Heat shock test	MIL-W-16878D
5	Wrapping test after heating	—
6	Cold bend test	MIL-W-16878D
7	Solderbility test	MIL-W-16878D
8	Abrasion test	JIS C 3003
9	Slow compression test	UL Subject 758
10	Cut-through test	UL Subject 758
11	Electrical tests	ASTM-D-149, 257, 1531

5. RESULTS AND DISCUSSION

The properties of insulation with percent gels are shown in Figure 1 - 6. As shown in Figure 1, the melting point of XLPE increases gradually up to about 40% gels, but increases rapidly above 40% gels according to the increase of percent gels. According to this result, it is necessary to get more than 50% gels to obtain good thermal properties.

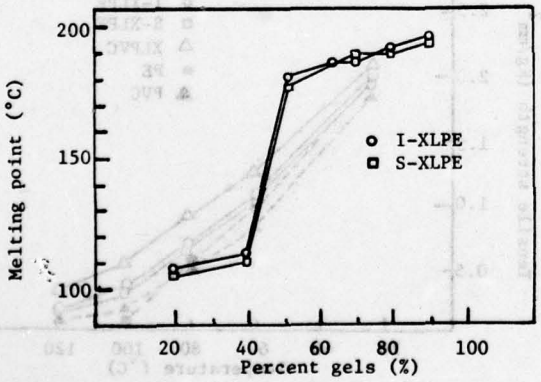


Figure 1 Change of melting point dependent on percent gels

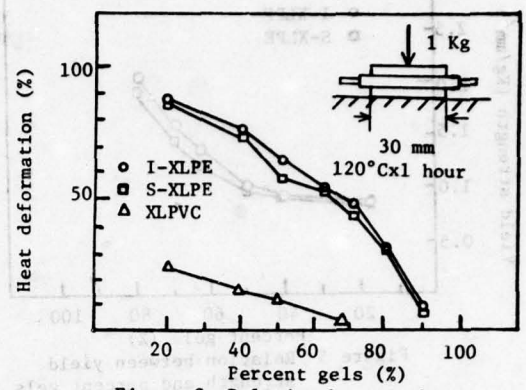


Figure 2 Relation between heat deformation and percent gels

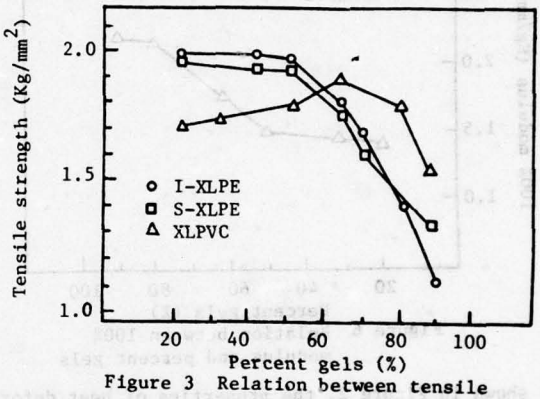


Figure 3 Relation between tensile strength and percent gels

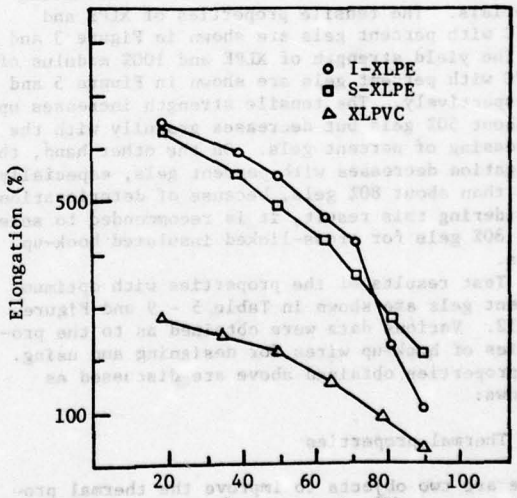


Figure 4 Relation between elongation and percent gels

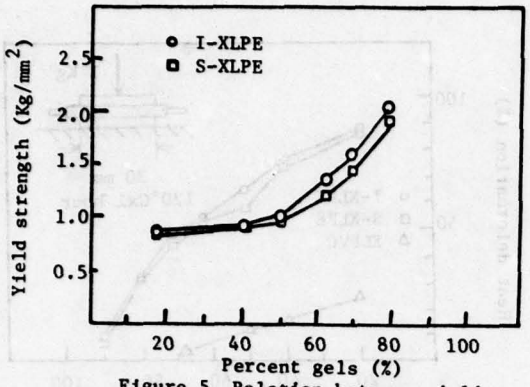


Figure 5 Relation between yield strength and percent gels

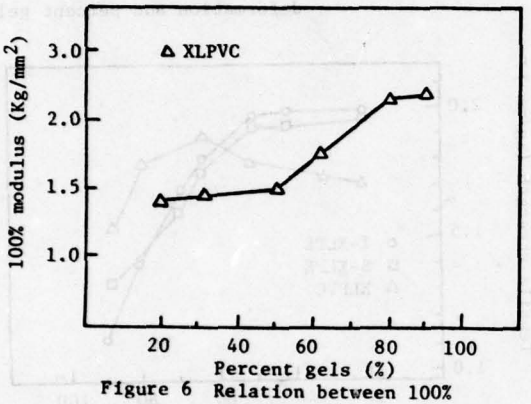


Figure 6 Relation between 100% modulus and percent gels

As shown in Figure 2, the properties of heat deformation are improved with increased percent gels. But it is undesirable to increase percent gels extremely because of deterioration of insulating materials. The tensile properties of XLPE and XLPVC with percent gels are shown in Figure 3 and 4. The yield strength of XLPE and 100% modulus of XLPVC with percent gels are shown in Fiugre 5 and 6 respectively. The tensile strength increases up to about 50% gels but decreases gradully with the increasing of percent gels. On the other hand, the elongation decreases with percent gels, especially more than about 80% gels, because of deterioration. Considering this result, it is recommended to select 50 - 80% gels for cross-linked insulated hook-up wires.

Test results of the properties with optimum percent gels are shown in Table 5 - 9 and Figure 7 - 12. Various data were obtained as to the properties of hook-up wires for designing and using. The properties obtained above are discussed as follows:

(1) Thermal properties

There are two objects to improve the thermal properties; one is improvement of the property of heat shock. The other is that of long term heat stability. We utilize the property of heat shock for such improvements as solderbility. The soldering

Table 5 Solderbility test

Specimens \ Properties	Melting	Shrinkage
PE	Deformed	Shrank
I-XLPE	None	None
S-XLPE	None	None
PVC	Deformed	Shrank
XLPVC	None	None

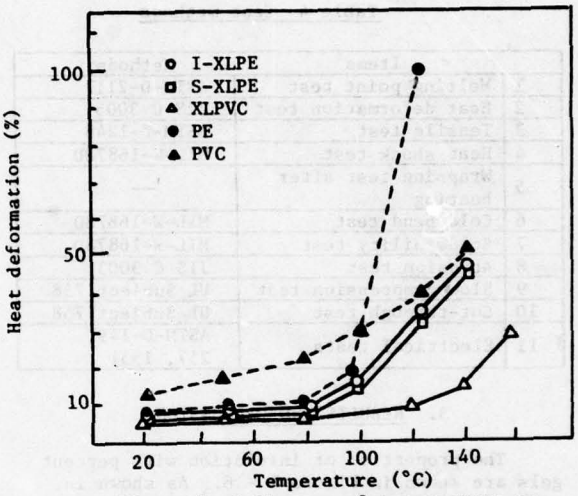


Figure 7 Influence of temperature on heat deformation

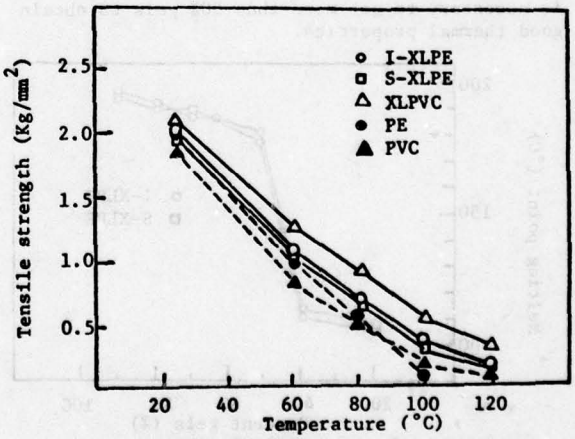


Figure 8 Influence of temperarure on tensile strength

Table 6 Thermal tests

Test itsms \ Specimens		PE	I-XLPE	S-XLPE	PVC	XLPVC
Heat shock test (150°Cx1 hour)	Cracks	Melted	None	None	Deformed	None
	Dielectric withstand (2 KV/1 min.)	Break down (melted)	Good	Good	Break down (deformed)	Good
Wrapping test after heating (150°Cx1 hour)	Cracks	Melted	None	None	Deformed	None
	Dielectric withstand (2 KV/1 min.)	Break down (melted)	Good	Good	Break down (deformed)	Good
Cold bend test (-50°Cx1 hour)	Cracks	None	None	None	None	None
	Dielectric withstand (2 KV/1 min.)	Good	Good	Good	Good	Good

Note: Mandrel diameter for wrapping or bending is as same as the diameter of wire

Table 7 Slow compression test

Specimens \ Radius of edge	0.15mm	1.6mm
PE	1.2kg	10.5kg
I-XLPE	1.4	13.0
S-XLPE	1.3	11.5
PVC	1.5	5.0
XLPVC	3.6	7.6

temperature is about 300°C, but we can prevent damage such as melting, deforming and shrinkage of insulation caused by contact with materials such as solder. Therefor, we can increase the efficiency of wiring for electronic appliances. The test result of solderbility is shown in Table 5. The un-cross-linked insulation shrank back and melted by soldering, but the cross-linked insulation did not. On the other hand, we utilize the long term heat stability for increasing the rating or using the hook-up wires at high temperatures. The heat deformation for various temperature is shown in Figure 7. The deformation of polyethylene increased extremely at temperatures greater than the melting point-about 100°C, but that of XLPE did not increase so much.

Table 8 Aging tensile properties

Temp.	Specimens / Properties / Period (days)	PE		I-XLPE		S-XLPE		PVC		XLPVC	
		T.S. (kg/mm^2)	EL. (%)	T.S. (kg/mm^2)	EL. (%)	T.S. (kg/mm^2)	EL. (%)	T.S. (kg/mm^2)	EL. (%)	T.S. (kg/mm^2)	EL. (%)
100	5	1.80	580	2.09	490	1.90	400	1.86	280	1.86	230
	10	1.83	560	1.97	470	1.87	380	1.79	260	1.82	230
	20	1.76	540	1.92	480	1.92	390	1.75	250	1.80	220
	30	1.91	560	1.92	470	1.78	350	1.82	230	1.89	210
120	5	Melted	Melted	2.11	470	1.81	360	1.88	240	2.01	220
	10	—	—	2.26	460	1.62	330	1.75	210	2.13	220
	20	—	—	1.96	440	1.17	250	1.71	210	2.04	210
	30	—	—	2.10	430	1.04	190	1.56	190	1.86	200
Unaged		1.85	660	2.0	550	1.95	430	1.75	290	1.80	230

Table 9 Electrical properties

Properties \ Specimens	PE	I-XLPE	S-XLPE	PVC	XLPVC
Volume Resistivity (Ω-cm)	Above $1x10^{16}$	Above $1x10^{16}$	Above $1x10^{16}$	$1x10^{15}$	$1x10^{15}$
Breake down voltage (A.C. KV)	Above 30	Above 30	Above 30	Above 30	Above 30
Dielectric constant (at 1MHz)	2.3	2.3	2.4	6.0	6.5
Dissipation factor (at 1MHz)	$3.0x10^{-4}$	$3.0x10^{-4}$	$5.0x10^{-4}$	$8x10^{-2}$	$9x10^{-2}$

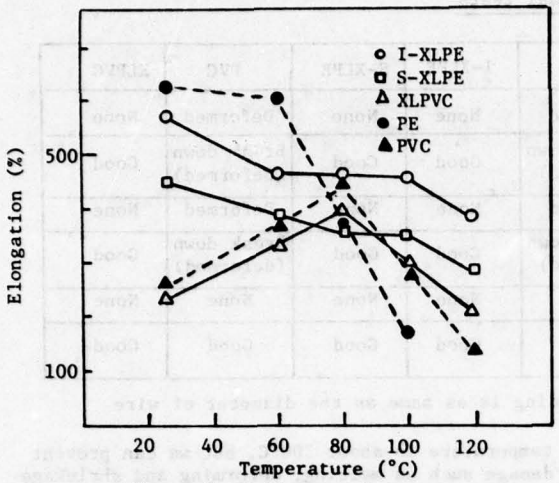


Figure 9 Influence of temperature on elongation

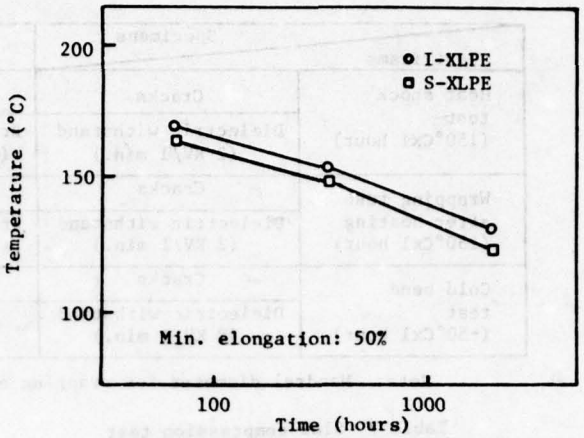


Figure 12 Long term heat stability

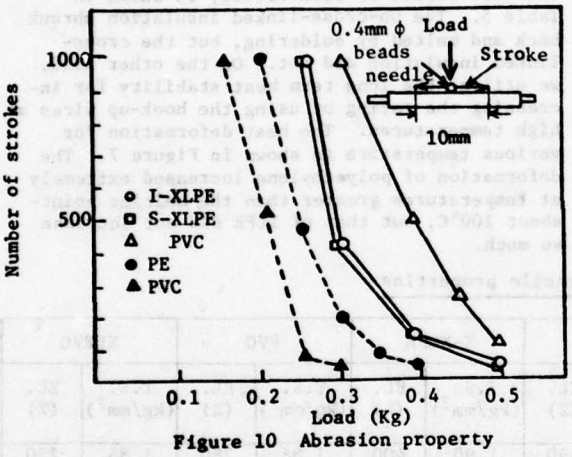


Figure 10 Abrasion property

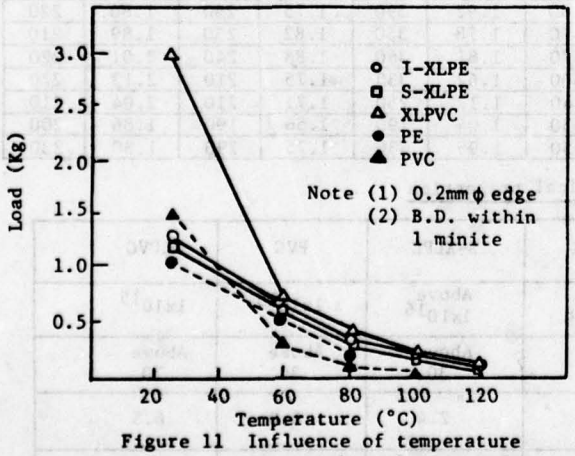


Figure 11 Influence of temperature on cut-through properties

We can use polyethylene at higher temperatures than the original melting point by cross-linking. This tendency is also seen in XLPVC. The tensile properties are shown in Table 8, Figure 8 and 9. As shown in these Table and Figures, the tensile properties show as same tendency as that of heat deformation.

(2) Mechanical properties

With increase of percent gels, the properties of tensile strength, abrasion, slow compression and cut-through are improved, but elongation properties are deteriorated. Improvement of abrasion properties are shown in Figure 10. The improvement of the property of XLPVC is evident compared with that of XLPE, therefore the XLPVC insulated hook-up wires are widely used for wire wrapping. This tendency is seen in the results of the slow compression test shown in Table 7 and the cut through test shown in Figure 11. This phenomenon relates to the hardness of the polymers. The yield strength of XLPE and the 100% modulus of XLPVC with percent gels are shown in Figure 5 and 6 respectively. The values increase at about 50% gels extremely. And at more than about 50% gels they increase gradually according to the increase of percent gels.

(3) Electrical properties

Generally polyethylene and polyvinylchloride possess excellent electrical properties, and are not affected by cross-linking practically. So, original electrical properties of these insulating materials can be utilized.

(4) The chemical properties

The chemical properties at high temperature are improved by cross-linking in the resistance to disolving in various solvents.

(5) Long term heat stability

The life of irradiated XLPE and siloxane XLPE is estimated in Figure 12 by means of Arrhenius' plots. Consequently the following typical results are obtained.

(A) With more than about 50% gels, the mechanical and especially thermal properties are improved remarkably, but with more than about 90% gels, the mechanical, especially tensile properties deteriorate.

(B) Greater deterioration of mechanical, especially tensile properties has been observed in irradiated XLPE than in siloxane XLPE, when percent gels are more than about 90%.

(C) In case of optimum percent gels, irradiated XLPE are superior to siloxane XLPE regarding mechanical properties and long term heat stability.

6. CONCLUSION

Property improvements of polyethylene and polyvinylchloride by cross-linking with various test results are described. This achievement can be applicable not only for hook-up wires but also for products in various fields such as shrinkable tube and highly expanded plastic, as melting points and softening temperatures increase. It is also advantageous for printing and adhesion because of oxidation and grafting on the surface of insulation. And we can use these cross-linked insulations for the control wires and cables in nuclear power plants by adding properties such as flame resistance, anti-radiation, and non-corrosion.

7. ACKNOWLEDGEMENT

The authors wish to express their thanks to many colleagues in The Fujikura Cablw Works, Ltd. who are engaged in the manufacturing and the development of hook-up wires.

8. REFERENCE

(1) Y. Tabata, Hoshasen Kako

(2) S. Machi et al, Japan Plastics, Vol. 125, No. 5, 70, 1974

(3) M. Ishibashi et al, Fujikura Technical Review, No. 45, 75, 1972

(4) H. Nishizawa, Rubber Digest, Vol. 28, 16, 1976

(5) W.A. Salmon and L.D. Loan, Journal of Applied Polymer Science, Vol. 16, 671, 1972

(6) M. Ishibashi et al, '76 National Convection of IECE of Japan, No.1670

(7) M. Ishibashi et at, '73 National Convection of IECE of Japan, No.1612

(8) L.D. Loan and W.A. Salmon, Bell Laboratory Record, 239, Sept. 1972.



Masashi Ishibashi

Head of Material Engineering Group, Telecommunications Research & Development Dept.
The Fujikura Cable Works, Ltd.,
1440 Mutsuzaki,
Sakura-shi, Chiba-ken,
Japan.

Mr. Ishibashi received B.S. degree in chemistry from Saitama University in 1959 and has been engaged in research and development of plastic materials and manufacturing method for electronic and telecommunication cables.
Mr. Ishibashi is a member of the Society of Polymer Science of Japan.



Tomohiro Yamamoto

Engineer of Telecommunication Cable Engineering Dept.
The Fujikura Cable Works, Ltd.,
1-5-1, Kiba, Koto-ku,
Tokyo, Japan.

Mr. Yamamoto received B.E. degree in electrical engineering from Kyusyu University in 1967 and has been engaged in engineering of electronic and telecommunication cables. Mr. Yamamoto is a member of the Institute of Electrical Engineers of Japan.



Akio Mogi

Engineer of Material Engineering Group, Telecommunications Research & Development Dept.
The Fujikura Cable Works, Ltd.,
1440 Mutsuzaki,
Sakura-shi, Chiba-ken,
Japan.

Mr. Mogi has been engaged in research and development of plastic materials and manufacturing method for electronic and telecommunication cables since 1965. Mr. Mogi is a member of the Society of Rubber Industry of Japan.

THE ROLE OF POLYMER PROPERTIES ON PERFORMANCE OF RETRACTILE CORD

Chong C. Ho

UNIROYAL CHEMICAL, Division of UNIROYAL, Incorporated
Naugatuck, Connecticut

ABSTRACT

A retractile cord offers space-saving and safety advantages over a straight cord. Retractile cords vary in size and design of the cord cross-section. Among the requirements for a retractile cord are pull-force and retraction after extension. Pull force and retractibility depend on cord design and polymer properties. An analysis of the mechanics of deformation of a retractile cord was made using the coil-spring equation which shows that the pull-force is related to the polymer modulus, and geometrical factors (coil radius, coil length, and cord diameter). Modulus of polymer is temperature, strain, and time dependent. Calculations show that in certain cord construction, the insulation is the load-carrying material despite the fact that its cross-sectional area is less than that of the jacket. Estimates of the shear-strain in the insulation upon extension of the retractile cord ranged from a few percents to over 20%, depending on cord construction.

INTRODUCTION

A familiar example of a retractile cord may be found in our telephone. Other applications of the retractile cord will be found in communication and test equipment. Retractile cord offers space-saving and safety advantages. When not in use, it retracts out of the way, thereby minimizing its potential of being a safety hazard.

A retractile cord is made by winding a straight cord on a mandrel, heat-setting, and unwinding. A cord generally consists of several insulated conductors wrapped by a jacket. The number of conductors varies from two for a simple test lead to more for communication application.

Retractile cords are made in various sizes. The coil diameter ranges from a fraction of an inch to several inches. The cross-section of the cord itself also varies - from ribbon-like to circular. In most cases, a major portion of the cord consists of polymeric materials.

Retractile Cord Performance Requirements

Performance requirement of retractile cord will, of course, vary depending on specific application. Two requirements are common to most applications. These are the pull force and retraction. Pull force refers to the effort required to extend the coil, and retraction refers to the ability of the cord to return to its coiled configuration when not in use.

Different manufacturers of retractile cords have developed their own methods of testing to meet these requirements. It is not the purpose of this paper to go into these testing methods. Rather, we are concerned with relating polymeric properties to cord performance.

MECHANICS OF A COIL SPRING

Force-Deflection Equation

The mechanics of deformation of a classical coil spring provides a basis in relating the retractile cord performance to polymer properties.

A coil spring is shown in Figure 1 as having a coil radius of R wound from a solid element having a diameter d and a length of l. We want to know the relationship between the force, F, required to extend the coil spring by a distance ΔY. The solution to this classical problem is given in the literature.[1]

$$\Delta Y = \frac{32\,FR^2l}{\pi\,G\,d^4}$$

or

$$\frac{F}{\Delta Y} = \frac{\pi\,G\,d^4}{32\,R^2l}$$

where

ΔY = extension of the coiled spring
F = force
R = radius of the coil
l = length of the unwound spring
d = diameter of the element
G = shear modulus of the spring material

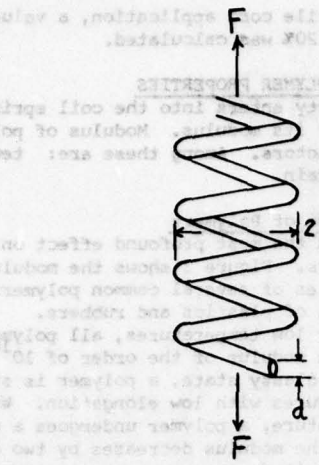
The derivation of the equation rests on the observation that the extension of the coil results from the twisting of the differential elements which result in the deflection or extension of the coil.

Geometrically, the equation states that the stiffness of the coil spring depends inversely on its radius squared, inversely to its length and depends strongly on the diameter of the element, namely, the diameter to the fourth power.

From a material standpoint, it is the modulus of the material which determines the stiffness of the coil. Modulus is defined as the ratio of stress/strain. Factors affecting the modulus of polymers will be briefly examined.

Stress and Strain Resulting from Coil Spring Deformation

As part of the derivation of the force-defletion



R = Radius of the coiled spring

d = Diameter of the spring element

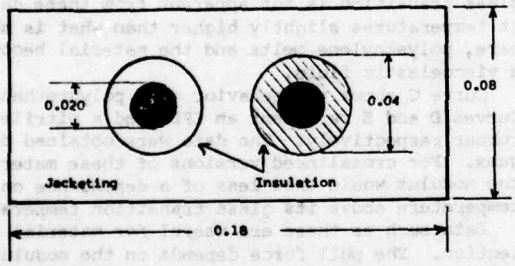
l = Length of the unwound spring

F = Force

ΔY = Extension of the coil

G = Shear modulus of the material

Figure 1: Model of a Coil Spring



Cross-Sectional Areas

Overall = $0.08 \times 0.18 = 0.0144$ in^2

Insulated wires = $\frac{2 \times \pi (0.04)}{4} = 0.00251$ in^2

Insulation only = $\frac{2\pi}{4}\left\{(0.04)^2 - (0.02)^2\right\} = 0.00188$ in^2

Jacketing material = $0.0144 - 0.00251 = 0.01180$ in^2

$$\frac{\text{Area of Jacketing}}{\text{Area of Insulation}} = \frac{0.01180}{0.001885} = 6.3$$

Figure 2: Cross-Section of a Simple Cord

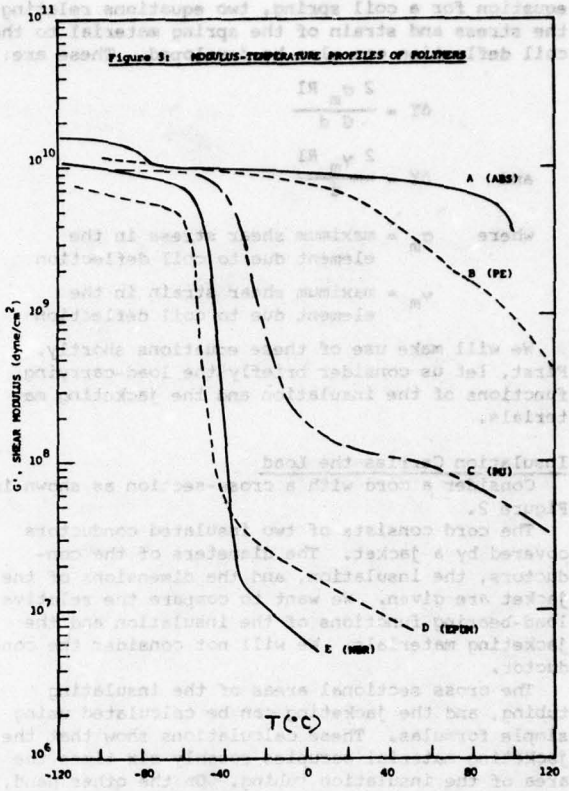


Figure 3: MODULUS-TEMPERATURE PROFILES OF POLYMERS

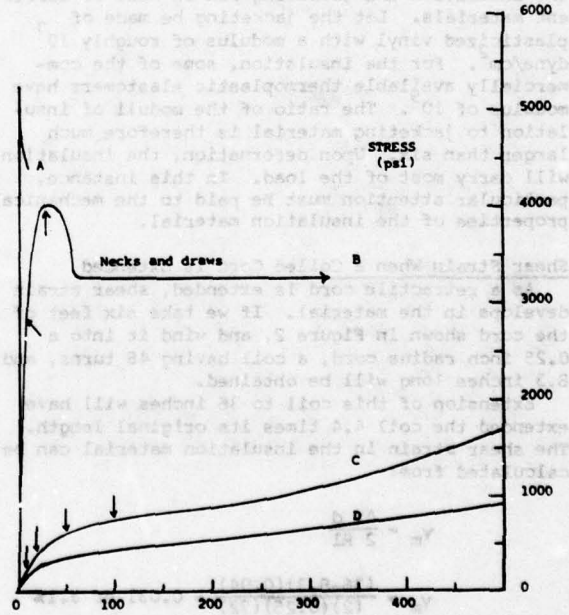


Figure 4: STRESS-STRAIN DIAGRAMS OF POLYMERS

equation for a coil spring, two equations relating the stress and strain of the spring material to the coil deflection can also be developed. These are:

$$\Delta Y = \frac{2\,\sigma_m\,R1}{G\,d}$$

and

$$\Delta Y = \frac{2\,\gamma_m\,R1}{d}$$

where σ_m = maximum shear stress in the element due to coil deflection

γ_m = maximum shear strain in the element due to coil deflection

We will make use of these equations shortly. First, let us consider briefly the load-carrying functions of the insulation and the jacketing materials.

Insulation Carries the Load

Consider a cord with a cross-section as shown in Figure 2.

The cord consists of two insulated conductors covered by a jacket. The diameters of the conductors, the insulation, and the dimensions of the jacket are given. We want to compare the relative load-bearing functions of the insulation and the jacketing materials. We will not consider the conductor.

The cross sectional areas of the insulating tubing, and the jacketing can be calculated using simple formulas. These calculations show that the jacketing material occupies roughly six times the area of the insulation tubing. On the other hand, the insulation and jacketing can be made of different materials. Let the jacketing be made of plasticized vinyl with a modulus of roughly 10^7 dyne/cm^2. For the insulation, some of the commercially available thermoplastic elastomers have modulus of 10^9. The ratio of the moduli of insulation to jacketing material is therefore much larger than six. Upon deformation, the insulation will carry most of the load. In this instance, particular attention must be paid to the mechanical properties of the insulation material.

Shear Strain When a Coiled Cord is Extended

As a retractile cord is extended, shear strain develops in the material. If we take six feet of the cord shown in Figure 2, and wind it into a 0.25 inch radius cord, a coil having 46 turns, and 8.3 inches long will be obtained.

Extension of this coil to 36 inches will have extended the coil 4.4 times its original length. The shear strain in the insulation material can be calculated from:

$$\gamma_m = \frac{\Delta Y\,d}{2\,R1}$$

$$\gamma_m = \frac{(36-8.3)(0.04)}{(2)(0.25)(72)} = 0.031 \text{ or } 3.1\%$$

This shows that although the overall extension of the coil is large, the actual strain of the material is quite low, of the order of a few percents in this example.

It is obvious that the value of the strain will vary depending on cord design and use requirement. In another retractile cord application, a value of strain as high as 20% was calculated.

POLYMER PROPERTIES

Material property enters into the coil spring equation simply by its modulus. Modulus of polymers depends on many factors. Among these are: temperature, time and strain.

Modulus-Temperature of Polymers

Temperature has the most profound effect on the modulus of polymers. Figure 3 shows the modulus-temperature profiles of several common polymers, including examples of plastics and rubbers.

At sufficiently low temperatures, all polymers become glassy with modulus of the order of 10^{10} dyne/cm^2. In its glassy state, a polymer is stiff, brittle, and fractures with low elongation. With increasing temperature, a polymer undergoes a glass transition where the modulus decreases by two or more orders of magnitude over a narrow temperature range. Above the glass transition temperature, the polymer becomes rubbery where the modulus is of the order of 10^6 - 10^7 dyne/cm^2. In its rubbery state, a polymer can be stretched to high elongation, and shows recovery when the force causing the elongation is released.

In Figure 3, A and B are examples of thermoplastics. C, D, and E are examples of rubbery materials.

More specifically, A is an ABS plastic. The decrease in modulus around -80°C. is due to the glass transition of the rubber which functions as the impact modifier.

Curve B is that of a high-density polyethylene. For polyethylene, the presence of crystallinity dominates its mechanical properties so that the glass transition is not apparent from these data. At temperatures slightly higher than what is shown here, polyethylene melts and the material becomes a viscoelastic fluid.

Curve C shows the behavior of a polyurethane. Curves D and E represent an EPDM and a nitrile rubber respectively. The data were obtained on raw gums. For crosslinked versions of these materials, the modulus would show less of a dependence on temperature above its glass transition temperature.

Data such as these are useful for material selection. The pull force depends on the modulus of the material. Where a retractile cord is to be used at low temperatures, the glass transition will determine whether a material is suitable.

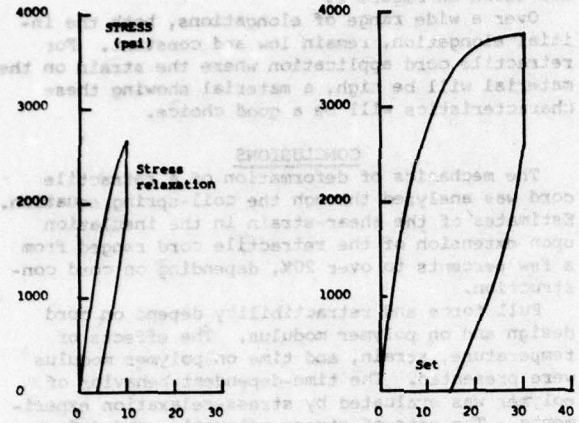
Stress-Strain Behaviors of Polymers

In comparing different polymers, it is common practice to compare their tensile strength and their elongation at break. For rubber compounds, the moduli at 100 and 200% elongations are often available.

For retractile cord application, it is necessary to look at the stress-strain behaviors of polymers in greater detail.

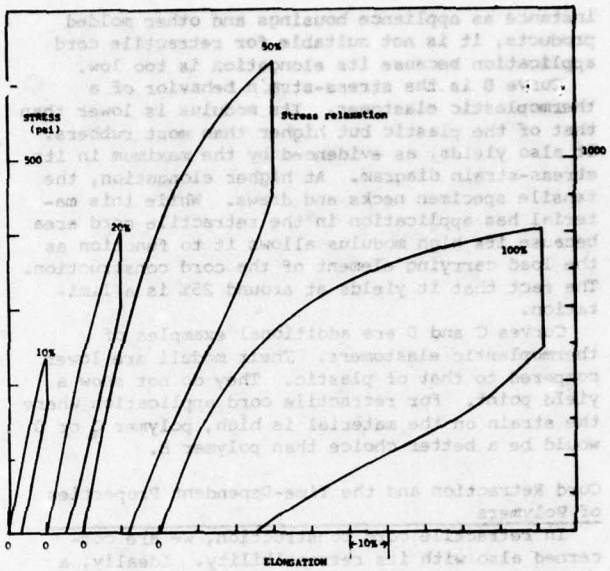
Figure 4 depicts the stress-strain behaviors of typical plastic and rubbers.

Curve A represents the behavior of a plastic. It is typified by high modulus. It exhibits a yield point at low elongation. At fracture, the percent elongation is about 15. While it finds wide application as an engineering plastic, for



	10%	30%
-b X 100	3.7	3.8
Set / Initial Elongation	35%	49%

Figure 5: STRESS RELAXATION ON POLYMER B



	10%	20%	50%	100%
-b X 100	4.0	3.6	4.1	5.2
Set / Initial Elongation	32%	25%	24%	25%

Figure 6: STRESS RELAXATION ON POLYMER C



instance as appliance housings and other molded products, it is not suitable for retractile cord application because its elongation is too low.

Curve B is the stress-strain behavior of a thermoplastic elastomer. Its modulus is lower than that of the plastic but higher than most rubbers. It also yields, as evidenced by the maximum in its stress-strain diagram. At higher elongation, the tensile specimen necks and draws. While this material has application in the retractile cord area because its high modulus allows it to function as the load carrying element of the cord construction. The fact that it yields at around 25% is a limitation.

Curves C and D are additional examples of thermoplastic elastomers. Their moduli are lower compared to that of plastic. They do not show a yield point. For retractile cord application where the strain on the material is high, polymer C or D would be a better choice than polymer B.

Cord Retraction and the Time-Dependent Properties of Polymers

In retractile cord construction, we are concerned also with its retractibility. Ideally, a retractile cord should return completely to its coiled configuration when it is not acted on by an external force.

Comparison of various polymers for retractibility can, of course, be achieved by constructing cables and simulation testing. This is time-consuming and expensive. Another approach is through the evaluation of the time-dependent properties of polymers.

Stress Relaxation

A very useful technique in studying the time-dependence of polymer properties is by stress relaxation. In a stress relaxation experiment, a specimen is extended rapidly to a predetermined elongation, and the force required to hold the specimen at that fixed elongation is measured as a function of time. The rate of change of the force provides a parameter for material comparison. At the end of the stress relaxation experiment, the deformation on the specimen can be reversed and the elongation at which the force drops to zero is measured. This gives a measurement of "set".

For correlation purposes, the force-time data from the stress relaxation experiments can be described by a linear logarithmic equation:[2,3]

$$\log (\text{stress}) = a + b \log (\text{time})$$

The parameter b is negative and is proportional to the percent decrease of the force per decade of time. The higher the absolute value of b, the more rapidly would the force decrease with time.

Stress relaxation results on polymer B (Figure 4) are shown in Figure 5 at 10 and 30% elongations. While the rates of stress relaxation as measured by the parameter b are not significantly different at 10 and 30%, the elongation set as a percent of the initial elongation is higher at 30% initial elongation compared to 10%. These results show that polymer B is not suitable in application where high strain on the cord material is expected.

Results of stress relaxation experiments on polymer C at 10, 20, 50 and 100% initial elongation are shown in Figure 6.

Over a wide range of elongations, both the initial elongation, remain low and constant. For retractile cord application where the strain on the material will be high, a material showing these characteristics will be a good choice.

CONCLUSIONS

The mechanics of deformation of a retractile cord was analyzed through the coil-spring equation. Estimates of the shear-strain in the insulation upon extension of the retractile cord ranged from a few percents to over 20%, depending on cord construction.

Pull force and retractibility depend on cord design and on polymer modulus. The effects of temperature, strain, and time on polymer modulus were presented. The time-dependent behavior of polymer was evaluated by stress-relaxation experiments. The rate of stress relaxation and deformation set at the end of stress relaxation were useful parameters for material comparison.

Much remains to be done, however, in the area of relating cord performance to polymer properties. Interaction between cord manufacturers and material producers is needed to develop the correlation between actual performance and laboratory measurements.

REFERENCES

1. Cottrel, A. H., Mechanical Properties of Matters, John Wiley & Sons, Inc., (New York, 1964), page 130.
2. Cotten, G. R. and Boonstra, B. B., J. Appl. Polymer, Sci., 9, page 3395-3408 (1965).
3. Meinecke, E. A., et al, Rubber Chem. & Tech. 51 (1), (1978), pages 117-125.



Chong C. Ho - Biographical Sketch

Chong C. Ho is a senior group leader at the Uniroyal Chemical Company at Naugatuck, Connecticut. He received his B.S. and M.S. in chemical engineering from the University of Idaho, and his Ph. D in chemical engineering from Reusselaer Polytechnic Institute. He joined Uniroyal in 1964 and has worked in the area of polymer physics: rheology, mechanical properties, and morphology of polymers and polymer blends. His mailing address is: Uniroyal Chemical Company, Spencer Street, Naugatuck, Connecticut 06770.

SHOULDER BREAKING PROBLEMS OF POLYETHYLENE SPECIMENS ON TENSILE STRENGTH TESTS

J. Cobo and M. Villarig

CABLES DE COMUNICACIONES S.A.
Zaragoza (Spain)

ABSTRACT

It is well known by all of us that test results obtained in a laboratory are greatly influenced by the conditions under which such tests are performed. Polyethylene tensile tests conducted on molded slabs well proves this fact.

A problem which we frequently come across on tension testing with different types of polyethylenes used for telephone cable insulation is the rupture of the "Dumbbell" specimen at the shoulder or at the widening point.

Some procedures and specifications normally used on tension testing on some polyethylenes do produce the above problem, thus causing the specimen to break before reaching its total extension.

The different testing procedures as requested by ASTM, REA, BS, VDE, UNE, etc. plus that of each individual user do not usually agree in type of specimen or in conditions. In some cases tolerance values are given which decisively influence the results.

In this Paper we have analyzed the influence which testing speed and shape of the specimen (including thickness and width) have upon the premature rupture of the specimen at the shoulder. We are also proposing a corrected method to obtain more reliable and consistent information.

1. The nature and importance of tension testing on polyethylenes

Tension testing is probably one of the most widely used requirements, however its theoretical aspect is not that well understood thus quite often overestimated. A good understanding of this test is important as the results obtained do greatly differ with changes in testing parameters. The most important ones are:

- Testing temperature
- Testing speed
- Thermal history of the specimen
- Molecular orientation of the specimen
- Shape, thickness and width

Should these factors not be properly chosen for each individual polyethylene or group of polyethylenes with the same behavior, one could obtain ruptures which are not within the reference marks of the test (at the shoulder or widening part of specimen). These results would obviously be incorrect and in turn would lead to an erroneous evaluation of the material.

1.1 The most important concepts of tension testing

Figure 1 shows us a typical experimental curve of a polyethylene tension test. This curve represents a load as a function of time or an increase in length ($L-L_o$), since the time and the increase in length are equivalent.

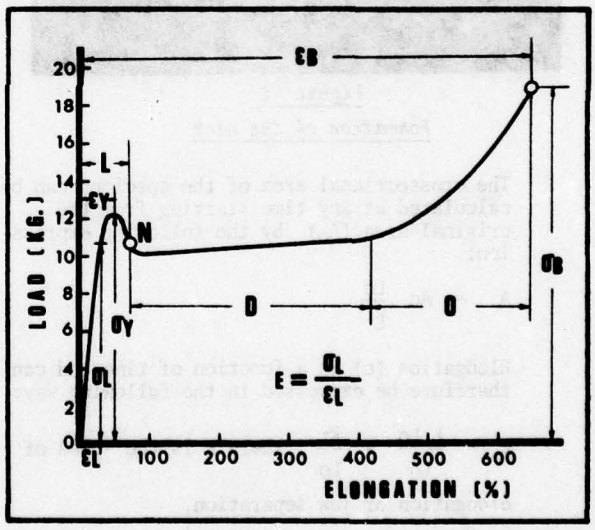


Figure 1
Tensile Curve

The symbols used are as follows:

L_o = Original length
L = Length at any given time
E = Young's modulus
σ_y = Yield stress
σ_L = Stress at inflexion point
σ_B = Tensile strength at break

ε_y = Elongaton at yield
ε_L = Elongation at inflexion point
ε_B = Elongation at break

One can calculate the tensile strength (σ) as a function of the original cross section. As the specimen cross section decreases during the stretching process, the true tensile strength is always greater than that calculated.

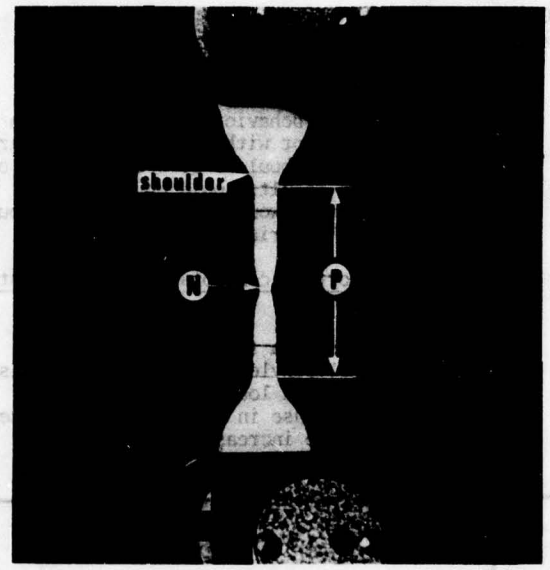


Figure 2

Formation of the neck

The crossectional area of the specimen can be calculated at any time starting from the original area (A_o) by the following expression:

$$A = Ao \frac{Lo}{L}$$

Elongation (ε) is a function of time and can therefore be expressed in the following way:

$$\varepsilon = \frac{L-Lo}{Lo} = \frac{Kt}{Lo}$$, where K is the speed of elongation or jaw separation.

The above mentioned elongation can sometimes be substituted by what is called "true elongation (ε_v) defined as:

$$\varepsilon_v = \int_{Lo}^{L} \frac{dL}{L} = \ln \frac{L}{L_o}$$

Tensile strength (σ_B) and elongation at break point (ε_B) are in practice the terms most commonly used. These terms are profoundly affected when the specimen breaks at the shoulder, thus not reflecting its true strength and elongation.

1.2 A study of the tension testing curve

The tension testing curve can be divided into the following regions:

Region L:

The part of the curve from origen to point N (where it begins to narrow down or where the neck starts to form as shown in figure 2).

In this region on which the curve shows the yield point, the specimen is subject to a more or less uniform deformation along this part (P) as shown in figure 2, where the elongation is proportional to the stress. Before reaching point N (where the narrowness or neck starts to form) the stress drops due to the formation of same.

From an applicational point of view this part of the curve in practice is the most interesting as it covers the maximum stress and elongation to which the conductor insulation is going to be submitted.

Region D:

This region also called "cold drawing" is where the stress rate of increase is very small compared to the elongation. The neck or narrow point which it has formed, gradually runs along the length of the specimen, the main extension or elongation being located in this region. During this process crystallite reorientation takes place due to the drawing of the polymer in the direction of the extension.

Region O:

In this region the narrow portion or neck has extended along the length of the specimen and once again the stress starts to rise at the same time as the specimen stretches.

A more uniform drawing takes place in this area, thus increasing considerably the molecular orientation of the material to rupture point.

1.3 Considerations

1.3.1 Thermal history

The thermal history of the sample from which the "dumbell" specimens are obtained is an important consideration. Variations in processing the molded slabs can greatly affect final results. An in-depth study of this factor would make this paper much too long. We shall try to explain this point in general terms which will help us to understand the remainder of this paper.

The polyethylene is formed by large molecules which make an orderly state

difficult to achieve as it is amorphously cooled (cast) to its solid state. The influence cooling has on highly branched polyethylenes is quite low. The branching points avoid the progression of crystallites above a certain level. Nevertheless there is an apparent influence on low chain branched polymers, which can themselves reach a high degree of crystallinity. For this reason and keeping in mind the low branch polymers, one can obtain a high level of crystallites with slow cooling from the melt stage to the solid.

A joint organization of the crystallites on slow cooling is also allowed, thus forming large spherulites (small associated and tridimensional ordinand glasses). On the other hand rapid cooled polyethylene contains smaller spherulites and greater amorphous regions. The problem we are working on in this paper is considerably accentuated when the specimen is slowly cooled from melt to solid. The effect of the treatment or thermal history in polyethylenes is greater the higher the density.

1.3.2 Molecule orientation

The molecules in compression molded materials have practically no orientation at all. Tension testing results and rupture problems for this reason are going to be influenced. A polyethlene which breaks before reaching its complete cycle may not experience this problem when tested with extruded material specimens. Extruded polymers possess a strong orientation in the direction of extrusion. The results of the tensile strength at break and elongation tests will be considerably improved when the material has its molecules orientated in the same direction of the stress imposed.

The granules of material for this study were first put through a rolling mill with its rollers properly heated to homogenize and melt the granules. The compound so obtained was then molded in a press which has an extremely high cooling capacity. The time taken up in lowering the temperature from 180°C to 30°C was approximately three minutes. The uniformity of the cooling was practically uniform at all points of the surface in the mold.

In this study we have centered ourselves on two factors which we consider extremely important; the speed of the test and the type of specimen (shape and crossection area).

1.4 Equipment and enviromental conditions

The apparatus used for testing plastics, as shown in figure 3 was an Instron dynamometer model 1026 equipped with special rubber jaws. The ambient temperature was maintained at 23°C and a relative humidity of 50%.

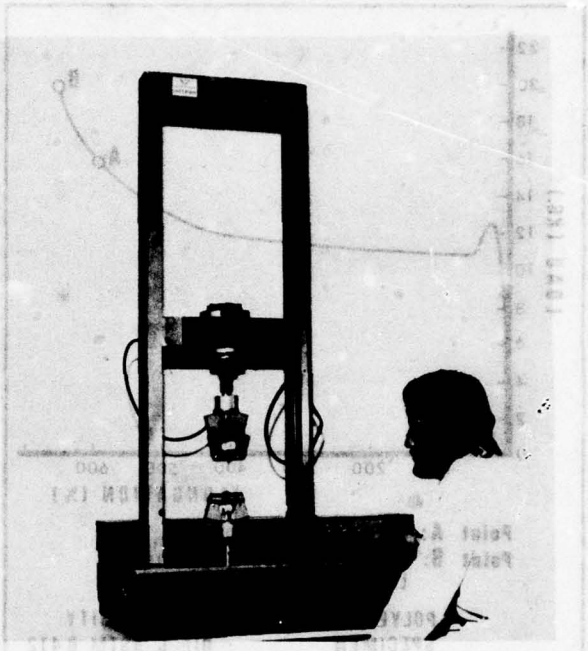


Figure 3
Dynamometer

1.5 Rupture problems

Figure 4 shows a typical curve of tension tests on low density high molecular weight polyethylenes used for cable insulation.

Point A corresponds to ruptures with the type of specimen and testing method, as described, which are commonly used in accordance to some specifications.

Point B corresponds to ruptures using a modified type of specimen.

In this case the specimen has only been modified with regards to its shape, keeping in this way the same width and thickness. Testing conditions have also been identical (speed of separation between jaws: 500 mm/min.).

With some types of polyethylenes a modification in the shape of the specimen, keeping constant other factors, may avoid ruptures at the shoulder or widening point.

The rupture of the specimen at point A is produced at the shoulder, whereas in point B the specimen broke within the specified marks.

If the specimen breaks at the shoulder as in the case of Point A, it has not finished its complete cycle and therefore will not show its maximum elongation and stress points.

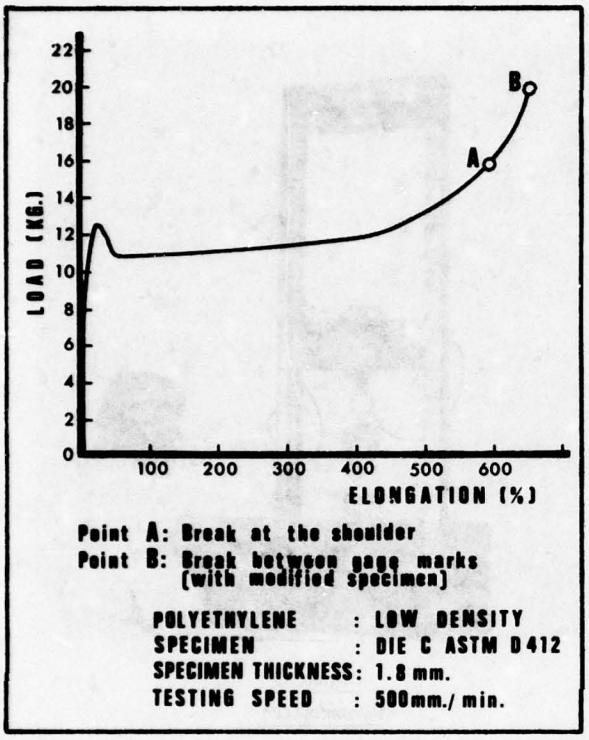


Figure 4
Tensile Test

Specimens which have been modified and break at the center do increase their elongation by 5% and their tensile strength at break by 20 to 25%.

Considering the high level of elongation obtained from these polymers, we should be careful in reaching conclusions about a given material based on a 5% difference. However this can and does influence the results, at different laboratories thus causing them to disagree in their results.

Regarding the tensile strength, the difference is more appreciable and could lead to a wrong interpretation when the value of a material is in question.

2. THE INFLUENCE OF TESTING SPEED

Table 1 shows us the results of the different types of ruptures with a speed of jaw separation of 50, 200 and 500 mm/min. Low, medium and high density polyethylenes commonly used as insulation on telephone cables were tested.

It can be seen that specimens prepared in accordance with ASTM 412 and tested at a speed of 500 mm/min. are more susceptible to failures as the compound density increases. Actually the rate of failures start to get pronounced on type I polyethylenes with a density closer to those of type II.

Medium and high density polyethylenes tested at speeds of 500 mm./min. do present mostly shoulder breaks of the specimens or the material only stretches a small part of the way, therefore breaking without hardly having extended. At speeds of 200 mm./min. the percentage of ruptures out of the specified marks on medium density polyethylenes is low, but the problem still exists on high density. To avoid this problem it is necessary to lower the speed down to 50 mm./min.

We all know that high density polyethylene molecules (long chains) have relatively few side branches, making them highly crystallite. On the other hand low density polyethylenes have highly branched chains and therefore present a greater quantity of amorphous regions and consequently less proportion of crystallite. Molecular slip in polymer stretching is much more difficult with a high level of crystallite. Its molecules are in order and closely packed together, thus presenting a linkage between them which oppose or resist deformation. The molecules do not have sufficient time to adapt themselves to the new positions when the testing speed is too high, consequently rupture takes place before the cycle can be completed. This problem takes a more serious aspect when the material has no molecule orientation in the direction of the stress.

The various types of polyethylenes tested can be seen on the graph in Figure 5, the curves correspond to the elongations experienced with the specimens up to the forming of the neck (the start of region D) as could be seen in Figure 2.

The elongation produced during this period, as we have already mentioned is distributed to nearly the whole specimen, this can therefore give us an idea of its attitude towards deformation.

Polyethylenes with a lower density (Young's modulus which is lower to those of higher densities) give higher elongation in the area mentioned to those which have a higher density.

We can see from the graph that as the testing speed decreases the elongation on the treated area increases with all the polyethylenes tested. Consequently deformation has a higher level of uniformity along the length of the specimen.

Figure 6 shows the elongation experienced in zones 2 and 3 of the specimen ASTM (figure 7) before the narrowing is reached. Speed of jaw separation of 50 and 500 mm/min. were used. One can clearly see that the specimens tested at low

TABLE I

PERCENTAGE OF BREAKS OCCURRING OUTSIDE GAUGE MARKS AT DIFFERENT TESTING SPEEDS

POLYETHYLENES	SPECIMEN THICKNESS (mm)	SPECIMEN ASTM TESTING SPEED mm/min. 50	200	500	SPECIMEN E TESTING SPEED mm/min. 50	200	500
B_{23}	1.8	10	10	50	10	10	10
	1.0	10	10	30	10	10	10
B_{25}	1.8	20	20	90	10	10	10
	1.0	20	10	80	10	20	10
M_{28}	1.8	10	40	100	10	10	10
	1.0	10	10	100	10	20	10
M_{30}	1.8	20	20	100	10	10	20
	1.0	20	20	60	20	20	20
A_{43}	1.8	40	100	100	10	70	100
	1.0	30	40	100	10	10	50

POLYETHYLENES

	Type	Density	Class	Category
B_{23}	I	0.923	A(Nat.)	5
B_{25}	I	0.925	A "	5
M_{28}	II	0.928	A "	5
M_{30}	II	0.930	A "	5
A_{43}	III	0.943	A "	4

speeds have produced greater deformation with the same elongation between the specified marks, therefore the speed per unit length at any given time has a higher and spread out uniformity. Further on in this paper it can be easily understood how this curve was obtained.

3. ANALYSIS OF THE REASONS WHY THE SPECIMENS BREAK AT THE SHOULDER AT HIGH TESTING SPEEDS

Polyethylenes from Type I were chosen for this study with a density of 0.925 gr/cm3, quite close to those of Type II.

This material presented rupture problems at the widening or shoulder area of the specimen with a speed of jaw separation of 500 mm/min. On specimens die cut per ASTM (see figure 7), we observed that on 90% of the cases the failures occurred in zone 3.

If we were to divide specimen type C (ASTM D-412) into zones as can be seen in figure 7, and examine the elongation which is experienced by each individual zone during the test, we would find that although the highest percentage of elongation corresponds to the narrowing zone, a

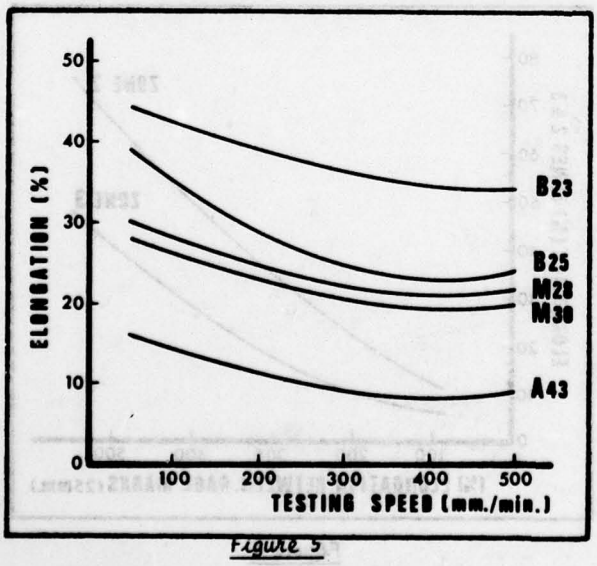


Figure 5

Relation of testing speed to elongation up to narrowing point

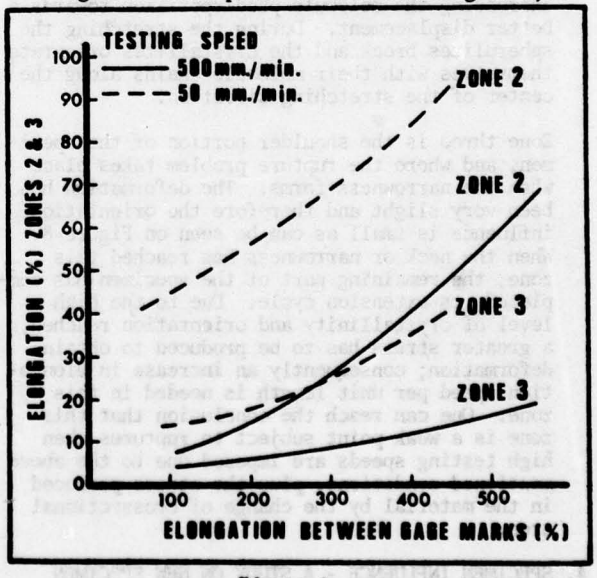


Figure 6

Relation of elongation in zones 2 and 3 to elongation between gauge marks at two testing speeds

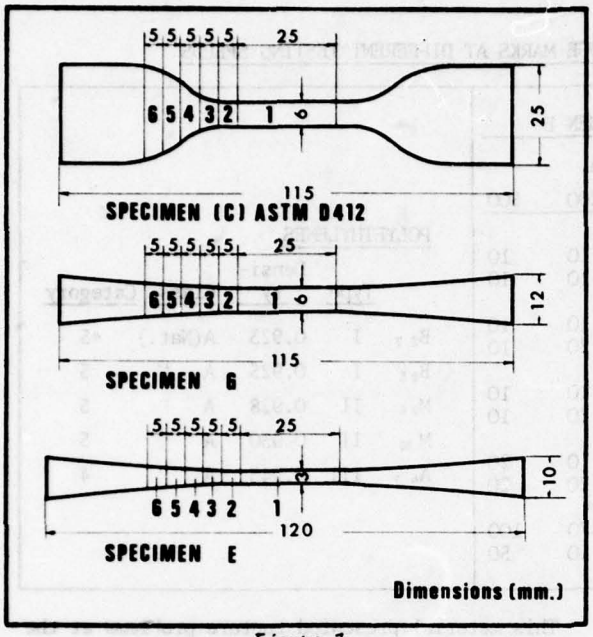


Figure 7

Types of specimens used showing areas studied

progresive stretching is being produced in other zones, which is not apparently affected.

Zone 2 with an identical width to that of the testing reference has shown considerable elongation just before producing its narrowness. Consequently this zone has formed a certain molecule orientation in the direction of the stress, thus increasing the molecule predisposition towards a better displacement. During the stretching the spherulites break and the crystallites orientate themselves with their molecule chains along the center of the stretching direction.

Zone three is the shoulder portion of the specimen, and where the rupture problem takes place when the narrowness forms. The deformation has been very slight and therefore the orientation influence is small as can be seen on Figure 8. When the neck or narrowness has reached this zone, the remaining part of the specimen has completed its extension cycle. Due to the high level of crystallinity and orientation reached, a greater stress has to be produced to obtain deformation; consequently an increase in elongation speed per unit length is needed in this zone. One can reach the conclusion that this zone is a weak point subject to ruptures when high testing speeds are imposed due to the above mentioned conditions, plus the stress produced in the material by the change of crossectional area.

4. SPECIMEN INFLUENCE - A STUDY ON NEW SPECIMEN DESIGNS

Our laboratory has designed two types of specimens

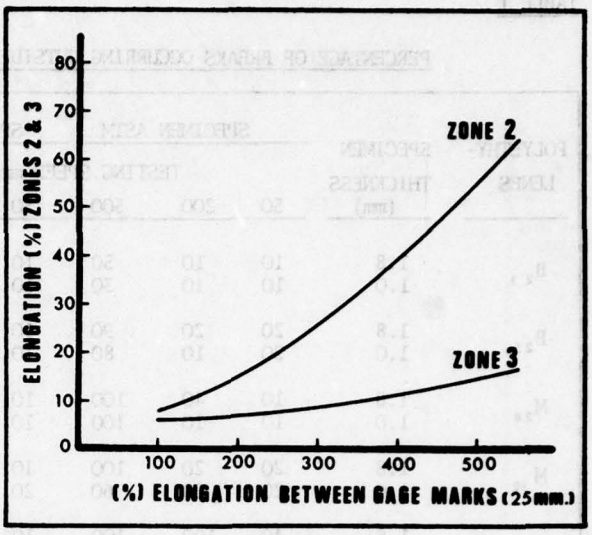


Figure 8

Elongation in zones 2 and 3 of the specimens per ASTM D-412

as can be seen in figure 7. Our intention has been to find ways of reducing the effects caused by ruptures of the widening areas (shoulder of specimen). This study has also been divided into zones.

Table I shows us the improvements obtained with the rupture using type E specimens. This has been the only modification in testing conditions.

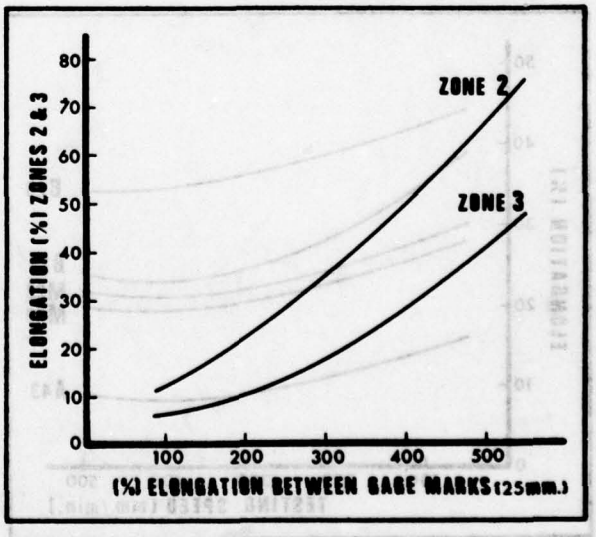


Figure 9

Elongation in zones 2 and 3 of specimen G

Excluding high density polyethylenes, ruptures at speeds of 500 mm/min. in most cases were produced within the specified reference or bench marks.

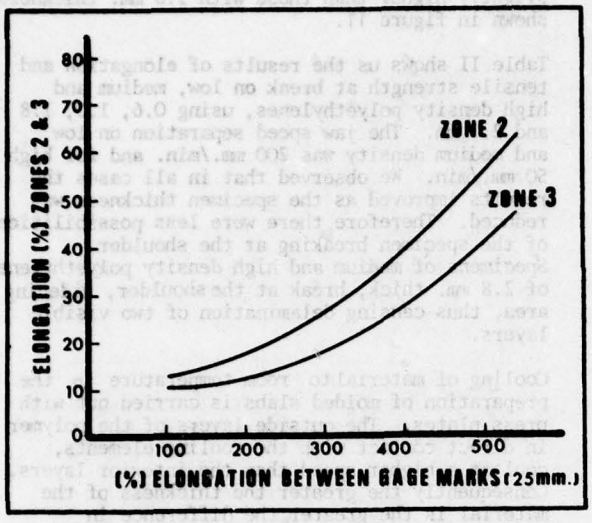


Figure 10

Elongation in zones 2 and 3 of Specimen E

Figure 8, 9 and 10 reflect the deformations experienced in zones 2 and 3 of the specimens, before reaching narrowness, in relation with the elongation increase of zone 1. (zone between reference marks where narrowness progresses). Deformation of zone 2 on the three types of specimens is very similar. However zone 3 of the specimen (ASTM D-412) experienced a substantial lower elongation compared to corresponding zones on specimen types G and E.

The graphs shown in Figures 11 and 12 demonstrate the deformations experienced by the different zones of the specimen, at the time the narrowness or neck produced by the elongation reaches these zones. The elongation percentage in zones 5 and 6 of specimen ASTM have been obtained by deduction due to the fact that the narrowing does not reach this zone. It can clearly be appreciated that specimen G as well as specimen E have produced a progresive and uniform deformation in the different zones, therefore the elongation speed per unit length at any point is slower or more gradual than ASTM specimens, when narrowness reaches these zones. On the other hand the stress experienced by the material with section change is lower due to its gradual change in crossection. The material also progresively orientates itself in the direction of the stress, in this way the molecules obtain a better disposition to withstand deformation. These tests were carried out under the same conditions with low density polyethylenes (0.925 gr./cm3).

We have found that on high density polyethylenes the elongation of the different zones, as the neck or narrowness is formed, is much lower than with low density polyethylenes. Figure 13 shows

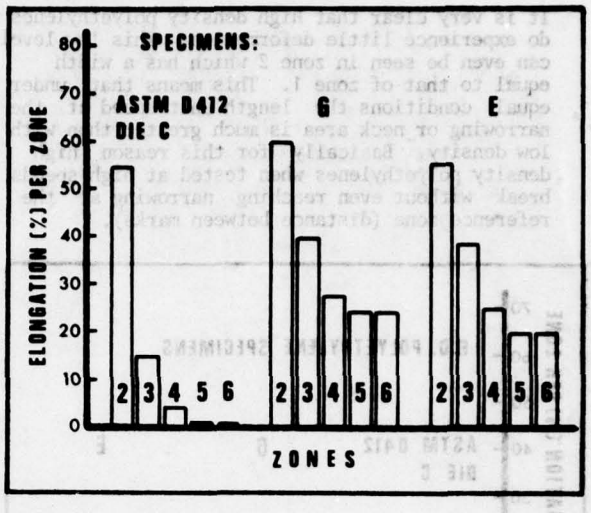


Figure 11

Elongation in different zones with 1.8 mm.thick specimens

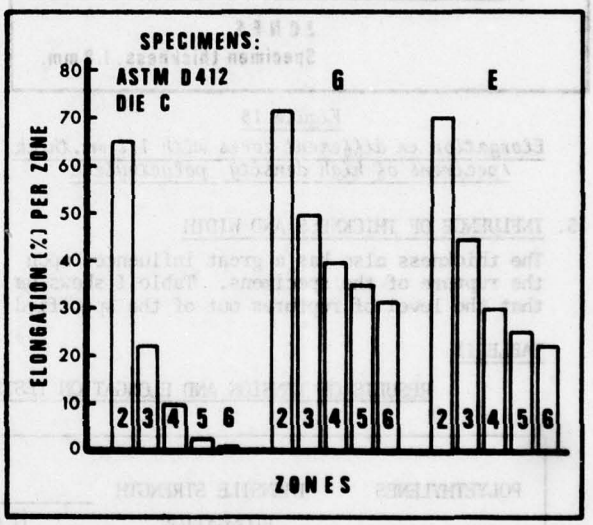


Figure 12

Elongation in different zones with 1.0 mm.thick specimens

us that the elongation is excesively low in zone 2 at the time when narrowness reaches it when compared to those formed of low density polyethylenes. One should keep in mind that the test in this case was performed at a speed of 50 mm./min. If it had been carried out at 500 mm./min. as with low density, deformation would have been even lower. A relative value could be obtained form figure 6 which showed us the difference in the deformation of low density(B_{25}) polyethylenes at speeds of 50 and 500 mm/min.

It is very clear that high density polyethylenes do experience little deformation. This low level can even be seen in zone 2 which has a width equal to that of zone 1. This means that under equal conditions the length unit speed at the narrowing or neck area is much greater than with low density. Basically for this reason high density polyethylenes when tested at high speeds break without even reaching narrowing at the reference zone (distance between marks).

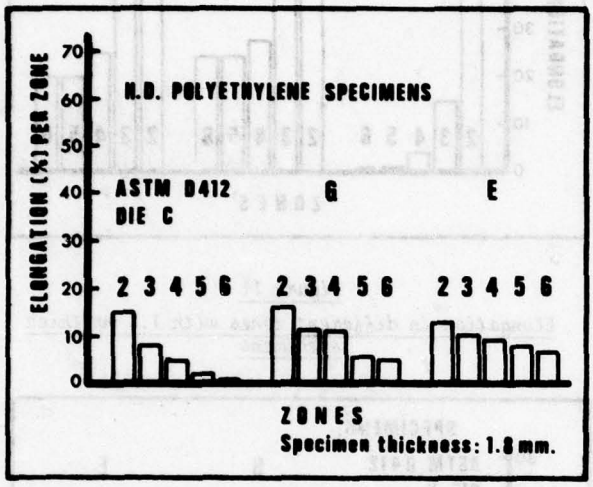


Figure 13

Elongation in different zones with 1.8 mm. thick specimens of high density polyethylene

5. INFLUENCE OF THICKNESS AND WIDTH

The thickness also has a great influence upon the rupture of the specimens. Table I shows us that the level of ruptures out of the specified reference marks is lower with 1.0 mm. specimen thickness. One can also appreciate from figure 12 how the deformation in the different zones of the specimen with the same thickness (1.0mm.) are slightly higher than those with 1.8 mm. thickness shown in figure 11.

Table II shows us the results of elongation and tensile strength at break on low, medium and high density polyethylenes, using 0.6, 1.0, 1.8 and 2.8 mm. The jaw speed separation on low and medium density was 200 mm./min. and for high 50 mm./min. We observed that in all cases the results improved as the specimen thickness was reduced. Therefore there were less possibilities of the specimen breaking at the shoulder. Specimens of medium and high density polyethylenes of 2.8 mm. thick, break at the shoulder, widening area, thus causing delamination of two visible layers.

Cooling of material to room temperature in the preparation of molded slabs is carried out with press plates. The outside layers of the polymer in direct contact with the cooling elements, cool at a higher speed than the interior layers. Consequently the greater the thickness of the material is the greater the difference in temperature of the outside layers with regards to the inside.

Different cooling speeds cause the formation of various grades of crystallite in the polyethylenes and a subsequent stress which affects the rupture. The above mentioned delamination phenomenon formed by the stretched material and quite frequently found with medium and high density polyethylenes has been previously explained. Figure 14 shows us layers L and L', which are the closest to the refrigerant and cool at a higher speed than the interior layer I. As the cooling in layer I is much slower, the

TABLE II

RESULTS OF TENSION AND ELONGATION TESTS WITH SPECIMENS OF VARIOUS THICKNESSES

POLYETHYLENES	THENSILE STRENGTH / ELONGATION	THICKNESS (mm) 0.6	1.0	1.8	2.8
B_{25}	Kgr/cm²	176	167	160	152
	%	700	680	710	660
M_{30}	Kgr/cm²	185	173	167	155 *
	%	740	770	685	640 *
A_{43}	Kgr/cm²	290	286	266	145 *
	%	870	855	845	620 *

* For the 2.8 mm. specimens of M_{30} and A_{43}, breaks occurring at the shoulder producing delamination

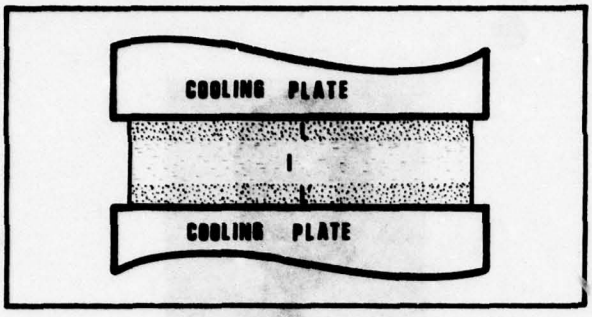


Figure 14

Layers formed in molded material due to rapid cooling

crystallinity of the material is greater than the outside layers, thus forming stresses which consequently affect the rupture. The stretching of the outside material due to its low crystallinity has a higher flexibility than that of the interior layer. We find that due to this at the end of the test the material separates and delaminates. This point becomes more acute the thicker the molded slab.

The width of the specimens is also an important point to keep in mind, although its influence is lower than the factors previously mentioned. Table III shows the results of the tensile strength at break and elongation tests carried out on low, medium and high polyethylenes, using 3, 4 and 6 mm. widths. The jaw separation speeds were 200 mm./min. for low and medium density and 50 mm./min. for high. An improvement has been noted with the reduction in the width of the specimen as it also reduces the possibilities of the specimen breaking at the shoulder. A more positive result has been obtained from E type specimens with a narrower width than that of type G.

6. CONCLUSIONS

The investigation has shown that the shape and thickness of the specimen as well as the test speed have an important influence on shoulder ruptures. This influence increases depending on the density of the polyethylenes, thus the higher the density the greater the influence.

The above mentioned rupture problems do slowly disappear when the test speed is lowered, therefore it hardly exists at low speeds.

A specimen design such as the ones studied in this paper does improve and avoid the problem with most types of polyethylenes, even at high speeds of separation between jaws.

There are large differences between the various procedures and specifications, in most cases concerning the application of the points stressed in this paper. If these parameters are not properly chosen to cope with the different peculiarities characteristic of the polyethylenes which form a group (type) the influence upon tension testing is a risk and does evidently cause the specimen to break before the material reaches its complete extension.

ACKNOWLEDGEMENTS

The authors gratefully acknowledge the colaboration of the Physic-Chemistry Laboratory staff and to Mr. J. Perez for all the tests performed. We are also grateful to Messrs. F.W.Horn and J.Z. Avalos for their comments and help in preparing this manuscript.

REFERENCES

1. The Nature and Properties of Polythene
Imperial Chemical Industries Ltd. 1964

2. Mechanical Properties of Polymers
L. Nielsen - Van Nostrand Reinhold Co. N.Y.1962

TABLE III

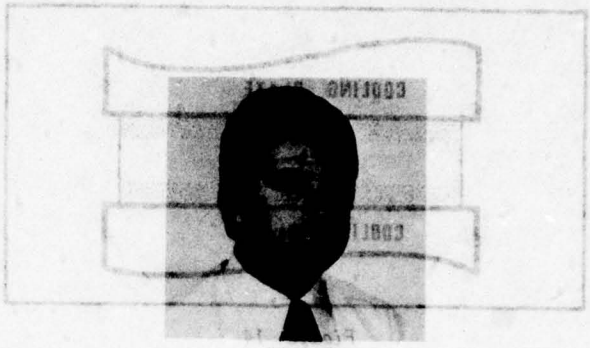
RESULTS OF TENSION AND ELONGATION TESTS WITH SPECIMENS OF VARIOUS WIDTHS

POLYETHYLENES	TENSILE STRENGTH / ELONGATION	WIDTH (mm) 3	4	6
$B_{2.5}$	Kgr/cm²	199	180	177
	%	730	740	700
$M_{.30}$	Kgr/cm²	205	188	165 *
	%	820	845	640 *
$A_{4.3}$	Kgr/cm²	321	293	275
	%	880	900	840

* Specimens broke at the shoulders



Manuel Villarig has a degree in telecommunications engineering from the E.T.S.I.T. (Escuela Tecnica Superior de Ingenieros de Telecomunicación) of Madrid and is Director of Research and Development with Cables de Comunicaciones, S.A. in Zaragoza, Spain. Mr. Villarig joined CCSA immediately upon graduation and started as a process technician. His assignments have included engineering projects related to the plant start-up and he was also assigned various special projects in process and product engineering until this year when he was promoted to his present position.



Julio Cobo graduated in 1969 from Escuela Universitaria de Ingenieria Tecnica Industrial de Santander with a degree of Ingeniero Tecnico Quimico. He joined C.C.S.A. located at Zaragoza, Spain in 1972 and is now in charge of the Physics-Chemistry Laboratory of the Research and Development Department.

THE RAPID EVALUATION OF THE PROCESSABILITY OF POLYETHYLENE RESINS FOR USE ON HIGH SPEED INSULATING LINES

by

E.P. Marsden

Northern Telecom Canada Limited
Montreal, Quebec

ABSTRACT

The shop trial is the arbiter of processability. As such trials are costly in lost production time, a laboratory method is needed which can predict processability. However, capillary rheometry indicates that at the shear rates encountered during insulating, all the polyethylenes being screened were virtually identical, although shop trials showed that some of these materials exhibited high spark rates, surface roughness and, occassionally, a tear-like separation of the insulation skin from the foam core. The results of simple experiments show that high speed insulating with polyethylene resins has more in common with melt spinning than with capillary extrusion. Using the Rheometrics mechanical spectrometer and a melt tension apparatus, it can be demonstrated that the extensional properties of the melt can predict the processability of polyethylene materials and readily distinguish between blends and homopolymers.

INTRODUCTION

In order to introduce a new insulating material, it is necessary to conduct a full-scale shop trial. If these trials are unsuccessful, the cost in lost production time and scrap charges is high. Thus, it is becoming increasingly important that some quick method of laboratory testing be available to identify and quantify those material properties which are critical to processability. A successful solution to this problem would enable a company to provide a list of requirements, "a processability passport", to its suppliers of PIC insulating resins.

Laboratory measurements of such fundamental physical properties of polymers as melting point, viscosity, tensile strength, etc. are routinely applied in industry as instruments of quality control and to predict behaviour under conditions of use.

A far more difficult exercise is to predict processability from laboratory experiments, since the latter are designed to be relatively simple and industrial processes are rarely so. A prerequisite of any attempt at predicting processability is to design a model which identifies those properties of the material which are relevant and which takes account of the relative importance of these properties in describing the overall process. Such a model, which will inevitably contain many simplifications should be such that it suggests measurements of certain fundamental properties of the polymer which will adequately describe the behaviour of the material under processing conditions. Oversimplification will lead to an incorrect analysis and hence will not adequately predict processability. Overcomplexity on the other hand will result in so many measurements being made in the laboratory that, even though the model allows processability to be accurately predicted, it would be easier, less time-consuming and less costly simply to conduct a shop trial.

In this report, an attempt is made to predict the processability of medium and high density polyethylene resins which are used, or are being considered for use for PIC insulation.

RESULTS AND DISCUSSION

Medium density and high density resins are used for filled core cables, both as a solid insulation and as a skin on the foam skin construction. These materials can be homopolymers or, in the case of some medium density materials, blends of high and low density polyethylene.

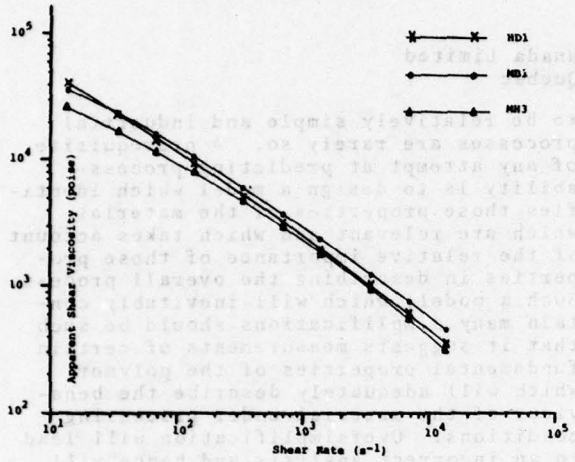
Shop experience has shown that some materials would run well on any construction at high line speeds whereas others could not be run even at low line speed. Clearly the key to the problem must lie in the rheological properties, but which properties and under what test regime?

Figure 1 illustrates the problem. The three resins are little different at the shear rate encountered during processing, i.e. $10^4 \rightarrow 10^5\ s^{-1}$, yet their processability is different. MB1 and HD1 process well but MH3 exhibits a very high spark

rate during insulating.

FIGURE 1

PLOT OF APPARENT SHEAR VISCOSITY AGAINST SHEAR RATE FOR VARIOUS POLYETHYLENES



Furthermore, although insulated conductors of the correct O.D. and with a smooth insulation surface are produced by the high speed insulating process, the same materials, when extruded through a capillary rheometer show marked die-swell and severe melt fracture[1].

Thus, it is clear that capillary rheometry is not descriptive of the wire insulating process and some mechanism other than simple visco-elastic response to an imposed shear stress must dominate the wire insulating process.

The flow field in the crosshead die is complex. Pressure flow from the extruder is augmented by drag flow due to the passage of the wire through the die[3]. Since the velocity profile of annular flow and drag flow differ significantly, the resulting velocity profile and shear flow fields will be complex[4,5].

Although it is widely accepted that the shear and elastic forces generated in the die influence such phenomena as die swell and surface finish, it is becoming increasingly clear that processes such as extrusion, injection moulding and foaming include significant extensional as well as shear flows[1,5,6]. And in processes such as melt spinning extensional forces will clearly dominate. Furthermore, there is evidence to suggest that extensional processes outside the die influence both the degree of die swell in melt spinning[7] and shear flow within the wire crosshead[4].

Conversely, visco-elastic responses of the melt to the extrusion process can influence many of the parameters critical to the melt spinning process, e.g. the degree of die swell will determine the take-up rate necessary to produce filament of a given diameter.

Furthermore, it is known that in melt spinning a smooth filament can be produced even when the extrudate from the spinerette die shows melt fracture[8], and that the smoothing effect is more marked the greater the extensional force, i.e. take-up rate, and the longer the extensional force is allowed to act, i.e. the longer the air gap[9].

It is, therefore, proposed that extensional forces outside the die dominate the wire insulating process, and that the balance of these external extensional forces and the visco-elastic forces within the die determine the ease and degree of drawdown and the surface finish of the insulation.

To test this proposal, two simple experiments were carried out, the aims of which were to produce, using the same material, insulated conductors and extruded filaments over a similar range of shear rates, and to compare the surface characteristics and die-swell of the two products.

Firstly, a 24 AWG wire was insulated with MB1 using a standard PIC 1.016 mm (0.040") die. When melt was spewed through the die with the conductor stationary, the surface of the tubular extrudate was extremely rough. The line speed was then increased stepwise until the insulation was smooth.

Table 1 summarizes the results which are also shown graphically in Figure 2.

TABLE 1

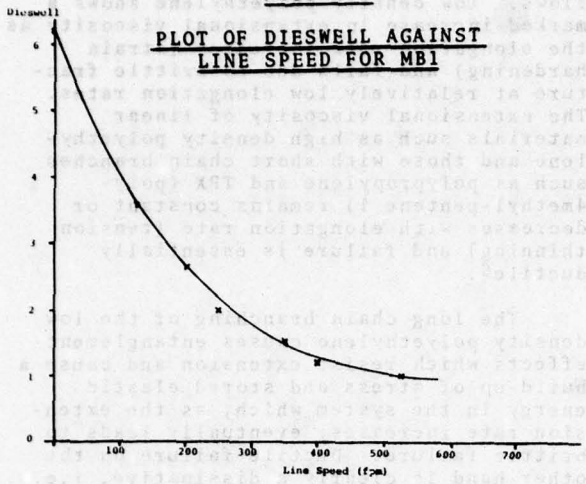
EXTRUSION OF MB1 ONTO A 24 AWG COPPER CONDUCTOR USING AN 1.016 mm (0.040") DIE

Line Speed mpm	(fpm)	Die Swell	Shear Rate* s^{-1}	Surface Appearance
0		6.25	9.90×10^4	Extremely rough
38	(125)	3.60	9.01×10^4 (1.80×10^3)	Very rough
61	(200)	2.65	8.54×10^4 (2.88×10^3)	Rough
76	(250)	2.00	4.25×10^4 (3.60×10^3)	Slight roughness
157	(350)	1.55	6.19×10^4 (5.04×10^3)	Slight roughness
122	(400)	1.20	4.76×10^4 (5.76×10^3)	Very slight roughness
160	(525)	1.00	4.26×10^4 (7.56×10^3)	Smooth

*Figures in brackets - contribution of drag flow to overall shear rate.

FIGURE 2

PLOT OF DIESWELL AGAINST LINE SPEED FOR MB1



At low line speeds the surface of the insulation is visibly rough and die swell is considerable. As the line speed increases, the surface roughness and die swell decrease until at 106 m/min. (525 fpm), the O.D. is at its nominal value and the insulation is smooth.

It is interesting to note that as the line speed increases, the overall wall shear rate decreases. As the contribution due to drag flow increases the back pressure, pressure drop across the die and hence output rate will decrease. The contribution to the overall shear rate of pressure flow will, therefore, also decrease. Similar effects have been observed by Han[4] in wire insulating and by White[7] in the melt spinning process.

It can be seen that at the line speed at which a smooth insulation is produced, drag flow contributes 20% of the total shear rate. Or, more pertinently, the line speed which is necessary to produce extensional forces sufficient to obtain a smooth insulation are such that 20% of the total shear within the die is due to drag flow.

In Table 2, the results of a second experiment in which MB1 was extruded through a 0.51 mm (0.020") standard PIC die is shown. At the shear rate at which a smooth insulation was produced during the wire coating process ($4.26 \times 10^4\ s^{-1}$), the extruded filament was rough and showed considerable die swell.

TABLE 2

EXTRUSION OF MB1 THROUGH AN 0.508 mm (0.020") Sh 400 DIE AS A SOLID FILAMENT

Extruder RPM	Output Rate g/min.	Die Swell	Shear Rate s^{-1}	Surface Appearance
2	1.66	2.08	2.29×10^3	Smooth
5	15.38	2.26	3.12×10^4	Bead-like Distortion
10	24.9	2.53	3.45×10^4	Bead-like Distortion
20	39.3	2.78	5.41×10^4	Sharkskin
30	58.6	2.98	8.07×10^4	Sharkskin

Process Model Conclusions

It is, therefore, concluded that wire insulating is essentially a melt spinning process and is, thus, dominated by extensional forces outside the die. Furthermore, as in melt spinning, visco-elastic and extensional forces within the die are relevant only insofar as the die-swell and surface roughness of the extrudate determine the magnitude of the extensional forces (i.e. line speed), and the time for which these forces must act (i.e. length of air gap) to produce a smooth insulation surface on a product of the correct O.D.

Thus, the critical rheological properties of the polymer are extensional - extensional viscosity, elongation rate, critical stretch ratio, i.e. that value of VT/VE, where VT is the take-up velocity and VE is the velocity of the extrudate in the absence of a take-up force, at which the strand fails, and drawdown ratio.

Part II - Materials Model

A material is said to exhibit poor processability if either the spark rate is excessively high or the surface is unacceptably rough. To be relevant, extensional parameters must explain these phenomena and distinguish between processable and non-processable resins where visco-elastic forces fail to do so.

A spark results when the insulation is so reduced in thickness that the potential imposed by the spark tester grounds the conductor. Sparks are almost invariably associated with impurities and the crater-like depressions in which these impurities are found clearly demonstrate flow. Breakaways, i.e. a tear-like separation of the skin from the foam core characteristic of some materials on F/S are an extreme case of "cratering". Since the failure which causes a spark is localized, the stresses and strains which cause it must also be short range and short lived, and it is proposed that these are due to the presence of a contaminant, causing high localized elongational stresses, elongational rates and stretch ratios. It should be noted that fracture of melts, like solids, is very sensitive to strain rate[6].

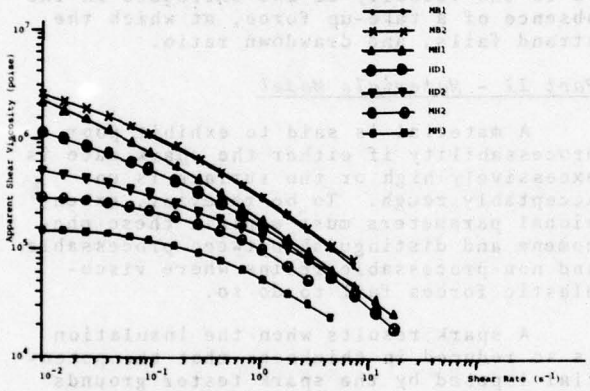
The extensional viscosity, η_E, is related to η_o, the true melt viscosity and at low elongation rates has a value $3\eta_o$.

(This viscosity is known as the Trouton viscosity η_T). Thus, it would be expected that, even though practically identical at high shear rates, that at extremely low shear rates, as obtainable on the Rheometrics Mechanical Spectrometer, materials with different extensional characteristics should also show significantly different shear rate behaviour. A further most important consequence of the relationship between an extensional viscosity is that $\eta_o \alpha \bar{M}_w^{3.4}$ *(10)*. Since $\bar{M}_w$ is determined by the reaction conditions during polymerization, it is a parameter which should be controllable by the manufacturer.

Figure 3 shows low shear rate data generated by using the Rheometrics Mechanical Spectrometer in the cone and plate mode. It is apparent that those materials which showed poor processability on both foam skin and solid PIC, MH3 and MH2 have the lowest values of η_{app} at $10^{-2}s^{-1}$.

FIGURE 3

PLOT OF APPARENT SHEAR VISCOSITY AGAINST SHEAR RATE FOR VARIOUS POLYETHYLENE RESINS



However, the processability of MH2 was significantly better than that of MH3. Since HD2, MH1 and HD2 have been successfully run in shop trials, it must be concluded that the minimum acceptable level for η_{app} at $10^{-2}s^{-1}$ must lie between that of MH2 and HD2. From Figure 2, it can be seen that MB2 and MB1 are almost identical in shear and have high values of η_{app}, yet MB1 is readily processable on regular F/S, whereas MB2 suffers from "breakaways". Clearly, there must be differences in the mechanism of extensional flow of the homopolymers and mechanical blends of high density and low density polyethylenes.

The extensional behaviour of polymers is markedly different to that in shear. All polymers shear thin, i.e. the shear viscosity decreases as the shear stress and shear rate increases. No such generalization can be made about extensional flows. Low density polyethylene shows a marked increase in extensional viscosity as the elongation rate increases (strain hardening) and fails due to brittle fracture at relatively low elongation rates. The extensional viscosity of linear materials such as high density polyethylene and those with short chain branches such as polypropylene and TPX (poly-4methyl-pentene 1) remains constant or decreases with elongation rate (tension thinning) and failure is essentially ductile[6].

The long chain branching of the low density polyethylene causes entanglement effects which resist extension and cause a build-up of stress and stored elastic energy in the system which, as the extension rate increases, eventually leads to brittle failure. Ductile failure on the other hand is clearly a dissipative, i.e. a flow phenomenon akin to necking down, and occurs at much higher elongation rates.

Figure 4 illustrates these effects for MB2 and its component resins. The low density material develops much higher stress in the line and breaks at a very much lower stretch ratio than the high density material. The presence of the high density material in a blend of these materials, i.e. MB2, increases the stretch ratio at which brittle failure occurs, as its tension thinning nature tends to dissipate the stored elastic energy of the low density component.

FIGURE 4

SPINNABILITY OF MB 2 ITS HIGH AND LOW DENSITY COMPONENTS

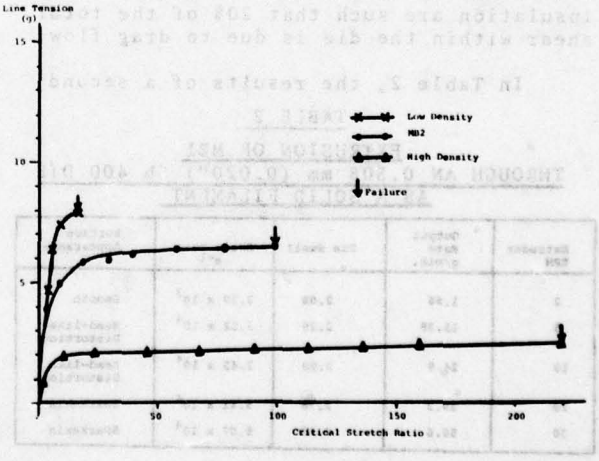
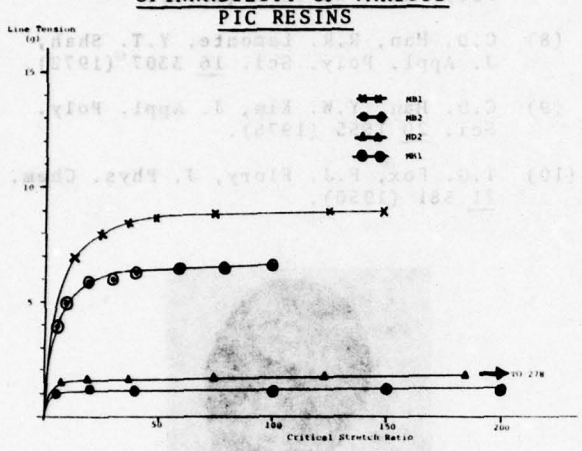


Figure 5 shows the results of melt spinning experiments using a melt tension apparatus, for various PIC resins. It can be seen that MB1 fails at a significantly higher stretch ratio than MB2.

FIGURE 5

SPINNABILITY OF VARIOUS PIC RESINS



Thus, the processability differences between MB1 and MB2 inexplicable using shear flow data are resolved when extensional flow parameters are considered. The higher critical stretch ratio of MB1 is attributable to the lower number of long chain branches in its low density component compared with the low density material in MB2, a consequence of the different polymerization process used by these companies. A reduced level of long chain branching results in a lower level of elastic memory in extensional flow.

During the above experiment, it was noticed that MB2 had a much lower freeze line than that of MB1 which was just below the die exit. DSC measurements confirmed that the crystallization rate of the high density component of MB2 was much lower than that of MB1 and that the disparity increased with cooling rate.

Since it was felt that the early establishment of a supportive matrix of high density polyethylene could influence the difference in critical stretch ratio of the two materials, an air cooling was applied to the emerging filament of the MB2 to increase its crystallization rate. Although increased crystallization was clearly observable as an increase in line tension and, although the crystallization rate could be made to exceed that of MB2, there was no increase in critical stretch ratio.

Although superior to MB2, MB1 shows the same quantitative behaviour. It is noteworthy that it tends to have higher spark rates than homopolymers and has an unacceptably high spark rate when processed under more stringent shear and drawdown regimes. It must, therefore, be concluded that elimination of elastic effects by the use of medium or high density homopolymers provided the extensional viscosity (and thus η_o) has a suitably high value, is an approach to obtaining processable PIC resins for F/S use which must be seriously considered.

Surface roughness is also associated with the elastic and extensional forces which are imposed on the melt by the extrusion process.

At the die exit, a molecule is subjected to an extensional force since part of the molecule will be still inside the die travelling relatively slowly and part will be outside the die accelerating rapidly to the much higher velocity of the line. These extensional forces will be greatest at the die wall since the melt velocity is lowest at this point (in theory the velocity of the molecular layer immediately adjacent to the die wall is zero). If the extensional force exceeds the breaking stress of the melt, melt fracture occurs. The stress at which melt fracture commences in low density polyethylenes has been shown by Cogswell[6] to agree well with the stress at which failure of a filament occurs during melt spinning.

Referring to Figure 5, the two medium density blends show melt fracture at much lower shear rates $10^2 s^{-1}$ than MH1 or HD2, MH1 shows melt fracture at shear rates in excess of $10^3 s^{-1}$ and HD2 does not show melt fracture even at a shear rate of $10^5 s^{-1}$. This would appear to confirm Cogswell's observations.

Materials Model - Conclusions

In conclusion, it can be said that a material suitable for high speed PIC insulating should have the following characteristics when evaluated using the indicated equipment.

1. Capillary Rheometer

   Apparent shear viscosity at 190°C < 1 x 10^3 poise (1 x 10^2Pa.s)
   Die; 50.8 mm (2.00") x 0.756 mm (0.03"), 90° included entrance angle.
   Shear rate 1 x $10^4 s^{-1}$.

2. Rheometrics Mechanical Spectrometer

Apparent shear viscosity at 190°C > 5 x 10^5 poise (5 x 10^4Pa.s)
Cone and plate mode.
Shear rate 1 x $10^{-2}s^{-1}$.

3. Melt Tension Apparatus

Critical stretch ratio at 190°C > 150
Die; 57.8 mm (2.275") x 1.3 mm (0.054"), 90° included entrance angle.

SUMMARY

Simple experiments in which a polyethylene resin was extruded as a filament and on a copper conductor at a similar shear rate have shown that wire insulating is essentially a melt spinning process. Thus, those parameters relevant to melt spinning-extensional viscosity (and hence shear viscosity at very low shear rates) critical stretch ratio, should also be relevant to high speed insulating.

Using the Rheometrics Mechanical Spectrometer and a melt tension apparatus, it was shown that the extensional parameters obtained using these instruments were capable of distinguishing between processable and non-processable resins where conventional visco-elastic measurements such as those obtained by using a capillary viscometer failed to do so.

REFERENCES

(1) D.C. Lau, M. Shannon, TR-4150-76-05, internal NTC report.

(2) T.C. Pound, TM-6360-77-19, internal NTC report.

(3) J.B. Paton et al, Processing of Thermoplastic Materials, Editor E.C. Bernhardt. SPE/Krieger, New York 1974,p. 271.

(4) C.D. Rao, C.D. Han,Proceedings, ANTECH, Montreal, 1977, 0.443.

(5) J. Meissner Rheol. Acta 10 230 (1971).

(6) F.N. Cogswell, Applied Polymer Symposia 27 1 (1975).

(7) J.L. White, J.F. Roman, J. Appl. Poly. Sci. 20 1005 (1976).

(8) C.D. Han, R.R. Lamonte, Y.T. Shah, J. Appl. Poly. Sci. 16 3307 (1972).

(9) C.D. Han, Y.W. Kim, J. Appl. Poly. Sci. 20 1555 (1976).

(10) T.G. Fox, P.J. Flory, J. Phys. Chem. 21 581 (1950).



Eric Marsden was born in Yeovil, England. He received a B.Sc. Honours degree in Chemistry from Leeds University in 1966, and a Ph.D. from Southampton University in 1976. At present, he is employed in the R&D group of Northern Telecom Canada Ltd. as a polymer scientist, in which capacity he has been engaged in the rheological characterization of materials and new product development.

BLOWN FILM ANALYSIS OF PVC WIRE AND CABLE COMPOUNDS

M. F. Marx

Western Electric Co., Inc.
Norcross, Georgia

Abstract

Blown film extrusion has been found to detect potential processing problems of PVC wire and cable compounds more so than other routine physical and chemical tests. Western Electric vinyl formulations are compounded to our recipe, hence melt flow processing characteristics are primarily controlled by compounding techniques and resin molecular weight. Other processing characteristics are then left to compound quality in terms of resin gels and ingredient dispersion.

This paper discusses vinyl compounding processes and possible extrusion problems. Identification of PVC resin gels as well as ingredient dispersion problems are discussed.

Since extruding blown film has proven to be useful in screening purchased PVC wire and cable compounds, it should be equally useful as a quality control measure for the vinyl compounder.

Summary

Extruding blown film is a practical raw material inspection test for the evaluation of wire and cable compounds. It produces a ready display of compound defects that can cause scrap rates to increase on the product line. By far the most significant shop extrusion problems can be attributed to degraded resin, unplasticized resin gels as well as poorly dispersed ingredients.

This test fills the gap between standard, physical inspection procedures and actual shop processing.

Introduction

Extruding wire and cable PVC compounds into blown film readily displays contamination, resin gels, and dispersion problems associated with that representative lot of compound. Imperfections that are difficult to find when examining pellets are more apparent when spread out over a large area. These potential extrusion problems are normally not uncovered when compound is inspected for routine physical properties such as tensile strength, elongation, specific gravity, shear, etc. Extruding flat tape does allow for subjective appraisal of the surface, however, it is not as revealing as extruding blown film.

Processing difficulties in the cable plant can most often be traced to contamination and poor dispersion rather than failure of physical requirements.

Although most extruded blown film is made from polyethylene, vinyl formulations having 25 to 80 phr plasticizer have been processed. Since Western Electric purchases in excess of 70 million pounds of PVC wire and cable compound annually made to specific formulas, the inspection and respective processibility of these compounds is of paramount importance.

Blown film extrusion was developed into an inspection test for incoming lots of compound primarily to identify inadequately mixed or contaminated compound. It was then necessary to look further into why certain lots of compound process well (extrude smoothly) while other lots from both the same as well as different suppliers do not process equivalently. Compound lots in question for comparative purposes were all within specification requirements. Viscosity vs. shear rate curves do not show significant differences between lots that were extruded and found to have different surface qualities. Surface smoothness is a highly desirable quality of finished wire in that it allows for contrasting ink color coding to be more discernible. This type of compound inspection has become necessary as a result of reductions in insulation and jacket thickness to conserve material.

Melt flow at very low shear rates on the order of one reciprocal second at 175°C using a modified Melt Index Test Procedure (ASTM-D-1238) has been found not to insure good extrusion quality nor does dynamic thermal stability testing using a torque rheometer. Although these processing type tests help to predict processibility there still remains a gap between compound processibility and routine inspection tests which it is hoped the film test will fill.

This paper discusses typical PVC wire and cable formulations and the reasons that have led to the evaluations of these compounds by extruding blown film. The film test is described along with typical PVC related defects. Actual shop extrusion experiences are also discussed.

Wire and Cable Compounds

Semirigid PVC compounds containing 30 phr of phthalate plasticizer are used to insulate 22, 24, and 26 gauge wire at speeds up to 5000 feet per minute. Insulation thicknesses of various product designs range from 4 to 8 mils. Extrusion shear rates under these conditions can reach $1X10^6$ reciprocal seconds. During insulating, wire is spark tested at 3000 volts DC.

Vinyl jacket formulations contain 40 phr linear alkyl phthalate plasticizer along with various levels of fillers and other additives to control specific properties. Jacket extrusion line speeds up 1000 feet per minute have two principal differences from insulating - there are no spark test requirements,and shear rates are significantly lower, by three to four orders of magnitude.

Compound formulations for wire and cable contain the following ingredients:

Resin, GP4 and GP5 per ASTM D-1755
Plasticizer
Lead Stabilizer
Filler, jackets only
Flame Retardant
Lubricant
Pigment

Knowing the composition of PVC compounds and their corresponding method of manufacture enables the analyst to identify material problems defined in the blown film test.

PVC Resin

PVC suspension grade dry blend resin in a fine particle size, free flowing white powder. To aid in manufacturing a uniform dry blend for subsequent compound fluxing, the resin should have a narrow particle size distribution range on the order of 100 to 200 microns.[1] The porosity structure which is based on particle size and bulk density is most important in that it enables resin to absorb plasticizer in the dry blend process.

Resin molecular weight, molecular weight distribution, along with plasticizer type, and loading as well as fillers, control processing and the final properties of the compound. As resin molecular weight decreases, plasticizer sorption is generally reduced which then leads to a higher resin gel count in the finished compound.

With an increasing demand for resin today, particularly for rigid applications, emphasis on good plasticizer sorption is reduced. Occupational Safety and Health Administration's exposure limits to vinyl chloride monomer (VCM)[2] have forced resin suppliers to modify their polymerization and resin drying process, hence stream stripping (SS) is being used. In contrast to the position of many resin suppliers concerning not degrading resin in SS, we often find a moderate number of amber resin gels in blown film.

Since reactors cannot be opened as frequently as in the past and new high pressure water cleaning techniques must be used, cleaning reactors becomes more difficult and thus increases the tendency for nonporous resin to form. In addition, gels can form due to deficiencies in the polymerization process. Nonporous resin is unable to absorb plasticizer and thus forms gels which are readily apparent in blown film. These gels can cause spark test failures (insulation faults) when compound is processed at high speed on thin wall (4-5 mil thick) insulation, specifically when the gels are not worked out in the extrusion process. Jacket extrusion on the other hand, produces a pimple-like surface when gels are present. Resin suppliers, by installing large reactors having less surface area per volume of monomer reacted, are reducing the tendency to form nonporous gel resin.[3]

Plasticizers

Organic high molecular weight liquids, termed plasticizers, are used to transform tough, horny vinyl resin into a useful flexible polymer. Various types and percentages are used to impart special end properties in the compound. High levels of plasticizer aid in compound processing, however, they also impart flammability to the detriment of finished wire and cable products.[4]

Levels of 30 phr plasticizer are used for semirigid insulating compound and 40 phr for flexible jacketing compounds. These use levels are a compromise between processing, flammability, long term aging, low temperature flexibility, and toughness. Although plasticizers are not usually responsible for compound processing difficulties and are not a factor in blown film defects, the high molecular weight phthalate types such as detridecyl phthalate (DTDP) are more difficult to flux than lower molecular weight counterpart plasticizers such as dioctyl phthalate (DOP). Compounds must therefore reach a particular minimum temperature in order to achieve complete plasticization during compounding.

Stabilizers

Lead salts near 5 micron median particle size are most commonly used to provide processing and aging stability. Tribasic lead sulfate and dibasic lead phthalate are the most widely used stabilizers for Western Electric wire and cable formulations. Their mean particle size is 4 to 6 microns, with the top size being 7 to 11 microns.

Dibasic lead phthalate is less reactive with phthalate plasticizers and is therefore recommended for long term stability, particularly at elevated temperatures. Both types of stabilizers are solid filler-like additives that must be thoroughly dispersed in the compound. Poor dispersion of lead stabilizers is the key problem that led to the

development of the blown film test. Several processing experiences will be discussed later.

Fillers - Flame Retardants

Antimony trioxide and aluminum trihydrate are both extensively used in Western Electric compounds to reduce product flammability. All formulations have a minimum of 2 phr antimony trioxide. Jacket formulations contain 15 phr aluminum trihydrate which is a flame retardant as well as a filler. Hydrated alumina, sold in a wide range of particle sizes, is required to have a mean particle size of 1 micron for Western Electric compounds having specific low temperature requirements. Pigment grade antimony trioxide has nominal ranges of 1.5 to 2.0 microns. Both additives can be dispersed in PVC formulations with a minimum of difficulty and are therefore not purchased with a lubricated surface coating.

Lubricants

Lubricants used consist of amide wax, dibasic lead stearate, paraffin wax, partially oxidized polyethylene and metallic stearates. In most cases, these ingredients melt and, therefore, their dispersion has not been a problem.

Pigments

Jacket compounds, particularly those formulations used for weatherable applications are purchased precolored. Furnace black and titanium dioxide are the principal pigments used in jacket formulations since they provide superior ultraviolet radiation screening protection. Chrome yellow, molybdate orange, and quinacridone red tint pigments are used to match the Bell System light olive gray color standard.

Poor pigment dispersion in jacket compounds causes appearance problems and clogs screens as well as offering potential tear points for thin wall jackets. They are also nuclei for low temperature cracks in finished jacket.

Nonweatherable colored insulation is obtained by blending a color masterbatch with natural compound at the extruder feed throat. Here the color concentrate if thoroughly dispersed, should not introduce spark test failures at the insulating line. Of the ten colors used to color code wire, carbon black which is used in the manufacture of black color masterbatch, is the most difficult pigment to disperse.

Compounding

Since compounding practices are as important for obtaining well mixed PVC wire compounds[5] as are the ingredients, a description of a typical compounding system is in order. Major wire and cable suppliers of bulk compound use the process described below to feed a two roll mill from which a continuous strip of compound is removed, cooled, and diced. The more significant steps in compounding are dry blending, and fluxing.

Dry Blend

Compounders dry-blend resin, plasticizer and other ingredients in either a high intensity mixer or a large ribbon blender. In the dry blend mix cycle, two important compounding practices should be followed:

First, the plasticizer must be evenly distributed within the resin matrix, allowing resin particles to be evenly plasticized.

Secondly, solids must be broken up and thoroughly dispersed[6] leaving the dry blend uniform and free flowing.

During the mix cycle, the resin becomes absorptive from frictional or conductive heating and the filler-like additives attach themselves to plasticized resin particles.

Fluxing

The next step is to fuse the dry blend in a Banbury® or a Farrel® continuous mixer, better known as an FCM. Banbury mixing is a batch process like dry blending and the compounder has the advantage of being able to extend the compound mixing time. An FCM unit, although more restrictive in this sense, is a more convenient continuous mixing process for fluxing compound.

Semirigid compounds are more shear heat sensitive to fluxing than flexible formulations having 40 or more phr plasticizer. In this vein, achieving high compound output rates requires the compounder to carefully control the flux melt temperature to achieve an optimum processible compound. Semirigid PVC compounded under a controlled flux temperature of 360°F has been found to have a higher melt flow than the same dry blend lot when fluxed at 380°F.

Blown Film Extrusion Test

As previously stated, extruding blown film reveals many defects. It readily displays compound ingredient quality as well as the compounder's competence.

BASIC BLOWN FILM LINE

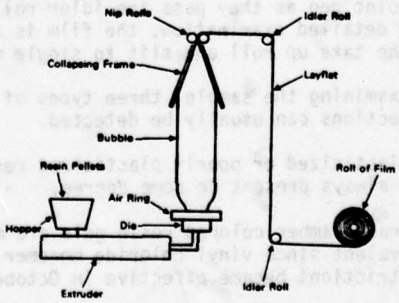


Figure 1

To extrude blown film, any size matched equipment can be used depending upon the compound sample size desired and the extrusion rate. Our 1-1/2" diameter 24/1 length to diameter ratio extruder processes about 25 pounds per hour of semirigid PVC at 40 rpm screw speed.

A typical system[7] consists of an extruder feeding a film die equipped with an air ring (Figure 1). The air ring (shown in Figure 2) can be fed with compressed air or, more conventionally a blower mounted on the film tower.

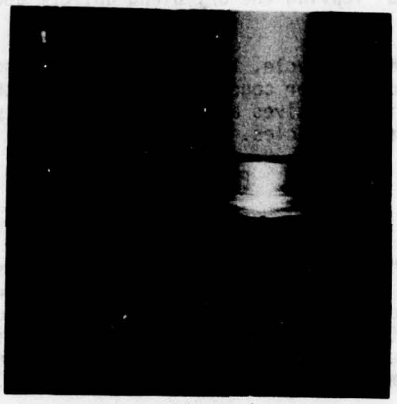


Figure 2

Film Die and Air Ring

From the die, a tube is blown outward and decreases in thickness down to approximately 2 mils as it is expanded and taken up by the tower. The bubble is then flattened by collapsing slats at the top while the volume of air within the bubble remains fixed.

The collapsed bubble (lay flat) is then fed over idler rolls to a surface winder, preferably one having a removable cardboard sleeve for a take up roll. During the process, the film, if wrinkle free, can be examined for general surface appearance. Surface appearance is the key property of the blown film test.

Obvious defects can be circled (Figure 3) with a ball point pen as they pass the idler roll. For a more detailed examination, the film is removed from the take up roll and slit to single thickness.

Upon examining the sample, three types of film imperfections can usually be detected.

1) Unplasticized or poorly plasticized resin gels are always present to some degree.

2) Degraded amber colored resin gels are more prevalent since vinyl chloride monomer (VCM) restrictions became effective in October, 1974.

3) Inadequate dispersion or agglomerated solids such as lead stabilizers, antimony trioxide, fillers, colorants and the like are seen as specks.

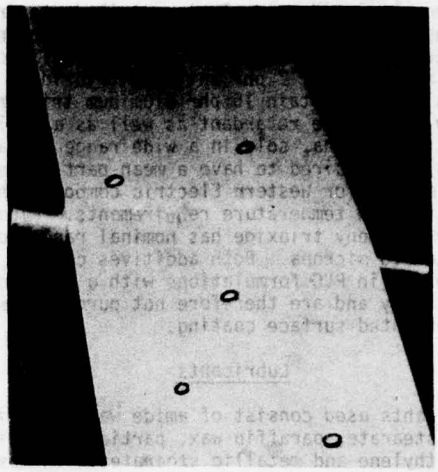


Figure 3

Circled Film Defects on
Film Feeding Over Idler Roll

In all cases the defects listed cause pimples or surface imperfections on the film. Defects 10 mils or larger can cause the film to tear. Frequent loss of entrapped air within the bubble is an indicator that there is possible contamination (provided that the die is centered and at the proper temperature). A relatively large 20 mesh screen is used to allow contamination to pass through and be seen in the film. If, however, some form of debris is caught within the die it will cause a continuous tear in the film at which time the die must be disassembled and cleaned.

A point of caution when extruding film is the die head pressure. Care must be exercised to insure that excessive pressure does not develop from a cold or clogged die. For some polymers, other than PVC, a critical melt temperature is important.

Typical conditions for extruding semirigid PVC,on our 1-1/2" diameter 24/1 extruder, are as follows:

Head Pressure		6000 psi
RPM		40
Temperature	^{o}F	
	Die	330
	Adaptor	330
	Melt	360
	Zone 3	330
	Zone 2	325
	Zone 1	320

Resin defects in blown film can be 3 or 4 times the thickness of the basic 2 mil film. To verify that the pimple defect is resin as opposed to a filler-like additive, the speck and surrounding film area are cut from the sample and pressed between two heated ($375^{o}+10^{o}F$) microscope slides. A clear area blending into the usually opaque surrounding area shown in Figure 4 indicates that the defect is resin.



Figure 4

Clear Resin Gel Pressed Out
Between Preheated Microscope Slides

For softer or more rigid formulations, temperatures should be adjusted down or up respectively. If, by raising the temperature profile in the extruder to obtain a higher melt temperature (380°) fewer resin gels are seen, then one can assume that the same effect can be obtained when extruding compound in the shop. On the other hand, if it is not necessary to raise the film extrusion temperature to reduce the gel count, then it can be assumed that the lot of compound is better mixed. By the same microscope slide test, an opaque speck that does not flow is a pigment or filler-like additive. These nontransparent defects will appear as dark specks when placed over a frosted light box. They will appear as white or pigment colored if placed over a contrasting black background and viewed with reflected light at preferably 3 to 5X magnification.

Lead stabilizer specks, imbedded in film (Figure 5a) turn black (Figure 5b) when sliced with a razor blade and exposed to a 30% sodium sulfide solution, while antimony trioxide will appear orange.

Pigments will appear as their natural color, sometimes streaked when the compound is pressed between preheated microscope slides. Other questionable film defects can be evaluated by appropriate analytical methods.



Figure 5a

Lead Speck (24X)



Figure 5b

Sliced Lead Speck Exposed to 30% Sodium Sulfide Solution (5X) (Turns Black)

Shop Extrusion Experiences

Lead stabilizer agglomeration and dispersion has caused more than its share of extrusion difficulties. Tribasic lead sulfate, for example, is a product of the chemical reaction between lead oxide (PbO "litharge") and sulfuric acid.

$$PbO + H_2SO_4 \text{ ----------} 3\,PbO\,PbSO_4H_3O \downarrow$$

In the manufacturing process, the precipitated slurry cake must be dried and pulverized to break up the agglomerates. If pulverization and air classification are inadequate, agglomerated lead particles will remain in the stabilizer batch. Tribasic lead sulfate contains one mole water of hydration and has a tendency to agglomerate. To prevent agglomeration and improve dispersion it is usually surface treated.

Lead Dispersion

In one incident a rail hopper car of semirigid natural insulating compound caused excessive faults in all insulating extruders. Screen packs showed an accumulation of white powder (Figure 6).

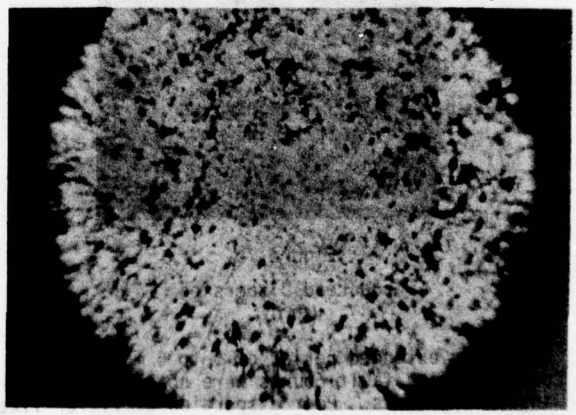


Figure 6
Lead Stabilizer Accumulated
on Extruder Screen Pack

After cleaning the extruder head, the spark test fault level at wire insulating was reduced until the screen pack (150 x 250 mesh dutch weave) became clogged forcing the contaminant through, causing faults. A sulfide solution stained the white powder black indicating a presence of lead. Blown film of that particular lot of semi-rigid PVC clearly revealed white lumps which also stained black. The remaining portion of that railcar was rejected.

Grainy Film - Poor Dispersion

Another example of poor surface smoothness can be attributed to a "grainy" film. Wire insulation with semirigid PVC, which produces a "grainy" surface when extruded as blown film also produces a rough textured surface when extruded in the shop.

Microscopic examination of the film seen in Figure 7a shows an abnormal number of particles larger than is seen in a uniform background sample Figure 7b which represents good dispersion.



Figure 7a

Poor Lead Dispersion
(24X)

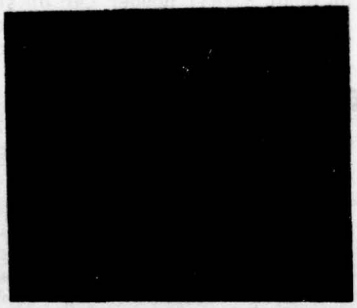


Figure 7b

Good Lead Dispersion
(24X)

During an extended period of 5 to 6 months, periodic high fault counts were noted at wire insulating lines. Poor dispersion of filler-like additives was seen in the blown film. A sieve analysis of particular lots of tribasic lead sulfate stabilizer indicated that up to .02% of the retained stabilizer had particles from 50 to 1000 microns. (Figure 8) In contrast, other lots of lead stabilizer had no retention of particles left on a #325 mesh screen when tested per standard wet screen procedure.

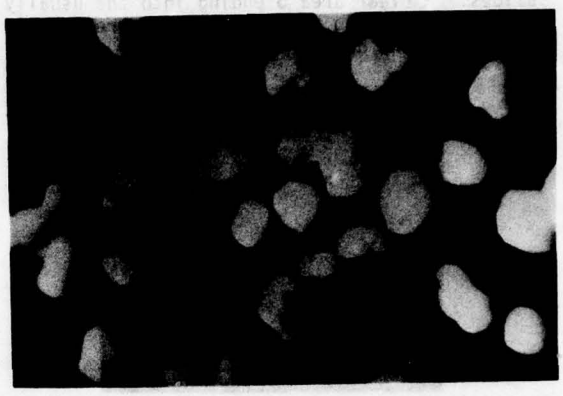


Figure 8

Retained Tribasic Lead
Sulfate on #325 Mesh Screen
(10X)

A #325 mesh sieve has 43 micron openings, however, and it is not a particularly good quality control inspection test for 5 micron and less PVC additives. A sedigraph or laser beam particle size analysis system is more desirable. These systems measure the particle size distribution over a range of 1 to 200 microns.

Also to be noted, is the fact that a particle size analysis may not represent what is actually fed to the dry blend mixer. Ideal particle size reduction could result from sample preparation, a process which would size reduce particles beyond what would be accomplished in compounding. Extruding blown film is therefore a prudent test for the user of purchased compound since he has only indirect quality control over ingredients. The compounder, on the other hand, can use the test to improve compounding procedures. In fact, it could be used to optimize compound quality as is being done in critical polyethylene film processes.

Black Color Concentrate

Spark test failures involving black pigments are particularly difficult to analyze since degraded compound, at the failure point, is indistinguishable from the base color. Several years ago one of our Western Electric locations isolated a sample of black color concentrate that was causing excessive spark test failures at the insulating line. Upon extruding blown film, using a known quality natural base compound and the questionable black color concentrate, it became readily apparent that poor pigment dispersion was responsible for the spark failure. Figure 9 shows a sample of

smooth black pigmented film placed over the rough textured film containing an inferior lot of dispersed black color concentrate. Microscopic examination of 1.5 mil film using transmitted light at 24X (Figure 10a and 10B) shows good and bad dispersion respectively.

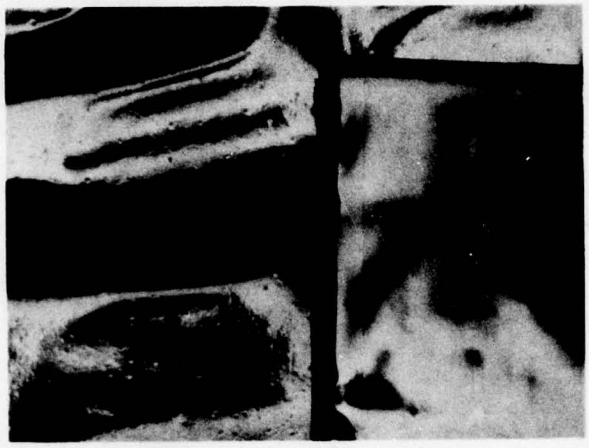


Figure 9

Photograph of Smooth Black Pigmented Film (right) Over Rough Textured Poor Carbon Black Dispersion Sample

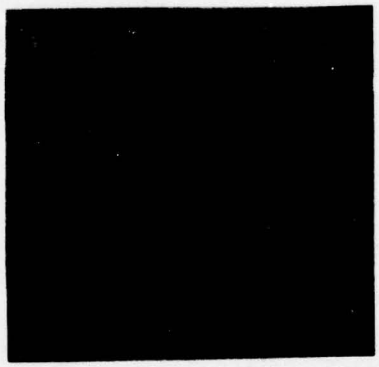


Figure 10a

Good Dispersion of Furnace Black Color Concentrate, 1 Part in Natural Semirigid PVC

The film sample provided the ready evidence for rejecting that particular lot of defective black color concentrate. Listed under the requirements for PVC color concentrates is the statement that the incorporation of concentrate into natural compound shall not degrade the surface appearance of natural compound blown film.

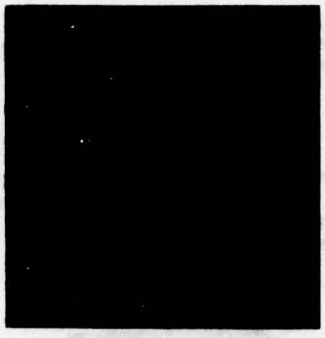


Figure 10b

Poor Dispersion of Furnace Black Color Concentrate, 1 Part in Natural Semirigid PVC

Summary

Extruding blown film is a practical raw material inspection test for the evaluation of wire and cable compounds. It produces a ready display of compound defects that can cause scrap rates to increase on the product line. By far the most significant shop extrusion problems can be attributed to degraded resin, unplasticized and partially plasticized resin gels as well as poorly dispersed ingredients.

This test fills the gap between standard, physical inspection procedures and actual shop processing.

References

1. Davis, Waveland D., "Testing and Characterization of Resins," Encyclopedia of PVC, Volume 1, Chapter 5.

2. "OSHA Exposure to Vinyl Chloride," Federal Register Vol. 39, No. 194, Part II, October 4, 1974.

3. Sorneson, Wayne R., "A Close Look at PVC Today," Plastics Engineering, April, 1977, pp 22.

4. Kaufman, S., Yocum, M. M., "The Behavior of Fire Resistant Communications Cables in Large Scale Fire Tests," Plastics in Telecommunications II Proceedings, London, England, September 18, 1978.

5. Prust, Randall S., "Quality Control in PVC Compounding," Plastics Compounding, May/June, 1978.

6. Levy, G. C., "Factors to Consider in PVC Dry Blend Preparation," Wire Journal, August, 1971, p. 39.

7. Prall, G. M., "How to Solve Blown Film Problems," Chemplex Corporation Product Information.

Acknowledgements

The author wishes to thank Ms. C. L. Hines and Ms. S. C. Perry for their assistance in extruding blown film. Also thanks are due Mr. E. L. Roberts for his cooperation in the project.



M. F. Marx is a Senior Engineer with the Western Electric Cable and Wire Product Engineering Control Center, Norcross, Georgia. He received a BS in Chemical Engineering from the University of Maryland in June, 1959, and is currently involved with wire and cable materials development.

He is a Senior Member of the Society of Plastics Engineers and a Registered Professional Engineer in North Carolina and Georgia.

IMPROVED RESISTANCE VALUES FOR CRIMPED TERMINATIONS OF NICKEL-PLATED ELECTRICAL WIRE

Ronald P. Fialcowitz
Michael T. Gromek
Norman R. Byrd

Douglas Aircraft Company
McDonnell Douglas Corporation
Long Beach, California

Summary

The generally inferior performance of crimped, nickel-plated wire terminations when compared to tin-plated wire was investigated. A comprehensive survey was made to delineate the particular troublesome wire/termination hardware combinations. Heat-aging large populations of such crimped terminations resulted in continuously increasing millivolt drop values across the contact wire interface. A variety of cleaning techniques applied to the conductors before crimping significantly improved performance. Electron scanning microscope photographs revealed contamination particles. Analysis identified them as residue of lubricants and cooling fluids used during the strand drawing operation. Alternate fluids were selected and trial production runs completed. It is believed the performance levels and long-term reliability of crimped, nickel-plated wire terminations will be improved by these new strand drawing procedures.

Discussion

The transition in the aerospace industry from soldering to mechanical crimping for wire terminations occurred approximately 20 years ago. It had long been recognized that soldering nickel-plated wire required more care than soldering silver or tinplate. An identical difficulty was soon observed with crimp terminations.

The experience at Douglas Aircraft Company has been largely with tin-plated conductors. The use of nickel-plated wires was limited to high-temperature applications such as engine pods. It was acknowledged that the crimping of nickel plate was a more marginal operation. But it was believed that tighter-toleranced tools and more frequent calibration procedures could compensate for the difficulty.

In the summer of 1976, an effort was made to convert from tin-plated wire to nickel-plated MIL-W-81381/12 type wire. An extensive survey was made of the common electrical terminations in use on Douglas commercial aircraft. Tests were conducted in which nickel-plated wire was terminated with the standard crimping tools and termination hardware commonly used with the tin-plated wire. Millivolt drop readings and breaking strength measurements were made and compared to MIL-W-22520 criteria and Douglas quality standards.

The results were interesting. Many lugs and contacts were found to be perfectly compatible with nickel-plated wire. Other terminations posted occasional poor readings. And still a third category appeared consistently bad.

An effort was made to determine the reason for this erratic situation. This paper describes in chronological sequence the steps taken in this investigation. Over 10,000 data points were noted, and it was with reluctance that most of them had to be omitted for this brief presentation. Although a potential cause of the nickel-plating crimp problem was observed, the researchers do not claim that the final solution has been reached. It is hoped that the following data will suggest other avenues of research that escaped the authors.

Test Results

Unless specified for tin-plated wire, all data are for nickel-plated conductor. Since the full reason for the nickel-plate problem cannot be laid to the manufacturer applying the insulation, it was deemed desirable to use letter designations to distinguish between sources. More than one manufacturer was used in this study. But the most impressive results were obtained from one particular quantity of wire, designated as from a "Wire Manufacturer A" in this paper.

Millivolt drop and crimp strength criteria for tin-plated wire from MIL-C-22520F are referenced on most of the graphs. These are indicated by short, horizontal lines, solid or dashed, at the appropriate level on the ordinate. Despite the fact that an amendment to MIL-C-22520 has relaxed the requirements for nickel-plated wire crimps so that they no longer need be as low as tin-plate values, this investigation was intended to achieve a quality level equivalent to tinplate. This became even more desirable when it was observed, as will be shown, that the high- millivolt drop readings of nickel-plated wire crimps could grow during heat aging to truly prohibitive heights.

Vendor part numbers for the applicable termination hardware and crimp tools are listed on each illustration. Their sources are summarized in Table 1.

Initial Survey

A sampling of the many crimped terminations that had acceptable values is given in Table 2. In this listing, the millivolt drop value cited is the maximum recorded among the indicated number of specimens. All results in Table 2 were obtained with one production batch of nickel-plated wire from Wire Manufacturer A.

TABLE 1

TOOL AND CONTACT MANUFACTURERS

CONTACT	MANUFACTURER
LRC12Z-5 WITH GSC071T SLEEVE	BURNDY THOMAS AND BETIS
LRC20W-5	BURNDY
LRM16W-2	BURNDY
LRM20W-5	BURNDY
YAE 18-N2-2	BURNDY
YAE 22-G15	BURNDY
012-0008-101	FLIGHT
012-1008-201	FLIGHT
012-1012-201	FLIGHT
016-0007-101	FLIGHT
030-1952-000	ITT CANNON
030-2062-000	ITT CANNON
030-2063-000	ITT CANNON
030-9081-003	ITT CANNON
031-1007-000	ITT CANNON
031-1046-002	ITT CANNON
031-1059-001	ITT CANNON
031-9081-001	ITT CANNON
031-9084-000	ITT CANNON
031-9084-001	ITT CANNON

CONTACT	MANUFACTURER
031-9134-001	ITT CANNON
031-9134-004	ITT CANNON
031-9174-003	ITT CANNON
031-9203-008	ITT CANNON
031-9206-000	ITT CANNON
200-12/30-3	DEUTSCH
200-12/30-7	DEUTSCH
800-20/32-1	DEUTSCH

TOOL	MANUFACTURER
M8ND	BURNDY
M10S	BURNDY
11210	BUCHANAN
15500-16-1	DEUTSCH
155000-12	DEUTSCH
612118	BUCHANAN
612548	BUCHANAN
613606	BUCHANAN

TABLE 2

LIST OF ACCEPTABLE CRIMPED TERMINATIONS

CONTACT PART NUMBER	WIRE GAGE	TOOL	NUMBER OF SPECIMENS	MAXIMUM MILLIVOLT DROP (MV)	MINIMUM BREAKING STRENGTH (POUNDS)
YAE22-G15	20	M8ND N14HET-25	6	3.77	36.3
YAE18-N2-2	20	M8ND N14HET-25	5	4.89	30.4
031-1046-002	20	M10S S-67	6	3.18	30.7
031-1046-002	20	M10S-1 S-6A	6	3.07	28.0
031-9174-003	20	M10S S-67	6	3.48	34.0
031-9174-003	20	M10S-1 S-6A	6	3.76	27.0
031-9134-001	20	M10S-1 S-8	6	3.43	29.0
031-9134-001	20	M10S-1 S-6A	6	3.61	27.3
031-9203-008	20	M10S-1 S-7	6	3.20	29.5
031-9203-008	20	M10S-1, S50, SL-83	6	3.98	30.5
031-9084-001	20	M10S-1 S-7	6	4.19	30.6
LRM16W-2	18	M10S-1 S-7	12	3.04	42.5
LRM16W-2	16	M10S-1 S-7	12	3.16	48.3
030-1952-000	20	11210	12	3.83	25.2
LRC12Z-5 GSC071T-SLEEVE	16	M10S-1 S-8	6	2.70	69.2
030-2063-000	18	M10S-1 S-8	6	3.98	48.5
800-20/32-1	18	M10S-1 S-41	12	2.00	42.0
030-2062-000	14	M10S-1 S-8	6	3.68	92.0
012-008-101	12	M10S-1 S-8	6	2.9	102.0
012-1008-201	12	M10S-1 S-8	6	3.0	115.0
031-1059-001	12	M10S-1 S-8	6	2.6	123.0
030-2062-000	12	M10S-1 S-8	6	3.3	136.0
200-12/30-3	12	155000-12	6	3.1	102.0

Table 3 gives some of the readings that were disappointingly outside the tin-plated criteria. This group has only a minor percentage of the test specimens with such a deviation. The table gives the various high values found among the cited number of total samples for each tool/contact combination.

Table 4 defines the connector contacts that gave consistently poor readings when crimped on nickel-plated wire. No special adjustments were made to the crimp tools. In all the work cited so far, the wire was processed as if it were tin-plated. These results were considered intolerable. The following text treats the subsequent investigation that was intended to eventually crimp these contacts onto nickel-plated wire, with the same success as shown in Table 2.

Crimp-Depth Study

A few explanatory comments on the figures in this paper should make them more understandable. Both millivolt drop

TABLE 3

LIST OF ERRATIC CRIMPED TERMINATIONS

CONTACT PART NUMBER	WIRE GAGE	TOOL	NUMBER OF SAMPLES	HIGH MILLIVOLT DROP (MV)	BREAKING STRENGTH (POUNDS)
012-1012-201	20	M10S-1 S-8	12	7.87	37.7
				4.44	37.75
				4.40	35.1
LRM 20W-5	20	M10S-1 S-6A	12	5.49	27.5
				4.02	30.0
				4.27	28.6
				4.18	27.5
LRC 20W-5	20	M10S S-67	12	4.79	30.25
				4.26	25.75
				4.44	24.0
				4.70	25.8
031-9206-000	20	M10S-1 S-7	6	4.60	30.5
				4.06	32.7
031-9134-004	20	M10S S-79	6	4.74	31.7
				4.07	32.5
031-1007-000	20	M10S S-79	6	4.84	33.3
				4.49	32.6
				4.04	33.5
				4.62	32.5
030-9081-003	20	M10S S-79	6	4.45	32.5
				4.26	30.8
				4.08	32.3
200-12/30-7	18	15500-16-1	6	5.49	49.0
				4.53	43.2

TABLE 4

LIST OF CONSISTENTLY POOR CRIMP TERMINATIONS

CONTACT PART NUMBER	WIRE GAGE	TOOL	NUMBER OF SAMPLES	MAXIMUM MILLIVOLT DROP (MV)	MINIMUM BREAKING STRENGTH (POUNDS)
031-9084-000	20	M10S-1, S50, SL-83	6	14.57	25.7
031-9134-004	20	M10S-1, S41, SL-68	6	5.50	33.0
031-1007-200	20	M10S-1, S41, SL-68	6	6.43	36.0
030-9081-003	20	M10S-1, S41, SL-68	6	5.84	35.4
031-9084-000	16	M10S-1 S-7	6	17.50	45.2
031-9081-001	16	M10S-1 S-7	6	5.86	45.0
031-9206-000	16	M10S-1 S-7	6	8.44	51.5
030-2003-000	16	M10S-1 S-8	6	7.23	56.0
012-0008-101	14	M10S-1 S-8	6	5.68	82.0
012-1008-201	14	M10S-1 S-8	6	5.7	80.0
200-12/30-3	14	15500-12	6	6.22	62.0
200-12/30-7	14	15500-16-1	6	7.98	73.0
031-1059-001	14	M10S-1 S-8	6	4.67	99.0

and breaking strength are frequently plotted on the same graph. Electrical characteristics are depicted with a solid line, mechanical with dashes.

A decision had to be made between showing average values or the entire observed span. Limiting a graph to only the maximum and minimum readings can be misleading, inasmuch as the sample population is never evenly distributed throughout the span. But aerospace vehicles do not fly on the average performance of their components. The few components operating outside their permissible tolerances have effects out of all proportion to their insignificant numbers. Therefore, the outermost measurements defining the envelope were used.

The measured gap between the fully collapsed dies of a crimping tool is known as the G dimension. Due to springback of the contact metal, the measured indentation affected by the dies is frequently larger than the intended G dimension. In all the original work, both the initial die clearance and the final crimp depth were measured and recorded. In this paper, only the G dimension will be given. In Figure 1, a nominal 0.035-inch G dimension was used for this survey of a standard tin-plated wire and versions of nickel-plated MIL-W-81381/12 from two wire manufacturers. Six specimens of tin-plated wire provided low-millivolt drop measurements which were extremely uniform. The span of millivolt drop measurements for the two nickel-plated versions is larger and each is obviously different from the other. Although samples from

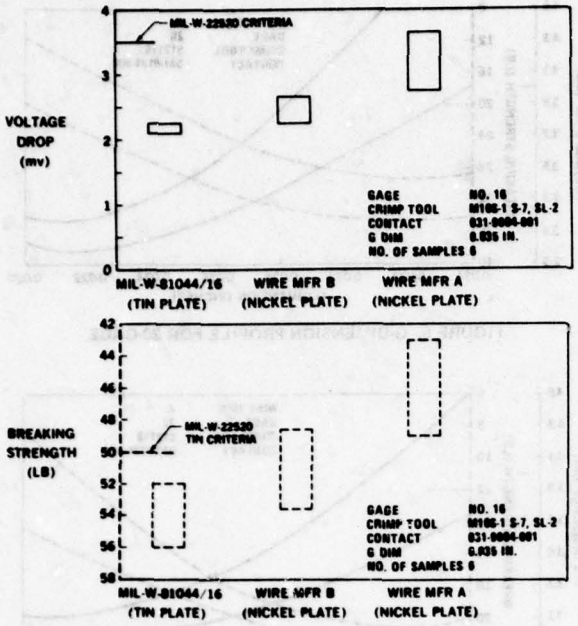


FIGURE 1. COMPARISON BETWEEN NICKEL AND TIN PLATE

Manufacturer A did yield acceptable millivolt drop readings at this G dimension setting, the corresponding breaking strength values are below the desired criteria.

The variation of millivolt drop and breaking strength performance shown in Tables 2 through 4 was further studied through the mechanism of constructing profiles. Using the same wire sample from Manufacturer A and the same crimping tool, MIL-C-22520/1, a range of G dimensions was imposed on two different contacts. Groups of six specimens were measured at each G-dimension setting. Figure 2 plots the maximum and minimum readings of each set of six.

Noting the MIL-C-22520 electrical and strength criteria on the ordinate in Figure 2, it can be observed that both parameters lie largely in the acceptable zones. However, they unfortunately wander out at opposite ends of the G range. As the tightening crimp improves the millivolt drop, the reduced cross-sectional area of the stranding is reflected in the lowering breaking strength. Consequently, the range where both are acceptable is quite narrow and in the center of the tool range. This could be a principal reason for the erratic results experienced by industry in crimping nickel-plated wire. In many instances, it has been reported that simple adjusting of the crimping tool was adequate to regain satisfactory performance. But it is questionable how long a tool can hold a narrowly optimum G setting.

There has been a popular theory that the successful crimping of nickel-plated wire requires an 8-indent tool. Most of the work defined this far has been with the standard 4-indent crimp tools commonly used with tin-plated wire.

Employing two different 8-indent tools, very detailed G-dimension profiles were constructed comparing Manufacturer

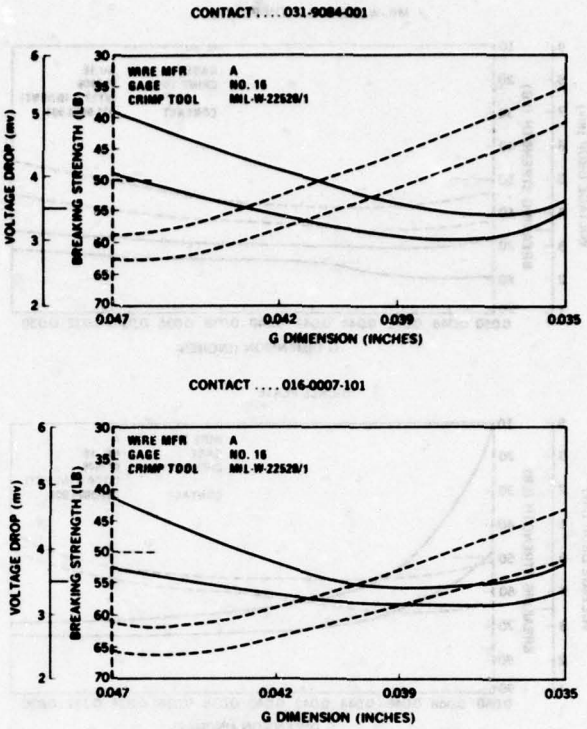


FIGURE 2. VARIATION BETWEEN CONTACTS

A's nickel-plated wire with a commonly used tin-plated wire. The same contact, P/N 031-9084-001, was used throughout. Settings were varied by only 0.002 inch and six specimens were used each time.

The Buchanan adjustable P/N 613606 provided excellent results on the tin-plated wire throughout the entire span of readings. Both millivolt drop and breaking strength are consistently acceptable in the top part of Figure 3. However, the bottom part of the figure for nickel-plated wire shows an abrupt increase in millivolt drop as the looser crimp settings are approached.

The Buchanan P/N 612548 also imposes an 8-indent crimp. But unlike the previous tool which steps the dimples, all eight indentations are of equal depth. The results shown in the top of Figure 4 are startling. The tin-plated wire preserves its desirable millivolt drop over the range of settings, but the tighter crimps seriously erode the physical strength of the termination. The corresponding nickel-plated wire graph, shown in the bottom part of the figure, likewise reveals disappointing breaking strength values.

To continue the demonstration of how revealing G dimension profiles can be, gauges 20, 22, and 24 are depicted in Figures 5 through 7. The narrowness of the acceptable combination of millivolt drop and breaking strength values is enhanced. The Buchanan 8-indent tool 612118, qualified to MS3198, was used for all terminations.

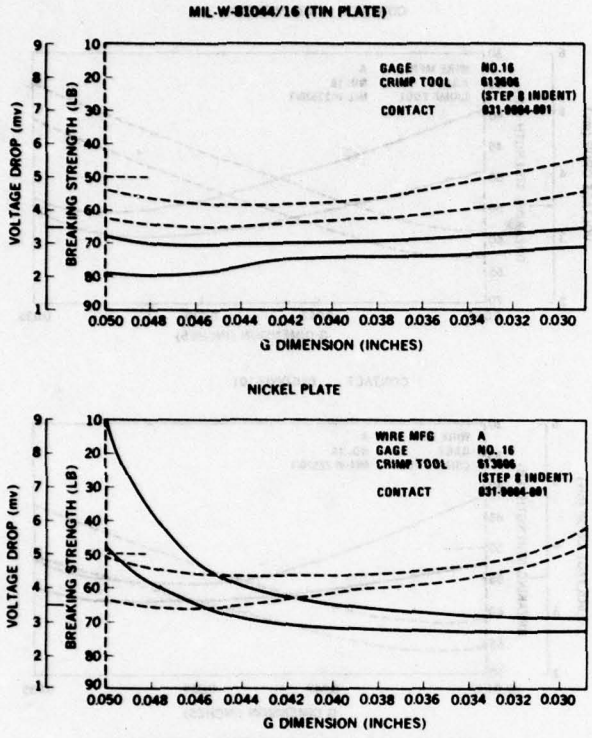


FIGURE 3. COMPARISON BETWEEN TIN AND NICKEL PLATE

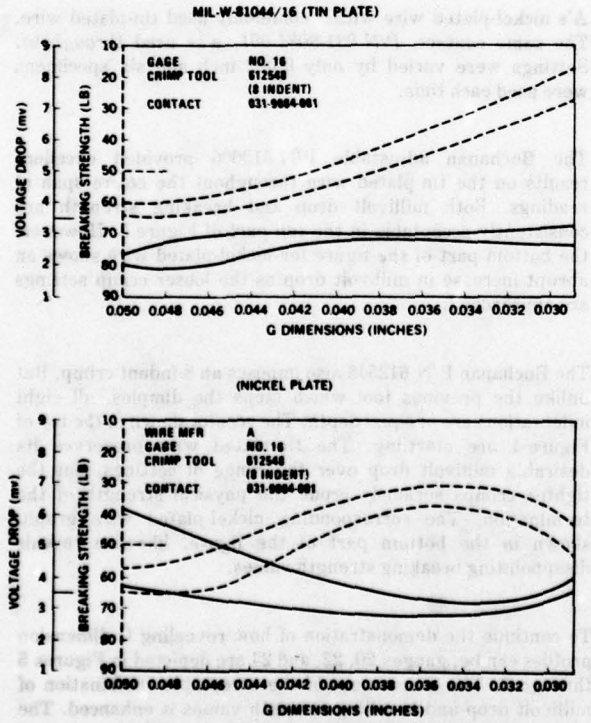


FIGURE 4. COMPARISON BETWEEN TIN AND NICKEL PLATE

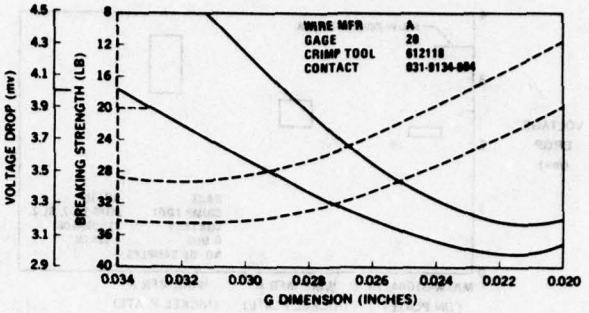


FIGURE 5. G-DIMENSION PROFILE FOR 20-GAGE

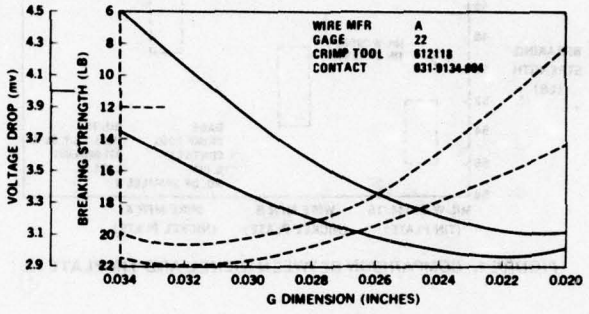


FIGURE 6. G-DIMENSION PROFILE FOR 22-GAGE

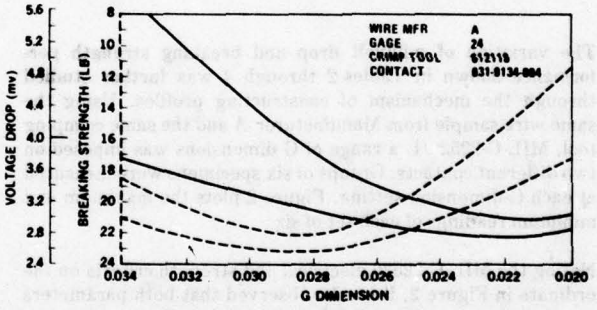


FIGURE 7. G-DIMENSION PROFILE FOR 24-GAGE

Heat Aging Study

As mentioned earlier, Amendment 1 to MIL-C-22520F permits virtually all millivolt drop values for nickel-plated wire that have been shown so far. A series of heat aging exposures was undertaken to determine how stable these initial voltage measurements are.

Six specimens each of tin- and nickel-plated wire were utilized. Gages 20 and 16 were crimped in the identical contact with an MS3191 tool. Millivolt drop values were monitored through a 28-hour exposure to 400°F. This is a severe exposure for tin. That element forms nonconductive intermetallic coatings at short-term exposures of 300°F. The deterioration of the tin-plated samples at this abuse, as shown in Figure 8, is therefore not surprising. What is significant is the vastly greater

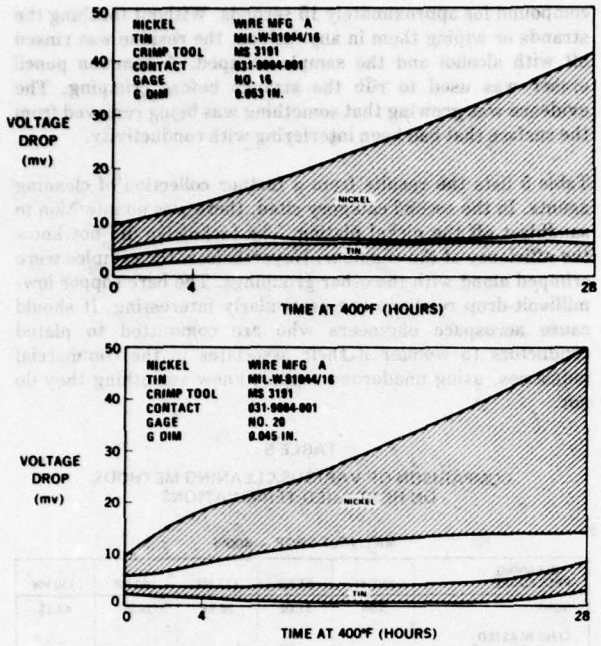


FIGURE 8. COMPARISON OF TIN AND NICKEL PLATE HEAT-AGED TERMINATIONS

increase in voltage drop experienced by the crimped terminations of nickel- plated wires.

It is acknowledged that nickel is little affected by an ambient temperature of 400°F. Therefore, this experiment was the first indication that an effect was being observed from some agent other than nickel.

The next logical investigation was to determine if a more mild exposure would affect a crimped nickel-plated wire termination. Figure 9 defines the deterioration observed after continuous and cyclic exposure to only 250°F. Inasmuch as the exposure varies between readings, a bar chart presentation is used. Once again, an undeniable trend toward an increasing drop in millivolt values became established.

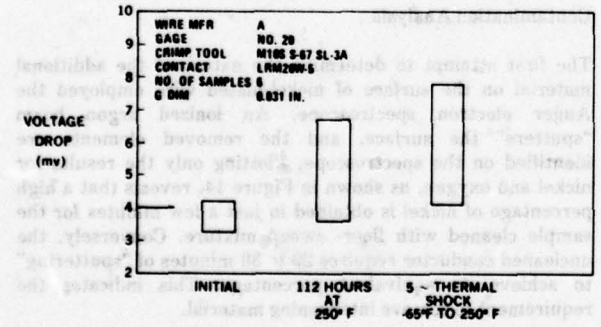


FIGURE 9. HEAT-AGING AND THERMAL SHOCK

To obtain an even clearer understanding of the phenomenon being studied, G-dimension profiles were generated for a set of 20-gage terminations that were successively heat-aged at two temperature levels. First, a 63-hour test at 250°F was used. After the millivolt drop readings were recorded, the specimens were returned for an additional 23 hours at 400°F. Six samples were used in each group at a G-dimension setting. In Figure 10, only the average of each set of six measurements is shown. Tensile values were obtained at the completion of the thermal aging. It is well that they were. The tighter G-dimension zone would indicate relatively stable millivolt drop readings, but the corresponding breaking strength trace reveals diminishing quality crimps.

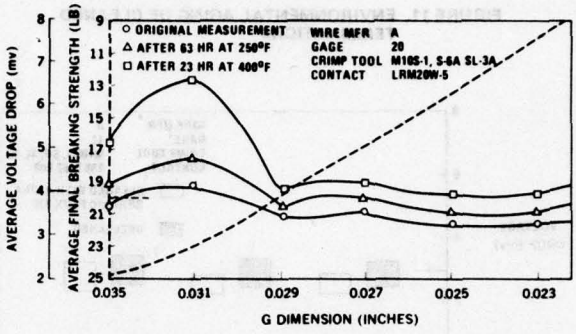


FIGURE 10. G-DIMENSION PROFILE OF HEAT-AGED TERMINATIONS

Cleaning Methods

The cumulative evidence of the catastrophic effect of heat on nickel-plated terminations could be satisfactorily explained only by the presence of some foreign material. An assumption was made that Alpha Organic Flux No. 830 would probably be effective in removing unknown surface contamination. Twelve 16-gage samples were cleaned with the flux and flushed with alcohol/distilled water. Six more bare, stripped wire specimens were untreated and used as a control. All were terminated in the P/N 031-9084-001 contact with a Burndy M10S-1 4-indent tool.

Figure 11 illustrates the results. The original uncleaned conductor millivolt drop readings quickly deviated from the cleaned population. The initial 250°F heat soak resulted in one termination of the control sample reaching a maximum drop of 17.88 mv. To conserve time, no subsequent attention was paid to the control group. The figure lists the various efforts made, including physical, environmental, and electrical, to induce deterioration in the cleaned specimens. The performance did broaden slightly, but obviously was stabilizing by the end of the experiment.

Most of the previous charts show results from Manufacturer A's wire. Other sources were used in the study, but normally with less striking values. An exception, however, was the effort to clean 12-gage wire. Alpha Organic Flux 830 could do little to improve the very satisfactory performance of wire from Manufacturer A. But, as Figure 12 illustrates, the control samples from conductor Manufacturer C quickly deteriorated in millivolt drop value under heat-aging exposure.

The search began for other efficacious cleaning agents. Figure 13 displays plots for some of the imaginative materials that were quickly investigated. "Sand dip" consisted of

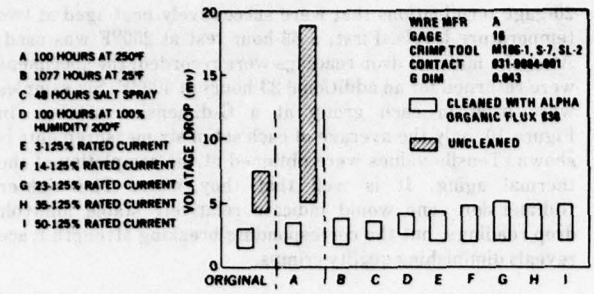


FIGURE 11. ENVIRONMENTAL AGING OF CLEANED TERMINATIONS

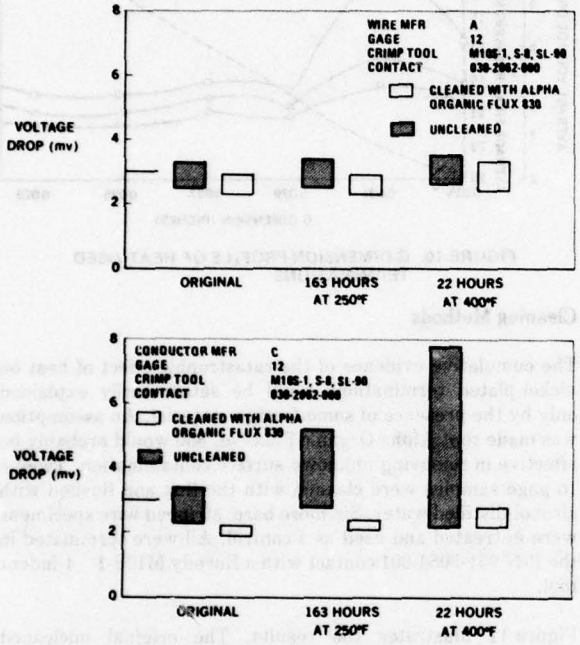


FIGURE 12. COMPARISON OF 12-GAGE FROM ALTERNATE SOURCES

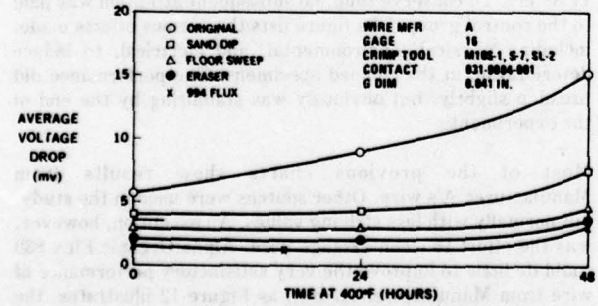


FIGURE 13. EFFECTS OF VARIOUS CLEANING AGENTS ON HEAT-AGED TERMINATIONS

inserting the stripped conductor a few times into a beaker of sand, followed by an alcohol rinse. Another procedure was to hold the conductor stationary in a beaker of floor-sweep compound for approximately 15 seconds. Without touching the strands or wiping them in any fashion, the residue was rinsed off with alcohol and the sample crimped. A common pencil eraser was used to rub the strands before crimping. The evidence was growing that something was being removed from the surface that had been interfering with conductivity.

Table 5 lists the results from a further collection of cleaning agents. In the second category cited, there was no intention to sandblast off the nickel plating. The technician did not know the efficiency of the chamber. Nevertheless, the samples were crimped along with the other groupings. The bare copper low-millivolt-drop readings are particularly interesting. It should cause aerospace engineers who are committed to plated conductors to wonder if their associates in the commercial industries, using unadorned copper, know something they do not.

TABLE 5

COMPARISON OF VARIOUS CLEANING METHODS ON HEAT-AGED TERMINATIONS

MILLIVOLT DROP – 400°F

CLEANING PROCEDURE	INITIAL	93 HR	117 HR	140 HR	330 HR
NONE	5.96	31.02	28.91	36.22	42.13
SAND BLASTED ALCOHOL RINSE PLATING REMOVED	2.75	2.85	2.79	2.74	3.03
200L FLUX, 2442 HOT H_2O ALCOHOL RINSE	4.05	6.66	6.10	8.36	10.53
ROTARY ERASER ALCOHOL RINSE	3.77	5.31	5.73	6.58	7.37
800 GRIT CROCUS CLOTH	3.03	3.63	3.56	3.67	4.13
200L FLUX, HOT H_2O ALCOHOL RINSE	3.05	3.08	3.3	3.1	3.27
SAND BLASTED PLATING INTACT	2.99	4.11	4.0	4.25	5.2

MILLIVOLT VALUES ARE AVERAGES OF 3 SAMPLES

The values given in the table are averages from three samples. The high measurement of the three samples for the initial control group was more than 103 millivolts.

Contamination Analysis

The first attempt to determine the nature of the additional material on the surface of nickel-plated wire employed the Auger electron spectroscope. An ionized argon beam "sputters" the surface, and the removed elements are identified on the spectroscope. Plotting only the results for nickel and oxygen, as shown in Figure 14, reveals that a high percentage of nickel is obtained in just a few minutes for the sample cleaned with floor- sweep mixture. Conversely, the uncleaned conductor requires 20 to 30 minutes of "sputtering" to achieve an equivalent percentage. This indicates the requirement to remove intervening material.

Plotting the oxygen reading, the Auger detects very little of that element on the cleaned sample. But it requires approximately 20 minutes or more to remove the additional surface oxygen from the uncleaned wire. The surface contaminant would appear to consist of an oxygen compound of some nature.

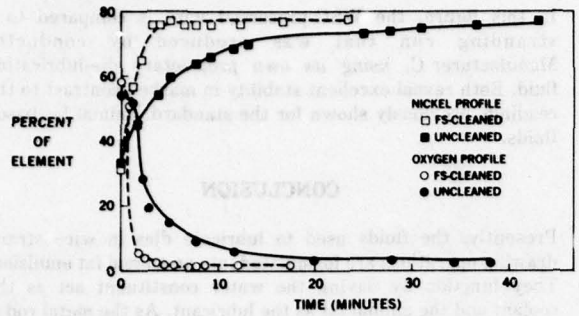


FIGURE 14. AUGER ELECTRON SPECTROSCOPIC COMPOSITIONAL DEPTH-PROFILES OF SURFACE REGIONS ON UNCLEANED AND FS-CLEANED WIRES

The scanning electron beam microscope was used for a series of magnifications. Figure 15 presents selected photographs. The cleaned samples were affected by dipping the stripped wire into the commercial floor-sweep mixture. The 220X photograph of the control specimen shows a concentration of material that is admittedly not standard. Contamination particles of this size were not normally observed at this magnification. The 1100X photograph of an uncleaned surface shows the more common sight. The surface of the nickel plate is covered by globules of some extraneous substance.

Drawing of nickel-plated wire requires the use of a die lubricant. In annealing the final strand, another fluid is used for quenching. These liquids are quite standard in metalworking operations and frequently are formulations of considerable antiquity, having been developed empirically many years ago. The die lubricant is a low-viscosity oil usually based in part on zoological products. Quantities of these fluids were secured from the principal conductor suppliers. They were evaporated and reduced to their solid residues. Infrared spectrographs were obtained not only from these substances but also from the globules illustrated in Figure 15. Needless to say, the comparative study of these spectrographs noted many lines of similarity. Both showed the unmistakable presence of straight chain hydrocarbons with minor amounts of ester linkages. A strong assumption can therefore be made that trace residues of the drawing and quenching fluids frequently remain in varying amounts on the surface of nickel-plated strands.

New Manufacturing Process

An alternate fluid was selected. It consisted of a water soluble gum (WSG), diluted with water to concentrations of from 1 to 3 percent. It is organic in nature, and acted to enhance the viscosity of the water. It is an efficient friction reducer during the passage of the strand through the dies, but showed little subsequent tendency to adhere to the nickel surface.

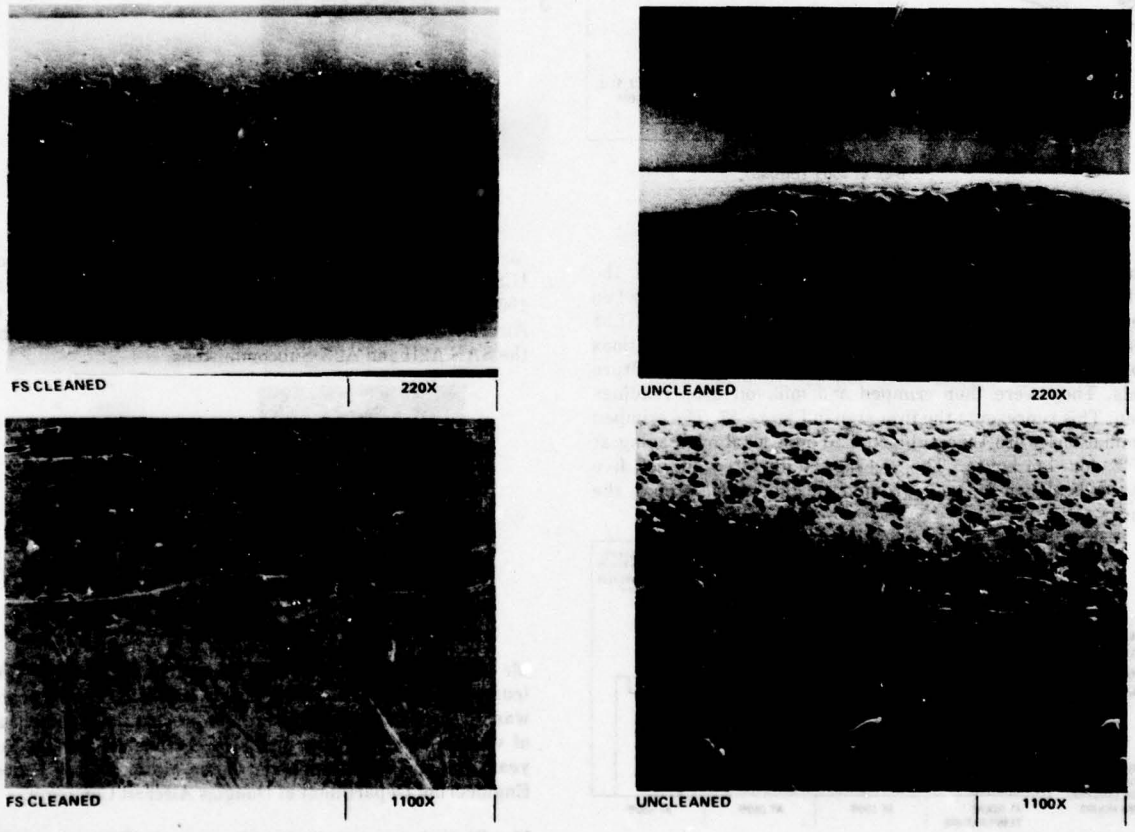


FIGURE 15. ELECTRON BEAM MICROSCOPE PHOTOGRAPHS

Cooperative stranding producers made special runs of nickel-plated conductor, utilizing WSG in place of the standard fluids. These wires were then crimped and studied in the previously described fashion. Figure 16 shows some of the results of the products from two stranding suppliers. Although the millivolt drop still does not quite correspond to tin-plated wire performance, the stability of the readings at elevated temperature over appreciable time is encouraging.

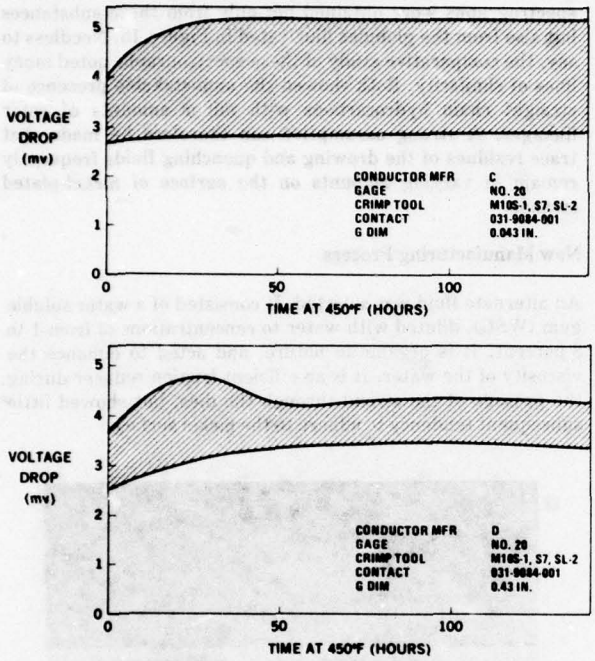


FIGURE 16. HEAT-AGING OF WATER SOLUBLE GUM PROCESSED WIRE

Figure 17 illustrates an investigation to detect if the performance of WSG-processed wire would deteriorate when appreciable time elapsed between fabrication and use. Time was simulated by temperature exposure. Sample populations of bare conductor were aged 884 hours at various temperature levels. They were then crimped and millivolt drop readings taken. This represents the first step in Figure 17. The crimped terminations were then subjected to additional oven-aging at 450°F for 144 hours. The average millivolt value of five samples is shown for each grouping in the second step of the figure.

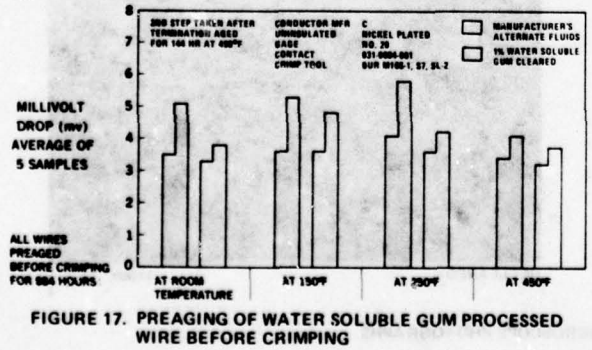


FIGURE 17. PREAGING OF WATER SOLUBLE GUM PROCESSED WIRE BEFORE CRIMPING

In this figure, the WSG-processed wire is compared to a stranding run that was produced by conductor Manufacturer C, using its own proprietary die-lubricating fluid. Both reveal excellent stability in marked contrast to the readings previously shown for the standard, animal fat-based fluids.

CONCLUSION

Presently, the fluids used to lubricate dies in wire strand drawing operations are formulated into an animal fat emulsion. They function by having the water constituent act as the coolant and the animal fat as the lubricant. As the metal rod is forced through the dies, the emulsion is broken and discrete animal organic products form a coat on the finished strand. The animal fat is not soluble in water, having to be emulsified with a soap to form a colloidal solution. Consequently, any residue deposited on the strand cannot be readily removed by redissolving it in water. The many millivolt drop experiments discussed in this paper would indicate this tenacious residue interferes with electrical connections.

An alternative production method is therefore proposed: to use an aqueous solution of a water soluble gum. This readily miscible mixture, depending upon the molecular weight of the material used, could be of a viscosity that will permit its use as a strand drawing coolant and lubricant.



Ronald P. Fialcowitz

Mr. Fialcowitz graduated in 1952 with a B.S. degree from the U.S. Merchant Marine Academy, Kings Point, N.Y. Since 1962, he has been an electrical components engineer at Douglas Aircraft Company, Long Beach, California. He is a member of the SAE A2H and A2X Subcommittees.



Michael T. Gromek

Mr Gromek graduated from Pennsylvania Military College (currently Widener) in 1955, with a B.S.M.E. For 13 years, he was involved in the equipment and process development areas of various semiconductor industry companies. For the last 10 years, he has been a member of the Materials and Processes Engineering Department of Douglas Aircraft Company.

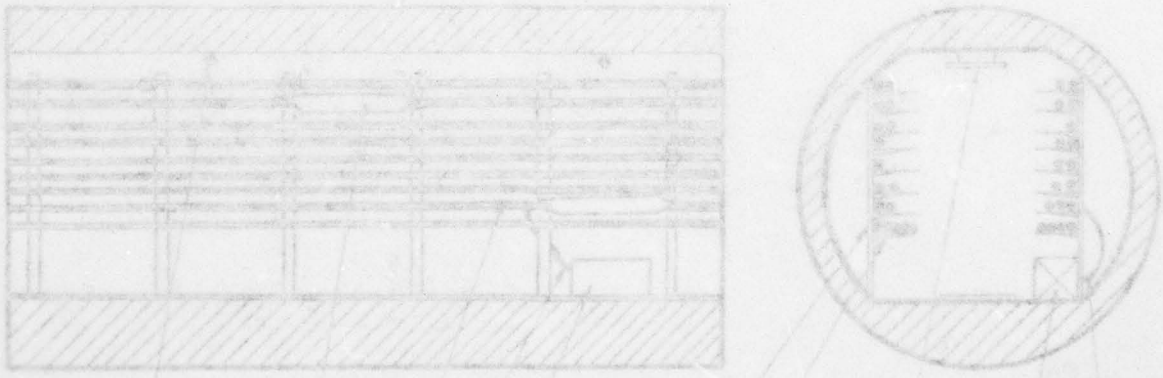
Mr. Gromek was awarded an Engineer-in-Training certificate from the State of Delaware in 1955.



Norman R. Byrd

Dr. Byrd graduated from the Polytechnic Institute of Brooklyn in 1948 with a B.S. degree in chemistry, and in 1954 with a Ph.D in organic chemistry. Since then, he has worked in chemical research with DuPont, Goodyear, Rayonier, and Ford Aeronutronic. Since 1962, he has been with Douglas Aircraft Company, and is currently in charge of chemical research.

Dr. Byrd is a member of the American Chemical Society, the Chemical Society of London, the American Association for the Advancement of Science, and the New York Academy of Science. He is also a member of Phi Lambda Upsilon (Honorary Chemistry Society), Sigma Xi (Honorary Scientific Research Society), and is a Fellow of the American Institute of Chemists. He has written numerous publications and holds many patents.



NEW JUNCTION CABLE WITH LOADING COILS FOR CABLE TUNNEL USE

K. Ishizaki and K. Mori
Nippon Telegraph and Telephone Public Corp.
Tokyo, Japan

K. Sugiyama
The Furukawa Electric Co., Ltd.
Tokyo, Japan

Y. Iwamoto
Sumitomo Electric Industries, Ltd.
Yokohama, Japan

H. Ishihara
The Fujikura Cable Works, Ltd.
Tokyo, Japan

Summary

In a cable tunnel system, cable outer diameter and length are not as limited as in a conduit system. Since 1971, NTT has investigated the most suitable junction cable for cable tunnel use. Field tests were made on cables from 1974 to 1976 and commercial tests have been conducted to examine various cable characteristics since 1977. These cables are now successfully in service. A series of these tests proved that a multi-pair and long-section cable with loading coils is an optimum cable structure for cable tunnel use.

This new junction cable includes new small loading coils at its midpoint. The part containing loading coils is almost the same as the cable alone in outer diameter and in mechanical characteristics to ease handling the cable.

This paper describes commercial test results regarding electrical and mechanical characteristics, as well as cable structures.

1. Introduction

A cable tunnel is one of several underground facilities to accommodate telecommunication cables. It is most effective in congested city areas. In the existing conduit system, it is difficult to install and maintain many cables in a manhole. Since most manholes are constructed in a street, it is difficult to reconstruct and to extend the system due to traffic congestion. The cable tunnel system has a large cable accommodation capacity and has the ability to protect telecommunication circuits in case of an earthquake. The total length of cable tunnels in Japan amounts to about 200km, and increases year after year. Furthermore, a "Cable Tunnel Network Project"[1] in urban areas is now under consideration. After accomplishment of this plan, the total length will amount to about 1,100km.

Figure 1 and photograph 1 show a cable tunnel.

In order to utilize the advantage of a cable tunnel where cable outer diameter and length are not as limited as in a conduit system, investigations have been conducted with regard to cable structures.

Junction cables, which are generally used in a cable tunnel, were studied to determine an optimum structure for cable tunnel use. As a result, a multi-pair and long-section cable, based on the existing junction cable, was designed to relax restrictions on outer diameter and length. Additionally, coil inclusion internally in the cable improves the reliability at cable splices and decreases the number of splices required during cable installation.

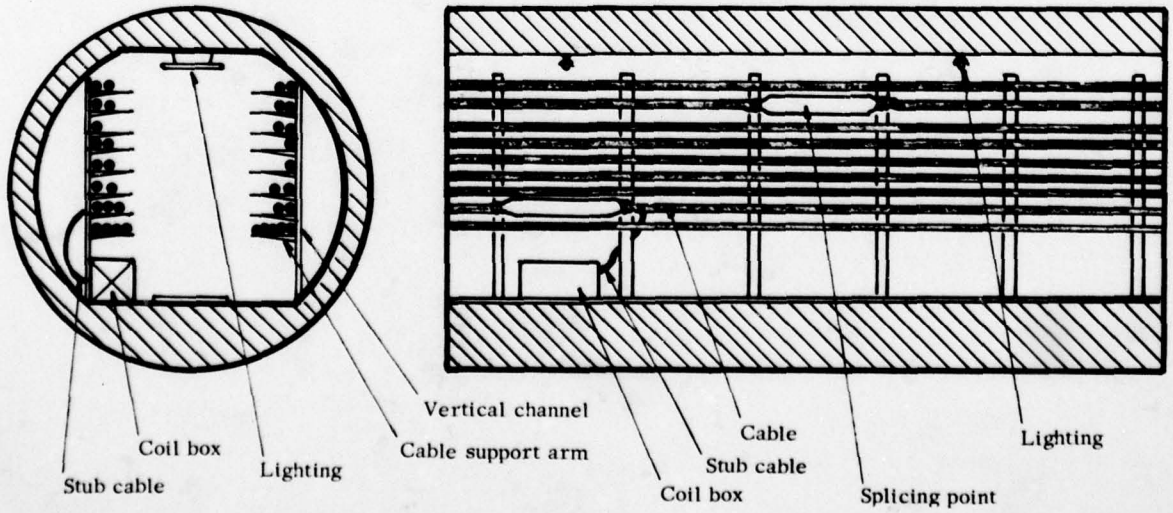


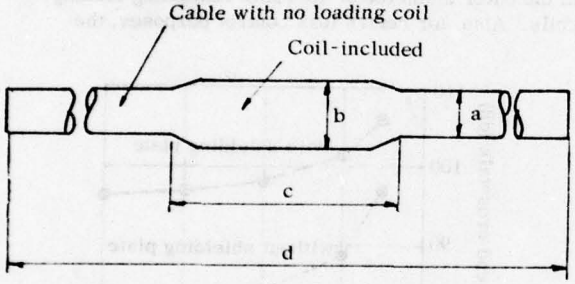
Figure 1 Cable tunnel



Photograph 1 Cable tunnel

2. Cable Structures

Figure 2 shows the cable for commercial tests under practical use environments.



a (Cable outer diameter)	: nominal	79 mm
b (Coil including outer dimater)	: maximum	99 mm
c (Coil including length)	: maximum	17 meters
d (Cable length)	: nominal	500 meters

Figure 2 Cable for commercial tests

This cable has foamed polyethylene (PEF) insulated conductors and laminated aluminum polyethylene (LAP) sheathing. The cable is 0.65mm–1,400 pair (containing 1,200 loaded pairs) which is 400 pairs more than the maximum for conventional 0.65mm conductor cable. Cable length, 500 meters, is almost twice conventional cable length. The cable is designed so as to include loading coils at its midpoint. Moreover, considering the cable laying ease, the outer diameter of the part containing loading coils is nearly the same as the cable alone.

2.1 Multi-pair and Long-section Design

.1.1 Multi-pair

The following restrictions are considered in designing a multi-pair cable.

(1) Restriction on transportation

In Japan, traffic rules generally restrict truck size to less than 2.5 meters wide, 12 meters long, 3.8 meters high and 20 tons in gross weight. These dimensions determine transportable cable drum size and truck weight loaded cable. When winding a cable on a cable drum for transportation, there are several limiting factors which must be taken into account. The cable bending ratio, determined by its radius of curvature, limits the size of the cable drum core. The width limitation set up for the transport facility – the truck – limits cable drum width. Also, the diameter of the cable itself limits the length which can be wound on a cable drum – the larger the diameter, the shorter the overall cable section length. Therefore, large multi-pair cable design (a great number of pairs accommodation in one cable) is contrary to long-section cable design (a cable-piece length enlargement) described in paragraph 2.1.2.

(2) Cable support arms interval

Upper and lower cable support arms are fixed at intervals of about 20cm in a cable tunnel. Hence, the outer diameter of both the cable and its splice must be less than the space between cable support arms.

(3) Cable laying workability

It is desirable to enlarge a cable outer diameter so as to accommodate a great number of pairs in one cable, not so far as the efficiency lowering in cable transporting and laying.

2.1.2 Long-section

In Japan, most of conduit systems are composed of rigid polyvinyl-chloride (PVC) pipes and cast iron pipes. A cable-piece length is restricted to about 250 meters due to friction between cable and conduit when pulling the cable into conduit.

On the other hand, in a cable tunnel, it is not necessary to consider the friction. This makes it possible to increase cable length.

Long-section design has, however, restrictions as well as multi-pair design. Especially, electrostatic coupling is the most important factor to be considered.

In Japan, junction circuits are generally loaded. Crosstalk in loaded circuits is chiefly because of electrostatic coupling. When a cable is manufactured, electrostatic coupling in each quad increases with complex characteristics of the following factors.

(i) Random coupling along cable
(proportional to square root of the cable length)

(ii) Uniform coupling along cable
(proportional to the cable length)

Therefore, the cable length cannot be increased freely because uniform coupling along the cable cannot be disregarded. A pair-type cable makes it relatively easy to increase the cable length. In Japan, however, a quad-type cable with a high rate of conductor accommodations is used. It was decided not to change the cable structure from the quad-type to the pair-type, because the change would have a major influence on the present telecommunication cable system.

Through consideration on the above restrictions in paragraph 2.1.1 and 2.1.2, 1,400 pairs and 500 meters was adopted as optimum values for 0.65mm conductor cable.

2.2 Coil Inclusion Concept

An internal loading coil structure is designed in order to use the cable tunnel space effectively, to improve reliability in splices and to save construction manpower due to splicing point decrease. Cable sections including coils can be handled in the same way as other parts of the cable.

2.2.1 New Small Loading Coil

A new small loading coil was developed, having the same electrical properties as the conventional loading coil, for inclusion into the cable during its manufacture and for use with existing loading coil systems.

Figure 3 illustrates the new small loading coil and Table 1 shows its dimensions and electrical characteristics compared with those of the conventional loading coil.

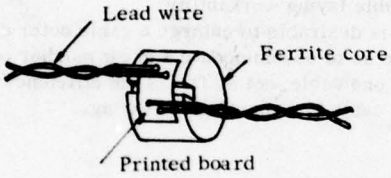


Figure 3 New small loading coil

Table 1 Comparison between new small coil and conventional coil

Item		New small coil	Conventional coil
Core size	Outer diameter	14 mm	17 mm
	Height	10.5 mm	13 mm
Inductance		100±1.5mH	100±1.5mH
Effective resistance		< 20 Ω	< 20 Ω

Here, an idea was worked out to facilitate splicing work between cable conductors and the winding coil wire involved in this new coil. A printed board is bonded to the ferrite core with an adhesive. Through this board, 0.14mm coil wires and 0.4mm lead wires are soldered to each other. The lead wire, as it is, does not have sufficient mechanical strength. Epoxy resin is painted over this contact area to give more strength. Therefore, the splice has higher mechanical tensile strength than the 0.4mm lead wire.

2.2.2 Coil Unit Structure

A coil unit is composed of a hundred new coils in a line. Since there would be crosstalk due to magnetic flux between coils, shielding plates are put between them. Figure 4 shows the near-end crosstalk improvement with shielding plate. A shock-absorbing material is used to reduce friction between coil and plate for flexibility, and to protect the vulnerable ferrite core from direct external stress. Lead wires are placed along the aligned coils.

Coil unit structure is shown in Fig. 5.

2.2.3 Coil Units Arrangement

Coil units are circular to prevent an increase in the outer diameter of the cable containing loading coils. Also, for return loss control purposes, the

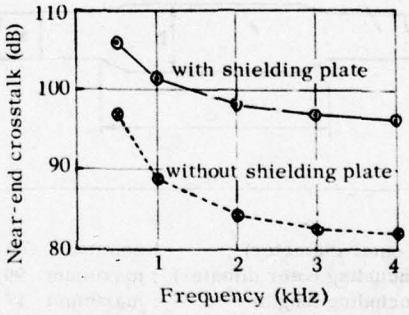
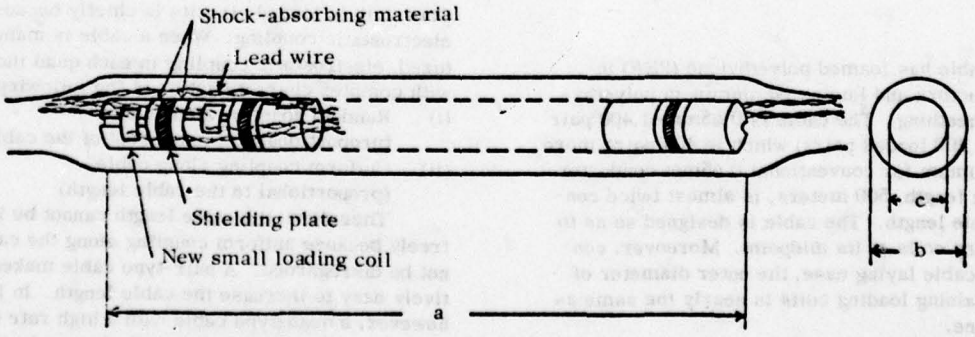


Figure 4 Near-end crosstalk improvement with shielding plate



a (Coil unit length) : about 1300 mm
b (Coil unit outer diameter) : about 27 mm
c (New small coil outer diameter) : 14 mm

Figure 5 Coil unit structure

allowable length of cable containing the loading coil is within 22 meters, which is a half of 5 percent loading interval deviation. This means that this part is made as short as possible. However, the loading coil units cannot be too bunched together. Loading coil units, each unit handling 100 pairs, are located in the cable as shown in Fig. 6. To ease installation, loading coil units are installed in pairs on opposite sides of the cable. Subsequent pairs of loading coil units are placed end on from the previous two loading coil units, but located at a different circumferential position. Figure 6 shows one pair of loading coil units in the A-A' position in the cross section view. The subsequent loading coil units are shown in the B-B' position in the cross section view.

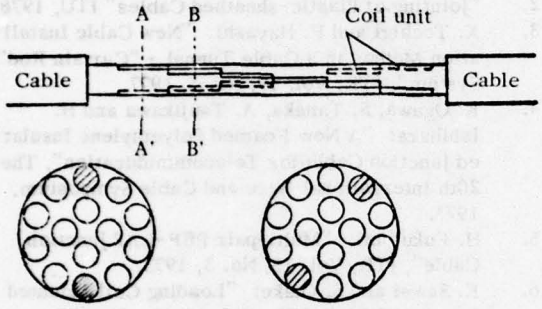


Figure 6 Coil unit arrangement

2.2.4 Splicing at Coil-including Part

Splicing between coil unit and cable conductors is made by manual twist and soldering. Spliced pairs are covered with a sleeve. This method makes it possible to reduce the outer diameter of the cable containing loading coils.

The coil units are sheathed with a polyethylene pipe with a thin metal layer. The pipe is jointed to the cable sheath by a heat-welding method.

2.3 Cable Splicing in Cable Tunnel

The cable conductors are spliced by using a conductor splicing machine. An auxiliary lead sleeve method[2] is adopted for cable sheath jointing. The splice is made longer to prevent an increase in lead sleeve diameter.

3. Commercial Tests

NTT began commercial tests on many kinds of cable characteristics in 1977.

3.1 Commercial Test Outlines

Commercial tests were held in about 6 km junction line between Shinjuku and Ikebukuro telephone office in Tokyo. These new junction cables were laid in cable tunnels by means of a "Curtain Rod" system[3].

The factors examined in these tests are described below.

(1) High frequency characteristics of non-loaded circuits (Attenuation constant, Near-end crosstalk, Far-end crosstalk)
(2) Voice frequency characteristics of loaded circuits (Attenuation constant, Characteristic impedance, Near-end crosstalk)
(3) Electrostatic coupling in each quad
(4) Gas pressurization characteristics (Gas flow resistance, Pneumatic volume, Gas flow rate)

3.2 Commercial Test Results

Cables were laid under conditions wherein the minimum radius is about 80cm on cable drum and the maximum vertical height from ground level to cable tunnel bottom is about 30 meters. Despite these severe conditions, neither mechanical nor electrical troubles occurred. This means that the cables have sufficient mechanical strength for cable laying.

The high frequency characteristics of non-loaded line are shown in Fig. 7. These characteristics are as good as those of the conventional multi-pair PEF-LAP junction cable[4,5].

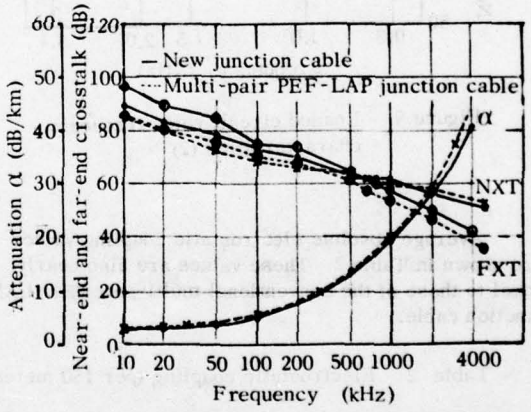


Figure 7 High frequency characteristics of non-loaded line

The voice frequency characteristics of loaded circuits are shown in Figs. 8 and 9. These characteristics are almost equal to those of the existing loaded circuit which includes conventional loading coils.

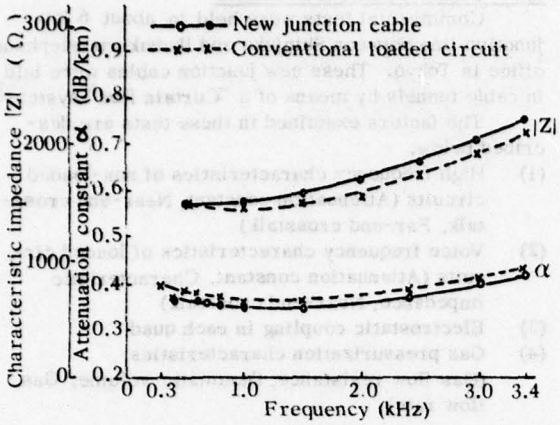


Figure 8 Loaded circuit voice frequency characteristics (1)

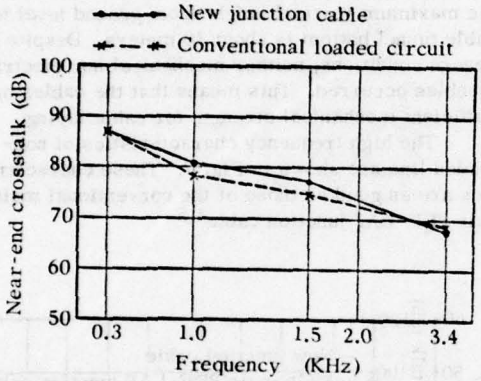


Figure 9 Loaded circuit voice frequency characteristics (2)

Average absolute electrostatic coupling values are shown in Table 2. These values are also nearly equal to those of the conventional multi-pair PEF-LAP junction cable.

Table 2 Electrostatic coupling (per 150 meters)

Item	Electrostatic coupling	
	Average	Maximum
New junction cable	15 pF	81 pF
Multi-pair PEF-LAP junction cable	19 pF	88 pF

Gas pressurization characteristics are shown in the following.

Gas flow resistance : 1.6×10^{-4} $\left[\frac{(kg/cm^2)^2}{m \cdot g/min}\right]$

Pneumatic volume : 2.8 $\left[g/(m \cdot kg/cm^2)\right]$

Gas flow rate : 4.7×10^3 (m^2/min)

4. Conclusion

This new junction cable increases overall working space in a cable tunnel due to elimination of loading coil boxes and stub cables. It improves reliablility due to loading coil inclusion during its manufacture, and saves construction manpower due to splicing point decrease.

Along with the growth of cable tunnel networks, this new junction cable with loading coils will be extensively introduced in Japan.

Reference

1. H. Shimura and N. Sugawara; "Cable Tunnel Network Projects in Large Cities", JTR, Vol. 15, No. 4, 1973.
2. "Jointing of Plastic-sheathed Cables" ITU, 1978.
3. K. Tochigi and F. Hayashi; "New Cable Installation Method in a Cable Tunnel - "Curtain Rod" System", JTR, Vol. 19, No. 4, 1977.
4. K. Ogawa, S. Tanaka, A. Tsujikawa and H. Ishihara; "A New Foamed Polyethylene Insulated Junction Cable for Telecommunication", The 20th International Wire and Cable Symposium, 1971.
5. H. Fukutomi; "Multi-pair PEF-LAP Junction Cable", JTR, Vol. 15, No. 3, 1973.
6. K. Sawai and S. Otake; "Loading Coil Mounted Junction Cable", JTR, Vol. 19, No. 3, 1977.



Kohsuke Ishizaki
Nippon Telegraph and Telephone Public Corporation
1-1-6 Uchisaiwai-cho, Chiyoda-ku, Tokyo, Japan

Mr. Ishizaki, Staff Engineer of NTT's Engineering Bureau, is now engaged in developmental research on junction cables with loading coils for cable tunnel use, local network system and aluminum conductor cables.



Yuhya Iwamoto
Sumitomo Electric *Industries, Ltd.*
1 Taya-cho, Totsuka-ku, Yokohama, Japan

Mr. Iwamoto is an engineer in Communication Cable Accessories Engineering Section of Sumitomo Electric Industries, Ltd. and is engaged in communication cable accessories development and designing.

He received B.E. degree in Tokyo Metropolitan University in 1972.



Kenji Mori
Nippon Telegraph and Telephone Public Corporation
1-1-6 Uchisaiwai-cho, Chiyoda-ku, Tokyo, Japan

Mr. Mori, Staff Engineer of NTT's Engineering Bureau, is now engaged in developmental research on protection of telecommunication outside plant, cable gas pressurization monitoring system and so on.

He is a member of the Institute of Electronics and Communications Engineers of Japan.



Hirofumi Ishihara
The Fujikura Cable Works, Ltd.
5-1, Kiba 1-chome, Koto-ku, Tokyo, Japan

Mr. Ishihara was born in 1942. He joined the Fujikura Cable Works, Ltd. as a member of technical staff after his graduation from Kyushu Institute of Technology in 1965.

He is now an assistant chief of Telecommunication Cable Engineering Department.



Kazuo Sugiyama
The Furukawa Electric Co., Ltd.
6-1, Marunouchi 2 chome, Chiyoda-ku, Tokyo, Japan

Mr. Sugiyama graduated from Osaka University in 1964 with a B.E. degree in electrical engineering.

Upon graduation he joined the Furukawa Electric Co., Ltd. and was engaged in research and development of telecommunication cables.

He is now an assistant manager of Technical Department of Telecommunication Division and a member of the Institude of Electronics & Communications Engineers of Japan.

LIGHTNING SURGES IN BURIED, FILLED TELEPHONE DISTRIBUTION CABLE

by

J. J. Refi and M. J. Swiderski
Bell Laboratories
Norcross, Georgia 30071

Abstract

Pair-to-pair and pair-to-shield peak voltage surges were monitored for 152 days during the 1977 lightning season on a buried, filled distribution cable in Munson, Florida. A total of 106 surges greater than 0.5 kV were recorded during 72 thunderstorm days. When normalized, these equate to 0.41 surges per thunderstorm day per monitoring channel (pair-to-pair or pair-to-shield). This frequency is about the same as that reported previously by other investigators. However, the Munson data differ significantly in that surge amplitudes were recorded which are substantially greater than previously reported.

Introduction

Conductor-to-conductor high voltage test requirements for multipair telecommunications cable have traditionally been based on the insulating material's inherent dielectric strength plus its ability to withstand normal manufacturing processes. For example, for cables used in the Bell System, the conductor-to-conductor high voltage requirements are 500 volts dc for pulp and from 2.4 to 5.0 kV dc for air core PIC (plastic insulated conductor) depending on gauge. (Of course the actual performance of these insulations, particularly plastic, is much higher than the factory test requirement.)

Because of its low dielectric strength, pulp cable is much more vulnerable to lightning than PIC. To lessen this vulnerability, cable protectors are used more frequently on pulp than in comparable PIC installations. However, there has been little field information on the magnitude of conductor-to-conductor surges that cable actually experiences. Such information is vital for setting high voltage requirements that cable must meet to insure a high probability of survival. Although a fair number of lightning surge measurements have been made in the past, all of these have been of pair-to-shield and pair-to-ground voltages.[1,2,3] Accordingly, a field measurement program was undertaken to measure pair-to-pair voltages in a buried filled distribution cable in a high lightning area.

Study Site

Cable Route

The measurement site is located in Southern Bell's Pensacola District in an extremely rural area of the Blackwater River State Forest in Munson, Florida - about 28 air miles northeast of Pensacola. The Pensacola District is generally assumed to have a soil resistivity of 1000 meter-ohms. However, measurements made at eight points along the Munson study route yielded an average soil resistivity of 3350 meter-ohms. This resistivity, along with the area's 93 thunderstorm days in 1977 gives a lightning exposure factor of $93\sqrt{3350} = 5380$ - about the highest known in the United States.

The cable route is a commercial distribution cable consisting of solid insulation PIC cable. As shown in Figure 1, a 50-pair filled cable runs south from the Munson C.D.O. (Community Dial Office) for a distance of about 47 kft, and then splits into a 25-pair filled cable that runs west and a 25-pair air core cable that runs east. The 25-pair air core cable is then spliced into a 50-pair air core cable. Some of the pairs continue out of both the 25-pair filled and the 50-pair air core cables into aerial open wire spans. The pairs which were monitored were terminated at Indian Ford Road - about 47 kft from the C.D.O.

All of the cable in the route is 22-gauge and buried, except at two creek crossings where aerial spans ($\approx$200') of 24-gauge 50-pair air core cable are used. All splices in the buried cable (except for a few encapsulated buried repair splices) are made with B wire connectors in

above-ground pedestals.

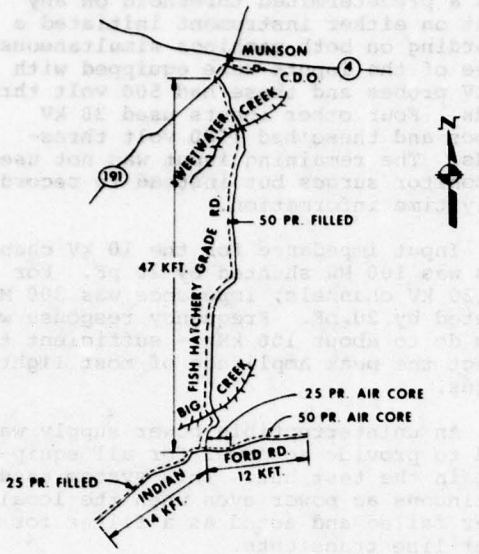


Fig. 1 - Buried distribution cable used in Munson lightning study.

A possible entry point for lightning surges into a cable core is through station protectors at the customer end of drop wires or via the drops themselves. Consequently, in order to provide lightning paths into our cable, thirteen simulated service drops were installed at the locations shown in Figure 2.

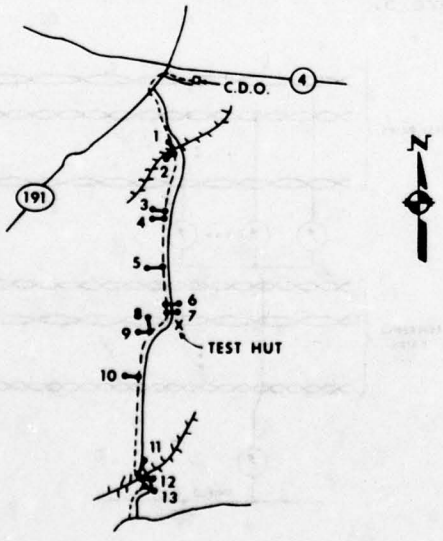


Fig. 2 - Drop and test hut locations.

Each drop was about 200' long and all were buried except for drops 1, 2, 11, 12 and 13 which were aerial. In addition, all of the aerial drops except for drop 12 were equipped with 6-mil gap carbon cable protectors (800V dc nominal breakdown) at the point of connection to the cable. All of the drops were terminated in 3-mil gap carbon station protectors (500V dc nominal breakdown) without a station set or anything else attached.

Measurements were made from a test hut located about midway along the cable route (Figure 2). The test hut exterior and the equipment in the interior are shown in Figure 3.

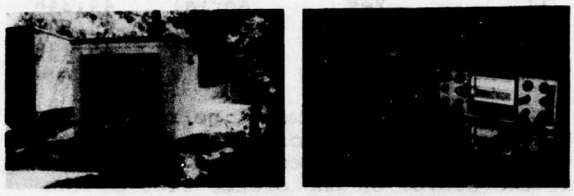


Fig. 3 - Test hut and equipment.

The test hut site is the first point from the C.D.O. at which commercial power begins paralleling the cable route (the test sets require 120V ac power). Since drops 11, 12 and 13 have their station protectors on the same side of the road as the electric power line, the ground connections for the station protectors on these drops were connected not only to ground rods, but also to the power line neutral. Station protector grounding for all other drops was accomplished via ground rods.

Each of the thirteen drops was connected to a "test" pair in the 50-pair filled cable. In addition to these thirteen test pairs, five more pairs were designated as "reference" pairs. These "reference" pairs differed from the "test" pairs only in that they did not have any drops attached. They served as a reference against which surges on the test pairs were measured.

To summarize, all reference and test pairs extend out of the C.D.O. and run for a distance of about 47 kft to the end of the 50-pair filled cable. At that point, they are cleared, cut dead and encapsulated. All of them were checked for continuity, had all loading coils removed, and had their splices encapsulated. This was done to insure that the measured surges were not clipped by electrical breakdown within load coils or splices. Details of each drop are given in Table 1.

TABLE 1

Drop Summary

Drop Number	Cable Protector	Type of Drop	Footage to C.D.O.
1	Yes	Aerial	8,519
2	Yes	Aerial	8,519
3	No	Buried	14,924
4	No	Buried	15,188
5	Yes	Buried	20,530
6	No	Buried	26,338
7	No	Buried	26,522
8	No	Buried	27,922
9	No	Buried	27,922
10	No	Buried	32,518
11	Yes	Aerial	44,346
12	No	Aerial	44,521
13	Yes	Aerial	45,138

To simulate normal line relays, all test and reference conductors were terminated in 450Ω resistors to ground at the C.D.O. on the office side of the fused office protectors (Figure 4).

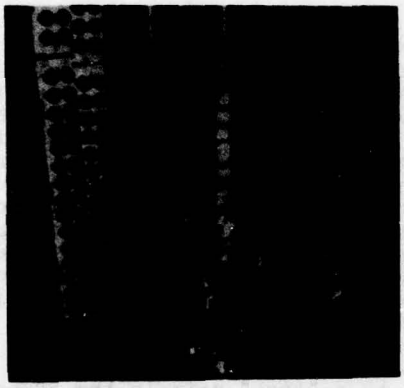


Fig. 4 - 450Ω resistors terminating test and reference conductors in the C.D.O.

Instrumentation

Pair-to-pair and pair-to-shield surges were measured using two memory voltmeters. Each voltmeter contained four independent monitoring channels sharing a common power supply and chassis. Each channel controlled one pen on a four pen pressure sensitive strip chart recorder. The instruments were "on-line" all the time even though the chart recorder might not be running. When a surge occurred, its peak amplitude was stored in a digital memory. If its amplitude exceeded a certain threshold, the chart recorder started running and the amplitude was recorded on the paper.

The two instruments were connected to run in parallel so that a surge greater than a predetermined threshold on any input on either instrument initiated a recording on both machines simultaneously. Three of the inputs were equipped with 10 kV probes and these had 500 volt thresholds. Four other inputs used 30 kV probes and these had 1500 volt thresholds. The remaining input was not used to monitor surges but instead to record daily time information.

Input impedance for the 10 kV channels was 100 MΩ shunted by 20 pF. For the 30 kV channels, impedance was 300 MΩ shunted by 20 pF. Frequency response was from dc to about 100 kHz - sufficient to detect the peak amplitude of most lightning surges.

An uninterruptible power supply was used to provide ac power for all equipment in the test hut. This system assured continuous ac power even when the local power failed and acted as a filter for power line transients.

Connection to Monitored Pairs

The conductors of all five reference pairs were connected together at the test hut and served as the signal common (not ground). Additionally, the tip conductor of each test pair was connected to its respective ring conductor. Longitudinal surges were then measured between selected test pairs and the grouped reference pairs. Pair-to-shield surges were measured between the grouped reference pairs and shield. The pair-to-pair and pair-to-shield connections are shown in Figure 5.

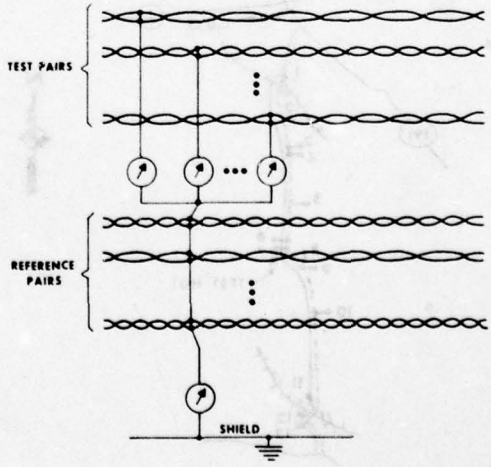


Fig. 5 - Connection to monitored pairs.

Of the thirteen test pairs available, six were monitored. Five of these (drops 6, 7, 11, 12 and 13) were monitored full-time whereas drops 3 and 4 took turns on the other channel. The seventh channel was used to monitor pair-to-shield surges and the eighth channel was dedicated solely for recording daily time information. In addition, some of the other drops were also monitored with quantized surge counters. These counters did not have a time base and, thus, their results are not included here. Their data, however, do support the results from the memory voltmeters.

Results and Analyses

Surge Day Correlation with Thunderstorms

The study period ran from May 27 to October 25, 1977. During these 152 days, 72 thunderstorm days were reported by the Naval Air Station at Whiting Field which is about 9 miles southwest of the test site. Surges were recorded at the test site on 22 days. Nineteen of these 22 surge days were reported as thunderstorm days at Whiting Field. It is likely that isolated local storms occurred in Munson on the other three days. This excellent correlation of surge days with thunderstorm days imbues confidence that the recorded surges are associated with storms and are not caused by power transients, crosses or other vagaries.

Lightning Damage to Drop 4

On July 30, 1977, an off-scale surge (greater than 10 kV) was recorded on the test pair connected to drop 4. Examination revealed extensive sheath and conductor damage to the buried drop over a distance of about 25 ft from the pedestal splice into the distribution cable. Figure 6 shows the shield damage to the drop at a point within the pedestal. Burning, charring and melting are evident.



Fig. 6 - Lightning sheath damage to drop 4 on length within the pedestal.

Removal of the sheath at a point two feet from the pedestal splice revealed extensive internal heat damage. Figure 7 shows the shield corrugations impressed into the softened conductor insulation. The melted plastic caused the conductors to short to the shield.



Fig. 7 - Lightning conductor damage to drop 4, two feet from the pedestal splice.

Although the area immediately surrounding the site of drop 4 was examined for physical evidence of a lightning stroke, none was found. However, the heat damage to the drop, the absence of any power lines and the large recorded surge leads to the inescapable conclusion that the drop was damaged by lightning.

Surge Amplitude Frequency

Figure 8 shows a histogram of the surge amplitudes normalized to a monitoring channel and a thunderstorm day. Note that the figure shows a surge frequency of 0.002 greater than 17 kV. This represents the occurrence of the surge that damaged drop 4. The surge went off scale on a 10 kV monitoring channel, and auxiliary instrumentation on this pair (a surge counter) indicated that it was greater than 17 kV.

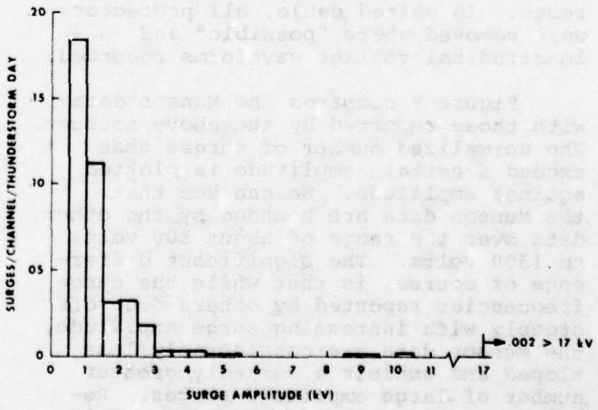


Fig. 8 - Normalized surge frequency as a function of amplitude.

Comparison of Data to Others

A fair number of measurements of lightning surge voltages in telephone cables have been made in the past. Messrs. D. W. Bodle and P. A. Gresh published a paper in 1961 on voltage surges that they measured in trunk telephone plant in areas with low and high degrees of lightning exposure.[1] The low exposure measurements were made on underground cable in Baltimore, Maryland; Pontiac, Michigan; and South Orange, New Jersey. The high exposure measurements were made on aerial cable in Buford, Georgia (100 pair, PIC, Alpeth) and Mt. Freedom, New Jersey and on buried cable in Griffin, Georgia (jute-protected, lead-sheathed, quadded with external shield wires). In each of the high exposure areas, open-circuit longitudinal surge voltages and resultant metallic voltages across a representative resistive termination were recorded. All of the measurements were made at the central office across standard 3-mil office protectors having a breakdown of about 500 volts dc.

In 1972, Mr. Yukinori Ishida published his results on lightning surges measured on toll and distribution cables in various areas in Japan.[2] Longitudinal voltage surges were measured at cable terminals using oscilloscopes and surge counters. The degree of plant exposure and the presence or absence of protectors are not discussed in the paper.

In 1973, Messrs. E. Bennison, A. J. Ghazi and P. Ferland published their results on lightning surges measured on toll facilities in ten areas of Canada.[3] Open wire, paired cable (aerial and buried) and coaxial cable (aerial and buried) were measured. The test site was located midway along each route. In paired cable, all protectors were removed where "possible" and longitudinal voltage waveforms recorded.

Figure 9 compares the Munson data with those reported by the above sources. The normalized number of surges that exceed a certain amplitude is plotted against amplitude. We can see that the Munson data are bounded by the other data over the range of about 500 volts to 1500 volts. The significant difference of course, is that while the surge frequencies reported by others drop off steeply with increasing surge amplitude, the Munson data are considerably less sloped and exhibit a markedly greater number of large amplitude surges. Recall that the Bodle-Gresh surges could not exceed about 500 volts because of the presence of central office protectors (the above plot shows an extrapolation of their data). Ishida does not mention protectors and so it is not clear whether his data are similarly limited. The Bennison, Ghazi and Ferland data, however, were presumably not amplitude limited. Perhaps the differences between their data and ours are due to their routes being toll whereas ours was distribution cable. Distribution cable might be more vulnerable to lightning because of the greater number of entry points.

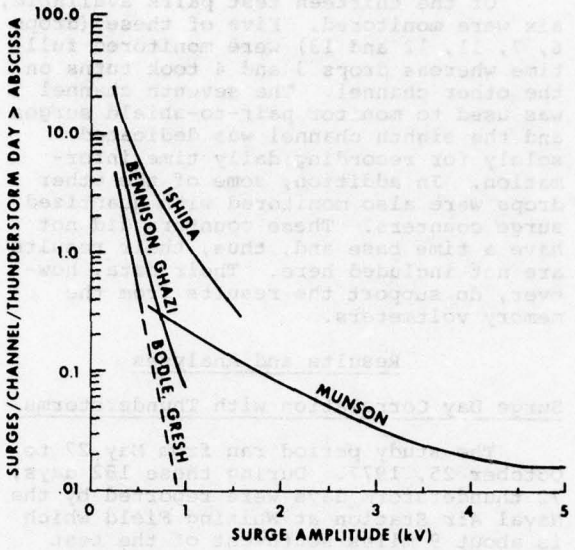


Fig. 9 - Comparison of Munson data to that obtained by others.[1,2,3]

Analytical Fit to Data

The histogram in Figure 8 suggests that the surge magnitudes are exponentially distributed. We will therefore fit an exponential probability density function to the data and then test its adequacy with a chi-square goodness of fit test.

Recall that some of the channels had a 0.5 kV threshold and some a 1.5 kV threshold. Insofar as it is the high amplitude surges that are important for cable design, we choose to fit the combined data from all channels that exceed 1.5 kV. In statistical parlance this is termed "truncation on the left," and it can be dealt with by taking the conditional distribution of surges given that they exceed 1.5 kV. For an exponential distribution, such a conditional distribution is also exponential and the probability density function is given by:

$$p(x) = \frac{1}{\lambda} e^{-(x-1.5)/\lambda} \qquad x \geq 1.5$$

where:

x = surge amplitude in kV

λ = fit parameter

A complication in fitting this equation to our surge data is that the exact magnitude of one of the surges is not known - we only know that there was one surge greater than 17 kV. This condition is termed "censoring on the right," and it can be accommodated by simply thinking of the surge as belonging to a cell which extends from 17 kV to infinity. With these imposed constraints, equation (6), Appendix A, is derived for obtaining the maximum likelihood estimate of λ. When this equation is applied to the observed data in Table 2, $\hat{\lambda}$ is found to be 1.9. We can now calculate the expected number of surges in each cell by substituting λ = 1.9 into equations (2) and (3) of Appendix A. Table 2 compares the expected surges with the observed number in each cell.

TABLE 2

Comparison of Observed and Fitted Surge Frequencies

Cell	Range (kV)	Number of Surges Observed	Number of Surges Expected From Fit
1	> 1.5 to 2.0	14	12.25
2	> 2.0 to 2.5	15	9.42
3	> 2.5 to 3.0	8	7.24
4	> 3.0 to 3.5	3	5.57
5	> 3.5 to 4.0	3	4.28
6	> 4.0 to 4.5	3	3.29
7	> 4.5 to 5.0	1	2.53
8	> 5.0 to 5.5	1	1.94
9 thru 14	> 5.5 to 8.5	0	5.14
15	> 8.5 to 9.0	1	0.31
16	> 9.0 to 9.5	1	0.24
17	> 9.5 to 10.0	0	0.18
18	>10.0 to 10.5	2	0.14
19 thru 30	>10.5 to 17.0	0	0.45
31	>17.0	1	0.02
Total		53	53

A chi-square goodness of fit test (Appendix B) leads to the conclusion that the exponential probability density function with λ = 1.9 fits the data well. This is visually confirmed in Figure 10.

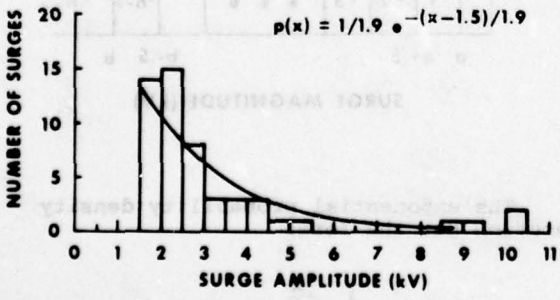


Fig. 10 - Exponential fit to observed surge data.

The fit, however, does tend to underestimate the number of high amplitude surges. For example, Figure 11 displays the fitted exponential and the experimental data for the probability that a surge exceeds a certain value.

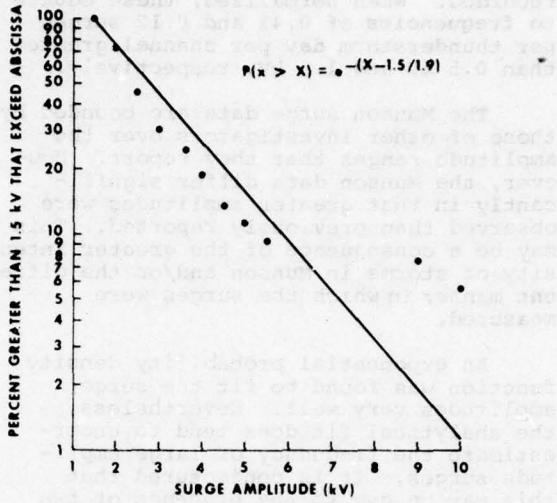


Fig. 11 - Percent of surges greater than 1.5 kV that exceed the abscissa.

It is clear from this figure that there are more observed surges above 8 kV than the fit predicts. This suggests that there may be two distinct surge populations. Looking back at Figure 10, it appears that the two populations cross one another at about 7 kV. It is conjectured that the high amplitude population is caused by direct lighting hits whereas the low amplitude population is due to induced voltages.

Similarity of Drops

The pair-to-shield surge data and the data from the various drops are insufficient to draw any strong conclusions about how the surge distribution for a particular drop compares to the data as a whole. However, the data do suggest that there are no significant differences in the surge distributions for the various drops and that pair-to-pair surges are the same as pair-to-shield.

Summary and Conclusion

Pair-to-pair and pair-to-shield voltage surges were monitored for 152 days during the 1977 lightning season on a buried, filled distribution cable in Munson, Florida. During this time, 72 thunderstorm days and 22 surge days occurred. Nineteen of these 22 surge days were thunderstorm days at Whiting

Field. Insofar as Whiting Field is about 9 miles from the test site, isolated local storms may have occurred in Munson on the other three days.

A total of 106 surges greater than 0.5 kV and 53 surges above 1.5 kV were recorded. When normalized, these equate to frequencies of 0.41 and 0.12 surges per thunderstorm day per channel greater than 0.5 kV and 1.5 kV, respectively.

The Munson surge data are bounded by those of other investigators over the amplitude ranges that they report. However, the Munson data differ significantly in that greater amplitudes were observed than previously reported. This may be a consequence of the greater intensity of storms in Munson and/or the different manner in which the surges were measured.

An exponential probability density function was found to fit the surge amplitudes very well. Nevertheless, the analytical fit does tend to underestimate the frequency of large amplitude surges. It is conjectured that this may be due to the presence of two distinct surge populations. One population has most of its surges above 7 kV and may be due to direct lightning hits. The other population has most of its surges below 7 kV and is more likely caused by induced voltages.

Insofar as previous investigators have not reported lightning environments as severe as that found here, the conditions in Munson are probably not typical of the majority of cable plant. It seems clear from our data, however, and from the actual lightning damage inflicted on the service wire during the study that large surges can occur sufficiently often in exposed rural plant to make dielectric strength an important parameter in cable design.

Acknowledgements

Messrs. J. Anderson and J. Lovelace of Southern Bell in Milton, Florida were indispensable in executing the route modifications, hut construction and day-to-day operating details of the study. Mr. R. Shupe gave helpful support and Mr. F. H. King made the soil resistivity measurements along the route. Their assistance and that of all those at Southern Bell who were involved in this study is gratefully appreciated.

Mr. P. A. Tukey of Bell Laboratories at Murray Hill was most helpful with the data analysis.

References

1. D. W. Bodle and P. A. Gresh, "Lightning Surges in Paired Telephone Cable Facilities," Bell System Technical Journal, March 1961, pp. 547-576.

2. Y. Ishida, "Induced Lightning Surges in Paired Telephone Cables," Review of the Electrical Communication Laboratories, Vol. 20, No. 3-4, March-April, 1972.

3. E. Bennison, A. J. Ghazi and P. Ferland, "Lightning Surges in Open Wire, Coaxial, and Paired Cable," IEEE Transactions on Communications, October, 1973.

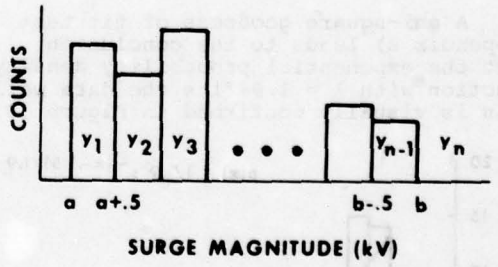
4. Paul G. Hoel, Introduction to Mathematical Statistics, John Wiley and Sons, Inc., 1971, p. 229.

Appendix A

Derivation of the Maximum Likelihood Estimate of the Fit Parameter of a Truncated Exponential Distribution with Censoring

(Derived by P. A. Tukey)

The data consist of n random variables, y_i, which are counts of the number of surges occurring within 0.5 kV wide cells. The first cell begins at some value, a, and the last closed cell contains y_{n-1} surges and ends at the value, b. The data contains a count, y_n, of surges greater than b. This censoring on the right is accommodated by simply taking the last cell as running from b to infinity.



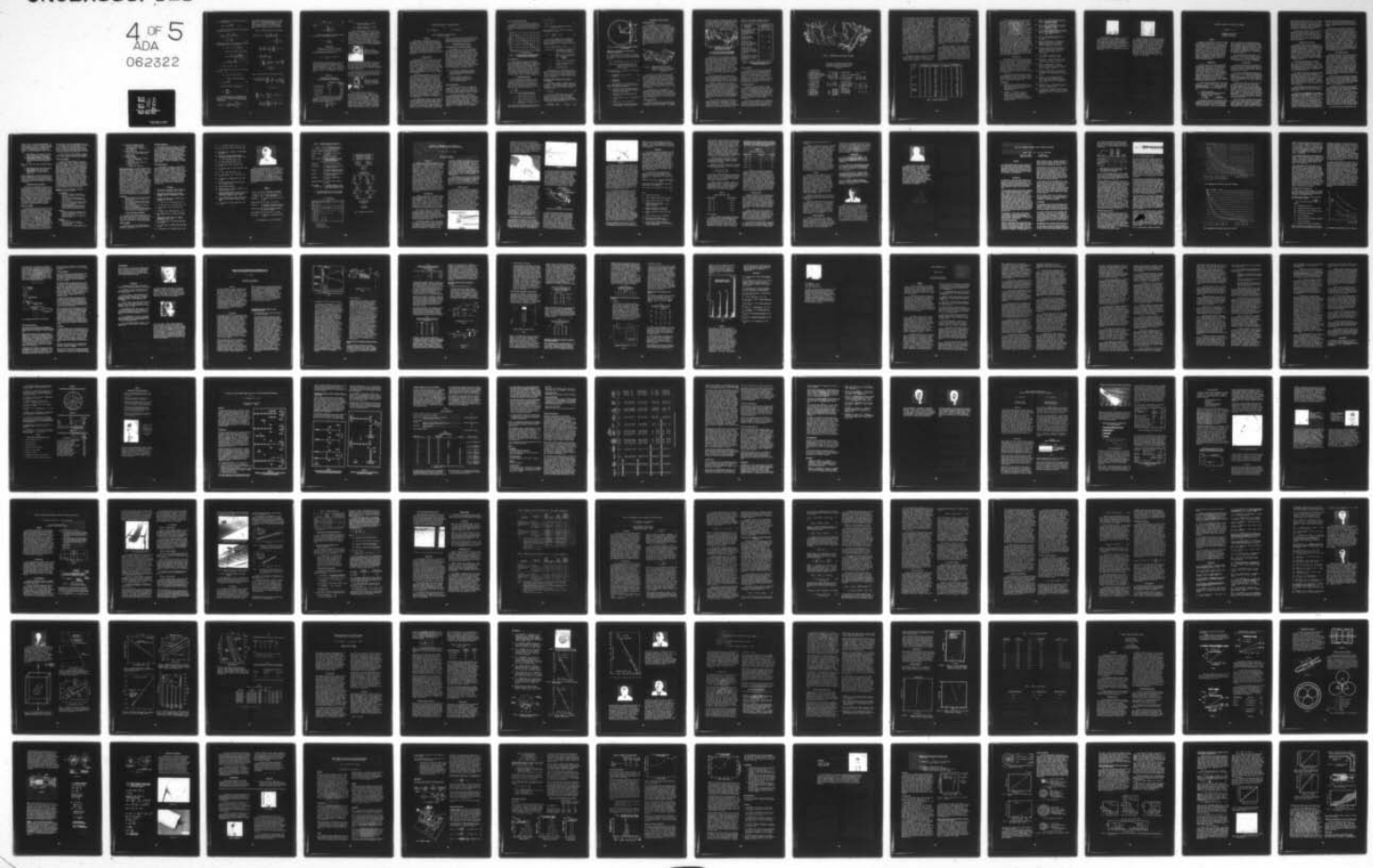
The exponential probability density function has the form:

$$p(x) = \frac{1}{\lambda} e^{-\frac{x}{\lambda}} \qquad x \geq 0$$

AD-A062 322 ARMY COMMUNICATIONS RESEARCH AND DEVELOPMENT COMMAND --ETC F/G 13/9
PROCEEDINGS OF THE INTERNATIONAL WIRE AND CABLE SYMPOSIUM (27TH--ETC(U)
NOV 78 E F GODWIN

UNCLASSIFIED NL

4 OF 5
ADA
062322



The conditional density function for $x \geq a$ is given by:

$$p(x) = \frac{1}{\lambda} e^{-\frac{(x-a)}{\lambda}} \qquad x \geq a$$

Let x be the voltage of a single surge. Then for any $X \geq a$,

$$P\{x \leq X\} = \int_a^X \frac{1}{\lambda} e^{-\frac{(x-a)}{\lambda}} dx$$

$$= 1 - e^{-\frac{(X-a)}{\lambda}} \qquad (1)$$

We can now use (1) to calculate the probability that x is in the i th cell.

$$P_i = P\{x \text{ is in i th cell}\}$$

$$= P\{[a+.5(i-1)] < x \leq (a+.5i)\}$$

$$= \left[1 - e^{-\frac{i}{2\lambda}}\right] - \left[1 - e^{-\frac{(i-1)}{2\lambda}}\right]$$

$$P_i = e^{-\frac{i-1}{2\lambda}}\left(1 - e^{-\frac{1}{2\lambda}}\right) \qquad (2)$$

for $i = 1,2,\ldots,n-1$

The probability that x is in the last cell is:

$$P_n = P\{x \text{ is in n th cell}\}$$

$$= P\{x > b\} = P\{x > [a+.5(n-1)\}$$

$$P_n = e^{-\frac{n-1}{2\lambda}} \qquad (3)$$

The total number of surges is:

$$y_T = \sum_{i=1}^{n} y_i \qquad (4)$$

The probability (or likelihood) of observing the particular allocation into y_1, y_2, etc., is given by the multinomial distribution:

$$\text{Lik}(y;\lambda) = \frac{y_T!}{y_1!y_2!\ldots y_n!} \prod_{i=1}^{n} P_i^{y_i}$$

The maximum likelihood estimate $\hat{\lambda}$ is that value of λ which maximizes $\text{Lik}(y;\lambda)$ with respect to λ, holding the observation $y = (y_1,\ldots,y_n)$ fixed. To calculate $\hat{\lambda}$, we differentiate $\ell n[\text{Lik}(y;\lambda)]$ with respect to λ, set the result to zero, and solve for λ.

First, taking the natural logarithm:

$$\ell n[\text{Lik}(y;\lambda)] = \ell n\left[\frac{y_T!}{y_1!y_2!\ldots y_n!}\right] + \ell n \prod_{i=1}^{n} P_i^{y_i}$$

$$= \ell n\left[\frac{y_T!}{y_1!y_2!\ldots y_n!}\right] + \sum_{i=1}^{n} y_i \, \ell n(P_i)$$

$$= \ell n\left[\frac{y_T!}{y_1!y_2!\ldots y_n!}\right] + \sum_{i=1}^{n-1} y_i\left[-\frac{(i-1)}{2\lambda} + \ell n\left(1 - e^{-\frac{1}{2\lambda}}\right)\right] - \frac{(n-1)y_n}{2\lambda}$$

Then, differentiating and setting to zero:

$$\frac{\partial\left[\ell n\left(\text{Lik}\left(y;\lambda\right)\right)\right]}{\partial\lambda} = \sum_{i=1}^{n-1} y_i\left[(i-1) - \frac{e^{-\frac{1}{2\lambda}}}{\left(1 - e^{-\frac{1}{2\lambda}}\right)}\right] + (n-1)y_n = 0$$

$$\sum_{i=1}^{n-1}(i-1)y_i - \frac{(y_T - y_n)}{e^{\frac{1}{2\lambda}} - 1} + (n-1)y_n = 0$$

$$\left(e^{\frac{1}{2\lambda}} - 1\right)\left[\sum_{i=1}^{n}(i-1)y_i\right] = y_T - y_n$$

$$e^{\frac{1}{2\lambda}} = 1 + \frac{1}{B} \qquad (5)$$

where

$$B = \frac{\sum_{i=1}^{n} (i-1)y_i}{y_T - y_n}$$

Taking the natural logarithm of both sides of (5) and solving for $\hat{\lambda}$:

$$\hat{\lambda} = \frac{1}{2\ell n\left(\frac{1+B}{B}\right)} \qquad (6)$$

Appendix B

Goodness of Fit Test to the Data

In order to determine whether the probability density function

$$p(x) = \frac{1}{1.9} e^{-(x-1.5)/1.9}$$

fits the data satisfactorily, we make use of the chi-square test to examine the differences between the observed and expected frequencies in Table 2. Since many authors[4] require at least five expected events in each of at least five cells, the data in Table 2 is reclassified in Table B-1.

TABLE B-1

Comparison of Observed and Fitted Surge Frequencies

Cell Range (kV)	Number of Surges Observed O_i	Number of Surges Expected From Fit E_i
> 1.5 to 2.0	14	12.25
> 2.0 to 2.5	15	9.42
> 2.5 to 3 0	8	7.24
> 3.0 to 4.0	6	9.85
> 4.0 to 5.0	4	5.82
> 5.0	6	8.42

The chi-square statistic is simply the sum of the square of the differences between the observed and the expected number of surges normalized by the expected number for each cell:

$$\chi^2 = \sum_{i=1}^{6} \frac{(O_i - E_i)^2}{E_i}$$

where

O_i = observed number of surges in the i th cell

E_i = expected number of surges in the i th cell

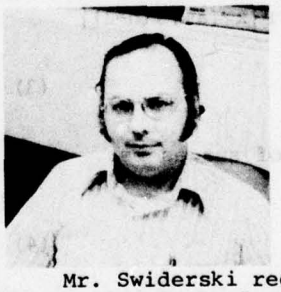
Doing the summation on the data in Table B-1, we find that $\chi^2 = 6.40$. Since one parameter (λ) has been estimated from the data, and we compared 6 cells, the number of degrees of freedom is 6-1-1 = 4. From statistical tables, it is found that at the 5% level of significance for 4 degrees of freedom $\chi_o^2 = 9.49$. Since χ^2 is less than χ_o^2, the hypothesis that the data were obtained from sampling an exponential population with $\lambda = 1.9$ is supported.



James J. Refi
Bell Laboratories
2000 N.E. Expressway
Norcross, GA 30071

Mr. Refi began work with Bell Laboratories in 1966 at the Baltimore Laboratory as a Member of Technical Staff. He has worked on land coaxial and multipair cables and has authored papers on T2-LOCAP and pair unbalance phenomena.

Mr. Refi received the B.S.E.E. from Villanova University in 1966 and the M.S.E.E. from the Polytechnic Institute of Brooklyn in 1968. He is a member of I.E.E.E., Tau Beta Pi and Eta Kappa Nu.



Michael J. Swiderski
Bell Laboratories
2000 N.E. Expressway
Norcross, GA 30071

Mr. Swiderski received his A.A. in Electronics Technology in 1968 from Baltimore Junior College. After graduation, he joined Bell Laboratories to work on coaxial cable development. Since then he has worked on DEPIC cable, sheath design, high voltage testing and lightning measurement. He is presently an Associate Member of Technical Staff in the Distribution Cable and Sheath Group of the Loop Transmission Division. Mike enjoys motorcycling and amateur radio for relaxation.

LIGHTNING PINHOLES IN CABLE SHEATHS

by

H.D. Campbell D.O. Lawrence

Northern Telecom Canada Limited
Montreal, Quebec

ABSTRACT

This paper presents an analysis of the major factors determining the degree of damage to buried cables in the form of pinhole punctures in the sheath resulting from lightning strokes to ground. A technique of predicting the levels of pinholing which might be experienced under a broad range of conditions is developed. The technique is illustrated using the Canadian environment and powder filled cable as examples.

INTRODUCTION

The sheaths of PIC cables are exposed to hazards during their installation and subsequent service in the buried environment. Once installed, the buried cable may be mechanically damaged by excavating machinery or electrically damaged by lightning in the immediate vicinity of the cable route. This paper deals with the probability of damage due to the well-known lightning pinholing of the jacket component of the sheath.

The pinhole phenomenon has long been considered a significant contributor to water entry of PIC cable cores that may lead to premature transmission problems and early cable replacement. The first approach to the moisture problem was the addition of an inner jacket — the so-called PAP sheath. Later, a further improvement in performance was realized by the introduction of grease filled cables with sealed sheaths. More recently, a powder filled construction has been introduced[1] that has been shown to have advantages over the conventional grease filled cores. Because none of these approaches is a complete solution to the lightning problem, the need to estimate the probability of damage is still apparent.

The impairment caused by the lightning induced pinholes may take the form of incipient damage wherein the energy released is not sufficient to puncture the metal substrate of the sheath. More severe conditions may rupture the complete sheath and expose the core to immediate moisture penetration. In either case, corrosion of the metal component of the sheath may occur, causing the eventual moisture incursion and/or loss of sheath continuity[2].

LIGHTNING DAMAGE FACTORS

The Frequency of Lightning Strokes

The probability of lightning damage to buried cables is a linear function of the number of strokes to ground per unit area. Isokeraunic maps indicate the level of thunderstorm activity on a large scale. This cartographic technique enables statistics obtained from discrete points (frequently airport weather stations) to be extrapolated to provide more general information. Field investigations conducted in North America have provided stroke factors which predict the average number of strokes to earth per unit area for each thunderstorm day. The stroke factors which have gained acceptance are[3]:

(1) 0.14 strokes to ground per square kilometre per thunderstorm day in areas experiencing predominantly frontal storms.

(2) 0.11 per square kilometre per thunderstorm day where convection storms are most common, e.g., in North America.

Earth Resistivity

Experience has shown that lightning damage is relatively severe in high soil resistivity areas. Earth resistivity is the single, most important factor in determining lightning damage to buried cables.

The earth's crust is composed of numerous different materials with large variations in their chemical, mineral and moisture contents. As a result, the resistivity of the earth varies over a large range between extremes of about 1 ohm·meter and approaching 10,000 ohm·meters. It is a general rule-of-thumb that the older the formation, the higher the earth resistivity.

Stroke Current Magnitudes

The magnitude of the peak current varies from a few kiloamperes to over 200 kiloamperes. The statistical distribution is well documented in the literature. A cumulative distribution curve is shown in Fig. 1.

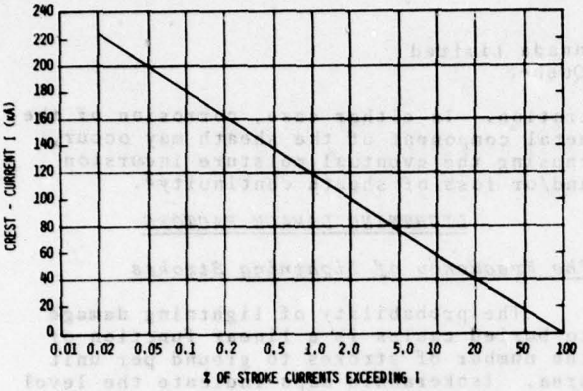


FIG. 1 DISTRIBUTION OF LIGHTNING STROKE CREST CURRENTS TO GROUND

Other Factors

Local conditions may significantly modify the extent of damage. Shielding may be provided by other cables, pipes and the like, while tall structures such as trees and towers tend to increase the number of strokes to cable in the vicinity. The severe lightning environment of high resistivity soils provides a high risk of pinholing, but such locations are likely to have lower risks of corrosion than the low resistivity soils in wet, swampy areas.

PINHOLE MECHANISM

The mechanism of breakdowns to the sheath of a buried cable has been described previously[4,5]. If the soil is assumed to have uniform resistance then the critical distance from the stroke point to the cable beyond which no breakdown in the jacket will occur is[5]:

$$r(I) = \frac{I\rho}{2\pi U} \qquad (1)$$

where r(I) is distance from stroke point to cable, meters.

I - peak stroke current, kA

ρ - earth resistivity, Ω·m

U - dielectric strength, cable jacket, kV.

The cumulative frequency distribution of the lightning current amplitudes, Fig. 1, can be written:

$$S(I) = e^{-bI} \qquad (2)$$

where b is the cumulative frequency constant, kA^{-1}.

The probability of a lightning stroke in the range dI is then:

$$W(I) = -\frac{dS(I)}{dI} = be^{-bI} \qquad (3)$$

The total number of all lightning strokes per year which have a current equal to or greater than I and which develop a voltage equal or greater than U on the cable is[5]:

$$N_G(I) = 2N_E \ell D \int_I^\infty W(I)\, r(I)\, dI \qquad (4)$$

where $N_G(I)$ - the number of strokes per year which may lead to cable jacket breakdowns.

N_E - number of strokes per unit area and per thunderstorm day, $\frac{\text{strokes}}{TD \cdot m^2}$

ℓ - length of the cable, meters

D - number of thunderstorm days per year.

TD - *thunderstorm day*

Expression (4) includes all breakdowns, including direct strokes and strokes that arc to the cable. The probability of a direct stroke or a stroke arcing to the cable is very much less than strokes causing only pinholes.

Length of Cable subject to Pinholing per Stroke

Consider a stroke to ground (Fig. 2) distance x from a buried cable at its nearest point. The length of cable subject to pinholes, d, may be expressed in terms of the distance r.

$$d = 2r \sin\theta \qquad (5)$$

If it is assumed that x may be any distance from 0 to r with equal probability then over a period of a large number of strokes of a given current magnitude, the average length of cable subject to pinholes per stroke will be:

$$d = \left(\frac{\pi r^2}{2}\right)\frac{1}{r} = \frac{\pi r}{2} \text{ meters} \qquad (6)$$

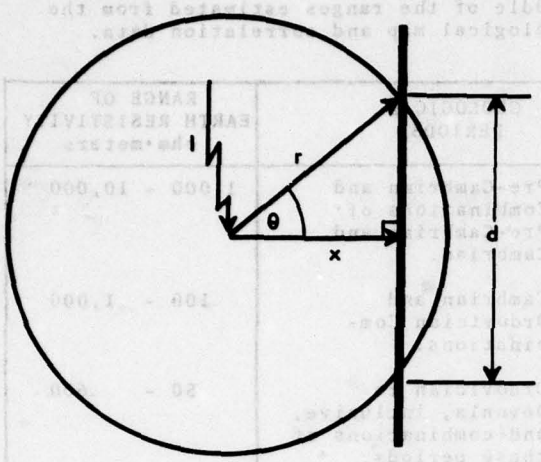


FIG. 2 AVERAGE LENGTH OF CABLE SUBJECT TO PINHOLING

Theoretical Estimates of Total Cable subject to Pinholes

The product of the number of strokes, N_G, and the distance, d, per stroke yields the length of cable subjected to pinholing, so that:

$$P(I) = 200\, N_E D \int_I^\infty W(I) \cdot r(I) \cdot d(I)\, dI \quad (7)$$

where P(I) is the percentage of cable subjected to pinholes per year in a given earth resistivity region.

Substituting (1), (3) and (6) and letting I = 0 (7) becomes:

$$P = \frac{100\, N_E D\rho^2}{4\pi U^2} \int_o^\infty bI^2 e^{-bI}\, dI \quad (8)$$

$$P = \frac{100\, N_E D\rho^2}{2\pi U^2 b^2} \quad (9)$$

From experimental and theoretical data, representative values can be assigned to the pinhole parameters:

N_E - a value of 0.11 (strokes/thunderstorm day $\cdot km^2$) has been indicated earlier in the paper.

D - available from isokeraunic maps (cf Fig. 3).

U - a mean value of 75 kV is representative.

b - from Fig. 1, $b \approx 0.041\ kA^{-1}$

ρ - value depends upon the region of interest and is discussed later.

ESTIMATES OF CABLE DAMAGE

Isokeraunic Data

Two sources of data were used to obtain information on the isokeraunic levels across Canada. An isokeraunic map of Canada was extracted from The Telephone Association of Canada[6]. Additional information in the form of spot lightning statistics was obtained from an Environmental Canada publication on climatic normals[7]. These spot statistics were accumulated by numerous airports and weather stations scattered across the country. When they were superimposed on the TAC isokeraunic map in Fig. 3, it was found that the majority of the spot statistics agreed with the generalized data of the isokeraunic map.

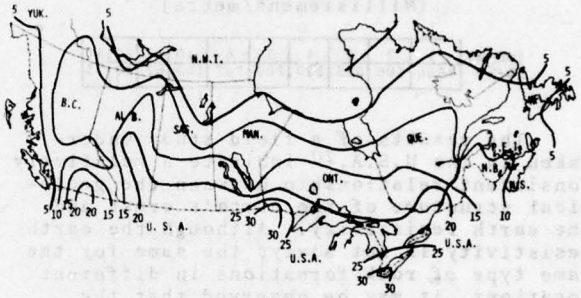


FIG. 3 ISOKERAUNIC MAP OF CANADA

(Numbers indicate the average number of thunderstorm days per year)

The level of thunderstorm activity increases from near zero in the extreme north of Canada to a high of between 30 and 35 thunderstorm days per year in both the S.W. and Lake Erie regions of Ontario. The highest point level is the 33.1 recorded at Windsor, Ontario. In addition to the increase in thunderstorm activity from north to south in Canada, there is a general increase inland from the east and west coasts.

In any one year, the number of thunderstorm days may be higher or lower than the levels indicated on the isokeraunic map, however, over the expected life of a cable, the average for any particular region should be close to the figure predicted by the map.

Earth Resistivity

Conductivity maps of the resolution required for accurate assessment of damage probability are not available. Two maps

of Canada based on limited data were identified as sources of reference for generalized earth resistivity information[8,9]. It is apparent that there is likely to be a fairly wide variation in earth resistivity within each region on such a map (Fig. 4).

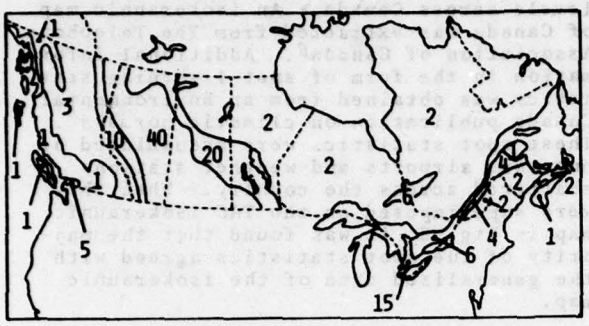


FIG. 4 ESTIMATED EFFECTIVE GROUND CONDUCTIVITY IN CANADA (Millisiemens/metre)

(mS/m)	1	2	3	4	5	6	10	15	20	40
(Ω·m)	1000	500	333	250	200	167	100	67	50	25

The results of a field study undertaken in the U.S.A.[10] indicate a relatively consistent relationship between the geological structure of the earth's crust and the earth resistivity. Although the earth resistivity is not always the same for the same type of rock formations in different locations, it may be observed that the variation for any particular material is within much narrower limits. Thus, from a knowledge of the composition of the earth's crust in a given area, the range of earth resistivities for that area may be predicted.

The principal correlation data between type of formation and earth resistivity is summarized in Table 1. The table shows the major geological periods and the corresponding ranges of earth resistivity.

A Magnetic Anomaly Map of Canada[11] was used to identify the principal physiographic regions of Canada. The regions are illustrated on the outline map of Canada in Fig. 5. By comparison with a Geological Map of Canada[12], the major geological features of each region were established. Using the earth resistivity/geological age correlation data [10], the range of earth resistivities in each of the physiographic regions and sub-regions were tabulated (Fig. 5).

The estimates of earth resistivity ranges were used to supplement the single values obtained for each region on the conductivity maps. In general, the magnitudes of earth resistivity indicated by the conductivity maps were somewhere in the middle of the ranges estimated from the geological map and correlation data.

GEOLOGICAL PERIODS	RANGE OF EARTH RESISTIVITY ohm·meters
Pre-Cambrian and Combinations of Pre-Cambrian and Cambrian.	1,000 - 10,000
Cambrian and Ordovician Combinations.	100 - 1,000
Ordovician to Devonia, inclusive, and combinations of these periods.	50 - 600
Carboniferous, Triassic, and combinations of carboniferous and earlier periods.	10 - 300
Cretaceous, Tertiary, Quaternary and combinations of these periods.	2 - 30

TABLE 1 SUMMARY OF PERIOD/RESISTIVITY CORRELATION (REF. 10)

Cable Location

In order to assess the probable pinholing statistics which may be expected with buried cables, a knowledge of the location of installations is necessary. A population distribution map, Census of Canada - 1971 was used to give a first approximation of cable locations. It was assumed that cable installations have a geographical distribution proportional to the population density.

Pinholing Growth

Estimates of the severity of pinholing may be determined from (9) from which it is readily found that by far the most critical parameter is the earth resistivity. In relatively common earth resistivities of 100 ohm·meters, the severity of pinholing will be theoretically two orders of magnitude less than that in the high earth resistivities of 1000 ohm·meters.

The effect of pinholes on cable performance depends somewhat on the cable construction. Because air core PIC cables permit entrance of large quantities of water when the sheath is ruptured, they

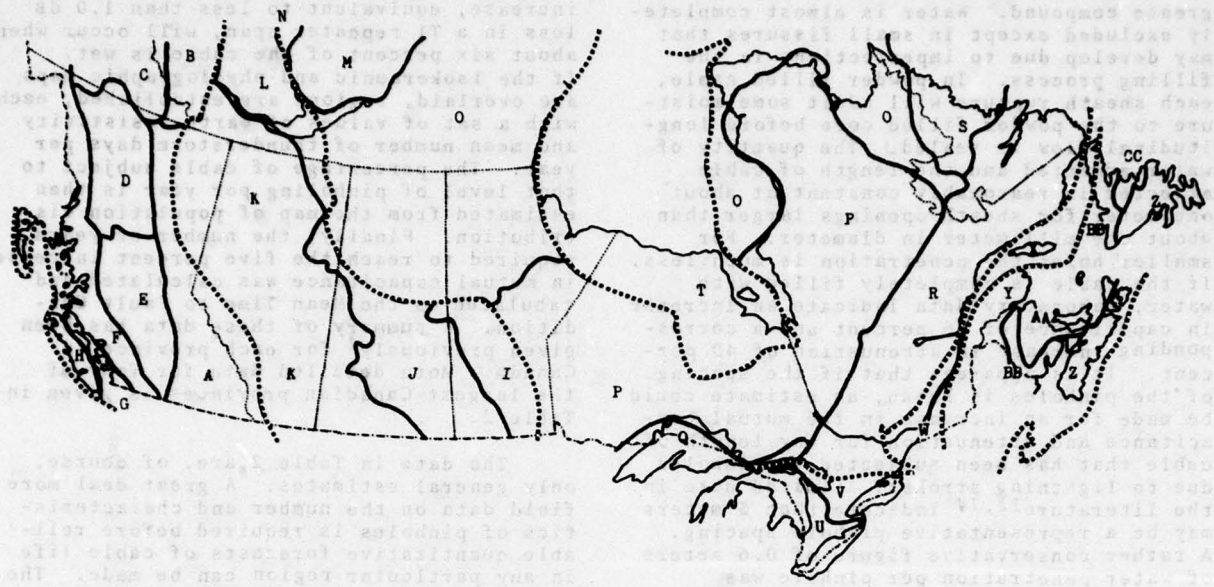


FIG. 5 PHYSIOGRAPHIC REGIONS OF CANADA

KEY TO FIG. 5 (PHYSIOGRAPHIC REGIONS OF CANADA)

The estimated earth resistivity ranges are given in ohm·meters (a) from the conductivity maps; (b) from the age/resistivity correlation in parentheses.

CORDILLERON OROGEN		
A. Rocky Mountain Area	300-1000	(200-5000)
B. MacKenzie Mountain Area	-	(10 -1000)
C. Northern Plateaus & Mountains	-	(50 -1000)
D. Central Plateaus & Mountains	300-1000	(10 -1000)
E. Southern Interior Plains	300-500	(20 -600)
F. Coastal Mountain Area	1000	(10 -1000)
G. Coastal Trough	200-250	(10 -300)
H. Outer Mountain Area	1000	(10 -1000)
INTERIOR PLATFORM		
I. 1st Prairie Level	50	(50-600)
J. 2nd Prairie Level	25 - 50	(2 -300)
K. High Plains	25 -100	(2 -100)
L. MacKenzie Lowlands	25 - 50	(2 -300)
CANADIAN SHIELD		
M. Slave Region	-	(500-5000)
N. Bear Region	-	(500-5000)
O. Churchill Region	500	(500-5000)
P. Superior Region	500	(500-5000)
Q. Southern Region	500	(500-5000)
R. Grenville Region	500	(500-5000)
S. Nain Region	-	(500-5000)
T. HUDSON PLATFORM	500	(500 - 2000)
GT. LAKES - ST. LAWRENCE LOWLANDS		
U. Huron & Erie Lowlands	70	(50 - 600)
V. Ontario Lowlands	170-250	(100 - 1000)
W. St. Lawrence Lowlands	170-250	(100 - 1000)
X. Anticosti Region	500	(100 - 600)
APPALACHIAN OROGEN		
Y. Quebec & New Brunswick Highlands & Uplands	500 - 1000	(50 - 1000)
Z. Atlantic Uplands	500 - 1000	(50 - 1500)
AA. Gulf of St. Lawrence Plain	500	(10 - 1000)
BB. New Brunswick, Nova Scotia & Newfoundland Highlands & Uplands	500 - 1000	(50 - 1500)
CC. Central Lowlands of Newfoundland	1000	(50 - 1000)

have been largely replaced for buried use by PIC cables having a core filled with a grease compound. Water is almost completely excluded except in small fissures that may develop due to imperfections in the filling process. In powder filled cable, each sheath rupture will admit some moisture to the powder filled core before longitudinal flow is sealed. The quantity of water admitted and the length of cable affected is reasonably constant at about one meter for sheath openings larger than about one millimeter in diameter. For smaller holes the penetration is much less. If the cable is completely filled with water, laboratory data indicate an increase in capacitance of 86 percent and a corresponding increase in attenuation of 40 percent. It is apparent that if the spacing of the pinholes is known, an estimate could be made for an increase in the mutual capacitance and attenuation for any length of cable that has been subjected to pinholes due to lightning strokes. Limited data in the literature[13,14] indicate that 3 meters may be a representative pinhole spacing. A rather conservative figure of 0.6 meters of water penetration per pinhole was assumed[1].

Using these data, estimates were made of the number of pinholes that can be tolerated before transmission parameters are significantly degraded. In the calculations, the average increase in mutual capacitance was limited to 5.0 percent. This increase, equivalent to less than 1.0 dB loss in a T1 repeater span, will occur when about six percent of the cable is wet. If the isokeraunic and physiographic maps are overlaid, regions are established, each with a set of values of earth resistivity and mean number of thunderstorm days per year. The percentage of cable subject to that level of pinholing per year is then estimated from the map of population distribution. Finally, the number of years required to reach the five percent increase in mutual capacitance was calculated and tabulated as the Mean Time to Fault Condition. A summary of these data has been given previously[1] for each province in Canada. More detailed data for four of the largest Canadian provinces is given in Table 2.

The data in Table 2 are, of course, only general estimates. A great deal more field data on the number and characteristics of pinholes is required before reliable quantitative forecasts of cable life in any particular region can be made. The dielectric breakdown in cable jackets will be far more extensive in high resistivity soil than in low resistivity soil, but the characteristics of the jacket rupture and the consequence of such ruptures may vary widely.

PROVINCE	THUNDERSTORM DAYS PER YEAR	EARTH RESISTIVITY OHM·METERS	ESTIMATED % OF TOTAL CABLE	MEAN TIME TO FAULT CONDITION (YEARS)
QUEBEC	20	150	6	360
	25	150	56	290
	15	250	6	170
	20	250	16	130
	10	500	4	65
	15	500	5	45
	20	500	5	30
	25	500	2	25
ONTARIO	25	100	10	650
	30	100	25	550
	25	200	56	160
	20	500	2	30
	25	500	3	25
	35	500	1	19
	20	1000	3	8
ALBERTA	25	25	46	10000
	20	100	46	800
	10	330	5	150
	15	330	3	100
BRITISH COLUMBIA	15	100	5	1100
	5	250	29	500
	10	200	32	410
	10	330	3	150
	15	330	5	100
	5	1000	4	30
	10	1000	11	16
	20	1000	11	8

TABLE 2 ESTIMATES OF PINHOLE GROWTH

In high resistivity soil, the partial currents are likely to cause many breakdowns that rupture only the cable jacket, leave the underlying shield intact and do not degrade the cable transmission properties, unless the shield is eventually corroded. On the other hand, in low resistivity soil, the ruptures that do occur are more likely to cause melting of the shield and water incursion. Direct strokes or arcs to the cable are relatively infrequent and will cause severe damage only in the immediate area of impact. Since it has been assumed in this study that all jacket pinholes, however small, will admit moisture to the cable, the estimates of fault conditions are believed to be conservative. For the more usual lightning environments, the estimates are generally much in excess of the usually accepted nominal cable life, while the severe lightning environments indicate that some additional protective measures may be required, particularly where the earth resistivity is greater than 1000 ohm·meters. This recommendation is also applicable, in general, to all other types of cable having a metal sheath with an insulating covering[15].

CONCLUSIONS

The relative extent of pinholing for all cables having an insulating covering over a metal sheath is primarily dependent on soil resistivity. For high soil resistivity areas, where lightning activity is severe, service life for all such cables, including powder filled cables may be adversely affected. In such cases, the addition of an inner jacket under the shield or other protective measures should be considered.

For the usual lightning environments, the estimates in Table 2 indicate, with a high confidence level, that powder filled cable having a conventional sealed sheath will be completely satisfactory.

References

(1) McManus, T.K. and Beveridge, R., "A New Generation of Filled Core Cable", 26th International Wire and Cable Symposium, Cherry Hill, N.J., November 1977.

(2) Baboian, R., Hartley, S.R. and Hyman, E.D., "High Strength, Corrosion Resistant Clad Metal Shielding for Telephone Wire and Cable", 23rd International Wire and Cable Symposium, Atlantic City, N.J., December 1974.

(3) Bodle, D.W., "Electrical Protection Guide for Land-base Radio Facilities", Joslyn Electronic Systems.

(4) Sunde, E.D., "Lightning Protection of Buried Toll Cables", Bell Telephone System Monograph, B-1396.

(5) International Telegraph and Telephone Consultative Committee (CCITT), Joint Working Party CDF, Contribution No. 13, April 1975.

(6) T.A.C., "The Telephone Association of Canada Lightning Survey", TAC3-1971.

(7) Canada - Department of Transport - Meteorological Branch, "Climatic Normals Volume III - Sunshine, Cloud and Thunderstorms", 1968.

(8) Canada - Department of Transport - Telecommunications and Electronics Branch, "Provisional Ground Conductivity Map", Sheets 1 & 2, June 1960.

(9) "ITT Reference Data for Radio Engineers", 5th Edition, 1970.

(10) Card, R.H., "Earth Resistivity and Geological Structure", Electrical Engineering, Volume 54, 1935.

(11) Canada - Department of Energy, Mines and Resources - Geological Survey of Canada, "Magnetic Anomaly Map of Canada", 1255A.

(12) Canada - Department of Energy Mines and Resources - Geological Survey of Canada, "Geological Map of Canada", 1250A.

(13) Ronald, U.P., "Conductive Plastic Sheath on Buried Communication Cable for Reduced Lightning Damage", Proc. IEEE Conference on Communications 1972.

(14) Connolly, R.A., "Soil Burial Tests", The Bell System Technical Journal, Volume 51, January 1972.

(15) International Telegraph and Telephone Consultative Committee (CCITT), Joint Working Party CDF, Contribution No.14, May 1975.



Hugh Campbell is a member of the R&D staff, Northern Telecom Canada Limited, Cable Division, and has been engaged in development and electrical measurements of both power and communications cable since joining the company in 1950. He holds a B.Sc. degree in Electrical Engineering from Nova Scotia Technical College and is a member of the Order of Engineers of Quebec and IEEE.



Derek Lawrence is a native of England and began his career there with BICC Ltd. as a student engineer. He graduated from The City University, London, in 1975 with a B.Sc. (Hons) in Electrical and Electronic Engineering, having specialized in communications. He then moved to Canada and joined Northern Telecom as an R&D Staff Member in the Telecommunications Cable Division. In 1978 he joined Anaconda Telecommunications as Systems Engineer at the Cable Products Headquarters in Overland Park, Kansas. He is a member of the IEEE.

LABORATORY EVALUATION OF BURIED SPLICE CLOSURES

by Norman A. Gac

Telecommunications Division
Raychem Corporation
Menlo Park, California

SUMMARY

Ideally, a buried closure for filled PIC cable splices should reconstitute the electrical and mechanical properties of the cable. In service, the closure may experience a variety of environmental stresses which may lead to the destruction of its basic function - providing a reliable water seal. Laboratory evaluations of the materials and engineering test criteria must define the performance levels required in service. This paper reviews some existing design and specifications criteria in use. It attempts to provide a meaningful approach, a proper balance between materials and engineering paramenters, and an assessment of currently accepted standards.

INTRODUCTION

A buried splice closure should reconstitute the electrical, mechanical, chemical and biological properties of the cable. For filled cable closures, this norm dictates that the splice closure should provide an adequate water seal. Pure mechanical weaknesses can interrupt transmission. However, field failure reports generally state water as the cause. Yet, suppliers and users expend considerable effort evaluating buried closures in the laboratory prior to field use. Apparently, the design evaluation criteria are too narrow or do not measure the relationships between laboratory and field conditions.

In 1975, the author participated in the introduction of a filled distribution cable-service wire pretermination product. This system is adequately described elsewhere.[1, 2, 3] The referenced articles describe several salient requirements. These are:

1. production assembly,
2. severe handling following installation,
3. exposure to four environmental conditions, namely,
   a. factory
   b. storage
   c. placement
   d. field service

An extensive laboratory evaluation was central to the wide-spread success of the pretermination buried splice closure. The product requirements listed were essentially those of a filled cable. Yet in the early 1970's filled cable improvements were still being made. No commercial closure product satisfactorily met the factory pretermination requirements. User specifications for even field installed products were unavailable. Therefore, evaluation standards were lacking. A costly test development program was required prior to making financial commitments for the expansion of our Engineering Test Laboratory. This situation has radically changed.

The overall objective of this paper is to review buried closure evaluation status. More specifically, it is written to summarize (1) background information, (2) industry requirements, (3) laboratory evaluations, and (4) suggestions.

FILLED CABLE

A meaningful discussion of buried closures requires a review of filled cable technology. The principal (1) technical considerations, (2) functional characteristics and (3) current trends are summarized in this section.

The technical requirements are found in discussions of air core PIC failures and reclamation approaches.[4, 5, 6, 7] Filling PIC cable seals conductor insulation faults and provides a stable dielectric medium between pairs. Thus, electrolytic corrosion is essentially eliminated and signal loss is minimized.[8]

The water which causes air core PIC to fail may enter by (1) moisture vapor transmission, (2) sheath damage, and (3) poor closure seals. Water vapor transmission is currently reduced to negligible levels by bonded aluminum shield constructions. Well filled cable makes sheath damage effects negligible relative to air core counterparts. Powder filled cable may provide additional improvements.[9, 10] Water can migrate in petrolatum filled cable into the splice closure. Thus, the splice closure becomes vulnerable both from cable and closure water entry.

Filled cable must be handled under a variety of conditions. Thermal expansions and contractions as well as mechanical stresses such as bending, tensile loading, and vibration, introduce an adhesion requirement.[11] Petrolatum based and similar hydrocarbon filling compounds adhere to the non-

polar polyolefin conductor insulations. An accomodating, self healing effect is also present. More rigid and/or more polar materials do not exhibit this materials combination. We have found that the "gasket seal" achieved with these latter materials is easily broken following thermal or mechanical displacements. Water paths are formed.

Filled cable has displaced air core PIC as the preferred distribution cable. Moreover, the 10 year trend toward filled cable appears to be continuing and starting to impact the larger pair count requirements.[12, 14, 15] This cable type can, in principal, replace pressurized cable designs. However, present closures may prove inadequate for large splice bundles.

CLOSURES FOR FILLED CABLE

A buried splice should be considered an integrated system. The three major components being (1) conductor connectors, (2) bonding hardware, and (3) the environmental seal. This review is directed toward the last item. However, the other two components cannot be totally ignored. If connectors prevented moisture ingress reliably, closure filling or seals would be less critical. Limitations also exist in some designs because bonding hardware acts as the tensile load bearing member. Movement of the splice seal relative to the splice is therefore possible.

Filled cable closures may be classed as: (1) direct buried encapsulations, (2) hermetic seals, and (3) above ground pedestals. This paper deals primarily with the available criteria and laboratory evaluation of the first category. However, some designs which appear to primarily depend on the encapsualnt also require a sealed outer shell for water exclusion.

Configurations vary widely in current closure designs. The CCITT published a handbook early this year attempting to compile this information.[16] Eight major categories: 3 based on cold and 5 based on hot installation methods are presented. Only one closure is explicitly recommended for filled cable. Neither some well known filled closures nor above ground pedestals are mentioned. Nonfilled hermetic seal varieties are not designated as used with filled cable.

No performance criteria are given in the CCITT publication. However, the need to define such criteria was discussed in the Group VI session in March, 1978.

Since 1971, the Proceedings of the International Wire and Cable Symposium have published only three papers on filled closures. In 1971, it was reported that closures were the main source of difficulty in filled cable field trials.[17] An inadequate sheath seal was the failure mode noted in every instance of the several approaches tried. The grease or polymeric filling compounds did not provide a secondary barrier. These served little purpose once the outer structure seal was broken. Two paper announced new reentreble polyurethane materials. A 1973 paper focused on methods only.[18] The second included performance results for a new material described as the primary moisture barrier.[19] It stated that other grease-like and polyurethane compounds available up to 1975 had shortcomings.

The difficulty in adhering to nonpolar polyolefin materials was discussed in four related papers. An injection welding technique was described in 1974.[20] A hot wire welding technique was described in 1975.[21] Both methods were used to overcome the difficulty in bonding to the nonpolar jacket surface. Thermal expansion and contraction effects were said to be overcome by fusion to the sheath. Another 1975 paper discussed the difficulty with blocking PIC cable with polyurethane materials.[22] Again, adhesion or wetting was noted as the technical problem. Finally, a closure technique for polyethylene jacketed submarine cable was described in 1976.[23] It stated that the welding techniques could be improved upon with new polymeric adhesives under pressure developed with heat shrinkable tubing. The closure filling was the polybutene cable compound.

USER PRODUCT CRITERIA

Documents specifying filled cable splice environmental seals include a wide range of inputs. User product criteria are a maze of system philosophy, experience and level of detail from the supplier's viewpoint. Requirements have been reviewed from agencies and organizaitons in Africa, Europe, the Middle East, North America, and the Pacific Basin. First, the level of detail varies considerably. Criteria may be so specified that only one closure design is acceptable. The other extreme is a statement that cable integrity must be maintained by the closure. North American organizations require filled closures. Generally. the various European agencies favor nonfilled hermetic seals for use with lower pair count filled distribution cable.

One major factor which influences the choice between filled and nonfilled closures is the practical need for reentry and reassignment of pairs. New construction in the United States is based upon direct buried, dedicated pairs. With this network design, a splice can be permanently sealed. Reentry is less important.

In attempting to adequately design and evaluate filled cable closure products, the supplier encounters various levels of demand for information which can be categorized as (1) materials, (2) methods, and (3) functional. There is good agreement on materials, i.e., chemical and biological, requirements. The reader is referred to REA Specification PE-74[24] as typical. It includes various (1) soils chemical, (2) corrosion, (3) connector, sheath and conductor insulations compatibility and (4) fungus resistance requirements. These same evaluations are generally required by those specifying other designs. Methods evaluations, e.g., installation conditions, vary considerably and therefore will not be considered here.

The remaining agreements between users and

suppliers center on functional requirements. As typical, Table 1 lists those required by REA for filled closures and Table 2 lists those acceptable to the German Post Office for a hermetic seal product.[25] Some important test details with respect to the REA requirements listed in Table 1 are:

1. Test Splice: ring cut cable, no connectors, no bonding, no cable end seals
2. Order of Test Execution: sequentially
3. Pass Criteria: maintain 5000 megohms, 500 VDC insulation resistance, tip/ring, ring/shield, tip/shield with moisture sensors

And for the German Post Office evaluation shown in Table 2:

1. Test Splice: none, cable stubs are used
2. Order of Execution: parallel tests
3. Pass Criteria: pressure retention, 40 KPa (6 psi), no visual leaks in a water bath

The two examples given show that user specifications are inadequate for supplier design use other than as a guide or for quality assurance purposes. In other words, meeting the laboratory specification does not insure that the product will function in the field.

LABORATORY EVALUATION PROGRAM

The previous sections point out that there is a considerable body of materials information from which to proceed. The technical problem is one of overcoming the difficulty in adhering to nonpolar paraffinic materials. The incorporation of material combinations, however, requires functional evaluation. The central question is not one of materials compatibility, but the effectiveness of the seal. Thermal and physical stresses impose analogous requirements on mechanical seals and encapsulations. However, current laboratory criteria do not functionally evaluate installed products. Spliced cable should be subjected to a test sequence which approximates field environments.

DESIGN TEST PROGRAM

After much effort, we have evolved the filled closure test program depicted in Figure 1. Splices are made with defined cable designs and specific connectors--plus moisture sensors. These sample splices are conditioned along with closure components at low, normal and high temperature extremes. The assembled test specimens are thermally cycled such that splice core temperatures stabilize at -30°C and 50°C. This temperature range subjects the outer surfaces to temperatures greater than -40°C and 60°C. This conditioning is followed by immersion in a 5% salt solution and measurement of insulation resistance. Tip/ring, ring/shield, and tip/shield values are recorded for 10 moisture sensors. A randomization program has yet to be developed for connector pairs. Currently we group tips and rings by binder group until low values are determined. Tests are discontinued when 10% of the pairs have values below 1000 megohms at 500 VDC. It is estimated that a calendar period of 4 to 5 months is required to conduct the entire program. The test sequence was developed primarily for products used in North America where a user commitment to totally filled plant is specified.[24, 26, 27, 28]

At this time, we have not subjected a product to this entire sequence. However, this recommendation is based on many similar completed programs.

TYPICAL TEST PROGRAM

A typical completed evaluation is included for clarification. Table 3 lists 8 combinations of 2 available housings and 4 commercial encapsulants that were sequentially tested. The housings are designated S and M. S was a prototype designed to seal to the sheath with an adhesive. The designer believed that a hermetic seal and a rigid shell would enhance various encapsulants. These would act as secondary water barriers. S(H) designates that filling plugs were left out of S. M was a semi-rigid shell or mold. Vinyl tape held M in place for filling. Therefore, no strain relief or tensile loading ability was provided by the shell. Encapsulants I and II were low elongation, cured-in-place materials. Encapsulants III and IV were thixotropic grease-like compositions. The objective was to gauge performance with a systematic variation of housing and encapsulant. Thus, relative performance could be established for additional design work. The same filled and nonfilled connector arrangement was used in all splices.

Procedures This early attempt at sequential testing included the following:

Splice Details
- 200 pair, 22 gauge in line splice
- fold back arrangement per Bell System Practices
- pairs selected for monitoring were 1 to 16 and 26 to 41 at each end of the splice bundle
- pairs 1 to 8 and 26 to 33 were connected with unfilled connectors; others used waterproof connectors
- bonding hardware was the load bearing variety compatible with the housing
- 7 feet cable stubs outside of closure

Criteria
- insulation resistance, tip/ring, ring/shield, tip/shield of 1000 megohms at 500 VDC minimum, 20°C
- failure was defined as 3 or more pairs below this level

Sequence
1. Thermal stress
   - 10 cycles, 12 hours per cycle
   - core temp extremes: -5°C (-20°F), +50°C (120°F)
   - 3 day 40°C (105°F) water immersion, 2 ft.

2. External environmental stress
   - 70 cycles, 24 hours per cycle
   - 1 foot sand, water, 5% NaCl
   - Core temperatures: -18°C (0°F), +50°C (120°F)
3. Internal water head
   - 30 days, 40°C, 2 feet head water bath
   - 1 in. x 1 in. hole in cable 1 foot from ring cut
4. Mechanical Stress
   a. Tensile loading
      - 250 lb to sheath held 15 minutes
      - 5 day water immersion
   b. Bend Stress
      - Manual bend, 45 to splice axis
      - 3 foot lever arm
      - 3 bends
      - 18 days water immersion

Results and Discussion The results obtained with the 8 closure systems are given in Table 3. It was found that the specific filled and nonfilled connectors and, as a result, the powered counterparts, were indistinguishable in these tests. Visual inspection on disassembly showed water in each closure and less than complete filling of the bundle core. As can be seen with sample 1, the hermetic seal prototype worked until a sheath fault was introduced. Samples 2 and 3 showed that encapsulant I functioned to block water entry with the sheath fault. The connectors in sample 2 were found to be well encapsulated. This was not so in sample 3. In the case of both samples 4 and 5, it is believed that encapsulant adhesion to the shell was sufficient to cause a pumping action in wet cycling. This view has been verified in related experiments with encapsulant II. Little need be said about encapsulants III or IV. The hermetic closure prototype design was clearly unacceptable as were all of encapsulants as primary barriers.

Conclusions

1. The waterproof connectors were inadequate without encapsulant or a hermetic seal water barrier.
2. Very limited sequential testing showed these commercial encapsulating materials to be ineffective.
3. Filling techniques need to be improved with all 4 encapsulants.
4. Every product system had at least one specific flaw which was clearly definable as a result of this sequential test.

RELATED FUNCTIONAL EVALUATIONS

The test sequences presented are long term, final engineering evaluations. They assess assembled closure capabilities. Direct, short term tests of bonding hardware, connectors and encapsulants are preferable for initial design studies.

BONDING HARDWARE

We have done little with bonding hardware evaluation. The reader is directed to two references for information.[26, 29]

WATERPROOF CONNECTORS

Our closure studies have shown a wide variability in waterproof connector performance. An apparatus was accordingly developed to functionally assess the effectivity of connector filling materials and design. The basic apparatus consists of a 5% NaCl solution bath into which connectors are immersed and powered. Current flow is measured with 50 VDC power supply in parallel with microamp and milliamp meters. These are connected to a switch bank leading to the connectors. Ground potential is maintained with an immersed stainless steel electrode. Failure is defined as a milliamp current flow.

ENCAPSULANT ADHESION

An experimental arrangement is under development to functionally rate encapsulant adhesion to conductor and connector surfaces. Tests in progress include experiments in which a central conductor is wrapped in short, uniformly spaced regions with stripped singles. The central member exits the top of an encapsulant plug while the monitors exit the bottom. A water head is placed over this wire array. Point to point insulation resistance readings of the bare wire segments to the water and each other are made. This allows the time dependence and extent of water ingress along the central vertical conductor to be quantitatively characterized.

REFERENCES

1. "Pre-fab Cable Plant Saves Time and Money for Mountain Bell," Telephony, June 21, 1976.
2. "Encapsulation System ups Splice Quality," Telephone Engineer and Management, September 1, 1976.
3. "Sharp Insight Improves Out-of-Sight Plant," Telephony, June 19, 1978.
4. C. L. Cox, et al., 21st IWCS, 1972, p. 47.
5. V. W. Pehrson, et al., 21st IWCS, 1972, p. 56.
6. S. Kaufman and R. Sabia, 21st IWCS, 1972, p. 64.
7. S. Kaufman, et al., 26th IWCS, 1977, p. 24.
8. M. C. Biskeborn and D. P. Dobbin, 17th IWCS, 1968.
9. "Powder Blocks Water from Cable," Design Engineering, January 1978.
10. T. K. McManus and R. B. Beverdige, 26th IWCS, 1977, p. 204.
11. T. E. Luisi and J. J. Kaufman, 24th IWCS, 1975, p. 374.
12. J. Pritchett, et al., 24th IWCS, 1975, p. 374.

13. H. J. C. Spencer, 26th IWCS, 1977, p. 149.

14. F. W. Horn and M. Villarig, 25th IWCS, 1976, p. 1.

15. See manufacturers' catalogs in the 2000-3000 pair range.

16. "Jointing of Plastics-Sheathed Cables," International Telephone Union, Geneva, 1978.

17. J. M. Lyon, 20th IWCS, 1971, p. 235.

18. G. Gillemot, 22nd IWCS, 1973, p. 201.

19. M. Brauer and R. Sabia, 24th IWCS, 1975, p. 104.

20. J. G. Nevison and D. T. Parr, 23rd IWCS, 1974, p. 375.

21. D. F. Gill, 24th IWCS, 1975, p. 99.

22. J. E. Billigmeier, et al., 24th IWCS, 1975, p. 112.

23. Y. Kubota and S. Yamakawa, 25th IWCS, 1976, p. 129.

24. "Filled Splice Cases," REA Specification PE-74, January 1, 1978.

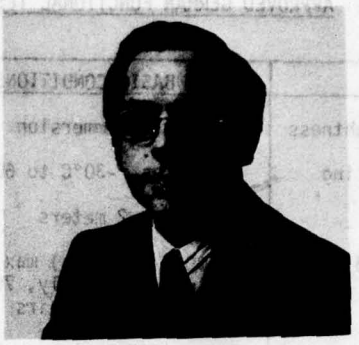
25. Raychem Internal Document.

26. "Product Criteria for Splice Closures," AT & T Engineering, March, 1978.

27. "Specification/GTS/8518 for Aerial, Buried and Underground Non Metallic Splice Closures," GTE Service Corporation, April, 1978.

28. "Test Program for Buried Cable Encapsulation Systems," Bell Northern Research, January, 1976.

29. L. Ance and H. M. Hutson, 25th IWCS, 1976, p. 129.



Norman A. Gac received a B.S. in Chemical Engineering from Purdue University and a Ph.D. from Rensselaer Polytechnic Institute. Prior to joining Raychem Corporation in 1971, he held engineering and scientist positions in industrial, academic and research organizations. Currently, he has responsibilities for product development and engineering evaluation in the telecommunications cable accessories area. His professional affiliations include membership in the International Telegraph and Telephone Consultative Committee (CCITT), Study Group VI.

APPENDIX

Table 1: REA PE-74 FUNCTIONAL TEST SEQUENCE

ITEM	BASIC CONDITIONS[a]
Preparation	3 samples each at 0°C, 20°C and 40°C
Thermal Cycling	25 cycles, -25°C and 45°C
Vibration	10 cycles, 5 and 20 Hz, ±0.1 in. amplitude, 0°C and 40°C samples
Tensile Loading	1/2 cable breaking strength or 250 lbs., maximum
Water Immersion	2 days at 20°C, 3 foot head
Wet Cycling	25 cycles, 3 foot head, 2°C to 45°C

a. All temperatures are at core locations

Table 2: APPROVED GERMAN FUNCTIONAL TESTS

ITEM	BASIC CONDITIONS[a]
Pressure Tightness	23°C water immersion
Thermal Cycling	10 cycles, -30°C to 60°C
Impact	500 g. at 2 meters
Tensile Load	1,000 N (225 lbs) max. per cable sequentially, 700 N (157 lbs) <100 pairs
Compression	700 N (157 lbs) on cable
Static Load	1,000 N (225 lbs) on 25 cm^2, 5 minutes each side
Flexure	45° cable deflections hold 5 minutes, 2 times each cable
Torsion	90° twist, both directions, holding 5 minutes
Vibration	10 Hz, 3 mm amplitude, 10 days
Bonding Continuity	10, -30°C to 60°C thermal cycles
Water Vapor Permeability	10°C water immersion, continuous helium purge to determine water permeability rate

a. Each test requires 3 or 5 closures pressurized to 6 psi which must be retained.

Table 3: CLOSURES AND RESULTS - PRELIMINARY TEST SEQUENCE

CLOSURE								
NUMBER	1	2	3	4	5	6	7	8
SHELL	S	M	S	S(H)[a]	S	M	S	S/S(H)[b]
ENCAPSULANT	NONE	I	I	I	II	III	III	IV
TEST RESULTS								
PHASE -								
1. THERMAL STRESS	PASS	PASS	PASS	PASS	PASS	FAIL	FAIL	PASS
2. FREEZE-THAW	PASS	PASS	PASS	FAIL	FAIL	--	--	(FAIL)[b]
3. WATER HEAD-CORE	FAIL	PASS	PASS	--	--	--	--	--
4. TENSILE LOAD	--	(PASS)[c]	(FAIL)[d]	--	--	--	--	--
5. BEND STRESS	--	NO CHANGE	NO CHANGE	--	--	--	--	--

a. plugs left out of shell

b. plug fell out during cycling

c. bonding hardware pulled out

d. failed connectors poorly encapsulated

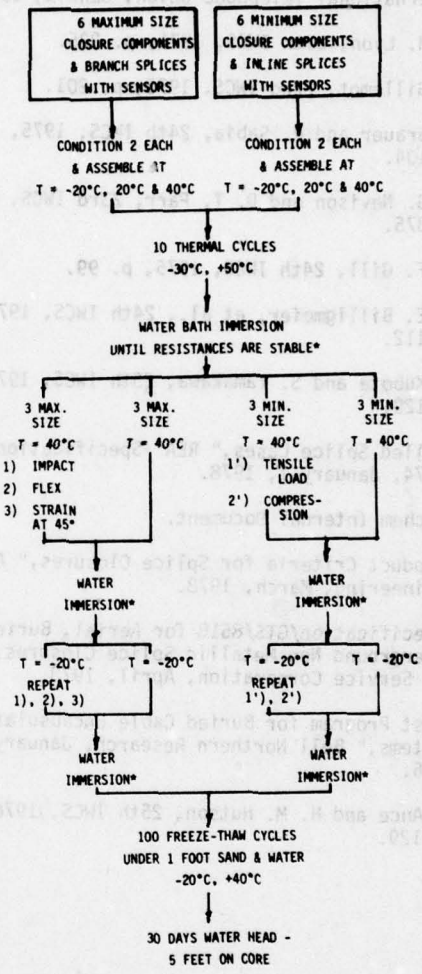


Figure 1. PROPOSED BURIED CLOSURE TEST SEQUENCE

CONECS - A COMPLETE SPLICING SYSTEM FOR AERIAL, BURIED AND UNDERGROUND TELEPHONE PLANT

by

D. R. Frey and G. S. Cobb

Bell Laboratories
Norcross, Georgia

Abstract

CONECS is a complete system for designing and installing connectorized multipair cable in aerial, buried, and underground plant. CONECS, developed by AT&T, Bell Labs, and Western Electric, includes hardware, documentation and training. CONECS utilizes the Western Electric 710 Connector System in 25 pair multiples and is fully compatible with 710 Connector field splices. A new Wire Holding Index Strip (WHIS) plugs into the connector module to form a splice, supplementing the conventional bridge module and connector module male/female option. The WHIS makes possible fully connectorized branch splices. Besides multipair cable, CONECS options are available for coil cases, inductor cases, and FDI's. Western Electric is manufacturing CONECS in all cable plants and many service centers. Telephone companies are realizing savings in both costs and installation time of new plant.

Introduction

CONECS, an acronym for CONnectorized Exchange Cable Splicing, is a Bell System development by AT&T, Bell Labs, and Western Electric. It is a practical solution to an old idea, plug-together telephone plant. Cables connectorized and tested at a Western Electric factory or service center are shipped to the field, installed in place using standard methods, and simply and quickly plugged together.

The central objective of CONECS is to reduce plant construction costs by removing tedious, repetitive and time consuming operations from the field and placing them in a more controlled environment where the working conditions are more pleasant and constant; thus, there is a higher efficiency potential.

The CONECS program, since its beginning in 1974, has been a very structured development effort. Each part of the program began with extensive field trials, followed by phased introduction, and general availability. Before any step proceeded, methods for field engineering, field construction, manufacturing, training courses, and installation hardware were developed and available. These were then tested in field trials, and fine tuned during a phased introduction period to assure a smoothly functioning system for general availability. Aerial and buried applications preceeded underground applications by about a year because they generally have fewer constraints and complexities.

The CONECS concept and early development was discussed in a paper by Frey and Hardee[1] at the 1976 Symposium. This paper briefly reviews the concept, and deals more extensively with system economics and implementation experience since 1976.

CONECS System

The heart of CONECS is the Western Electric modular 710 Connector System,[2,3] which is the standard modular system and preferred high production system in most Bell System companies for conventional field splicing of multipair cables. Initially, the basic configuration of CONECS used the plug-in bridge feature of the 710 Connector System. Typically, at a straight CONECS splice, one cable end was terminated in connector (female) modules and the mating cable end was terminated in bridge (male) modules. These are quickly plugged together with the aid of a simple plier-type hand tool. The concept is illustrated in Figure 1.

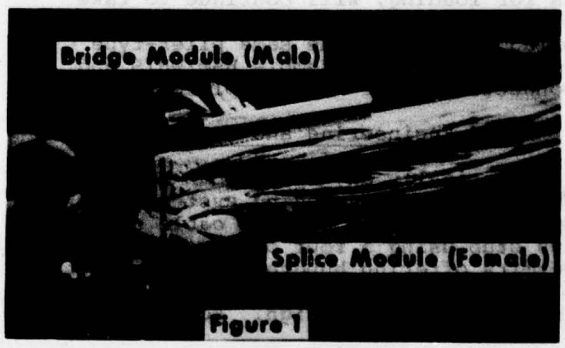


Figure 1

These splices can be unplugged and replugged to other modules to rearrange splices. This feature is very convenient for unloading during a conversion to carrier service. At branch splices using this configuration a third (branch) cable can be added in the field to the top of the connector module using a pair-at-a-time hand tool (Figure 2).



Figure 2

A new component, called Wire Holding Index Strip (WHIS), has been added to the 710 Connector System for CONECS for dedicated straight splices where disengagement and rearrangement are not required. The two piece WHIS assembly captivates the conductors of one cable end. Otherwise, WHIS is similar to a conventional index strip and mates with the connector module as shown in Figure 3. A connector module used to terminate a cable end and mate with a WHIS is called a Bottomless Splice Module (BSM). A straight BSM/WHIS splice can be simply branched by plugging into the connector modules of a cable terminated with bridge modules. The BSM/WHIS splices are smaller, which is a decided advantage for large feeder cables. Planned activity splices, such as for loading, will continue to take advantage of the plug-in connector/bridge feature. The same plier-type tool is used to assemble BSM/WHIS and connector/bridge module splices.

Field Engineering and Construction

Basically any splice can be made a CONECS splice. A coding system, which specifies the end of each cable or apparatus stub using a four or five letter code, permits offering hundreds of splice and closure combinations for full flexibility in Outside Plant design. Both ends of

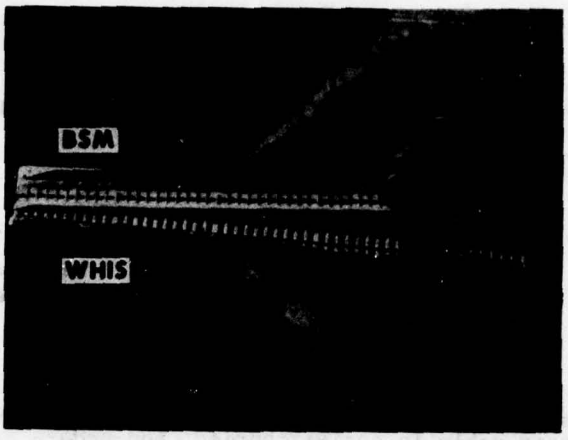


Figure 3

a cable may be connectorized for buried or aerial applications, however constraints in splice location or placing may restrict the reels to single end CONECS. Good route planning will purposely include several conventional field splices for length adjustments and verification testing. Underground applications are necessarily single ended as shown in Figure 4. The cable cannot be pulled into a duct by the CONECS end, nor would a connectorized end fit through a duct. Thus,

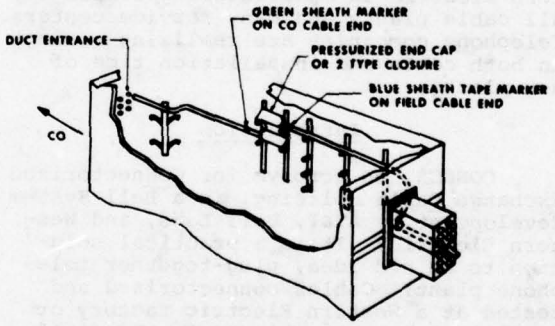


FIGURE 4

UNDERGROUND CONNECTORIZED ENDS OF CONECS CABLE IN PLACE

a typical underground CONECS job would have alternating 710 field and CONECS splices. Standard methods can be used to place aerial, buried or underground CONECS. During placing, a special bar, see Figure 5, attaches to the ends of aerial and buried cables to align them for splicing, and a special feed tube with a hinged seam opens to pass over the CONECS bundle in underground installations. Accurate placement and handling of the CONECS end adds only about 7-1/2 minutes to the placing time per reel.

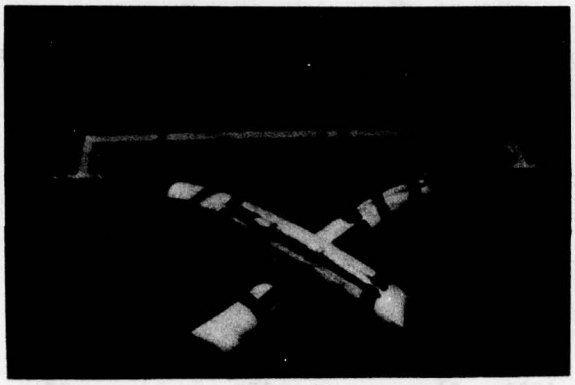


Figure 5

Several important factors were verified over and over during the field trials and phased introductions, and remain true now. First, training of engineering and construction management, and craft persons is essential before starting to use CONECS. Second, joint planning of the job by engineering and construction is essential prior to ordering the cable. Finally, the construction supervisors must plan and direct the work of their people to gain the full benefits of the potentially higher productivity. Since plugging modules together is much faster, less than 1/3 the time for conventional splicing the construction job must be coordinated to take advantage of this. In many jobs CONECS cable can be spliced as quickly as it is placed - no open pits, repeat visits, etc.

In ordinary construction, the craft person or contractor often determines placing methods and directions, location and configuration of splices, types of closures, and the direction of branch, load coil, or apparatus stubs entering a splice at the field location. But with CONECS these affect the connectorization code and must be determined before the cable is ordered. Revisions or late decisions could cause a connectorized end to be cut off. Thus, the initial cost of engineering a CONECS job is higher, about 1/2 hour per splice, but on the positive side, construction changes and reengineering are sharply decreased or eliminated. Further, it results in more planned utilization of ducts and manhole space. The training packages, comprising manuals with audio-visual aids, emphasize the need for good joint planning. Methods are included for preparing a simple schematic that provides a quick, accurate means for accounting for all details.

A policy adhered to during all phases of the program required potential users to be thoroughly trained before participating Members from each operating area were taught how to train management and craft persons. They were supported in the field by Bell Labs and Western Electric Application Engineers.

Economics

The higher field productivity, higher quality, and operational benefits have made CONECS extremely attractive from the start, but the questions of economics could not be fully answered until an experience base was developed. At first, it appeared that, overall, CONECS was econimical but that first costs may be slightly higher. Now we know, taking into account only well defined first cost parameters, that properly planned and managed CONECS jobs cost less on a splice for splice basis for most areas of the Bell System, and there are other, less tangible benefits.

A formula has been developed for comparing the cost of making a field splice with and without CONECS. To be economical or equivalent on a first cost basis:

$$\text{CONECS Splice Costs} \leq \text{Conventional Splice Costs} \quad (1)$$

Substituting the appropriate terms into each side of the equation:

$$2CC + H_c \cdot R + P \cdot R + E \leq H \cdot R + M + C_s + T_c \cdot R \quad (2)$$

where:

CC = CONECS price $/end

H_c = Total CONECS splicing time, hours

R = Telco loaded labor rate, $/hour

P = CONECS placing penalty, 15 min./splice x 4 men = 1 hr./splice (average)

E = Extra engineering effort for CONECS, $20/splice (average)

H = Total conventional splicing time, hours

M = Module material cost, $/splice

C_s = Net scrap cable costs for conventional splice, $/splice

T_c = Time to clear cable end with conventional splice, 1 hour/splice (very conservative)

Many of these terms are familiar and self-explanatory. Some, however, require elaboration. H_C and H are the total number of manhours charged to the splice. This would include travel time, closing and reopening partially completed splices if needed, personal time, clean up, etc. C_S is the net scrap cable cost, for excess cable eliminated at CONECS splices, thus it is only charged to the conventional splice. A survey has shown an average of fifteen feet of excess cable is removed by a splicer at each underground splice.

Time to clear a cable end (T_C) is a cost to conventional splicing to permit verification testing. CONECS ends are automatically cleared.

The local loaded labor rate (R) varies throughout the country, therefore equation (2) is solved for (R):

$$R \geq \frac{2CC + E - M - C_s}{H - H_C + T_C - P} \qquad (3)$$

If the local telephone company loaded labor rate is equal to or greater than the calculated value for (R), then CONECS is economical on a first cost basis in that operating area for that splice.

Table I shows the typical break-even loaded labor rate for several splices in underground plant. Average splicing productivity was used for both CONECS and conventional field splicing, based on field trial and recent survey data.

TABLE I

BREAK-EVEN LABOR RATE

Cable Size*	Dollars/Hour
600 - 22	16.24
1200 - 22	14.07
1800 - 24	14.95
2700 - 26	15.33
3600 - 26	14.49

*Pairs-Gauge

Table II shows corresponding savings in costs and time, using average Bell System loaded labor rate and productivity for conventional splicing. First cost savings range from 7% to 16% and labor hours are reduced by about 63 to 70% for underground splicing. Labor savings are comparable in larger aerial and buried splices, but the dollar savings are less. Typically a buried splice which takes about six hours with conventional methods will take only 1-1/2 hours with CONECS.

TABLE II

SAVINGS PER SPLICE

Cable Size	$ Dollars	% Labor
600 - 22	7	63
1200 - 22	16	66
1800 - 24	15	67
2700 - 26	14	69
3600 - 26	16	70

In addition to readily quantified costs, there are additional benefits of CONECS. Construction intervals can be shortened resulting in substantial reduction in the period capital investment is in a nonearning status, which reduces carrying charges. Nonproductive time of manhole guards and costs of guarding open buried splices is reduced. These are additional savings which can be calculated for each job. Other savings which are harder to quantify are: fewer capital tools required, less lost time due to restricted work hours in busy streets, and a reduction in overtime and borrowed craft persons to cover peak loads.

Manufacturing

CONECS cables are now connectorized in all Western Electric cable factories and sixteen regional service centers. Most large orders are made in the factories. The service centers can respond more rapidly to special requests and routine orders for stock cable and apparatus. Interfaces, load coils, apparatus cases, stub cables, and pressure plugs are connectorized in a manner similar to cable reels.

CONECS cables are fully tested before shipping, and 100% good pairs are shipped in the modules. Sheath ends are prepared for the closure specified. Compound is removed from waterproof cable ends, which eliminates an undesirable field operation and improves the reliability of encapsulated splices.

It has been a manufacturing challenge to keep up with the enthusiastic demand for CONECS with a quality product. Growth has been especially fast in underground

cables because the savings there are largest.

CONECS is basically foreign to normal cable factory operations and some think it should not be part of a cable factory.[4] Cable manufacturing is a high capital, low labor technology and CONECS is the opposite. Different quality control procedures and sampling are required. Much of the quality of cable is machine controlled where the quality of CONECS is labor sensitive. Connectorization is further complicated by the many options permitted by CONECS - over 1500 permutations for each type of cable. The type of connector chosen (male/female, etc.) on which wall of the manhole the cable is placed, the type of splice (straight, branch, etc.), the configuration (in-line, fold-back, etc.) and the type of closure to be used all affect the measurements and orientation for manufacturing.

Future

Most Bell System companies are now using CONECS for all types of plant. Nearly any splice that can be made in the field can be ordered as a CONECS splice. Our experience thus far indicates the system is more comprehensive and complex than it need be. The next step will simplify the system and mechanize the engineering and coding. This will have a potential for reducing codes and errors in both the field and manufacturing. A large field trial of a simplified system is underway in one operating company. Results should be known by the years' end.

Western is applying more technology to mechanize connectorization which will reduce costs and put more machine control in quality.

CONECS has demonstrated a potential for providing lower cost, higher quality telephone plant, which can be realized with reasonable management. It has been accepted more enthusiastically than expected. At this point, we can expect upwards of 75% of all underground cable reels and 50% of all buried and aerial cable reels will be candidates for connectorization in the future.

Acknowledgements

CONECS is the result of a joint effort of the Engineering and Customer Services Organization of AT&T, the Cable Joining Department of Bell Labs, and the Western Electric, Loop Transmission Apparatus and Cable Product Engineering Control Centers. Many in all three companies contributed to the work reported. It is difficult to acknowledge specific individuals in a development like this without unintentionally omitting some very deserving person, but we feel it is necessary to give special acknowledgement for the efforts of the Western Electric, Loop Transmission Apparatus, Product Engineering Control Center.

References

1. D. R. Frey and A. G. Hardee, 1976 Proceedings of the 25th International Wire and Cable Symposium, pp. 125-128, "CONnectorized Exchange Cable Splicing (CONECS)."

2. R. W. Henn, 1973 Proceedings of 22nd International Wire and Cable Symposium, pp. 195-200, "Systematic Encapsulated Cable Splicing Connector for Aluminum and Copper Wire."

3. D. R. Frey and D. C. Borden, 1976 Proceedings of 2nd Intl. Symposium on Subscriber Loops and Systems, pp. 68-117, "A System of Wire Joining with Connection Verification."

4. O. D. McMahon, 1978, USITA Mid-Western Telephone Showcase, Technical Seminar, "Preconnectorization of Cables and Related Equipment."



Dean R. Frey is a Member of the Technical Staff at Bell Laboratories in Norcross, Georgia and supervises the Wire Joining Development Group of the Cable Splicing Department. For the last 12 years he has been active in developing splicing apparatus and hardware for the Bell System. Prior to this he was involved with the development of hardware for underwater systems. Mr. Frey received a BSME degree from the Pennsylvania State University and a MME degree from New York University.



Gary S. Cobb is a member of the Technical Staff in the Cable Joining Department of Bell Laboratories in Norcross, Georgia. He is presently the Project Engineer for CONECS. Prior to this assignment, he was active in the development of Sea Plow IV, a vehicle for burying ocean cable. Before that, he was involved in the design and development of ocean cable and associated hardware. Mr. Cobb received a BSME from Virginia Polytechnic Institute and State University and a MSME from the University of Maryland.

A NON-FLAME PROPAGATING TELEPHONE CABLE FOR INDOOR INSTALLATION

James M. Daly and Dipl.-Ing. Georg Maltz

The Okonite Company
Ramsey, New Jersey

Kabelmetal
Hannover, Germany

Abstract

An inside telephone cable has been developed for use in high-rise and high occupancy buildings. This cable design, which utilizes a continuously welded and corrugated aluminum sheath, will not propagate a fire even after the aluminum sheath and the conductor insulation have been destroyed in the area of flame impingement.

Introduction

In recent years, there have been numerous fires where the fire was carried from one location to another by electrical cables that burned. The TVA Brown's Ferry Nuclear Generating Station, the Telephone Building and the World Trade Center, both in Manhattan, being the most publicized cases.

Power and control cables that would not propagate a fire had been developed during the past several years and were readily available. Telephone cables, however, had not been changed and the common cables used for inside wiring were still the flammable constructions that would emit dense smoke and continue to burn even after the heat source was removed, thus transmitting a fire to other locations. These undesirable features become even more threatening when the cables are installed above false ceilings in offices where that space is also used for the air return to the air conditioning system. Burning cables can introduce dense smoke into the air system and increase the danger to personnel both directly from the fumes and indirectly through reduced visibility and possible panic.

The Okonite Co., who was one of the leaders in the development of non-propagating power and control cables, undertook the development of a flame-retardant, non-propagating, low smoke telephone cable for inside wiring.

National Electrical Code

Since all wiring must comply with the National Electrical Code (NEC),[1] this Standard was used to provide an initial design criteria. Also, the intent was to design one cable that would be suitable for installation anywhere in a building regardless of location. The requirements for cables installed in ducts, plenums, and other air handling spaces are more restrictive than for cables installed elsewhere so these requirements established the minimum design criteria.

Section 300-22 of the 1978 NEC specifies the wiring methods permitted to be used in ducts, plenums, and other air handling spaces. In ducts or plenums used for environmental air, Type MI mineral-insulated metal-sheathed cable, Type MC (Metal-Clad) cable employing a smooth or corrugated impervious metallic sheath, electrical metallic tubing, flexible metallic tubing, intermediate metal conduit, or rigid metal conduit are the only wiring methods permitted.

In other spaces used for environmental air, such as the space above false ceilings used for the air return, only Type MI mineral-insulated metal-sheathed cable, Type MC cable and Type AC cable commonly referred to as "BX", are permitted. Other type cables and conductors must be installed in electrical metallic tubing, intermediate metal conduit, rigid metal conduit, metal surface raceway with metal covers where accessible, or flexible metal conduit.

The final design criteria was to provide an economical installed cost. This eliminated the use of conduit or raceways and indicated a factory assembled cable would be the answer.

UL Standards

No UL Standard exists for inside telephone cable or communication cables under Article 800 of the 1978 NEC. The closest Standard that was applicable was UL Subject 13 which covers Power-Limited Circuit Cable under Article 725 of the 1978 NEC.

UL elected to include the inside telephone cable with Subject 13[2] and due to the application and intended use of the cable type, the voltage rating of 300 Volts was eliminated. The cable discussed in this paper is UL Listed as Power-Limited Circuit Cable for use in Class 2 circuits which are power limited as defined in Section 725-31 of the 1978 NEC.

Considerations for an Optimum Cable Construction

In recent years a number of improved telephone cable constructions have been developed for indoor use which offer better flame resistance character-

istics than conventional PVC insulated and jacketed cables[3]. The possible cable constructions and their behavior under different conditions of exposure to fire have been summarized in the following table.

Cable Construction \ Type of fire	Locally confined limited heat source	Locally confined medium heat source	Major fire
Conventional PVC	1 - 3	1 2 3	1 2 3
Slow-burning PVC	1 - 3	1 - 3	1 2 3
Slow-burning PVC with low HCl emission	1 - -	1 - (3)	1 2 (3)
C-L-X cable	- - -	1 - -	1 - 3

1 Cable damaged at point of exposure to flame
2 Cable damaged and propagates flames
3 Cable emits corrosive smoke

The C-L-X inside telephone cable, like any other cable, will be destroyed when exposed to a major fire, however, it will not propagate the fire and offers substantial additional advantages when the cable is subjected to local fires.

While the potential fire hazard of indoor cable installations is widely recognized, existing cable constructions have remained unchanged in many countries. Instead, the efforts to contain fire damage have been directed to structural measures. The primary approach being to install fire-stops along the cable ducts. However, when structural changes are undertaken, which occurs frequently in high-rise buildings, these fire stops are often removed. It is under these circumstances, particularly when welding work is being done, that fires break out. Hence, a conscientious approach towards improving the fire safety of a building cannot limit itself to structural measures. It is essential that the cable itself be made fire-resistant and non-propagating. The C-L-X indoor telephone cable represents such a design. It will fail at the point of prolonged exposure to a massive flame or fire but it will not propagate the fire. Thus, it is only necessary to splice in a new cable section for the damaged piece and normal service can be restored in a short time.

Design of the C-L-X Cable

In recent years, several new cable types for indoor communication applications have been proposed. The improvements were based on the use of new resins with enhanced fire resistance. However, these cables, in addition to being more costly, suffered one major draw-back, namely, when exposed to flame, they will propagate the fire! Since this condition is the cause of many spreading fires, a new cable design which would contain the fire to the immediate area of exposure to flame seemed urgently needed. The Okonite Company has developed such a design *.

* U.S. and foreign patents pending.

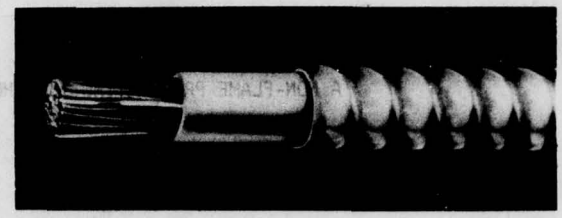


Fig.1 CLX Inside Telephone Cable

The final cable selected to comply with the 1978 NEC and UL 13 consists of solid bare copper conductors, sizes 0.205 and 0.324 mm^2 (#24 and 22 AWG). The conductors are insulated with a flame-retardant PVC, color coded in accordance with telephone industry standards. The insulated conductors are twisted into pairs and then assembled into the common configurations from 3 to 400 pairs. A flame-retardant PVC jacket is extruded over the core and a continuously welded and corrugated aluminum sheath is applied overall. The jacket under the metallic sheath permits terminating the sheath at a wall or enclosure and continuing with the jacketed cable to the instrument or termination point.

While the sheath can be applied either smooth or corrugated, the corrugated sheath was selected to facilitate installation since the corrugated sheath is much more pliable than the smooth sheath. The aluminum sheath is identical in every respect to that used on Type MC power and control cable. Also, like MC cable, the aluminum sheath when used with approved terminators, may be used as the equipment grounding conductor since it exceeds the requirements of NEC Table 250-95 in all sizes. This feature provides a positive equipment ground between all interconnected equipment.

The aluminum sheath is applied by the Kabelmetal process in which a strip of metal is continuously formed into a tube around the cable core, longitudinally welded and transversely corrugated.[4] The corrugated cable has excellent crush resistance, good pliability and is impervious to the ingress of moisture. In most installations, the cable can be used without any plastic jacket over the metal sheath and, in fact, it is recommended that non-jacketed constructions be used in air ducts or plenums,

In addition to the excellent mechanical properties of the C-L-X cable, it offers superior electrical characteristics. The low sheath resistance is effective [illegible] broad frequency range. This represent[illegible]tant advantage for all high-freque[illegible]ions, particularly for digital appl[illegible]a transmissions carried on C-L-X ca[illegible] nearly free of interference from outsi[illegible]ources which can lead to bit errors. Thus the C-L-X cable provides circuit integrity which cannot be obtained with cables without a tubular metallic sheath.

The C-L-X cable offers a level of protection

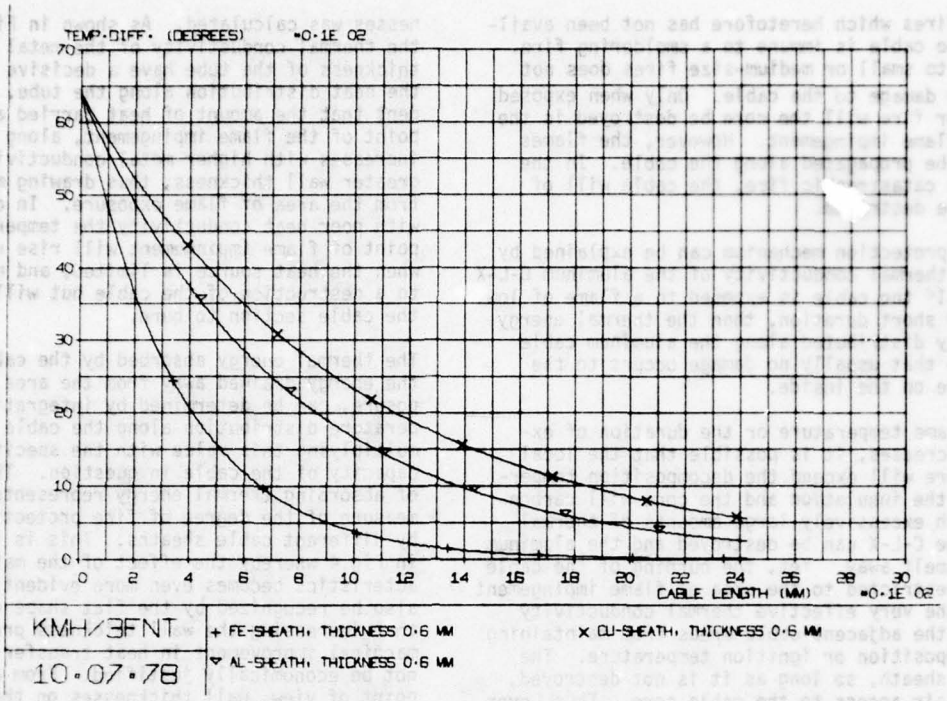


Fig.2 Temperature Distribution Along Metallic Sheath

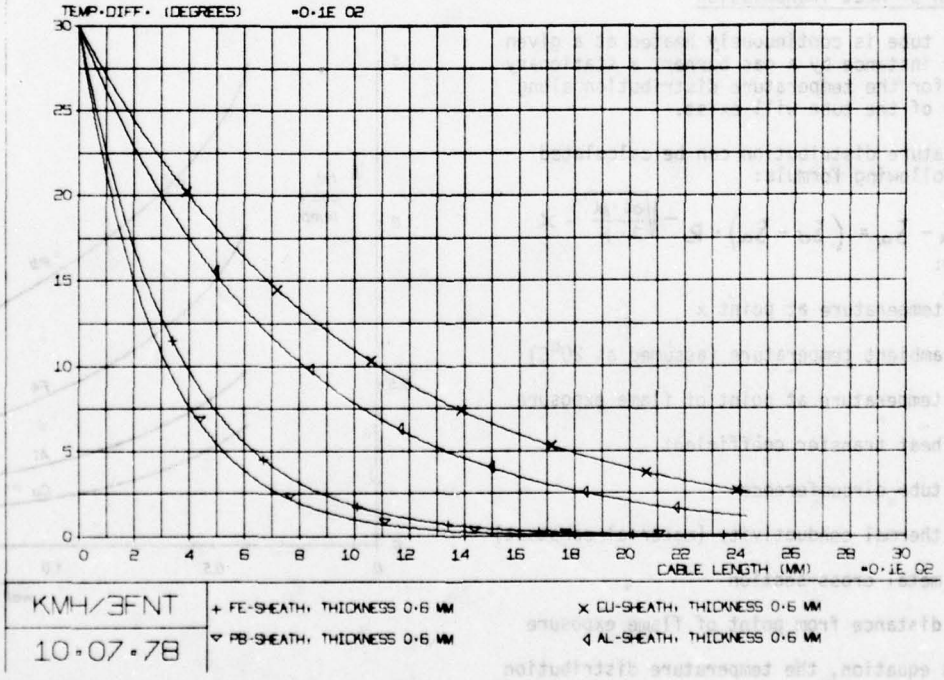


Fig.3 Temperature Distribution Along Metallic Sheath

against fires which heretofore has not been available. The cable is immune to a smoldering fire. Exposure to small or medium-size fires does not cause any damage to the cable. Only when exposed to a major fire will the core be destroyed in the area of flame impingement. However, the flames will not be propagated along the cable. In the case of a catastrophic fire, the cable will of course, be destroyed.

The fire protection mechanism can be explained by the good thermal conductivity of the aluminum C-L-X sheath. If the cable is exposed to a flame of low energy or short duration, then the thermal energy is rapidly distributed along the aluminum cable sheath so that usually no damage occurs to the cable core on the inside.

As the flame temperature or the duration of exposure increases, it is possible that the local temperature will exceed the decomposition temperature of the insulation and the core will carbonize. With excessively large amounts of thermal energy the C-L-X can be destroyed and the aluminum can even melt away. Yet, the burning of the cable will be restricted to the area of flame impingement because the very effective thermal conductivity prevents the adjacent cable areas from maintaining the decomposition or ignition temperature. The aluminum sheath, so long as it is not destroyed, prevents air access to the cable core. Thus, even under adverse circumstances and arrangement of the cables, the cables can only burn at the place of the fire source and only as long as sufficient energy is supplied from the outside.

Calculation of Heat Transmission

If a metal tube is continuously heated at a given point, for instance by a gas burner, a stationary condition for the temperature distribution along the length of the tube will exist.

The temperature distribution can be calculated with the following formula:

$$\vartheta_x - \vartheta_a = (\vartheta_\sigma - \vartheta_a) \cdot R^{-\sqrt{\frac{\alpha \cdot \mu}{\lambda \cdot F}} \cdot x}$$

whereby:

ϑ_x = temperature at point x

ϑ_a = ambient temperature (assumed as 20°C)

ϑ_σ = temperature at point of flame exposure

α = heat transfer coefficient

μ = tube circumference

λ = thermal conductivity (material constant)

F = metal cross-section

x = distance from point of flame exposure

Using this equation, the temperature distribution along a tube for different metals and wall thicknesses was calculated. As shown in Figs.2 and 3, the thermal conductivity of the metal and the wall thickness of the tube have a decisive influence on the heat distribution along the tube. It is evident that the amount of heat carried away from the point of the flame impingement, along the tube, increases with higher metal conductivity and greater wall thickness, thus drawing more heat from the area of flame exposure. In cable sheaths with poor heat conductivity the temperature at the point of flame impingement will rise rapidly, even when the heat source is limited, and not only lead to a destruction of the cable but will also cause the cable section to burn.

The thermal energy absorbed by the cable, that is, the energy drained away from the area of flame exposure, can be determined by integrating the temperature distribution along the cable length and multiplying this value with the specific heat capacity of the cable in question. The capability of absorbing thermal energy represents a relative measure of the degree of fire protection provided by different cable sheaths. This is illustrated in Fig.4 whereby the effect of the material characteristics becomes even more evident. It can also be recognized by the flat shape of the curves that increasing the wall thickness provides only a marginal improvement in heat transfer which could not be economically justified. From a practical point of view, wall thicknesses on the order of 0.4 mm (0.016 in.) for copper and 0.8 mm (0.032 in.) for aluminum represent optimum solutions. For economic reasons, preference is usually given to aluminum.

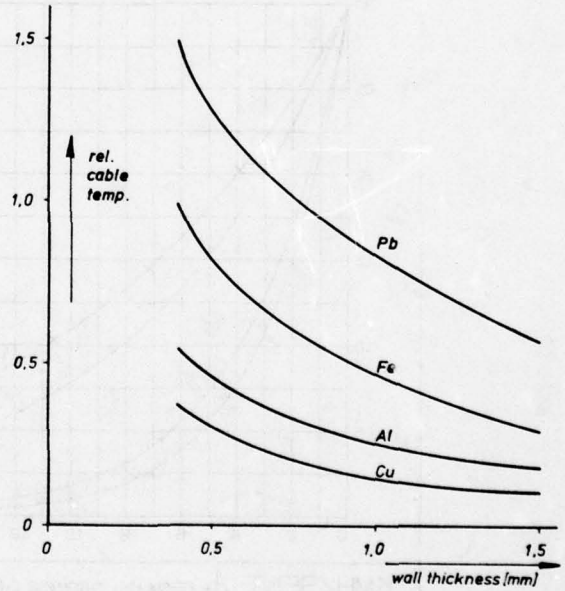


Fig.4 Temperature Distribution vs Wall Thickness

A confirmation of the computation illustrated in Figs.2 and 3 can be readily obtained through a simple experiment, simulating a brazing operation, whereby tubes of different metals are heated with a brazing torch. Fig.5 shows the calculated and measured values for the temperature distribution along a steel and an aluminum tube with 0.3 mm (0.012 in.) and 0.6 mm (0.024 in.) walls, respectively. This only confirms the well known fact that much more heat is needed to braze or solder an aluminum pipe than a steel pipe.

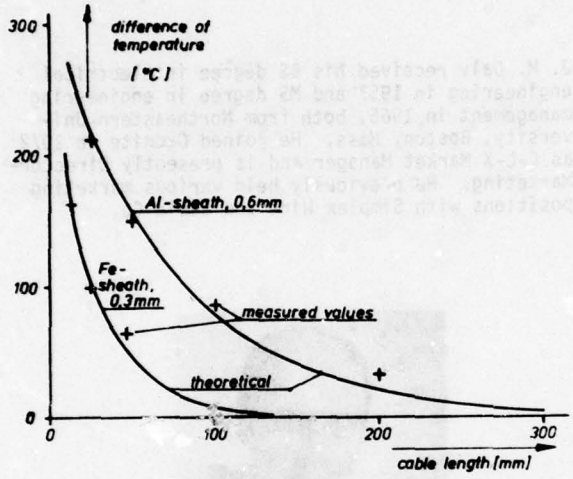


Fig.5 Temperature Gradient vs Cable Length

Flame Testing Procedure

The criteria used to determine the propagation qualities of the cable was the Vertical Tray Flame Test as defined in UL Subject 13 and IEEE Standard 383.[5]

Basically the flame test consists of placing six lengths of 12.7 mm (0.5 inch) diameter cable in a single layer in a vertical steel cable tray with a separation of one-half the cable diameter between adjacent cables. A ribbon-type gas burner is mounted horizontally behind the tray, 1.8 m (6 ft.) from the top of the vertical tray and 76.3 mm (3 in.) behind the tray. The burner is adjusted to provide 17640 kcal/h (70,000 BTU/h) and then turned on for 20 minutes.

The cable may be destroyed in the area of flame impingement, but it shall not propagate the flame. Upon removal of the flame after 20 minutes, the cable must self-extinguish and there shall not be any damage (blistering or charring) to the insulated conductors, the jacket, or the sheath at the top of the tray, which is 1.8 m (6 ft.) above the burner.

Flame Test Results

The initial flame tests were conducted on a telephone cable consisting of 25 pair 0.324 mm^2 (#22 AWG) with polyethylene insulation and jacket. The lengths of cable were totally engulfed in flames in 5 minutes and completely consumed in less than 10 minutes.

The identical cable was then enclosed in the continuously welded and corrugated aluminum sheath and retested. This time, the cables not only passed the test, but dramatically limited the fire damage. The cables were consumed in the immediate vicinity of the flame source but there was no damage to the insulation or jacket 1.2 m (48 in.) above the flame source. This test clearly proved the effectiveness of the aluminum sheath by changing a highly flammable cable into a non-propagating cable.

A standard PVC insulated and jacketed inside telephone cable was tested with essentially the same results as the polyethylene; namely, the cables propagated and were completely destroyed in less than 10 minutes. Again, addition of the C-L-X sheath made the cable non-propagating and passed the test satisfactorily.

While the aluminum sheath alone was sufficient to prevent propagation of a fire regardless of the core, we further improved the cable by changing the insulation and jacket on the core from the flammable PVC to a non-propagating PVC. This construction not only passed the 17640 kcal/h (70,000 BTU/h) test discussed above but it also passed a similar test using a heat source of 53,000 kcal/h (210,000 BTU/h). Actually once a cable successfully passes the 17640 kcal/h test, it can also pass any test using a higher heat input, only the length of damage to the cables will change.

Conclusion

An inside telephone cable is now available for use in commercial buildings and occupancies that will provide significantly greater fire protection than that presently available. The C-L-X inside telephone cable is UL labeled and complies with the 1978 National Electrical Code. The cable, while designed primarily for use in air ducts, plenums, or other air handling spaces, may also be used anywhere else in the building, eliminating any need to change wiring methods for different locations.

The C-L-X cable offers ease of installation and provides a much more economical installed cost than wire or cable in raceways.

Finally, use of this cable will prevent any future occurrences of a localized fire being transmitted throughout the building by the communication cables.

Acknowledgement

The authors wish to express their appreciation to Messrs. Stobaeus and Verdenhalven of Kabelmetal, for the experimental work and calculations performed in the preparation of this paper and to Cable Consultants Corporation for their translation services between the authors.

References

1. National Electrical Code, 1978 Edition, National Fire Protection Association, Boston, Mass.

2. Subject 13, Power Limited Circuit Cable, Underwriters Laboratories, Inc., Melville, L.I., N.Y., March, 1978

3. Dr. O. Leuchs, "A New Flame Self-Extinguishing Hydrogen Chloride Binding PVC Jacketing Compound For Cables", Proceedings of the 19th International Wire and Cable Symposium, 1970, pp. 239-255.

4. Dr. H. Martin, "High Power Radio Frequency Coaxial Cables, Their Design and Rating", Proceedings of the 22nd International Wire and Cable Symposium, 1973, pp. 70-98

5. Standard 383, Type Test of Class 1E Electric Cables, Field Splices, and Connections for Nuclear Power Generating Stations, Institute of Electrical and Electronic Engineers, N.Y., N.Y., 1974

6. R. A. Nelson and J. M. Daly, "Corrugated Metallic Sheathed Cable - Design and Applications" IEEE Transactions on Industry Applications, Vol. IA-11, No.2, March/April 1975

7. Dr. Ing. Gerhard Ziemek and James M. Daly, "Welded Aluminum Cable Sheaths", Wire Journal, March 1976



J. M. Daly received his BS degree in electrical engineering in 1957 and MS degree in engineering management in 1965, both from Northeastern University, Boston, Mass. He joined Okonite in 1972 as C-L-X Market Manager and is presently Director-Marketing. He previously held various marketing positions with Simplex Wire and Cable Co.



G. D. Maltz, born at Riga in 1930, received his Dipl.-Ing. degree in communication engineering from the Technical University of Hannover, Germany, in 1958. He has been engaged in research, development, and design of telecommunication cables since 1955, except the years 1962/65 when he was head of the test department of a radio link equipment manufacturing company. Since 1965 he has been Director of the research and development department for telephone and carrier frequency cables, Kabel- und Metallwerke Gutehoffnungshutte Aktiengesellschaft, Hannover, West Germany.

PYROLYSIS OF PVC AND EXPERIMENTAL PVC COMPOUNDS USING TGA, FURNACE AND OVEN TECHNIQUES WITH RECOVERY STUDIES OF HCl

A. B. Carel

Continental Oil Company
Ponca City, Oklahoma 74601

Abstract

A thermal gravimetric analysis instrument (TGA) and a tube furnace were used to pyrolyze modified polyvinyl chloride (PVC) at 600°C. The effluents were collected in dilute caustic, and both effluent and residue portions were analyzed for chloride by titration with silver ion using a modified Volhard method. The total recovered chloride was determined and compared to the theoretical chloride values. The evolution of chloride at low temperatures was measured using a thermostated oven that was equipped to contain multiple specimens. Inert gas carried the evolved chloride through gas impingers containing dilute caustic. Analyses were made with a chloride specific ion electrode using an AutoAnalyzer system.

Introduction

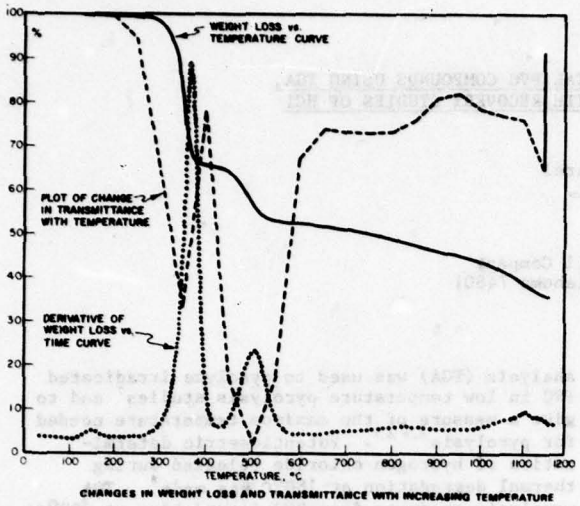
As polyvinyl chloride (PVC) becomes more popular as a building material, electrical insulator and general replacement for industrial materials, it becomes more important for health reasons to reduce the amount of hydrogen chloride that is released during heating or pyrolysis. This reduction in evolution of hydrogen chloride can be achieved by the addition of ingredients to retain the hydrogen chloride in the residue. In order to determine the success of hydrogen chloride retention, reproducible methods were needed for heating the samples under carefully controlled conditions for completely pyrolyzing the PVC while analyzing the effluent and residue fractions (from the pyrolysis) for chloride. In this way, the recovered chloride could be compared to the theoretical amount of chloride in the original sample.

Many techniques have been used to measure hydrogen chloride evolution from PVC and other types of chlorinated plastic compounds. A combination of laser, infrared (IR), and phototube technology[1] was used to measure combined hydrogen chloride and smoke evolution. A specific ion electrode[2,3] was used to measure hydrogen chloride evolution and an IR gas analyzer to measure gases[2] and hydrocarbon types from PVC pyrolysis. Thermal gravimetric analysis (TGA) was used to pyrolyze irradicated PVC in low temperature pyrolysis studies[7] and to give a measure of the maximum temperature needed for pyrolysis[4,5,6,7]. Potentiometric determination of hydrogen chloride released during thermal degradation at 180°C was made[8]. TGA pyrolysis products from PVC degradation at 300°C were examined by IR, gas chromotography (GC), and mass spectrometry[9]. None of these methods or other literature methods were concerned with the recovery of total chloride from both effluent and residue fractions.

Thermogravimetric (TGA) Method for High Temperature Pyrolysis

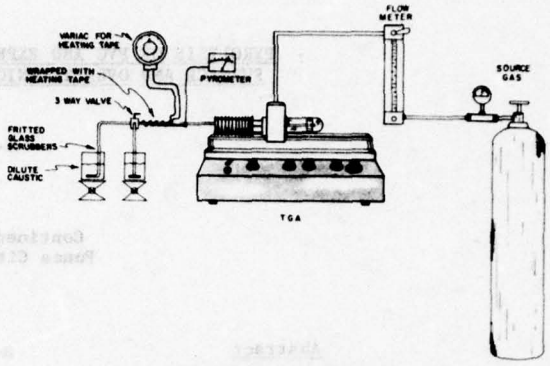
1. Preliminary Work Using a Light Transmittance Cell and Gas Scrubbers.

   In our initial work we attempted to obtain a variety of information from a single TGA (DuPont Model 951) pyrolysis run by placing 100 mg of the experimental PVC sample in the platinum pan attached to the quartz rod and then pyrolyzing the sample to 1150°C. We recorded the weight loss vs temperature curve and the derivative of weight loss vs time curve. The effluent gas (air) from the TGA apparatus was passed through a 5-cm flow cell contained in a Spectronic 70 spectrophotometer to measure the light transmittance (650 nm) vs temperature. Finally, the gas was scrubbed by passing it through dilute caustic, and the caustic solution was acidified and titrated for chloride with silver ion. Attempts were also made to obtain chloride data on the residue portion from pyrolysis. Figure 1 shows the weight loss and percent transmittance data that were obtained for an experimental PVC sample. While all this information is interesting, we could not obtain the total chloride recovery data sought on the effluent and residue portions. A more efficient gas scrubber arrangement was needed to recover products for chloride measurement.



CHANGES IN WEIGHT LOSS AND TRANSMITTANCE WITH INCREASING TEMPERATURE

FIGURE 1



TGA APPARATUS FOR PYROLYSIS OF EXPERIMENTAL PVC COMPOUNDS

FIGURE 2

2. TGA Apparatus and Gas Collection Assembly.

A drawing of the TGA apparatus for pyrolysis of experimental PVC compounds is shown in Figure 2. Either air or nitrogen purge gas can be used. Nitrogen purge gas was used for all of the experiments with both the TGA and tube furnace methods. Nitrogen gas was chosen since pyrolysis data and not combustion data were desired. It has been shown[10,11] that the dehydrochlorination of PVC is essentially a thermal decomposition process and flaming combustion conditions are not required. The amount of hydrogenchloride released depends upon the temperature and time of exposure. This author[10] has further shown that the rate of release of hydrogenchloride from PVC is much faster with air than with nitrogen and is greatly influenced in combustion where oxygen concentrations may vary from 2 to 21 percent. Nitrogen was then used based on these and other criteria in order to provide uniform thermal pyrolysis conditions. Selected commercial samples were run using both air and nitrogen carrier gas for comparison. All results obtained using the two gases were identical. The gas is metered through the TGA furnace containing the experimental PVC compound, and the evolved chloride (HCl) is collected with a fritted glass scrubber. A three-way valve with ball and socket joint connections is used to divert the flow from one collector to another. The incoming line and valve assembly is heated with a heating tape to prevent condensation of HCl. This arrangement provided quantitative collection of all degradation products for subsequent analysis.

3. Testing Procedure

Approximately 0.5 g of sample is cut into ribbons of about 5 mm square, accurately weighed, and placed in a platinum spoon shaped to the inner contour of the quartz heating tube. The platinum spoon is inserted 7 cm into the quartz heating tube to place it directly under the thermocouple, and the quartz tube is placed in the TGA furnace. A 20-mm coarse frit immersed in 50 ml of 0.2N sodium hydroxide solution is connected to a three-way valve and the valve to the quartz tube. All lines leading to the frit are maintained at 250°C. Nitrogen is passed through the system at 50 ml/min, and the sample is heated at 50°C/min to 600°C and maintained there for 15 minutes. The solution used to trap the effluent is transferred to a beaker and the residue in the heating pan is transferred to an Erlenmeyer flask. The residue is crushed, boiled in dilute nitric acid, and filtered. Both effluent and residue portions are titrated with silver ion according to the modified Volhard method[12] to determine chloride content. The method consists of adding potassium thiocyanate and ferric nitrate solution to the sample containing 75 mls of 3M nitric acid. Silver nitrate is added until the solution turns clear (absence of red ion thiocyanate color) at the end point.

Data Obtained by the Thermogravimetric Analyzer Method

It was necessary to establish the maximum temperature necessary for pyrolysis to obtain the maximum chloride evolved. Table 1 contains chloride data on effluent fractions for Samples 1, 2, and 3 taken in the temperature range of 25° to 600°C.

TABLE 1

PERCENT CHLORIDE IN VARIOUS TEMPERATURE INCREMENTS OF THE EFFLUENT OF TGA PYROLYZED EXPERIMENTAL PVC COMPOUND SAMPLES

		TEMPERATURE °C										
Sample	Run No.	25	200	250	300	300	400	400	500	550	600	Total
1	1		0.05	0.55	27.14	6.28	0.04	0.07	0.05	Nil	Nil	34.18
	2						35.03				0.01	35.04
	3						35.90				0.01	35.91
2	1					28.32	0.33				0.77	29.42
	2						28.42				0.22	28.64
3	1					21.16	0.30				0.68	22.14
	2						21.93				1.12	23.05

Program conditions were 20°C/min to 200°C, and then 10°C/min to 600°C. Nine effluent fractions were taken on Sample 1. The evolved chloride was 27.14% in the 250°-300°C fraction with 6.28% in the 300°-360°C fraction, and only 0.12% chloride was found in fractions from 400°-600°C. Two repeat runs were made collecting only two fractions, 25°-400°C and 400°-600°C. The evolved chloride in the 25°-400° fraction was >35% with only 0.01% in the 400°-600°C fraction.

Samples 2 and 3 were both analyzed in duplicate. In the first analysis of each sample, fractions were taken from 25-360, 360-400, and 400°-600°C. In the second analysis of each sample, fractions were taken from 25-400 and 400°-600°C and the results were compared. Significant chloride (>5% of the total evolved) was found in the 400°-600°C fractions.

The residues from these three samples were then analyzed for chloride. Table 2 includes the total recovered chloride and the theoretical chloride values for these samples. The data show that most of the chloride was recovered, although many fractions were taken and analyzed.

TABLE 2

SUMMARY OF EVOLVED, RETAINED, AND TOTAL CHLORIDE DETERMINED FOR EXPERIMENTAL PVC COMPOUND SAMPLES PYROLYZED BY TGA

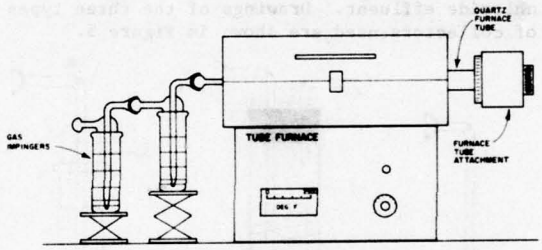
Sample	EFFLUENT 25-600°C	Residue	Total	Theory
1	35.91	2.26	38.17	37.97
	35.04	2.24	37.28	
			Avg. (37.32)	
2	29.42	2.56	31.98	31.32
	28.64	2.59	31.32	
			Avg. (31.65)	
3	22.14	8.14	30.28	32.13
	23.05	7.93	30.98	
			Avg. (30.63)	
4	24.31	12.47	36.77	37.83
	25.60	12.63	38.23	
			Avg. (37.5)	
5	29.09	9.71	38.80	37.83
6	24.88	12.84	37.72	37.97
7	34.77	0.28	35.05	–

In order to reduce the time required for pyrolysis, we increased the program heating rate to 50°C/min from ambient to 600°C, then switched to isothermal heating and maintained the sample at 600°C for 15 minutes. Finally, we took a second effluent fraction for an additional 5 minutes at 600°C. No significant chloride was found in this fraction. Examples of the data obtained from pyrolysis of PVC compounds by this procedure are shown in Table 2. Samples 1 through 6 are experimental PVC compound samples. By adding certain additives we were able to increase the chloride in the residue from only 2.25% for Sample 1 to 12.84% for Sample 6. The agreement between total recovered chloride and the theoretical value ranged from 0.03 to 1.50% for the six samples with an average deviation of 0.52%. Sample 7 is a commercially available[2], rigid PVC compound said to have a 40% calculated reduction in hydrogen chloride evolution. We found only 0.28% chloride in the residue after pyrolysis.

Tube Furnace Method for High Temperature Pyrolysis

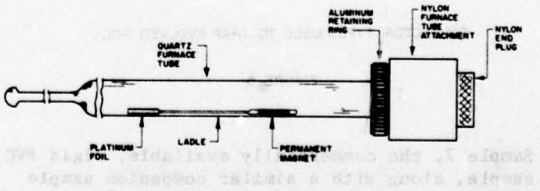
1. Apparatus for Pyrolysis of PVC

   A Lindberg tube furnace (Model 55035), capable of maintaining >1000°C temperature was purchased. A quartz furnace tube, a nylon furnace tube attachment, and a quartz ladle with magnet were fabricated. Figure 3 shows a drawing of the assembled apparatus complete with two impingers. A drawing of the furnace tube assembly is shown in Figure 4.



TUBE FURNACE ASSEMBLY FOR PYROLYSIS OF EXPERIMENTAL PVC COMPOUNDS

FIGURE 3



FURNACE TUBE ASSEMBLY

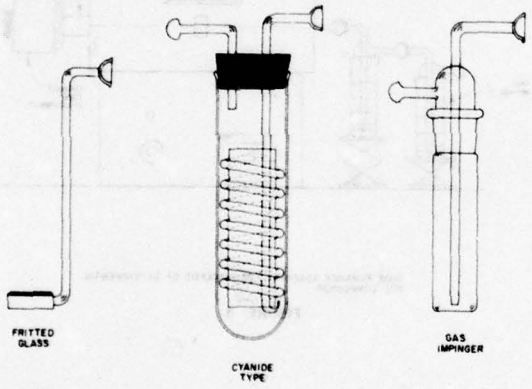
FIGURE 4

2. Sample Pyrolysis Procedure

Two gas impingers containing 0.2N sodium hydroxide solution are connected in series to the furnace tube that is heated at 600°C. The experimental PVC sample (≈0.5 g accurately weighed) is placed on the platinum foil in the ladle and covered with platinum foil. The ladle is placed in the cool zone and nitrogen flow started. When the air is purged, the ladle is pushed into the furnace zone, and the sample is maintained there for 20 minutes. The effluent from the two impingers is transferred to a beaker and acidified. The residue is transferred to an Erlenmeyer flask, crushed, boiled in dilute nitric acid, and filtered. Both effluent and residue portions are titrated with silver ion according to the modified Volhard method [12] to determine chloride content as previously described.

Data Obtained by the Tube Furnace Method

The glass frit (immersed in dilute caustic) previously used to scrub the effluent gas by the TGA method could not be used with the tube furnace method because it was plugged with oil and carbon. Both cyanide and gas impinger collectors were investigated for collecting the chloride effluent. Drawings of the three types of collectors used are shown in Figure 5.



COLLECTOR TYPES USED TO TRAP EVOLVED HCL

FIGURE 5

Sample 7, the commercially available, rigid PVC sample, along with a similar companion sample (Sample 8), was selected to determine the preferred type of collector to be used under these rapid pyrolysis conditions. Table 3 summarizes the chloride data obtained on Samples 7 and 8. The volatile chloride was collected using a cyanide collector, a gas impinger, or two gas impingers connected in series containing 0.2N sodium hydroxide solution. The total chloride found in the effluent fractions from Samples 7 and 8 was 34.92 and 35.09% respectively, using the cyanide collectors, and 35.07 and 35.32% respectively, using dual gas impinger collectors. From 0.31 to 0.44% chloride was recovered with the second impinger showing that at least two impingers are needed for total recovery. Chloride in the residue from five runs on the No. 7 sample ranged from 0.28 to 0.41%. The chloride ranged from 0.31 to 0.44% in the residue of Sample 8 for four runs. The total chloride (effluent and residue) recovered from pyrolysis of both samples is essentially the same and within experimental error. The cyanide and gas impinger scrubbers are comparable in collection efficiency of chloride.

TABLE 3

COMPARATIVE DATA FOR COLLECTION OF CHLORIDE FROM THE PYROLYSIS EFFLUENT OF COMMERICALLY AVAILABLE COMPOUND SAMPLES OBTAINED WITH TUBE FURNACE

	PERCENT CHLORIDE EFFLUENT				
Sample	1	2	Residue	Total	Type Effluent Collector
7	35.35	–	0.30	35.65	
	34.48	–	0.33	34.81	CN Scrubber
	Avg. 34.92		0.32	35.23	
7	34.31	–	0.28	34.59	1 Gas Impinger
	34.53	0.31	0.41	35.27	2 Gas Impingers
	34.94	0.35	0.35	35.69	2 Gas Impingers
	Avg. 34.74	0.33	0.38	35.48	
8	34.72	–	0.44	35.16	
	35.46	–	0.43	35.85	CN Scrubbers
	Avg. 35.09	–	0.44	35.53	
8	35.12	0.40	0.31	35.83	
	34.68	0.44	0.43	35.55	2 Gas Impingers
	Avg. 34.90	0.42	0.37	35.69	

Table 4 shows data obtained on experimental PVC Samples 4, 5, and 6 using two gas impingers. From two to four analyses were made on each sample. The deviation from theory ranged from 0.02 to 0.67% for the average analyses of these samples. The data also show that the second gas impinger is necessary to recover all of the evolved chloride.

TABLE 4

PVC PYROLYSIS OBTAINED USING A TUBE FURNACE AT 600°C AND COLLECTING THE EFFLUENT GAS WITH TWO GAS IMPINGERS

	PERCENT CHLORIDE EFFLUENT				
Sample	1	2	Residue	Total	Theory
4	22.98	0.38	14.74	38.08	
	22.95	0.38	14.20	37.53	
	Avg. 22.96	0.38	14.47	37.81	37.83
5	23.7	0.53	13.35	37.58	
	24.1	0.33	12.92	37.35	
	24.19	0.41	12.25	36.85	
	23.1	0.45	13.31	36.84	
	Avg. 23.78	0.43	12.96	37.16	37.83
6	22.78	0.49	14.66	37.93	
	23.08	0.30	14.01	37.39	
	Avg. 22.93	0.40	14.35	37.68	37.37

Comparative Pyrolysis Data Obtained by TGA and Tube Furnace Methods

Three experimental PVC compounds (Samples, 4, 5, and 6) were pyrolyzed by the TGA and tube furnace methods. Comparative data for chloride found in the effluent and residue fractions are shown in Table 5. Also included is the total

chloride obtained by each method and the theoretical value for each sample. The deviation from theory for total chloride ranged from 0.02 to 0.67% and 0.25 to 0.97% by the tube furnace and TGA methods, respectively. The chloride was 1.55 and 4.89% higher in the effluent fraction and 1.51 to 3.25% lower in the residue fraction by the TGA method as compared to the tube furnace method. The temperature of both furnaces was 600°C ± 10°C as determined using a potentiometer. The higher percentage of chloride in the pyrolysis residue from the tube furnace method is probably related to the rapid pyrolysis with this method. Surface contact of the evolved chloride with the chloride scavenger could increase due to rapid swelling of the sample when inserted into the hot furnace.

TABLE 5

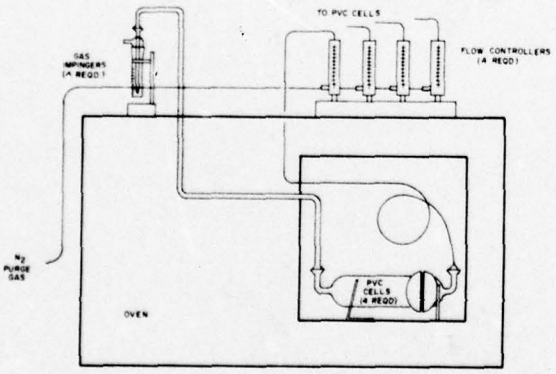
COMPARATIVE PYROLYSIS DATA
FOR EXPERIMENTAL PVC COMPOUND SAMPLES
FOR TUBE FURNACE AND TGA METHODS

	PERCENT CHLORIDE						
	EFFLUENT		RESIDUE		TOTAL		
Sample	Tube	TGA	Tube	TGA	Tube	TGA	Theory
4	23.34	24.95	14.47	12.55	37.81	37.50	37.83
5	24.21	29.1	12.96	9.71	37.16	38.80	37.83
6	23.33	24.88	14.35	12.84	37.68	37.72	37.97

Oven Method for Low Temperature Pyrolysis (HCl Evolution)

1. Apparatus

A laboratory oven (Precision Scientific, Cat. No. 1077), was equipped with a temperature controller capable of maintaining ±0.5° at 90, 105, and 130°C. Four cells, each 15 cm long x 40 mm ID were fabricated from both members of a No. 40 glass joint. Each cell was sealed with O-rings and U-clamps. Four flow controllers controlled the nitrogen purge gas at 100 ml/min through each cell. Glass lines connected the cells to four gas impinger scrubbers, one of which was connected to each cell. A drawing of the apparatus is shown in Figure 6.



OVEN ASSEMPLY FOR EVOLUTION OF LOW LEVEL CHLORIDE ION FROM EXPERIMENTAL PVC COMPOUND SAMPLES

FIGURE 6

2. Measurement Procedure

About 50 g of sample are accurately weighed, placed in a cell, and sealed. In order for samples to be directly compared, they must have comparable surface areas. The all glass lines and cells are connected and placed in the oven, the nitrogen sweep gas is turned on, and the oven is equilibrated at the desired temperature. Dilute sodium hydroxide solution (≈0.01N) is added to the gas impingers and then connected to the cells. The impingers are removed and replaced with fresh scrubber solution at 24-hour intervals, until three samples have been collected from each PVC sample. The process is repeated until each temperature of interest has been examined. The scrubber solutions are analyzed with an AutoAnalyzer system using a chloride specific ion electrode as the detector.

Data Obtained by Low Temperature Oven Methods

Four samples of compounded PVC were tested with the oven apparatus. Thirty-six fractions were collected, three for each sample at 90, 105, and 130°C. Table 6 contains the data for the four samples tested.

TABLE 6

CHLORIDE ION EVOLVED FROM THREE-DAY OVEN TEST
FROM EXPERIMENTAL PVC COMPOUND SAMPLES

	μg Cl⁻ /g SAMPLE/24 HOURS			
	90°C			
Day / Sample	1	2	3	Avg.
A	0.49	0.08	0.08	0.22
B	0.63	0.12	0.12	0.26
C	0.78	0.22	0.22	0.41
D	2.27	1.70	1.31	1.76
	105°C			
Day / Sample	1	2	3	Avg.
A	1.02	1.23	0.94	1.06
B	1.58	1.91	2.02	1.84
C	4.37	3.24	3.67	3.76
D	9.92	9.26	9.24	9.48
	130°C			
Day / Sample	1	2	3	Avg.
A	16.1	23.0	33.7	24.3
B	22.4	35.4	56.4	38.2
C	33.6	40.6	61.3	45.2
D	97.4	95.2	90.8	94.5

In the 90°C test, an average of 0.22, 0.26, 0.41, and 1.76 μg Cl^-/g sample/24 hours was evolved for Samples A, -B, -C, and -D, respectively. The chloride ion decreased with time indicating the elimination of entrapped chloride.

The 105°C test produced an average of 1.06, 1.84, 3.76, and 9.48 μg Cl^-/g sample/24 hours for Samples A, -B, -C, and -D, respectively. No particular trend in chloride ion content over the 3-day test period was found.

In the 130°C test, the evolved chloride ion increased significantly over that obtained from the 105°C test and increased for

Samples A, -B, and -C from day 1 to day 3. Sample D showed the reverse trend. An average of 24.3, 38.2, 45.2, and 94.5 μg Cl^-/g sample/24 hours was evolved for Samples A, -B, -C, and -D, respectively. The data are shown in histogram form in Figure 7.

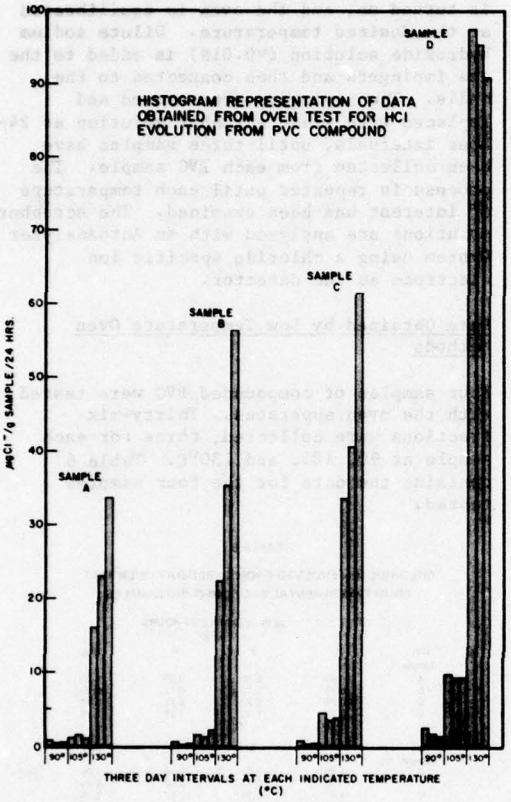


FIGURE 7

Summary

Data presented in this paper demonstrate that various types of PVC compounds can be reproducibly pyrolyzed by either TGA or tube furnace techniques. Data obtained by either TGA or tube furnace methods are comparable. Equipment costs for the two methods are about $20,000 and < $1,000 respectively. Appropriate collectors are described for collecting the evolved chloride. The modified Volhard titration method is used to analyze the effluent and residue fractions for chloride. Recovery of total chloride in both fractions is in all cases comparable to the theoretical chloride present. An oven test method was devised for simultaneous evolution of chloride from multiple PVC compound specimens at varying low temperatures. This test is sensitive and reproducable. It allows for the analysis for chloride at less than 1 ppm and can be used to simultaneously compare several PVC compound specimens for relative hydrogen-chloride evolution at preselected temperatures.

References

[1] J. J. Comeford and M. Birky, Fire Technology, 6, 85 (1972).

[2] J. E. Hartizle and R. A. Youst, B. F. Goodrich Company, presented in part at the PVC Flamability Minitec meeting of the Society of Plastics Engineer, Saddlebrook, New Jersey, January 1977.

[3] J. W. Wimberley and A. B. Carel, Automated Method for Measuring the Thermal Degradation of Polyvinyl Chloride. To be published.

[4] R. Savoley and R. G. Badger, J. Appl. Polym. Sci., 16, 3265 (1972).

[5] R. L. Hassel, Amer. Lab., 9, 35 (1977).

[6] P. Dunn and B. C. Ennis, J. Appl. Polym. Sci., 14, 355 (1970).

[7] P. Dunn and B. C. Ennis, J. Appl. Polym. Sci., 14, 713 (1970).

[8] V. Zdenek, et al, Plasty Kauc 11, 260 (1974).

[9] E. A. Boettner, et al, J. Appl. Polym. Sci., 13, 377 (1969).

[10] W. D. Woolley, Plastics and Polymers, 40, 203 (1972).

[11] W. D. Woolley, Plastics and Polymers, 41, 280 (1973).

[12] E. H. Swift, et al, Anal. Chem., 22, 306 (1950).



A. B. Carel
Continental Oil Company
P. O. Box 1267
Ponca City, Okahoma 74601

The author is a Senior Research Scientist in the Analytical Research Section of Continental's Research and Development Department. He was graduated from Central State University with a BS degree in 1956 and joined Continental Oil in that year. He has been active in Gas and Preparative Gas Chromatography and is presently primarily concerned with inorganic analysis including Conoco's "CONOSTAN" analysis and with Thermal analysis. He holds 8 patents and has authored 18 published papers.

FLAME RETARDANTS IN PVC

Eugene R. Cox

Continental Oil Company
Ponca City, Oklahoma 74601

ABSTRACT

PVC is an inherently flame retarded polymer by virtue of the halogen in its molecular structure. A useful finished compound is achieved by adding other ingredients such as stabilizers, plasticizers, and the like. These additives are capable of altering PVC combustibility performance.

Rigid PVC has excellent flammability properties and flame retardants are generally not required. The addition of flame retardant additives helps to reestablish combustion properties reduced by the addition of plasticizers which is necessary to achieve flexible PVC compounds. As a result, the PVC industry is a major consumer of fire retardant additives. Judicious choices have to be made employing fire retardant additives that will not only give good flame suppression but also provide low smoke and inhibit toxic gas formation.

Fires have occurred since the beginning of time. Man has learned that it can be both friend and foe. Moderating its adverse characteristics is the task before us. Controlling flammability, smoke, and degradation of products and materials is the key to acceptance and wider use of our products in an ever-demanding environment where safety and life hazard have become paramount issues. Hazards due to fire are complex phenomena and the combined effect of many factors. The major factors causing death or serious incapacity of persons are compiled on Table I.

Studies of full-scale fires in recent years have defined the major source of danger to imperiled personnel as not being the flame but rather the by-products of combustion: toxic gases, oxygen depletion, superheated atmosphere, and the psychological and physiological effects of smoke. Perhaps the most important factor affecting life and property in a building fire is smoke.[1] It can damage property, prevent easy exit of occupants, and cause injury or even death by inhalation. An inverse relationship between flammability and smoke generation is known to exist for most materials, and as Federal regulations begin to stipulate the wider use of flame-retardant materials, smoke generation will become one of the major problems in the area of flammability.

A simplified model for the combustion of polymeric materials can be described as follows (Table II):

1. Ignition. A heat source causes the material temperature to rise until phase and chemical changes occur.

2. Fire Growth. Fuel gases thus generated mix with ambient air in the surrounding environment and support combustion.

3. Burning Intensity. Sustained burning results from the establishment of a balance of the mass flux of fuel gases outward to the diffusion flame and the radiant heat flux from the flame back to the pyrolyzing surface.

4. Generation of Smoke and Toxic Components. Pyrolytic degradation and decomposition of the flammable substrate promote evolution of smoke and toxic gases.

5. Extinction-Suppression. Cessation due to introduction of suppression from an outside source or formation of products that create an atmosphere that will not support combustion.

Since 1965 there has been a general upsurge of interest in fire retardance and fire-retardant polymeric materials. This growth is indicated by the data found in Table III. It appears to be on target, as 1978 data indicate sales of 610 Mlbs.[2] Industry's long-range interests require the achievement of products that are more fire-resistant and yield lower smoke and toxic gas levels when involved in fires.

Some of the unique properties of PVC make it an excellent material for use in today's demanding environment. PVC is an inherently flame-retarded polymer by virtue of the halogen (chlorine) in its molecular structure. By itself, PVC polymer is virtually useless. A useful finished compound is achieved by adding

other ingredients such as stabilizers, plasticizers, and the like. These ingredients are capable of altering PVC combustibility performance. Rigid PVC has excellent flammability properties, and flame retardants are generally not required. On the other hand, addition of flame-retardant additives helps to reestablish combustion properties reduced by the addition of plasticizer which is necessary to achieve flexible PVC compounds. As a result, the PVC industry is a major consumer of fire-retardant additives.

Today I want to overview for you our key considerations when formulating flexible PVC for improved flame retardancy. Additionally, I want to highlight the trend we see toward legislation directed at reducing smoke and toxic combustion gases and how this not only affects PVC but many other polymer systems as well.

This versatile polymer PVC has found extensive application in plumbing pipe, electrical conduit, wire and cable, flooring, furniture, profile, wall coverings, house siding, houseware, phonograph records, and appliances. And, of course, most building wire, with the approval of recognized electrical code authorities, is vinyl-insulated and vinyl-jacketed.

To date, more than 1,500 communities have approved PVC pipe for home construction. More than 50,000 miles of vinyl plumbing pipe have been installed and are giving excellent performance in homes of America. Conservatively, it is estimated that more than 2 billion feet of PVC electrical conduit and more than 50 billion conductor feet of PVC insulated building wire have been installed during the last 20 years. United States' usage of PVC is projected to increase from 2300 thousand metric tons in 1977 to 2500 thousand metric tons in 1978.

Despite an excellent history of product performance and safety, more stringent standards are being demanded for applications where this and other polymers are used. PVC will remain a factor because of a number of desirable combustibility characteristics including low flame spread, relatively high ignition resistance, low fuel load contribution (about 87 percent that of wood), slow burning, lack of flaming drips, and the necessity of high external heat to maintain combustion.

To prevent any misunderstandings, I want to say that my use of the term "flame-retarded," or similar terms, does not mean that PVC will not burn. PVC, like all organic materials, will burn, given a large enough heat source. Because a halogen is part of its molecular structure, PVC maintains a high level of flammability performance. Chlorine constitutes about 57 percent of its molecular structure. Compounds containing chlorine and other halogens are, of course, effective additive type fire retardants for plastics. PVC is just that--a halogen-rich organic material. So, not surprisingly, PVC is used to improve flammability performance of other polymers such as ABS.

Various thermal degradation studies[3,4,5,6] have shown that PVC decomposes in a number of steps into carbon monoxide, carbon dioxide, and hydrogen chloride as the major combustion gases and minor amounts of a complex mixture of aliphatic, olefinic, and aromatic hydrocarbons, primarily benzene, toluene, ethylene, and naphthalene. A quantitative breakdown reveals that at the decomposition temperatures studied (280°C-600°C), approximately 57 percent of the PVC is degraded to hydrogen chloride, 38 percent to various low- and high-molecular-weight hydrocarbons, and 4 percent to a carbonaceous ash. The presence of the non-combustible gas, hydrogen chloride, and the relatively low yield of organic degradation products provides a reasonable explanation for the low flammability level of rigid PVC and its high oxygen index (the minimum percentage of oxygen required to maintain a standard burning rate).

Fire retardancy, whether inherent or by additive chemicals, can have undesirable effects, notably increased smoke due to incomplete combustion and production of irritating or toxic combustion gases. Fire researchers are concerned that smoke and toxic gases inhibit the ability of occupants to escape a fire. Thus the emphasis on flame-retardant additives must include smoke reduction and reduced production of toxic gases, along with lower flame propagation.

Some have criticized PVC for toxic gas production during combustion.[7] It is our strong belief that other polymer systems can expect the same type of criticism as increased amounts of smoke and gases are produced as a trade-off for improved flame retardancy. It should be understood that most combustion products from the burning of any organic material are toxic. The combustion products from PVC are no exception. A major combustion gas of PVC is CO; another is hydrogen chloride, HCl, which, unlike the combustion products from many other organic materials, is easily detectable by odor. It is the evolution of this acid gas that inhibits the burning reaction in PVC.

Flammability and smoke problems are introduced when compounding PVC. Compounding additives, notably plasticizers, are used to make flexible PVC compounds for wire and cable insulation, upholstery, and wall covering. Plasticizers are combustible and alter the combustibility performance of PVC. Ignition resistance is lowered and flame spread increased by these modifiers. Addition of flame-retardant additives helps to reestablish combustion properties altered by compounding. Factors to be considered when designing a compound with improved flame retardance are cost and the

maintenance of physical properties of the polymer system. Most PVC compounds have found a position in the marketplace due to their cost effectiveness. Expensive and extensive modification would force them into an uneconomical market position. The key in selecting a flame-retardant system is not only its effectiveness at low cost but also finding one with a minimum effect upon processing, physical properties, and aging.

How do flame retardants or other additives affect these properties? Processing problems can occur through changes in flow so the finished product is not formed properly during extrusion, molding, or other fabrication. Physical property problems can include reduced resistance to heat-distortion or deformation, loss of tensile, modulus or tear strengths, lowered elongation, reduced flexibility, clarity, gloss, and oil resistance. The normal useful life of a product can be reduced considerably by the loss of certain strength characteristics. Volatilization of the additive, for instance, may cause unacceptable appearance and less flexibility. In the markets we serve, any significant change in the inherent properties of the products usually cannot be tolerated. Thus we must be careful in selecting the proper flame-retardant system suitable for each compound and its expected use.

About 20 percent of PVC compounds contain flame retardants.[8] Phosphate esters, chlorinated hydrocarbons, antimony oxide, and boron compounds are the major products used in PVC. These materials in 1976 totaled 50 million pounds valued at 40 million dollars, accounting for approximately 33 percent of the volume by weight and 28.5 percent by dollar volume of the total flame-retardant chemicals used in plastics. The growth rate for flame retardants in PVC compound should outstrip the projected growth of PVC as more demands are made for flame-retarded polymer systems. As more regulations directed at reducing smoke and toxic gas emissions are promulgated, it is a certainty that these changes will be forced upon the industry.

PVC resin may be compounded with stabilizers, pigments, lubricants, fillers, and plasticizers to provide a range of applied products from rigid to flexible, from clear transparent to opaque, and in a complete range of colors. PVC compounds are characterized by excellent resistance to the deteriorating influence of weather, superior electrical properties, and a low order of flammability.

On a weight basis, plasticizer is the most important compounding ingredient used in making flexible PVC compound. For the most common hardness and flexibility requirements, plasticizer levels used normally are in the range of 40 to 100 parts by weight per hundred parts PVC resin. The widest used plasticizers are high-boiling esters of dibasic aliphatic and aromatic acids, and most are flammable. Common primary plasticizers have a flash point of from around 200°C-315°C and are thus combustible. Listed on Table IV are flash points of typical PVC plasticizers.

The burning characteristics of plasticized PVC vary according to the type and amount of plasticizer and other combustible materials in the formulation. Once the plasticizer ignites, the PVC molecules in contact with the flame front decompose. The decomposition products are present in the smoke and char.

Our problem is to flame retard the PVC compound, not the PVC resin. In many typical formulations, the amount of PVC resin is less than 50 percent and the main fuel contributor is the plasticizer. Therefore, the combination of a reduced level of chlorine plus the presence of combustible plasticizer makes the compound more susceptible to ignition. A typical nonfire retarded flexible PVC will have an OI of 22-26 percent. At this oxygen index level, plasticized PVC is still less combustible than many other plastics. Use of appropriate flame retardants plus selection of other ingredients based on their combustibility characteristics allows production of flexible PVC compounds with OIs of up to about 35 percent.

The most commonly used flame-retardant additive for PVC is antimony trioxide, because it acts as a synergist with the chlorine contained in the polymer. Typically, as little as 2-5 parts of antimony trioxide per 100 parts of PVC resin give excellent results in compositions containing up to 50 parts of primary plasticizer, such as dioctyl phthalate.

The cost of vinyl formulations is usually calculated on a volume cost basis, since most products are manufactured to meet size rather than weight specifications. The high specific gravity of antimony oxide thus magnifies the cost consideration in compounding. The pigmenting strength of antimony oxide precludes its use in clear formulations, and it adds an additional parameter to color-matching considerations as well.

Some of these disadvantages of antimony oxide have been circumvented through preparation of flame retardants in which antimony oxide is coated on inert carriers, such as silica. One proprietary antimony oxide blend is said to contain 25 percent antimony oxide, to have only 25 percent of the tinting strength of pure antimony oxide, and to have a specific gravity of 3.3 (vs 5.3-5.6 for Sb_2O_3). A second is said to contain 50 percent antimony oxide. On an activity basis they claim to impart equivalent flame retarding at lower antimony levels than pure antimony oxide.

Next to antimony oxide, the most useful inorganic compounds for the flame retardation of PVC are the borates. Crystalline

borohydrates, which retain their water of hydration to 480°F - well above vinyl-processing temperatures - can be used with lower levels of antimony oxide to achieve flame retardancy. Data generated by O'Mara[9] shows that zinc borate, though relatively ineffectual as the sole fire-retarding ingredient, is an effective adjunct in formulations containing antimony oxide. Molybdenum compounds are being actively promoted as flame retardants and smoke suppressants for vinyl compounds, either alone or in combination with antimony oxide. Another metallic oxide offered is stannic oxide hydrate. Several other proprietary metallic additives are on the market or in various levels of development.

With some exceptions "inert" fillers like calcium carbonate, clay, and silica contribute to flame retardancy in vinyl by simply diluting the organic fraction of the compound. Calcium carbonate in some cases absorbs part of the HCl from burning PVC without lowering the oxygen index.

Aluminum trihydrate acts in both the condensed and gas phases of burning PVC to aid in flame retardation. In the condensed phase, it aids in the development of a good residual surface char, and in the gas phase, it acts to dilute and cool the flame by virtue of the released water of hydration.

When clarity is a requirement, one must choose from one of three classes of compatible liquid retardants: the phosphate plasticizers, the chlorinated hydrocarbon extender plasticizers, or any of various plasticizing halogenated organic phosphates.

Phosphorus compounds have long been used as flame retardants, and they are thought to act by directing decomposition toward production of less hydrocarbon fuel and more carbonaceous char. Chlorinated paraffins and aromatics are also used. These normally range from 40 to 70 percent chlorine content and are similar in flammability properties to PVC polymer. They are generally classified as secondary plasticizers since they can migrate to the surface when used at concentrations above about 30 percent of the total plasticizer system. Some adverse color properties may also be encountered when using chlorinated paraffins and aromatics.

Halogenated phosphate esters combine some of the attributes of both the phosphate and chlorinated-hydrocarbon flame retardants. Part for part, they reduce flammability more than straight alkyl or aryl phosphates. They are, however, more expensive, less compatible, and less resistant to the adverse effects of heat and light. They provide the vinyl compounder with a route to flame retardation that requires minimum modification.

Key considerations, when designing a flexible PVC compound for improved flame retardance, include:

Influence of the additive on the cost constraints dictated by the end application.

Ability to achieve required physical and chemical properties.

And, very important, the effect the additive will have on smoke generation and toxic gas emission.

Smoke generation and toxic gas emission are serious concerns. Many, if not most, regulations in existence address ignitability. Flame retardants have mainly been used, therefore, to upgrade materials by making them more difficult to ignite and reducing flame spread. These mechanisms are listed on Table V.

We know that fire-retardant additives generally alter the burning characteristics of a polymer in such a way that the fire-retarded plastic will produce more smoke when burned than its non-fire retarded counterpart. This is because the fire-retardant mechanism inhibits flame, resulting in incomplete combustion. Thus the positive benefits of achieving materials which are difficult to ignite, have reduced flame spread, and are slow burning are threatened by the concern about increased smoke. Modified PVC, typical of many flame-retarded plastics, emits considerable smoke.

There is no panacea for the suppression of smoke during combustion; a trade-off with other properties is always present when reduced smoke is desirable. Commercially available additives include certain bimetallic inorganics, ferrocene, and molybdenum and extended molybdate compounds. These may be incorporated singly or in combination with other compounds to achieve the desired performance.

Incomplete combustion may also lead to increased toxic gas formation. During combustion of any organic material, numerous flammable and nonflammable combustion products may be produced. Howard Emmons writing in Scientific American,[10] reported that analysis revealed the presence of some 175 different organic compounds in the combustion products from wood, the most toxic components being carbon monoxide and acrolein. Complete combustion burns off combustible products, reducing the number and quantity of organic compounds or gases in the fire atmosphere. Incomplete combustion, or smoldering in a "nonflaming" mode, maximizes

organic off-gases. In a fire, both flaming and nonflaming conditions invariably exist simultaneously.

Admittedly, all the questions on the problems of flame and smoke are not answered. Much work remains to be done, as scientifically acceptable test methods to evaluate the hazards from burning materials do not yet exist. Many reputable scientists in industry, government, and academia are working on test methodology.

The fact that few smoke and combustion gas regulations for burning materials exist should not be interpreted to mean that there is not concern. Rather, it is indicative of the difficulty in developing meaningful test procedures. Dr. M. M. Birky of the National Bureau of Standards[11] notes that investigations in combustion toxicity require studies on "methodology for generating the products" as well as "methodology for determining the biological response elicited from exposure to the products."

Approximately fifteen years ago, building code administrators began writing provisions, which said, in effect, that plastics and other building materials are approved only if their combustion products are no more toxic than those of untreated wood burned under similar conditions. For a number of years, apparently, code officials did not actively seek such information. Gradually the situation changed. Officials, having a responsibility to enforce the code, found compliance nearly impossible due to the lack of a scientifically acceptable means of evaluating life safety hazards of burning materials. In an effort to standardize a procedure, the International Conference of Building Officials (ICBO) proposed a bioassay test for cellular plastics used in construction. This created a strong response from industry, government, and academia. The National Bureau of Standards concurred that no suitable method then existed and stepped in to assume the responsibility of developing a standardized test which ultimately could be used for building code regulations. As a result, the "no more toxic than wood" requirement was dropped from the ICBO code. However, the requirement still appears in some other codes, and industry at times still faces a dilemma in how to comply.

NBS is diligently working to develop a combustion toxicity protocol, or test. The intent of the NBS test method will be for screening purposes only to identify unusually toxic materials and not to rank materials. NBS issued a draft protocol late in 1977, and assembled an advisory group from industry and academia to critique, revise, and finalize the method. It can be expected that the Bureau of Standards protocol, when finalized, will be incorporated into building codes. Other groups, such as FAA, are also working on toxicity tests for application in areas other than building codes.

Smoke generation regulations already exist to varying degrees. The three major model performance building codes in the United States, as well as National Fire Protection Association's Fire and Life Safety Code, all set smoke generation limits for interior finish materials based on the ASTM E-84 test. Some individual cities expand that to include plastics in all construction uses. Other tests, including the NBS Smoke Density Chamber and the Ohio State Release Rate Apparatus, are being evaluated by ASTM, and these devices may be referenced in future codes.

Another test, a modification of the Steiner tunnel, is being developed by Underwriters Laboratories and Bell Laboratories to evaluate wire and cable. This test may be used to classify cables for flame spread and smoke for the National Electrical Code.

The Federal Aviation Administration is also active. A few years ago, FAA proposed smoke rules for aircraft cabin materials based on Smoke Density Chamber testing. Last year, FAA backed off on their proposal, not because they do not want it but because they believe that the risks to life safety posed by flame, smoke, and toxic gases in an actual fire are interrelated. It appears that FAA will move towards a standard integrating these three combustion characteristics.

We see a trend, therefore, toward legislation directed at reducing smoke and toxic combustion gases. The current thrust in fire circles appears to be more towards early warning devices (smoke detectors), prevention (low ignition properties), and control (sprinkler systems).

For PVC the technology exists to achieve good flame retardance characteristics in most product applications. Product performance equals or surpasses economically competitive thermoplastics.

The trend within the PVC industry will be an increased effort to produce products with reduced smoke and toxic combustion gases without seriously affecting other performance characteristics while maintaining competitive economics in the process.

BIBLIOGRAPHY

1. Task Group of Subcommittee IV of ASTM E-5, "The Control of Smoke in Building Fires - A State-of-the-Art Review," Materials Research and Standards, Vol 11, No. 4, April 1977, pp 16-23, 42.

2. Avon, "Plastics Market in 1978 Is Growing but More Slowly," Plastics Engineering, June 1978, pp 33-35.

3. Zapp, J. A., "Fires, Toxicity and Plastics," Physiological and Toxicological Aspects of Combustion Products: International Symposium, March 1974, pp 58-74.

4. Brandt, B., and F. L. Mohler, J. Res. Natl. Bur. Stds., 55, 323 (1955).

5. Strombers, R. R.; S. Straus; and B. Achhammer, J. Polymer Sci., 35, 355 (1959).

6. Noffz, D.; W. Bery; and W. Pfab, Z. Anal. Chem., 235, 21 (1968).

7. O'Mara, M. M., J. Polymer Sci., A-1, 8, 1887 (1970).

8. Kidder, R. C., "Additives for Plastics-Flame Retardancy," Plastics Engineering, February 1977, pp 38-42.

9. O'Mara, M. M.,; W. Ward; D. P. Knechtges; and R. J. Myer, "Fire Retardation of Polyvinyl Chloride and Related Polymers," Flame Retardancy of Polymeric Materials, ed. Marcel Dekker, Inc., 1973, pp 195-272.

10. Emmons, H. W., "Fire and Fire Protection," Scientific American, Vol 231, July 1974, pp 21-27.

11. Punderson, J. O., "Toxicity and Fire Safety of Wire Insulation: A State-of-the-Art Review," Wire Technology, 9/10:77, pp 64-72.

TABLE I

Major Factors Causing Death in a Fire

1. Direct consumption by fire
2. High temperatures
3. Oxygen depletion
4. Presence of carbon monoxide
5. Presence of toxic gases
6. Presence of smoke
7. Development of fear, shock, and panic
8. Secondary fire effects (trauma, fracture)

TABLE II

Components of the Flammability of Plastics

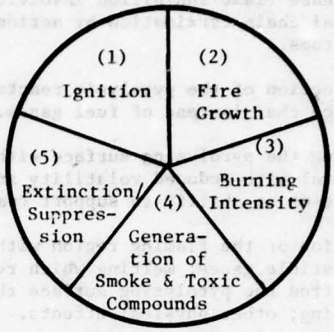


TABLE III

Consumption of Flame Retardants by Plastic Industry

	M Lbs	M Dollars
1965	94	45
1970	200	100
1975*	280	198
1980*	800	640

*Projections from Plastics World Research Department, July 21, 1975, Plastics World.

TABLE IV

Flash Points of Some Common Plasticizers for PVC

Plasticizer	Flash Point °F (COC)
Di-(2 ethyl hexyl) phthalate (DOP)	420
Di-isodecyl phthalate (DIDP)	450
Di-tridecyl phthalate (DTDP)	455
Di-isooctyl phthlate (DIOP)	420
Normal-octyl,-decyl phthalate (NODP)	430
Di-butyl phthalate (DBP)	340
Di-octyl adipate (DOA)	390
Di-isodecyl adipate (DIDA)	425
Di-isooctyl adipate (DIOA)	390
Di-octyl sebacate (DOZ)	450
Tri-octyl trimellitate (TOTM)	490
Epoxidized soya oil (ESO)	600
Octyl epoxy tallate (OET)	450

TABLE V

Mechanisms for Flame Retardation

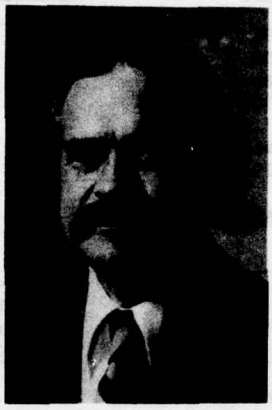
1. Gas phase flame inhibition involving fire-radical chain termination by action of halogen atoms.

2. Redirection of the pyrolysis reactors to produce char instead of fuel gases.

3. Coating the pyrolyzing surface with residual material with reduced volatility and with little or no ability to support combustion.

4. Dilution of the flaming region with non-combustible gases; melting which removes heat from the pyrolyzing surface through dripping; other physical effects.

5. Removal of heat from the pyrolyzing surface by endothermic decomposition or dehydration of additives.



Eugene R. Cox

Continental Oil Co.

Research and Development Dept.

P. O. Box 1267

Ponca City, OK 74601

Mr. Cox is a Senior Development Engineer in the Plastics Applications Section of Conoco Chemicals Research and Development Department. He received his education at Louisiana State and Oklahoma State Universities. He is a member of ASTM E-5 and SPI's Coordinating Committee on Consumer Safety and has been a member of PPI's Fire Test Committee.

THE EFFECT OF SILANE COUPLING AGENTS ON FILLED PVC JACKETING FORMULATION PROPERTIES

by

J.L. Rodriguez and J. Cobo

CABLES DE COMUNICACIONES S.A.
ZARAGOZA - SPAIN

ABSTRACT

One economic procedure which is followed in order to improve flame retardant properties on vinyl compounds is increasing the amount of fillers such as calcium carbonate and aluminum hydroxide. Since these larger quantities of filler are detrimental, to some extent, to the physical characteristics of the compound, we have explored the possibilities of adding silane coupling agents. In this study we present the various results which the addition of these agents have on the mechanical properties, accelerated aging, and melt flow of non-rigid PVC jacketing compound formulations with a high proportion of fillers.

INTRODUCTION

In recent years we have seen an increased emphasis on studies towards optimizing the addition of inorganic fillers in PVC formulations for the cable industry in order to meet new fire regulations among other reasons. These new formulations must also be economically feasible. Thus the addition of calcium carbonate (to absorbe the acid gases released in the pyrolysis or combustion) and the aluminum hydroxide (to raise the value of the oxygen index limit), are becoming common practice in proportions which reach up to 100 parts per hundred of resin (p.h.r.).

However the addition of high amounts of inorganic fillers to a polymeric system such as in the case of non-rigid PVC compounds does demand a readjustment of its components in order to avoid deterioration of the properties in the compound obtained; plus a knowledge of the filling characteristics and techniques in the preparation of the compound (for example by means of adding the various components, in a pre-arranged sequence to the industrial mixer).

The component readjustment can be carried out by:

1. varying the resin/plasticizer relationship
2. using a new polymer in the mixture as an additional plasticizer or as an "alloy"
3. altering the particle surface of the filler and/or polymer at the interphase, for example, by means of coupling agents or by
4. a combination of all three.

This paper shows the tests which have been carried out on the possibilities of using silane coupling

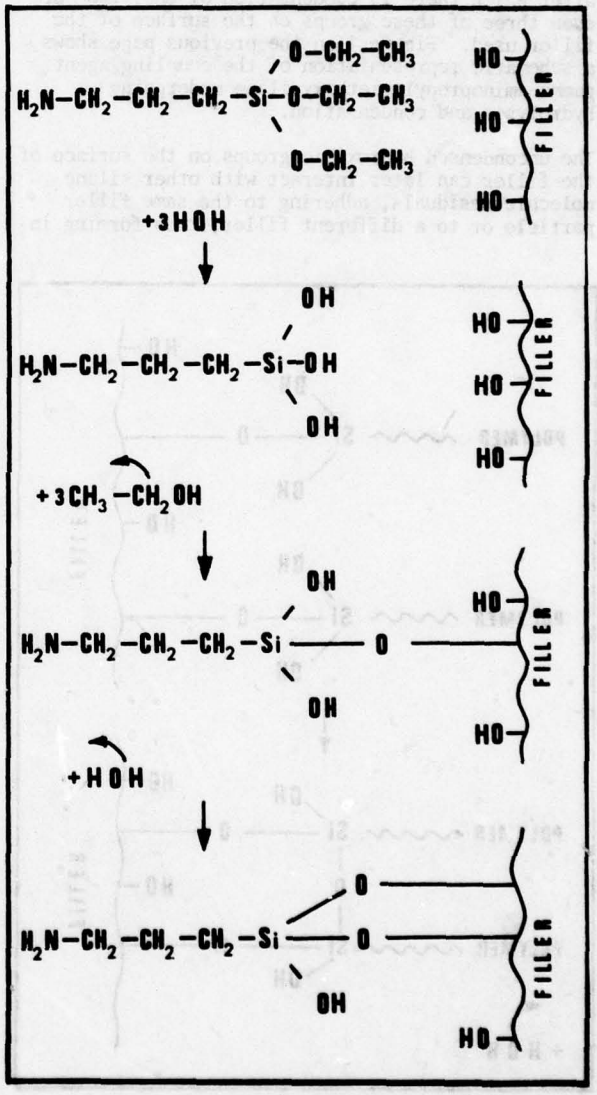


Figure 1

Hydrolysis of the silane coupling agent and bonding to the filler surface

agents for highly filled PVC formulations and the results which have been obtained. The use of calcium carbonate (conventional particles ≈ 5 μ) is an additional incentive due to its availability in the Spanish market.

MECHANISM OF COUPLING FILLER TO POLYMER BY MEANS OF SILANE AGENTS

Silane coupling agents present a dual function on which its bonding capacity between the polymeric phase and inorganic fillers is based. In accordance with scientific literature, one can interpret the coupling mechanism by means of hydrolysis of the silane alkoxy groups to form hydroxilic groups, after which there is condensation of one, two or even three of these groups on the surface of the filler used. Figure 1 on the previous page shows a schematic representation of the coupling agent gamma-aminopropyltriethoxysilane undergoing hydrolysis and condensation.

The uncondensed hydroxilic groups on the surface of the filler can later interact with other silane molecule residuals, adhering to the same filler particle or to a different filler, thus forming in this way a bond between 2 silicon atoms through the oxygen atom (the same as with silicones). This later reaction takes place under elevated temperatures which results in a cross-linking of the polymer (see figure 2).

If an overdose of silane agent is added to that required to form a monomolecular layer around the filler, or in the absence of this filler, an after cross-linking between polymeric chains is produced with no intervention of adhered silane groups to the filler (see figure 3).

The bond between the aminopropylic radical of the silane molecule and the polymer chains takes place by adding amino groups to conjugated unsaturation formed by dehydrochlorination when PVC decomposes at molding temperature range.

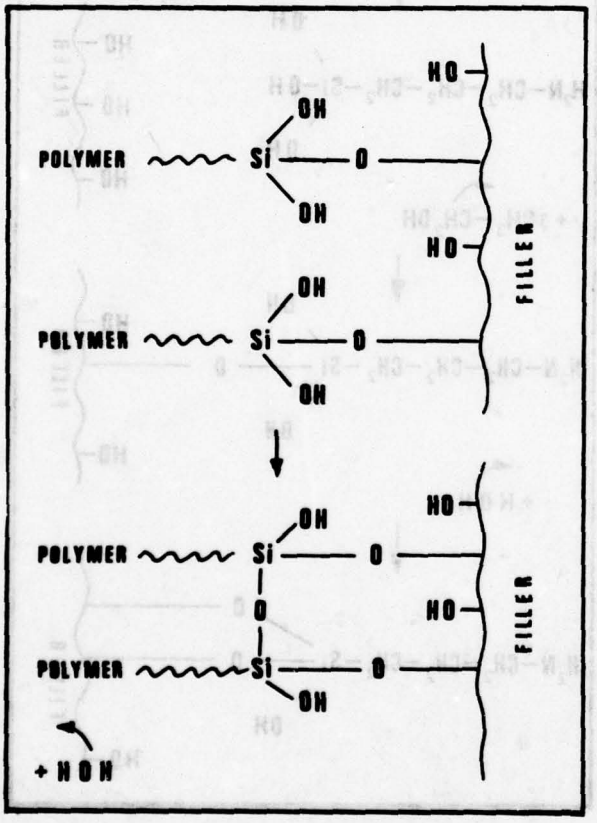


Figure 2
Mechanism of the polymer crosslink through the coupling agent bonded to the filler

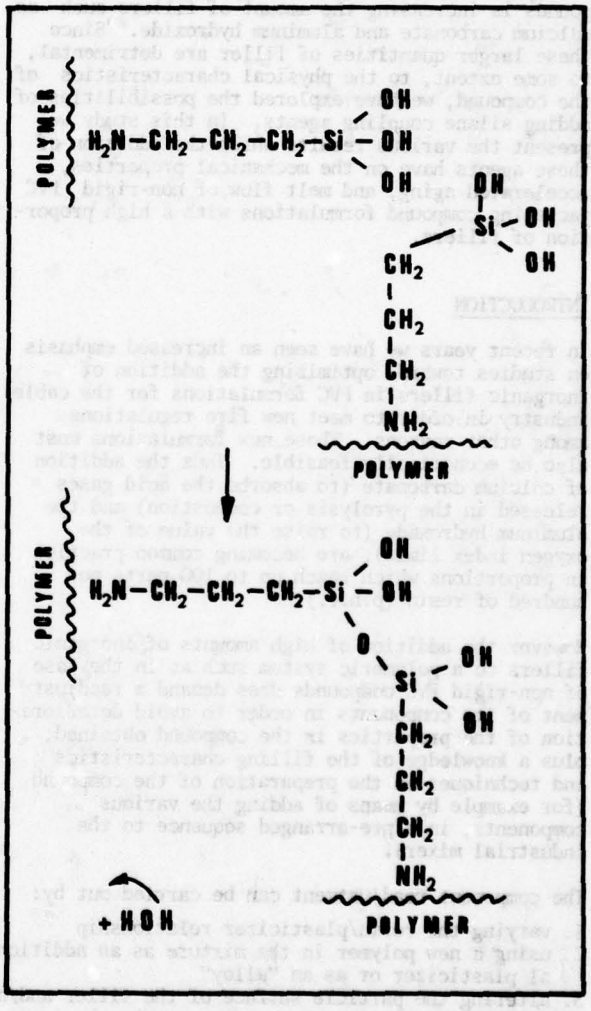


Figure 3
Polymer crosslink through the coupling agent not bonded to the filler

COMPOUND FORMULATIONS AND TESTING METHODS

Our aim, as previously mentioned, is to study the influence of silane coupling agents on properties such as thermal aging, processability, oxygen index limit, acid gas absortion, and volume resistivity, when these agents are incorporated as bonding in PVC formulations with a high percent of mineral fillers. A non-filled formulation has been used as a control as well as the corresponding ones filled without a coupling agent. The silane coupling agent used in all cases has been gamma-aminopropyltriethoxysilane, (Silane A-1100, by Union Carbide Corp.) at a set proportion of 1.7 parts per 100 of filler. Tables 1 and 2 show us the formulations used.

TABLE 1

BASIC FORMULATION

PVC Resin (Suspension process, K value 67)		100
Stabilizer (87% Tribasic lead sulfate)		5
Plasticizers:	DOP (DI-ISO OCTYL PHTHALATE, DIELECTRIC)	As specified in table 2
	CHLORINATED PARAFFIN (52% Cl)	Id.
Antimony Oxide		5
Fillers:	Calcium carbonate (Medium particle size 5μ)	As specified in table 2
	Hydrated alumina (medium particle size 6 μ)	Id.
Lubricants:	Polyethylene waxes	0.8
	Glycerol esters	0.2
Silane Coupling agent		As specified in table 2

TABLE 2

VARIABLE COMPONENTS

FORMULATION No.	DOP	CHLORINATED PARAFFIN	CO_3 Ca	$Al(OH)_3$	COUPLING AGENT
1	35	10	-	-	-
2	35	10	60	-	-
3	35	10	60	-	1.7 p.h.f. (Method 1)*
4	35	10	120	-	-
5	35	10	120**	-	-
6	35	10	120	-	1.7 p.h.f. (Method 1)
7	35	10	120	-	1.7 p.h.f. (Method 2)
8	35	10	-	60	-
9	35	10	-	60	1.7 p.h.f. (Method 1)
10	35	10	-	120	-
11	35	10	-	120	1.7 p.h.f. (Method 1)
12	35	10	-	120	1.7 p.h.f. (Method 2)
13	35	10	120	40	-
14	35	10	120	40	1.7 p.h.f. (Method 2)
15	35	10	120	40	1.7 p.h.f. (Method 3)
16	35	10	120	40	1.7 p.h.f. (Method 1)
17	40	12	120	40	-
18	40	12	120	40	1.7 p.h.f. (Method 2)
19	40	12	120	40	1.7 p.h.f. (Method 3)
20	40	12	120	40	1.7 p.h.f. (Method 1)

* Methods of adding coupling agents are given below

** Coated CO_3Ca

The molded slabs for testing have been prepared by the conventional method consisting of component weighing and shaking (stirring) to obtain a dry mixture. This dry blend is then kneaded by two milling rolls and this obtained plastic sheet is molded for a period of five minutes at 180°C. This method is not used in cases where the formulation contains silane as will later be explained. The temperature of the milling rolls was 155°C for formulations without silane and 125°- 130°C on those with silane.

The influence of a thourough mixing (stirring) has been noted in the preparation of the dry mixture when the incorporation of the filler is studied, but unfortunately we do not have a high speed mixer in our laboratory. However, this work is comparative and the possible influence of hand mixing equipment to obtain proper filler dispersion should equally affect all formulations.

The coupling agent was incorporated in the filler or in the resin prior to component mixing by means of the following alternative steps:

1. The required quantity of silane coupling agent was added to the corresponding proportion of filler, followed by mixing and dispersion, thus obtaining an even distribution. After a period of 2 to 3 hours exposed to air, the filler coated with the coupling agent was then weighed together with the rest of the components. Following this procedure the components were mixed to obtain the dry blend which was then milled and molded.

2. The calculated quantity of silane as determined from the weight of the filler was added to the PVC resin. It was then thoroughly mixed to obtain a complete and uniform distribution. The mixture was then left exposed to air for a period of 18 hours. The object of this procedure was to obtain a partial hydrolysis of the coupling agent (this hydrolysis can also be detected by the slight odor of ethyl alcohol), which allows its easy adhesion to the filler when it is used in dry mixture operations.

3. The third procedure consists of a modification to procedure No.2, in which once the dry blend is prepared it should be held for a period of 3 to 4 hours before milling.

We have not studied other methods,such as adding silane to the plasticizer because it was considered that the two basic procedures described are more representative.

One experimental fact we should be aware of is that silane residues adhere to aluminum surfaces. For this reason in the preparation of molded slabs with formulations containing silane it was found necessary to place a polyester sheet between the aluminum sheet and the compound. However no adherence to steel was detected (in the mill or the press mold). This could possibly be due to a hydrocarbon layer formed on the steel surface from its continuous use.

Table 3 indicates the testing methods used to determine the properties measured.

TABLE 3

TEST METHODS

- Tensile strength and elongation

  ASTM D-412; Specimen Die C and jaw separation speed of 500 mm./min.

- Accelerated Aging

  Forced circulating air oven; 100°C, 120 hours

- Density

  ASTM D-792, Method A

- Tear Resistance

  Internal method similar to ASTM-D-624. Jaw separation speed 200 mm./min. The results are expressed in % to that obtained in formulation No.1, which was used as a control.

- Melt flow

  ASTM D-1238 at 170°C and/or 190°C. Die with 51° entry angle and 2.1 mm. diameter - 10 Kg. load.

- Oxygen index limit

  ASTM D2863; B type specimen (1.92 mm. thickness)

- Acid gas absorption

  Ratio of Cl retained in ash (as soluble chloride) to theoretical Cl, in percentage. The chloride retained in four washing bottles was also tested. Weighed samples are calcinated for 30 minutes at 650°C with circulating air.

- Volume Resistivity (dry)

  ASTM D-257. 500V after 1 minute electrification.

RESULTS AND DISCUSSION

Mechanical characteristics and oven aging

In general, we can see from table 4 on the following page that silane added formulations which contain aluminum hydroxide as a filler behave differently than those with calcium carbonate. Formulations with the latter as a filler have a lesser effect on the mechanical properties. On the other hand, we observed that in all the formulations tested the mechanical characteristics change according to the method used in adding the silane coupling agents to the resin (methods 2 and 3) or to the filler (method 1). The addition of coupling agents in accordance with method 1 results in an improvement in the tensile strength and a decrease in the elongation when compared to the equivalent formulations without silane and also when compared to the formulations in accordance with methods 2 and 3. However these values, regardless of method used, are comparably the same after accelerated aging.

When calcium carbonate is used as a filler, the addition of silane in moderate amounts (determined by the percentage of filler used) generally results in slight changes of the mechanical characteristics. It can be seen that the formulation 3 results in an increment of 9% in tensile strength, 6% in tear resistance, and a slight decrease in elongation when compared to formulation 2 without silane. We can also see that formulation 3 has better aging characteristics than formulation 2.

The formulations with larger amounts of filler (120 p.h.r. of $Ca\ CO_3$) and consequently higher amounts of silane are sensitive to the method used in adding the coupling agent. A mixed blend per method 1 (formulation 6) shows an increase of 32% in tensile strength and 24% in tear resistance with a loss in elongation. Accelerated aged values were better retained by formulation 6 than formulation 4 as can be seen in Table 4. When silane is added to the resin (formulation 7), the increase in tensile strength is 14%, and 19% in tear resistance with little change in elongation when compared to formulation 4. However after accelerated aging there are drastic changes probably because of a cross-linking action taking place when exposed to high

TABLE 4

TEST RESULTS

FORMULATION No.	TENSILE STRENGTH Kg/cm2	ELONGATION %	PERMANENT ELONGATION %	AGED TENSILE STRENGTH Kg/cm2 (% O.V)	AGED ELONGATION % (% O.V.)	DENSITY g/c.c.	TEAR RESISTANCE % per 1	MELT FLOW g/10 min. at 170°C	OXYGEN INDEX LIMIT	VOLUME RESISTIVITY Ω cm.
1	185	330	85	166 (90)	276 (84)	1.326	100	3.979	30.3	7.10^{13}
CALCIUM CARBONATE AS FILLER										
2	136	260	50	122 (90)	162 (62)	1.51	85	2.600	30.3	$1.4.10^{14}$
3	148	245	48	136 (92)	170 (70)	1.51	90	0.148	30.8	$8.0.10^{13}$
4	106	211	34	89 (84)	112 (53)	1,69	66	1.776	30.4	$1.9.10^{14}$
5	109	220	36	90.5 (83)	121 (55)	1.69	68	1.809	29.0	
6	140	121	15	127 (91)	76 (63)	1.69	82	3.200*	32.4	$6.8.10^{13}$
7	121	203	34	124(102)	81 (40)	1.69	79	3.658*	33.0	
HYDRATED ALUMINA AS FILLER										
8	133	253	50	128 (96)	150 (59)	1.49	84.4	1.347	34.6	$1.8.10^{14}$
9	188	120	15	186 (99)	84 (70)	1.49	92	3.778*	34.7	$9.2.10^{13}$
10	120	178	43	91 (76)	122 (69)	1.657	73.2	0.778	41.4	$3.2.10^{14}$
11	190	58	9	185 (97)	35 (60)	1.636	91	0.178	41.3	$8.0.10^{13}$
12	150	88	13	179 (120)	38 (43)	1.64	89	3.015*	41.5	$8.2.10^{13}$
MIXTURE OF CALCIUM CARBONATE AND HYDRATED ALUMINA										
13	94	187	28	76 (81)	88 (47)	1.75	50.4	0.699	33.2	$1.3.10^{14}$
14	119	108	12			1.755	73.7	3.781*	33.3	
15	119	106	11	153 (128.5)	28 (26.5)		73.9	3.336*	33.4	$9.8.10^{13}$
16	161	47	7	141 (87.5)	31 (66)	1.75	85	1.027*	33.4	$6.0.10^{13}$
MIXTURE OF CALCIUM CARBONATE AND HYDRATED ALUMINA WITH AN INCREASE IN PLASTICIZER (40/12)										
17	85	202	30	68 (80)	102 (55)	1.74	46.2	1.885	32.0	$7.6.10^{13}$
18	104	120	14			1.735	66.7	4.497*	32.1	$4.2.10^{13}$
19	109	109	11	142 (130)	30 (27.5)		70.7		32.1	$4.2.10^{13}$
20	153	40	5	155 (101)	33 (82)	1.74	75.3	2.4605*	32.5	$2.5.10^{13}$

* Tested at 190°C because values at 170°C were too low

temperatures. Therefore it was observed that there were less differences in tensile strength and elongation values between formulations 6 and 7 after aging.

Formulations which contain aluminum hydroxide are also sensitive to the method used. Actually, addition of coupling agents increases tensile strength and tear resistance values to a greater degree than those with calcium carbonate. On the other hand there is a substantial loss in elongation which is more pronounced with increments of silane (brought about by increases in percent of filler). An interesting result is that tensile strength (before and after aging) is practically the same in the formulations 9 and 11 containing silane, while the elongation values under the same circumstances is approximately half with formulation 11. After aging the tensile strength and elongation values are very similar on formulations with coupling agent added either in the filler or in the resin. Moreover the tensile strength value, after aging, is approximately equal (in both of the above cases) to the value obtained from the formulation without fillers and used as a control. These facts suggest that a more consistent linking between the filler and the polymer takes place through the coupling agent than the link obtained when calcium carbonate is used. Tear resistance is also practically the same in the formulations with silane added to the filler and have 60 and 120 p.h.r. of $Al(OH)_3$. In comparison to their equivalent formulations without coupling agents we observe an increase of 9 and 24% respectively.

Formulations with a mixture of calcium carbonate and aluminum hydroxide gave values lower than those with aluminum hydroxide only but higher than those with calcium carbonate as the only filler. It was also observed that tensile strength (before and after accelerated aging) in the group of formulations with mixed fillers had a value higher than any of the group containing only calcium carbonate as filler, nonwithstanding that formulation 20 had a greater amount of plasticizer. Regarding tear resistance we can see a wide spread in readings with the best performance obtained from formulation 16. This value falls between the ones obtained from formulations 7 and 12 which respectively have calcium carbonate and aluminum hydroxide as fillers.

Values of tensile strength and elongation after accelerated aging tend to approach each other regardless of whether the coupling agent was added to the resin or to the filler. In the case of adding silane to the filler (low original elongation), satisfactory values are retained after aging.

Processability

The basic operations for the compounding of PVC are a) the dry blend mix in order to get a uniform distribution of the various components, and b) extrusion to either pelletize or to apply directly on the cable as a jacket.

The addition of coupling agents improves the dry blend mixing process because the layer which is formed over the particles of filler and/or resin prevents the formation of component conglomorates.

Our studies show that adding silane affects unfavorably the melt flow level, a characteristic which to some extent measures extrusion performance. At a temperature of 170°C its value drops abruptly on all the formulations tested. However, at 190°C the melt flow is comparable to that obtained from a control formulation without fillers (tested at 170°C). This presumes that formulation with silane may have to be extruded at temperatures 15 to 20°C higher than normal compounds.

Dielectric characteristic

On formulations containing silane, we have obtained volume resistivity values which are slightly lower than those corresponding formulations which do not contain coupling agents. This could be due to the presence of ethyl alcohol produced by hydrolysis during a melting process. Nonetheless, we do not think this slight variation will affect its use as a compound formulation.

We have not attempted to measure dielectric constant on these formulations since our studies are on jacket compounds. However we do not expect a substantial change in this characteristic which may prevent its use as an insulation material.

Flame retardant properties

The oxygen index limit has been taken as the criteria to determine flame retardant properties of all our formulations tested. On those with a large amount of calcium carbonate (formulations 6 and 7), the addition of this silane coupling agent raise this index 2 to 2.5 units compared to formulation 4 without the coupling agent. However on formulations which contain aluminum hydroxide the index value does not seem to be affected by the addition of coupling agents. It may be because the values obtained are already of considerable magnitude. In the formulations with mixed fillers the increase of the oxygen index limit due to the addition of coupling agents is negligible. It should be noted that formulations with uncoated calcium carbonate maintain the same index level as that of formulation 1 which is used as control.

Regarding the release of gases, the addition of silane coupling agents does not seem to have an appreciable effect. Values obtained by the absorption of chlorhydic acid were equivalent to those obtained on formulations without the coupling agent.

CONCLUSIONS

The addition of silane coupling agents in non-rigid PVC formulations, which have a high percentage of fillers, greatly affect their mechanical properties. Substantial improvements are found in tensile strength and tear resistance especially when aluminum hydroxide is used as a filler. However the compound flexibility is negatively affected, except

when the formulations are moderately filled with calcium carbonate.

Good mechanical properties are retained after oven aging on those formulations for which coupling and cross-linking have taken place prior/or during the milling process. On the other hand a detrimental effect is observed on those materials whose cross-linking takes place at a later time.

Consequently in order to obtain a good coupling, the best mixing method is adding the coupling agent to the filler prior to the preparation of the dry blend.

Other characteristics affected to a lesser degree are the oxygen index limit which increases to 2.5 units on formulations with 120 parts of calcium carbonate, and the slight decrease of volume resistivity. Regarding compound processability the addition of coupling agents improves in great measure the dry blend operation but may require higher extrusion temperature than conventional compounds.

In summary, the addition of coupling agents has been found very useful in correcting the detrimental effect which large amount of inorganic fillers have on non-rigid PVC formulations. However these same agents have an unfavorable effect on the compound flexibility depending on the amount used. Therefore it may be necessary to use concentrations of silane lower than those used on this study. Another possible solution could be the use of an "alloy" polymer to obtain additional flexibility without affecting flame retardant characteristics. In any event, the formulation to be used may be chosen considering the characteristics required from the compound and the cost of the raw material.

ACKNOWLEDGEMENTS

The authors wish to thank the personnel who have helped in this study especially to Messrs. Molleda and Gómez Madrazo of C.I.E.-C.T.N.E. for their help in determining the oxygen index limit, to Messrs. Alibert and Sisó of Saenger S.A. and Messrs. Esqués, Diaz and Pérez of C.C.S.A. for their laboratory help.

We also wish to express our thanks to Messrs. F. Horn and J. Avalos for their valuable suggestions and to Mrs. Maria P.Mendoza for her patience and understanding in typing this document.

REFERENCES

1. Sterman, S; Marsden, J.G.; "Theory of Mechanisms of silane coupling Agents in glass reinforced - and filled thermoplastic and thermosetting resin systems" - Published by Union Carbide Corporation.

2. Monte, S.J.; Sugerman, G.; Sharpe, P.D.,"ORGANO TITANATE COUPLING AGENTS FOR FILLED POLYMERS" 24th I.W.C.S. Proceedings, 1975. Pages 300-324

3. Falter, J.A.; Warren, P.E. - "Filled Vinyl Jacket compounds" - 25th I.W.C.S. Proceedings 1976. Pages 356-361.

4. Roesler, F.; M.C. Broom, J. - "Polymer Alloys for Flexible Cable Jacketing" - 24th I.W.C.S. Proceedings, 1975 - Pages 335-339.

5. Brown, M. - "Thermoplastic Polyester Copolymers and their blends with vinyls for molded and extruded Electrical Applications" - 24th I.W.C.S. Proceedings, 1975 - Pages 292-299.

6. Nota Editorial - Perspectivas de las cargas" Rev. Plásticos Modernos, 31 - Pages 395-398 March 1976.

7. Plueddman, E.P.; Stark, G.L. - "Agentes de Acoplamiento para modificar cargas", Rev. Plasticos Modernos, 34 - Pages 710-715, November 1977.

8. Plueddman, E.P.; Stark, G.L. - "Aspectos reológicos de cargas - agentes de acoplamiento" Rev. Plásticos Modernos, 35 - Pages 93-98, January 1978.



Jose Luis Rodriguez, graduated in Chemistry Sciences in 1968. After 4 years as Assistant Professor in the Faculty of Sciences of Zaragoza, he joined Cables de Comunicaciones in 1973 and was an active member in the start-up of the Investigation Laboratory. His present responsibilities cover plastic raw materials and dielectrics.



Julio Cobo graduated in 1969 from Escuela Universitaria de Ingenieria Tecnica Industrial de Santander with a degree of Ingeniero Tecnico Quimico. He joined C.C.S.A. located at Zaragoza, Spain in 1972 and is now in charge of the Physics-Chemistry Laboratory of the Research and Development Department.

CABLE DESIGN AND MATERIALS FOR HIGH RELIABILITY, SEVERE DUTY AND CIRCUIT INTEGRITY

B. C. Milliken

MiliBride, Inc.
Williston, Vermont

R. S. Armstrong

General Electric Co.
Schenectady, New York

Abstract

Creative cable engineering and newer high performance materials have reduced to practice cable designs with improved thermal capability and extended circuit integrity to meet the most critical application, environmental and safety demands. High temperature, industrial heating cables, elevator control and interlock cables, appliance wire, thermocouple lead wires, and specialty power and control cables developed mark new advances in the state of the art for high reliability cable design. Combinations of micaceous tapes and space age polymeric materials have enabled the cable designer to incorporate radiation, steam, and chemical resistance and flame retardancy into cable construction. Performance exhibited suggests further possibilities for other severe duty demands imposed by nuclear power and control, fire alarm, aircraft, high voltage electronic power, oil well logging, mass transit and other applications.

Introduction

Cable designs that offer improved thermal capability and extended circuit integrity have been developed through creative cable engineering and incorporation of new high performance materials. Cables now on the market offer the specifier and end user a wide choice of performance characteristics and designs that satisfy specific requirements of Underwriter Laboratories, Canadian Standards Association, National Electrical Manufacturers Association and the City of New York's Department of Public Works.

Unique constructions, materials, and performance aspects have brought about new advances in the state of the art for high reliability cable design. These advances are particularly applicable to high temperature industrial heating cables, elevator control and interlock cables, appliance wire, thermocouple lead wires and specialty power and control cables.

Combinations of micaceous tapes, and polymeric materials including silicones, fluorocarbons and polyimides allow radiation, steam and chemical resistance and a high degree of flame retardancy to be designed into cable construction. Designs that exceed the requirements of IEEE 383 indicate that severe duty demands imposed by nuclear power and control, fire alarm, aircraft, high voltage electronic power, oil well logging, mass transit and other applications can be satisfied through incorporation of high performance mica tapes.

Use of mica in cable construction is not particularly new, having been used for a number of years in specialty high temperature applications such as aircraft hook-up wire. However, growing demands for higher temperature wire in general and increasing concern for safety and reliability in more traditional markets have motivated the cable designer to expand the use of micaceous insulation in cable construction. This not only has led to development of superior tapes and new levels of performance, but has opened the way for dramatic functional improvement by combining the micaceous insulation with other high performance materials.

With few exceptions, deployment of mica paper is directly over the bare conductor as depicted in Figure 1.

TYPICAL CABLE CONSTRUCTION

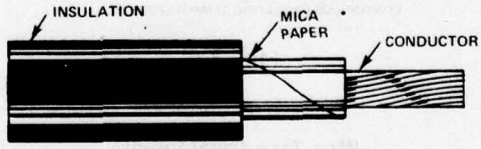


Fig. 1

Figure 2 demonstrates the use of mica paper in a typical multiconductor configuration.

In the event of thermal overload, flame exposure or other catastrophic condition, the conductors remain electrically protected in carrying out their specified mission. Figure 3 illustrates the thermal capability attainable in 600-volt cable with circuit integrity utilizing mica as opposed to traditional and other high temperature materials.

TYPICAL MULTI-CONDUCTOR CABLE CONSTRUCTION

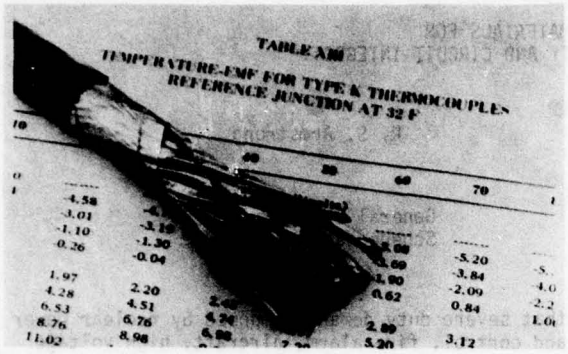


Fig. 2

Areas where mica cable is successfully used include steel mills (furnaces, soaking pits, coke ovens, cranes, safety and emergency equipment), continuous casting plants (machinery exposed to highly corrosive hydraulic fluids), chemical plants, electric generating stations, and for high temperature plastic processing equipment.

TEMPERATURE CAPABILITY COMPARISON OF CABLE MATERIALS

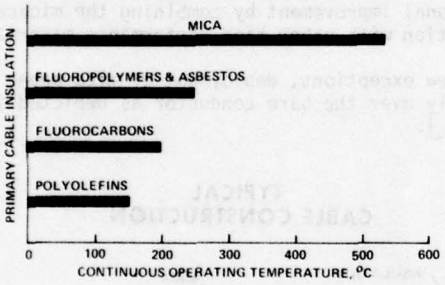


Fig. 3

Mica Tape Development

Designers of electrical equipment have recognized the high temperature, high dielectric, non-burning, non-toxic value of mica for decades, hence it was logical that they should utilize it in cable applications. The challenge was to develop a practical, thin form of insulation that could be easily handled. The result has been tapes that impart a level of circuit integrity beyond that obtainable through the use of any other polymer or tape, organic or inorganic, currently in commercial production.

Reconstituted, fired, muscovite paper of higher than normal density is combined with glass (cloth or unidirectional yarns) reinforcement and bonded with a high performance cured methyl polysiloxane resin.

A composite tape construction is able to withstand severe electrical and thermal overload conditions. The high density mica paper permits tape designs with a minimum binder content (the weakest link thermally and in flame resistance) and designs that electrically retain 60 to 70 percent of original dielectric strength after 1200 to 1500°F exposure. Such constructions are highly resistant to radiation and withstand 10^9 rads at a 10^8 rads per hour dosage rate. They are so highly insensitive to moisture that electrical integrity remains unchanged between one and 24-hour water immersion with over 50% retention of original dielectric strength.

Typical properties of two commercially available mica paper tapes are detailed in Figure 4:

Thickness, inches nominal	0.004	0.005
Construction		
Mica paper thickness, in.	0.0018	0.0018
Reinforcement	glass yarn/ polyester film	glass cloth
Shelf Life, normal storage	> 1 year	> 1 year
Yield, approx. Lb/Yd^2	0.23	0.27
Kg/M^2	0.124	0.146
Tensile Strength, Avg. Lb/In	75	85
Elongation to final break, O/O	< 3	< 3
to mica fracture, O/O	0.4	0.4
Electric Strength, Avg. VPM S.T., R.T., 1/4" Electrodes	1,000	600
Dielectric Constant, 60 Hz, 200°C	< 2	< 3
Flexibility - Helically Tapable (with proper width selection) on AWG wire size [minimum])	28	20

TYPICAL PROPERTIES - MICA PAPER TAPES
Fig. 4

Tapes are specifically designed for application by high speed helical taping or by longitudinal folding at normal extruder wire line speeds. Their inert nature enables them to be combined compatibly with other insulating compounds. Under catastrophic conditions, mica paper tapes emit no known toxic or noxious fumes and meet OSHA standards at extended high temperatures. Typical test performance characteristics of mica paper tapes are shown in Fig. 5:

Insulation Resistance	- Multi layer, Helical warp	- 20 megohms
	- Multi layer, Helical warp, exposed to propane flame - at 1200°F, 15 min.	- 2 megohms
Moisture Resistance	- Electric strength after water immersion for 1 hr.	- 50% of original
	24 hrs.	- Unchanged
Radiation Resistance (Gamma)	- Withstands	- 10^9 Rads
	Dosage Rate	- 10^8 Rads/Hr.
Dissipation Factor	- At 200°C, 50 VPM	- 5-10%

TYPICAL PERFORMANCE CHARACTERISTICS
OF MICA PAPER TAPES
Fig. 5

Cable Development

A variety of cable designs incorporating mica paper insulation utilize a number of materials applied over the mica in various combinations to meet requirements of specific applications. Among the materials used are:

Glass and asbestos braids
Fluoropolymers
Silicones
Ethylene propylene rubber
Cross linked polyethylene
Fluorocarbon resins

Specific constructions have been approved by Underwriters Laboratories and by Canadian Standards Association for 450°C, 600-volt rating. Operational capability of these cables ranges from -55°C to 538°C, and the constructions are widely accepted in both single and multi-conductor configurations. Still other designs have been produced for control cable applications and have met or exceeded the requirements of IEEE 383. They have also passed qualification tests consisting of exposure to radiation, extreme heat, steam and chemical spray simulating a nuclear station environment and loss of coolant accident (LOCA) conditions.

The value of mica in providing for extended circuit integrity is further demonstrated in Figure 6. Two cables (7-conductor, #12 AWG stranded copper) differing only by inclusion of mica paper over the conductor singles in one case were installed in a horizontal ladder tray. Both cables employed a widely specified flame-resistant design. The cables were exposed to flame adjusted to 1900°F (± 50°F) supplied by a 21000 Btu burner. Insulation resistance was monitored using alternate conductors in the outer layers as one electrode, and the remaining conductors as the other. Measurements were made with a 500-volt DC megometer. Repetitive tests have confirmed the results shown in Figure 6:

INSULATION RESISTANCE OF TWO FLAME RESISTANT CABLE DESIGNS EXPOSED TO A 1900°F FLAME TO A 10,000 MEGOHM FAILURE POINT

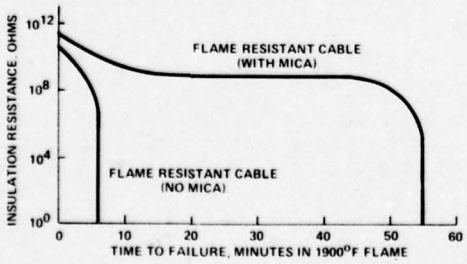
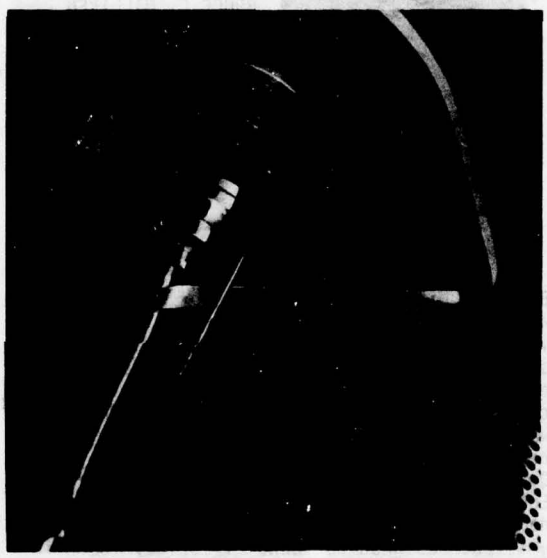


Fig. 6

Typical multi-purpose high temperature cables in current production employ stranded 27% nickel coated copper conductors insulated with mica paper tape applied in concentric layers (Figure 7). Tapes are available in narrow (to 1/4") slit widths in both pad and spool form, suitable for conventional cable-taping machine application at normal speeds (35-40 FPM). A wall of inorganic braid impregnated with flame retardant completes the basic design.

For cabling, singles and appropriate fillers are wrapped with mica paper tape as the binder and jacketed with a heat, moisture and abrasion resistant braid. These cables are capable of 538°C continuous service temperature and offer corrosion resistance, high dielectric strength, low power factor and flexibility without cold flow or heat distortion.



MICA PAPER TAPING OPERATION
Fig. 7

Miniaturization that requires high temperature wire is now a reality. Conductors as small as 28 AWG are being taped in diameters that do not exceed 40 mils overall. The smaller wires and cables greatly simplify installation in conduit as well as meeting market demands for miniaturization.

Conclusion

Cables utilizing mica paper as a design component have attained levels of performance never before achieved. Mica paper insulation has made possible dramatic advances in thermal operating capabilities, has extended circuit integrity and has enabled cable designers to offer specifiers and users a margin of safety that has not previously been

possible. Space age tapes developed from long established technology provide a reasonable economic approach to satisfying steadily increasing performance demands in the cable field. Designs have demonstrated their reliability in protection from extremes of heat, fire, high voltage, radiation, chemical exposure, and water immersion. New designs providing vastly superior performance are currently gaining acceptance in a growing number of applications and can be expected to achieve further recognition as they are extended to rapid transit, aircraft, automotive and other applications.



BRUCE C. MILLIKEN
President
MiliBride, Inc.
Industrial Avenue
Williston, VT 05495

Bruce C. Milliken is President of MiliBride, Inc., Williston, Vt., a company he formed in 1976, devoted to the manufacture of high temperature specialty wire and cable. Mr. Milliken has an extensive background in the field of wire and cable, having joined Haveg Industries in 1962, where he held a variety of assignments. In 1966 he joined Harbour Industries, Shelburne, Vt., as Quality Control Manager and in 1970 became Engineering Manager. In 1973 Mr. Milliken was named Vice President/Engineering, a post held until he resigned to found MiliBride. Born in Maine, Bruce holds a B.A. degree from Moncton University and has studied at the University of Vermont. He is a member of the American Society for Quality Control.

RICHARD S. ARMSTRONG
Market Development
Specialist
Insulating Materials
General Electric Co.
1 Campbell Road
Schenectady, NY 12345



Richard S. Armstrong is a Market Development Specialist with General Electric Company's Insulating Materials Business in Schenectady, N.Y. He joined GE in 1957 as a technical service engineer for coated materials and mica products. Since that time he has held a variety of assignments in field sales, product planning and market research in the insulating materials area. His current position includes market responsibility for coated materials, films and cable tapes. Prior to working for GE he was employed by E.I. du Pont de Nemours & Co., Inc. in Kingston, N.C. Mr. Armstrong holds a B.S. in Chemistry from Tufts University and is a member of A.S.T.M.

EFFECT OF FIRE-PROTECTIVE COATING ON AMPACITY OF CABLES IN CABLE TRAYS

D.V. Paulson, G.C. Gambs, Jr., and S.P. Carfagno

Franklin Research Center
Philadelphia, Pennsylvania 19103

ABSTRACT

The effect of a sprayable fire-protective coating on the ampacity (i.e., current-carrying capacity) of a 1/C #4/0 AWG and a 7/C #12 AWG cable (both XLPE/PVC) was determined with the cables tightly packed (46 to 47% fill with three layers of cable) in individual 12-in (0.3-m)-wide ladder-type cable trays. The steady 60-Hz current was measured that produced a stable conductor temperature (at the center of the cable tray) of approximately 75°C, and subsequently 90°C, for tray conditions of no coating, a 1/8-in (3.1-mm)-thick wet coating (approximately 1/16-in (1.6-mm) when dry) and a second 1/8-in (3.1-mm) thick wet coating of the fire-protective material. The results indicated that with a 90°C conductor temperature (and 50°C temperature rise), the ampacity was reduced by 2% with one 1/8-in (3.1-mm) thick wet application and, at most, 3% with a second 1/8-in (3.1-mm)-thick wet application of the fire-protective coatings.

INTRODUCTION

The fire-proofing of cables in trays is conveniently obtained by the application of suitable sprayable materials. Because such applied materials provide additional thermal barriers to the dissipation of electrical resistive heat generated within the cables, it was of interest to measure the actual effects of such coatings on the ampacity capabilities of typical cables used in nuclear power generating stations. This paper describes the design and results of the investigation.

TEST ARRANGEMENT

The test arrangement was based on previous investigations by Lee[1] and Stolpe[2] on ampacities for cables in open trays.

Two open, horizontally-mounted cable trays were uniformly and tightly packed with three layers of cable, with 16 runs of power cable per layer and 17 runs of control cable per layer, as shown in Figure 1. The trays were commercially available galvanized-steel open-rung ladder types. The nominal dimensions were 12 in (0.3 m) wide by 3 in (76 mm) deep by 8 ft (2.4 m) long with 6 in (0.15 m) rung spacing. The test cables were the following types:

- 1/C #4/0 AWG copper-stranded insulated with XLPE and an overall jacket of PVC. The nominal cable diameter was 0.72 in (18.3 mm).
- 7/C #12 AWG copper-stranded insulated with XLPE, individual conductor jacket of PVC and an overall jacket of PVC. The nominal cable diameter was 0.71 in (18.0 mm).

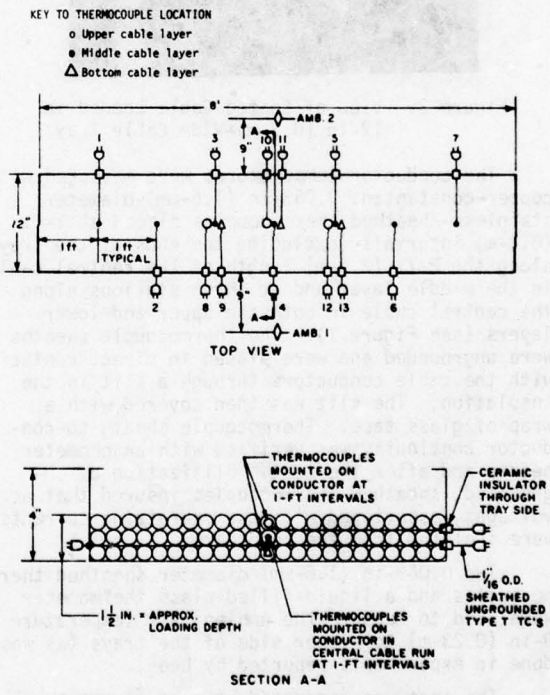


Figure 1. Sketch of Tray Loading and Thermocouple Location

One tray was 47% filled with the 7/C #12 cable, and the other tray was 46% filled with the 1/C #4/0 cable. The percent cable fill was calculated by dividing the total cable cross-sectional area $\left[\frac{\pi \times (\text{cable OD})^2}{4} \times \text{no. of cables}\right]$ by the

available cross-sectional tray area [inside width x inside height above the rungs]. A 47% fill represents about the maximum capacity of a tray containing three layers of cable. After each cable run through the tray, the cable was looped back into the tray for the next run, so that all runs were connected in series and the same current flowed in all the conductors. See Figure 2.



Figure 2. View of Coated Cable Loaded in 12-in (0.3-m)-Wide Cable Tray

The conductor temperatures were measured with copper-constantan, 0.063-in (1.6-mm)-diameter stainless-sheathed thermocouples placed at 1-ft (0.3-m) intervals (excluding the ends of the tray) along the 8-ft (2.4-m) length of the central cable* in the middle layer and at three stations along the central cable in both the upper and lower layers (see Figure 1). The thermocouple sheaths were ungrounded and were placed in direct contact with the cable conductors through a slit in the insulation. The slit was then covered with a wrap of glass tape. Thermocouple sheath-to-conductor continuity was verified with an ohmmeter before and after the test. Utilization of ungrounded, sheathed thermocouples insured that ac voltages, associated with the energizing currents, were isolated from the recorders.

Two 0.063-in (1.6-mm) diameter sheathed thermocouples and a liquid-filled glass thermometer were used to measure the ambient air temperature 9-in (0.23-m) to either side of the trays (as was done in experiments reported by Lee[2]).

The test was conducted at room temperature (27°C nominal) with negligible air circulation around the trays.

*The 12-in (0.3-m) tray was not wide enough to hold 17 power cables, so there was a small space between the 16th cable and the side channel of the tray. In this case, the thermocouples were installed in the eighth cable from this side, which was not more than one-half of a cable diameter from the vertical centerline of the tray.

The temperature indications from the thermocouples were continuously recorded on multipoint strip-chart temperature recorders. The calibration of the temperature recorders was checked at the beginning and end of each day of testing by use of a reference thermocouple (of the same type as that used in the cable trays), which was sequentially immersed in a stirred ice-water bath and an insulated flask of boiling water.

TEST PROCEDURE

Phase 1 - Uncoated Cables

The 60-Hz current load was supplied at a level adjusted by a variable autotransformer. The 7/C #12 cable was energized directly, while the 1/C #4/0 cable required the use of a low-voltage current transformer. The currents were measured with a precision current transformer and ammeter.

The current was adjusted in each of the two trays until a steady current provided an average conductor temperature of 75°C in the central cable run (center cable in middle layer). This condition was then readjusted to obtain an average conductor temperature of 90°C. The average temperatures were determined from the three centermost thermocouple locations (TC #3, 4 & 5 of Figure 1) along the central cable run.

Phase 2 - Initial Coating

The fire-protective coating[Δ] was applied to a thickness of 1/8 in (3 mm) (wet depth) to all exposed surfaces of the cables (top and bottom) within the cable trays.

After application of the coating, it was cured by energizing the cables to a current level which provided an average middle-layer conductor temperature of approximately 38°C (100°F) for 24 h, with an ambient air temperature of 27°C (80°F). (The conductor temperatures were less than 38°C (100°F) in the top and bottom layers.) The cure was extended for another 44 h at ambient air temperature only.

Following the cure, the ampacities at 75°C (167°F) and 90°C (194°F) were determined as in Phase 1.

Phase 3 - Final Coating

A second coating of 1/8-in (3-mm) (wet depth) thickness was sprayed onto the cable trays and cured for 24 h with the cables energized to provide a top layer temperature at 38°C (100°F). The final total dry thickness resulting from the initial and final coating was approximately 1/8 in (3 mm). The ampacities at 75°C (167°F) and 90°C

[Δ]The fire-protective coating was described by the supplier as a sprayable, non-intumescent, water-borne, air-drying, paste-consistency, fire-retardant coating, based on a binder of polyvinyl acetate copolymer emulsion and filled with both active and inert fire-retardant ingredients.

(194°F) conductor temperatures were then determined as in Phases 1 and 2. Views of the final coating are shown in Figures 3 and 4.



Figure 3. Top View of Typical Cable Tray Coated with Two Thicknesses of Cable Coating

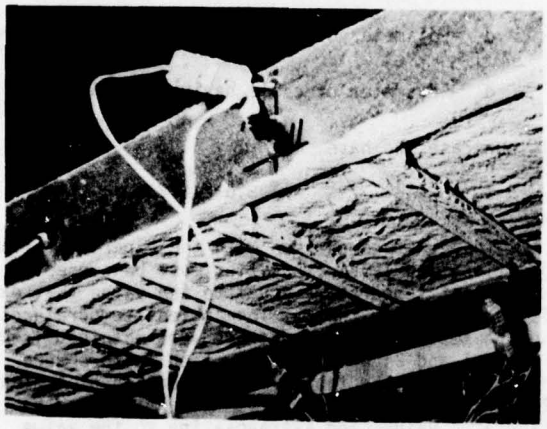


Figure 4. Bottom View of Typical Cable Tray Coated with Two Thicknesses of Cable Coating

Phase 4 - Additional Curing of the Final Coating

After completion of Phase 3, the coated cable trays were additionally cured by maintaining them at ambient room conditions (approximately 27°C) for 9.7 d, and then the ampacities were redetermined at 75°C and 90°C, as in Phases 1 through 3.

TEST RESULTS

The temperature measurements along the central cable run (center cable of middle layer) showed that end effects were noticeable as much as 2 ft (0.6 m) from the ends of the tray. Therefore, only the temperature measurements 3 ft (0.9 m) from each end plus the ones at the center were used to compute the average conductor temperature. The thermocouples in the upper and lower cable layers verified that these were cooler than the middle layer, by approximately 10°C.

The test results are summarized in Tables 1 and 2. In Figures 5 and 6, the log ΔT has been plotted against log I, where ΔT is the conductor temperature rise above the ambient temperature and I is the current through the conductor. This form of plotting is based on the work of Lee[1] and Stolpe[2], who found that log ΔT is approximately proportional to log I.

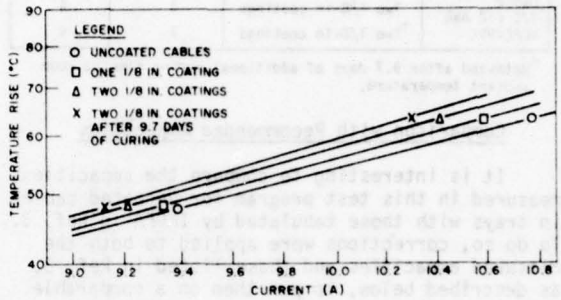


Figure 5. Ampacity Vs. Temperature Rise for 7/C #12 AWG Cables in a 12-in (0.3-m)-Wide Tray (Range of Ambient Temperatures: 26.7° to 27.8°C)

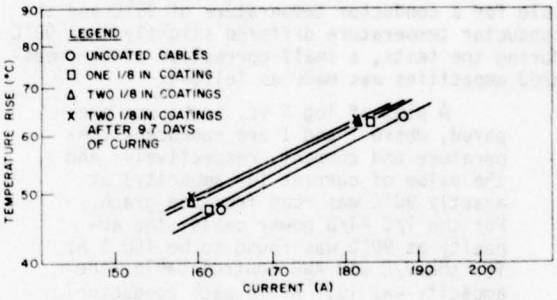


Figure 6. Ampacity Vs. Temperature Rise for 7/C #12 AWG Cables in a 12-in (0.3-m)-Wide Tray (Range of Ambient Temperatures: 26.7° to 27.8°)

Figures 5 and 6 show that the coating had a small effect on the ampacity for a given conductor temperature rise.

The percent reductions[¶] in ampacity resulting from the coating are given in Table 3. The deratings appear to be slightly dependent on the value of temperature rise and coating thickness; but they are all very small, the highest value being only 4%. In the case of the power cable there was a small change after approximately 10 additional days of curing under ambient room conditions, but there was no change in the case of the control cables.

[¶]Expressed as percent reduction of ampacity from measured ampacity without coating.

Table 3. Ampacity Deratings

Cable Type	Coating Thickness (Measured when wet)	Ampacity Deratings (%) Vs. Temperature Rise	
		$\Delta T = 50°C$	$\Delta T = 60°C$
Power Cable 1/C #4/0 AWG XLPE/PVC	One 1/8-in coating	2	2
	Two 1/8-in coatings	2	3
	[+]Two 1/8-in coatings	3	4
Control Cable 7/C #12 AWG XLPE/PVC	One 1/8-in coating	1	2
	Two 1/8-in coatings	3	4
	[+]Two 1/8-in coatings	3	4

[+]Retested after 9.7 days of additional curing time at room ambient temperature.

Comparison with Recommended Ampacities

It is interesting to compare the ampacities measured in this test program for uncoated cables in trays with those tabulated by IPCEA in Ref. 3. To do so, corrections were applied to both the measured ampacities and those listed in Ref. 3, as described below, to put them on a comparable basis.

Correction of Measured Ampacity for Conductor Temperature

Since ampacities listed in Ref. 3 are available for a conductor temperature of 90°C and the conductor temperature differed slightly from 90°C during the tests, a small correction of the measured ampacities was made as follows:

> A plot of log T vs. log I was prepared, where T and I are conductor temperature and current, respectively; and the value of current (or ampacity) at exactly 90°C was read from the graph. For the 1/C #4/0 power cable, the ampacity at 90°C was found to be 188.3 A; for the 7/C #12 AWG control cable, the ampacity was 10.7 A (in each conductor).

Calculation of Loading Depth

The depth of tray loading in our tests was calculated using the formula given in Ref. 3, page i, as follows:

$$h = \text{Cable Depth} = \frac{\text{No. of Cables} \times (\text{Cable OD})^2}{\text{Inside Width of Tray}}$$

For the 1/C #4/0 AWG power cable, this yields

$$h = \frac{48 \times (0.72)^2}{11.8} = 2.11 \text{ in } (53.6 \text{ mm})$$

and for the 7/C #12 AWG control cable, we find

$$h = \frac{51 \times (0.71)^2}{11.8} = 2.18 \text{ in } (55.4 \text{ mm})$$

IPCEA Ampacities

For these cable depths, IPCEA ampacities can be found in Ref. 3 for the following conditions:

Conductor temperature = 90°C

Air ambient temperature = 40°C

From Table 4 of Ref. 3, the ampacity for the 1/C #4/0 cable is found to be 137.5 (by plotting the tabulated ampacities as a function of "calculated depth of cables in tray" and reading the value of ampacity at 2.11 in).

For the 7/C #12 AWG cable, it is necessary first to obtain the ampacity for a 3/C cable and then to make a correction. From Table 6 of Ref. 3, using the procedure described above for the power cable, the ampacity for the 3/C #12 AWG cable is found to be 8.6 A for a cable depth of 2.18 in (55.4 mm). This is converted into the ampacity for a 7/C #12 AWG cable by use of a formula from Section B of Ref. 3:

$$I'_x = \frac{d'_x}{d'_o} \sqrt{\frac{3}{n_x}} \; I'_o$$

where

I'_o = ampacity for 3/C cable from table

I'_x = ampacity for cable having n_x conductors

d'_o = diameter of 3/C cable from table

d'_x = diameter of cable having n_x conductors

In our case, we have

$$I_7 = \frac{0.71}{0.49} \sqrt{\frac{3}{7}} \times 8.6 = 8.2 \text{ A}$$

To permit comparison with the experimental ampacities, the IPCEA ampacities must be corrected to an ambient temperature equal to the value that existed during the tests. The ambient temperatures during tests of uncoated trays were obtained from Tables 1 and 2; and the correction factors were obtained from the table for "Correction of Ambient Temperature," page i of Ref. 3, by plotting the tabulated values and extrapolating to the value of ambient temperature during the tests.

Cable Type	Ambient Temperature (°C)	Temperature Correction Factor
1/C #4/0 AWG	26.7	1.124
7/C #12 AWG	27.2	1.119

(Since the ambient temperature during the test was only a few degrees below 30°C, the lowest value in the IPCEA table, the extrapolation should not introduce a significant error.)

The ambient temperature corrections of the IPCEA ampacities (for a 90°C conductor temperature) are as follows:

1/C #4/0 AWG power cable: $137.5 \times 1.124 = 154.6$ A

7/C #12 AWG control cable: $8.2 \times 1.119 = 9.2$ A

The ampacities measured here in the same conditions were 188.3 and 10.7 A, respectively. Therefore, the IPCEA ampacities are conservative.

Thickness Measurement After Curing

After completion of the ampacity tests, the tray loaded with control cables was cut through with a band saw 4.5 ft (1.4 m) from one end to permit thickness measurements on the cured coating. A view of the cross section is shown in Figure 7. The measurements confirmed that the dry coating thickness was 1/8 in (3 mm) over the crests of the cables in the top and bottom layers, which is where the wet thickness had been measured.

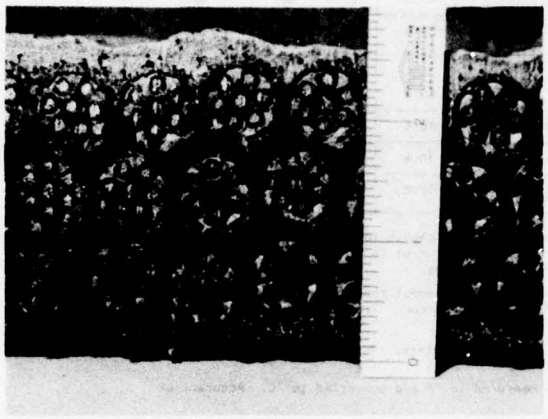


Figure 7. Cross Section of Coated Cable Tray

CONCLUSIONS

To determine the effect of a fire-protective coating on ampacity, two tightly-packed 12-in (0.3-m)-wide cable trays were tested without being coated, after curing of a 1/8-in (3.1-mm)-thick wet coating, after curing of a second 1/8-in (3.1-mm)-thick wet coating on all exposed cable surfaces in the cable tray and after an additional 9.7 days of curing at room temperature. The cured (dry) coatings were approximately 1/16 and 1/8 in (1.6 and 3.1 mm) thick based upon coating-supplier information, which was confirmed by actual measurement in the case of the 1/8-in (3.1-mm) thickness. In one tray, 1/C #4/0 AWG power cable was tightly packed into approximately 46% of the available tray space while the other tray was approximately 47% filled with 7/C #12 AWG control cable; there were 3 layers of 16 power cables in one tray and 3 layers of 17 control cables in the other tray.

The ampacities measured after each coating was cured indicates that, with a 90°C conductor temperature and 50°C temperature rise, the ampacity was reduced by a maximum of 2% with one 1/8-in (3.1-mm)-thick wet application and at most 3% with a second 1/8-in (3.1-mm)-thick wet application of the coating.

In conclusion, based on data derived from this test, the effect of a sprayable fire-protective coating on the ampacity of typical power and control cables, tightly packed in cable trays to more than 40% fill, is very small.

ACKNOWLEDGEMENT

The authors wish to thank the Vimasco Corporation of Nitro, WV, who manufactures the fire-protective coating used and who sponsored this project.

REFERENCES

1. Lee, R. H., IEEE Transaction Paper 71-TP-543-PWR, *Ampacities of Multiconductor Cables in Trays* (see IEEE Transaction on Power Apparatus & Systems 91:1051-1056, May/June, 1972). New York, The Institute of Electrical and Electronics Engineers, Inc., 1971.

2. Stolpe, J., IEEE Transaction Paper 70-TP-557-PWR, *Ampacities for Cables in Randomly Filled Trays* (see IEEE Transaction on Power Apparatus & Systems 90:962-974, May/June, 1971). New York, The Institute of Electrical and Electronics Engineers, Inc., 1970.

3. IPCEA Pub. No. P-54-440 (Second Edition), NEMA Pub. No. WC 51-1975, *Ampacities, Cables in Open-Top Cable Trays*, Washington, D.C., The National Electrical Manufacturers Association, 1975.

BIOGRAPHICAL NOTES

David V. Paulson graduated from the University of Redlands in 1950 with a B.S. in Physics. He has an extensive background in applied research and testing in explosive ordnance, aerospace and, more recently, in the qualification of equipment for nuclear power generating stations. He is currently the Chief of the Environmental Testing Section of the Franklin Research Center (FRC).

Gerard C. Gambs, Jr., received a B.S. (1970) and an M.S. (1976) in Mechanical Engineering from Villanova University. He has experience in a variety of positions involving application of engineering to hardware-associated experimental design problems. He is a Research Engineer on the staff of FRC.

Dr. Salvatore P. Carfagno joined The Franklin Institute Research Laboratories (FIRL) soon after its organization in 1946. During his nearly 30 years with FIRL he has participated in studies involving heat transfer, fluid mechanics, magnetohydrodynamics, gaseous ignition and energy conservation. During the last 9 years his activities have been concentrated in the qualification of safety-related equipment for nuclear service. During this time he has contributed to the development of a number of IEEE and ANSI standards. He received his B.S. in Mechanical Engineering from Drexel (1949) and a Ph.D. in Physics from Temple University (1963). Dr. Carfagno is Manager of the Performance Qualification Laboratory at FRC.

Table 1. Ampacity Test Results (Measured Data at ∿90°C Conductor Temperature)

Cable Size and Tray Configuration	Thickness of Fire-Protective Coating (Note 1)	Central Conductor Average Temperature (Note 2) °C	°F	Current (Note 3) A	Ambient Room Temperature (Note 4) °C	°F	Calculated Temperature Rise Above Room Ambient Temperature °C
1/C #4/0 AWG. 46% fill in a 12 in. wide by 3-3/4 in. deep, ladder-type, open tray. (3 layers of 16 cables each)	No coating	90.4	194.8	189.0	26.7	80	63.7
	1/8 in. (wet)	90.9	195.7	184.8	28.3	83	62.6
	Additional 1/8 in. (wet)	90.5	194.9	181.6	27.8	82	62.7
	After final cure period (Note 5)	90.2	194.3	181.6	27.2	81	63.0
7/C #12 AWG. 47% fill in a 12 in. wide by 3-3/4 in. deep, ladder-type, open tray. (3 layers of 17 cables each)	No coating	90.7	195.3	10.8	27.2	81	63.5
	1/8 in. (wet)	90.9	195.7	10.6	27.8	82	63.1
	Additional 1/8 in. (wet)	90.9	195.8	10.4	27.8	82	63.1
	After final cure period (Note 5)	90.5	194.9	10.3	27.2	81	63.3

Notes:
1. Coating was applied to all (top and lower) exposed surfaces of cables in the tray. Thicknesses measured while the coating was wet. Coatings cured for a minimum of 24 h while a cable temperature of ∿100°F was maintained by current flow through the cables.
2. Average temperature calculated from indications of the 3 center-most thermocouples (TC 3, 4 and 5) located on the conductor(s) of the cable at the center of the array. Temperatures measured in °F and converted to °C. Accuracy of measurement: ± 2°C.
3. Currents measured using current transformers and 5-A current meters. Accuracy of measurement: ± 0.65% of full scale.
4. Ambient room temperature near the cable trays was measured in °F and converted to °C. Accuracy of measurement: ± 2°C.
5. After 9.7 days @ room ambient temperatures.

Table 2. Ampacity Test Results (Measured Data at ∿75°C Conductor Temperature)

Cable Size and Tray Configuration	Thickness of Fire-Protective Coating (Note 1)	Central Conductor Average Temperature (Note 2) °C	°F	Current (Note 3) A	Ambient Room Temperature (Note 4) °C	°F	Calculated Temperature Rise Above Room Ambient Temperature °C
1/C #4/0 AWG. 46% fill in a 12 in. wide by 3-3/4 in. deep, ladder-type, open tray. (3 layers of 16 cables each)	No coating	74.3	165.7	163.0	26.7	80	47.6
	1/8 in. (wet)	74.3	165.7	161.6	26.7	80	47.6
	Additional 1/8 in. (wet)	74.8	166.7	159.2	27.2	81	47.6
	After final cure period (Note 5)	75.7	168.2	159.0	27.2	81	48.5
7/C #12 AWG. 47% fill in a 12 in. wide by 3-3/4 in. deep, ladder-type, open tray. (3 layers of 17 cables each)	No coating	75.0	167.0	9.38	26.7	80	47.8
	1/8 in. (wet)	74.8	166.7	9.35	26.7	80	48.1
	Additional 1/8 in. (wet)	75.4	167.7	9.1	27.2	81	48.7
	After final cure period (Note 5)	75.5	168.3	9.1	27.2	81	48.3

Notes:
1. Coating was applied to all (top and lower) exposed surfaces of cables in the tray. Thicknesses measured while the coating was wet. Coatings cured for a minimum of 24 h while a cable temperature of ∿100°F was maintained by current flow through the cables.
2. Average temperature calculated from indications of the 3 center-most thermocouples (TC 3, 4 and 5) located on the conductor(s) of the cable at the center of the array. Temperatures measured in °F and converted to °C. Accuracy of measurement: ± 2°C.
3. Currents measured using current transformers and 5-A current meters. Accuracy of measurement: ± 0.65% of full scale. The current value is for a single conductor.
4. Ambient room temperature near the cable trays was measured in °F and converted to °C. Accuracy of measurement: ± 2°C.
5. After 9.7 days @ room ambient temperatures.

EFFECT OF MOISTURE ON THE STRENGTH OF OPTICAL FIBERS

David Kalish, B. K. Tariyal
and H. C. Chandan

Bell Telephone Laboratories
2000 Northeast Expressway
Norcross, Georgia 30071

Summary

A major concern in achieving satisfactory performance of optical fibers for a long service life is the effect of moisture on strength. This paper illustrates, both analytically and experimentally, how the environment can degrade the strength of fibers under a constant stress (static fatigue), a constant stressing rate (dynamic fatigue) and zero stress aging. Time-dependent fracture originating from submicron flaws in polymer-coated optical fibers can be described by conventional fracture mechanics concepts using a power function for the crack growth rate. Static and dynamic fatigue results on fused silica fibers support the stress-corrosion mechanism for time dependent failure. Finally, it is shown how proof testing of optical fibers can be used to guarantee a minimum time-to-failure in static fatigue.

Introduction

The theoretical strength of fused silica[1] is determined by the interatomic force-separation curve of the constituent atoms (silicon and oxygen) and is approximately 16 GPa*. In contrast, most glass objects exhibit fracture strengths in the range of 35 to 140 MPa while carefully prepared fused silica fibers have attained strengths of up to about 6 GPa. It is well established, both theoretically and experimentally, that the discrepancy between the theoretical and observed strengths in glass (and in other brittle solids) is due to the presence of flaws (inhomogeneities or cracks). In a classic paper in 1920, Griffith used a thermodynamic argument to show that a flaw in an elastic solid becomes unstable when the rate of release of stored elastic energy is equal to the rate of increase of energy from creating new surfaces.[2] The fracture strength (σ_f) is thereby related to the flaw size (a_c) by:

$$\sigma_f = \frac{1}{Y}\left(\frac{E\gamma}{a_c}\right)^{1/2} \qquad (1)$$

where E = Young's (elastic) modulus, γ = surface free energy, and Y = geometric constant for the specimen-flaw configuration, Figure 1. The inverse relationship between strength and the square root of flaw size as first described by Griffith remains the fundamental law governing the strength of optical fibers.

An alternative approach to establishing a fracture criterion for a linear elastic solid was developed by Irwin[3] who analyzed the stresses close to the crack tip rather than throughout the body. Irwin defined a parameter called the stress intensity factor (K_I), which has the units of stress (MN/m^2) multiplied by the square root of a dimension ($m^{1/2}$). He showed that fracture will occur when a critical value of the stress intensity factor (K_{Ic}) is reached

$$\sigma_f = \frac{K_{Ic}}{Ya_c^{1/2}} \qquad (2)$$

where K_{Ic} ≡ critical stress intensity factor in the tensile mode.* The value of K_{Ic} for a particular material is a constant and can be determined with Equation (2) by creating a flaw of a known size (a_c) in a simple geometry specimen which establishes Y and measuring the fracture strength (σ_f). The critical size of a crack in a fused silica optical fiber can be estimated with Equation (2). The dimensionless geometric constant Y for a part-through semicircular crack at a fiber surface with a crack plane normal to the fiber axis is 1.24 and K_{Ic} for fused silica is 0.8 $MN/m^{3/2}$ so that the fracture strength versus crack size relationship in Figure 2 is obtained. As an example, a fracture strength of 1 GPa is a result of a 0.4 μm flaw.

*1 GPa = 1 GN/m^2 = 1×10^9 N/m^2 = 145,038 psi
1 MPa = 1×10^6 N/m^2

*This simplified example is part of the field known as fracture mechanics; there are numerous review papers and books on the subject of the mechanics of fracture including (4) and (5).

In order to understand the strength of glass, one must also recognize that glass contains many flaws, with a distribution of flaw sizes. Moreover, the largest crack will usually be different in each glass body. Thus one must apply statistics to describe glass strength. Weibull[6] empirically postulated a simple power law for the distribution of strength (flaws) in engineering materials. The "Weibull" expression,

$$\ell n \ell n \frac{1}{1-F} = \ell n\, V + m\, \ell n \frac{\sigma}{\sigma_o} \qquad (3)$$

where F = cumulative probability of failure, V = volume of sample, and m and σ_o are characteristic constants of the distribution, has often been applied to the analysis of the fracture of brittle materials. In the case of glass, since surface flaws normally control the fracture strength, V in Equation (3) can be replaced by A(Area), L(Length) or d(diameter) whichever variable principally characterizes the surface.

The strength of glass must be reported either as a complete distribution or for convenience by some statistically representative value; it is common to use the median strength where F = 0.5 and that is what is used in this paper.

A basic assumption of the Griffith or Irwin analyses is that the critical size flaw is stable (does not grow) at $\sigma < \sigma_f$, but becomes unstable and propagates rapidly across the specimen at $\sigma = \sigma_f$. This assumption is valid only for very high stressing rates or in an inert environment (e.g., vacuum or a dry gas). At normal loading rates the local environment at the surface of a glass can have a substantial detrimental effect on the strength. The basic phenomenon involved is the slow growth of flaws in an active environment (often referred to as "subcritical crack growth"). This slow flaw growth results in fracture at a lower stress than would occur in an inert environment, where flaws are stable until the fracture criterion is satisfied and unstable rapid fracture takes place. It is this slow surface-flaw growth that leads to time-dependent fracture in glass.

There are two common manifestations of time-dependent fracture which result from the manner in which the stress is applied. If the applied stress is maintained at a constant value below the inert strength then the glass can fracture after a period of time in an active environment and this behavior is known as "static fatigue." On the other hand, if the applied stress is continually increasing (such as in a standard tensile test), then the strength in an active environment will be lower than in an inert environment and this behavior is known as "dynamic fatigue."

In glass, water in the environment is primarily responsible for slow crack growth. Relatively low concentrations of water can cause long term failures by static fatigue at stresses well below one-half of the inert strength. Fused silica shows a time-dependent strength so that this phenomenon is of concern for the survival of optical fibers under the stresses and environments encountered during manufacturing, installation and service. Time-dependent fracture is the focus of this paper.

Analytical Description of Time-Dependent Fracture

The most prominent theories for the specific mechanism of time-dependent fracture in glass are critically reviewed by Wiederhorn,[7,8] Adams and McMillan[9] and Pavelcheck and Doremus.[10] The stress-corrosion mechanism developed by Charles[11-13] and later by Charles and Hillig[14,15] can be used to explain most of the available data for static fatigue and dynamic fatigue in a variety of glass compositions, temperatures and chemical environments. The stress-corrosion mechanism postulates a stress-and-temperature-dependent chemical reaction which controls the rate of growth of the pre-existing surface flaws. The analytical description of stress corrosion leads to a relationship between the nominal applied stress (away from the flaw) and the time-to-fracture. The maximum size surface flaw gives the highest stress concentration at the flaw tip, and hence the fastest rate of stress assisted chemical breaking of primary atomic bonds at that point.

In this paper, we do not attempt to establish the suitability of any particular mechanism for static fatigue. Instead, for analytical convenience, we choose at first to adopt the stress-corrosion model of Charles[11,12] and examine the static fatigue and dynamic fatigue behavior of polymer coated fused silica optical fibers.

The static fatigue model of Charles,[12] where the flaw growth rate is a power function of stress, results in

$$\log t_s = -n \log \sigma_s + \log k_s \qquad (4)$$

where n (the exponent in the power function) and k_s are characteristic constants

for a material, geometry and environment. Similarly, Charles[13] showed that for dynamic fatigue

$$\log\sigma_d = (1+n)^{-1}\log\dot{\sigma} + (1+n)^{-1}\log k_d \quad (5)$$

or

$$\log t_d = -n\log\sigma_d + \log k_d \quad (6)$$

where σ_d = dynamic fatigue strength, $\dot{\sigma}$ = stressing rate, t_d = time to failure in dynamic fatigue and[16]

$$\log k_d = \log k_s + \log(n+1). \quad (7)$$

Further insight into the characteristic parameter k_s is provided by the fracture mechanics analysis of Evans[17,18] who used a power law for flaw velocity (v) analogous to that proposed by Charles,[12] except that the former employs the stress intensity factor (K_I) as the independent variable:

$$v = \frac{da}{dt} = AK_I^{\,n} \quad (8)$$

where A and n are characteristic crack growth parameters. Equation (8) can be combined with the basic fracture mechanics relationships:

$$a = \left(\frac{K_I}{Y\sigma}\right)^2 \text{ and } a_c = \left(\frac{K_{Ic}}{Y\sigma_f}\right)^2 \quad (9)$$

where a = flaw size, Y = geometric constant, σ = applied stress, a_c = critical crack size for fracture, K_{Ic} = critical stress intensity factor and σ_f = inert environment strength to give an equation that is the analog of Equation (4):

$$\log t_s = -n\log\sigma_s + (n-2)\log\sigma_f + \log\frac{2}{AY^2(n-2)K_{Ic}^{\,n-2}} \quad (10)$$

Similarly for dynamic fatigue, the fracture mechanics analysis[17] leads to an equation that is the analog of Equation (5).

$$(n+1)\log\sigma_d = \log\dot{\sigma} + \log(n+1) + (n-2)\log\sigma_f + \log\frac{2}{AY^2(n-2)K_{Ic}^{\,n-2}} \quad (11)$$

An independent measurement of σ_f involves tensile testing under conditions where slow crack growth is completely inhibited, e.g., at a very low temperature, at a very high strain rate or in a dry environment. The parameter K_{Ic} can be determined for the glass composition of interest by bulk sample fracture mechanics tests and the parameter Y can be calculated if the flaw shape is known.

Examples of Time-Dependent Fracture

Kalish and Tariyal[19] measured the effect of stress rate from 3.0 to 0.061 GPa/S on the tensile strength (σ_s) of 5.0cm gage length specimens of a polymer (ethylene vinyl acetate) coated fused silica optical fiber tested at each of four relative humidities (RH) from 2 to 97% at 23°C. The plots of log median σ_d versus $\dot{\sigma}$ are shown in Figure 3 along with the values of the flaw velocity exponent n obtained from each slope $(n+1)^{-1}$. The value of n decreases from 29.0 at 2% RH to 15.9 at 97% RH showing a very pronounced effect of humidity on the dynamic fatigue of the fused silica fibers.

The crack growth parameter A in Equation (8) was calculated for each humidity from the intercepts in Figure 3 by using Equations (5) and (11) and the results are summarized in Table 1.

The dynamic fatigue measurements at the four humidities can be used to calculate the median static fatigue behavior according to Equation (4) where the n values are listed in Table 1 and k_s are calculated with Equation (7). The predicted effect of humidity on the time-to-failure is dramatic; for example, for a static fatigue strength of 2.5 GPa the 97% RH environment gives a life of about one hour while the 2% RH environment gives a life of several years.

The static fatigue of 61cm gage length specimens of a polymer (ethylene vinyl acetate) coated fused silica optical fiber in 97% RH is shown in Figure 4.[19] The range of measured failure times in Figure 4 can be evaluated in terms of the cumulative probability of failure.[18] Equations (3) and (10) can be combined[6,19] to give:

$$\log t_s = -n\log\sigma_s + \frac{(n-2)}{m}\log\log(1-F)^{-1} + (n-2)\log\sigma_o - \frac{1}{m}\log L + \log D \quad (12)$$

In the Kalish and Tariyal study,[19] the parameter $\log\sigma_o = 0.762$ was calculated for the measured median t_s at each σ_s (the data in Figure 4), and the constant logD =

-0.413 contains the constants Y, K_{Ic}, n and A for the 97% humidity static fatigue condition, the values of which were previously noted. Consequently, calculated probability plots for static fatigue condition, the values of which were previously noted. Consequently, calculated probability plots for static fatigue failure times were generated for the three stress levels used in the measurements; the calculated curves and measured points are shown in Figure 5. The measured t_s, which typically span about 2 to 3 decades, all lie in a reasonable range between F = 0.1 and 0.9, which supports the fracture mechanics description of the static fatigue process in optical fiber.

The static fatigue behavior as predicted from dynamic fatigue measurements can be compared to calculated static fatigue behavior based upon static fatigue measurements. The 97% RH results for the ethylene vinyl acetate coated optical fiber in Figures 3 and 4 provides a convenient basis for such a comparison. First, the parameter log k_s, Table 1, as determined by dynamic fatique measurements must be adjusted to account for the difference between the 5cm gage length used in those measurements and the 61cm gage length used in the static fatigue measurements. This is done by comparing dynamic and inert strength measurements at equal probabilities of failures,[19] and it is found that the gage length adjusted log k_s from Table 1 is 9.31 for the 97% RH case. In Table 2, the static fatigue strength levels predicted from the two types of tests for three nominal failure times are compared and found to be in excellent agreement. This illustrates the validity of making short term dynamic fatigue measurements for the purpose of engineering predictions of longer term static fatigue performance.

Crack Growth Law

Minnear and Bradt[22] collected crack growth results for a number of ceramics and glasses, and showed a reasonable linear correlation between logA and n. A similar correlation between the crack growth parameters n and logA for fused silica only is presented in Figure 6; the data used to establish this correlation is summarized in Table 3. The data points in Figure 6 represent dynamic fatigue and static fatigue measurements on fused silica fibers and, in one case, direct crack-growth measurements on fused-silica sheets where sufficient information was available for us to calculate logA and n. There is an excellent correlation between logA and n (correlation coefficient = 0.998) according to:

$$\log A = 3.387n - 11.598 \qquad (13)$$

where from Equation (11) K_I is in $GNm^{-3/2}$ and v is in ms^{-1}. This correlation supports the stress-corrosion mechanism for time-dependent fracture of glass and the applicability of fracture mechanics concepts to the submicron range of flaws that exist in fused silica optical fibers. The strong correlation between logA and n can be utilized to simplify the mechanical characterization of fused silica optical fibers. Now it should only be necessary to establish the n parameter, for example, by using Equation (5), to calculate logA from Equation (13), and to calculate the inert strength σ_f with Equation (11). Once these parameters are known, it is possible to calculate what changes in environment or fiber strength are needed to provide a specified fiber lifetime.

An important feature of Figure 6 and Table 3 is that the results for different polymer coatings as well as uncoated fused silica cannot be distinguished from one another; they are all correlated by Equation (13). This fact leads to the conclusion that the polymer coatings do not influence the kinetics of the static and dynamic fatigue but merely serve to protect the fiber against mechanical damage. Of course, the latter is very important since small initial size flaws take longer to grow to a critical size at a given stress level.

Zero Stress Aging

The preceding discussion of static and dynamic fatigue shows that they are different manifestations of the same phenomenon. Under ideal circumstances, a cable could be installed with no residual stresses on the fibers. However, the fibers may still be stressed at a later time during routine maintenance, repairs or other work done in the vicinity of the cable. Consequently, whether exposure to moisture under zero stress is detrimental to the subsequent strength of the fibers is of interest.

Tariyal and Kalish[26] recently studied the effect of aging in different environments on the strength of polymer-coated optical fibers. The effect of aging in deionized water for either 10 or 100 days at 23°C and of drying at 50°C in a vacuum of 0.05 mm Hg for 7 days are summarized in Figure 7 in terms of median strengths.[26] A 13% decrease in ambient (~50% relative humidity and ~23°C) strength to 4.78 GPa

occurs after 10 days of aging (no drying) and a further 3% decrease in ambient strength to 4.63 GPa occurs upon aging for 100 days. The observation that the rate of strength degradation decreases with aging time is in agreement with the observations of Fox et.al.,[27] and of Wang and Zupko.[28] The ambient strength of fibers aged for 10 days is recovered to within 3% of the original ambient strength by drying. The ambient strength of fibers aged for 100 days is not recovered to the same extent by drying; here the strength comes back to within only 11% of the initial ambient strength. The ambient strength results alone are not conclusive with respect to the question of permanent damage to the fibers under zero-stress aging. When the fiber aged for 100 days and dried is tested in inert conditions, the strength is equivalent to (within 1%) the initial inert strength. In addition, it was found that aging for 5 months under ambient conditions has no effect on either the ambient or the inert strength of coated optical fibers (not shown here), in agreement with Fox et.al.[27]

Since fibers do not show a decrease in the inert strength on aging either in ambient or in deionized water, the loss of ambient strength after aging in water cannot represent flaw growth. Aging in the presence of water evidently prepares a crack surface to undergo dynamic fatigue on subsequent testing by saturating the polymer coating with water and establishing a high humidity environment at the crack tip, due to absorption of water molecules at the polymer-glass interface as well as flaw surfaces. The incomplete recovery on drying, Figure 7, indicates that 7 days at 50°C under a partial vacuum of 0.05 mm of Hg is not sufficient to get all the chemisorbed water off the glass surface.[29] Again, the fact that the inert strength is recovered to within 1% of the original strength indicates that no permanent damage (i.e., flaw growth) occurs during aging.

Design Considerations

The survival of long lengths of fibers exposed to stresses arising from the manufacture and installation of optical cables is crucial to an economically successful application of long distance optical communication. From an engineering design point of view one needs to guarantee that long lengths of fibers have a certain minimum strength, and a certain minimum static fatigue life under service conditions. It is very difficult to demonstrate compliance with these two requirements because of the size and time dependence of glass strength as discussed in this paper and as is reviewed by Kalish et.al.[30]

One way of establishing the long length strength is through a suitable statistical analysis of the short length data in order to obtain the pertinent statistical distribution parameters; see for example References 6, 31 and 32. These parameters can then be used to estimate long length strengths.[33-35] However, fiber strengths in general show multimodal strength distributions, arising from flaw populations of different physical origins. The predominant mode in any sample population is determined by factors such as gage length, number of tests, and various fiber processing parameters[35-36] and this may not correspond to the flaw population in the entire sample which is controlling the strength in long lengths. Consequently, the estimation of the long length strength from short length data cannot be accomplished with any useful degree of reliability. In the absence of a reliable analytical estimation method, there are two possible alternatives for ensuring a minimum strength in long optical fibers, namely nondestructive inspection (NDI) and proof testing. At the present time, a suitable NDI technique to detect the appropriate flaw size range (0.02 μm to 2 μm) in fibers is not available and therefore, proof testing offers an attractive means of ensuring the mechanical reliability of glass fibers.

Theory of Proof Testing

In proof testing, an optical fiber is subjected to a tensile load greater than that expected in any subsequent step during cable manufacturing, installation or service. The fibers which fail the proof test are rejected. The mathematical foundation for the selection of the proof test load and establishment of the proof test conditions for brittle materials is well developed.[37-39] All specimens containing flaws larger than the critical flaw size will fail because the stress intensity factor at the crack tips will exceed the critical stress intensity factor K_{Ic}. For the fibers which survive the proof test,

$$K_{Ic} > K_p = \sigma_p Y \sqrt{a_i} \qquad (14)$$

where K_p is the stress intensity factor developed during the proof test at the largest flaw in the surviving fiber, Y is the geometric constant, σ_p is the proof stress and a_i is the initial size of the largest flaw. Thus, for any applied stress σ_o below the proof stress level, the maximum initial stress intensity factor K_{Ii} is:

$$K_{Ii} < K_{Ic}\left(\sigma_a/\sigma_p\right) \qquad (15)$$

Equation (15) describes the protection against short term overload on the fiber, i.e., a simple result of the fracture mechanics analysis is that the fiber will not break at instantaneous stresses below the proof test stress.

If the applied stress $\sigma < \sigma_p$ is maintained for a long time in an active environment then static fatigue can occur. However, since the fiber survived the proof test, a maximum possible size flaw has been guaranteed failure time due to static fatigue is also established.[40] The development of the expression for the time-to-failure follows the arguments presented earlier except that Equation (15) is used in place of Equation (9). The result for the power law flaw growth model is:

$$t_{s(min.)} = B\sigma_p^{n-2}\sigma_s^{-n} \qquad (16)$$

where $B = 2/AY^2(n-2)K_{Ic}^{(n-2)}$ and σ_s is now the applied stress that leads to a static fatigue failure in time t_s (min) or greater.

The benefits of proof testing of long length optical fibers on the subsequent survival of these fibers in lightguide cables have been documented by Tariyal et.al.[41] The cable tests showed that cables containing fibers which had been proof tested at 207 MPa showed no fiber breaks until the strain on the cable core (containing the fibers) was approximately equal to or greater than the prior proof test strain level. In contrast, a cable containing fibers that were not proof tested showed fiber breaks at cable core strains well below the equivalent proof test strain level.

The relation between the time-to-failure and the applied stress for a proof tested fiber, Equation (16) can be used to provide a graphical aid for predicting service life. In Figure 8, failure time is plotted as a function of applied stress for three different proof stress levels. Such a diagram is called a life prediction diagram.[38]

Life prediction diagrams can be used in several ways: to predict the lifetimes under certain residual loads, or to specify the maximum allowable residual stress in an installed cable for a specific service life. In addition, if the residual load is constrained at some minimum value then the life prediction diagrams can be used to determine the proof stress which will assure adequate service life under the given conditions. The reliability of all these predictions, however, depends on, (1) conducting a proper proof test and (2) obtaining accurate values of the material parameters to use in Equation (16).

Sequence of Loading

The time-to-failure in static fatigue predicted by Equations (10) or (16) accounts for only a single applied stress level throughout the lifetime. As a practical matter, an optical fiber which is drawn, polymer coated, and proof tested will probably be subjected to a sequence of stress-time interval combinations representing cable construction, storage on a reel, installation in the field, and residual stresses in service. The analyses presented in previous sections do not consider the accumulation of damage (flaw growth) that can occur in each stage of sequential loading. The physical model to be considered is to start with an initial maximum size flaw a_p as established by the proof test stress σ_p and then let that flaw grow in an active environment under stress σ_i for time t_i where t_i is less than the static fatigue time-to-failure at σ_i. If the fiber eventually is placed in service under stress σ_a, what is the expected lifetime? The analytical solution to this problem simply involves following the flaw growth through each stress-time interval and leads to

$$t_{s(min)} = B\sigma_p^{n-2}\sigma_s^{-n} - \sigma_s^{-n}\sum_{i=1}^{m}\sigma_i^{n}t_i^{n} \qquad (17)$$

The first term on the right hand side of Equation (17) is the same as in Equation (16), i.e., a minimum time-to-failure based upon the proof test alone. The second term represents the further reduction in lifetime because of various stressing sequences. Since the second term is independent of the sequence of summation, the time-to-failure will depend upon the proof test stress, the final applied stress and the intermediate applied stress/time combinations but not on the sequence of the intermediate stress/time combinations.

Conclusions

1. Polymer-coated fused-silica optical fibers are susceptible to static fatigue and to dynamic fatigue, independent of the presence or type of coating.

2. Time-dependent fracture in fused-silica optical fibers can be described from a fracture mechanics viewpoint with crack growth rate being represented by a

power function of the stress intensity factor.

3. Dynamic fatigue and static fatigue of polymer-coated fused-silica fibers appear to be two manifestations of the same phenomenon, i.e., the stress-corrosion of glass following the mechanism proposed by Charles[11-13] and elaborated upon by Charles and Hillig.[14-15]

4. There is a strong correlation between the crack-growth parameters A and n for fused silica in the power function crack-growth law $v = AK_I^n$, independent of the test method or environment used for establishing A and n and of whether the glass has a polymer coating or not. This provides a convenient analytical tool for predicting failure times due to static fatigue.

5. The aging of polymer-coated fused-silica optical fibers in water under zero stress leads to a decrease in strength but no growth in flaw size during aging. The effect is thought to be due to the establishment of a high humidity environment at the crack tip which promotes rapid dynamic fatigue during subsequent testing.

6. Proof testing of optical fibers provides a guaranteed minimum fracture strength and minimum lifetime due to static fatigue. However, the complete stress-time interval history following the proof test must be considered in order to make a useful prediction of the service lifetime guaranteed by the proof test.

References

1. B. R. Lawn and T. R. Wilshaw, Fracture of Brittle Solids, Cambridge Univ. Press, Cambridge (1975) p. 160.

2. A. A. Griffith, Philos. Trans. Roy. Soc. London, A221 (1920) p. 163.

3. G. R. Irwin in Encyclopedia of Physics, Vol. 6 (1958) p. 55.

4. J. F. Knott: Fundamentals of Fracture Mechanics, Butterworth, London (1973).

5. D. Broek: Elementary Engineering Fracture Mechanics, Noordhoff Int. Publ., Leyden, (1974).

6. W. Weibull, "A Statistical Theory of the Strength of Materials," Proc. Royal Swedish Inst. for Eng. Research, #151 (1939).

7. S. M. Wiederhorn, J. Non-Cryst. Sol. 19, 169-191 (1975).

8. S. M. Wiederhorn in Fracture Mechanics of Ceramics Vol. 3, ed. R. C. Bradt et al (Plenum Press, N.Y.), 549-89 (1978).

9. R. Adams and P. W. McMillan, J. Mater. Sci., 12, 643-657 (1977).

10. E. K. Pavelchek and R. H. Doremus, J. Non-Cryst. Sol., 20, 305-321 (1976).

11. R. J. Charles, J. Appl. Phys. 29 (1) 1449-53 (1958).

12. R. J. Charles, J. Appl. Phys. 29 (1) 1554-60 (1958).

13. R. J. Charles, J. Appl. Phys. 29 (11) 1657-1662 (1958).

14. R. J. Charles and W. B. Hillig, in Symposium on the Mechanical Strength of Glass and Ways of Improving It. (Union Scientifique Continentale du Verre) paper II-3 (1961).

15. W. B. Hillig and R. J. Charles, in High Strength Materials ed. V. F. Zackay (Wiley, New York) pp. 682-701 (1965).

16. R. J. Charles, J. Non-Cryst. Solids 18, 273-74 (1974).

17. A. G. Evans, Int. J. Fract. 10(2) 251-259 (1974).

18. A. G. Evans and S. M. Wiederhorn, Int. J. Fract. 10(3)379-92 (1974).

19. D. Kalish and B. K. Tariyal, J. Amer. Ceram. Soc., 61(11-12), (1978) to be published.

20. Fracture Mechanics in Ceramics ed by R. C. Bradt et. al., (Plenum Press, NY), Vols. 1 and 2 (1974), Vols. 3 and 4 (1978).

21. S. M. Wiederhorn and L. H. Bolz, J. Amer. Ceram. Soc. 53(10) 543-548 (1970).

22. W. P. Minnear and R. C. Bradt, J. Amer. Ceram. Soc. 58(7-8), 345-346 (1975).

23. S. M. Wiederhorn, A. G. Evans and D. E. Roberts in Fracture Mechanics of Ceramics, Vol. 2 ed. R. C. Bradt, D. P. H. Hasselman and F. F. Lange (Plenum Press, New York), pp. 829-841, (1974).

24. B. A. Proctor, I. Whitney and J. W. Johnson, Proc. Roy, Soc., London, 297A, 534-557 (1967).

25. J. E. Ritter, Jr., J. M. Sullivan, and K. Jakus, "Applicability of Fracture Mechanics Theory to Failure Predictions

for Optical Glass Fibers," Paper 20-G-78 presented at American Ceramics Society 80th Annual meeting, Detroit, May 9, 1978.

26. B. K. Tariyal and D. Kalish, "Effect of Zero Stress Aging on the Strength of Optical Fibers," Proceedings of Conference on Physics of Fiber Optics, (Plenum Press, N.Y.) 1978, in press.

27. A. Fox, E. O. Fuchs and R. L. Key, Topical Meeting on Optical Fiber Transmission II, O.S.A. Williamsburg, Virginia, Technical Digest, paper TuA4, February, 1977.

28. T. T. Wang and H. M. Zupko, J. Mater. Sci. 13 (1978-in press).

29. R. S. McDonald, J. Phys. Chem., 62, 1168 (1958).

30. D. Kalish, P. L. Key, C. R. Kurkjian, B. K. Tariyal and T. T. Wang, Chapter 12 in Optical Fiber Communications, ed. by S. E. Miller and A. G. Chynoweth (Academic Press, New York), 1978 (in press).

31. Phoenix, S. L., Composite Materials Testing and Designm American Society for Testing and Materials, Philadelphia, Pa., 130 (1973).

32. McClintock, F. A., in Fracture Mechanics of Ceramics, Vol. 1, ed. R. C. Bradt et al (Plenum Press, New York) N.Y., p. 93 (1974).

33. Maurer, R. D., Appl. Phys. Letts., 27, 220 (1975).

34. Kurkjian, C. R., Proc. XI Intl. Congress on Glass, Prague, 469 (1977).

35. Kalish D., Tariyal, B. K. and Pickwick, R. O., Cer. Bull., 56, 491 (1977).

36. Tariyal, B. K. and Kalish, D., Mater Sci. Eng. 27, 69 (1977).

37. Wiederhorn, S. M., J. Amer. Ceram. Soc., 56, 226 (1973).

38. Evans, A. G. and Widerhorn, S. M., Int. J. Fract., 10, 379 (1974).

39. Ritter, J. E., Jr. and Meisel, J. A., J. Amer. Ceram. Soc., 59, 478 (1976).

40. Tariyal, B. K. and Kalish, D., Fracture Mechanics of Ceramics," Vol. 3, ed R. C. Bradt, D. P. H. Hasselman and F. F. Lange, Plenum Press, N.Y., 161 (1978 (1978).

41. Tariyal, B. K., Kalish, D. and Santana M. R., Ceram. Bull., 56, 204 (1977).

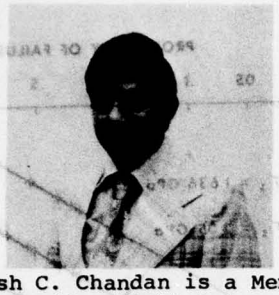
42. Evans, A. G. and Fuller, E. R., Mat. Sci. Eng., 19, 69 (1975).



David Kalish is Supervisor of the Metallurgical Engineering Group of Bell Labs in Norcross, Georgia, which he joined in 1971. He earned his S.B. (1960), S.M. (1964) and Sc.D. (1966) Degrees in Metallurgy from M.I.T. Dr. Kalish was at Man Labs Inc., Bambridge, Massachusetts from 1960-63 and 1966-68, and at the Lockheed-Georgia Company Research Lab from 1968-71. His current activities involve research and development of materials for communications wire and cable and associated joining apparatus. This effort includes studies on the manufacturing and physical behavior of optical fibers. Dr. Kalish is a Fellow of ASM and a member of AIME and the Wire Association.



Basant K. Tariyal is a member of the Materials Engineering and Chemistry Department at Bell Labs, Norcross, Georgia. He received his B.S. in physics, chemistry and mathematics from Lucknow University, India, in 1960, his Bachelor of Technology degree in metallurgical engineering from Indian Institute of Technology in 1964, and his M.S. in 1967 and Ph.D. in 1969, both in materials science from the University of Toronto. With Bell Labs since 1970, Dr. Tariyal is working on the effects of materials and processing variables on the mecahnical and optical properties of optical fibers. Dr. Tariyal is a member of Amer. Ceram. Soc., ASM and AIME.



Harish C. Chandan is a Member of Technical Staff at Bell Labs, Norcross, Georgia which he joined in 1977. A graduate of the Indian Institute of Technology, Kanpur, he received a B. Tech. in 1969 and an M. Tech. in 1971, both in metallurgy. Dr. Chandan earned an M.S. from Syracuse in 1974 and a Ph.D from Penn State in 1978. He is currently working on the mechanical properties of optical fibers. He is a member of the Amer. Ceram. Soc. and ASM.

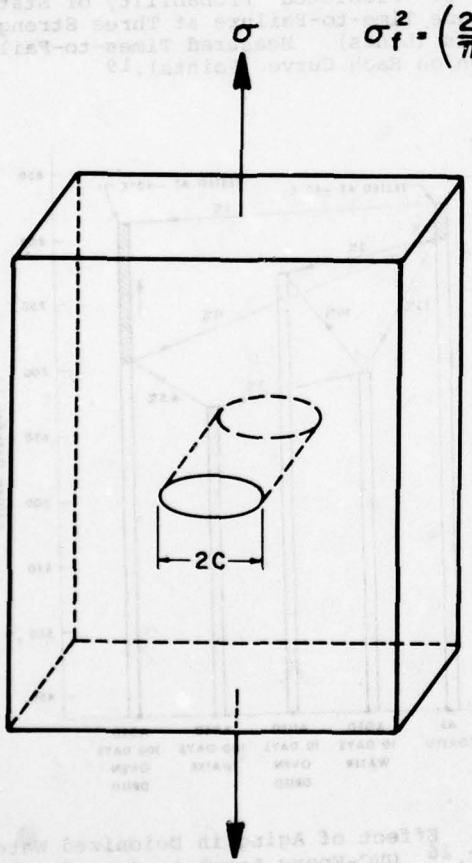


Fig. 1. Griffith Model[2] for Brittle Fracture in Glass Initiating at Pre-existing Elliptical Flaw of Length 2C.

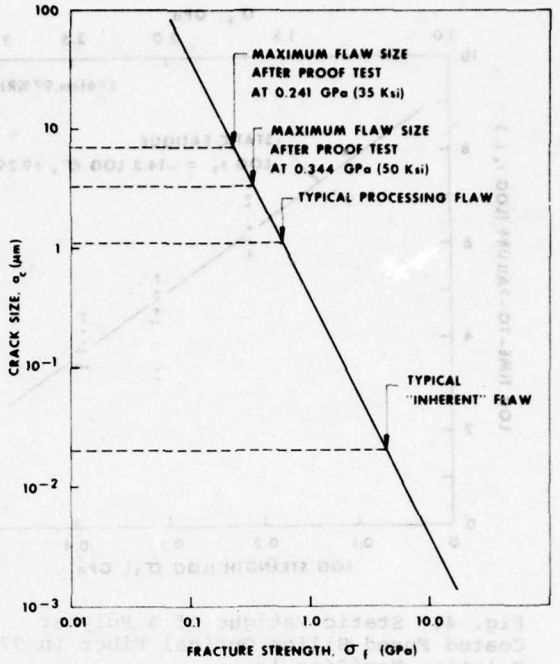


Fig. 2. Flaw Size Versus Fracture Strength Relationship Based Upon Fracture Mechanics Model of Part Through Semi-circular Surface Flaw Normal to the Axis of a Fused Silica Fiber.

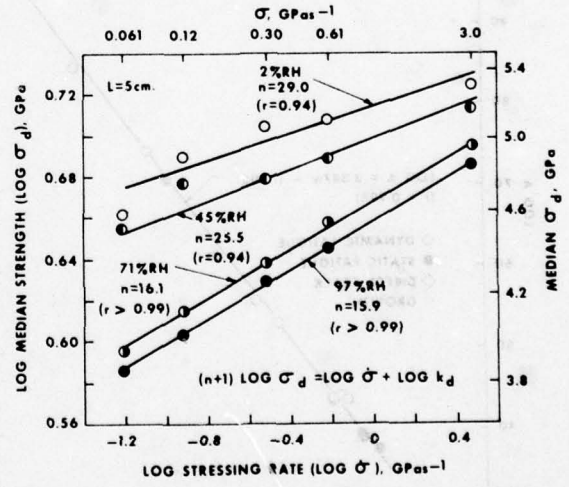


Fig. 3. Effect of Relative Humidity on Dynamic Fatigue of a Polymer Coated Fused Silica Optical Fiber. Linear Regression Correlation Coefficient = r.[19]

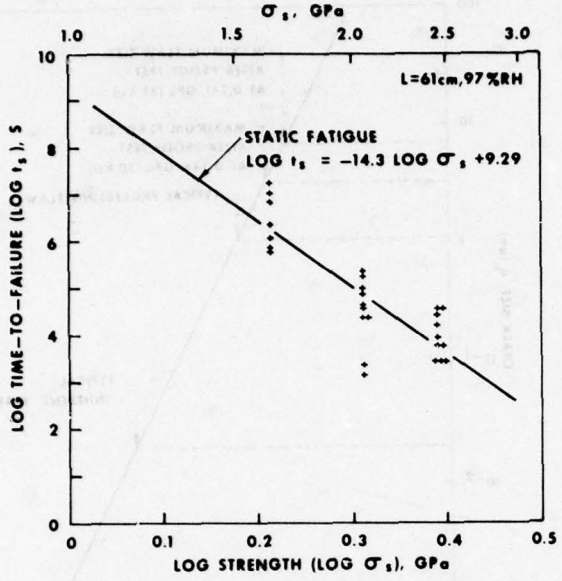


Fig. 4. Static Fatigue of a Polymer Coated Fused Silica Optical Fiber in 97% Relative Humidity.[19]

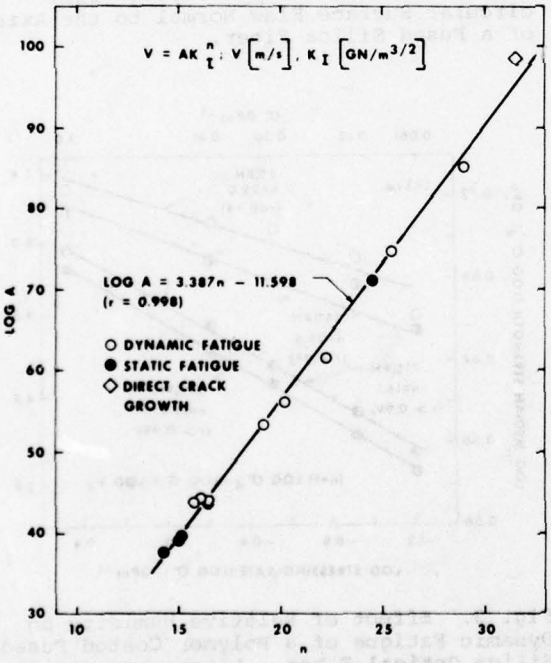


Fig. 6. Correlation Between Crack Growth Parameters n and A for Fused Silica.

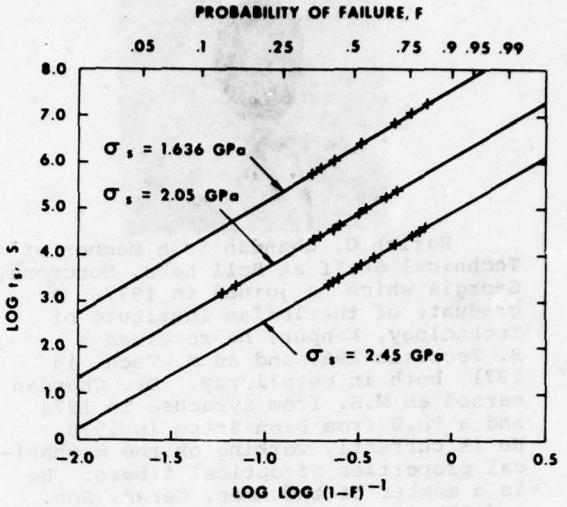


Fig. 5. Predicted Probability of Static Fatigue Time-to-Failure at Three Strength Levels (Lines). Measured Times-to-Failure Shown on Each Curve (Points).[19]

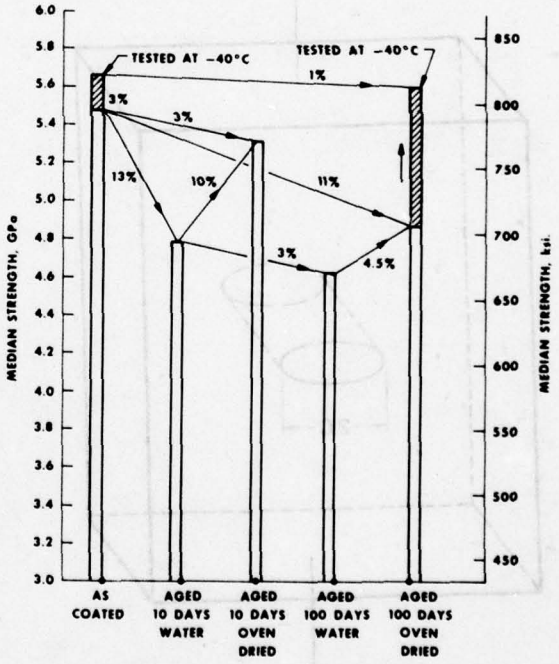


Fig. 7. Effect of Aging in Deionized Water at 23°C.[26] UVC-Epoxy Acrylate Coated Fiber Furnace Drawn and Aged (Gage Length = .05m, Strain Rate = .04S^{-1}, 50 Replicate Tests).

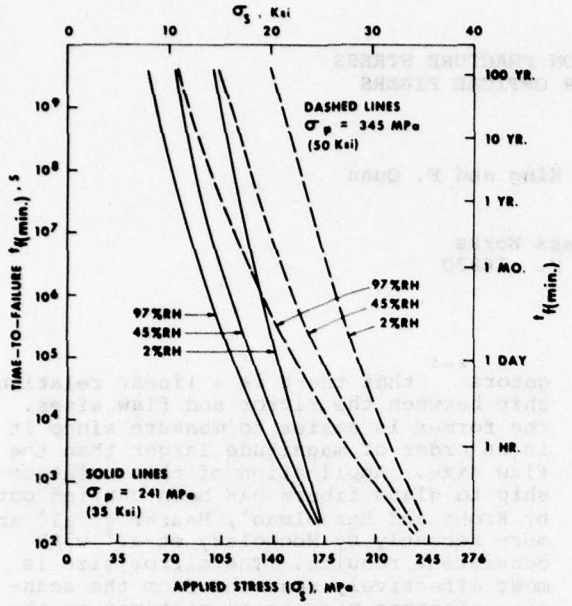


Fig. 8. Calculated Minimum Time-to-Failure (t_{fm}) versus Constant Applied Stress (σ) for Polymer Coated Fused Silica Optical Fibers Loaded in Very High (~97%), Ambient (~45%) and Very Low (~2%) Relative Humidities.

TABLE 1

Summary of Results of Stress Rate Tests for Fused Silica Fiber

Relative Humidity	n	$\log k_s$	Correlation Coefficient	logA
2%	29.0	19.96	0.94	85.03
45%	25.5	17.04	0.94	74.11
71%	16.1	10.18	>0.99	44.26
97%	15.9	9.87	>0.99	43.75

NOTES:

1. Using median strengths on 5cm gage length specimens.
2. k_s from $\log k_d = \log k_s + \log(n+1)$.
3. For stress in GPa and time in seconds.

TABLE 2

Comparison of Predicted Static Fatigue Strengths Based Upon Dynamic Fatigue Measurements and Static Fatigue Measurements*

Failure Time (t_s)	Predicted Static Fatigue Strength, σ_s From Measurements of: Static Fatigue	Dynamic Fatigue
1 month	1.58 GPa	1.52 GPa
1 year	1.33	1.23
10 years	1.14	1.12

*Coated Fused Silica Optical Fiber in 97% RH, 61cm gage length.

TABLE 3

Summary of Crack Growth Parameters* for Fused Silica

Type of Measurement	Type of Specimen	Environment	Gage Length cm	σ_{Ic} GPa	n	log A	Ref.
Dynamic Fatigue	Coated Optical Fiber	97%RH	5	6.76	15.87	43.750	19
Dynamic Fatigue	Coated Optical Fiber	71%RH	5	6.76	16.08	44.257	19
Dynamic Fatigue	Coated Optical Fiber	Ambient	5	6.76	25.47	74.621	19
Dynamic Fatigue	Coated Optical Fiber	2%RH	5	6.76	29.01	85.031	19
Static Fatigue	Coated Optical Fiber	97%RH	61	6.16	14.29	37.566	19
Direct Crack Growth	Bulk Sheet Uncoated	Water	-	-	31.56	98.279	23
Static Fatigue	Uncoated Silica Fiber	Ambient	~10	7.52	20.24	56.004	24
Dynamic Fatigue	Coated Optical Fiber	55%RH	30	5.67	22.23	61.493	25
Dynamic Fatigue	Coated Optical Fiber	97%RH	5	5.43	19.18	53.195	
Static Fatigue	Coated Optical Fiber	97%RH	61	5.65	15.19	39.618	
Dynamic Fatigue	Coated Optical Fiber	97%RH	5	5.29	16.54	44.153	
Dynamic Fatigue	Coated Optical Fiber	Ambient	5	5.29	16.53	43.807	
Static Fatigue	Coated Optical Fiber	Ambient	5	5.29	24.55	71.044	
Static Fatigue	Coated Optical Fiber	97%RH	61	5.17	15.05	39.327	

*σ in GPa, K_I in $GNm^{-3/2}$, V in ms^{-1}, t in s

SOME RECENT RESULTS ON FRACTURE STRESS AND MIRROR SIZE FOR OPTICAL FIBERS

S. T. Gulati, C. B. King and F. Quan

Corning Glass Works
Corning, N. Y. 14830

This paper presents some recent data on the strength and the corresponding fracture mirror size of optical fibers. The cladding glass compositions considered are: borosilicate glass with 15 ~ 20% B_2O_3, 96% silica glass and 100% silica glass. The data confirms the constancy of the product of fracture stress and the square root of mirror radius. The latter can be conveniently measured with the aid of an optical microscope and provides an efficient, reliable way for the fiber user to access the fracture stress.

Introduction

This paper presents some recent data on the strength and the corresponding mirror size of optical fibers with three different cladding compositions. The cable manufacturers and other fiber users are often interested in assessing the stress at which fiber fails, particularly during handling and the cable manufacturing process. The technique described here uses an optical microscope and should enable the fiber user to analyze the failures quickly and reliably. The three cladding glass compositions considered in this work are (i) borosilicate glass with 15 ~ 20 per cent B_2O_3 or the OVPO (outside vapor phase oxidation) fiber (ii) 96 per cent silica glass, or the IVPO (inside vapor phase oxidation) fiber and (iii) 100 per cent silica glass fiber (Suprasil II). Earlier data on strength vs mirror size for the OVPO fiber with < 15% B_2O_3 in the cladding glass and for the silica fiber were reported by Maurer et al[1] in 1974.

It is well known that the fracture stress is related to the flaw size. However, if the flaw size is very small as is commonly the case for high strength fibers, an accurate measurement of its size to determine the failure stress can be difficult. Fortunately, it has been shown empirically by previous investigators[2-5] that there is a linear relationship between the mirror and flaw sizes. The former is easier to measure since it is an order of magnitude larger than the flaw size. Application of this relationship to glass fibers has been carried out by Krohn and Hasselman[6], Maurer et al[1] and more recently by Mecholsky et al[7] with consistent results. The mirror size is most effectively measured from the scanning electron microscope pictures of the fracture surfaces but can also be approximated with the aid of a good optical microscope with a filar eyepiece.

In addition to the fracture stress, the mirror size is also a function of the glass composition. In the case of the graded-index optical fibers, composition varies continuously in the core and is relatively constant in the cladding. Thus, if the mirror extends to the core region as in the case of weak fibers it becomes difficult to assess the fracture stress accurately since the appropriate constants for the core glass are not available. This is one limitation of the method under discussion.

Analysis

The mirror is the flat, smooth region of the fracture surface with the original flaw near its center.[4] It is surrounded by a region of small radial ridges called the mist. The mist region is surrounded by a region of larger radial ridges called the hackle. Finally, the hackle region is surrounded by the macroscopic crack branching. The four regions[3] of a typical fracture surface are shown in Fig. 1, in which "a" and "r" denote the flaw and mirror sizes respectively. A photomicrograph of the actual fracture surface of 100% silica fiber appears in Fig. 2 and shows the various regions including the mirror. Previous investigators[4] have

* Kpsi = 1000 psi

shown that the product of the fracture stress (or strength) and the square root of the distance from the origin to the onset of mist (or the mirror radius) is constant in most silicate glasses. Mathematically,

$$\sigma_f = \frac{A}{\sqrt{r}} \quad , \qquad (1)$$

where σ_f is the fracture stress and A is the mirror constant for the particular glass and is a function of glass composition.

In their recent work on silica fibers, Mecholsky et al[7] were able to distinguish between the inner mirror (mirror-mist boundary) and the outer mirror (mist-hackle boundary) and observed that the mirror to flaw size ratio was 12.5 for the inner mirror and 16.7 for the outer mirror. Their stress computations based on the inner mirror were in good agreement with those of Maurer et al.[1] It should be pointed out, however, that unless extreme care is taken, it is difficult to distinguish between the inner and outer mirror boundaries. In the present work the average mirror size was used for computing the fracture stress.

The mirror constant A has been reported by Kerper and Scuderi[5] for different glass compositions including the three mentioned earlier. These values were determined from flexure tests on relatively large specimens. In the present work the mirror constant was determined by carrying out the regression analysis of the tensile strength vs mirror size data for the actual fibers. Any discrepancies in the A values determined here and those of Ref. 5 are attributed to mode of testing, specimen size and the differences in glass composition (notably the OVPO fiber which has a somewhat different composition than the borosilicate glass, Corning Code 7740, considered by Kerper and Scuderi).

Results and Discussion

The fracture surfaces of approximately 20 fibers, 125 μm in diameter, in each of the three categories were examined under the scanning electron microscope. The mirror radius was measured from the SEM pictures and the corresponding fracture strength at 20m gage length was measured by the rapid fiber tensile tester[8] at a strain rate of 0.04/min. This data is plotted on a log-log paper in Figs. 3 through 5 with stress along the X-axis and mirror radius (in μm) along the Y-axis. The dotted line through the data is based on the mirror constant given by Kerper and Scuderi[5] while the solid line is based on the regression analysis of the fiber data. The values of mirror constant A as given by Kerper and Scuderi[5] and by the fiber data are compared in Table 1.

Table 1 Mirror Constant A
(Kpsi $\mu m^{1/2}$)

Glass Composition	Kerper & Scuderi[5]	Present Work
Borosilicate	287	268
96% Silica	266	270
Suprasil II	275	285

The agreement is good, particularly for 96 per cent silica and Suprasil II glasses. The considerable deviation in the case of borosilicate glass reflects the substantial differences in the composition of Corning Code 7740 glass and the OVPO cladding glass. It is believed, however, that the constant based on actual fiber data is a better estimate for assessing the fracture stress for optical fibers. It is interesting to note in Fig. 3 that for $r > 40$ μm the data deviates considerably from the straight line indicating that the mirror has extended into the variable-composition-core area for which A is not known. If the composition of the cladding glass is not known, an average value of 274 for A should be used to estimate the fracture stress.

The above discussion pertains to fibers which fail from a uniform tensile stress. The fiber may also fail during handling and the cable manufacturing process from a bending stress which is nonuniform across the fiber cross-section. The relation between mirror size and the fracture stress in such a situation is more complex than eqn. (1) and will not be covered here.

Conclusions

Recent data on optical fibers confirm the constancy of the product of fracture stress and the square root of mirror radius. The mirror constant A is in good agreement with the previously published values, notably for 96 per cent and 100 per cent silica glasses. The assessment of fracture stress from the measured mirror size is an efficient, reliable and a useful technique, notably for cable manufacturers and other fiber users.

References

(1) R. D. Maurer, R. A. Miller, D. D. Smith and J. C. Trondsen, "Optimization of Optical Wave Guides - Strength Studies", Final Technical Rept. on ONR Contract No. N00014-73-C-0293, March, 1974.

(2) E. B. Shand, "Breaking Stress of Glass Determined from Dimensions of Fracture Mirrors", J. Am. Ceram. Soc., Vol. 42, pp. 474-478 (1959).

(3) J. W. Johnson and D. G. Holloway, "On the Shape and Size of the Fracture Zones on Glass Fracture Surfaces", Phil. Mag., Vol. 14, pp. 731-743 (1966).

(4) J. J. Mecholsky, R. W. Rice and S. W. Freiman, "Prediction of Fracture Energy and Flaw Size in Glasses from Measurements of Mirror Size", J. Am. Ceram. Soc., Vol. 57, No. 10; pp. 440-443 (1974).

(5) M. J. Kerper and T. G. Scuderi, "Modulus of Rupture in Relation to Fracture Pattern", Ceramic Bull., Vol. 43, No. 9; pp. 622-625 (1964).

(6) D. A. Krohn and D. P. H. Hasselman, "Relation of Flaw Size to Mirror in the Fracture of Glass", J. Am. Ceram. Soc., Vol. 54, No 8; p. 411 (1971).

(7) J. J. Mecholsky, S. W. Freiman and S. M. Morey, "Fractographic Analysis of Optical Fibers", Ceramic Bull, Vol. 56, No. 11; pp. 1016-1077 (1977).

(8) Ben Justice and Suresh Gulati, "Tensile Tester for Long Optical Fibers", Ceramic Bull. Feb., 1978.

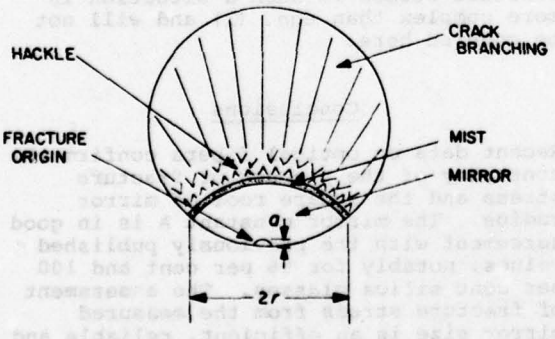


Fig. 1 Fracture Surface Showing Different Regions



Fig. 2 Photomicrograph of Fracture Surface of 100% Silica Fiber

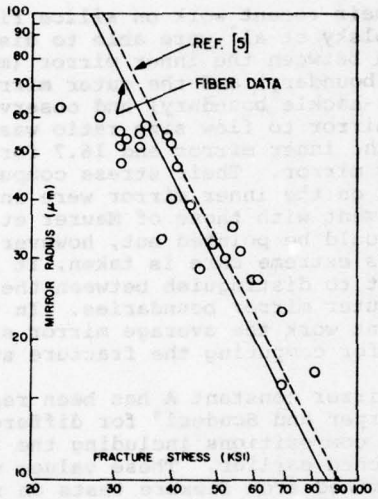


Fig. 3 Mirror Radius vs. Fracture Stress; OVPO Fiber

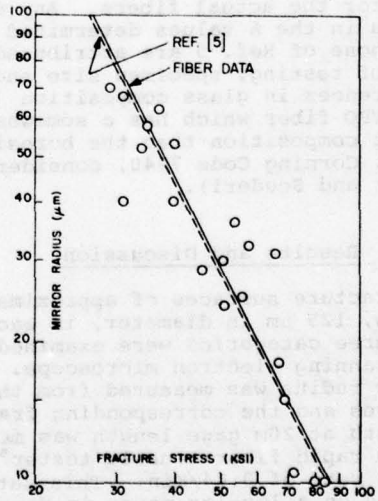


Fig. 4 Mirror Radius vs. Fracture Stress; IVPO Fiber

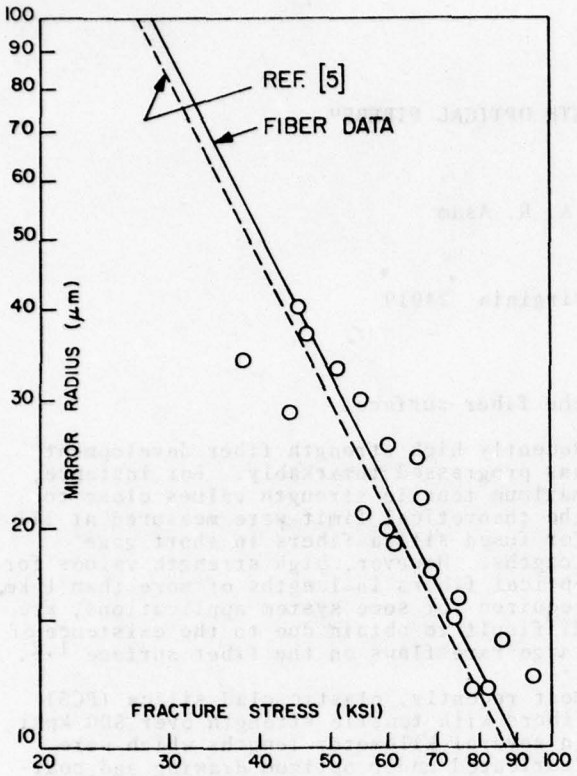


Fig. 5 Mirror Radius vs. Fracture Stress; Suprasil II Fiber



Charles B. King is a senior associate in process development at Corning. He graduated from Oberlin College with a B.S. in chemistry in 1937 and a Ph.D. in physical chemistry in 1940 from the Massachusetts Institute of Technology. Dr. King is primarily interested in glass strength problems and has been associated with glass tableware, glass cookingware, radomes, windshields, memory discs, and more recently optical fibers.



Suresh Gulati is a research supervisor in the Physical Properties Research Dept. at the Corning Glass Works, Corning, NY, 14830. He received a B.S. in mechanical engineering in 1957 from the University of Bombay, India, an M.S. from Illinois Institute of Technology in 1959 and a Ph.D. in mechanics from the University of Colorado in 1966. Dr. Gulati's research interests include thermal, mechanical and rheological properties, stress analysis and fracture mechanics.



Frederic J-Y Quan is a senior applications development engineer for the Telecommunication Products Department at Corning. He received his B.S.E.E. in 1969 from the Polytechnic Institute of Brooklyn and an M.B.A. in finance and marketing from Adelphi University in 1974. Prior to his work at Corning, he has been associated with the R & D programs at the Electronics Command at Ft. Monmouth and at Hazeltine Corp. in Greenlawn, NY. His present interests include new applications for optical waveguides and related transitional problems in applying the technology from the lab to practical use.

"LONG LENGTH, HIGH STRENGTH OPTICAL FIBERS"

M. S. Maklad and A. R. Asam

ITT EOPD - Roanoke, Virginia 24019

Low loss and low dispersion graded index fibers have been fabricated in multi-kilometer length. Fiber lengths more than 5 km each have passed proof testing at 150 kpsi without mechanical failure. Improvements in fiber strength have been related to superior quality of substrate material, fiber drawing temperature and fabrication environments. Characteristics of optical fibers such as optical transmission, pulse dispersion, numerical aperture, static fatique and dynamic strength will be discussed.

INTRODUCTION

The long length tensile strength of low loss optical fibers is an important parameter which determines stress levels allowed along the fiber length during cabling and under service environment. Long length high strength low loss fiber development is needed to achieve high production yield as well as to meet some systems strength requirements.

In glass optical fibers, the minimum tensile strength is determined by the existence of stress concentration at flaw tips on the fiber surface. Under tensile loading, the stress at the flaw tip reaches a much higher value over that of the externally applied stress due to the leverage introduced by the flaw geometry. Failure takes place when the stresses reach the theoretical limit for the Si-O bond which is about 2×10^6 psi. Furthermore, in the presence of moisture, the flaws over the fiber surface would enlarge at a stress level well below that of the Si-O bond strength. This effect is known as static fatigue or stress corrosion.

In order to improve the tensile strength of the optical fibers, it is important to develop flaw free preform and fiber surfaces, to maintain the pristine surface quality by providing a low abrasion coating for mechanical protection, and to reduce or prevent moisture from reaching the fiber surface.

Recently high strength fiber development has progressed remarkably. For instance, maximum tensile strength values close to the theoretical limit were measured at ITT for fused silica fibers in short gage lengths. However, high strength values for optical fibers in lengths of more than 1 km, required for some system applications, are difficult to obtain due to the existence of large rare flaws on the fiber surface [1,2].

Most recently, plastic clad silica (PCS) fibers with tensile strength over 500 kpsi in several kilometer lengths which were fabricated under optimum drawing and coating conditions have been reported [3,4]. However, few data are available on the strength of long CVD fibers. The strength of CVD fibers depends on the preform fabrication parameters including substrate quality.

This paper describes the fabrication technique for 3 - 11 km long CVD fibers and also discusses the optical and mechanical performance characteristics of these fibers.

EXPERIMENTAL PROCEDURES

CVD preforms ranging from 40 cm to 110 cm

1. Metcalfe, A.G. and G.K. Schmitz. "Effect of Length on the Strength of Glass Fibers," ASTM Proc. 64: 1075-1093 (1964).
2. Justice, B. and S. Gulati. "Tensile Testor for Long Optical Fibers," Bull. Amer. Ceram. Soc. 57 (2) 217-219 (1978).
3. Miller, T.J. and A.C. Hart. "Silicone-Coated Fused Silica Fibers with Tensile Strength >3.5 GN/m^2 (500 kpsi) in >1 km Gage Lengths," presented at the annual meeting of Amer. Ceram. Soc., Detroit, Michigan (May 1978).
4. DeMarcello, F.V., A.C. Hart, Jr., J.C. Williams and C.R. Kurkjiaan. "Effect of Drawing Conditions on the Strength of Silica Fibers," ibid.

in length and a diameter of 1.3 cm were fabricated by chemical vapor deposition of cladding and core materials inside a high purity synthetic or natural fused quartz tube and by collapsing the composite tube into a solid preform. The CVD preforms were polished with a CO_2 laser beam prior to fiber drawing in order to improve the preform surface quality by removing surface flaws. The optimum parameters of CO_2 laser polishing have been established [5]. The preforms were drawn into fibers in a clean environment with an O_2/H_2 torch. As CO_2 laser drawing is limited to small diameter preforms [6], the CO_2 laser heat source could not be employed to draw long length fibers from large diameter CVD preforms.

Fiber drawing and the application of protective coatings of silicone and Hytrel^R were performed in an on-line operation in order to reduce degradation of the pristine fiber strength. A high drawing temperature was selected to minimize the drawing tension. The fiber was drawn in a clean environment, and coating parameters and techniques were optimized to achieve high coating concentricity, to properly cure coating materials and to minimize mechanical abrasion of the fiber during coating.

The proof test was performed either on-line or off-line. The method and procedures of proof testing were described elsewhere [7]. Static fatigue tests were performed on short gauge length samples by winding the fiber over a series of mandrels of different sizes, which simulate different tensile strength loads. Time for the first failure to appear on the fiber was recorded and plotted as a function of stress. The fibers were then evaluated for optical loss, pulse dispersion and numerical aperture.

RESULTS AND DISCUSSION

The lengths of fibers drawn from 13 mm diameter and 40 - 110 cm long preforms varied from 4.5 km to 11 km. The low attenuation losses of 3.8 dB/km @ 0.85 μ and low pulse dispersion of <1ns/km were measured in long length graded index fibers and are shown in Table 1.

Two types of silica substrates, synthetic silica suprasil 2 and natural fused silica TO8FB, were used for this investigation. The effects of substrate quality such as impurity and/or inclusion content on long length strength of CVD fibers have been evaluated by proof testing the entire fiber length to a specified tensile stress. The results of proof tested fibers are listed in Table 2, which shows the low failure probability of CVD fibers produced with suprasil substrate tubing and have demonstrated the importance of using a high quality substrate material for the fabrication of high strength fibers.

Dynamic strength testing was performed on 2 meter gauge lengths of CVD fibers. The probability of failure as a function of stress is shown in Figure 1. All points fall on a straight line with a slope m = 36, indicating the absence of large flaws and the high strength of CVD fibers. However, the existence of rare large flaws was detected by proof testing the entire fiber length at 100 kpsi and 150 kpsi levels.

Figure 2 shows a Weibull plot of a PCS fiber tested in 2 m gauge length. Also shown in the graph are the probabilities of failure of long length CVD fibers produced from natural (FB) fused silica and synthetic silica substrates (SS-2). The probability of failure of long length fiber was calculated from proof test data. From Figure 2, it can be seen that fibers drawn from preforms fabricated using synthetic silica substrates, which are relatively free of stress concentrators such as bubbles, inclusions and other impurities, exhibit lower probability of failure as compared to those drawn from natural fused silica substrate preforms [8]. Plastic clad synthetic silica fibers show an even lower probability of failure.

The differences of long length strengths for these fibers are attributable to the surface and bulk qualities of preforms prior to drawing. In the case of the PCS fiber, the quality of the synthetic silica rod is high. In the case of the CVD fiber, the quality of the preform depends on the substrate tube. The synthetic silica substrate tube is made by core-drilling, surface polishing and drawing to the final substrate dimensions. This technique causes deterioration of the original quality of the synthetic silica. In addition, the

5. Schlef, C.L., S.M. Oh, and A.R. Asam. "Characterization of CO_2 Laser Polished Glass Surface," to be published.

6. Saifi, M.A. "Limitation in CO_2 Laser Fiber Drawing," presented at the Topical Meeting on Optical Fiber Transmission II, Williamsburg, Virginia (February 1977).

7. Kao, C., M. Maklad, J.E. Goell. "Testing of Tensile Strength of Optical Fiber Waveguides," ibid.

8. Mecholsky, J.J., S.W. Freiman and S.M. Morey. "Fractographic Analysis of Optical Fibers," Bull. Amer. Ceram. Soc. 56 (II) 1016-1017 (1977).

process involved in fabricating a CVD preform could introduce some additional surface contamination.

Static fatique mandrel tests showing the time to failure for CVD fibers at different stresses is illustrated in Figure 3. The n value was calculated from Figure 3 and was found to be 20. Therefore, CVD fibers which are free of large and rare surface flaws when subjected to a 100 kpsi service load are expected to last indefinitely, even in the presence of moisture.

CONCLUSIONS

Long length, high strength CVD fibers with low loss and low dispersion were fabricated in 3 - 11 km lengths with proof test stresses ranging from 100 kpsi to 150 kpsi by controlling the synthetic silica substrate quality, preform processing environment, CVD preform surface treatment, drawing conditions and environment, coating materials and coating technique.

ACKNOWLEDGEMENT

The writers thank P. Oh, C. Schlef, P. Pureza and R. Spencer for performing fiber drawing and mechanical testings.

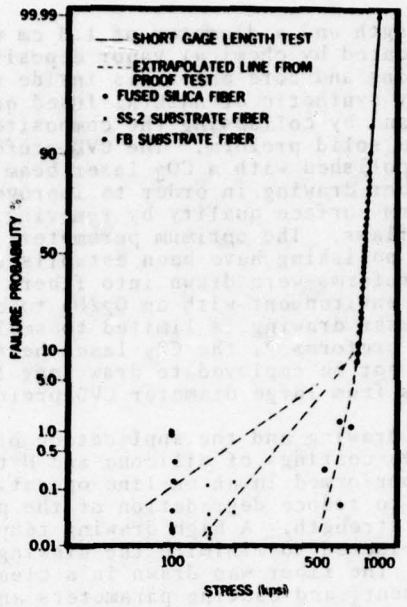


Figure 2. Effect of Silica Substrate Quality on the Long Length Strength of Optical Fibers.

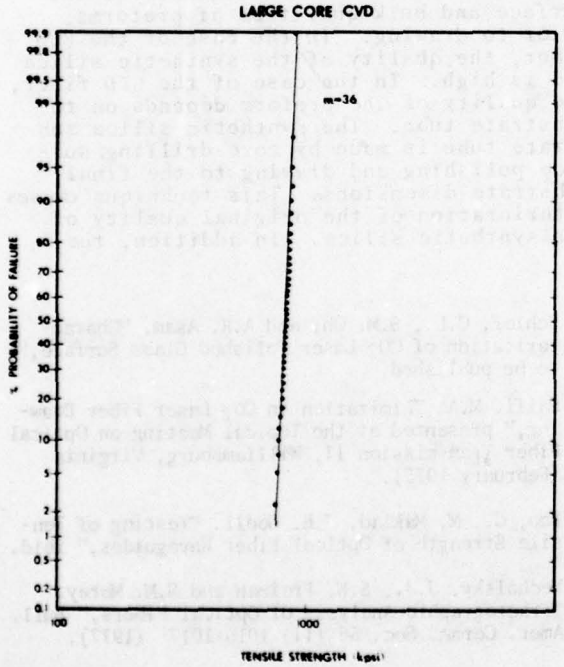


Figure 1. Dynamic Strength Test Results of CVD Fiber (2 m Gauge Length).

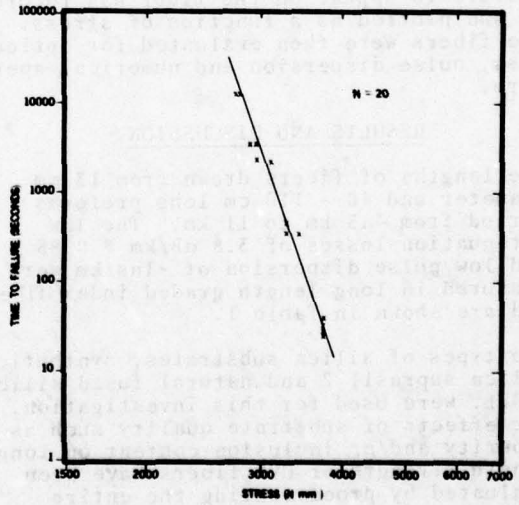


Figure 3. Mandrel Test Results of the CVD Fibers Static Fatigue.

TABLE 1. OPTICAL EVALUATION DATA

SUBSTRATE MATERIAL	FIBER LENGTH (m)	NA	DISPERSION (ns/km)	LOSS (dB/km @ 0.85 μm)
FB	5353	0.26	0.66	4.02
FB	5076	0.23	0.81	4.38
FB	5430	0.28	-	4.19
FB	5252	0.23	1.10	3.79
SS-2	4368	0.27	0.63	3.93
SS-2	4307	0.24	0.95	3.68
SS-2	4432	0.25	0.67	4.15
SS-2	5404	0.25	1.08	4.40
SS-2	11020	0.24	0.68	4.05 (@ 0.87 μm)
SS-2	8320	0.23	0.47	2.98 (@ 1.05 μm)
SS-2	9340	0.22	3.32	2.57 (@ 1.05 μm)

TABLE 2. PROOF TEST RESULTS

SUBSTRATE MATERIAL	P. T. STRESS (kpsi)	PASS/FALL RATIO
SS-2	150 - 200	0.44
FB	100	0.2

A SINGLE FIBER ALIGNMENT SYSTEM

L. M. Borsuk
ITT Cannon Electric
Santa Ana, California

and

M. Pomerantz
US Army CORADCOM
Fort Monmouth, New Jersey

ABSTRACT

With the increasing use of fiber optics for data communication, it has become apparent that there is an urgent need for field usable interconnection hardware for single fibers. This hardware must be simple to terminate and must provide efficient optical power transmission, or low coupling losses. One requirement for such hardware is the Army's need for a six-channel hermaphroditic connector in its tactical fiber optic communications systems. This paper describes a new single fiber alignment concept, developed under U.S. Army Communications Research and Development Command contract with ITT Cannon Electric, that accomplishes these requirements.

The alignment concept is based upon the use of three precision spheres arranged in a plane nesting together at 120° increments. At the geometric center of the spheres is an interstitial space to retain the fiber. This assembly (or ferrule) is mated to an opposing identical ferrule by causing the spheres of each to nest together at 60° increments. The fibers thereby are aligned coaxially.

Concept, required accuracies for efficient coupling, design features, and performance data are described on the following pages.

INTRODUCTION

A major barrier for implementation of Army fiber optic communications systems is the absence of a reliable, rugged, outdoor environment resistant connector having low coupling loss. The connector is needed in one-kilometer length cable assemblies containing six individual optical fiber channels. For the long haul time division multiplexed (TDM) system, high bandwidth graded index multimode fibers will be employed for the transmission of digital data at rates up to 20 megabits per second for distances of eight kilometers without repeaters. System loss constraints dictate that cable-to-cable coupling loss through the mating connectors must be under 1.0 dB repeatedly, on an optical channel-to-channel basis. Other desired features are hermaphroditic design (identical connectors mate with each other), protection of fiber mating surfaces, ease of cleaning, ease of assembly, simplicity of design, low cost and compactness. Although all these features are important, the driving objective is the 1.0 dB coupling loss. One of two techniques is generally used for fiber coupling in the design of separable connectors. The first is direct fiber-to-fiber alignment and the second is the interposition of a lens system between the two fibers. With the exception of one particular lens design approach, which, however, does not appear to lend itself to a hermaphroditic connector configuration, the most efficient coupling achieved to date by various vendors has been with direct fiber-to-fiber alignment approaches. This paper deals with one such approach currently being investigated by ITT Cannon Electric under contract with the U.S. Army Communications Research and Development Command (CORADCOM).

DESIGN REQUIREMENTS

Accuracy of alignment of opposing/mating fibers is the key feature of a fiber optic separable connector that determines the efficiency of coupling optical energy. The coupling loss is comprised of both intrinsic and extrinsic losses:

- Intrinsic are those associated with fiber characteristics (i.e., diameter variation, NA variation, Fresnel reflection, etc.).
- Extrinsic are losses associated with the connector hardware, the accuracy of alignment provided.

In order to establish the extrinsic design requirements, an analysis first was made of the three major misalignment loss mechanisms. They are lateral, gap and angular. By physically varying the alignment of bare fibers and measuring the

coupling loss, the analysis was verified emperically.

LATERAL LOSS is due to deviation from optimum coaxial alignment of the mating fibers. Figure 1 defines coupling loss in dB as a function of misalignment to core diameter ratio.

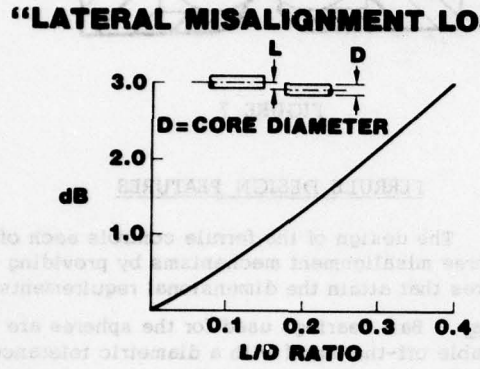


FIGURE 1

GAP LOSS is due to the separation between end faces of mating fibers and is a function of numerical aperture as well as separation distance. Figure 2 defines gap loss in dB.

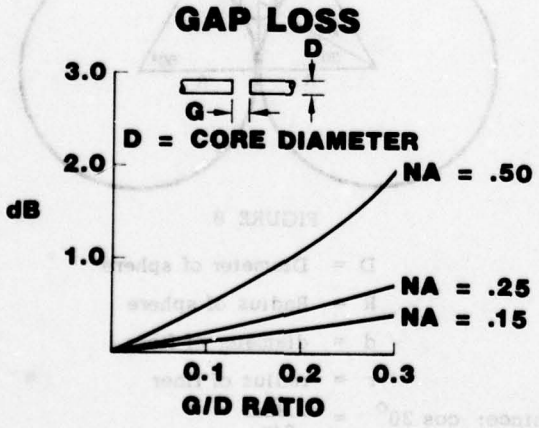


FIGURE 2

ANGULAR LOSS, as shown in Figure 3, is also a function of numerical aperture.

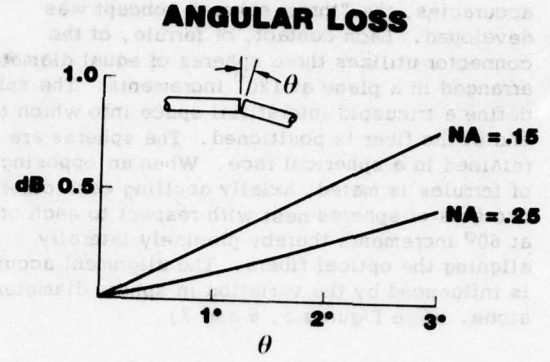


FIGURE 3

Each of these foregoing losses, both intrinsic and extrinsic, assume uniform distribution of optical energy over all modes. Each is independent of the other; therefore, all must be added to calculate a fiber-to-fiber termination coupling loss.

In order to determine the dimensional alignment requirements, the fiber and system parameters must be considered. A long length telecommunication link will use small diameter single fiber. This connector concept is designed to provide a *less than 1 dB coupling loss* (79.4% coupling efficiency) when terminating a 125 micron (0.00492 inch) diameter fiber. The optical core diameter is 85 microns (0.0033 inch) with an 0.18 NA.

Using the loss misalignment curves involves a budgeting of the 1 dB to each parameter based upon achievable dimensional control of the connector components. The following chart lists the accuracies which must be held considering manufacturing tolerances to achieve a < 1 dB fiber-to-fiber interconnection.

Misalignment	Accuracy	dB
Lateral	< 0.00018 inch	0.3
Gap	< 0.00020 inch	0.2
Angular	< 1/4 degree	0.1
	Total extrinsic	0.6
	Fresnel loss	0.32
		0.92

FIGURE 4

ALIGNMENT CONCEPT

In order to achieve the above dimensional accuracies, the "three-sphere" concept was developed. Each contact, or ferrule, of the connector utilizes three spheres of equal diameter arranged in a plane at 120° increments. The spheres define a tricuspid interstitial space into which the end of the fiber is positioned. The spheres are retained in a spherical race. When an opposing pair of ferrules is mated, axially abutting each other, the two sets of spheres nest with respect to each other at 60° increments thereby precisely laterally aligning the optical fibers. The alignment accuracy is influenced by the variation in sphere diameter alone. (See Figures 5, 6 and 7)

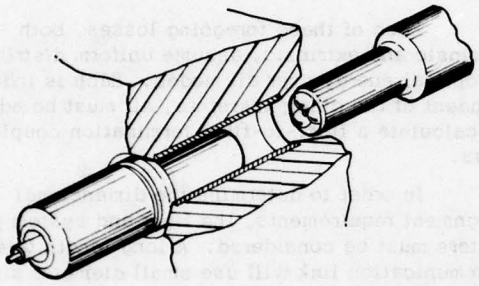


FIGURE 5

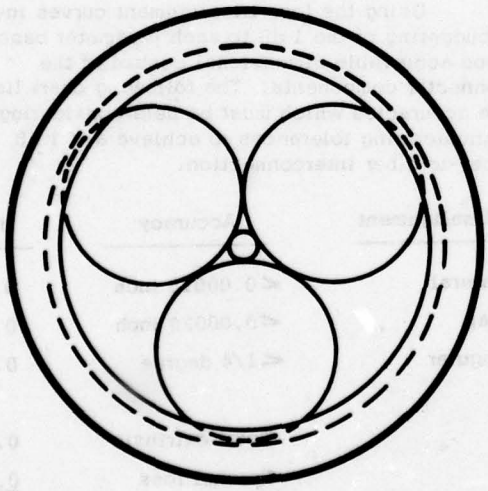


FIGURE 6

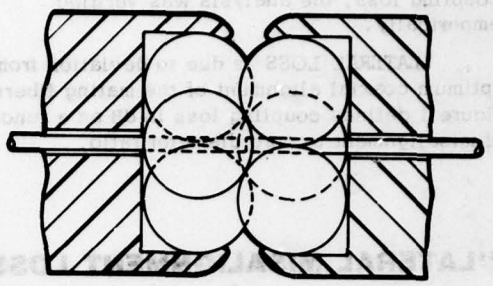


FIGURE 7

FERRULE DESIGN FEATURES

The design of the ferrule controls each of the three misalignment mechanisms by providing features that attain the dimensional requirements.

Lateral - Ball bearings used for the spheres are available off-the-shelf with a diametric tolerance of 0.000010 inch. An interstitial space equal to the fiber diameter is created by calculating a specific diameter of the ball bearings. The relationship of the sphere diameter to the fiber diameter has been derived geometrically (see Figure 8).

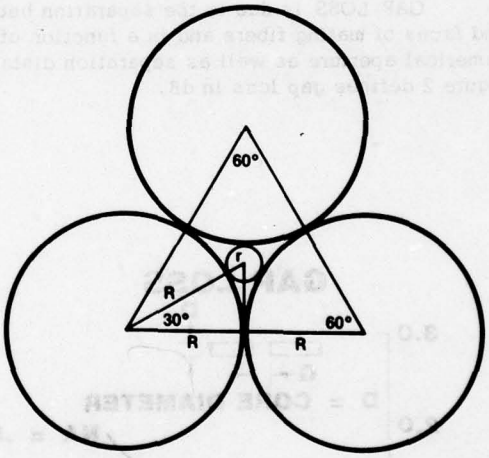


FIGURE 8

D = Diameter of sphere

R = Radius of sphere

d = diameter of fiber

r = radius of fiber

since: $\cos 30^\circ = \frac{R}{R+r}$

then: $D = 6.464d$

for a 0.00492 inch fiber, D = 0.0318 inches

A ramped bearing race retains the spheres at the internal leading edge of the cap (see Figure 9). Since the cap is threaded to the adaptor body, relative rotation will result in radial movement of the spheres. Tightening of the cap will close the spheres upon the fiber thus accommodating the varying fiber diameters (caused by fiber manufacturing tolerances). As opposing ferrules mate, the ferrules rotate about their longitudinal axis until the spheres nest under load at 60° increments as shown in Figures 7 and 9. The fibers are aligned coaxially and affected only by the sphere diametric tolerance.

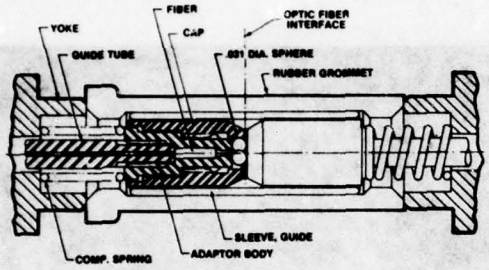


FIGURE 9

Gap - Accurate separation of fiber end faces is controlled by proper positioning of the fiber during assembly. It is accomplished easily by using a fourth and larger sphere nested among the three spheres shown in Figure 11. The fiber end face, when positioned against this sphere, will be at the precise recessed location required to provide a zero gap when aligned with an opposing fiber. The location of the fiber end face required when two ferrules are nested and the diameter of the sphere that will position it are calculated geometrically as shown in Figures 10 and 11.

Angular - Control of the angular alignment between mating fibers is accomplished through the use of a guide tube (refer to Figure 9). This tube precludes the pivoting of the fiber as it passes through the spheres. By choosing a proper length to inside diameter ratio (or inside fiber clearance), the angularity of the fiber is limited. The concentricities of the threaded parts were taken into account also in determining the tube inside diameter.

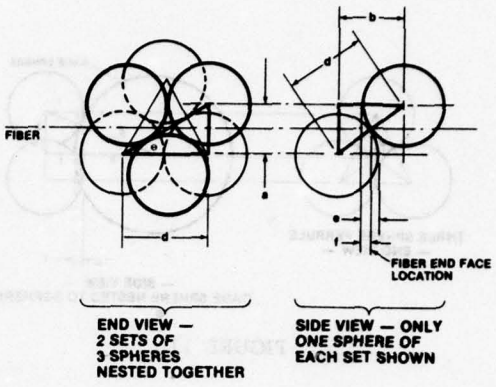


FIGURE 10

d = SPHERE DIAMETER

$\theta = 30°$, $\tan\theta = 1/\sqrt{3}$

$$\tan\theta = \frac{a}{d} = \frac{1}{\sqrt{3}}$$

$$\text{①} \therefore a = \frac{d}{\sqrt{3}}$$

then: $d^2 = b^2 + a^2$

and substituting ①

$$b^2 = d^2 - \frac{d^2}{3}$$

$$\text{②} \therefore b = d\sqrt{\tfrac{2}{3}}$$

now $b = d - e$

and $f = e/2$

$$\text{③} \therefore b = d - 2f$$

substitute ③ into ②

$$d - 2f = d\sqrt{\tfrac{2}{3}}$$

$$\therefore f = \frac{d - d\sqrt{\frac{2}{3}}}{2}$$

f is the amount of fiber end face recess

If $d = 0.0318$ inches
then $f = 0.00292$ inches

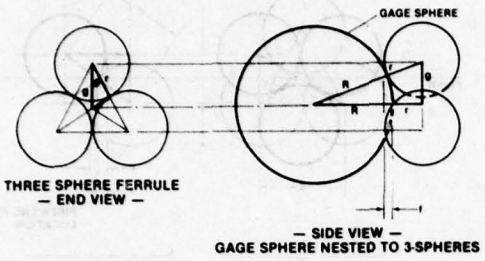


FIGURE 11

R, D = Radius, Diameter of gage sphere
r, d = radius, diameter of ferrule sphere
f = fiber end face recess

$\theta = 30°$, $\cos 30° = \frac{\sqrt{3}}{2} = \frac{r}{g}$

$\therefore g = \frac{2r}{\sqrt{3}}$

and $(R+r)^2 = g^2 + (R+r-f)^2$

substituting for g and f:

$$(R+r)^2 = \left(\frac{2r}{\sqrt{3}}\right)^2 + \left[R+r-\left(\frac{d-d\sqrt{3/4}}{2}\right)\right]^2$$

$$(R+r)^2 = \frac{4r^2}{3} + \left(R + r - \frac{d}{2} + \frac{d\sqrt{3/4}}{2}\right)^2$$

$$(R+r)^2 = \frac{4r^2}{3} + (R + r\sqrt{3/4})^2$$

$$R^2 + 2rR + r^2 = \frac{4r^2}{3} + R^2 + 2rR\sqrt{3/4} + \frac{2r^2}{3}$$

$$2rR + r^2 = 2r^2 + 2rR\sqrt{3/4}$$

$$R + \frac{r}{2} = r + R\sqrt{3/4}$$

$$R - R\sqrt{3/4} = \frac{r}{2}$$

$$R = \frac{r}{2(1 - \sqrt{3/4})}$$

$$R = \frac{r}{0.367}$$

$$\text{or } D = \frac{d}{0.367}$$

if d = 0.0318 inches
$\therefore$ D = 0.0866 inches

ASSEMBLY TECHNIQUES

The first step in termination of a fiber is to prepare the end face. It must be perpendicular to the fiber axis and optically clear. The method chosen for use with this connector was that of cleaving.[1] To cleave a fiber, it is pulled in tension and scribed with a diamond or other suitably hard material. Fibers made of different glass or by different processes require development of the specific tension used to cause the fracture to propagate at 90° to the axis without any lip or hackle (imperfections in the optical end face). Figures 12 and 13 are a cleaved fiber end face photographed using a scanning electron microscope.

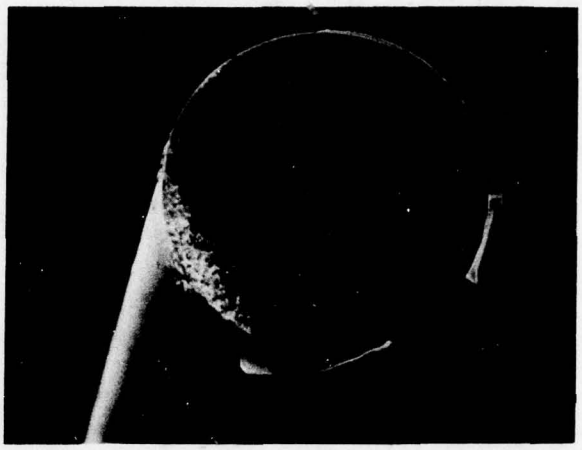


FIGURE 12

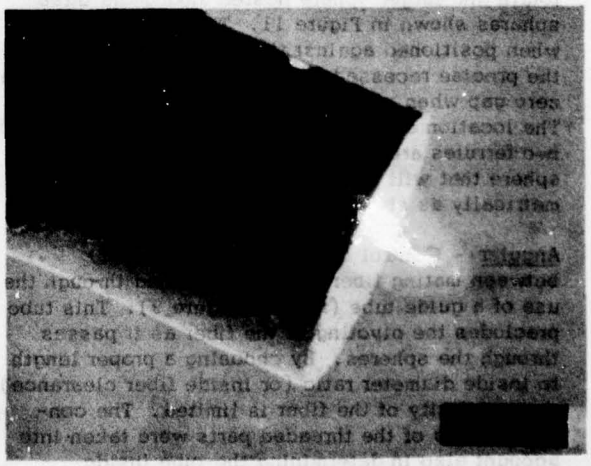


FIGURE 13

Once the fiber is prepared, it is threaded through the ferrule. To allow the spheres to spread the cap and adaptor body are loosened; the fiber is positioned approximately even with the front of the spheres; then, the spheres are clamped lightly to the fiber. By nesting the large sphere to the three in the ferrule, the fiber is pushed back to its proper location and the cap is tightened to hold the fiber. Epoxy is used for permanent fiber retention.

The ferrules are mated with the help of a loose guide sleeve (see Figure 9) to guide the spheres in to a nesting position. The ferrules are free to rotate within the connector to allow the spheres to seat at 60° increments. Compression springs drive the spheres together and overcome the sliding friction.

PERFORMANCE

Single channel connectors have been produced for the fiber parameters and sphere diameters discussed. Termination of 85 μ core fibers resulted in a statistical mean coupling loss of 0.621 dB and a three sigma distribution of 1.04 dB. Furthermore, these connectors exhibited good stability under -55°C to 105°C temperature cycling (negligible effect before and after cycling, and 0.5 dB variation during cycling) and shock and vibration cycling (negligible effect before, during and after cycling).

Prototype six-channel hermaphroditic connectors employing this concept will be fabricated and evaluated under the CORADCOM contract. This evaluation will assess the feasibility of the design with respect to stability of performance in the Army's tactical field environment.

# # #

REFERENCE

1. D. Gloge, P. Smith, D. Bisbee and E. Chinnock, Optical Fiber End Preparation for Low-Loss Splices, Bell System Technical Journal, Vol. 52, No. 9, Nov. 1973.

Les Borsuk is an Engineering Manager in the Advanced Development Engineering Department at ITT Cannon Electric in Santa Ana, California. He is responsible for the development of fiber optic interconnections.

Prior to joining ITT Cannon Electric in 1971, Mr. Borsuk held the positions of Engineering Manager and General Manager at Elco Corporation, Pacific Division. His experience includes 11 years in the interconnection field and ten years of electronic packaging. He holds numerous patents in these fields.

Mr. Borsuk received his BSME in 1956 from the University of Connecticut. He attended graduate school at UCLA and is President of the Southern California Chapter, Electronic Connector Study Group, Inc.



MORT POMERANTZ



LES BORSUK

Mr. Morton Pomerantz served in the US Army in World War II from 1943 to 1946. He received his BEE degree from New York University in 1955. He has been employed at Fort Monmouth since 1952 as an Electronics Engineer. In that time, he has been engaged in R&D activities, principally in the areas of RF cables and connectors and tactical communications cables. For the past six years his principal interest has been in the development of tactical fiber optic cables and connectors for the Army's fiber optic communication systems.

Mr. Pomerantz is a member of IEEE. He serves as the Army member of the Working Group on Cables and Connectors of the Tri-Service Fiber Optics Coordinating Committee.

SPLICE LOSSES IN FUSION-SPLICED OPTICAL WAVEGUIDE FIBERS WITH DIFFERENT CORE DIAMETERS AND NUMERICAL APERTURES

By D. R. Briggs and L. M. Jayne

Corning Glass Works, Corning, N. Y.

ABSTRACT

Fusion (butt) welding experiments were performed on graded-index optical waveguide fibers. Mean extrinsic (technique-related, due to the fusion process) losses were 0.18 dB for mating unlike fibers and 0.30 dB for joining like fibers. Intrinsic (fiber-related) losses due to deliberate mismatching of core diameters, numerical apertures and alpha profiles were studied, and basic splice-loss theory was essentially verified. Tensile testing of welded fibers was also done; mean tensile strength remaining after fusion was 0.41 times the original strength, but there was definite improvement in values as the experiment progressed. Strength loss was found to be partly the result of handling damage and partly from thermal stresses arising from volatilization of B_2O_3 from the cladding in the fusion zone. Extrinsic splice losses were mainly the result of a change in numerical aperture in the core caused by evaporation of B_2O_3 from the cladding in the fusion zone.

INTRODUCTION

Fusion splicing has been explored by several workers[1-3] as a practical method for joining optical waveguide fibers. The technique has been of interest because it offers a way to cable fiber lengths greater than those now commercially available. The technique may also be used for repair of occasional breaks during the cabling operation or during installation of cable in the field. In addition, a welded joint is not likely to come apart or to become angularly misaligned under stress, which might happen with a mechanical connection device.

Much of the previous work in the field involved cutting and resplicing the same fiber, and splicing step-index fibers. This paper expands upon the previous work and covers splicing graded-index fibers, especially different ones to each other.

SCOPE

All 16 possible joining combinations of four carefully selected production fibers were studied. These fibers were chosen for the widest practical variation in numerical aperture, core diameter, and alpha profile. The theory of intrinsic splice loss was compared to the data generated. The effect of the welding process on fiber tensile strength was also explored, and some analysis was done in an attempt to explain the underlying causes for splice and strength loss.

SAMPLES

Samples came from four different production reels of Corning Glass Works graded-index optical waveguide fiber. Nominal O.D. was 125 microns. Nominal core diameter was 63 microns, and there was a spread of 5 microns between maximum and minimum fibers. Nominal numerical aperture was 0.21, with a maximum spread of 0.015. The nominal alpha profile number was 2.0, and the maximum spread was 0.42. Two separate property measurements were made on each sample. Initial specimen length of 3m was gradually reduced to 2m as cuts and resplices were made. All samples were selected for excellent roundness of core and the concentricity of the core with respect to the O.D.

EQUIPMENT

Fig. 1 shows the general arrangement of the equipment. In addition to the welder itself, the key components are the source LED and the detector.

Fig. 2 shows the fusion welder device.[4] Vacuum chuck (1) is stationary and holds the receiver fiber. Vacuum chuck (2) holds the transmitter fiber, and it can be manipulated in three planes by means of the micropositioner (3). The operator moves the handle (4) to move the welding rods (5) vertically into and out of the fusion zone. The operator can also move the handle sideways approximately $\pm$ 1.5mm to achieve complete fusion at the weld.

The source is a Plessey LED, Model HR 952F, with an optical waveguide fiber pigtail cemented to the face. The pigtail is a step-index fiber with an 86-micron core and a numerical aperture of 0.16. Light from the pigtail completely fills the 63-micron core of the transmitter fiber butted against it in the three-rod holder.

The detector comes from EG&G Corporation and has a code number PV 444A. The 2lmm diameter window

assures complete collection of light leaving the receiving fiber.

The following apparatus is not shown in Fig. 1, but was used in the experiment:

1. A 90X stereo microscope was used for viewing the fibers in the splice area: aligning them prior to splicing and monitoring progress during the welding process.
2. A commercially available fiber cutter made square, clean cuts. This was essential for achieving a proper welded joint.
3. A tensile testing machine measured the breaking stress of fused fibers. Control fibers were also tested.

TEST METHOD

Each fiber end was carefully stripped of protective coating and then cut. The reference light reading, I_R, was taken on the transmitter fiber. The detector end was withdrawn from the detector and placed into chuck (2). One end of the receiver fiber was placed in chuck (1) and its other end in the detector. The two butt ends were aligned visually. Small adjustments were then made with the micropositioner in order to maximize the light throughput of the unspliced ends, thereby assuring the best alignment of the two cores. The fiber ends were separated slightly, and the cut ends slightly firepolished with the welding rods. The two ends were then brought together until they just touched and were tack welded at a somewhat higher voltage on the power supply. The voltage was stepped up still further to complete the weld.

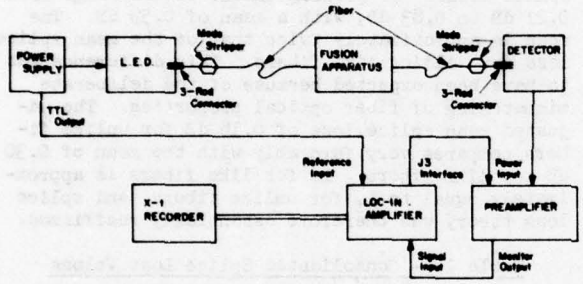


FIG. 1 – ARRANGEMENT OF APPARATUS

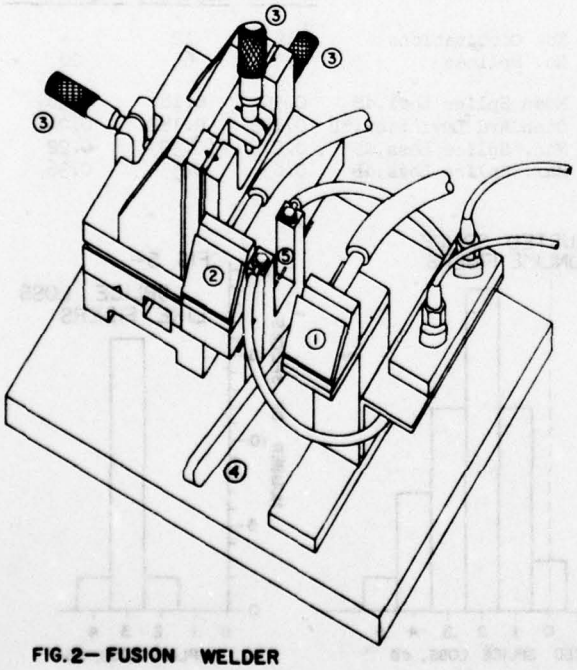


FIG. 2– FUSION WELDER

The light output reading, I_o, of the spliced fiber was read and the splice loss, L, calculated by:

$$L = -10 \log \left[\frac{I_o}{I_R}\right] \quad \text{in dB} \qquad (1)$$

Five splices were made for each of the 16 (4 x 4) joint combinations possible. When an obvious imperfection such as an air bubble was seen at the weld, the welded section was immediately cut out, and the complete weld was reworked.

For the sake of efficiency, fusion of samples for tensile testing was conducted separately from the fusion for the splice-loss portion of the experiment. Four welds were made for each of the 16 possible splice combinations, and they were tensile tested, using a 0.6m gauge length.

All welding and testing was performed in random order.

THEORY ON SPLICE LOSS

Intrinsic losses are related to the properties of the mating fibers. They occur when the transmitting fiber has a higher value than the receiving fiber for one or more of the following properties: core diameter, numerical aperture, and alpha profile. The effects are additive. If the transmitting fiber has a lower value for a particular property, there is no loss, nor can there be a gain. Mode-coupling losses caused by distortions of the waveguide have been considered negligible.

Using the approach of Hawk and Thiel,[5] and Gloge and Marcatili,[6] the individual intrinsic-loss terms may be calculated as follows:

$$L_{NA} = -10 \log \left[\frac{NA_r}{NA_t}\right]^2 \quad \text{for } NA_r < NA_t \text{ only} \qquad (2)$$

$$L_D = -10 \log \left[\frac{D_r}{D_t}\right]^2 \quad \text{for } D_r < D_t \text{ only} \qquad (3)$$

$$L_\alpha = -10 \log \left[\frac{\alpha_r(\alpha_t + 2)}{\alpha_t(\alpha_r + 2)}\right] \quad \text{for } \alpha_r < \alpha_t \text{ only} \qquad (4)$$

where L = splice loss, dB
NA = numerical aperture
D = core diameter
α = alpha profile number
sub r = receiver fiber
sub t = transmitter fiber

Extrinsic splice losses are related to the techniques used in the joining procedure. There are at least 5 possible sources of loss:

1. The fusion process itself.
2. Lateral misalignment of the fiber cores.
3. Angular misalignment of the fiber cores.
4. Distortion of fibers.
5. Fiber end finish and Fresnel reflections.

The effects of items 2 through 5 are considered negligible because of the techniques used in the fusion process. Therefore only the effect of the fusion process itself will be considered.

The total measured splice loss equals the sum of the intrinsic losses plus the extrinsic loss, as follows:

$$L = L_f + (L_{NA} + L_D + L_\alpha) \qquad (5)$$

where L = splice loss, dB
L_f = extrinsic splice loss due to fusion
sub NA = numerical aperture
sub D = core diameter
sub α = alpha profile number

RESULTS AND DISCUSSION

Splice Loss

Fig. 3 shows the measured splice loss distribution for the 60 splices involving unlike fibers. Fig. 4 is a histogram of the above splice loss distribution adjusted to eliminate the effects of intrinsic splice losses. These adjusted values are actually the extrinsic splice losses and are calculated by rearranging equation (5) as follows:

$$L_f = L - (L_{NA} + L_D + L_\alpha) \qquad (6)$$

In five of the 12 cases, numerical aperture mismatch was the sole contributor to an intrinsic loss; alpha profile alone to 1 case; NA plus core diameter to 1 case; and core diameter plus alpha to 5 cases. The mean intrinsic splice loss due to NA was 0.15 dB, core diameter 0.18 dB, and alpha difference 0.08 dB.

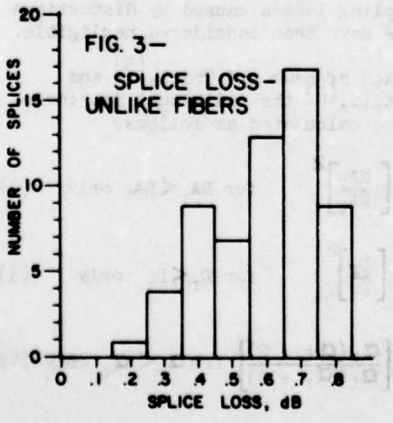
As shown in Fig. 4 there are five negative values, which of course is not possible. All negative values came from the five welds made in one particular case, and can only be explained by a measurement error made somewhere during the procedure.

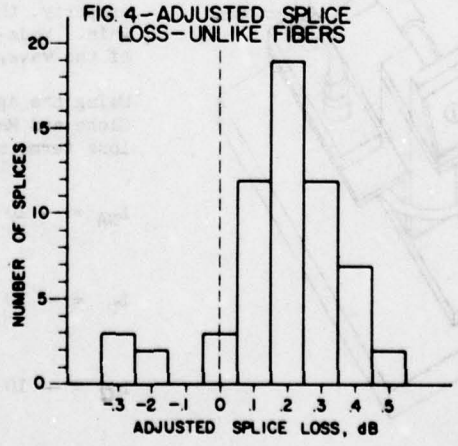
Fig. 5 is a histogram of the measured splice loss distribution for the 20 splices involving like fibers. In the fusion of like fibers, the intrinsic-loss terms in equation (5) drop out, and $L = L_f$. At this point, the value for L_f for like-fiber fusion can be directly compared to the L_f calculated for the fusion of unlike fibers.

Table 1 consolidates splice loss data. Measured splice losses for joining unlike fibers range from 0.21 dB to 0.83 dB, with a mean of 0.59 dB. The mean is approximately twice that of the mean splice loss for welding like fibers. This difference was to have been expected because of the deliberate mismatching of fiber optical properties. The adjusted mean splice loss of 0.18 dB for unlike fibers compares very favorably with the mean of 0.30 dB for like fibers. L_f for like fibers is approximately equal to L_f for unlike fibers, and splice loss theory was therefore essentially reaffirmed.

Table 1 -- Consolidated Splice Loss Values

	Unlike Fibers		Like Fibers,
	Actual	Adjusted	Actual
No. Combinations	12	12	4
No. Splices	60	60	20
Mean Splice Loss,dB	0.59	0.18	0.30
Standard Deviation,dB	0.156	0.182	0.041
Min. Splice Loss,dB	0.21	(0.33)	0.22
Max. Splice Loss,dB	0.83	0.53	0.36





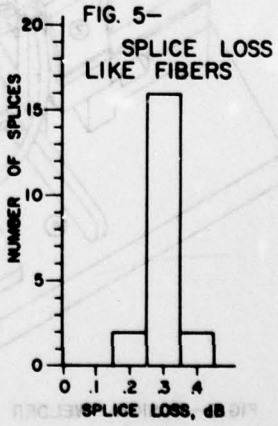


Table 2 -- Changes in Fiber Strength

	Strength, kpsi		Ratio Fused
	Unfused	Fused	to Unfused
Mean	185.	75.5	0.41
Standard Deviation	63.2	22.7	0.36
Maximum	353.	117.	0.33
Minimum	81.1	23.3	0.29

Spliced Fiber Strength

Fiber strength was diminished by the fusion process, as shown in Table 2. Mean strength of fused fibers dropped 59% from that of the control, or unfused, fibers. Maximum and minimum values fell even further percentage-wise.

Great care was taken to pinpoint the exact location of the tensile break with respect to the fusion line. The location distribution of the 64 tensile breaks is shown in the histogram Fig. 6. Approximately 84% of the breaks occurred in the splice area -- that is, within ± 18mm of the splice line, and between the two chucks. Despite the considerable care taken to prevent handling damage to the fibers, 16% of the breaks occurred at the vacuum chucks or beyond. This was certainly well beyond the region affected by the fusion process. It should be noted that uncoated fiber is vulnerable to handling damage and that the plastic protective coating on each fiber end had to be stripped away approximately 80mm for two reasons:

1. *Prevent the plastic coating from interfering* with the cleanliness of both the cut and the weld.
2. Make sure that each fiber end seats properly in the vacuum chuck.

Mean tensile strength values for the 16% of the fibers which broke outside the splice region were virtually identical to the mean values for the tensile breaks in the splice region. The net

FIG. 6 – DISTRIBUTION OF TENSILE BREAKS ON FUSED FIBER

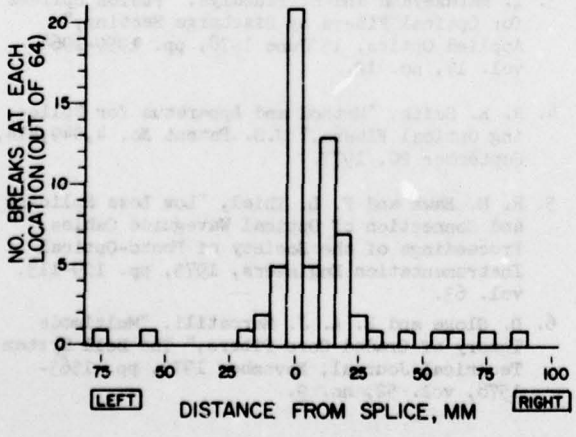
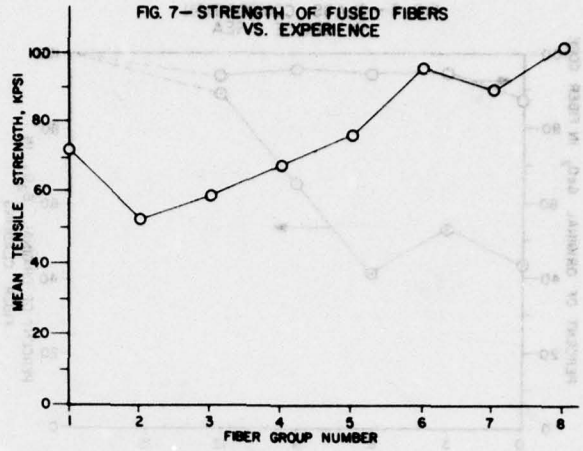


FIG. 7 – STRENGTH OF FUSED FIBERS VS. EXPERIENCE



effect of taking all 64 tensile break values is to present a somewhat pessimistic view of the effect of the fusion process.

Fig. 7 gives evidence that tensile strength improved with welding experience. The tensile data were arranged in sequence, in groups of 8 each. The tension experiment was started only after considerable practice on the technique itself. The mean strength of the first batch was 72 kpsi. Before the second group was started there was a two-week intermission due to the pressure of other laboratory activity. The values fell to the 53 kpsi mean level, but then increased gradually right up to the final group at a mean of 102 kpsi. The mean tensile strength of unfused fibers was 185 kpsi.

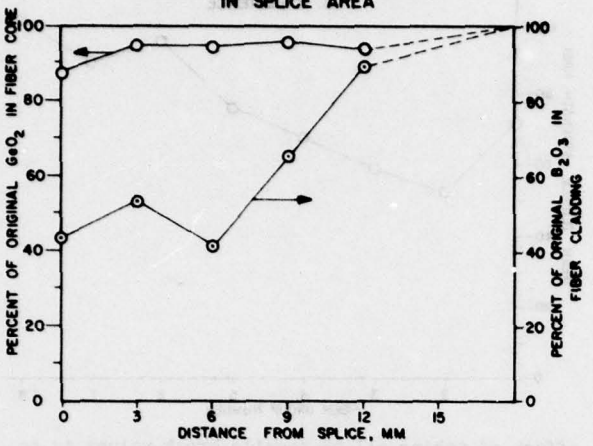
The key to achieving good fiber tensile strength seems to be the amount of time the fibers are subjected to the heat of the welding process, as well as to the temperature applied. In a separate experiment it was determined that shortening the welding time led to weak fibers, and increasing the welding time beyond a certain point caused rapid falloff in tensile strength. The strongest joints involved the best balance of time and temperature.

Obviously, tensile strength was lost because of the fusion process. Indeed, only six out of the 64 control specimens tested at lower strength than the very highest fused sample. The overlap is extremely narrow.

Changes in Chemical Composition

There are two possible explanations for strength loss: damage during handling, and changes of some sort to the glass itself as a result of the fusion process. Splice losses, on the other hand, can only be explained by whatever change took place in the glass during fusion. The effect of handling damage was held to the most practical minimum and has already been discussed. It remains, therefore, to explore what effects the fusion process had on the glass in the splice area.

FIG. 8 — GLASS COMPOSITION IN SPLICE AREA



Samples of fused fiber were very carefully cut at the splice line and at 3mm intervals on either side of the splice line. Scanning electron microscope probes were made at 2-micron intervals across the face of the sectioned fibers. The glass "cladding" layer is 31 microns thick and contains mostly silica plus boric oxide to achieve the proper balance of refractive index and thermal expansion. The core is 63 microns in diameter and contains silica plus germania for the desired optical properties.

It can be seen from Fig. 8 that approximately 50% of the B_2O_3 cladding content evaporated in the section 6mm on either side of the splice line. It is well known in the glass industry that B_2O_3 is quite volatile in the temperature range used. The effect of the B_2O_3 loss is to produce a localized reduction in linear expansion of approximately 50%. Upon cooling, this region was placed under a permanent strain roughly estimated to be 4 kpsi. This residual strain accounts for a portion of the observed weakness, but a detailed model of the strain condition was not developed.

It was estimated that the effect of losing approximately 50% of the B_2O_3 in the cladding in the fusion zone was to increase its refractive index approximately 0.003. This effectively narrows the differential in refractive index between the core and the cladding by 0.003. The net effect is to produce a localized reduction in the numerical aperture of the waveguide fiber in the core. Thus, some of the higher order modes have a chance to escape the core in the splice region. The most likely explanation for the measured extrinsic splice losses, both for like and unlike fibers, is, therefore, the localized reduction in numerical aperture arising from the volatization of B_2O_3 in the splice zone.

The effect of the fusion process on the chemical composition of the core was much less pronounced, as is shown in Fig. 8 for the germania remaining in the core. Less germania was volatilized than was B_2O_3 because its vapor pressure is considerably lower at the fusion temperature. A maximum of 11% of the GeO_2 in the core was evaporated. This difference in chemical composition may have had some effect on either strain or refractive index in the core, but the effect was not explored further at the time.

CONCLUSIONS

1. Graded-index optical waveguide fibers can be fused, although the process is still dependent upon operator skill.
2. Strength of fused fiber was adequate, but the mean was only 41% of the control-fiber strength.
3. Strength improved with experience and was highly dependent upon time and temperature.
4. Mean extrinsic splice loss was 0.18 dB for unlike fibers and 0.30 dB for like fibers.
5. Theory regarding intrinsic splice losses was essentially verified.
6. Strength loss can be explained partly by handling damage and partly by stresses induced by chemical composition changes due to evaporation.
7. Extrinsic splice losses result mainly from localized changes in numerical aperture of the fiber caused by evaporation of B_2O_3 from the cladding.

Acknowledgements

The authors appreciate the many suggestions and observations made by R. M. Hawk, D. B. Keck, and J. G. Racki.

References

1. Y. Kohanzadeh, "Hot Splices of Optical Waveguide Fibers," Applied Optics, March 1976, pp. 793-794, vol. 15, no. 3.

2. D. L. Bisbee, "Splicing Silica Fibers with an Electric Arc," Applied Optics, March 1976, pp. 796-798, vol. 15, no. 3.

3. I. Hatakeyama and H. Tsuchiya, "Fusion Splices for Optical Fibers by Discharge Heating," Applied Optics, 15 June 1978, pp. 1959-1964, vol. 17, no. 12.

4. R. E. Smith, "Method and Apparatus for Splicing Optical Fibers," U.S. Patent No. 4,049,414, September 20, 1977.

5. R. M. Hawk and F. L. Thiel, "Low Loss Splicing and Connection of Optical Waveguide Cables," Proceedings of the Society of Photo-Optical Instrumentation Engineers, 1975, pp. 109-113, vol. 63.

6. D. Gloge and E. A. J. Marcatili, "Multimode Theory of Graded-Core Fibers," The Bell System Technical Journal, November 1973, pp. 1563-1578, vol. 52, no. 9.



Biography

Douglas R. Briggs
Corning Glass Works
Corning, New York

He received his B.S. in Chemical Engineering from Northeastern University in Boston, then his M.S. in Chemical Engineering from MIT. His early work experience was as a Process Chemical Engineer with Stauffer Chemical Company. He then joined Corning Glass Works and held a variety of Sales and Marketing positions in the company's Chemical Systems Department. He is now Supervisor of the Optical Waveguide Product Engineering Laboratory in Corning's Electronics Division.

STRESS IN FIBERS DURING OPTICAL CABLE MANUFACTURING PROCESS AND INSTALLATION

by

T. Kobayashi*, Y. Sugawara*, R. Yamauchi*
K. Inada* and N. Uchida**

* The Fujikura Cable Works, Ltd.
Sakura-shi Chiba-ken 285 Japan
** Electrical Communication Laboratories, N.T.T.
Ibaraki Tokai Ibaraki-ken 319, Japan

Abstract

This paper present design concepts for stable structures of optical fiber cable considering mostly the stress in fibers as well as transmission characteristics during optical cable manufacturing process and installations. The stress in fibers is directly concerned with cable structures. Four types of cable have been manufactured and their transmission characteristics have been compared with each other. Unit type structure of eight fibers has been found to be very stable and the stress in fibers of the unit type cable has been measured from the pulse delay due to the elongation of the fibers during the installation.

Introduction

It is considered that the following two points are the most important for the design of optical fiber cables;

(1) Fibers do not suffer changes in the transmission characteristics,

(2) Fibers do not break.

during cabling process and installation.

Recently, transmission loss of fiber becomes remarkably low and the loss below 3 dB/km is easily obtained in the wavelength region around 0.85 μm. In the longer wavelength region such as 1.2 μm - 1.3 μm, the losses of the fibers are less than 1 dB/km. Therefore, investigation of optical fiber cable structure without loss increase under cable manufacturing process and installation has become very important.

As for the mechanical properties of fiber, improvement in tensile strength is also remarkable [1] - [3]. It is reported that the Weibull distribution of the strengthfor the fiber made by synthetic silica is composed of single mode and that its slope is very steep. However, the Weibull distribution for the fiber manufactured by the MCVD method using a fused quartz tube is generally composed of two or three modes and low tensile strength is observed for long span. Fig. 1 shows the typical Weibull distribusions of the fiber strength of synthetic silica fibers and MCVD fibers.

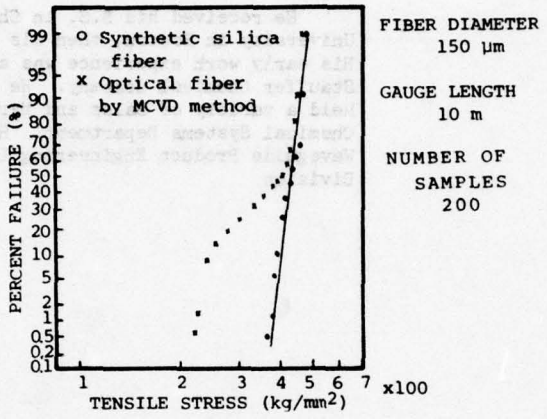


Fig.1 Weibull distribution of tensile stress of fibers

Considering the above two points, various types of cables have been disigned and manufactured, and compared with each other in the aspect of transmission characteristics. The stress in the cable under installation has been investigated and measured with pulse delay. The results show that the unit type cable is a very suitable structure in the aspects of transmission characteristics and mechanical properties.

Fiber structures and transmission characteristics of the fibers

Graded-index fibers manufactured by the MCVD method are used in this experiment, and the structure and parameters of the fibers are illustrated in Fig.2. Core diameter, outer diameter, and index difference Δn of the fibers are 60 μm, 150 μm and 1.0 %, respectively. The fibers are coated with thick and soft silicone resine with 450 μm in diameter so as to prevent the microbending due to side pressure [4]. Nylon with 0.9 mm in outer diameter is coated on the fiber.

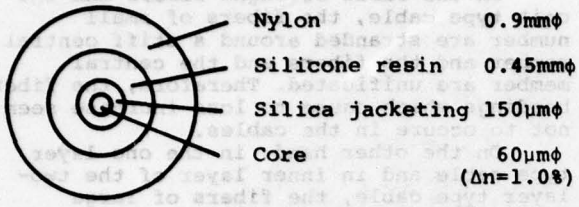


Fig. 2 Structure and fiber parameter of graded index fiber

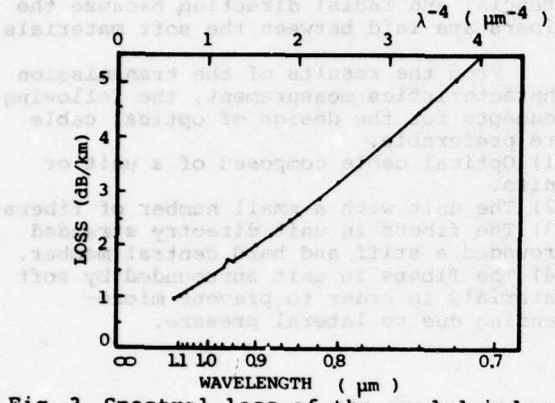


Fig. 3 Spectral loss of the graded index fiber

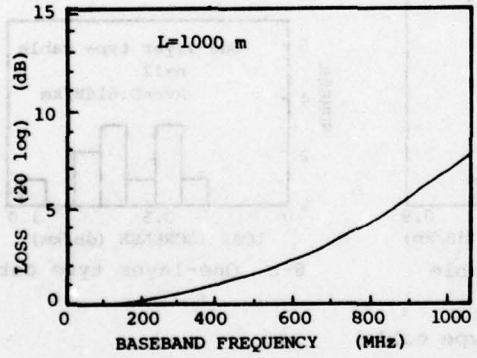


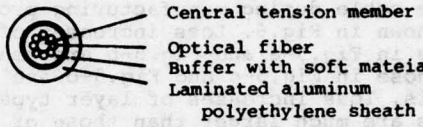
Fig. 4 Baseband frequency response of the graded index fiber

Average loss increase by Nylon coating is less than 0.1dB/km.

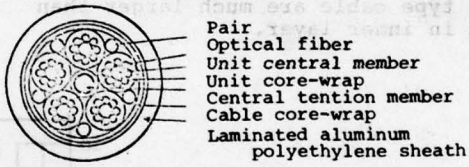
Typical loss and baseband frequency response of the graded-index fibers are shown in Fig.3 and 4, respectevely. Losses at λ=0.84μm and λ=1.1μm are typically 2.5dB/km and 1.0dB/km, respectively, and the 6-dB electrical bandwidth at 1km is about 900MHz.

Cable structure

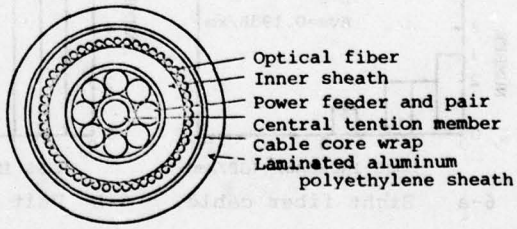
In this experiment, four types of optical fiber cables are designed and manufactured. Fig.5 shows the cable structures. Fig.5-a is an optical cable with eight fibers. These fibers are stranded around a stiff central tesion member and are surrounded by soft materials as buffer. Fig.5-b is a unit type optical cable with forty fibers. This cable is composed of five units whose structure is similar to the cable core with eight fibers shown in Fig.5-a. These units are stranded around the central tension member and are wrapped with plastic tapes. Fig.5-c is a one-layer type cable with fifty fibers. These fibers are stranded around the copper feeders and pairs, and are surroundedby soft materials as buffer.



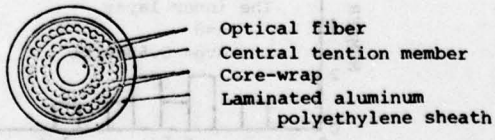
5-a Optical cable with eight fibers



5-b Unit type cable



5-c One-layer type cable



5-d Two-layer type cable

Fig.5 The structures of the optical cables

Fig.5-d is a two-layer type cable with fifty fibers. Twenty fibers are wound in inner layer around the central member and are surrounded by soft materials. In outer layer, thirty fibers are laid and are also surrounded by the soft materials. Laminated-aluminum-polyethylene sheath is used for those cables. The cable length are approximately 1km.

Loss increases of the cable during manufacturing processes

The loss increases of those cables are measured during cable manufacturing processes. In spectral measurement, a 500m-long fiber whose parameter is the same as used in this experiment is inserted in front of the measured fiber in order to attain a steady state modal distribution.

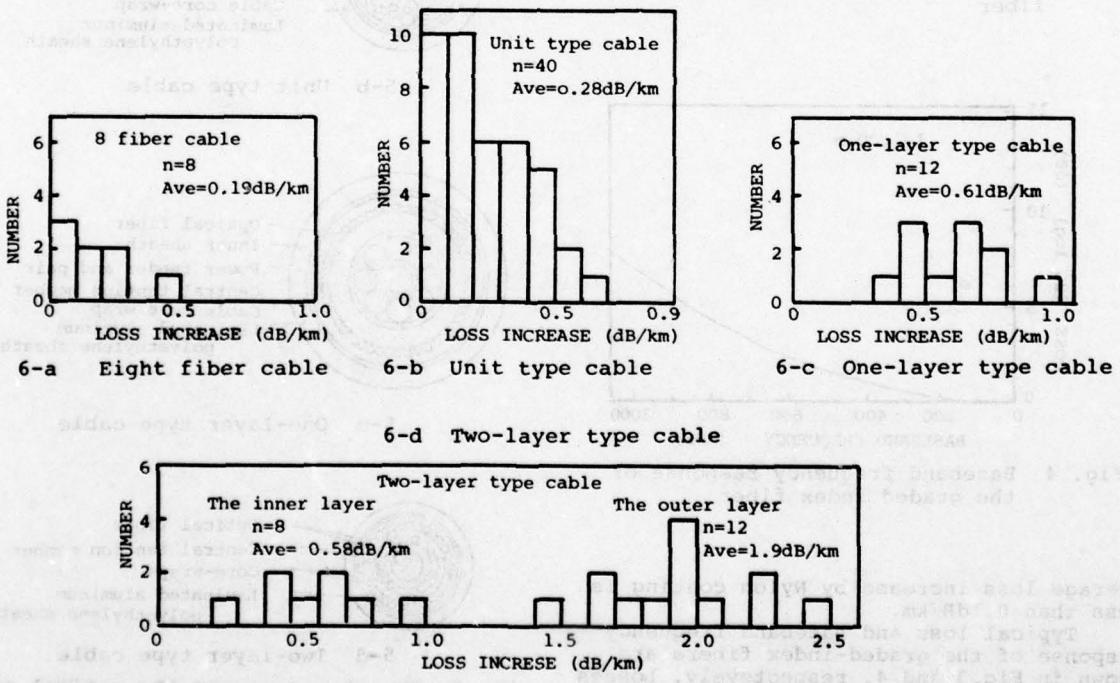
The histogram of the loss increases of the cable during manufacturing processes are shown in Fig.6. Loss increases of the cables in Fig.5-a and Fig.5-b are small and those in Fig.5-c and Fig.5-d are large. That is, loss increases of layer type cables are much larger than those of unit type cables. Moreover, the loss increases of the fibers in outer layer of the two-layer type cable are much larger than those in inner layer.

In the cable of eight fibers and the unit type cable, the fibers of small number are stranded around a stiff central member and the fibers and the central member are unificated. Therefore, the fiber bendings which cause to loss increase seem not to occure in the cables.

On the other hand, in the one layer type cable and in inner layer of the two-layer type cable, the fibers of large number are stranded. Because of large number of fibers, fibers are easy to be bent in circumstancial direction. Moreover, in outer layer of the two-layer type cable, the fibers are easy to be bent in circumstancial and radial direction, because the fibers are laid between the soft materials.

From the results of the transmission characteristics measurement, the following concepts for the design of optical cable are preferable.

1) Optical cable composed of a unit or units.
2) The unit with a small number of fibers.
3) The fibers in unit directry stranded arounded a stiff and hard central member.
4) The fibers in unit surrounded by soft materials in order to prevent micro-bending due to lateral pressre.



6-a Eight fiber cable

6-b Unit type cable

6-c One-layer type cable

6-d Two-layer type cable

Fig. 6 The histagram of the loss increases of the cables during manufacturing proceses

Measurment of elongation of fibers in the cable under installation

Investigation of the fiber strain in the cable is one of the important factors to designing a cable structure. The eight fiber cable and the unit type cable have been used in the elongation test, because these cables have good transmission characteristics. The elongation of the fiber in the cable was measured by the change of optical pulse delay time which was caused when the fiber was lengthened under installation.

The travelling time of an optical pulse in a graded-index fiber is given by

$$\tau_0 = N_1 L / c \qquad (1)$$

where L is the length of fiber free from stress, c is the light velocity in vacuum, and N_1 is the material group index which is given by

$$N_1 = n_1 - \lambda \frac{dn_1}{d\lambda} \qquad (2)$$

with n_1 the refractive index along the fiber axis. When a tension is applied to a fiber along the fiber axis, both the fiber length and the refractive index change. Therefore, the travelling time of optical pulse in the fiber under tension becomes

$$\tau_1 = (N_1 + \Delta N_1)(L + \Delta L) / c \qquad (3)$$

Normally, refractive index difference between core and cladding is small, and the electric field vector of light in the fiber can be assumed to by approximately perpendicular to the fiber axis. Then, the change of N_1 is given by [5]

$$\Delta N_1 = -\frac{1}{2} N_1^3 (P_{12} - \sigma P_{11} - \sigma P_{12}) \frac{\Delta L}{L} \qquad (4)$$

where σ is the Poisson's ratio, P_{ij} is the strain-optics tensor component and only two values are necessary for an isotropic material. Using (1)-(4) and neglecting the term ΔL , the relation between the delay time difference $\Delta\tau$ and the fiber elongation is given by

$$\Delta\tau = \tau_1 - \tau_0 = [N_1 - \frac{1}{2} N_1^3 (P_{12} - \sigma P_{11} - \sigma P_{12})] \frac{\Delta L}{c} \qquad (5)$$

On the condition that P_{ij} of doped silica is the same as that of pure silica glass (P_{11}=o.121, P_{12}=0.270 [5]), N_1=1.478 [6] for a germenium doped graded index fiber Δn is 1%, and σ=0.17, the change of optical pulse delay per change of fiber length under tension becomes

$$D_{cal} = \frac{\Delta\tau}{\Delta L} = 38 \text{ psec/cm} \qquad (6)$$

Fig.7 shows the calculated and experimental results of the changes of pulse delay when a tension is applied to graded index fiber. Fig.8 shows the photograph of measurement of pulse delay. The changes of pulse delay time were measured by the pulse peek. The calculated and experimental results agree with each other, and the incline D_{exp} is determined as

$$D_{exp} = \frac{\Delta\tau}{\Delta L} = 40 \text{ psec/cm} \qquad (7)$$

Fig.9 shows the relation between the fiber strain and the cable strain under installation of the eight fiber cable shown Fig.5-a, and Fig.10 shows of the unit type cable shown in Fig.5-b by using the measurement pulse delay. Both pulling end is fixed with epoxi resin, and pulling span is 100m-long. In the eight fiber cable, the fiber strain is equal to the cable strain. On the other hand, in the unit type cable, fiber strain is about 0.1% smaller than that of the cable. Therefore, in the unit type cable, fiber strain in the unit is quite the same as the strain of the unit central member. However, when the several units are stranded around the cable central strength member, the strain of the fiber is about o.1% lower than the strain of the cable itself.

For example, if screening tests of the fibers are carried out with the stress of 28kg/mm^2 (500g at 150μm) which corresponds to the strain of 0.4%, the strain of the unit type cable is allowed up to 0.53% from Fig.10.

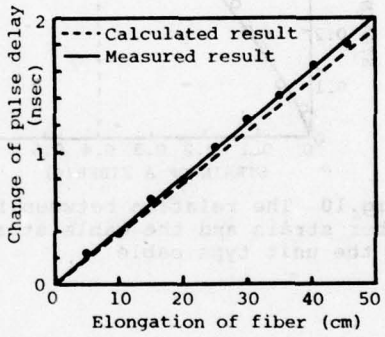
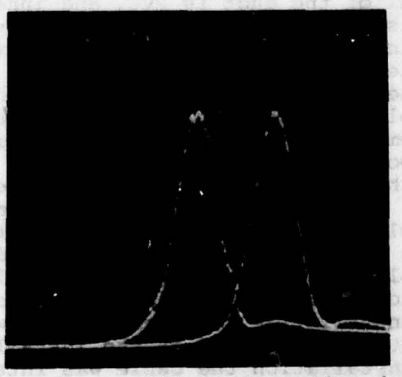


Fig.7 Relation between the changes of pulse delay and elongation of fiber under tention



Fiber elongation is 20cm.

Fig.8 The photograph of pulse delay measurement

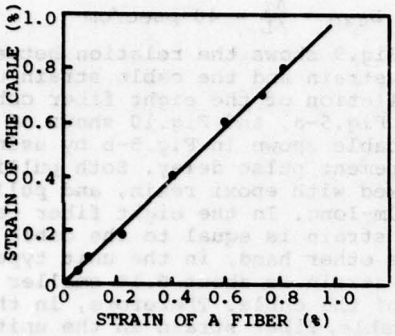


Fig.9 The relation between the fiber strain and the cable strain in the eight fiber cable

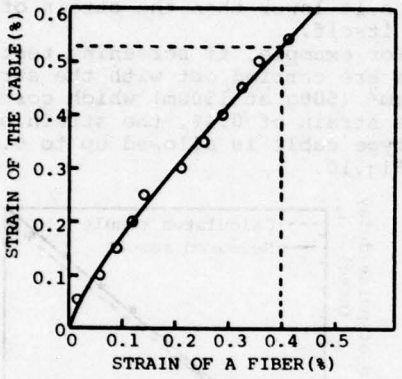


Fig.10 The relation between the fiber strain and the cable strain in the unit type cable

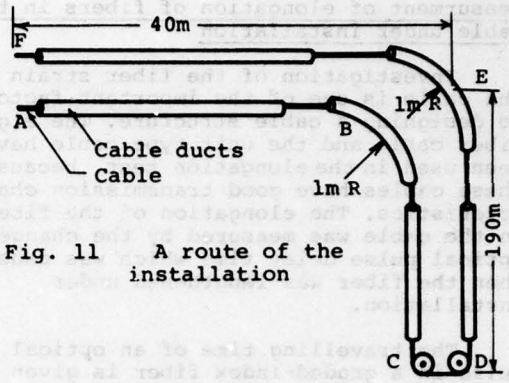


Fig. 11 A route of the installation

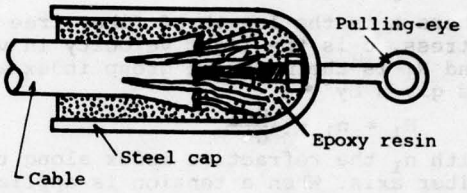


Fig.12 The structure of the pulling end of the cable

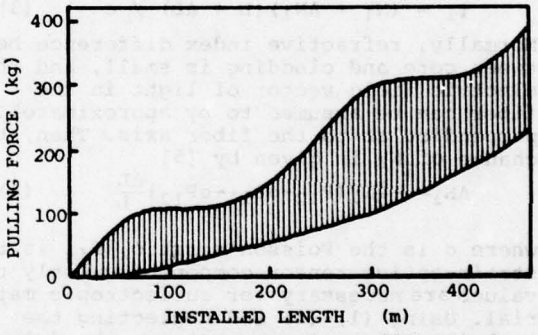


Fig. 13 A tention of the pulling end of the cable

Installation test of the unit type cable

The unit type cable,(Fig.5-b), was installed along an experimental duct. Fig.11 shows a route of the installation. Material of the duct is PVC, and inner diameter is 80mm. The route has two curved ducts and two rollers for severe curves. Total length of the route is 460m.

The structure of the pulling end of the cable is shown in Fig.12. Central tension member, fibers and sheath are fixed with epoxi resin in a metal cap. The strength of the pulling end can stand up to 1000kg. The tensions of the pulling end of the cable are measured by inserting the tension meter between the pulling end of the cable and the pulling wire. Fig.13 shows a tension of the pulling end of the cable under installation. Maximum tension was about 300kg at the end of the installation. After installation the cable was intentionally pulled with the tension of 700kg. Before and after the installation, transmission losses were measured in all the fibers in the cable. Loss changes were found to be less than 0.1dB/km and any failur of fiber was not observed.

Mechanical property of the unit type cable

Various mechanical tests such as squeezing test, bending test, vibration test, tensile test and twist test, were carried out for the unit type cable. Loss change and failure of the fibers are mainly tested. Table 1 shows the results of the mechanical tests.

Conclusion

Four types of optical cable have been designed and manufactured, and compared with each other in aspect of transmission

AD-A062 322 ARMY COMMUNICATIONS RESEARCH AND DEVELOPMENT COMMAND --ETC F/G 13/9
PROCEEDINGS OF THE INTERNATIONAL WIRE AND CABLE SYMPOSIUM (27TH--ETC(U)
NOV 78 E F GODWIN

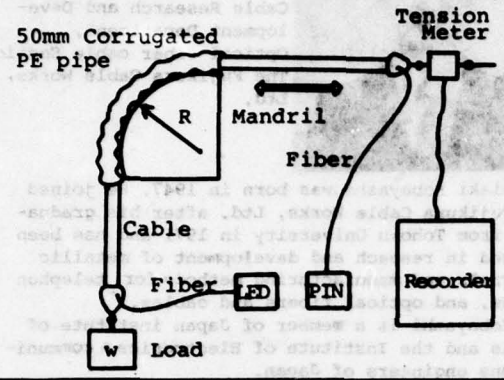
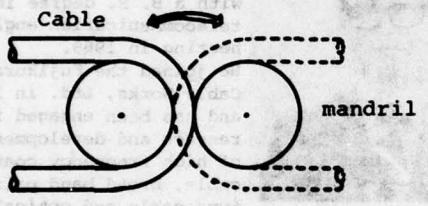
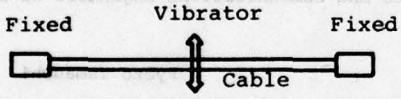
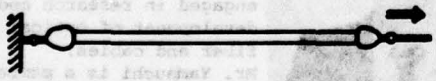
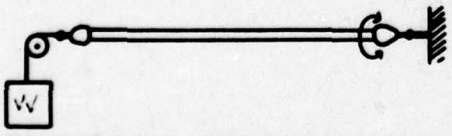
UNCLASSIFIED NL

5 OF 5
ADA
062322



END
DATE
FILMED
3 79
DDC

TABLE 1 Mechanical properties of the unit type cable

METHOD	CONDITION	RESULT
(1) Squeezing test 	Bending Radius 600mm Cable Length 5000mm Stroke 3000mm Load 200kg 300kg 500kg Times 10 times in both ways Sample Number 5	Loss change: Below 0.05dB Broken fiber: 0/600 Load / Flatness of cable 200kg 21.4x22.3 300kg 20.9x22.8 500kg 20.1x23.6
(2) Bending test 	Bending Radius 120mm 240mm Times 10 times in both ways Sample Number 5	No change in loss Broken fiber: 0/400
(3) Vibration test 	Span 1000mm Amplitude ±5mm Frequency 10HZ Times $5x10^6$ Sumple Number 5	No change in loss Broken fiber: 0/400
(4) Tensile Strength test 	Gauge Length 2000mm Pulling Speed 0.5%/min Sample Number 5 Maximum Tension 500kg	No change in loss Broken fiber: 0/200 Tension / strain 300kg 0.26% 500kg 0.40%
(5) Twist test 	Gauge Length 4000mm Torsion angle ±360° Sample Number 5	No change in loss Broken fiber: 0/200

characteristics.

A unit type cable with following structure has been found to be very stable under the cable manufacturing process

1) Optical cable composed of a unit or units.
2) The units with a small number of fibers.
3) The fibers in unit directly stranded aroud a stiff and hard central member.
4) The fibers in the unit sorrouded by soft materials in order to prevent microbending due to lateral pressure.

A measurement method of the elongation of fiber fiber in cable was presented and discussed.

The measured elongation of the fiber in the unit was quite the same as the elongation of the unit central member. However, when the several units were strunded around the cable tension member, the straun of the fiber was about 0.1% lower than the strain of cable itself.

Moreover, other several mechanical properties of the unit type cable were tested. The unit type cable has been found to be very stable for the mechanical property as well as the transmission characteristics.

Acknowledgement

Authors would like to express appeciation to Mr. K. Masuno and Mr. K. Ishihara of the Ibaraki Electrical Communication Laboratories, N. T. T. and Mr. s. Tanaka of the Fujikura Cable Works, Ltd., for their encouragement through this work.

Reference

[1] T. Kobayashi, et al, IOOC'77 B9-4.
[2] C. R. Kurkjian, et al Optical fiber transmission II, Feb. 1977
[3] C. K. Kao, et al. IWCS 223-225 1976
[4] T. Naruse, et al. Electron. Letters, March 1977,vol 13
[5] R. J. Pressley, "Handbook of laser with Selcted data on Optical Technology"
[6] S. kobayashi, et al. IOOC '77, B8-3.

Authors



Toshiaki Kobayashi

Engeneer, Telecommunication Cable Research and Development Department, Optical fiber cable Section The Fujikura Cable Works, Ltd.

Toshiaki Kobayashi was born in 1947. He joined The Fujikura Cable Works, Ltd. after his graduation from Tohoku University in 1971 and has been engaged in reseach and development of metallic materials and manufacturing methods for telephon cables, and optical fibers and cables.
Mr. Kobayashi is a member of Japan institute of metals and the Institute of Electronics & communications engineers of Japan.

Yasuyuki Sugawara



Yasuyuki Sugawara was born in 1947 and graduated from Tohoku University with a B. E. degree in telecommunication engineering in 1969.
He joined the Fujikura Cable Works, Ltd. in 1969, and has been engaged in reseach and development of high frequency coaxial cable, broad band pair type cable and optical fiber cables
He is Engineer in Telecommunication Cable Rsearch and Development Department, Optical fiber Cable Section, and is a member of the Institute of Electronics and Communications Engineers of Japan.

Ryozo Yamauchi



Ryozo Yamauchi was born in 1949. He joined the Fujikura Cable Works. Ltd. after his graduation from Nagoya University with a M.A. degree and has been engaged in research and development of optical fiber and cables.
Mr. Yamauchi is a member of the Institute of electronics & Communications Engineers of Japan.



Koichi Inada

Koichi Inada was born in 1941. He joind the Fujikura Cable works, Ltd. After his graduation from Yokohama National University in 1963 and has been engaged in research and development of high frequency coaxial cable, leaky wave coaxial cable, super conducting coaxial cable, milimeter waveguide and optical fibers. In 1976 he received Ph.D. degree in engineering from Tokyo institute of Technology.
Dr.Inada is now a head of optical fiber and cable development section and a member of the Institute of Electronics and Communications Engineers of Japan and the IEEE of the U. S. A.



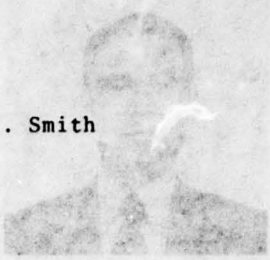
Naoya Uchda

Naoya Uchida was born in 1939, graduated from Kyoto University in 1962, and joined the Electrical Communication Laboratory in 1963 and has been engaged in reseach and development of acousto-optic light deflector and modulator, electro-optic waveguide modulator, and now disgning, fabrication and evaluation of optical fiber cables.
Mr. Uchida is a staff engineer, Optical Transmission Line Section in Ibaraki ECL, and a member of the Institute of Electronics and Communications Engineers of Japan and the Japan Society of Applied Physics.

MECHANICAL/ENVIRONMENTAL PERFORMANCE OF RUGGED LIGHTWEIGHT FIBER OPTIC CABLES FOR TACTICAL FIELD APPLICATIONS

Robert J. Freiburger, George A. Gasparian and John C. Smith
ITT Electro-Optical Products Division
P. O. Box 7065, Roanoke, Virginia 24019

Morton Pomerantz
U.S. Army Communications R&D Command
Fort Monmouth, New Jersey 07703



Abstract

Fiber optic cables developed under an ECOM contract were subjected to rigorous mechanical and environmental tests to determine survivability under simulated field conditions. Tests included impact, bend, twist, fatigue under load, roadway survival, high temperature, low temperature, minimum storage radius, and gripping and slippage. The testing indicated that fiber optic cables are extremely rugged, but that some parameters required improvement. Subsequently, a modified cable was developed which exhibited improved impact resistance, lower optical losses, and reduced jacket slippage. Areas requiring still further development and test effort were identified.

Introduction

For the past five years, the U.S. Army Communications R&D Command (formerly ECOM) has been engaged in the development of ruggedized fiber optic cables for tactical communications systems. For the long haul time division multiplexed (TDM) system, high bandwidth graded index multimode fibers will be employed for the transmission of digital data at rates up to 20 megabits per second for distances of 8 km without repeaters. The standard CX-11230 dual coaxial cable would require repeaters every 1/4 mile at these data rates and the system would weigh 8636 kg. By contrast, the 64 km system using fiber optics would weigh only 1815 kg. The ITT Defense Communications Division was awarded a contract for the development of such a system, consisting of two special optical modems, 7 optical signal repeaters, 10 one-kilometer lengths of low loss multifiber optical cable, one cable repair kit, an optical test set, and 7 optical cable simulators. Demonstration of the system will begin in late 1978. The CX-4566 (26 pair) cable is currently used in local distribution telephone and data systems within Army command posts. The cable runs range from 100 meters to one kilometer. Consequently, the attenuation of the fiber optic cable replacement for the local distribution systems need not be as low as that for the long haul TDM system. This less severe attenuation requirement resulted in the development of cables employing plastic cladded silica fibers under a contract awarded to ITT Electro-Optical Products Division in May 1975. During that program cables were developed which had attenuation less than 20 dB/km at .82 μm and which exhibited considerable resistance to rugged handling and adverse environmental conditions. The subject of this paper is the further development of those cables under an additional contract awarded to ITT EOPD in May 1977. The aim of this contract effort was to more fully characterize the performance of cables developed under the first program and to improve upon their performance through design changes and further testing.

Program Goals

The primary goal of this program was the development of an improved fiber optic cable having the optical and mechanical characteristics listed in Table 1. A reduction in fiber attenuation to 12 dB/km at .82 μm and an improvement in cable impact resistance to 4 Nm were of greatest interest. In addition, the cable should retain the desirable mechanical/environmental characteristics developed during the previous program.

Testing of Previous Cable Designs

During the May 1975-May 1976 program, two cable types were developed. As shown in Figure 1, the central strength member design (ECOM 1) consists of a 19-strand Kevlar® strength member surrounded by a Kevlar® braid. Six optical fibers are helically laid around the strength member along with polyester fillers. A helically

wrapped TFE tape is applied, followed by an extruded polyurethane jacket. The external strength member design (ECOM-3) consists of a bundle of seven helically laid optical fibers at the center surrounded by a polyurethane jacket. Kevlar® strength members are helically laid around the jacketed bundle, followed by TFE tape and an extruded jacket of polyurethane.

Both cable types exhibited good resistance to mechanical abuse[1], however it was determined that further testing was required to more fully characterize cable performance. Table 2 lists the tests performed and the following paragraphs describe the tests and their results.

Impact Resistance Test

Samples of cable types ECOM 1 and ECOM 3 were tested for impact resistance in accordance with MIL-C-13777F except that impact testing ranged from 1.2-4.7 Nm. Both cable types were found to be more impact resistant at high and low temperatures than at room temperature. Earlier[1] impact resistance test findings at room temperature were confirmed in that the maximum impact energy at which the ECOM 1 and ECOM 3 type cables sustained no broken fibers was approximately 2.6 Nm and 2.0 Nm[2], respectively. At +85°C both cable types survived 200 impacts at 3.4 Nm with no fiber breakage and at low temperatures[3] both cable types survived 200 impacts at energies up to 4.75 Nm.

The data presented above shows that the original program goal of developing a cable capable of withstanding impact forces over a wide temperature range is achievable. The data also shows that polymer coating materials, strength members, and fibers can be combined to form an impact resistant cable if properly selected.

Bend Test

Samples of cable types ECOM 1 and ECOM 3 were bend tested in accordance with MIL-C-13777F. All fibers in the ECOM 3 cables survived bend testing at low temperatures[3], room temperature, and high temperatures. Two fibers in one of the ECOM 1 samples failed during bend testing at +85°C.

Twist Test

Samples of cable types ECOM 1 and ECOM 3 were twist tested in accordance with MIL-C-13777F. The two cable types survived the twist test with no fiber breakage. The test equipment employed in the room temperature test allowed the cable to be twisted the specified 180 degrees. However, the test equipment employed for the high and low temperature tests restricted the twist angle to approximately 100 degrees instead of 180 degrees due to the particular design of the equipment.

Attenuation vs Tension

Attenuation vs tension testing was performed using the apparatus shown in Figure 2 to simulate the effect of tensile loading in the field. The tensile load was increased in eight increments to 181 kg and attenuation was measured at each increment. Neither cable type showed significant increases in attenuation over the 24 meter gauge length.

Fatigue

Fatigue testing was performed using the same test apparatus as that for the attenuation vs tension test. The objective of this test was to simulate a field condition in which the cable might experience tensile loads for a period up to two months. Moderate reductions in transmitted power were noted toward the end of the test period, but were felt to be within the system power budget. No fibers fractured during the two month period.

Roadway Survival

ECOM 1 and ECOM 3 cables were tested for cable survivability during a two-month test during which heavy vehicular traffic traveled over each cable type. Both cable types survived two weeks without any fiber breakage. During the third week, one fiber stopped transmitting in the ECOM 1 cable. At this inspection, it was noticed that tire tracks were located over the cables due to intentional acceleration. All fibers were transmitting in the ECOM-3 cable. Additional damage occurred during the fifth week of testing and four fibers in the ECOM 3 cable stopped transmitting. At this time, two additional fibers stopped transmitting in the ECOM 1 cable.

At the conclusion of the two-month test period, the attenuation was measured in the remaining fibers in the ECOM 1 cable. The results were comparable to pre-test values for ECOM 1. The polyurethane cable jackets remained intact, having a slightly "dulled" appearance. Internal components were frayed or distorted, but remained intact.

High Temperature Attenuation

ECOM 1 and ECOM 3 cables were evaluated to determine the effect of high temperatures (+85°C) on attenuation. Cables were evaluated on reels and in loose coils. Test data for cable types ECOM 1 and ECOM 3 are listed in Table 3. Neither cable type exhibited significant increases in attenuation when exposed to high temperature. The storage configuration appeared to have no influence on the results since average optical performance was nearly the same in a loose coil configuration as on a spool, but some fibers incurred significant increases in attenuation. This may be attributed to cable effects rather than reel configuration.

Low Temperature Attenuation

Both cable types were evaluated at -55°C to determine optical properties. As shown in Table 4, ECOM 1 and ECOM 3 cables exhibited no detectable light transmission at -55°C (attenuation equipment dynamic range ~87 dB). Although post-test results showed slightly reduced average attenuation compared to pre-test results, some individual fibers showed increased attenuation. The samples were the same as used in the high temperature tests. Between the pre-test results for high temperature and post-test results for low temperature there was an overall increase of attenuation.

The test was repeated at -45°C, and the results are summarized in Table 4. ECOM 1 showed increased attenuation of 25-30 dB/km but the attenuation of the ECOM 3 samples increased by only 5-10 dB/km. The attenuation of fibers in both cable types show some degradation due to exposure to the low temperature.

Both cables failed to transmit light at -55°C. The cause is believed to be a temperature induced density change in the silicone RTV resulting in a significant change in its refractive index. This results in a fiber that is very susceptible to microbending losses. Raising the temperature to -45°C improved transmission characteristics significantly for the ECOM 3 design, but losses in the ECOM 1 design remained moderately high compared to room temperature. The difference in performance between the two cable designs is felt to be related to the cable designs rather than the silicone.

Experiments to improve the low temperature performance of these cables will continue, with emphasis placed on the evaluation of alternate silicone materials. The interaction at low temperatures between the fibers and other cable materials will also be studied.

Minimum Storage Radius

ECOM 1 and ECOM 3 type cables were evaluated to determine the effect of storage on small diameter reels after cycling to -55°C and +85°C. In addition, the smallest diameter reel at which optical and mechanical degradation is negligible was to be determined. Reel diameters of 11 cm, 15 cm, and 25 cm were selected for evaluation. The 25 cm metal reel evaluation showed an average increase in attenuation of 8-9 dB/km after the temperature tests. The exact cause of this increase is not known, however, this particular test specimen had been respooled several times prior to testing. The mechanical effect was a slight set in the cables after the evaluations. The polyurethane jacket showed no degradation.

Cables on 15 cm metal reels showed an increase in attenuation of 2-3 dB/km. A slight set in the cables was observed. The attenuation increase was negligible for most fibers. Since there were attenuation increases in both the 15 cm and 25 cm diameter reel configuration, an additional evaluation was conducted with an ECOM 3 cable on a 11 cm metal reel to determine the minimum storage radius. The 11 cm reel was felt to be the smallest practical reel size for field applications. No significant increases in attenuation were noted for most fibers, however a slight set in the cables was noted after the completion of the test. A 30 cm section of ECOM 3 cable was stripped, and no damage to the Kevlar® strength members or inner polyurethane jacket was noted. No degradation was noted in the outer polyurethane jacket.

Contrary to the results that might be expected of such an evaluation, cables stored on the smallest reels exhibited the least increase in attenuation. The data indicate, however, that cables of the ECOM 1 and ECOM 3 designs can be stored on reels as small as 10-15 cm diameter without significant increases in attenuation after temperature cycling.

Gripping and Slippage

Both cable types were evaluated for jacket slippage characteristics using commercially available Kellems grips and Dead End grips. The objective was no slippage at 181 kg. Using the Kellems grips, slippage occurred at 45 kg. The Dead End grips held until 112 kg for both cable types. Aside from differences in grip types, a contributing factor to slippage was felt to be the helically wrapped TFE tape employed in both cable

types beneath the outer jacket.

Modified Cable Design

The extensive testing performed on the ECOM 1 and ECOM 3 cable designs formed the basis for a number of experiments that would produce a cable design meeting the program objectives listed in Table 1. Various designs were investigated with effort concentrating in the following areas:

1. Improvement of fiber buffers to minimize microbend effects and maximize impact resistance
2. Jacket material modifications to reduce jacket slippage
3. Elimination of the TFE tape to reduce jacket slippage

The resultant cable design is shown in Figure 3 and consists of seven plastic clad silica fibers buffered to a diameter of 1 mm. The seven fiber bundle is surrounded by an extruded polyurethane jacket, followed by a layer of Kevlar® strength members and a final polyurethane jacket.

Testing of Modified Cable

Representative samples of the modified external strength member cable were subjected to impact and bend tests at -55°C to +85°C and were evaluated for jacket slippage. Fatigue testing over a two-month period will begin during August, 1978.

Impact Testing

Impact testing was performed on six cable samples at each temperature in the range of +85°C to -55°C. As shown in Figure 4, survivability was high within the range of +85°C to -30°C, but 38% of the fibers failed at -55°C at the specified impact energy of 4 Nm. Additional testing at 4.4 Nm and 4.7 Nm confirmed the results. The high failure rate at -55°C was a result of the fracture of the outer polyurethane jacket which became brittle at that temperature. The jacket material employed was a slightly modified grade of polyurethane intended to provide a "matte" finish and a green color. Since the data presented earlier in this paper indicated high survivability at -45°C for ECOM 1 and ECOM 3 types, additional testing will be performed at -45° to -55°C on cables employing various grades of polyurethane to determine survivability.

Bend Testing

Bend testing was performed at +85°C, room temperature, and -55°C. Three cable samples were tested at each temperature with no fiber failures.

Gripping and Slippage

The modified cable design was tested for jacket slippage using commercially available Kellems grips and Dead end grips. In contrast to the performance of the ECOM 1 and ECOM 3 designs, the modified external strength member cable showed no slippage with either type grip up to the specified load of 181 kg. This drastic improvement is felt to be a result of the change in outer jacket material and the elimination of the TFE tape.

Summary

The modified external strength member cable developed under this program represents another step forward toward the eventual replacement of conventional conductors with fiber optics. It has been shown that optical fiber cables can withstand rugged tactical field conditions over wide temperature ranges without significant mechanical degradation. The modified external strength member design has met the impact resistance goal of 4 Nm at temperatures ranging from +85°C to -30°C. It has exhibited average attenuation of 12 dB/km at .82 μm, far below the 1975 goal of 50 dB/km. A question still to be answered is the lowest temperature at which plastic cladded silica fibers are operational, current data indicating -40 to -45°C. Work will continue in this area, concentrating on fiber and cable materials research.

References

1. "Low Cost Fiber Optic Cables for Local Distribution Systems," Research and Development Technical Report ECOM-75-1328-F.
2. Nm - (Newton-meters).
3. -45°C

Table 1. Program Goals.

Parameter	Goal
Attenuation	<12 dB/km @ .82 μm
Impact Resistance	4 Nm @ 200 impacts, -55°C, RT, +85°C
Bend	Survive 2000 cycles @ RT, 1000 cycles at -55°C and +85°C
Fatigue	No fiber breakage nor significant increases in attenuation @ 45 kg over two months
Jacket Slippage	No slippage at loads up to 181 kg

Table 2. Tests Performed on Previous Cable Designs.

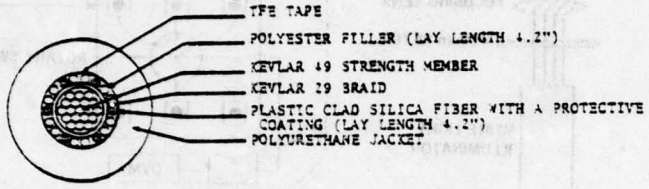
1.	Impact Resistance	Survive 200 4 Nm impacts @ -55°C, RT, +85°C
2.	Bend	Survive 2000 cycles @ RT, 1000 cycles @ -55°C, +85°C
3.	Twist	Survive 2000 cycles @ RT, 1000 cycles @ -55°C, +85°C
4.	Attenuation vs Tension	Minimum increase in attenuation at loads up to 181 kg
5.	Fatigue	No fiber breakage during two month period at 45 kg
6.	Roadway Survival	No fiber breakage during two month test period
7.	High Temperature Attenuation	No increase in attenuation at +85°C
8.	Low Temperature Attenuation	No increase in attenuation @ -55°C
9.	Minimum Storage Radius	Determine smallest diameter reel on which cables can be stored at temperature extremes
10.	Gripping and Slippage	Determine slippage characteristics with Kellems and Dead End Grips

Table 3. High Temperature Attenuation.

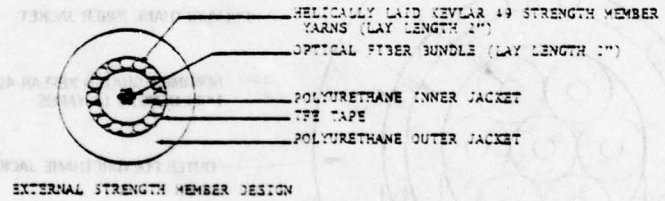
	Attenuation (dB/km @ .82 μm)		
	Pre-Test 24°C	Test 85°C	Post-Test 24°C
ECOM 1			
15 cm Reel	13.9	13.1	16.5
15 cm Coil	13.6	14.0	16.3
ECOM 3			
15 cm Reel	9.9	11.3	11.6
15 cm Coil	10.2	12.7	13.8

Table 4. Low Temperature Attenuation.

	Attenuation (dB/km @ .82 μm)		
	Pre-Test 24°C	Test -55°C	Post-Test 24°C
ECOM 1			
15 cm Reel	16.6	No light	15.2
15 cm Coil	16.3	No light	15.5
ECOM 3			
15 cm Reel	11.8	No light	12.7
15 cm Coil	13.6	No light	12.4
	Pre-Test 24°C	Test -45°C	Post-Test 24°C
ECOM 1			
15 cm Reel	15.2	38.0	17.2
15 cm Coil	15.5	40.4	15.9
ECOM 3			
15 cm Reel	12.7	20.6	16.2
15 cm Coil	12.3	15.0	13.7



Central Strength Member Design.
(ECOM-1)



External Strength Member Design
(ECOM-3)

Figure 1. Previous Cable Designs.

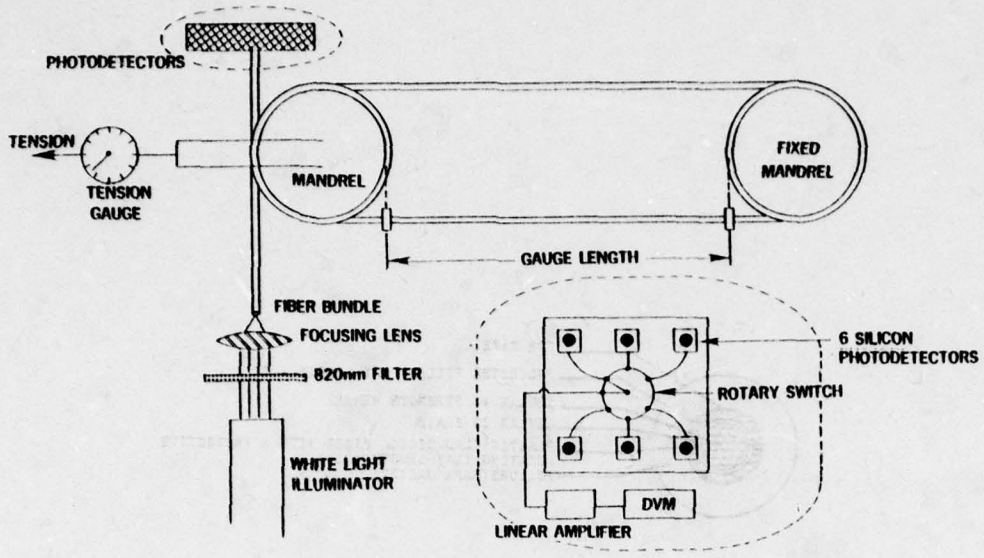


Figure 2. Attenuation vs Tension.

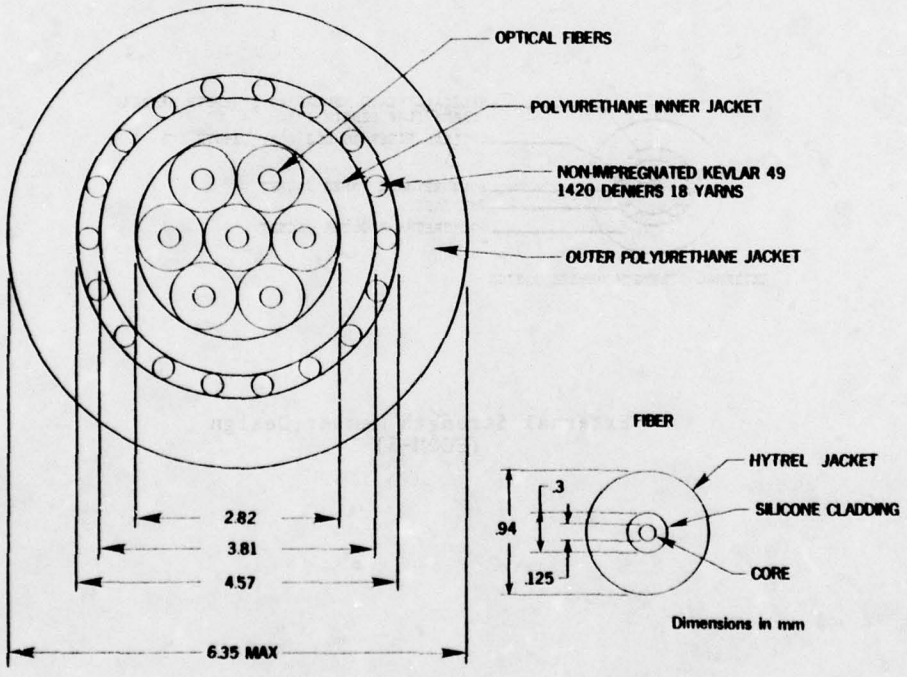


Figure 3. Optimized Low Cost Fiber Optic Cable.

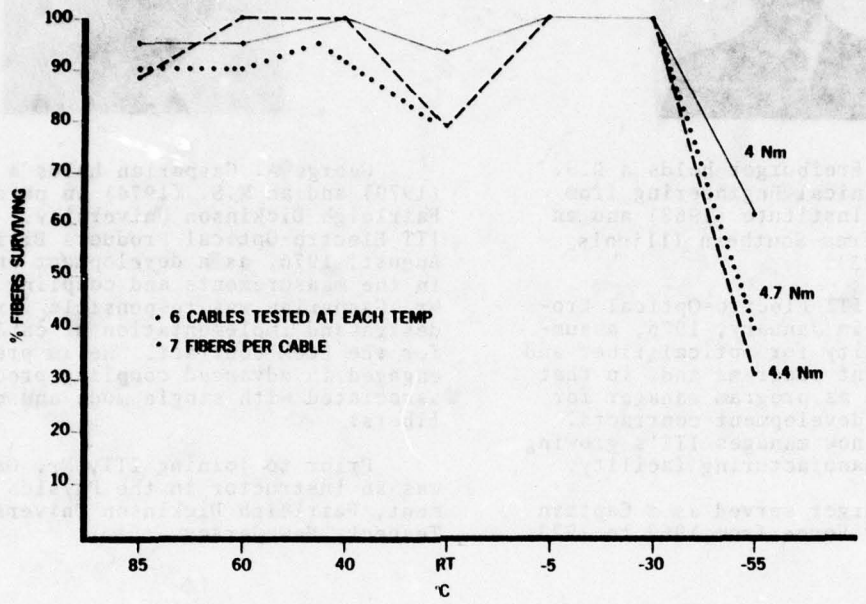


Figure 4. Impact Test.



Robert J. Freiburger holds a B.S. degree in Mechanical Engineering from General Motors Institute (1968) and an M.B.A. degree from Southern Illinois University (1973).

He joined ITT Electro-Optical Products Division in January, 1976, assuming responsibility for optical fiber and cable development programs and, in that capacity, acted as program manager for the ECOM cable development contracts. Mr. Freiburger now manages ITT's growing optical fiber manufacturing facility.

Mr. Freiburger served as a Captain in the U.S. Air Force from 1969 to 1973.



George A. Gasparian holds a B.S. (1970) and an M.S. (1974) in physics from Fairleigh Dickinson University. He joined ITT Electro-Optical Products Division in August, 1976, as a development engineer in the measurements and coupling group. Mr. Gasparian was responsible for the design and implementation of cable testing for the ECOM contract. He is presently engaged in advanced coupling processes associated with single mode and multimode fibers.

Prior to joining ITT, Mr. Gasparian was an instructor in the Physics Department, Fairleigh Dickinson University, Teaneck, New Jersey.



Mr. Morton Pomerantz served in the U.S. Army in World War II from 1943 to 1946. He received his B.E.E. degree from New York University in 1955. He has been employed at Fort Monmouth since 1952 as an Electronics Engineer. In that time, he has been engaged in R&D activities principally in the areas of RF cables and connectors and tactical communications cables. For the past six years his principal interest has been in the development of tactical fiber optic cables and connectors for the Army's fiber optic communication systems. Mr. Pomerantz is a member of IEEE. He serves as the Army member of the Working Group on Cables and Connectors of the Tri-Service Fiber Optics Coordinating Committee.



John C. Smith graduated from the Universided Tecnica del Estado - Santiago, Chile in 1958. He joined ITT Electro-Optical Products Division in 1974, where he is presently engaged in the development and design of fiber optic cables, including evaluation and selection of equipment and materials. He is also involved in the development of fiber optic coatings and related processes.

Prior to joining ITT, he was associated with General Cable Corp. (Philadelphia Insulated Wire) where he was Supervisor of Products Engineering. Earlier he was associated with Simplex Wire and Cable, Power and Control Division.

FIBER OPTIC CABLE DESIGN, TESTING AND INSTALLATION EXPERIENCES

Peter R. Bark
(Siecor Optical Cables, Inc., Horseheads, NY)

Ulrich Oestreich and Günter Zeidler
(Siemens AG, Munich, West Germany)

Abstract

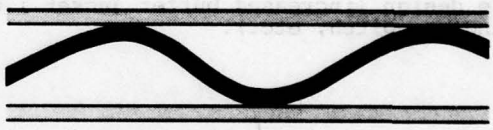
This paper deals with design considerations for Siecor® optical cables usable in various fields of applications. A loose tube fiber protection has been specially developed in order to decouple the fiber from forces applied to the cable. This construction preserves all optical properties of the glass fiber during and after cable manufacturing, during installation and over the operating range of environments. Fiber excess length, tube dimensions and cable materials are discussed for a great variety of cable constructions, such as: indoor cables, hook-up connections, duct and conduit cables, burial and direct plow-in cables, aerial cables for severe weather conditions, maximum pole distances, and for extreme high pull strength values. The cable performance is described by a number of test procedures put into practice and by some installation experiences.

1. Design Considerations

The mechanical properties and transmission characteristics of optical waveguide cables are mostly determined by microbends, attenuation change with temperature, and strain of the optical fibers. In high-performance, low-loss optical fiber cables one has to minimize these effects.

As reported before[1,2], Siecor protects the optical fibers* against microbending by applying a loose plastic tube. This buffer jacket consists of an inner Halar layer, a material providing low friction between fiber and buffer; and an outer layer of PBTP, a high-modulus polyester which provides high mechanical strength. The buffer jacket has an i.d. ranging from 0.8 to 1.3 mm and an o.d. ranging from 1.1 to 2.0 mm depending on cable type and application. The fiber can move freely inside the buffer jacket and can automatically adjust to a position of minimum bending strain, i.e. the position of minimum excess attenuation caused by bends.

Because of the special buffering process, the fiber is longer than the buffer jacket. This well-defined excess length, typically 0.1%, is chosen in such a way that practically no measurable excess loss is caused by the statistical fiber bends (macrobends) of the fiber helix inside the loose tube[3]; see Figure 1a. When loading the cable, first the strength members get stressed without transferring stress to the fiber. If, at increased cable load, the buffer jacket is strained, the fiber still remains stress-free and can freely adjust to a nearly "straight" position (see Figure 1b). All long-term ratings given later on for the different cable designs are based upon this fiber position inside the loose tube.



a. Fiber in Buffer Jacket After Cable Manufacturing



b. Decrease of Fiber Excess Length Caused by Strain Of Buffer Jacket During Cable Stress



c. Increase of Fiber Excess Length Caused by Shrinkage Of Buffer Jacket Materials During Cooling

Figure 1: Optical Fiber with Excess Length Inside a Loose Buffer Jacket

* Supplied by Corning Glass Works, cladding o.d. 125 µm, overall o.d. (including cellulose acetate lacquer) 138 µm

If the buffer jacket strain surpasses the fiber excess length, the fiber is in a tensile stress state causing microbending losses, especially at the points where the fiber is supported by the buffer jacket. This situation causes attenuation increase and probably fatigue effects. In order to prevent irreversible attenuation changes and/or fiber breakage, the cable should be loaded to this stress level for a short period only. This is the short-term rating for installation.

Figure 1c shows the case for increased fiber excess length caused by shrinkage of the buffer jacket plastic materials during cooling. The attenuation remains stable until the shortened mechanical period of the fiber helix creates macrobending losses and this, together with the increased pressure between the fiber and the inner wall of the buffer jacket, creates microbending losses.

The above described effects are summarized in Figure 2, where the attenuation change α_B of a cable in dB/km is given for both elongation and compression in percent for a buffer jacket with 0.8 mm i.d. The attenuation increases drastically if the buffer jacket is strained or shortened beyond $\pm$.1%. For negligible attenuation change the allowed elongation/compression has to stay within the small window of approximately $\pm$.1%. All needed additional strain has to be covered by the subsequent cable design (increased buffer jacket i.d., stranding, pitch, etc.).

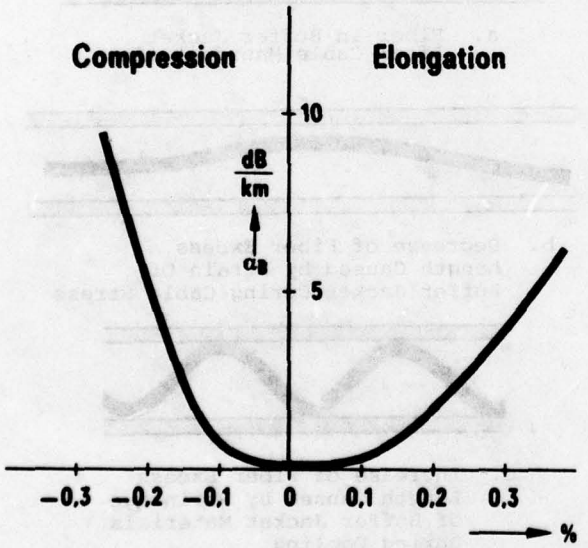


Figure 2: Attenuation Change α_B vs. Strain (Buffer Jacket i.d. 0.8 mm)

2. Cable Designs

2.1. Standard Cables - In the following we are describing several standard cable designs which have been proven as indoor and outdoor cables for tray, duct and underground installations.

Figure 3a shows the cross sectional diagram of an indoor one-fiber cable. A layer of reinforcing fiberglass yarn is spun around the buffer jacket and protected by a polyurethane (PUR) jacket. This light-duty cable was designed for use in a variety of environments over moderate installation distances. The fiberglass strength member is used to impart to the cable a degree of longitudinal stiffness. The tightly-extruded PUR sheath is still flexible and provides, together with the glued fiberglass, a longitudinal stiffness for a broad operating temperature range (-30° to +50° C). This cable can be reinforced by an additional layer of Aramid-yarn (Figure 3b) which is covered by an outer PVC sheath. For a two-fiber cable construction, two subunits as shown in Figure 3c are used and reinforced by a layer of Aramid-yarn. The material of the outer sheath of this flat cable is either PVC or PUR.

Cables for a larger number of fibers and for higher performance levels are made by stranding the loose tube buffers with perfect backtwist around a central element. In standard cables this central element consists of a buffered high-modulus steel wire, operating as an anti-buckling element. The performance of stranded cables is determined by the stranding induced fiber excess length, the value of which can be an order of magnitude higher than for unstranded cables. By properly selecting the stranding parameters and defining the cross section of Aramid yarns, operating temperature range and allowable installation forces are determined. Typical values of these for stranded standard cables are -40° to +70°C and 600N.

2.2. Modified Cable Designs - In order to meet special requirements, the standard cable design can be modified easily. The following design changes have been achieved in our product line:

All dielectric cables are desirable in environments with a high probability of lightning. In these cases the central element can be replaced by a fiberglass reinforced plastic element, e.g. 40% fiberglass rovings incorporated in an epoxy matrix.

Flame retardant cables are required for building installations and for nuclear power plant applications. Cables meeting the IEEE-383 flame test have been designed, manufactured and installed.

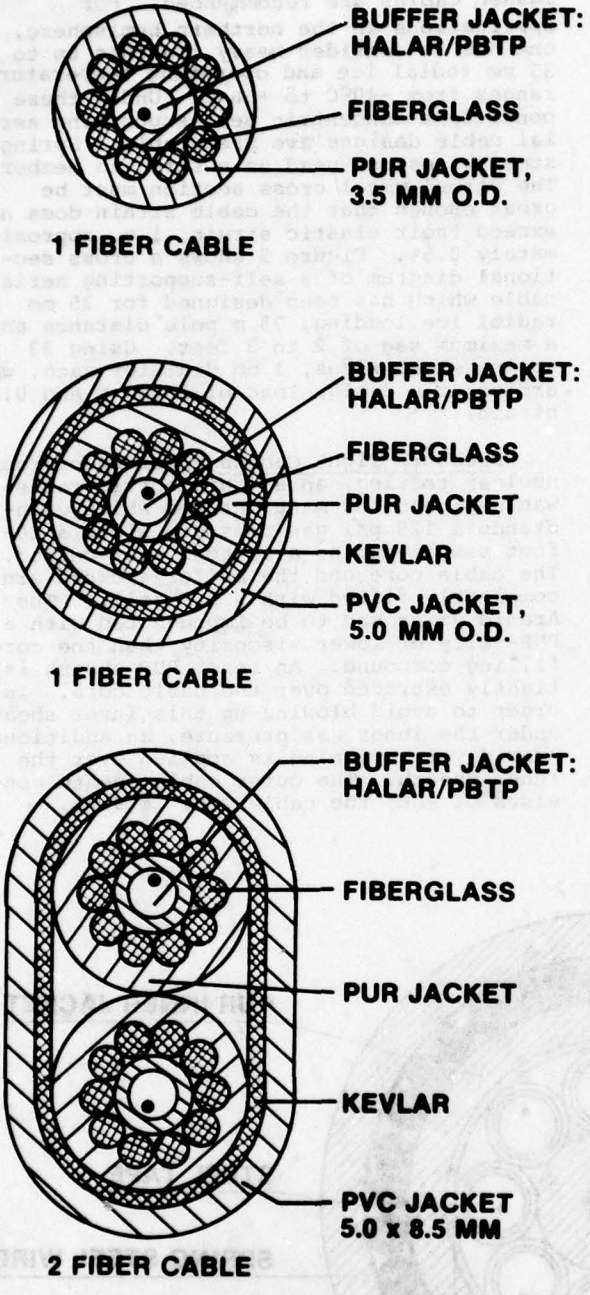


Figure 3: Standard One- And Two-Fiber Cables

Copper wires incorporated into fiber cable designs are needed, where repeaters have to be powered. These cables have been successfully tested.

Filled cables are recommended in all cases where the presence of water due to damage to the cable jacket, together with freezing temperatures, is to be expected (see paragraph 2.3).

Rodent protection for underground cables can be achieved by an additional outer PUR sheath or a steel tape armoring.

2.3. Filled Cables - Aging and fatigue tests in the presence of water or moisture with bare fibers which are under no stress indicate that no deterioration of optical and mechanical properties can be observed.

In the case of cable jacket damage, water can penetrate into the cable core and further into the buffer jacket. Presence of water and temperatures below 0°C may lead to ice forming inside the buffer jacket and may create attenuation increase due to expansion of the ice and microbending. These effects can be avoided by filling the buffer jackets. A suitable filling compound used in our cables is a plastified PUR-jelly. The cured resin is adjusted to be sufficiently soft and partly self healing to still allow the necessary fiber movements with a time constant below one second (see Figure 4).

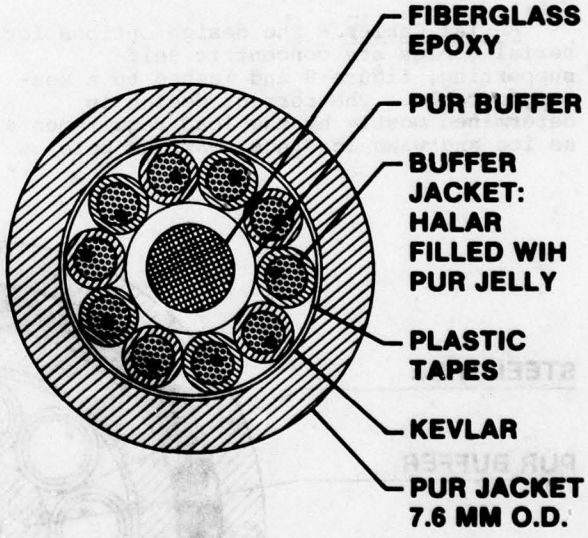


Figure 4: All Dielectric 10-Fiber Cable Containing Buffer Jackets Filled with PUR-Jelly

For cables containing both fibers and copper wires, the cable core can be filled also. The core filling compound, also a PUR-jelly, is selected to ease buffer jacket slippage when the cable is bent.

2.4. Special Application Cables - Fiber optic cables which are exposed to environments requiring extreme loads and broad operating temperature ranges during

life and/or during a short period of time (installation) have to be designed differently.

Direct Burial Cables - Direct burial cables are exposed to high pulling forces and additional mechanical loads (crushing, impact) during the plow-in procedures. Once the cables are installed, earth displacements caused by frost may give the direct buried cables additional loads. In addition, underground cables can be attacked by rodents. On the other hand, the operating temperature range is likely to be moderate.

Mainly, two different plow-in cables have been designed, characterized and successfully tested. One cable design consists of an inner cable core similar to standard cables with filled buffer jackets. The outside jacket is reinforced by one layer of stainless spring steel wires and two layers of steel tape. This armoring has been designed for plow-in procedures (5 feet deep) requiring up to 3000 N tensile force. For standard plow-in procedures up to 3 feet deep and soft ground, we have designed an all dielectric plow-in cable. This cable is protected by an additional layer of Aramid reinforcement yarns and an outer scuff- and rodent-proof PUR jacket.

Aerial Cables - The design options for aerial cables are concentric self-supporting, figure-8 and lashed to a messenger cable. The correct design is determined mostly by the load requirements, as ice and wind loadings, maximum pole distance and maximum allowable sag. For moderate temperature zones, figure-8 and/or lashed cables are recommended. For applications in the northern hemisphere, one has to consider heavy loadings up to 35 mm radial ice and operating temperature ranges from -40°C to +50°C. Under these conditions concentric self-supporting aerial cable designs are preferable. Spring steel wires are used as a strength member. The wires' total cross section must be great enough that the cable strain does not exceed their elastic strain, i.e. approximately 0.5%. Figure 5 shows a cross sectional diagram of a self-supporting aerial cable which has been designed for 35 mm radial ice loading, 75 m pole distance and a maximum sag of 2 to 3 feet. Using 33 spring steel wires, 1 mm diameter each, we arrive at a design load of 25000 N and 0.6% strain.

Pressure Tight Cables - For underground nuclear testing, an all dielectric cable was designed and manufactured which withstands a 125 psi gas pressure along a 10-foot sample during a 24-hour test period. The cable core and the buffer jackets are completely filled with a PUR-jelly. The Aramid yarns had to be impregnated with a PUR-jelly of lower viscosity than the core filling compound. An inner PUR sheath is tightly extruded over the cable core. In order to avoid blowing up this inner sheath under the inner gas pressure, an additional Aramid yarn spinning is applied over the inner sheath. The outer cable sheath consists of PUR; the cable O.D. is 9 mm.

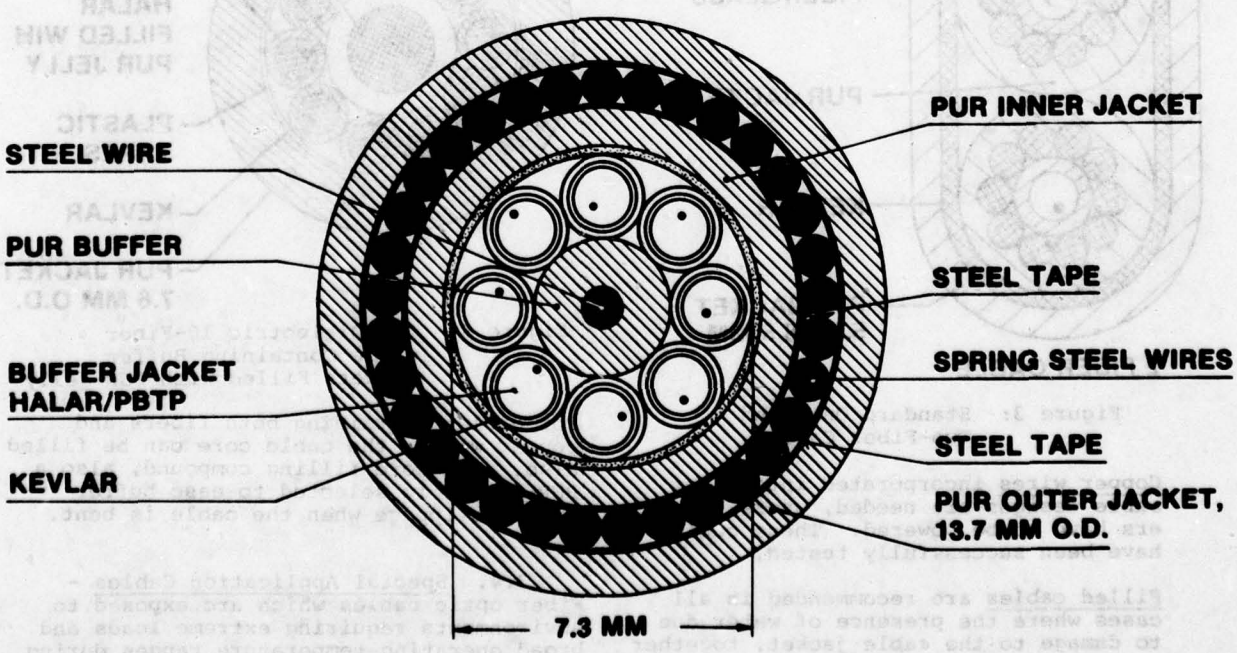


Figure 5: Self-Supporting Aerial Cable

3. Cable Testing

To insure reliability over a life time, all Siecor cable designs are subjected to optical, mechanical and environmental tests. The following mechanical tests are meaningful tools to characterize cable capability and field of application:

- Tensile test
- Temperature test
- Impact test
- Crush resistance test
- Bending test
- Flexibility test

Most of these tests are carried out according to MIL-DOD-STD 1678.

In order to simulate actual installation and handling conditions, all our cables are subjected to both long and short gauge-length tests after manufacturing (see Figures 6 and 7).

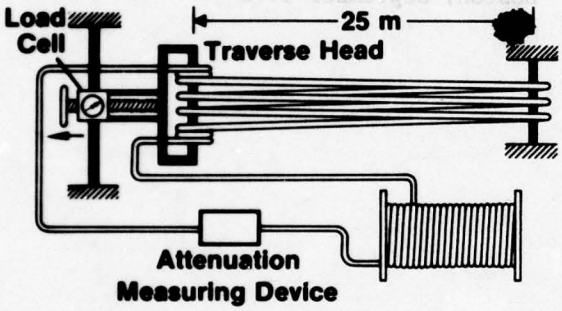


Figure 6: Long-Length Tensile Test

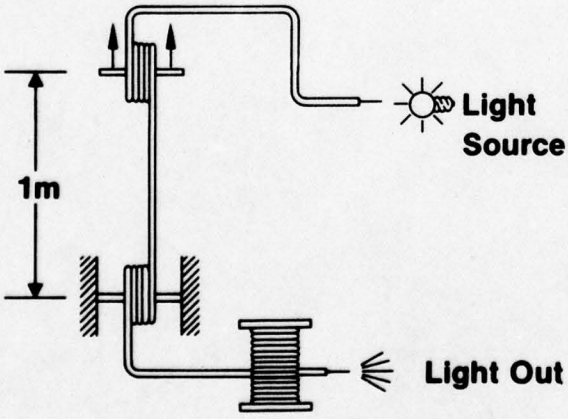


Figure 7: Short-Length Tensile Test

In the long-length test a 150 m cable portion of the manufacturing length is loaded. The cable is fixed with two chuck-drums and looped three times between two shafts which are 25 m apart. With the help of an insertion loss measuring device, the attenuation change versus pulling force is measured. In the short-length test the structural cable strength, determined by the cross section of the strength members, is measured. Optical fiber breakage is monitored visually. Figure 8 shows, qualitatively, changes in cable attenuation and the probability of optical fiber breakage as a function of tensile force. Cable ratings are derived from this model, based upon empirical results using the equipment and test procedures described above.

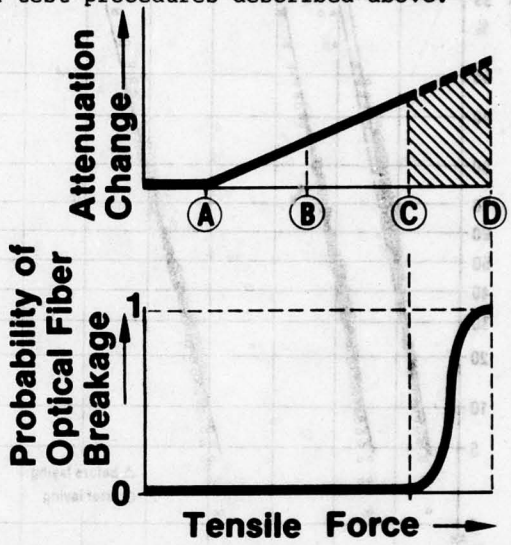


Figure 8: Effect of Tensile Force On Cable Properties

A. Recommended residual stress for no change in transmission properties

B. Recommended tensile force for installation (reversible change in transmission properties)

C. Force at which the first optical fiber may break

D. Force at which the cable may rupture (structural cable strength)

4. Installation Experiences

A series of installations have been carried out using the above-described fiber optic cable designs. Some of these cable links have been operating for more than two years without failure.[4] This includes duct as well as direct burial and aerial cables. In all installations it became obvious that fiber optic cables can be installed in the same way as conventional copper or coaxial cables using most of the same installation equipment. In many cases it was even easier to handle fiber optic cables.

Figure 9 shows attenuation data of cables

before and after installation for a duct system.[5,6] The figures indicate that there is no measurable change of fiber attenuation. These cables were installed using conventional tools. The major advantage, however, was that longer cable length over a greater number of bends could be installed in one run. Easy-to-handle splicing and measuring equipment is available and was successfully used in the field.

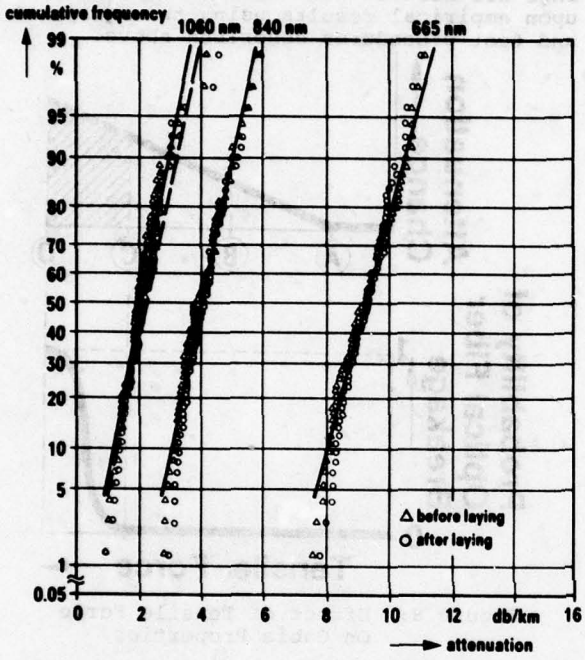


Figure 9: Cumulative Frequency Distribution of the Attenuation of Cables Before and After Installation

References

1 U. Oestreich, G. Boscher, G. Schöber, H. Liertz:
Optical Waveguide Cables
3rd European Conference on Optical Communication
Munich, September 1977, p. 44-46

2 P. R. Bark:
Optical Waveguide Cables: Design Considerations and Evaluation
1st International Symposium on Optical Communications (IBM)
Research Triangle Park, NC, October 18-20, 1977, p. 16-20

3 G. Zeidler:
Effects of Mechanically Induced Periodic Bends on the Optical Loss of Glass Fibres
Optics Communications (1976)

4 P. Bark, G. Boscher, J. Gier, H. Goldmann, G. Zeidler:
Installation of an Experimental Optical Cable Link and Experiences Obtained With the Transmission of TV and Telephone Signals
3rd European Conference on Optical Communication
Munich, September 1977, p. 243-245

5 H. Liertz, H. Goldmann, D. Schicketanz:
Laying and Properties of an Optical Test Link in Berlin
4th European Conference on Optical Communication
Genoa, September 1978

6 P. R. Bark:
Field Experiences with Fiber Optical Transmission Systems
10th Annual Electro Optics/Laser 78 Conference
Boston, September 1978

DESIGN AND MANUFACTURE OF AN EXPERIMENTAL LIGHTGUIDE CABLE FOR UNDERSEA TRANSMISSION SYSTEMS

R. F. Gleason and R. C. Mondello

Bell Laboratories
Holmdel, New Jersey

B. W. Fellows and D. A. Hadfield

Simplex Wire and Cable Company
Newington, New Hampshire

ABSTRACT

This paper describes the design of an experimental lightguide cable for use in long haul, high capacity undersea communication systems. It goes on to describe the methods used to manufacture a series of test lengths. Preliminary results from physical and transmission tests are discussed.

Design Requirements

Mechanical

The mechanical design of undersea cable is constrained at least as much by considerations of installation and recovery as by the stable pressure and temperature conditions on the ocean floor. It is usually more economical, and introduces no performance penalty, to fit the cable to the capacities of existing cable handling machinery than to significantly increase the equipment capability.

During installation, the cable experiences tension varying from essentially zero at the ocean bottom to a value at the ship equal to the weight per unit length of the cable in sea water multiplied by the depth of the water. The tension capability of the cable engine at the desired laying speed thus determines the maximum weight limit for the cable design. For the Bell System cable ship C.S. LONG LINES, the tension capability is 72 kN, so for use in maximum ocean depths, the weight of the cable must not exceed 8.4 kN/km.

If an emergency situation occurs during cable installation or recovery where the cable tension becomes extremely high, it is more preferable for the cable to break than for the cable engine to suffer structural damage. The cable can be recovered and repaired by equipment and personnel on the ship. With the brakes set to protect the motors, the strength of the LONG LINES cable engine is 180 kN; this then is the maximum acceptable cable breaking strength.

It is necessary to minimize the occurrence of cable suspensions on the ocean floor since these introduce undesirable static tension and are vulnerable to snagging by ships' anchors and fishing trawler gear. To achieve this, calculations based on ocean bottom profiles and ship handling characteristics show that the minimum satisfactory sinking rate for a cable, when sinking horizontally, is 0.97 km/hr. For a given cable diameter, this establishes the minimum acceptable cable weight in water. For example, a 20 mm cable must weigh at least 1.89 kN/km, and a 25 mm cable at least 2.52 kN/km.

In order to be able to recover a cable from the ocean floor the cable must be strong enough to support its own weight in a catenary between the surface and the bottom. In addition, dynamic stresses are introduced by the motion of the ship in response to wave action. Experience has shown that a satisfactory cable must have a breaking strength greater than the weight of 19 km of cable in water.

For a given diameter, the above considerations give maximum and minimum cable weight and, for a given weight, maximum and minimum strength. The results for a 25 mm cable are shown in Figure 1.

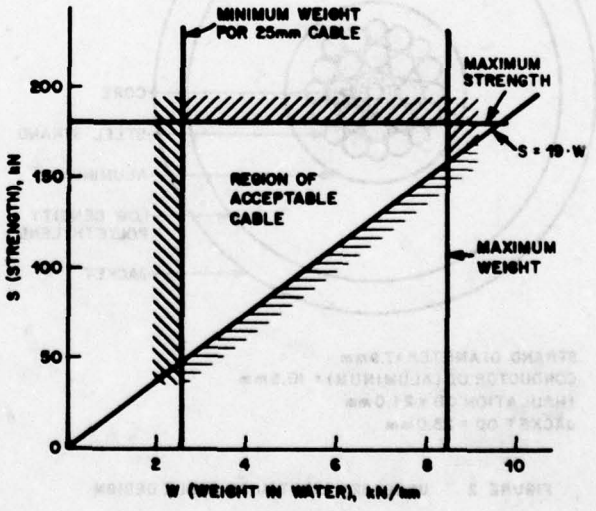


FIGURE 1 STRENGTH-WEIGHT DIAGRAM FOR UNDERSEA CABLE

Under normal laying conditions, a cable as shown in Figure 2, will experience approximately 0.25 percent strain. During recovery, however, strains as high as 1 percent can be expected. At the same time the cable will be bent around sheaves of 1.0 to 1.5 meter radius. Our goal is to develop a cable which will withstand 1 percent strain and repeated bending over a 1 meter radius without damage.

Electrical and Transmission

Since repeaters in undersea cable systems are series powered, the transmission cable also provides the DC power path. Consideration of power separation filter design led to establishing a maximum power feed voltage of 11 kV. For a 6500 km system, using the best available estimates for repeater power requirements, the maximum acceptable DC resistance for the cable is 0.65Ω/km.

To establish the insulation thickness, the maximum field strength was set at 3 kV/mm. This is low by normal power cable standards, but we believe it is justified when considering the sea water environment and the long history of problems with splices and molded joints in the ocean.

For the lightguide fibers, we established a target of no more than 1 dB/km cabling loss, which has been achieved in land cable. Further, to permit handling there must be no permanent attenuation change when the cable is flexed repeatedly over a 1 m radius and when tensioned to 1 percent strain.

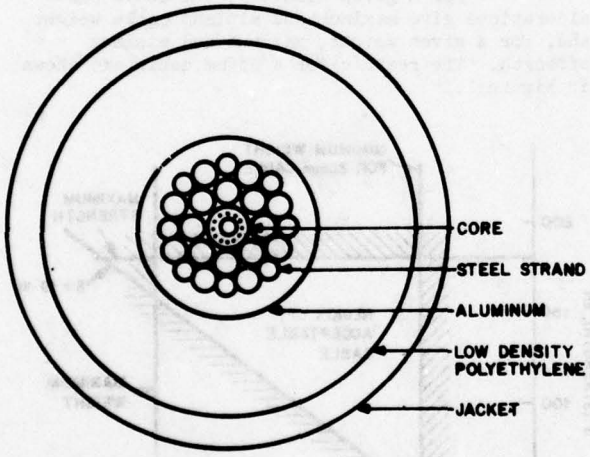


FIGURE 2 UNDERSEA LIGHTGUIDE CABLE DESIGN

Trial Design

A basic cable design which satisfies the mechanical and electrical requirements outlined above already exists. Undersea coaxial cable has the required strength, weight, strength to weight ratio, DC resistance, and maximum field strength. This cable also has a long history of manufacture, installation, and service. We need only modify its design to provide for fiber communication, choose an appropriate size based on systems considerations, and take advantage of any cost reductions associated with the fiber medium.

Cable Design

Figures 2 and 3 show the design of an experimental lightguide cable for undersea transmission. Figure 2 gives the overall cable design, while Figure 3 provides details of the central fiber core. Beginning with Figure 2, we have a fiber core which is discussed below in detail, a steel strand, a metallic conductor, high voltage insulation, and a protective jacket. The strand consists of 24 helically wound steel wires which provide the cable strength, weight, and modulus. This strand is surrounded by a conductor which allows us to satisfy the constraint on DC resistance. Copper has been used for this conductor in all our test cables to date, as it has in all undersea coaxial cable. However, we ultimately plan to use aluminum for this conductor because of its potentially significant cost savings. Note that this metallic conductor also provides a moisture barrier for the fibers. High voltage insulation is provided by a low density polyethylene layer whose thickness is determined by maximum field strength considerations. Finally, a high density polyethylene jacket may or may not be provided for the cable. This question is presently under investigation.

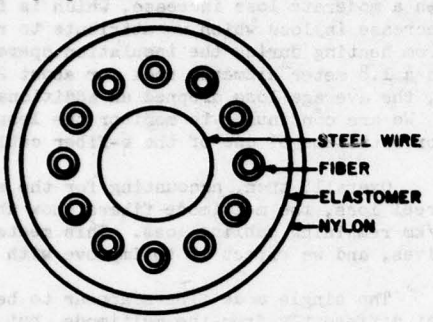
Fiber Core Design

In considering the fiber core design we will first discuss its location and the fiber encapsulation scheme. Note that the core has been placed within the steel strand at the center of the cable. This location provides maximum protection for the fibers, places them close to the cable's neutral bending axis, and provides for an essentially symmetric loading due to applied sea bottom pressure. The fibers have been completely encapsulated within the core by an elastomeric buffer which completely surrounds each fiber. This buffer isolates the fibers from any highly localized loads which could cause microbending and excess fiber loss, holds the fibers in a predetermined array, and makes handling of the core during manufacture a straightforward procedure.

Examining the fiber core in detail, Figure 3, we find a central steel wire, the fibers themselves, an encapsulant material, and an outer sheath. The central wire is required to provide strength to the core structure for manufacturing purposes. The fibers, which may be single mode or multimode, are helically wrapped within the encapsulant to provide for strain equalization in large diameter bending. The encapsulant is ideally an easily strippable material which has a low Young's modulus and a moderately high melting point. Finally, an outer sheath of a higher modulus

material is provided to ensure dimensional stability during subsequent manufacturing operations.

Based on present estimates for system parameters, the design described above has been optimized to provide a minimum cost cable. The dimensions used in our experimental cable are shown in Figures 2 and 3, and Table 1 provides a listing of cable properties.



CENTER WIRE OD = 0.8mm
NUMBER OF FIBERS = 12
FIBER OD (COATED) = 280μm
SHEATH THICKNESS = 0.1mm
CORE OD = 2.6mm

FIGURE 3 CORE DESIGN

PROPOSED LIGHTGUIDE EXPERIMENTAL CABLE

	DESIGN	OBJECTIVE
STRENGTH	85 kN	≤180
WEIGHT IN WATER	2.7 kN/km	≤8.4
STRENGTH/WEIGHT RATIO	31 km	≥19
SINKING VELOCITY	1.0 km/hr	≥0.97
DC RESISTANCE	0.65Ω/km	≤0.65
MAXIMUM E FIELD	3.0 kV/mm	≤3.0

TABLE 1

Manufacture of Trial Lengths

Manufacture of the experimental lightguide cable involves three basic operations: (a) fabrication of the fiber core, (b) fabrication of the composite strand-conductor structure, and (c) insulation extrusion. Ancillary operations include rewinding of optical fibers, optical testing, and physical testing of the cable.

Fiber Core

Manufacture of the experimental cable begins with receipt at Simplex Wire & Cable Company of optical fibers from Bell Laboratories, where they have been manufactured and proof tested to 240 MPa. To establish initial conditions, insertion loss is measured in each fiber using equipment calibrated to ±0.10 dB. Fibers are connected to the test leads using vacuum chucks and an index-matching fluid. The testing is performed in an environmentally controlled room, and to confirm the accuracy of measurements, test results are compared with measurements made previously at Bell Laboratories.

Following testing, fibers are rewound on equipment developed by Simplex Wire and Cable Company. The present design for a fiber rewinder includes a low tension (50 mN) payoff and high tension (50 mN-1470 mN) fail-safe take up, a precision traversing device and an in-line, frictionless, electronic footage counter. A static eliminator with air wiper is also provided for cleaning the fibers.

Manufacture of the fiber core is completed in a double pass sequence. The first of these passes is a tandem extrusion operation in which the fibers are stranded and encapsulated in a low modulus elastomer. During this tandem extrusion the steel center strand is preheated and sheathed with an elastomer. While this elastomer is still soft, the lightguides are stranded and partially embedded in it. This composite structure is then encapsulated with a secondary elastomeric jacket. In the next pass, this structure is sheathed with nylon in a tubing extrusion operation. This completes the fabrication of the fiber core. The insertion loss of the fibers is measured after each manufacturing pass to determine if any change has occurred due to the stranding or extrusion operations. If necessary, an optical time domain reflectometer is used to pinpoint breaks in the fibers.

The prototype line used for fabrication of the fiber core was developed by Simplex Wire and Cable Company. Its unique features include:

1. Minimum bending diameter restrictions of 150 mm for the optical fibers, and 1.83 m for the fiber core in order to minimize short-term stress in fibers.

2. Independent supply and take up tension controls which minimize the long-term fiber stress during storage of the fiber core.

3. A 12-bobbin lightguide strander with 200 mN to 1470 mN bobbin tension magnetic controls and a precision closing die assembly for embedding the fibers in the core.

4. Constant line tension control at less than 100 N independent of line speed control.

5. Precision line speed and extruder speed controls to maintain core diameter to within 25 μm.

6. Fully coordinated, regenerative line drives.

Composite Strand-Conductor

The composite steel strand and copper conductor used in prototype lengths of undersea lightguide cable is fabricated on conventional undersea coaxial inner conductor stranding, tube forming, welding and reducing equipment. The addition of a special, constant tension payoff stand for the fiber core was the only modification required. Future lengths of composite steel and aluminum conductor will be manufactured on a new stranding and aluminum extrusion line currently in development at Simplex Wire and Cable Company. In this operation, the fiber core will be paid off and the steel wires stranded as in the coaxial inner conductor stranding operation, but no forming, welding or reducing will be required as with copper. Rather, aluminum will be extruded directly over the steel strand.

The new conductor stranding and extrusion line will include a constant tension fiber core payoff stand, a high-speed planetary steel wire strander, a linear solid phase aluminum extruder and a high tension pull-out caterpuller. In addition, the extruder and line drives will be fully coordinated because the long lay strand is not coherent and therefore cannot be reeled. Hence, the aluminum extrusion and steel stranding operations must occur in tandem.

Insulation Extrusion and Final Testing

After the loss of the fibers is measured in the composite conductor, the insulation is extruded. This operation is performed on a conventional core extrusion line. Thereafter, loss is measured in the cable periodically to determine whether aging occurs, and if handling of the cable contributes to loss.

To conduct physical testing, special equipment for temperature, pressure, tension, torque, twist, bend and flex testing of lengths of lightguide cable is being developed by Bell Laboratories and Simplex Wire and Cable Company. This equipment simulates conditions anticipated during installation, operation and recovery of the cable. The facilities permit simultaneous optical and physical testing.

Test Results

Cabling Loss

Sample lengths of cable have been completed which contain 3, 6, and 12 fibers. These lengths have been tested for loss at each stage of manufacture. The results of these tests are shown in Figure 4, where the average loss at each stage is given. While the various fibers differed from one another at each stage of manufacture, they all followed curves similar in shape to the average curve shown.

First we will discuss the multimode fibers. At the fiber stage, the lightguides were wrapped on 150 mm diameter reels which we believe from other data introduces about 0.6 dB/km excess loss. We attribute the higher loss at the elastomer stage to microbending resulting from cabling of the fiber and cooling of the elastomer. The reheating which occurs in applying the nylon sheath allows relaxation and a decrease in loss. Again the handling associated with the application of the steel strand wires and the copper conductor produces a moderate loss increase, which is followed by a decrease in loss which we attribute to relaxation from heating during the insulation operation. Left on a 1.8 meter diameter reel for about 2 months, the average loss dropped an additional 0.6 dB/km. We are continuing to monitor the loss behavior with time of one of the 6-fiber cables.

Overall, then, accounting for the excess fiber reel loss, the multimode fibers show about 0.5 dB/km remaining cabling loss. This meets our objectives, and we expect it to improve with time.

The single mode fibers appear to behave somewhat differently from the multimode, but the general pattern is similar. The excess loss of these fibers on reels is approximately 2 dB/km, which exceeds the loss change introduced by the elastomer application. Subsequent changes are similar to those of multimode fibers except the loss increase during the steel stranding operation is much larger. We expect a decrease in loss with time.

Through the insulation stage, the cabling loss of the single mode fibers exceeds our objective. We will not be able to assess the seriousness of this problem until aging data is available.

Temperature Coefficient

Loss as a function of temperature has been measured over the range from 20° to 0° for a 1 km cable. The results are reproducible and show a change of 0.35 dB/km for the multimode fibers and 0.15 dB/km for the single mode for the 20° temperature change.

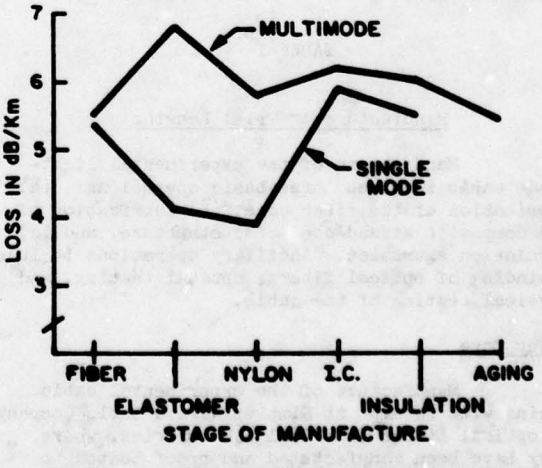


FIGURE 4 AVERAGE LOSS DURING PROCESSING

Effect of Tension

Tension tests on short lengths have shown that fiber continuity is maintained up to a cable tension of 66 kN, or about 0.85 percent strain. The fibers were proof tested in 1 kilometer lengths to 240 MPa (0.35 percent strain) which is less than we believe necessary and achievable for production cable.

Conclusion

The design and manufacture of trial lengths of an undersea lightguide communications cable have been discussed. While preliminary test results are encouraging, the deep-sea applicability of the design has not yet been established.



Bruce Fellows received his B.S. and M.S. degrees in Mechanical Engineering from the University of New Hampshire. He joined Simplex Wire and Cable Company in 1976 as Development Engineer for the Research and Development Group. In that position he has been responsible for the development of facilities and equipment, and manufacture and testing of prototype lengths of undersea lightguide cable.



R. F. Gleason received a B.S. in Engineering Science in 1961 from Case Inst., an M.S. in Engineering Mechanics in 1963 from N.Y.U. and a Ph.D. in 1967 from Stanford Univ. He has been with Bell Laboratories since 1961, working on the physical design of undersea cable systems. He presently supervises a group with responsibilities including coaxial and lightguide cable and cable termination design and development of cable handling equipment and methods.



Donald Hadfield is a graduate of Lowell Technical Institute, in Lowell Massachusetts, where he received his B.S. degree in Mechanical Engineering. Mr. Hadfield began work at Simplex as Design Engineer in 1971 and has since designed improved cable terminations and cable handling machinery for both plant and shipboard use. He has been chiefly responsible for the design of facilities and equipment for the manufacture of lightguide fiber core.



Richard C. Mondello received his Ph.D. degree in Applied Mechanics from the Polytechnic Institute of Brooklyn in December of 1971. After graduation he began working as a Member of the Technical Staff of Bell Laboratories in the Undersea Cable Laboratory. He has worked on the design and testing of both coaxial and lightguide undersea cables. Most recently, he was involved in the design and construction of an Ocean Simulating Facility at Holmdel, New Jersey.

INSTALLATION OF A FIBER OPTIC SYSTEM IN AN ELECTRIC POWER STATION

O.L. BISHOP ITT Telecommunications

J.C. SMITH ITT Electro-Optical Products Division

ABSTRACT

A fiber optic link was installed for a T1 rate PCM System. The optic system was selected because of its unique ability to operate in a harsh EMI environment.

The cable was optically evaluated at -40°C where it experienced only a slight increase in attenuation. The cable flexibility was virtually unchanged at the installation temperature of -18°C.

INTRODUCTION

Electric utility high voltage substations present some unique problems for communications circuits. The circuits are required for alarms, telemetering, protective switching, and telephone service. Normally, the circuits are provided by individual copper wire pairs operating at voice frequency and tied to the local telephone lines or to the power company's private microwave system. Interference voltages may be induced on the copper wires from the high voltage lines. The problems are compounded during ground fault conditions or switching surges when communications can be most critic during transients, induced voltages may reac amaging or hazardous levels. As voltage current levels increase, the communicati difficulties also increase.

The classic solution to the problem has been isolation transformers with voltage ratings as high as 30KV for each information channel. Neutralizing transformers and optic couplers (not fiber optic systems) are also in use. The insulation qualities of fiber optic cables are now being exploited as an alternative to copper wire systems.

A 1.544 Mb/S (T-1 Rate) Fiber optic system has been designed by ITT that satisfies the communications needs of most electric utility installations. The system was installed at the Arrowhead station of Minnesota Power and Light Company (MP&L) in February and March 1978. The MP&L power station converts plus and minus 250KV interference within the station is quite high in spite of a ground grid and a completely shielded SCR room. The communications service was provided by copper wire pairs from a microwave station to the main building - a distance of 1200 feet. The wires were in ducts underneath the ground grid, but still had 180V spires during switching transients.

SYSTEM CHARACTERISTICS

The 1.5Mb/S Fiber Optic Transmission System installed at MP&L was designed as an extention of the ITT T324 24 channel PCM system. The optic units are designed to physically replace two existing channel cords or be operated in a separate housing. When the units are mounted in the basic T324 shelf as in the MP&L installation, the channel capacity is reduced by two. The optic units are compatible with any T-1 rate system.

A T-1 signal consists of a binary PCM signal with alternate ones inverted to eliminate the DC component and lower the average frequency. The ternary signal format is referred to as AMI (Alternate Mark Inversion). The AMI signal is not suitable for best optic transmission. The signal could be rectified to unipolar and transmitted at 1.544Mb/S, but certain system monitoring information is transmitted by purposely violating the AMI pattern (bi polar violation). This monitoring function is most important for repeatered systems. To retain all of the input information including bipolar violations, the 1.544Mb/S AMI signal is coded into a 3.088Mb/S signal with a unique pattern for each of the original ternary levels. The receiver converts the signal back to the 1.544Mb/S AMI format. Although the receiver sensitivity is reduced 3 dB by this technique, the sacrifice is worthwhile for complete transparency of signal transmission.

Optic Transmitter

The fiber optic transmitter uses an LED as the emitter. The operating wavelength is 850nM and the nominal output power is 10 μW (-20 dBm) average in the fiber core at 25% duty cycle. The LED is assembled and sealed with an optic fiber

positioned near the LED chip face for maximum launch efficiency. This pigtail fiber is terminated by a jeweled ferrule connector. The connector is mounted at the rear of the optic unit such that the connector can be accessed from the rear of the equipment when the unit is inserted. Electrically, the LED is positioned between a constant current source and a high current sink line driver which is switched on and off by the singal. The peak output power is controlled by the current source. The constant current source can be adjusted by a KIP switch to obtain an extra 3 dB output power in long systems or up to 9 dB less power in short systems with an accompanying improvement in reliability.

Optic Receiver

The fiber optic receiver uses a PIN detector and an integrating transimpedance amplifier with an FET input. The bandwidth of the integrating preamp is narrow for improved sensitivity, but the pulses must be reshaped in a later stage. The receiver recovers and retimes the signal and converts it to a ±3 Volt ternary signal completely compatible with a T-1 system. The receiver sensitivity is -50 dBm for a 10^{-8} Bit Error Rate.

Optic Connector

The ITT-Leeds jeweled ferrule connector was chosen for the system because of its proven performance in field installations. The connector loss with 55 uM core, graded index fiber is less than 2 dB. The transmitter uses such a combination, but the receiver PIN has a 135 uM core step index fiber attached. The receiver connector joins a 55 uM and a 135 uM core fiber in the favorable direction and has a loss of .5 dB.

System Gain

With a -20 dBm transmitter output and a -50 dBm receiver sensitivity, the system has a 30 dB system gain (or margin). System calculations must account for connectors, splices, cable loss, and margin for uncertainties. Normally, a 6 dB margin is allowed for time and temperature degradation. The maximum path length is then conservatively established as 3.5 km with 6 dB/km fiber in 1 km lengths. Dispersion is not a factor at 3 Mb/S.

FIBER OPTIC CABLE

The cable used in this system was required to meet the specifications shown in Table 1. In addition to these requirements, it was also specified that:

--The concentricity, diameter uniformity and circularity of the core and cladding must be such that if any two ends of fibers are cut, polished and spliced together, then the loss of splicing then must not exceed 1 dB.

--The fibers must be color coded for easy identification.

TABLE 1

Cable Specifications

Number of Fibers	3
Fiber Core	Graded Index
Core diameter ±6%	55 um
Numerical Aperture	.25 min.
Cladding diameter ± 6%	125 um
Protected Fiber diameter	1 mm ± 0.0 0.1
Minimum Bend Radius	10 cm
Tensile Strength	150 Kg
Attenuation	10 dB/km max. @ .85 um
Dispersion	3 ns/km max.

--The fibers must be continuously proof tested at a level of 1 % elongation, before cabling.

--No metallic cable elements are allowed.

--Cold bend. Cable should be bent once around a 50 mm radius mandrel with 5 kg. tension at -20°C.

--Impact. A 2 kg load with a diameter of 12.5 mm will deliver a blow from 100 mm height onto cable laid on a flat anvil for 200 cycles.

--Environmental conditions. The cable shall meet all its requirements over the temperature range of -15°C to +60°C. The attenuation shall not exceed more than 1.5 dB/km at -40°C.

It was also known that the cable would be installed in a trough which could be opened for inspection and at that time, people would walk on the cables. This consideration played a heavy role in the selection of the amount of strength member for the cable and the wall thickness of its jacket.

The fiber optic cable consists of a central optical bundle with a thin polyurethane jacket. Eighteen strands of strength members are helically laid around the jacket of the cable core. The strength members and the outer polyurethane jacket provides the handling characteristics needed in the cable installation and operation.

Figure 1 depicts the cable design. The optical core is formed by a central Kelvar® yarn ans three graded index fiber optic wave-guides alternated with three Kevlar® yarns.

The experience accumulated from previous cable development work indicated that the outer layer of strength member would be sufficient to provide the 150 kg load required during installation. However, it was felt that additional Kevlar® in the optical bundle would further ruggedize the cable and at the same time would serve as a filler and stress relief for the fibers.

Polyurethane was selected not only because of its abrasion and tear resistance, but also because of its contribution to lower the increase of attenuation due to the cabling processes.

Table 2 shows the attenuation and dispersion of the fiber optic waveguides in this cable.

TABLE 2

Fiber	Attenuation	Dispersion
Red	5.36 db/km @.85 um	.78 ns/km @ 9 um
Yellow	7.06 " " " "	1.93 " " " "
Blue	7.37 " " " "	1.47 " " " "

The attenuation of this cable was measured when the whole reel was left in a chamber at -40°C. It was found that the average change of attenuation was 1.3 dB/km.

INSTALLATION

The MP&L site required 335 meters of cable over a route including ducts between manholes, covered trough, and a vertical run in the operating building. Plastic water pipe was installed in the trough to protect the cable. The cable was left outside overnight at the installation site to check cold temperature handling. The cable prove to be flexible at the -18°C installation temperature.

The original reeled cable length was used in the installation began in the middle through the trough and duct into the building. Each part of the pull was divided into easily definable segments such as between manholes. The cable was pulled through each segment and laid out on the snow before starting the next segment. Polywater C[R] lubricant was liberally applied to the cable at each duct entry point and all pulls were made without mechanical assistance. Measurements made for comparison indicated that the maximum applied force was less than 100 pounds though it was not measured during the installation. Portions of the duct were clogged with ice and required steam and rodding before the cable installation. The total time required for the cable pull was five hours and the cable was frozen in place within two hours of completion.

Connector assembly started immediately after the cable installation. The ferrules were cemented to the clean fiber ends using an epoxy that cures in three hours at 65°C or 24 hours at 25°C. The first set of ferrules at one cable end was prepared and cured during a dinner break. The other end was prepared and cured overnight. The next day the fibers protruding through the ferrules were polished using relatively standard manual polishing techniques. The entire installation, including connectors, had taken place in 26 hours elapsed time.

The cable was looped in all possible combinations at one end and the two-way loss was measured from the other using an Optic Measurement Set manufactured by ITT-Leeds. The measured two-way loss was 8 dB typical. The measurements indicated excess loss for the short cable, but the discrepency probably resulted from the short cable length (355 Meters). In long fiber lengths, high order modes are stripped in the first portion and additional lengths appear to have less attenuation. The cable was continuously monitored by optic measurement for the next month with no changes noted. The electronics equipment was then installed and the system began carrying the normal MP&L communications traffic.

CONCLUSIONS

The MP&L installation is thought to be typical of a large number of electric power station requirements. The installation showed that the cable can co-exist with other cables and does not require any special equipment or handling for installation. The jeweled ferrule connector can be installed in the field wihtout undue difficulties.

The system is now operational carrying protective switching, telemetering, and telephone signals as a permanent part of the communications network instead of as a field trial. This is an important step in the maturity of Fiber Optics.

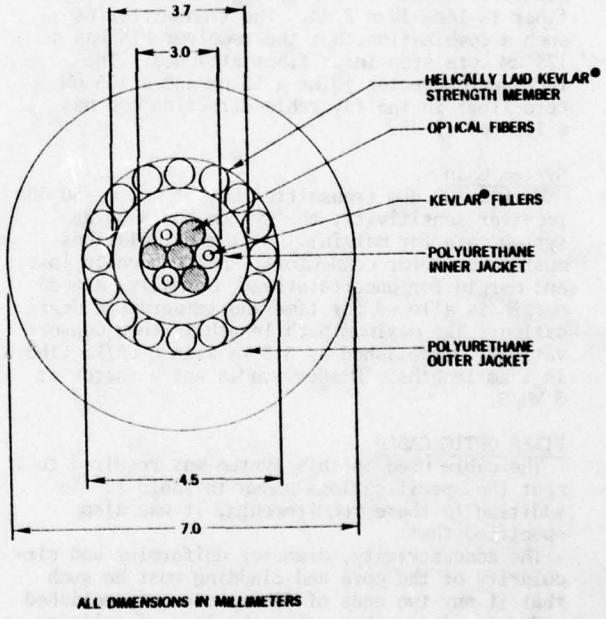
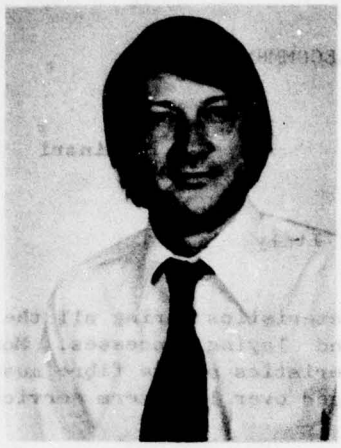


Figure 1

Fiber Optic Cable Design



O. L. (Lamar) Bishop received a B.E.E. degree from Georgia Institute of Technology in 1960 and an M.S.E.E. degree from the University of Maryland in 1967. He worked for Westinghouse Aerospace from 1960 to 1967 in airborne radar microwave and atenna design. In 1968, he joined ITT Telecommunications as a microwave radio design engineer. He is currently Project Engineer for the Fiber Optics program. He holds one antenna related patent and is a member of IEEE.



John C. Smith graduated from the Univerisded Tecnica del Estado - Santiago, Chile in 1958.

He joined ITT Electro-Optical Products Division in 1974, where he is presently engaged in the development and design of fiber optic cables, including evaluation and selection of equipment and materials. He is also involved in the development of fiber optic coatings and related processes.

Prior to joining ITT, he was associated with General Cable Corp. (Philadelphia Insulated Wire) where he was Supervisor of Products Engineering.

Earlier, he was associated with Simplex Wire and Cable, Power and Control Division.

From 1960 to 1966, he held the position of Supervisor of Compounding Laboratory in MADECO, Santiage, Chile, where he was responsible for compounds development for wire and cable.

HIGH QUALITY OPTICAL FIBRE CABLE FOR TELECOMMUNICATION

G. Grasso M. Pizzorno A. Portinari

Industrie Pirelli S.p.A. - Milan, Italy

Summary

The paper gives some results relevant to the research on optical fibre cables for medium and long distance telecommunications.
Firstly the problems which arise in manufacturing optical fibres cables are outlined after which the solutions which have been adopted are discussed.
In the second part the results obtained on the experimental production of cables having attenuation lower than 5 dB/km and bandwidth higher than 700 MHz·km are presented.

Introduction

As from 1973 a research programme for the manufacturing of long and medium distance telecommunication cables suitable for incorporating high quality optical fibres has been under way.
The research followed a development agreement signed in 1973 by Industrie Pirelli S.p.A. with Centro Studi e Laboratori Telecomunicazioni and Corning Glass Works (for the supply of optical fibres).
These fibres are multimode graded index fibres of 62 μm diameter core, 0.2 numerical aperture and with optical transmission characteristics which are of the highest quality currently available.
However, due to their small numerical aperture, these kinds of fibres are to be considered as a rather weakly guiding structures.
These fibres have therefore to be carefully protected against outside strain which may lead to a considerable amount of optical loss and, for this reason, a sophisticated cabling technique is needed.
The objective of the research has been to develop special types of fibre protections and cable structures that are capable of maintaining unchanged the fibre transmission characteristics during all the manufacturing and laying processes. Moreover the characteristics of the fibre must remain unchanged over long-term service contingencies.

Fibre coating

As it is well known, primary coated optical fibres cannot be incorporated in cables without resorting to a further protection. This protection is particularly necessary for the fibre to withstand axial and transversal stresses during cabling and laying operations.
Furthermore lateral strains could induce microbendings which in turn could lead to unacceptable increases in attenuation.
It has been established by theoretical considerations[1] that the optimum coating design should include a double protection made of one hard shell and another soft one.
As an extreme alternative to this solution the soft part of the protection can be substituted by a clearance (loose jacket).
It is also well known that, because of the possible damages to the optical characteristics that the protection itself can induce in the fibre, care must be taken in implementing these kinds of protections.
These damages stem mainly from the shrinking of the plastic materials which constitute the protection.
The plastic material shrinking can be chiefly associated with (1) the short-term cooling of the jacket during the coating operation (2), the long-term relaxation of the jacket and (3) the environmental thermal variations.
During the development of the optical fibre cables here described, both kinds of protection, namely (a) tight double jacket (with an inside soft layer) and (b) loose jacket, have been investigated.

- Jacket shrinking effects

(a) With regard to the tight jacket, all the above mentioned causes of shrinking make a significant contribution.
Due to the shrinking of the hard material, the fibre incorporated in the soft material buckles and takes on a helical configuration with a well defined pitch that, for a given fibre, depends mainly on the elastic characteristic of the soft material.
The extra attenuation derives from the main curvature of the helix and from the microcurvatures which arise when the soft layer is so compressed that the manufacturing irregularities of the hard layer can produce local distortions on the fibre's axis.

(b) The fibre inserted in the loose jacket behaves differently.
Firstly, the plastic material shrinking has minor importance, because the effect of the short-term cooling on the extrusion line can be minimized by letting the fibre slide inside the jacket, until the cooling is completed.
Secondly, the configuration of the fibre, due to the shrinking of a loose jacket, is not well defined.
As a matter of fact, this configuration can be considered helical but it is characterized by random variable parameters whose probability distributions depend, for a given fibre, on the inside dimension of the jacket, on the local frictions and on the excess fibre length.
In this case, microcurvature may arise when the fibre is pressed against the irregularities of the jacket's inner surface.
Therefore the optical transmission loss of a loose jacketed fibre, deriving from its main and local curvature, is not a defined function of the jacket shrinking.

- Type of jacket material

From the above mentioned considerations it follows that the choice of the plastic material, which is to be used as either the hard layer of the double protection or as the loose jacket, becomes very important.

The main requirements can be summarized as follows:

. high tensile modulus

. surface smoothness of the extrudate

. low shrinking due to the cooling after extrusion

. long-term stability

Many plastic materials were investigated.
Some data and experimental results are shown in Figs. 1, 2, 3.

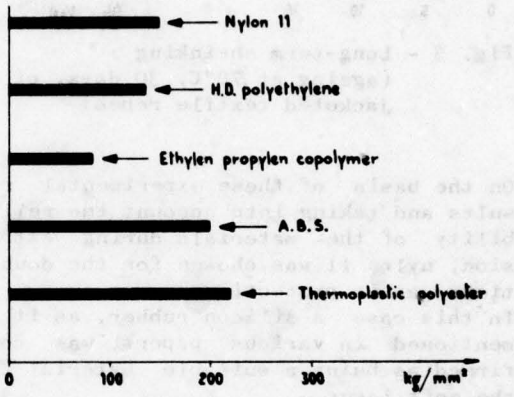


Fig. 1 - Tensile moduli of tested plastic materials

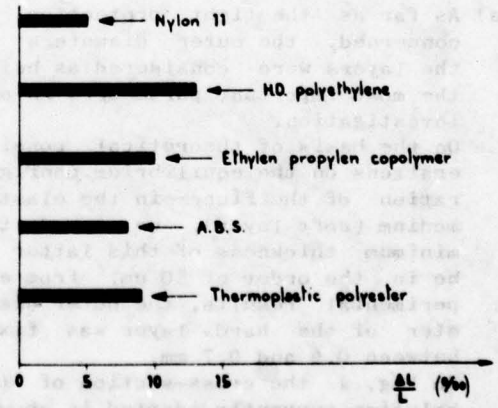


Fig. 2 - Shrinking due to the cooling after extrusion (material extruded on textile ropes)

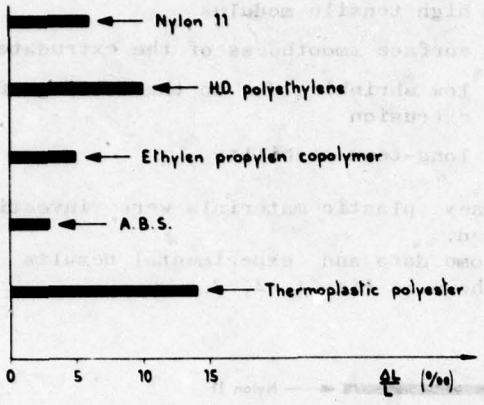


Fig. 3 - Long-term shrinking (ageing at 70°C, 30 days, of jacketed textile ropes)

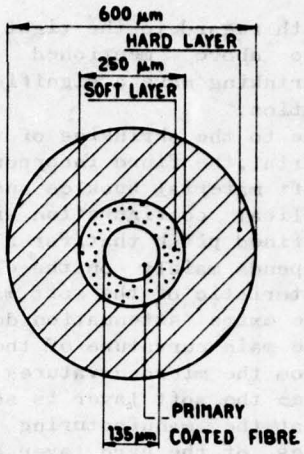


Fig. 4 - Cross-section of tight jacketed fibre

On the basis of these experimental results and taking into account the reliability of the materials during extrusion, nylon 11 was chosen for the double tight jacket protection.
In this case a silicon rubber, as it is mentioned in various papers, was confirmed as being a suitable material for the soft layer.
Because of the good compromise between long-term shrinking and inner surface smoothness, polypropylene was used for the loose protection.

- Jacket design and characteristics of the jacketed fibres

(a) As far as the tight protection is concerned, the outer diameters of the layers were considered as being the most important parameters in our investigation.
On the basis of theoretical considerations on the equilibrium configuration of the fibre in the elastic medium (soft layer), we found the minimum thickness of this latter to be in the order of 50 um. From experimental results, the outer diameter of the hard layer was fixed between 0.6 and 0.7 mm.
In Fig. 4 the cross-section of the solution currently adopted is shown.

The jacketing operation generally causes marginal increases (approximately 0.5 dB/km) in the fibre attenuation. As regards the behaviour when temperature variations occurr, we can say that, as the temperature lowers, the fibre attenuation gradually increases in a regular pattern. The increase may also be fairly significant with relatively small temperature variations and depends mainly on the geometric uniformity of the two layers.
A tipical attenuation-temperature characteristic is shown in Fig. 5.

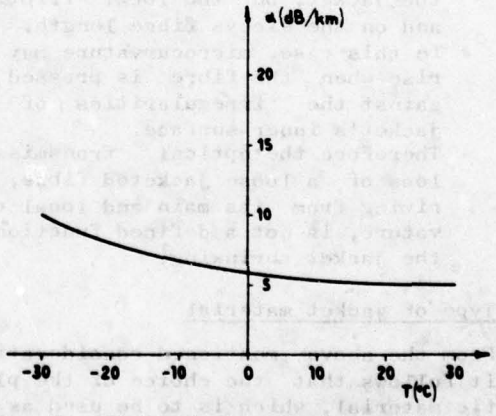


Fig. 5 - Tight double jacketed fibre: Indicative behaviour of the attenuation versus temperature

The protection of the fibre against lateral stresses is not very satisfactory because even small loads can induce extra attenuation.
The compression test results are shown in Fig. 6.

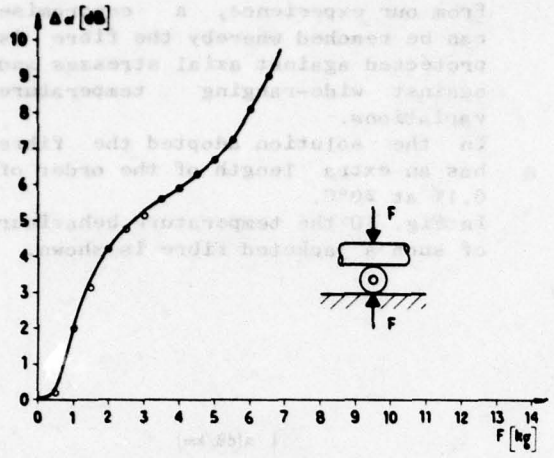


Fig. 6 - Tight jacketed fibre:
Increase of attenuation versus lateral compression force
(fibre compressed between a plate and a cylindrical body with R = 1 mm)

Moreover the tensile strength of the jacketed fibre is not much improved owing to the fact that the jacket dimension is very small.
At the moment this kind of protection is still under development and for the time being we do not consider it as the most suitable solution for use in long distance cables.

(b) The design of the loose jacketed protection was defined in two stages.
Object of the first stage was to establish the actual dimensions of the jacket. The inside diameter was determined in such a way as to minimize the effects of the short-term shrinking of the jacket after the extrusion: 0.7 mm was found to be the minimum acceptable diameter.
On the other hand, the thickness and the outer diameter were chosen on the basis of mechanical considerations.
In Fig. 7 the cross-section of the solution adopted is shown.
This kind of jacket provides a good protection against lateral stresses and its dimension can be considered as still being small enough for long distance cables.
Fig. 8 shows the results of the compression test on the chosen solution.

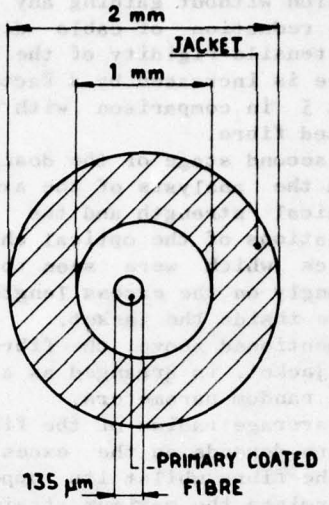


Fig. 7 - Cross-section of loose jacketed fibre

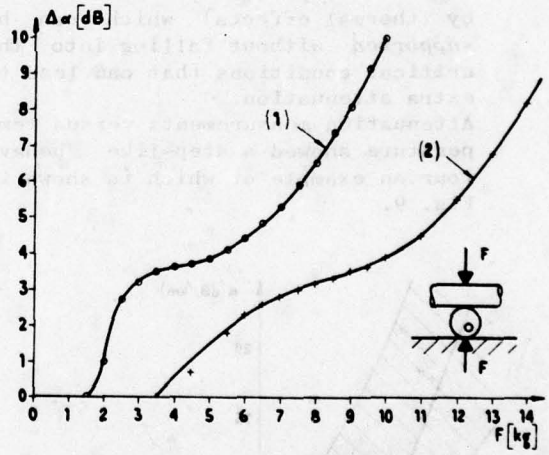


Fig. 8 - Loose jacketed fibres:
Increase of attenuation versus lateral compression force
(fibre compressed between a plate and a cylindrical body with R = 1 mm)

(1) jacket with outside/inside diameters 1.5/0.7 mm

(2) jacket with outside/inside diameters 2/1 mm

In this figure the performance of a smaller diameter jacket is also shown.

From the comparison it results that by using this last size one would considerably worsen the lateral protection without gaining any substantial reduction of cable dimension.

The tensile rigidity of the jacketed fibre is increased by a factor of about 5 in comparison with the uncoated fibre.

The second stage of the design dealt with the analysis of the axial mechanical strength and the thermal variations of the optical characteristics which were seen to depend strongly on the excess length of the fibre inside the jacket.

As mentioned above, the fibre, inside the jacket, is arranged as a helix with random parameters.

The average radius of the fibre curvature depends on the excess length of the fibre whilst its upper limit determines the maximum strain which can be applied to the jacketed fibre without causing dangerous stresses to the fibre itself; on the other hand, its lower limit determines the maximum compression strain (caused by thermal effects) which can be supported without falling into the critical conditions that can lead to extra attenuation.

Attenuation measurements versus temperature showed a step-like behaviour an example of which is shown in Fig. 9.

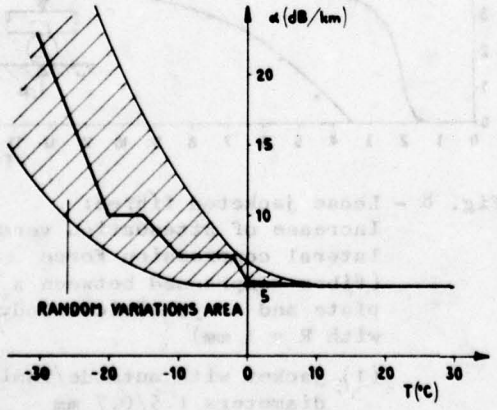


Fig. 9 - Loose jacketed fibre: Typical behaviour of the attenuation versus temperature

The attenuation remains nearly constant right down to a critical temperature below which random increases arise.

It was found that there is a quasi-definite relationship between the excess fibre length and this critical temperature.

From our experience, a compromise can be reached whereby the fibre is protected against axial stresses and against wide-ranging temperature variations.

In the solution adopted the fibre has an extra length of the order of 0.1% at 20°C.

In Fig. 10 the temperature behaviour of such a jacketed fibre is shown.

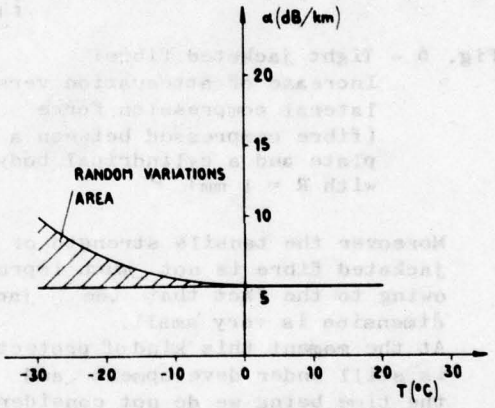


Fig. 10 - Loose jacketed fibre with extra length of 0.1% at 20°C: Attenuation versus temperature

Moreover it must be considered that the jacketed fibre can be temporarily submitted to axial strains of the order of 0.3% without any damage.

This results from the known Weibull survival distribution for this kind of fibres[2], taking into account the fibre excess length inside the jacket.

The extrusion line for jacketing the fibre has been carefully set up. In particular a sophisticated pay-off system was developed (Fig. 11).

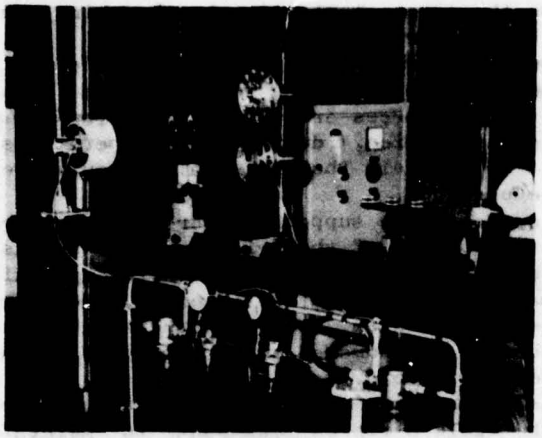


Fig. 11 - Fibre coating line:
Pay off system

The desired extra length for the fibre is achieved both by carefully controlling the back tension of the fibre and the cooling conditions of the plastic jacket.

The development of this kind of protection has now almost been completed. Its characteristics appear satisfactory in many respects.
It has subsequently been employed for the research on cabling operations in that, for the time being, it has been considered the most reliable for a high quality cable production.

Fibre cabling

On account of the dimensions and the strength of the protection selected, a traditional stranded cable structure was adopted.
Particular attention was devoted to the reinforcement, in order to allow long lengths of cable to be pulled inside ducts.
As a result of the above mentioned considerations, the jacketed fibre axial strain has to be kept under 0.3%, in order to ensure a safety margin.
Moreover, when designing the reinforcing element, its compression rigidity must also be taken into account.
We must in fact take into consideration that, in order to provide the external protection, a polyethylene sheath was selected. As a result of our investigation, even if a medium elastic modulus material was to be employed, owing to its thermal shrinking during the extrusion process, the cable core becomes compressed, thus causing a distortion of the jacketed fibres with a considerable increase in attenuation if no compression resistant element is incorporated into the cable.
Another important feature of a compression resistant element is that it improves the behaviour of the cabled fibres in temperature variations by increasing the range in which the attenuation of the fibres can be kept practically constant.
On the basis of these considerations, a wire, or a suitably stranded cord, of high tensile steel, was chosen as a central strength element.
In Fig. 12 the stress-strain diagram of the steel wire, adopted for the 8 fibre cable, is shown.

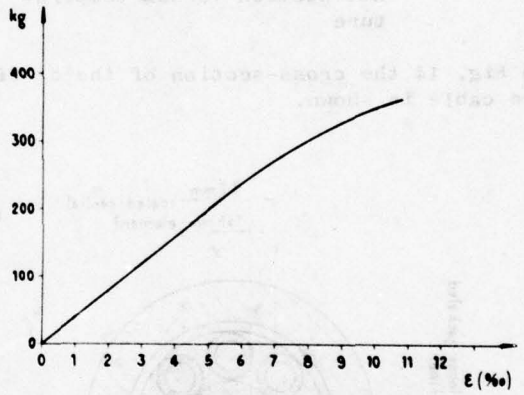


Fig. 12 - Special steel wire with o.d. 1.65 mm:
Pulling force versus elongation

Through experiments it was verified that it is possible to select the make-up of the reinforcing element in such a way as to withstand the compression caused by the external plastic sheath application and the pulling forces required during the installation.
Moreover, with regard to the behaviour in low temperature, the range in which the attenuation of the cabled fibres is constant may be increase by almost twice as much as that of the jacketed fibre and this because of the low thermal coefficient of the steel, which is effective in substantially reducing the thermal shrink-

ing of the cable (compare Figs. 13 and 10).

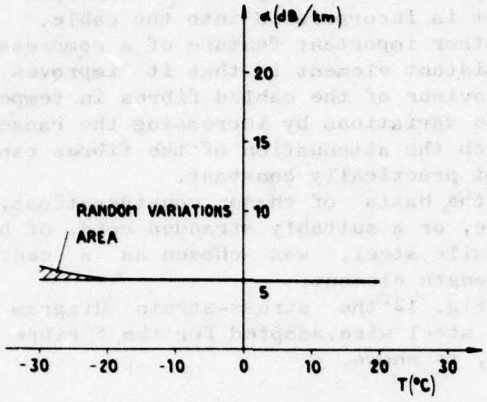


Fig. 13 - Cabled fibre (loose jacket, extra length 0.1% at 20°C): Attenuation versus temperature

In Fig. 14 the cross-section of the 8 fibre cable is shown.

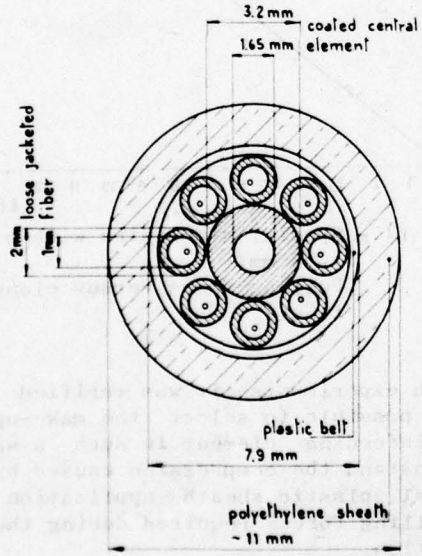


Fig. 14 - Cross-section of 8 fibre cable

A problem which is peculiar to cables, in which the reinforcing elements are placed in the central part of the core, is that of the possible slipping of the elements themselves.

The slipping may arise as a consequence of strong localized friction forces occurring on the external plastic sheath during the laying operations.

On short cable lengths, tested for this purpose, no slipping occurrs when these friction forces are maintained below 2 kg/m. In our opinion, during laying operations, it is unlikely that this value should ever be exceeded.

In practice, supposing there is a uniform distribution of the friction force and assuming its actual value as being approximately that of the cable weight, the force per unit length, acting on the sheath, is about a few hundred grams per metre for the heaviest cable.

As regards the stranding operation, if on the cable's fibres we want to maintain the same maximum strains that are allowed for the jacketed fibres, very low back tension has to be applied.

The cable core is then manufactured on a special floating bobbin stranding machine (Fig. 15) with a properly studied pay off system.

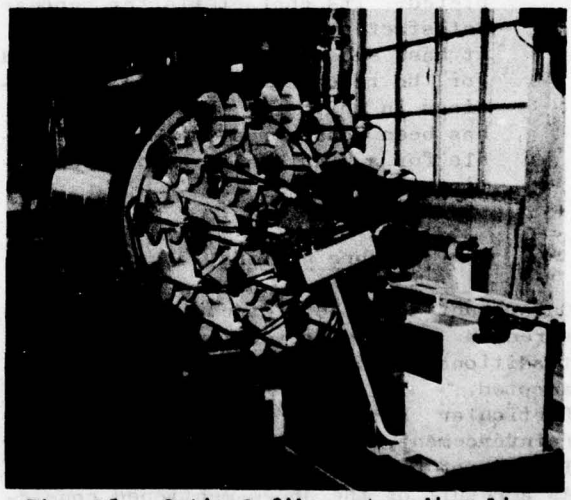


Fig. 15 - Optical fibre stranding line

Final protections

As the structure of the cable core is particularly strong, additional armourings can be avoided and the final protection can be ensured by a mere polyethylene jacket.

However, since the pneumatic resistance of

this type of cable is rather high, pressurization may be difficult.
In case of particular requirements for moisture protection, either an aluminium polylam sheath or a double polyethylene sheath can be used. From tests carried out on short samples, with both protections, the flexibility of the cable did not appear substantially reduced, in comparison with the single polyethylene jacket.
Thus the using of these above-mentioned protections should not lead to any consistent reduction of cable lengths that can be pulled during the installation.

Cable production

Cables with different fibre capacity, particularly 6, 8 and 12 fibres, have been experimentally produced.
For the time being, the production is mainly concentrated on 8 fibre cables.
Last year, of this 8 fibre cable (Fig. 16), 5 lengths of 1 km each were successfully installed in Turin's urban telephone ducts, in cooperation with S.I.R.T.I. and C.S.E.L.T. (COS 2 experiment[3]).
On this installed line an experimental transmission system at 140 Mbit/sec on 9 km length, without repeaters, was also successfully tested.

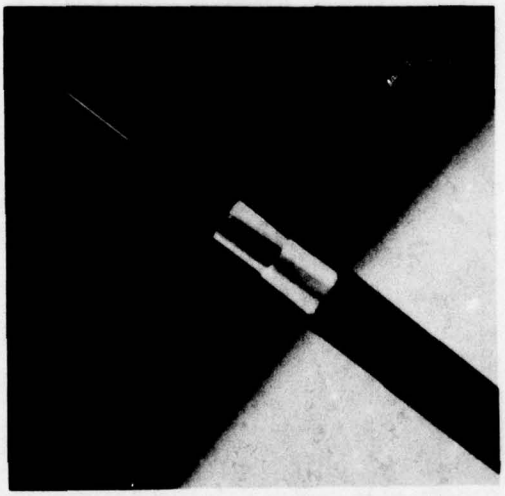


Fig. 16 - COS 2 experimental cable

An 18 fibre cable is now under development for the Italian Post Office Administration.

Cable performances

As an example of the performances of the tested optical cables, the characteristics of the 8 fibre COS 2 experimental cable (for which the most reliable statistical data are available) are listed hereunder, along with some information about the measurement methods developed. We point out that this cable is protected with a 1.5 mm single polyethylene jacket.

a) Optical transmission characteristics

In the COS 2 experimental cable the highest quality Corning fibres available were used: i.e. attenuation below 4.5 dB/km and bandwidth larger than 700 MHz·km at 820 nm.
According to our experience, the above two characteristics stayed practically unchanged throughout the cable manufacturing process. In fact, 95% of the fibres tested showed variations below $\pm$ 0.1 dB/km, for the attenuation, and below $\pm$ 50 MHz·km, for the bandwidth.
This range is to be considered consistent with the measuring errors.
For the remaining 5%, the variations were only marginally higher.
We therefore consider this cable suitable for incorporating the highest quality fibres without any practical deterioration of their optical characteristics.
It has to be stressed that the attenuation measurements (insertion loss method) and the bandwidth measurements (pulse method) were performed using a carefully studied "mode mixer" which allows the results of both measurements to be indipendent of the launching conditions.

b) Mechanical and environmental characteristics

The main cable characteristics are the following:

- max. allowed pulling force: 80 kg
  (cable weight approx. 100 kg/km)
- min. allowed bending radius: 30 cm
- impact test
  (the test is done by dropping a 10 mm diameter cylinder body onto the cable from a height of 1 metre)

  min. weight for fibre breaking : 3 kg

- compression test
  (the test is done by pressing the cable between two flat plates;
  compression speed 5 mm/min
  min. force, per unit length for fibre breaking: 100 kg/cm

- attenuation variation in temperature:
  no significant variations in the range - 20°C ÷ + 50°C.

Conclusions

It has been demonstrated that optical fibres with attenuation lower than 5 dB/km and bandwidth higher than 700 MHz·km can be incorporated into regularly manufactured cables without any appreciable decrease in their optical transmission characteristics.
On top of these results, successful COS 2 experimental laying operations and mechanical tests have established that, even if a greater awareness is needed of their particular characteristics, as compared with traditional cables, nevertheless conventional handling techniques can be used. Finally the stability of the transmission characteristics of cabled fibres against environmental variations has been checked. The conclusion that can be drawn is that this cable seems well suited for a reliable optical fibre transmission system.

Acknowledgments

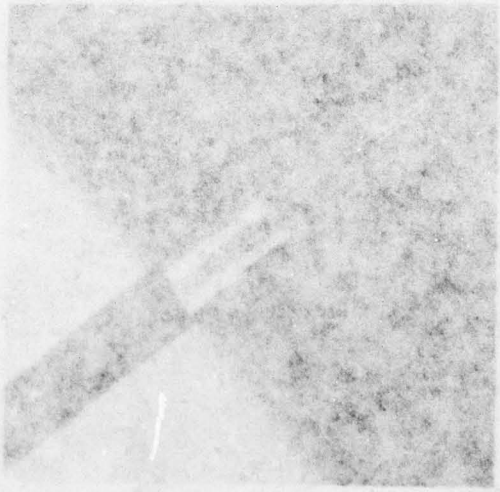
The authors wish to thank Industrie Pirelli S.p.A. for having given the permission to publish the results of their research activities on optical cables.
They also wish to thank S.I.R.T.I.'s staff who carried out the installation trials and tests and C.S.E.L.T.'s staff who were responsible for the on-site measurements and the transmission trials which, during the COS 2 experiment, have demonstrated the reliability of the cables developed.

References

1. Gloge D.; Optical Fibre Packaging and its Influence on Fibre Straightness and Loss, Bell System Tech. J. 1975, V54, 245-262.

2. Occhini E.; Mechanical Properties of Optical Fibres for Cables, Proceeding of 3rd European Conference on Optical Communication, Munich 1977.

3. Cocito G., Longoni S., Michetti L., Silvestri L., Tibone D., Tosco F., Vago A.; First Report on COS 2 Experiment Results, NTZ Bd 31 (1978) Heft 2, 135-137.





Giorgio Grasso was born in 1949. Degree in Electronic Engineering from the University of Bologna. He joined R. & D. Cable Laboratories of Industrie Pirelli S.p.A. in 1973. At present he is involved with optical fibre cables for telecommunication.



Massimo Pizzorno was born in 1943. Degree from Industrial Technology Institute of Milan. He joined R. & D. Cable Laboratories of Industrie Pirelli S.p.A. in 1969. At present he is working in the field of optical fibre cables for telecommunication.



Antonio Portinari was born in 1933. Degree in Electrical Engineering from University of Padua. He joined Industrie Pirelli S.p.A. in 1961. At present he is the manager of the Optical Fibre Cables Research and Development Laboratory.

UNIT CORE CABLE STRUCTURES FOR OPTICAL COMMUNICATION SYSTEMS

by

T.S. Swiecicki

Northern Telecom Canada Ltd.
Montreal, Quebec

F.D. King
F.P. Kapron

Bell-Northern Research
Ottawa, Ontario

ABSTRACT

An analysis of the design, fabrication and characterization of unit core cable structures for optical waveguides is presented. A mathematical model is developed which allows optimal dimensional values to be calculated for varying fiber parameters. Manufacturing methods are discussed, together with test results of prototype unit core cables utilising a reverse lay configuration.

INTRODUCTION

In order to obtain the maximum cost savings in telecommunication networks, resulting from the reduction or elimination of field electronics by using fiber optic systems, low attenuation and low cost cable structures are required.

Currently, low loss, high bandwidth optical waveguides are sensitive to microbending[1]. Low loss cables are most readily made by the 'loose containment' of the optical waveguides within the cable structure. A common method of achieving this is to enclose the fibers in a loose tube, which is extruded over individual or small groups of fibers. Multi-fiber cables can then be constructed by the planeterary cabling of a number of these tubes around a central member. Frictional forces occurring between the tubing, the central member and the cable jacket serve to constrain the linear expansion or contraction of the polyolefin tubes with respect to temperature, which would otherwise cause stresses in the fibers. While the loose tube construction has been successfully employed at Northern Telecom[2] and elsewhere to manufacture cables with attenuation lower than 4 db/km at 0.85μ, the designs do suffer from some disadvantages. These include:

(1) The individual tubing of fibers involves additional cost.

(2) The additional weight of the loose tube buffer results in an increase in inertial forces during cabling and the associated tension control problems.

(3) Effective water blocking of the loose tubes is not practical at present.

This last factor is of particular concern in the Canadian outside plant environment since ice crushing of optical fibers can substantially increase losses.

UNIT CORE STRUCTURES

As an alternative to the loose tube design, low loss optical fiber cables may be fabricated using a unit core structure. In this approach, a core structure is used consisting of a tensile member, surrounded by a profile extrusion containing a series of helical slots in its outside perimeter. In the cabling operation, the fibers are loosely placed in the helical slots and constrained by a tape wrap. Fig. 1 shows a cross section of a unit core fiber optic cable.

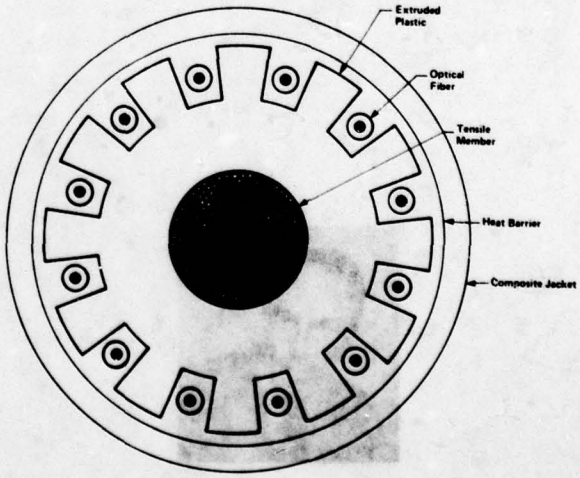


FIG. 1 CROSS SECTION OF UNIT CORE CABLE

The advantages of a unit core design include:

(1) An intermediate handling operation of the fibers during cable manufacture is omitted.

(2) Lower inertia of the reels during cabling allows tensions to be controlled more readily.

(3) The bonding of the extruded profile to the central member minimizes thermal effects.

(4) The structure is amenable to the introduction of some form of a water blocking medium.

Helically slotted unit core cables have been successfully developed by a number of manufacturers,[3,4] however, fabrication of the structure presents some practical difficulties. Firstly, the extrusion of a slotted core profile with a continuous helical lay requires either a rotating extrusion die or a rotating capstan/take up. Such equipment imposes limitations on the processing speed and has a high capital cost. Secondly, the cabler which lays the fibers in the helical slots must carry the fiber reels around the cable axis in exact synchronism with the helical slot lay. This requirement, together with the inertial forces involved, requires the cabler to be equipped with sophisticated position sensing and feedback control and as such limits manufacturing speeds and increases costs.

As an alternative to a continuous helically slotted core, the structure shown in Fig. 2 has been investigated, in an attempt to overcome these limitations.

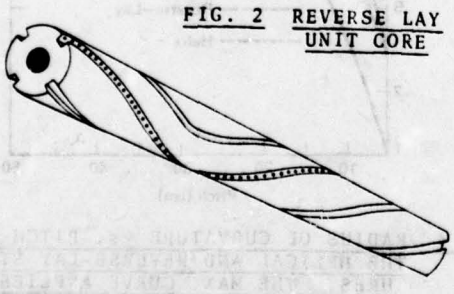


FIG. 2 REVERSE LAY UNIT CORE

In this structure, rather than spiral continuously around the core axis, the slots reverse their direction after each 360 degrees of rotation. (A further variation may use several rotations or less than one full rotation between reversals).

This modified structure preserves all the advantages of the basic unit core cable with the following processing improvements.

(1) No net rotation of the equipment used to produce the core is required. This simplifies the process and equipment and improves the potential line speed.

(2) There is no movement (other than unwinding) of the drums carrying the fiber in the cabling operation. The fiber cabling device may, therefore, have low inertia, allowing for simple control and higher line speeds.

MATHEMATICAL ANALYSIS

A mathematical model has been developed which allows optimum dimensions of the slot to be calculated for selected core outer diameters and fiber parameters (e.g. numerical aperture, core/cladding ratio and coating thickness). The temperature characteristics of the slotted core structure have also been predicted.

The locus of the fiber axis within the cable for either structure is given in the usual cylindrical coordinate system by the position vector.

$$\vec{r}(L) = \hat{x}\rho \cos\varphi + \hat{y}\rho \sin\varphi + \hat{z}\, L. \qquad (1)$$

Here x, y are unit vectors transverse to z along the cable axis, the radius ρ is constant, and the rotation angle φ as a function of cable length L and full-rotation pitch P is given by

$$\varphi_1(L) = 2\pi \frac{L}{P} \quad \text{.....helix} \qquad (2a)$$

$$\varphi_2(L) = 2\pi \sin^2\left(\frac{\pi}{2}\frac{L}{P}\right) \quad \text{....reverse-lay} \qquad (2b)$$

Equations (2) are displayed in Fig. 3; here

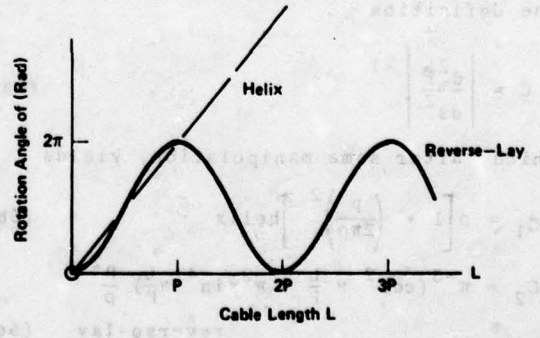


FIG. 3 ROTATIONAL POSITION OF THE FIBER AXIS vs. CABLE LENGTH IN BOTH THE HELICAL AND REVERSE-LAY STRUCTURES

the contrast between the geometrical properties of the two structures is apparent. The analytical form of (2b) is chosen as the simplest function that can satisfy the oscillatory behaviour of the reverse-lay structure in a minimum curvature fashion.

Fiber length S as a function of cable length L is obtained by integrating the incremental path length

$$ds = \sqrt{(\rho d\varphi)^2 + (dL)^2} \qquad (3)$$

to give

$$S_1 = L\left[1 + (2\pi\frac{\rho}{P})^2\right]^{\frac{1}{2}} \ldots \text{helix} \qquad (4a)$$

$$S_2 \simeq L\left[1 + (\frac{\pi^2}{2}\ \frac{\rho}{P})^2\right] \ldots \text{reverse-lay}, \quad P \gtrsim 20\rho \qquad (4b)$$

The result (4a) is well known, while the approximation (4b) avoids elliptic integrals and is accurate for practical values of pitch and radius. It is convenient to write both of these in the unified form

$$S \simeq L\left[1 + A(\frac{\rho}{P})^2\right] \qquad (4c)$$

$A_1 = 2\pi^2$ in the case of the helix,

$A_2 = \pi^4/4$ for the reverse lay,

from which, for example, the fractional excess fiber length ΔS is

$$\frac{S-L}{L} = \Delta S = A(\frac{\rho}{P})^2 \qquad (5)$$

Some properties of the structure with respect to curvature, tension and temperature change can now be investigated. The radius of curvature C is evaluated from the definition

$$C = \left|\frac{d^2\vec{r}}{ds^2}\right|^{-1} \qquad (6a)$$

which, after some manipulation, yields

$$C_1 = \rho\left[1 + \left(\frac{P}{2\pi\rho}\right)^2\right] \text{helix} \qquad (6b)$$

$$C_2 = \pi^{-3}(\cos^2 \pi\frac{L}{P} + \pi^2 \sin^4 \pi\frac{L}{P})\frac{P^2}{\rho}$$

reverse-lay (6c)

From equations 6(b) and 6(c), it is evident that whereas for the full helix, the curvature radius (C_1) remains constant, that for the reverse lay structure (C_2) varies from a maximum value P^2/π^3 at the turning points L = 0, P, 2P .... (see Fig. 3) to a minimum value P^2/π^4 midway between. This result is plotted in Fig.4.

The incremental effect on the radius of curvature when the core is wound onto a reel can be calculated, but because the direction (and magnitude in the reverse lay case) of the curvature vector $\left|\frac{d^2\vec{r}}{ds^2}\right|$ varies along the fiber axis, the result is analytically complex. A worst/best case estimate can, however, be made when the fiber and cable curvatures lie parallel or anti-parallel respectively. If R is the cable curvature radius, then the resultant minimum and maximum curvature radii are respectively

$$\text{Worst case} \ldots\ (\frac{1}{C} + \frac{1}{R})^{-1} \qquad (7a)$$

$$\text{Best Case} \ldots\ (\frac{1}{C} - \frac{1}{R})^{-1} \qquad (7b)$$

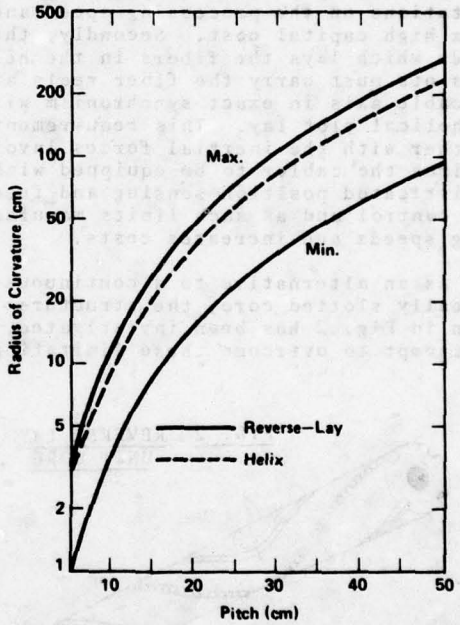


FIG. 4 RADIUS OF CURVATURE vs. PITCH FOR THE HELICAL AND REVERSE-LAY STRUCTURES. THE MAX. CURVE APPLIES TO THE REVERSE-LAY TURNING POINTS, THE MIN. CURVE FOR POINTS MIDWAY BETWEEN

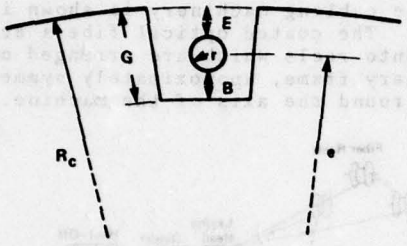
Tension and temperature effects are calculated using the geometry of Fig. 5. Differentials of (4c) are taken with the definitions of Young's modulus Y and Poisson's ratio σ applied to the cable

core; the fiber is not stressed. As tension is applied to the cable, the fiber lowers into the slot until contact with the groove bottom is made. At this point, the cable elongation is

$$\frac{\Delta L}{L} = \frac{2B}{\rho(D-1)-2\sigma(R-G)}, \quad D = \frac{1}{A}\left(\frac{P}{\rho}\right)^2 \qquad (8a)$$

with the associated tension across the core area a

$$\tau = Ya\,\frac{\Delta L}{L} \qquad (8b)$$



G = Groove Depth
r = Radius of Coated Fiber
B = Distance of Fiber From Groove Bottom
E = Distance of Fiber From Groove Top
R_c = Outer Radius of Core Structure

FIG. 5 GEOMETRY OF THE FIBER WITHIN THE GROOVE SLOT

These quantities are plotted in Fig. 6, using the values of Table 1 and assuming that the fiber is initially midway in the slot.

TABLE 1

Fiber OD	$2r = 0.4$ mm
Core OD	$2R_c = 6.4$ mm
Slot Depth	$G = 1$ mm
Fiber Axis Cyl. Radius	$\rho = R_c - \frac{1}{2}\sigma = 2.7$ mm
Elongation under Tension	$\frac{\Delta L}{\tau L} = Ya = 1.39 \times 10^{-5}$/lb
Initial Fiber Groove Separation	$B, E = \frac{1}{2}(G - 2r) = 0.3$ mm
Expansion coeff. of cable	$\alpha_c = 13 \times 10^{-6}$/C°
Expansion coeff. of Fiber	$\alpha_f = 0.5 \times 10^{-6}$/C°

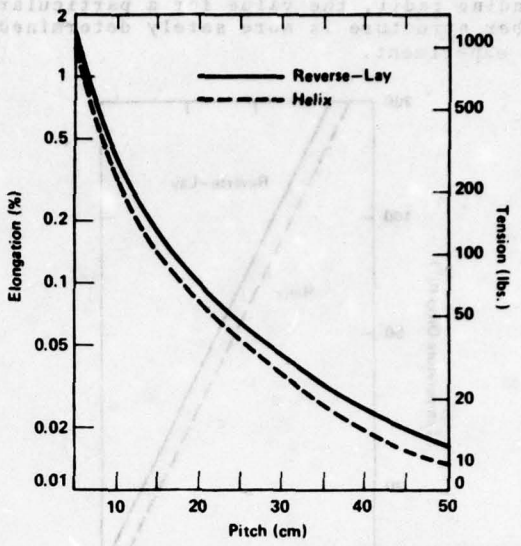


FIG. 6 MAXIMUM CABLE CORE ELONGATION AND ASSOCIATED TENSION FOR ZERO FIBER STRESS VERSUS PITCH

As the cable temperature is lowered, the fiber will rise in the slot since the liner coefficient of thermal expansion of the cable core greatly exceeds that of the fiber ($\alpha_c >> \alpha_f$). In a manner similar to that used above, equation (4c) gives the temperature drop ΔT which causes fiber contact with the groove top. Neglecting small terms,

$$\Delta T = \frac{2E}{\rho[D(\alpha_c - \alpha_f)-(\alpha_c + \alpha_f)]} \qquad (9)$$

Once the fiber has reached the top of the slot, further temperature contractions of the structure must be accommodated by fiber buckling. However, such buckling will reduce the net radius of curvature and can eventually add to the fiber loss. The temperature reductions required to produce fiber contact with the top of the slot are shown in Fig. 7.

Summary of Analysis

It is apparent from the preceding analysis that maximum elongation of the cable for minimum fiber stress is obtained by using the shortest possible pitch for the structure. However, with a reducing pitch the radius of curvature also reduces and eventually reaches a value where finite bending effects, especially on reeled fibers, become significant. The minimum curvature radius which can be tolerated, without loss, by a particular fiber structure depends on its numerical aperture, and core/cladding ratio. While there exist some published works[5] in this area which allow estimates to be made of acceptable

bending radii, the value for a particular fiber structure is more safely determined by experiment.

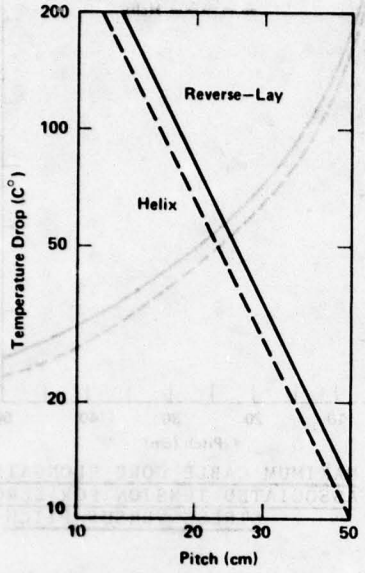


FIG. 7 ALLOWABLE TEMPERATURE DROP, TO PRODUCE FIBER CONTACT WITH GROOVE TOP vs. PITCH

FABRICATION

Fabrication of the cable is, at present, confined to three separate stages. Firstly, a suitable slotted core with a precalculated slot width, depth and pitch is manufactured. The fibers are then laid into the slots under low tensions and retained within the slots by a helically applied binder tape. Finally, a heat barrier tape and composite cable jacket are applied overall.

The machinery used to fabricate the reverse lay unit core is shown schematically in Fig. 8.

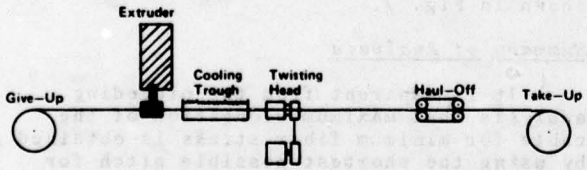


FIG. 8 UNIT CORE FABRICATION

A tensile strength member is passed through an extruder crosshead containing a profile extrusion die arrangement. The extrudate is twisted around its own axis by a twisting head located downstream of the cooling trough. Plastic deformation of the extruded profile occurs between the crosshead and the cooling trough, which induces a helical lay into the slots. Reversing the direction of rotation of the twisting head produces helical slots but of opposite hand. During this process the extruded core between the twisting head and the haul off deforms elastically. This elastic deformation is allowed to relax prior to the cable being wound onto a cable drum. Considerable care is required in the selection of the die profile, in order to achieve the correct dimensional properties of the core. In addition, cooling of the extrudate has been found to be critical if an imperfection-free and undistorted profile is to be obtained.

The cabling machinery is shown in Fig. 9. The coated optical fibers are wound onto reels which are arranged on a stationary frame, approximately symmetrically around the axis of the machine.

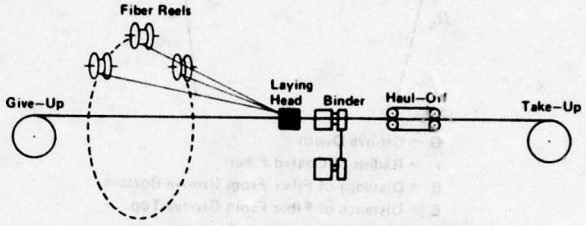


FIG. 9 FIBER LAYING

A low inertia laying head, which is driven directly by the slotted core, guides and places the fibers into their appropriate slots. The core is then taped by a conventional tape binding head. The torsional rigidity of the fibers was calculated to be sufficient to neutralise the finite positive and negative torsions that a reverse lay structure imposes. Prototype cable test results have confirmed this prediction.

The cable jacket is applied using conventional cable making equipment. Initial cable lengths have been jacketed with a sealed aluminum/polyolefin jacket over a longitudinally applied heat barrier tape. This type of jacket has been found to provide adequate mechanical protection, as well as acting as a barrier to prevent the permeation of moisture into the cable core. Other jacket constructions are also being considered.

CABLE TESTING AND MECHANICAL CHARACTERISTICS

Any fiber optic cable design has to withstand tension, bending, torsion and abrasion encountered during installation, as well as the extreme seasonal temperature fluctuations prevalent in Canada.

A number of prototype cable lengths utilising the reverse lay slotted core construction have been manufactured to date. The core profile used in all these cables resembles that shown in Fig. 1 and can accept a maximum of 12 fibers.

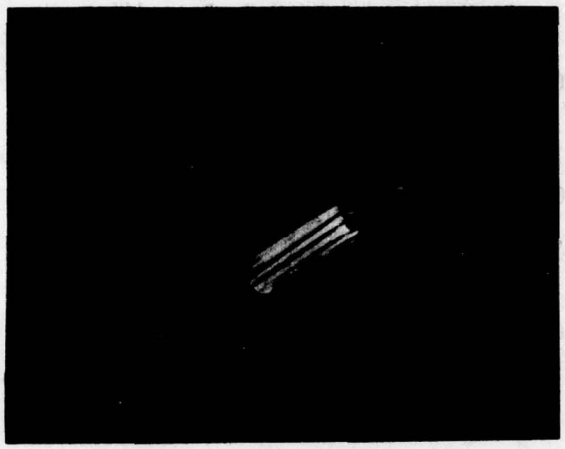


FIG. 10 12-FIBER REVERSE LAY SLOTTED CORE CABLE

The tensile strength member used was a multi-strand steel wire rope selected to give adequate stress/strain characteristics, as well as flexibility. The use of a non-metallic strength member is also being considered. All other materials used during manufacture are standard cabling grades with proven outside plant performance.

Testing Program

These cable lengths were subjected to a testing program initially developed during the manufacture of optical fiber cables for a field trial in Montreal during 1977[2]. In this program, the mechanical characteristics of the cable were determined by a series of tests aimed at assessing the radial and axial properties of the cable such as crush resistance, impact resistance, torsion, bending and repeated flexing properties. Short lengths of the slotted core cable were subjected to these stresses while the light power through the cable was monitored.

The test conditions are summarized in Table 2.

In all these tests, there was no detectable change (<0.01 dB) in attenuation.

The tensile strength of a cable can be defined as its ability to withstand axial tension, such as that encountered during cable installation, without any degradation of the optical properties of the waveguides. Ideally, tests to determine the tensile strength should be conducted on long cable lengths, since in short samples relative movement between the fibers and the cable can be exaggerated and thereby distort the results. The test apparatus subjected a 100 m length of cable to a tensile load as shown in Fig. 11.

TABLE 2

TEST	TEST CONDITION
Crush Resistance	87 kg load applied over 100 mm for 90 mins.
Impact Resistance	2 impacts with 25 mm dia. hammer on same location, 12Nm per blow.
Torsion	±360° over 2 m length, 10 cycles.
Bending	Two 360° turns around 60 mm radius mandrel.
Repeated Flexing	30 cycles (±90°) around 120 mm radius mandrel.

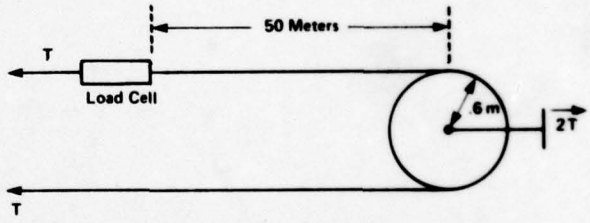


FIG. 11 APPARATUS FOR TENSION TESTING

After applying a load and maintaining it for a period of 10 mins., the cable was allowed to relax and the attenuation of the waveguides was measured. Tests on prototype lengths indicate that axial tensions greater than 1100N are easily withstood. Different values can be obtained with alternative strength members.

Temperature Characteristics

The coefficient of attenuation in respect of temperature (γ_t) was determined by subjecting a loose coil of cable (160 m in length) to varying temperatures in an environmental chamber. After allowing sufficient time for temperature equalisation, the attenuation of the cabled fibers was measured. Eary test results indicate that σ_t is less than 0.02 db/km/°C in the temperature range -20°C to +30°C.

CONCLUSIONS

Test results on prototype cable lengths of a new reverse lay/unit core design have proved to be encouraging both in terms of mechanical and optical properties. The reduction in intermediate handling of individual fibers promises to significantly improve the yield of low loss optical cable during manufacture. The cabling of fibers around a reverse lay slotted core structure has considerably reduced the inertial problems generally associated with the low tension cabling required by optical fibers. This will allow the use of higher cabling speeds with the potential of cabling in tandem with either jacketing or core extrusion. These factors, together with the low cost equipment required, make the reverse lay slotted core cables attractive for the production of economical low loss cables.

ACKNOWLEDGEMENTS

The authors would like to acknowledge the contribution of the many individuals in both Bell-Northern Research and Northern Telecom Canada Ltd. who have contributed to the work outlined in this paper.

References

(1) W.B. Gardner, Bell Systems Tech. Journal, Feb. 1975, p.457.

(2) An Overview of a Fiber Optic Exploratory Trial in Montreal, K.Y. Chang, E. Marthaler and H.K. Basmadjian, ICC/78.

(3) Present State of the Optical Cable Design, Splicing Processes & Interconnection Systems, G. Le Noane, CNET France, NTC/77.

(4) "Spectral Loss Performance of Optical Fiber Cables using Plastic Spacer & Metal Tube", T. Mizuicami, T. Hatta, S. Fukada, K. Mikoshiba and Y. Shimohori, IEE Conf./75.

(5) Laminated Fiber Ribbon for Optical Communication Cables, C.M. Miller, Bell Systems Tech Journal, Sept. 1976, p. 934.



Tom Swiecicki graduated from King's College, London University, England with an honours degree in Mechanical Engineering in 1970. Before emigrating to Canada in 1976 he was employed by Pirelli General Cable Works Ltd. in a number of positions associated with the production of telecommunication cables. Since 1976 he has been with Northern Telecom (Canada) Ltd., firstly in the Cable Division R&D Laboratories in Lachine, Quebec, presently he is a Manager with the Optical Systems Division and is based in Ottawa, Ontario.



Dave King was born in Drogheda, Ireland in 1946. He received his B.Sc. and M.Sc. degrees from Trinity College, Dublin in 1967 and 1968 respectively and his Ph.D. degree in Physics from McMaster University in Hamilton, Ontario in 1973. Since 1973 he has been with Bell-Northern Research in Ottawa where he has been involved in the development of light emitting diodes, low loss optical fibers and optical fiber cables for use in optical communication systems. He is currently manager of the component capability group in the Optoelectronics department.



Felix P. Kapron received a B.A.Sc. degree in engineering physics from the University of Toronto in 1962, and an M.Sc. and Ph.D. in physics from the University of Waterloo in 1964 and 1967, respectively.

After joining Corning Glass Works, Corning, N.Y. in 1967, Dr. Kapron participated in the realization of the first low-loss waveguides, and later predicted minimum chromatic dispersion near 1.3 μm. Since coming to Bell-Northern Research, Ottawa, Ontario in 1973, he has expanded into analytical work on other optical communications components and is presently senior scientist in Optoelectronics.

Dr. Kapron is a member of the Optical Society of America, the Society of Photo-Optical Instrumentation Engineers, and the Canadian Association of Physicists.

AUTHOR INDEX

Adams, J. E. 206
Armstrong, R. S. 321
Asam, A. R. 346
Bark, P. R. 379
Beaud, G. 74
Bishop, O. L. 390
Biskeborn, M. C. 139
Bissell, D. R. 191
Bolza, A. 394
Borsuk, L. M. 350
Briggs, D. R. 356
Bright, J. E. 7
Bruggendieck, S. 35
Byrd, N. R. 249
Campbell, H. D. 273
Carel, A. B. 299
Carfagno, S. P. 325
Chadwick, D. 191
Chan, M. G. 99
Chandan, H. C. 331
Clark, R. A. 7
Cobb, G. S. 281
Cobo, J. 225
Cobo, J. 313
Cox, E. R. 306
Daly, J. M. 293
Eoll, C. K. 156
Falquero, E. A. 92
Fellows, B. W. 385
Fialcowitz, R. P. 249
Freiburger, R. J. 370
Frey, D. R. 281
Fuchigami, T. 176
Fuse, K. 62
Gabriel, A. P. 200
Gac, N. A. 281
Gambs, G. C., Jr. 325
Gasparian, G. A. 370
Gilroy, H. M. 99
Gleason, R. F. 385
Grasso, G. 394
Groenendaal, G. C. 20
Gromek, M. T. 249
Gulati, T. 342
Hadfield, D. A. 385
Hall, L. J. 51
Hatta, T. 107
Heyward, I. P. 130
Ho, C. C. 220
Inada, K. 362
Ishibashi, M. 213
Ishihara, H. 258
Ishizaki, K. 258
Iwamoto, Y. 258
Jayne, L. M. 356
Johnson, L. 99
Justiss, J. D. 200
Kalish, D. 331
Kapron, F. P. 404
Kawawata, S. 107
Kertscher, E. 74
King, C. B. 342
King, F. D. 404
Kiss, K. D. 116
Kiss, K. D. 139
Kobayashi, T. 362
Kojima, N. 176
Lawler, J. D. 84
Lawrence, D. O. 273
Maklad, M. S. 346
Malawer, E. G. 116
Maltz, G. 293
Mangaraj, D. 139
Marsden, E. P. 235
Martin, W. M. 99
Marx, M. F. 241
McIntosh, T. F. 15
Milliken, B. C. 321
Mogi, A. 213
Mondello, R. C. 385
Mori, A. 27
Mori, K. 258
Nakagawa, S. 107
Nantz, T. D. 187
Nerer, P. 7
Noda, H. 107
Normanton, J. K. 44
Oestreich, U. 379
Ohmura, M. 176
Orimo, K. 62
Paulson, D. V. 325
Pomerantz, M. 350
Pomerantz, M. 370
Portinari, A. 394
Quan, F. 342
Robert, Ph. A. 171
Robinson, J. E. 44
Rodriguez, J. L. 313
Rossi, R. 84
Rossi, R. 200
Refi, J. J. 264
Sato, M. 107
Sato, S. 27
Schmidt, B. 74
Shibata, K. 62
Smith, D. C. 191
Smith, J. C. 370
Smith, J. C. 390
Sugaware, Y. 362
Sugiyama, K. 258
Suzuki, F. 27
Suzuki, Y. 27
Swiderski, M. J. 264
Swiecicki, T. S. 404
Tariyal, B. K. 331
Uchida, N. 362
Villarig, M. 225
Virkus, K. J. 84
Warren, P. C. 206
Wilson, R. R. 20
Woodard, D. P. 1
Yamamoto, T. 213
Yamauchi, R. 362
Zeidler, Günter 379



International Wire & Cable Symposium

SPONSORED BY U.S. ARMY COMMUNICATIONS RESEARCH AND DEVELOPMENT COMMAND (CORADCOM)

13, 14 & 15 November 1979

Cherry Hill Hyatt House, Cherry Hill, N. J.

Please provide in the space below a 100-500 word abstract (12 copies) of a proposed technical paper on such subjects as design, application, materials, and manufacturing of Communications and Electronics Wire & Cable of interest to the commercial and military electronics industries. Such offers should be submitted no later than 9 April 1979 to the Commanding General, U.S. Army Communications Research & Development Command, ATTN: DRDCO-COM-RM-1 (E. Godwin), Fort Monmouth, NJ 07703.

Title: _____

Authors: _____

Company: _____

Address: _____

Staple



Fold here

Stamp

Commanding General
US Army Communications R & D Command
ATTN: DRDCO-COM-RM-1 (E. Godwin)
Fort Monmouth, NJ 07703

Fold here

SECURITY CLASSIFICATION OF THIS PAGE (When Data Entered)

REPORT DOCUMENTATION PAGE

READ INSTRUCTIONS BEFORE COMPLETING FORM

1. REPORT NUMBER: N/A	2. GOVT ACCESSION NO. (9)
3. RECIPIENT'S CATALOG NUMBER: Final rept.	
4. TITLE (and Subtitle): (6) Proceedings of the [redacted] International Wire and Cable Symposium [redacted] (27th) held at Cherry Hill, New Jersey on November 14, 15 and 16 1978.	5. TYPE OF REPORT & PERIOD COVERED: Final 14-16 November 78
	6. PERFORMING ORG. REPORT NUMBER: N/A
7. AUTHOR(s): Various (10) Chairman: Elmer F. Godwin	8. CONTRACT OR GRANT NUMBER(s): None (16)
9. PERFORMING ORGANIZATION NAME AND ADDRESS: Fiber Optic Team (DRDCO-COM-RM-1) Multichannel Trans. Div. CENCOMS, US Army Communications R&D Command	10. PROGRAM ELEMENT, PROJECT, TASK AREA & WORK UNIT NUMBERS: Proj. No. 1L1 62701 AH92 AMC Code [redacted] 11.01
11. CONTROLLING OFFICE NAME AND ADDRESS: Fiber Optic Team (DRDCO-COM-RM-1) Multichannel Trans. Div., CENCOMS US Army Communications R & D Command	12. REPORT DATE (11) Nov[redacted]978 13. NUMBER OF PAGES: 414
14. MONITORING AGENCY NAME & ADDRESS (if different from Controlling Office): Same as 11 above. (12) 432p.	15. SECURITY CLASS. (of this report): UNCLASSIFIED 15a. DECLASSIFICATION/DOWNGRADING SCHEDULE

16. DISTRIBUTION STATEMENT (of this Report)

Approved for Public Release: Distribution Unlimited.

17. DISTRIBUTION STATEMENT (of the abstract entered in Block 20, if different from Report)

18. SUPPLEMENTARY NOTES

Proceedings of technical papers presented at 27th International Wire and Cable Symposium sponsored annually by US Army Communications Research & Development Command.

19. KEY WORDS (Continue on reverse side if necessary and identify by block number)

Aerospace electronics, cable design, cable evaluation, cable manufacture, cable materials, cable performance, cable testing, electronic wiring, fiber optics, interconnections, military electronics, telephone communications, wire insulation, wire materials, wire testing.

20. ABSTRACT (Continue on reverse side if necessary and identify by block number)

The International Wire and Cable Symposium is the only symposium of its kind in the world. The proceedings include fifty-three (53) papers in the field of electrical and electronic wire and cable, materials, testing, evaluation, connections, splicing, installation, applications, fire retardancy, fiber optics, manufacturing, processing, wire/cable design and manufacturing.

410 489

DD FORM 1 JAN 73 1473 EDITION OF 1 NOV 65 IS OBSOLETE

UNCLASSIFIED

SECURITY CLASSIFICATION OF THIS PAGE (When Data Entered)